Fach Geologie

Provenance analysis of sediments from IODP Expedition 341 sites U1417 and U1418 – Implications on climate-tectonic interactions at the southern Alaska continental margin

Inaugural-Dissertation
zur Erlangung des Doktorgrades der Naturwissenschaften
im Fachbereich Geowissenschaften
der Mathematisch-Naturwissenschaftlichen Fakultät
der Westfälischen Wilhelms-Universität Münster

Vorgelegt von
Barbara Huber
aus Hannover
2018

Dekan: Prof. Dr. Harald Strauß

Erstgutachter: Prof. Dr. Heinrich Bahlburg

Zweitgutachter: Dr. István Dunkl

Tag der mündlichen Prüfung: 26.04.2019

Tag der Promotion: 26.04.2019

Table of Contents

Abstract

Interactions of climate and tectonics during orogen formation are a subject of ongoing research with many open questions concerning their cause and effect relationship. The southern Alaska continental margin hosts the highest coastal mountain range on earth, the St. Elias Mountains. Its formation during the last ca. 10 Ma coincides with substantial climate alteration leading to strong glaciation, offering prime conditions for research on climate-tectonic interactions. Most of the detritus produced during the formation of this orogen is transported into the Surveyor Fan and its precursor in the Gulf of Alaska that were drilled during IODP expedition 341.

In this case study, we present a multi-method provenance analysis of sediments from two sites in the distal and proximal Surveyor Fan (site U1417 and U1418, respectively) using single grain geochemical analysis of amphibole, garnet, pyroxene and epidote along with zircon U/Pb and (U-Th)/He dating and REE analysis, Ar-Ar dating of amphibole and mica and point counting of light and heavy minerals. These data are compared to results from onshore studies and are interpreted in the context of changes in glaciation and tectonics.

Our results are in line with tectonics as prevalent factor in determining the main erosion centers with substantial modifications caused by the changing glacial cover. The recovered Miocene to Pleistocene sediments have been almost exclusively fed from long-term sources on the Chugach, Prince William and Yakutat terranes. Additional input from the Coast Plutonic Complex cannot be excluded but seem to have been minor. Differences in the characteristics of the sediments from the distal and proximal site are in line with the position of the sites in relation to the tributary system of the Surveyor Fan to impact their provenance hampering direct correlation and complementation of the two datasets.

The oldest Miocene sediments reveal high amounts of coaly material being very likely fed from the Kulthieth formation. A change in sediment composition implies rising input from the Chugach metamorphic complex from ca. 11 Ma onwards, leaving tectonic processes associated with the collision of the Yakutat terrane as the most likely cause. Input from the Chugach terrane in the late Miocene implies the existence of an effective transport system from the mountain range into the Gulf of Alaska, draining to the south east.

Single grain analysis of heavy minerals and zircon age spectra point to a progressive change in provenance from Miocene to Pliocene, very likely triggered by the advancing glaciation and erosion of the nearshore Yakutat terrane areas. This indicates the increasing glaciation to have enhanced erosion in the newly glaciated areas downslope in the spine of the orogen affecting the main area under erosion causing modifications of erosion centers.

The provenance affiliations of the sediments are in line with changes associated with the northern hemisphere glaciation at the Plio-Pleistocene transition while a homogenous sediment petrography and geochemistry during the Pleistocene imply climatic changes at the mid-Pleistocene transition did not cause significant changes in the main area under erosion. Glaciers seem to have remained in their topographically defined positions over time.

1 Introduction

Climate and tectonics are competitively discussed for being the main driver of exhumation and erosion (e.g., Molnar 1990; Berger et al., 2008a; Roe et al., 2008; Enkelmann et al., 2009, 2010, 2015, 2017; Yanites and Ehlers, 2012; Lease, 2018). Source-to sink studies of coastal mountain belts and their adjacent marine sediment sinks offer the potential to use sedimentation rates and changes in sediment petrography to unravel information on the orogen evolution and the impact of climatic and tectonic forces. Especially areas affected by variable degrees of glaciation are considered to be strongly affected by climate-tectonic interactions. The Southern Alaska continental margin hosts the highest coastal mountain range on Earth (Enkelmann et al., 2015). Its formation coincided with ongoing accretion and subduction of the Yakutat terrane and climatic changes leading to strong glaciation of the mountain range (Reece et al., 2011) (fig. 1). With its accretional character, its transitional setting of subduction to strike-slip conditions, the occurrence of some of the largest historical earthquakes, tsunami, high rates of convergence and exhumation, rapid orogenic deformation, extremely high sedimentation rates and the occurrence of the thickest and oldest glacial record of Cenozoic northern Hemisphere glaciation it is a prime location to answer key questions concerning continental growth and climate-tectonic interaction (Gulick et al., 2004, 2015). One of the main questions is how the increasing but variable glaciation impacted erosion centers and the tectonic stress regime of the active orogen (e.g., Berger et al., 2008a; Enkelmann et al., 2015, 2017; Worthington et al., 2018). Current research is mainly interested in the reaction of the orogen to the increasing glaciation since the Miocene and modification of glacial-interglacial cycles at the mid-Pleistocene transition (e.g., Gulick et al., 2015; Dunn et al., 2017; Enkelmann et al., 2017; Worthington et al., 2018). Glaciation of wide parts of the orogen hinders direct sampling of bedrocks, leaving river and offshore sediments as major sources for information on orogen formation (fig. 1).

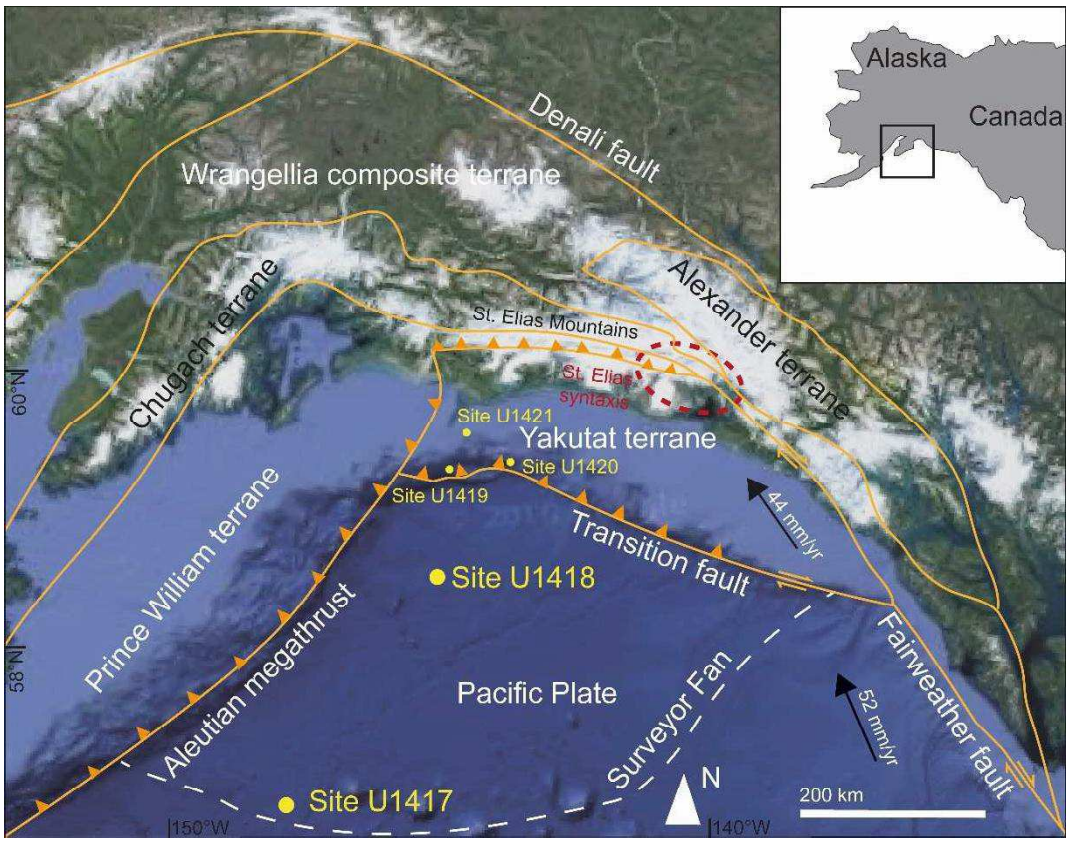

Figure 1: Generalized terrane map of the southern Alaska continental margin. IODP Expedition 341 sites are displayed in yellow. Modified after Perry et al., 2009; Expedition 341 Scientists, 2014; Enkelmann et al., 2017; Worthington et al., 2018.

The proximity of the orogen to the Gulf of Alaska and the absence of major onshore sediment basins allow fast transport of the orogenic detritus into the offshore sediment sinks without major modifications (Gulick et al., 2004). The bulk of these sediments is transported into the relatively confined area of the Surveyor Fan on the Gulf of Alaska abyssal plain. During IODP expedition 341 five sites were drilled on the Surveyor Fan recovering Miocene to Pleistocene sediments (Expedition 341 Scientists, 2014). The most distal site on the Alaska abyssal plain recovered the only complete Miocene to recent archive of orogenic detritus shed from the Southern Alaska margin.

The scope of IODP expedition 341 was to (I) trace how climate change since the Miocene affected the tectonic regime of an active orogenic system; (II) unravel the timing of advance/retreat phases of the northwestern Cordilleran ice sheet and its relation to the timing of other global ice sheets; (III) perform an expanded source-to-sink study against the background of interacting glacial, tectonic, and oceanographic processes that led to the formation of one of the thickest Neogene high-latitude continental margin sequences; (IV) explore how productivity, nutrients, freshwater input to the ocean, and surface and subsurface circulation in the northeast Pacific are connected and how they are related with the global carbon cycle; (V) establish a high temporal resolution record of the spatial and temporal behavior of the Neogene geomagnetic field using a multidisciplinary approach (Expedition 341 Scientists, 2014).

While the general source area for the Surveyor Fan sediments is known on the large scale, the details of this source-to-sink connection are not. Sedimentary provenance analysis is a key instrument to unravel the details of this connection and the denudation history of the source area from the sedimentary record. The goal of this study is to discover the following aspects by performing a provenance analysis of samples from the distal (U1417) and one proximal (U1418) site in the deep part of the Gulf of Alaska:

1. Document changes in sediment petrography and single grain geochemistry in the Miocene to Pleistocene Surveyor Fan and precursor sediments.
2. Perform a source-to-sink study to connect the offshore deposits with their onshore source rocks.
3. Examine the changes in provenance in the context of interactions between glacial and tectonic processes.
4. Link the findings from onshore studies with the new offshore data.

We use a multi-method approach of petrographic and single grain geochemical and geochronological methods. **Chapter 2** examines the single grain geochemistry of amphibole and garnet and variations in heavy mineral composition from Miocene to Pleistocene. Changes in heavy mineral composition during the Miocene, predating the onset of glaciation, imply tectonically-induced changes associated with the rise of the St. Elias Mountains to affect erosion centers and sediment transport. Garnet and amphibole data as well as U-Pb zircon age spectra presented in **Chapter 3** suggest that the Chugach metamorphic complex was the main sediment source at the end of the Miocene. Changes from the Miocene to Pliocene in geochemical compositions of amphibole and garnet and zircon U-Pb age spectra point to a climatically induced change in erosion centers associated with the advance of glaciers towards the tidewater line funneling increasing input from the lower grade metamorphic lithologies at the southern flanks of the orogen on the Chugach, Prince William and Yakutat terranes. No such changes could be found for the mid-Pleistocene transition implying a homogenous provenance during the climatic changes at the mid-Pleistocene transition. In **Chapter 4** abundant rock fragments imply high input from a metamorphic source area during the Miocene and Pliocene and slightly higher input from sedimentary rocks in the Pleistocene being in line with increased erosion of predominantly un- or low-grade metamorphic sedimentary formations in the areas closer to the shore during phases of strong glaciation after the onset of the Northern Hemisphere glaciation. This is also supported by the pyroxene and epidote data. No implications for a changing provenance at the mid-Pleistocene transition could be found in either of the data. The framework compositions are slightly different at the proximal and distal

sites indicating the positions of the two sites relative to the tributary system of the Surveyor fan to impact provenance which is also implied by the heavy mineral spectra and zircon data in **Chapter 2 and 3.**

1.1 Climate tectonic interactions at the southern Alaska continental margin

Numerical modelling as well as empirical studies have shown that climate and tectonics are not acting as separate processes but rather interact in a complex manner, connected through erosion and exhumation (Molnar and England, 1990; Raymo and Ruddimann, 1992; Roe et al., 2008). Modelling of surficial and tectonic processes as well as studies of orogens indicate modification of tectonic stress through erosion and redistribution of mass (Berger et al., 2008b; Roe et al., 2008; Worthington et al., 2010, 2018; Pavlis et al., 2012; Meigs et al., 2008; Tomkin and Roe, 2007). Tectonic uplift can directly impact erosion by creating higher relief and increasing the basin size and thereby accumulation space for the orogenic detritus. Another option is an indirect coupling of erosion and tectonics by changing climate caused by the rise of mountain belts, leading to changes in surface temperature, precipitation and circulation patterns (fig. 2). The resulting glaciation or enhanced precipitation can amplify erosion. Both scenarios are followed by mass redistribution which then can impact tectonics and further iterate (fig. 2).

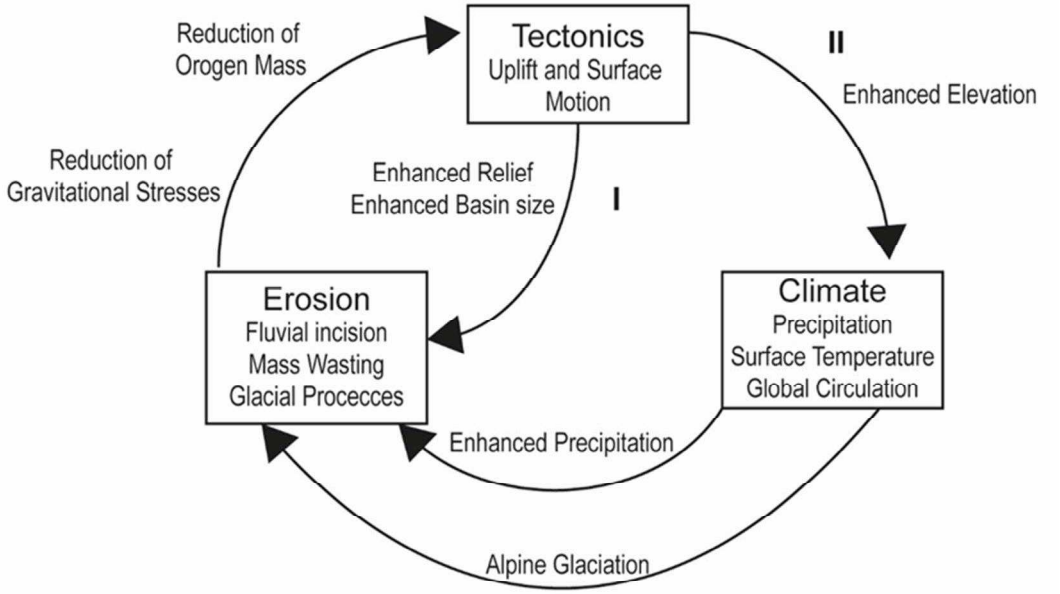

Figure 2: Basic loops of feedbacks and interactions between tectonics, climate and erosion. Loop I directly couples tectonics and erosion with tectonics increasing erosion rates by increasing elevation, relief and drainage basin size and an indirect loop II where enhanced elevation leads to changes in climate by means of precipitation, surface temperature and global circulation, resulting in glaciation and precipitation funneling erosion. Both loops result in a redistribution of mass that effects tectonics. After Willett et al., 2002.

Increasing rates of sedimentation have been found during the Neogene in on- and offshore sedimentary basins worldwide (Donnely, 1982; Zhang et al., 2001; Molnar, 2004). They are assumed to have resulted from increasing erosion rates caused by substantial changes in climate (Donnely, 1982; Molnar and England, 1990; Zhang et al., 2001; Molnar, 2004). Still, the details on how climate and tectonics interact are part of ongoing research (e.g., Molnar and England, 1990; Raymo and Ruddiman, 1992; Meigs and Sauber, 2000; Molnar, 2004; Clift, 2006; Huntington et al., 2006; Clift et al., 2008; Wipple, 2009; Whitaker, 2012; Gulick et al., 2015; Enkelmann et al., 2015; Worthington et al., 2018). Constraining information on climate

and tectonics and their interactions in the Earth system can be best addressed by the direct study of orogens or by analysis of orogen-derived sedimentary deposits in parts of the world where intensive tectonic and climatic processes have interacted or are still going on. One example are the St. Elias mountains where active tectonics as well as changes in climate and glaciation coincided during the last ca. 8 Ma leading to the formation of the highest coastal mountain range on Earth (e.g., Berger et al., 2008a, b; Reece et al., 2011; Gulick et al., 2004, 2015; Enkelmann et al., 2008, 2010, 2015, 2017).

How tectonic and climatic processes at the South Alaskan continental margin are interacting is still poorly understood and in the focus of current research (e.g., Berger et al. 2008a; Berger and Spotila 2008; Enkelmann et al. 2015; Enkelmann et al. 2010, 2017; Meigs et al. 2008; Spotila et al. 2004; Spotila and Berger 2010; Worthington et al. 2010; 2018; Dunn et al., 2017). Rapid exhumation in the St. Elias orogen started as the result of the final collision of the Yakutat terrane with the South Alaskan margin and accretion along the Chugach-St. Elias fault between ca. 11–8 Ma (Enkelmann et al., 2009; Falkowski et al., 2016; Dunn et al., 2017) (fig. 1). Impact of the Yakutat collision at the indenting plate corner has been found to be spatially limited to max. 30 km while flat subduction of the Yakutat slab caused deformation and exhumation up to 500 km further landward to the west (Enkelmann et al., 2017). Highest exhumation rates in the St. Elias mountains appear together with the highest precipitation rates, highest topography and the center of active deformation in the Syntaxis area (fig.1) (Spotila et al., 2004).

Alpine glaciation at the southern Alaska continental margin started when mountains were high enough at ca. 7 Ma and expanded to tidewater glaciation between 6.7 and 5.0 Ma (Lagoe et al., 1993). Glaciation became more intense with the onset of Northern Hemisphere glaciation at 2.5 Ma and the mid-Pleistocene transition at 1 to 0.7 Ma (Lagoe et al., 1993). The overall long-term erosion and exhumation pattern is characterized by focused erosion on the seaward side of the orogen where precipitation is high (>3m/a) while the dry northern side (<0.6 m/a) erodes much slower (Pewé 1975; Spotila et al., 2004; Berger et al. 2008a). Denudation rates in the subaerial parts of the orogenic wedge were relatively low predating the mid-Pleistocene transition (35 km^2/Ma unit flux, Berger et al. 2008a). Increasing sedimentation rates in the Yakataga Formation starting at ~6-5 Ma (Lagoe and Zellers 1996) and a small population of young ZFT (Zircon Fission Track) ages in the Miocene Surveyor Fan sediments support rising erosion and exhumation rates at the southern Alaska continental margin in the Miocene (Dunn et al. 2017). Sedimentation rates of the Yakataga formation rose even further at the Miocene-Pliocene boundary (Lagoe and Zellers, 1996). During the Pleistocene and especially after the mid-Pleistocene transition, denudation increased strongly resulting in denudation rates of ca. 190 km^2/Ma unit flux) (Berger et al. 2008a). Recent exhumation rates as revealed by ZFT and (U-Th)/He zircon ages from glacial sediments show strong variations in exhumation along strike, especially in the area of the St. Elias Syntaxis (fig. 1), where strike slip motion changes to convergence at the Yakutat plate corner (Enkelmann et al. 2010).

Sedimentation rates on the Surveyor Fan record a strong enhancement during the Pleistocene. Starting with rates of ~30–70 m/My between 5.2 Ma to 2.8 Ma for the distal fan, sedimentation rates doubled to peak values of 120 ± 20 m/My between 2.4 Ma and 2.0 Ma in response to the expansion of Northern Hemisphere glaciation at the Plio-Pleistocene boundary (Gulick et al. 2015). Reduced sedimentation rates of ~60 m/Ma from 1.6 Ma to 1.2 Ma indicate an apparent reduction of regional glacial erosion (Gulick et al. 2015). Coinciding with the mid-Pleistocene transition sedimentation rates rose to peak rates of ~140 m/Ma by 0.8 Ma, being even higher at more proximal sites (80 cm/ka at site U1418; 130 cm/ka on the shelf; up to 300 cm/ka on the slope (Gulick et al. 2015). Enkelmann et al. (2017) infer that the feedback mechanism between tectonics and erosion causing extremely rapid exhumation at the Syntaxis was initiated by the geometry of the subducting Yakutat plate, with increasing crustal thickness and a cuspate shape, and not by the onset of glaciation. The highly erosive glacial system that evolved since the end of the Miocene is supposed to have caused erosion centers to focus on the more windward positions of the orogen (Berger et al., 2008a, b; Meigs et al., 2008). Glacial systems are effective erosion agents creating high rates of sediment flux which can be as high as in large rivers (Nygard et al., 2007; Koppes et al., 2015; Jaeger et al., 1998; Gulick et al., 2015). Enkelmann et al. (2017) found exhumation in the orogen to be shifting on a local scale since the Miocene caused by tectonic uplift and global climate change. Berger et

al. (2008a) suggested that enhanced glaciation in the St. Elias orogen at the mid-Pleistocene transition and the resulting enhancement in erosion in the orogen and deposition of the eroded material on the active deforming wedge caused a structural reorganization of the orogen. A change in faulting patterns has been found for the offshore deformation front in response to increased sediment accumulation at the mid-Pleistocene transition from distributed all over the shelf to away from the glacial depocenters (Worthington et al. 2018). In contrast, Enkelmann et al. (2015) infer the change in climate at the Plio-Pleistocene transition to have already caused structural changes in the orogen.

Further west along the southern Alaska continental margin, where rock uplift is slower, an initial pulse of rising erosion rates has been discovered during the amplification of glaciation in the Pliocene (4.2–2.9 Ma) whereas erosion decreased after 2.9 Ma when glaciation was still strong but glacial erosion had outpaced rock uplift (Lease, 2018). Tectonic influx into the St. Elias orogen has also been exceeded by erosion and efflux of material from the orogen since the mid-Pleistocene transition (Gulick et al., 2015). Still, sedimentation rates in the Gulf of Alaska rose in the following period (Gulick et al., 2015) very likely because of the higher relief of the orogen providing more material for erosion.

1.2 Sedimentary provenance analysis-from offshore sink to onshore source

In sedimentary provenance analysis, an inverse approach is used to draw information from the sedimentary product of exhumation and erosion on the source rocks using diverse tools of mineralogy, petrography and geochemistry as the key to decipher the linkages. Provenance analysis of offshore sediments has already been used successfully in other areas to unravel regional tectonic changes and modifications of sediment dispersal mechanisms and pathways (e.g., Usman et al., 2014; Pandey et al., 2016). Improving technical methods allow to extract detailed information on the source rocks like metamorphic grade, source lithology, crystallization age of single grains as well as on the exhumation history of the source area from sedimentary deposits (e.g., Sircombe, 1999; Sha and Chappell, 1999; von Eynatten and Gaupp, 1999; Morton et al., 2004; Zack et al., 2004; Triebold et al., 2007; Whipp et al., 2009). While the most traditional approach in sedimentary provenance analysis is sediment petrography (Dickinson and Suczek, 1979; Ingersoll et al., 1984; Dickinson et al., 1985, Weltje and van Eynatten, 2004; Garzanti, 2016), advancements in heavy mineral analysis, analysis of the geochemistry of single grains, isotope geochemistry, geochronology and geothermochronology have decisively enhanced the tool kit for provenance analysis (Mange and Morton, 2007). Use of multi-method approaches has been found to be best to reveal as much information from sediments as possible (Garzanti, 2016). Especially the study of heavy minerals and rock fragments is considered most promising (Garzanti, 2016).

Various processes influence the sediment composition on the way from source to sink, starting with the source rock lithology and tectonic processes as well as relief and climate in the source region, followed by modifications during transport and intermittent storage, reworking and deposition in the sink that is finally sampled (e.g., Johnsson, 1993; Weltje and von Eynatten, 2004) (fig. 3). These processes leave their imprint in the sediment composition and petrography. In quantitative provenance analysis, vertical or lateral trends in sediment composition are related back to tectonic processes in the source area, changes in sediment dispersal or variations in climate during the generation of the sediments using an inverse approach (Weltje, 2012). The term sediment generation has been introduced to sum up this complex network of processes. Figure 4 illustrates how sediment composition changes during successive filling of a fault bounded sedimentary basin with two tributary systems (source I and II) at two different sites (sites a and b). The parent lithologies, being of plutonic, metamorphic and sedimentary character, are assumed to be distinguished unambiguously. The ternary diagram illustrates how the composition of the generated sediment changes if only source area I or II contributes sediment to the basin or how a mixture of both sources would develop. In a natural system, the source areas might be much more diverse and mixing much more complex. These complex networks of different process allow sediments derived from the

same sources to show different compositions when the path of sediment generation differs as well as different sediment sources to generate the same kind of sediment (von Eynatten and Dunkel, 2012). Notwithstanding these pitfalls, sedimentary provenance analysis is successfully applied as events in the hinterland are often reflected by sudden changes in the sedimentary record that can be revealed supported by the improving analytical methods that allow precise dating of crystallization age, analysis of source rock type and metamorphic conditions as well as the cooling and exhumation history of the source rocks (e.g., Carter and Bristow, 2003; Morton 2004, 2005; Andò et al., 2014; Moore et al., 2015; von Eynatten and Dunkl, 2012; Dunn et al., 2017).

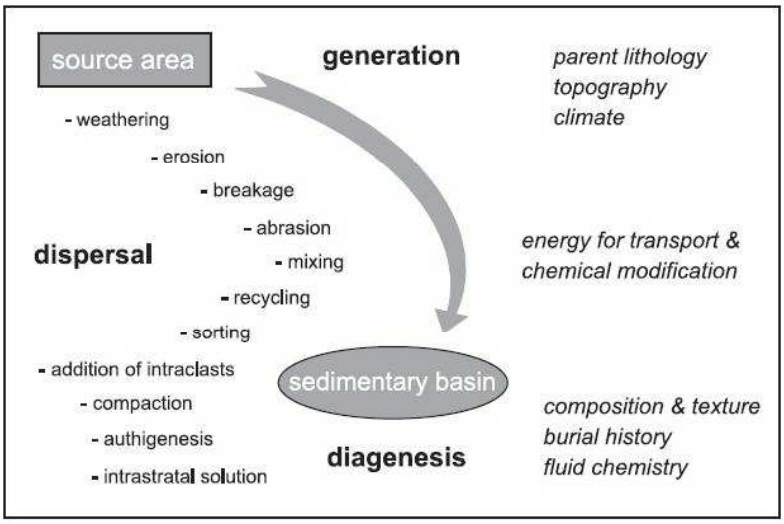

Figure 3: Process during the main stages of sediment evolution (bold) and controlling factors altering sediment composition on the way from source to sink (Weltje and von Eynatten, 2004).

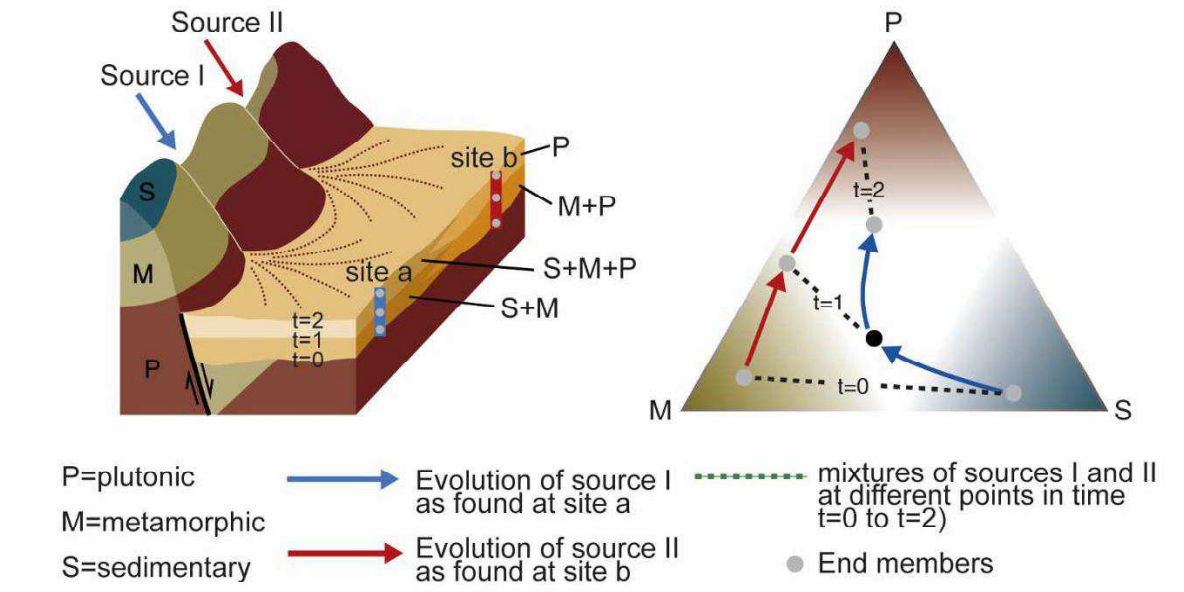

Figure 4: Evolution of sediment composition in a fault-bounded sedimentary basin during successive incision of a fluvial system and erosion of a heterogenous source area with two drainage areas of different composition. A illustrates how uplift affects the source rocks types available for erosion during successive unroofing. B shows how the sediment composition changes at three points in time. Dashed lines illustrate how mixtures of sediments derived from both source areas would develop. M = metamorphic source rock, P = plutonic source rock, S = sedimentary source rock. Modified after Weltje et al., 2012.

1.3 References cited

Andò, S., Morton, A., Garzanti, E., 2014. Metamorphic grade of source rocks revealed by chemical fingerprints of detrital amphibole and garnet. In: Scott, R.A., Smyth, H.R.,

Morton, A.C., Richardson, N. (Eds.). Sediment Provenance Studies in Hydrocarbon Exploration and Production. 386. Geol. Soc. London, Spec. Publ., pp. 351–371.
Berger, A.L., Gulick, S.P.S., Spotila, J.A., Upton, P., Jaeger, J.M., Chapman, J.B., Worthington, L.A., Pavlis, T.L., Ridgway, K.D., Willems, B.A., and McAleer, R.J., 2008a. Quaternary tectonic response to intensified glacial erosion in an orogenic wedge. Nature Geosci. 1, 793–799.
Berger, A.L., Spotila, J.A., 2008. Denudation and deformation in a glaciated orogenic wedge: The St. Elias orogen, Alaska. Geology 36, 523-526.
Berger, A.L., Spotila, J.A., Chapman, J.B., Pavlis, T.L., Enkelmann, E., Ruppert, N.A., Buscher, J.T., 2008b. Architecture, kinematics, and exhumation of a convergent orogenic wedge: A thermochronological investigation of tectonic–climatic interactions within the central St. Elias orogen, Alaska. Earth Planet. Sci. Lett. 270, 13–24.
Carter, A. Bristow, C.S., 2003. Linking hinterland evolution and continental basin sedimentation by using detrital zircon thermochronology: a study of the Khorat Plateau Basin, eastern Thailand. Basin Res., 15, 271-285.
Clift, P.D., 2006. Controls on the erosion of Cenozoic Asia and the flux of clastic sediment to the ocean. Earth Planet. Sci. Lett. 241, 571–580.
Clift, P.D., Hodges, K.V., Heslop, D., Hannigan, R., Van Long, H., Calves, G., 2008. Correlation of Himalayan exhumation rates and Asian monsoon intensity. Nature Geosci. 1, 875-880.
Dickinson, W.R., Suzeck, C.A., 1979. Plate tectonics and sandstone compositions. Am. Assoc. Petroleum Geologists Bull. 63, 2164-2182.
Dickinson, W.R., 1985. Interpreting Provenance Relations from Detrital Modes of Sandstones. In: Zuffa, G.G., (Ed.). Provenance of Arenits. D. Reidel Publishing, Company, p. 333-361.
Donnelly, T.W., 1982. Worldwide continental denudation and climatic deterioration during the late Tertiary: Evidence from deep-sea sediments. Geology 10, 451–454.
Dunn, C.A., Enkelmann, E., Ridgway, K.D., Allen, W.K., 2017. Source to sink evaluation of sediment routing in the Gulf of Alaska and Southeast Alaska: A thermochronometric perspective. J. Geophys. Res. Earth Surf. 122, 711–734.
Enkelmann, E., Garver, J.I., Pavlis, T.L., 2008. Rapid exhumation of ice-covered rocks of the Chugach–St. Elias orogen, Southeast Alaska. Geology 36, 915–918.
Enkelmann, E., Zeitler, P.K., Pavlis, T.L., Garver, J.I., Ridgway, K.D., 2009. Intense localized rock uplift and erosion in the St Elias orogen of Alaska. Nat. Geosci. 2, 360–363.
Enkelmann, E., Zeitler, P.K., Garver, J.I., Pavlis, T.L., Hooks, B.P., 2010. The thermochronological record of tectonic and surface process interaction at the Yakutat-North American collision zone in southeast Alaska. Am. J. Sci. 310, 231–260.
Enkelmann, E., Koons, P.O., Pavlis, T.L., Hallet, B., Barker, A., Elliott, J., Garver, J.I., Gulick, S.P.S., Headley, R.M., Pavlis, G.L., Ridgway, K.D., Ruppert, N., Van Avendonk, H.J.A., 2015. Cooperation among tectonic and surface processes in the St. Elias Range, Earth's highest coastal mountains, Geophys. Res. Lett., 42, 5838–5846.
Enkelmann, E., Piestrzeniewicz, A., Falkowski, S., Stübner, K., Ehlers, T.A., 2017. Thermochronology in southeast Alaska and southwest Yukon: Implications for North American Plate Response to Terrane Accretion. Earth Planet. Sci. Lett. 457, 348–358.
Expedition 341 Scientists, 2014. Southern Alaska Margin: interactions of tectonics, climate, and sedimentation. IODP Prel. Rep. 341. doi:10.2204/iodp.pr.341.2014.
Falkowski, S., Enkelmann, E., Drost, K., Pfänder, J.A., Stübner, K., Ehlers, T.A., 2016. Cooling history of the St. Elias syntaxis, Southeast Alaska, revealed by geochronology and thermochronology of cobble-sized glacial detritus. Tectonics 35, 447–468.
Garzanti, E., 2016. From static to dynamic provenance analysis—Sedimentary petrology upgraded. Sed. Geol. 336, 3-13.
Gulick, S., Freymueller, J., Koons, P., Jaeger, J., Pavlis, T., and Powell, R., 2004. Examining tectonic-climatic interactions in Alaska and the northeastern Pacific. Eos Trans. AGU, 85, 433–439.
Gulick, S.P.S., Jaeger, J.M., Mix, A.C., Asahi, H., Bahlburg, H., Belanger, C.L., Berbel, G.B.B., Childress, L., Cowan, E., Drab, L., Forwick, M, Fukumura, A., Ge, S., Gupta, S.,

Kioka, A., Konno, S., LeVay, L.J., März, C., Matsuzaki, K.M., McClymont, E.L., Moy, C., Müller, J., Nakamura, A., Ojima, T., Ribeiro, F.R., Ridgway, K.D., Romero, O.E., Slagle, A.L., Stoner, J.S., St-Onge, G., Suto, I., Walczak, M.D., Worthington, L.L., Bailey, I., Enkelmann, E., Reece, R., Swartz, J.M., 2015. Mid-Pleistocene climate transition drives net mass loss from rapidly uplifting St. Elias Mountains, Alaska. Proceedings of the National Academy of Sciences of the United States of America 112, 15042-15047.

Huntington, K.W., Blythe, A.E., Hodges, K.V., 2006. Climate change and Late Pliocene acceleration of erosion in the Himalaya. Earth Planet. Sci. Lett. 252, 107–118.

Ingersoll, R.V., Bullard, T.F., Ford, R.L., Grimm, J.P., Pickle, J.D., Sares, S.W., 1984. The effect of grain size on detrital modes: a test of the Gazzi-Dickinson point-counting method. J. Sed. Res. 54, 103–116.

Jaeger, J.M., Nittrouer, C.A., Scott, N.D., Milliman, J.D., 1998. Sediment accumulation along a glacially impacted mountainous coastline: North-east Gulf of Alaska. Basin Res. 10, 155–173.

Johnsson, M.J., 1993. The system controlling the composition of clastic sediments. In: Johnsson, M.J., Basu, A. (Eds.). Processes Controlling the Composition of Clastic Sediments. Geol. Soc. Am. Spec. Pap. 284, 1-19.

Koppes, M., Hallet, B., Rignot, E., Mouginot, J., Smith Wellner, J., Boldt, K., 2015. Observed latitudinal variations in erosion as a function of glacier dynamics. Nature 526, 100–103.

Lagoe, M.B., Eyles, C.H., Eyles, N., Hale, C., 1993. Timing of late Cenozoic tidewater glaciation in the far North Pacific. Geol. Soc. Am. Bull. 105, 1542-1560.

Lagoe, M.B., Zellers, S.D., 1996. Climates and Climate Variability of the Pliocene Depositional and microfaunal response to Pliocene climate change and tectonics in the eastern Gulf of Alaska. Mar. Micropaleontol. 27, 121-140.

Lease, R.O., 2018. Pliocene erosional pulse and glacier-landscape feedbacks in the western Alaska Range. Earth Planet. Sci. Lett. 497, 62–68.

Mange, M.A., Morton, A.C., 2007. Chapter 13 Geochemistry of Heavy Minerals. In: Mange, M.A., Wright, D.T., (Eds.). Developments in Sedimentology, Elsevier, 58, pp. 345-391.

Meigs, A., Johnston, S., Garver, J., Spotila, J., 2008. Crustal-scale structural architecture, shortening, and exhumation of an active, eroding orogenic wedge (Chugach/St Elias Range, southern Alaska). Tectonics 27, TC4003, doi:10.1029/2007TC002168.

Meigs, A., Sauber, J., 2000. Southern Alaska as an example of the long-term consequences of mountain building under the influence of glaciers. Quat. Sci. Rev. 19, 1543-1562.

Molnar, P., 2009. The state of interactions among tectonics, erosion, and climate: A polemic. GSA Today 19, 44-45.

Molnar, P., 2004. Late Cenozoic Increase in Accumulation Rates of Terrestrial Sediment: How might Climate Change Have Affected Erosion Rates? Annu. Rev. Earth Planet. Sci. 32, 67–89.

Molnar, P., England, P., 1990. Late Cenozoic uplift of mountain ranges and global climate change: chicken or egg? Nature 346, 29-34.

Moore, T.E., O'Sullivan, P.B., Potter, C.J., Donelick, R.A., 2015. Provenance and detrital zircon geochronologic evolution of lower Brookian foreland basin deposits of the western Brooks Range, Alaska, and implications for early Brookian tectonism. Geosphere, 11, 93–122.

Morton, A.C., Hallsworth, C., Chalton, B., 2004. Garnet compositions in Scottish and Norwegian basement terrains: a framework for interpretation of North Sea sandstone provenance. Mar. Petrol. Geol. 21, 393–410.

Morton, A.C., Whitham, A.G., Fanning, C.M., 2005. Provenance of Late Cretaceous to Paleocene submarine fan sandstones in the Norwegian Sea: integration of heavy mineral, mineral chemical and zircon age data. Sed. Geol. 182, 3–28.

Nygard A, Sejrup, H.P., Haflidason, H., Lekens, W.A.H., Clark, C.D., Bigg, G.R., 2007. Extreme sediment and ice discharge from marine-based ice streams: New evidence from the North Sea. Geology 35, 395–398.

Pandey, D.K., Clift, P.D., Kulhanek, D.K., Expedition 355 Scientists, 2016. In: Pandey, D.K., Clift, P.D., Kulhanek, D.K., Expedition 355 Scientists (Eds.), Expedition 355 summary.

Pavlis, T.L., Chapman, J.B., Bruhn, R.L., Ridgway, K., Worthington, L.L., Gulick, S.P.S., Spotila, J. 2012. Structure of the actively deforming fold-thrust belt of the St. Elias orogen with implications for glacial exhumation and three-dimensional tectonic processes. Geosphere 8, 991–1019.

Perry, S., Garver, J., Ridgway, K., 2009. Transport of the Yakutat Terrane, southern Alaska: evidence from sediment petrology and detrital zircon fission-track and U/Pb double dating. J. Geol. 117, 156–173.

Pewé, T.L., 1975. Quaternary geology of Alaska. U.S. geol. Surv. Prof. Pap. 835, 145 p.

Raymo, M.E. and Ruddiman, W.F., 1992. Tectonic forcing of late Cenozoic climate. Nature 359, 117–122.

Reece, R.S., Gulick, S.P.S., Horton, B.K., Christeson, G.L., Worthington, L.L., 2011. Tectonic and climatic influence on the evolution of the Surveyor fan and channel system, Gulf of Alaska. Geosphere 7, 830-844.

Roe, G.H., Whipple, K.X., Fletcher, J.K, 2008. Feedbacks among climate, erosion, and tectonics in a critical wedge orogen. Am. J. of Sci. 308, 815-842.

Sha, L.K., Chappell, B.W., 1999. Apatite Chemical Composition, Determined by Electron Microprobe and LaserAblation Inductively Coupled Plasma Mass Spectrometry, as a Probe into Granite Petrogenesis. Geochim. Cosmochim. Ac., 63, 3861-3881.

Sircombe, K.N.,1999. Tracing provenance through the isotope ages of littoral and sedimentary detrital zircon, eastern Australia. Sed. Geol. 124, 47-67.

Spotila, J.A., Buscher, J.T., Meigs, A.J., Reiners, P.W., 2004. Long-term glacial erosion of active mountain belts: Example of the Chugach–St. Elias Range, Alaska. Geology 32, 501-504.

Spotila, J.A., Berger, A.L., 2010. Exhumation at orogenic indentor corners under long-term glacial conditions: Example of the St. Elias orogen, Southern Alaska. Tectonophysics 490, 241–256.

Tomkin, J.H., Roe, G.H., 2007. Climate and tectonic controls on glaciated critical-taper orogens. Earth Planet. Sci. 262, 385–397.

Triebold, S., von Eynatten, H., Luvizotto, G.L., Zack, T., 2007. Deducing source rock lithology from detrital rutile geochemistry: An example from the Erzgebirge, Germany. Chemical Geology 244, 421-436.

Usman, M.O., Masago, H., Winkler, W., Strasser, M., 2014. Int. J. Earth. Sci. (Geol. Rundsch.) 103, 1141-1161.

von Eynatten, H., Gaupp, R., 1999. Provenance of Cretaceous synorogenic sandstones in the Eastern Alps: constraints from framework petrography, heavy mineral analysis and mineral chemistry. Sed. Geol. 124, 81-111.

von Eynatten, H., Dunkl, I., 2012. Assessing the sediment factory: The role of single grain analysis. Earth-Science Reviews, 115, 97-120.

Weltje, G.J., von Eynatten, H., 2004. Quantitative provenance analysis of sediments: review and outlook. Sed. Geol. 171, 1-11.

Weltje, G.J. 2012. Quantitative models of sediment generation and provenance: State of the art and future developments. Sedimentary Geology, 280, 4-20.

Whipp, D.M.Jr., Ehlers T. A., Braun, J., Spath, C.D., 2009. Effects of exhumation kinematics and topographic evolution on detrital thermochronometer data, J. Geophys. Res., 114, F04021, doi:10.1029/2008JF001195.

Whittaker, A.C. 2012, How do landscapes record tectonics and climate? Lithosphere 4, 160–164.

Willett, S., Brandon, M.T., Dorsey, R., Vendeville, B., Whipple, K., 2002. Dynamic Interactions Between Tectonics, Climate and Earth Surface Processes. In: Polard, D.D., et al., (Ed.). New Departures in Structural Geology and Tectonics. White Paper, Denver Colorado, September 22nd and 23rd, 2002, Tectonics Program, Earth Sciences Division, National Science Foundation (GEO/EAR). Department of Geol. and Env. Sciences, Stanford University, 63 p. http://pangea.stanford.edu/~dpollard/NSF/main.html (accessed on 26.7.2018).

Wipple, K.X., 2009. The influence of climate on the tectonic evolution of mountain belts. Nat. geosc. 2, 97-104.

Worthington, L.L., Daigle, H., Clary, W.A., Gulick, S.P.S., Montelli, A., 2018. High sedimentation rates and thrust fault modulation: Insights from ocean drilling offshore the St. Elias Mountains, southern Alaska. Earth. Planet. Sci. Lett. 483, 1-12.
Worthington, L.L., Gulick, S.P.S., Pavlis, T.L., 2010. Coupled stratigraphic and structural evolution of a glaciated orogenic wedge, offshore St. Elias Orogen, Alaska. Tectonics 29, TC6013, doi:10.1029/2010TC002723.
Yannites, B.J., Ehlers, T.A., 2012. Global climate and tectonic controls on the denudation of glaciated mountains. Earth Planet. Sci. Lett. 325–326, 63-75.
Zack, T., von Eynatten, H., Kronz, A., 2004. Rutile geochemistry and its potential use in quantitative provenance studies. Sediment. Geol. 171, 37-58.
Zhang, P., Molnar, P., Downs, W.R., 2001. Increased sedimentation rates and grain sizes 2–4 Myr ago due to the influence of climate change on erosion rates. Nature 410, 891–897.

2 Single grain heavy mineral provenance of garnet and amphibole in the Surveyor fan and precursor sediments on the Gulf of Alaska abyssal plain — Implications for climate-tectonic interactions in the St. Elias orogen

This chapter has been published as Huber, B., Bahlburg, H., Pfänder, J.A., 2018. Single grain heavy mineral provenance of garnet and amphibole in the Surveyor fan and precursor sediments on the Gulf of Alaska abyssal plain — Implications for climate-tectonic interactions in the St. Elias orogen. Sedimentary Geology 372, 173-192.
https://doi.org/10.1016/j.sedgeo.2018.05.007

Abstract

The St. Elias orogen formed as a result of the northwestward drift of the Yakutat terrane along and final collision with the Alaska margin in the Miocene. Its exhumation coincided with changing glacial conditions that are considered to have strongly interacted with mountain building processes. A significant part of the record of these tectonic-climatic interactions is stored in sediments on the Gulf of Alaska abyssal plain including the Surveyor fan. Our study examines temporal provenance changes of Miocene through Pleistocene sediments of the Surveyor fan, Gulf of Alaska, to constrain the dynamics of exhumation and mass transfer from the evolving St. Elias orogen to the adjacent Surveyor deep sea fan. We present single grain geochemical data of amphibole and garnet and $^{40}Ar/^{39}Ar$ cooling ages of biotite and amphibole together with point counting data of heavy minerals from sands and silts from two sites in the distal and proximal fan, drilled by IODP expedition 341 in 2013 (sites U1417 and U1418, respectively).

A shift in heavy mineral composition during the Miocene, predating the onset of glaciation, points to a tectonically-induced change in erosion centers and sediment transport, probably caused by the rise of the St. Elias Mountains. Garnet and amphibole data suggest the Chugach metamorphic complex is the main sediment source, implying input to the Surveyor fan from sources relatively far in the north during the Miocene. Changing provenance signals from the Miocene to Pliocene suggest rising input from the lower grade metamorphic areas at the southern flanks of the orogen, indicating the advance of glaciers to the tidewater line, providing material from this flanking region. Higher input from the Chugach metamorphic complex in all Pleistocene sediments suggests the Northern Hemisphere glaciation at the Plio-Pleistocene boundary caused erosion and sediment yield from the interior of the orogen. Climatic changes at the mid-Pleistocene transition did not cause significant changes in the provenance signal.

2.1 Introduction

In active orogens, tectonically-driven deformation and climate-induced removal and redistribution of mass show complex interactions (e.g., Molnar and England, 1990; Meigs et al., 2008; Adlakha et al., 2013). The style of feedback between and coupling of climate and tectonics continues to be controversially discussed (e.g., Molnar and England, 1990; Raymo and Ruddiman, 1992; Meigs and Sauber, 2000; Peizhen et al., 2001; Molnar, 2004; Clift, 2006; Huntington et al., 2006; Clift et al., 2008; Gulick et al., 2015; Enkelmann et al., 2015a; Worthington et al., 2018). The evolution of the St. Elias orogen at the southern Alaska continental margin (fig. 1A) is connected to subduction of the Yakutat plate under the North American Plate, and coincides with pronounced climatic changes. The relative contribution of climate and tectonics to exhumation is the subject of ongoing research (e.g., Spotila et al., 2004; Berger and Spotila, 2008; Meigs et al., 2008; Berger et al., 2008a, b; Enkelmann et al., 2009, 2010, 2015b, 2017; McAleer et al., 2009; Headley et al., 2012, 2013; Pavlis et al., 2012; Gulick et al., 2015). Onshore studies in the St. Elias Mountains are hampered by the ongoing glaciation (fig. 1B). Most of the orogenic detritus has been delivered to the Gulf of Alaska forearc, shelf and abyssal plain including the Surveyor deep sea fan, potentially storing information on the evolving orogen and sediment routing into the ocean (Jaeger et al., 1998; Expedition 341 Scientists, 2014).

Provenance research on offshore sediments in other regions has demonstrated its usefulness in deciphering regional changes in tectonics and sediment dispersal mechanisms and pathways (e.g., Usman et al., 2014; Pandey et al., 2016). Zircon U-Pb ages and Hf-isotope data obtained for IODP sites U1417 and U1418 drilled in the Surveyor fan (Huber et al., unpublished manuscript) identify the Chugach-Prince William and Yakutat terranes and the Chugach metamorphic complex (CMC) in particular as important sources, and suggest a change in provenance at the Miocene/Pliocene boundary. Zircon and apatite fission-track ages reveal input to the Surveyor fan from the rapidly exhuming St. Elias Syntaxis from the Miocene onwards (Dunn et al., 2017). If and how climatic change at the mid-Pleistocene transition affected the provenance signal remains unresolved (Dunn et al., 2017; Huber et al., unpublished manuscript).

In this contribution, we attempt to further constrain the mass transfer from the St. Elias orogen into the Surveyor fan as a function of the evolving orogen's exhumation by application of single grain geochemical methods to heavy minerals. We present results of a provenance study focusing on the geochemistry of detrital amphibole and garnet and $^{40}Ar/^{39}Ar$ dating of amphiboles and mica, along with a quantification of the heavy mineral spectra by point counting of Miocene to Holocene sediments from IODP 341 sites U1417 and U1418 (distal and proximal Surveyor fan, fig. 1B). Single grain geochemical analyses are less affected by chemical and physical fractionation compared to bulk methods and have been used successfully in provenance analysis given that the source rocks show heterogeneous compositions for certain minerals (Mange and Morton, 2007; Andò et al., 2014; Aliazi et al., 2016; Garzanti, 2016). Amphibole and garnet in particular constrain information on the metamorphic grade of the source lithologies (Morton, 1984; Andò et al., 2014; Aliazi et al., 2016) that varies along the southern Alaska continental margin (Plafker, 1987; Gasser et al., 2011; Bruand et al., 2014).

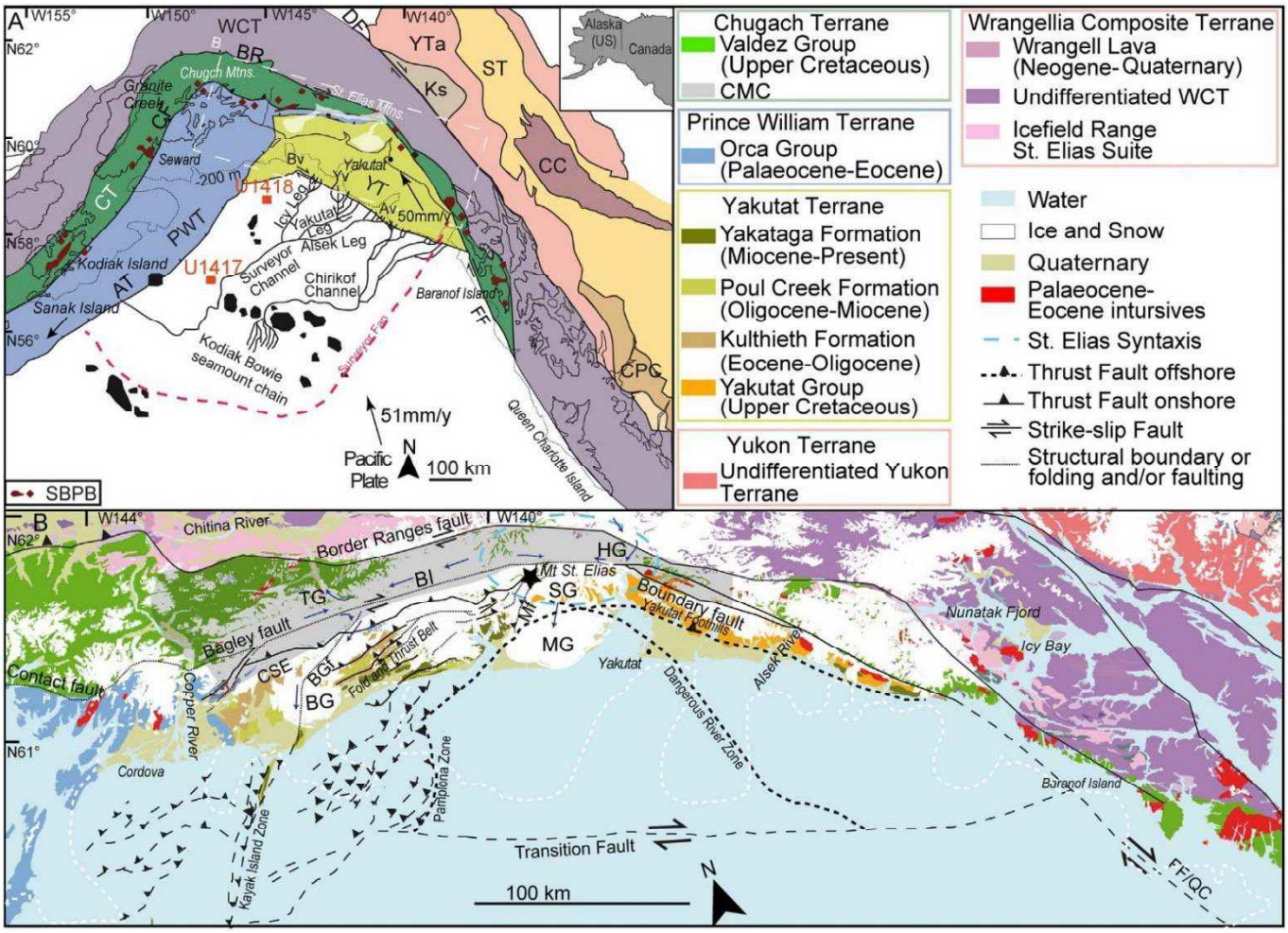

Figure 1: (A) Terrane map of the southern Alaska continental margin (modified after Plafker, 1987; Carlson et al., 1996; Colpron and Nelson, 2011; Reece et al., 2011; Gasser et al., 2012). Plate velocity vectors after Elliott et al. (2010). AT = Aleutian trench; Av = Alsek valley; BR = Border Ranges fault; Bv = Bering valley; CC = Cache Creek terrane; CF = Contact fault; CPC = Coast Plutonic Complex; CT = Chugach terrane; KS = Kluane Schist; FF = Fairweather Fault; PWT = Prince William terrane; SBPB = Sanak Baranof Plutonic Belt; ST = Stikinia terrane; WCT = Wrangellia composite terrane; YT = Yakutat terrane, YTa = Yukon-Tana terrane; Yv = Yakutat valley. Red dots mark the distal (U1417) and proximal (U1418) sites of IODP Expedition 341. (B) Simplified geological map of the southern Alaska continental margin. BG = Bering Glacier, BGf = Bering Glacier fault, BI=Bagley Icefield, FF/QC = Queen Charlotte- Fairweather Fault System; CSE = Chugach-St. Elias Fault, HG = Hubbard Glacier, Mf = Malaspina fault, MG = Malaspina Glacier, SG = Seward Glacier, TG = Tana Glacier. Map data from: Bruhn et al. (2004, 2012), Colpron and Nelson (2011), Wilson et al. (2015), Lipovsky and Bond (2014) and Cui et al. (2015). Glacial flow directions are indicated by dark blue arrows after Post (1972). White line indicates glacier extent during LGM (Last Glacial Maximum) after Manley and Kaufman (2002). Gray shaded area marks the extent of the Chugach metamorphic complex (CMC).

2.2 Background

2.2.1 Geological setting

The St. Elias Mountain range is characterized by a high local relief of over 5000 m (e.g., Mt. St. Elias, 5489 m), rising from sea level to high peaks over a short distance of 55 km. Ongoing flat slab subduction of the Yakutat terrane under the North American Plate since the Oligocene and final oblique collision with the North American Plate in the Miocene led to the rise of the mountain range (Plafker et al., 1994; Bruhn et al., 2004; Enkelmann et al., 2008; Finzel et al., 2011; Falkowski et al., 2014; Finzel et al., 2015). The Yakutat terrane sits at the termination of the Aleutian trench, in the gap between the North American continent to the north and the Pacific Plate to the south (fig. 1A). To the west, it is bordered by the Kayak Island zone, to the south by the Transition fault and to the north and east by the Chugach-St. Elias fault and the Fairweather-Queen Charlotte transform fault respectively (fig. 1A). Presently it is moving to the northwest at ca. 50 mm/yr (Elliott et al., 2010). Thermochronological data reveal an area of extreme high exhumation rates, the St. Elias Syntaxis, at the Yakutat plate corner where transform motions along the Fairweather fault changes to flat-slab subduction (Enkelmann et al., 2009, 2010, 2015a; Falkowski et al., 2014; Falkowski and Enkelmann, 2016; Dunn et al., 2017). The Yakutat terrane has been transported northwestwards along the Fairweather-Queen Charlotte transform fault system since ca. 30 Ma; its initial position is still under debate (Bruns, 1983; Plafker, 1987; Plafker et al., 1994; Perry et al., 2009). U-Pb and fission track data suggest short transport (ca. 600 km) of the terrane from an Eocene position off today's coast of British Columbia (Plafker, 1987; Perry et al., 2009). However, a much longer northward translation of the terrane from northern California (Bruns, 1983) cannot be ruled out completely.

The transform motion of the wedged shaped Yakutat terrane crust, thickening to the east, along the Fairweather fault changes to collision along the Chugach-St. Elias fault (Plafker et al., 1994; Worthington et al., 2012). Eastward of the Dangerous River Zone (fig. 1A), the Yakutat basement is made up of the Yakutat Group, part of the flysch and mélange of the Chugach accretionary complex, that is locally metamorphosed to greenschist facies (Plafker, 1987; Plafker et al., 1994). The western part is covered by eastward thinning sedimentary deposits of up to 15 km thickness, consisting mainly of the Kulthieth (Lower Oligocene to Eocene), Poul Creek (upper Eocene/Oligocene to Miocene) and Yakataga (Miocene to Pleistocene) Formations (Plafker et al., 1980; Plafker, 1987; Plafker et al., 1994; Worthington et al., 2010; Enkelmann et al., 2015b) (fig. 1B). The sediments westward of the Pamplona zone, the offshore deformation front, have been offscraped forming the thin-skinned Yakutat fold and thrust belt, accommodating ca. 6 mm/yr of shortening (Plafker, 1987; Worthington et al., 2010; Chapman et al., 2013).

Landwards of the Yakutat terrane follows the Chugach-Prince William terrane, forming a ca. 2100 km long accretionary prism of deformed late Triassic to early Cretaceous mélange, late Cretaceous to Eocene flysch, and oceanic basalt (Plafker et al., 1994) (fig. 1A). The Chugach-Prince William terrane was accreted in the late Cretaceous- early Tertiary (Plafker, 1987). The ice-covered Contact fault (named Bagley fault under the Bagley ice field) separates both terranes (fig 1B). While the western part is metamorphosed at pumpelleyite–greenschist facies grade, the eastern part underwent up to upper amphibolite facies metamorphism within the CMC (Hudson and Plafker, 1982; Sisson et al., 1989) (fig. 1B). The CMC is rimmed by a belt of metabasalts and greenschist- to amphibolite facies metasedimentary rocks along the southern side (metabasite belt) (Hudson and Plafker, 1982; Bruand et al., 2011; Gasser et al., 2011). Eastward of the CMC, most rocks are of lower metamorphic grade but rocks of metamorphic grade similar to the CMC can be locally found at least until the Nunatak Fjord and on Baranof Island (Dusel-Bacon et al., 1993; Dusel-Bacon et al., 1996; Zumsteg et al., 2003) (fig. 1A). Granitoid intrusions of the Paleocene-Eocene Sanak-Baranof Plutonic Belt are distributed across the CMC but also intrude the Chugach-Prince William terrane outside the CMC (e.g., Hudson and Plafker, 1982; Sisson et al., 1989; Bruand et al., 2011) (fig. 1A, B).

The Border Ranges fault separates the Wrangellia composite terrane and the Chugach-Prince William terrane (fig. 1). The Wrangellia composite terrane accreted to the North American continent in the Middle Jurassic to mid Cretaceous (e.g., Plafker et al., 1989, 1994). It consists

mainly of intraoceanic Paleozoic and Mesozoic magmatic arc-assemblages, upper Triassic green- and limestone with a cover of Upper Jurassic-Lower Cretaceous flysch, Paleogene alluvial strata and Oligocene– Recent lava with generally low metamorphic overprint (up to greenschist facies) but locally reaches amphibolite facies grade at the border to the Chugach terrane (Hillhouse, 1977; Plafker, 1987; Gehrels and Berg, 1994; Nokleberg et al., 1994; Plafker et al., 1994; Trop et al., 2002). Eastward of the St. Elias Mountains, plutonic and metamorphic rocks of the Coast Plutonic Complex form the coast range of British Columbia, reaching to northern Washington State (Stowell et al., 2002). It consists of a central gneiss belt intruded by late Cretaceous to Tertiary plutonic rocks and low to medium grade metamorphic rocks on the west and east flanks (Crawford et al., 1987).

2.2.2 Surveyor fan depositional system

The precursor of today's Surveyor fan has been active since the Miocene (ca. 9.7 Ma; Rea and Snoeckx, 1995). The fan has moved to the northwest by dextral translation as part of the Pacific Plate since the beginning of its deposition (Stevenson and Embley, 1987; Reece et al., 2011). The present Surveyor fan spans a distance of over 600 km from the continental shelf to the Aleutian trench (Stevenson and Embley, 1987; Dobson et al., 1998; Reece et al., 2011) (fig. 1A). Turbidite fans are commonly linked to fluvial systems. Contrastingly, the Surveyor fan is being fed directly by a glacial system (Ness and Kulm, 1973; Carlson et al., 1996 ; Reece et al., 2011). Today, it is fed by the Surveyor channel system, starting offshore the Malaspina and Bering glaciers and the glacially-formed sea valleys that are concentrating sediment delivery (Carlson et al., 1996; Reece et al., 2011). The Surveyor channel might have acted as transport system from 5 Ma onwards (Hogan et al., 1978; Reece et al., 2011), but a recent study places its inception at ca. 2.7 Ma (Gulick et al., 2015). At the base of the slope, several small shelf-crossing gullies merge to three channels (Icy, Yakutat and Alsek Leg; fig. 1A) (Carlson et al., 1996). The Yakutat Leg is connected to the Yakutat Sea Valley, capturing input from the Malaspina and Hubbard glaciers (Reece et al., 2011) (fig. 1A). The Alsek Leg conjoins to the Alsek Sea Valley and Alsek glacial system. It is considered to have existed since the onset of glaciation at the Miocene/Pliocene boundary (Reece et al., 2011). The Icy Leg connects to partially buried sea valleys between Icy Bay and the Pamplona Spur, a tectonically controlled basement high of the Pamplona Zone, experiencing input from the Bering glacier before it was shut off some when after the onset of glacial interval C (Reece et al., 2011) (fig. 2). Around 150 km from the continental margin, these channels join to form the main Surveyor channel that discharges into the Aleutian trench at ca. 700 km distance (Carlson et al., 1996).

2.2.3 Glaciation at the southern Alaska continental margin

After warm middle Miocene conditions, cooling started in the late middle to early late Miocene, resulting in alpine glaciation in the late Miocene (ca. 7 Ma; Lagoe et al., 1993) (fig. 2). Tidewater glaciers were established between 6.7 and 5.0 Ma during glacial interval A (Lagoe et al., 1993). The mid-Pliocene was characterized by a warm period from 4.2 to ca. 3 Ma that was followed by the Northern Hemisphere glaciation starting at ca. 2.5 Ma (glacial interval B; Lagoe et al., 1993). At the mid-Pleistocene transition, glaciation increased during glacial interval C because of a change in global glacial-interglacial climate cycles from 40 to 100 kyr at 0.7 to 1 Ma (Lagoe and Zellers, 1996).

Today, glaciers cover ca. 50% of the Chugach-St. Elias orogen, overlying many faults including the Malaspina fault, Bering Glacier fault and parts of the Fairweather fault (Enkelmann et al., 2010; Bruhn et al., 2012) (fig. 1B). The Bering, Malaspina and Hubbard glaciers are the largest glaciers at the Gulf of Alaska (Molina, 2008) (fig. 1B). The Bagley ice field connects to the Bering glacier but its ice flow is separated from the adjacent Seward glacier (Bruhn et al., 2012). Glaciers have been previously thicker and covered large parts of the continental shelf during phases of stronger glaciation (Péwé, 1975; Mann and Hamilton, 1995; Berger et al., 2008a; Worthington et al., 2010; Headley et al., 2013; Expedition 341 Scientists, 2014) (fig. 1B). The high relief of the orogen leads to mean annual precipitation at

the southern flanks of ca. >2.5 m a^{-1}, while precipitation decreases strongly at its northern side to < 0.6 m a^{-1} (Péwé, 1975; Spotila et al., 2004).

2.3 Site descriptions

2.3.1 Site U1417-distal site

Site U1417 was drilled to a total depth of 709.5 m CCSF-B (CCSF-B = core composite depth below seafloor corrected to the true drilled interval; for details see Expedition 341 Scientists (2014)), recovering Miocene to Holocene sediments (Expedition 341 Scientists, 2014) (fig. 2). It is situated on the distal Surveyor fan ca. 60 km west of the Surveyor channel, which delivers sediment to the site via overbank processes (Expedition 341 Scientists, 2014) (fig. 1A). The Miocene and Pliocene sediments that were deposited prior to the onset of the main Surveyor channel are turbiditic deposits (Reece et al., 2011). Five lithostratigraphic units were identified (Expedition 341 Scientists, 2014) (fig. 2). These units are grouped into subunits, defined by the amount of mud, silt, sand, lonestones, ash, diamict, and biosilicious material as well as the style of interbedding (Expedition 341 Scientists, 2014). The most prominent lithology is mud with varying amounts of biogenic and coarser material. Between 5.2 Ma and 2.8 Ma, sedimentation rates were at ~30–70 m/Myr (Gulick et al., 2015). Near the Plio- Pleistocene boundary, sedimentation rates rose to ca. 120 ± 20 m/Myr at 2.4–2.0 Ma associated with development of northern hemisphere glaciation (Gulick et al., 2015). After a short-term reduction of sedimentation to 60 m/Myr from 1.6–1.2 Ma, sedimentation rates increased from the middle-Pleistocene transition onwards to values up to 140 m/Myr by 0.8 Ma (Gulick et al., 2015).

2.3.2 Site U1418-proximal site

The proximal site is situated between a modern channel that feeds the Aleutian trench and a presumably inactive channel-like structure named the Bering channel that is also supposed to have fed the Aleutian trench while active (Expedition 341 Scientists, 2014) (fig. 1A). Sediments were delivered from these channels to the site by hemipelagic settling and gravity flows (Expedition 341 Scientists, 2014). The recovered sediments extend from Early/Middle Pleistocene to Holocene (fig. 2). Sedimentation rates (810 m/Myr) are higher than at the distal site (Gulick et al., 2015).

A thick deposit at the base of the recovered sediments represents a chaotic seismic sequence that has been interpreted as an Early Pleistocene massive slope failure deposit (Mass Transport Deposit; unit IV; fig. 2) (Reece et al., 2011; Expedition 341 Scientists, 2014). The top of the Mass Transport Deposit correlates with the onset of ice streams and increased sedimentation during the mid-Pleistocene transition (Expedition 341 Scientists, 2014). Lithologic units IIC and IID represent deposition in the abandoned Bering channel while units IIA and IIB are supposed to have been deposited in a now abandoned channel that might have fed the Aleutian trench (Expedition 341 Scientists, 2014). Unit I is interpreted to have formed through suspension settling and mud-rich gravity flows from the shelf/slope (Expedition 341 Scientists, 2014).

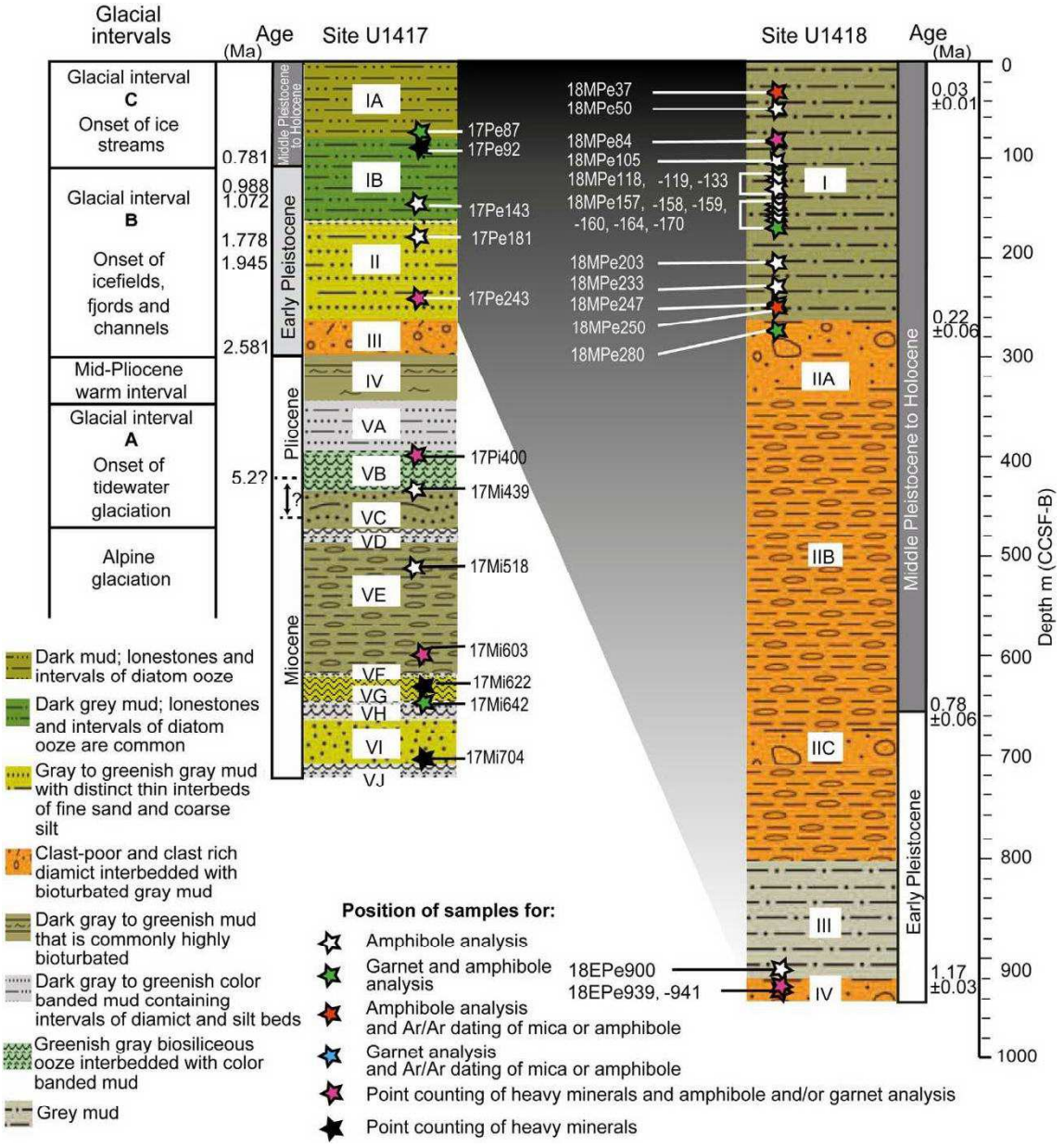

Figure 2: Lithostratigraphic units and climatic events at the Gulf of Alaska with sampling positions for amphibole and garnet analysis, point counting and $^{40}Ar/^{39}Ar$ dating. Modified after Expedition 341 Scientists (2014) and references therein.

2.4 Sampling

Sampling focused on sands and silts of IODP Expedition sites U1417 (9 samples) and U1418 (21 samples). Samples between ca. 1 and 14 cm thickness were taken from the one core half provided for sampling (core diameter of 6.2 cm), limiting the sample volume. Samples depths are given in m CCSF-B. Sample names start with the abbreviated name of the site (17 for U1417 or 18 for U1418) followed by the abbreviated name of the stratigraphic interval (Mi = Miocene, Pi = Pliocene, Pe = Pleistocene, EPe = Early Pleistocene, MPe = Middle Pleistocene) and the depth from which the sample was taken (fig. 2). The IODP code of each sample can be found in Appendix A. The time of deposition was deduced from bio- and

magnetostratigraphic reconstructions and the resulting age model (Expedition 341 Scientists, 2014; Jaeger et al., 2014; Gulick et al., 2015).

2.5 Sample preparation and analytical methods

We performed point counting of heavy minerals, analysis of single grain geochemical compositions of amphiboles from 30 samples (9 from site U1417, 21 from site U1418) and garnets from 9 samples (5 from site U1417, 4 from site U1418) using a microprobe. The grain size fractions 63–250 µm were chosen for analysis. Most of the samples contain no or very few grains >0.25 mm (0–2%). Grains <0.063 mm provide the largest fraction in all samples, making up over 90% in some samples. The heavy mineral content in all samples is moderately rich (<5%) but limited sediment volumes because of the diameter of the drill core (6.2 cm; sample weights of ca. 10 g to 70 g) and grain size, with many samples providing <1.5 g of material of 0.063–0.25 mm, the absolute heavy mineral volume for analysis is small. Still, this size fraction was the only one providing valuable amounts of heavy minerals for analysis. The small sample volume also made the calculation of sample indices like the Heavy Mineral Concentration index (Garzanti et al., 2007) unfeasible. Restriction to this narrow grain size fraction might lead to some information being lost because of grain size dependence of mineral compositions (e.g., Garzanti et al., 2008; Krippner et al., 2015). Still, inter-sample comparison is not invalidated.

To evaluate possible zonation of garnets, microprobe measurements along lines from rim to rim across 32 representative garnets, with 12 measurements per line, were acquired. We determined $^{40}Ar/^{39}Ar$ ages of eight biotite and amphibole grains from samples of the Miocene to Pleistocene sediments of sites U1417 and U1418 on the distal and proximal Surveyor fan, respectively (fig. 2). For details of sample preparation, analytical methods and measurement results see Appendix B–E.

2.6 Amphibole and garnet as provenance indicators

The geochemistry of amphibole and garnet depends on source rock geochemistry and P-T conditions of formation, allowing analysis of their major element geochemistry to reveal information on the genetic type of the source rock (Leake, 1978; Morton, 1984; Mange and Maurer, 1992; Leake et al., 2004; Mange and Morton, 2007; Andò et al., 2014). We classify the amphiboles according to the rules of the IMA 2004 (International Mineralogical Association) (Leake et al., 2004) to evaluate changes in the compositional spectra with depositional age. For information on metamorphic grade, we plot the SiO_2 vs. TiO_2 content and Al^{IV} vs. Al^{VI} values of amphiboles. Continuous spectra of increasing Ti with reduction of Si are typical for rising metamorphic grade of the source rock (Fleet and Barnett, 1978; Andò et al., 2014). $Al^{IV}/Al^{VI} = 2$ is considered to be the boundary between low pressure metamorphic amphiboles and high pressure amphiboles (<2) (representing ca. 5 kbar; Leake, 1965; Fleet and Barnett, 1978; Li et al., 2015). $Al^{IV}/Al^{VI} \geq 3.3$ is the limiting value for unaltered igneous amphibole (Fleet and Barnett, 1978).

For classification of the source rock of garnets, we use a multivariate discrimination scheme that provides probabilities for the affiliation of garnet to one of five main source rock types (eclogite-, amphibolite- and granulite- facies metamorphic rocks, ultramafic and igneous rocks) (Tolosana-Delgado et al., in press). To display the diversity of the garnet compositions and changes therein, we use the triangular diagram of Mange and Morton (2007) that has almandine + spessartine, grossular, and pyrope as apices, which are the most abundant garnet endmembers in our samples (fig. 3A). The discrimination fields are not intended to be diagnostic for certain garnet bearing rock types but evaluation of natural garnet populations indicates the respective genetic types (Mange and Morton, 2007; Tolosana-Delgado et al., in press). Strong overlap of three facies groups in the lower left part of field Ci (i.e., Fe and/or Mn rich) occur and igneous rocks as well as amphibolite facies metasedimentary rocks may plot in the same field (Bi-type garnets; Krippner et al., 2014) and could therefore be misinterpreted.

We keep the discrimination fields, but to avoid misleading indications for provenance we refer to the garnets in the different fields as “x-type” garnet where x is the fieldname in the triangular diagram. For more detailed information on the methods for amphibole and garnet data analysis see Appendix F.

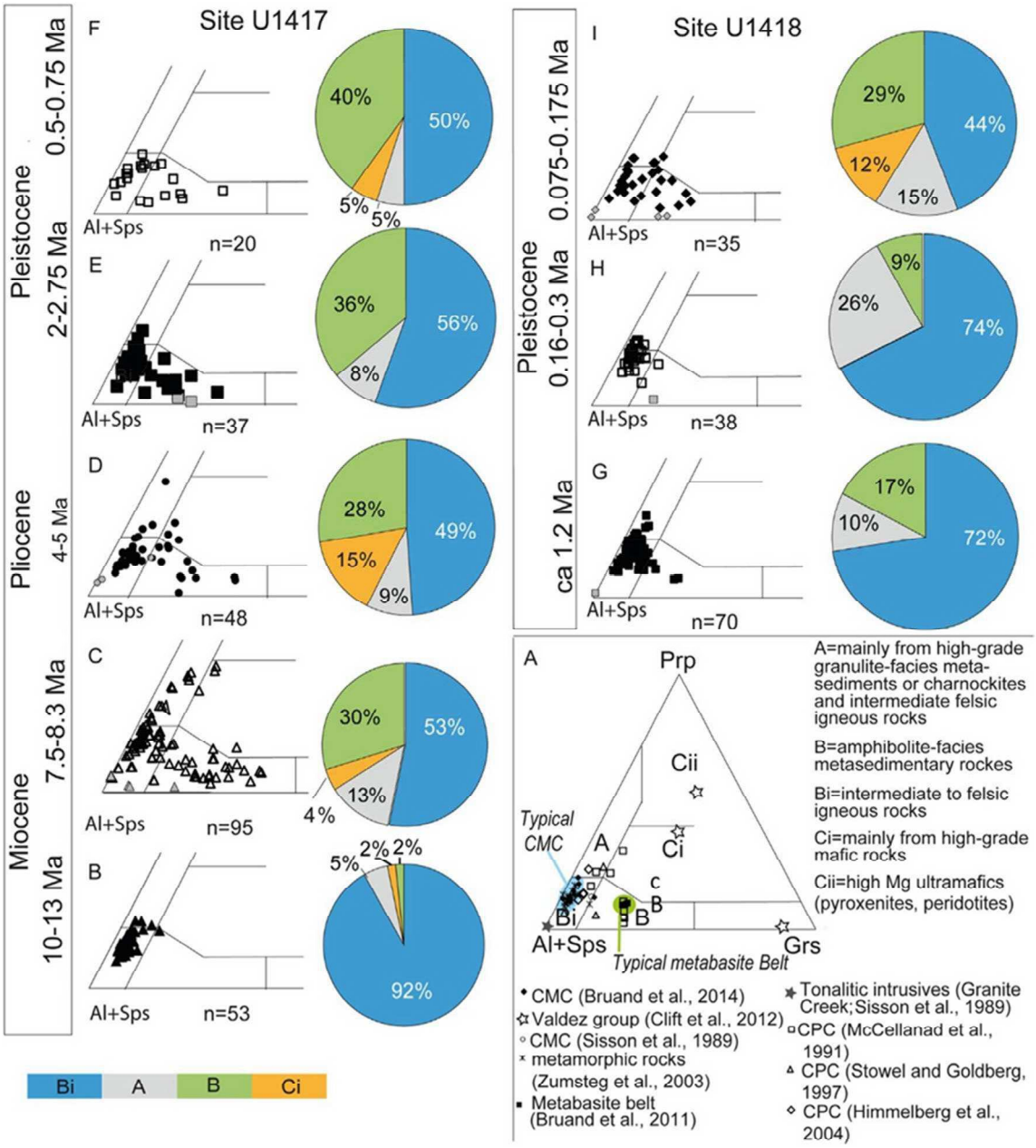

Figure 3: Garnet discrimination diagram after Mange and Morton (2007) using pyrope, almandine + spessartine and grossular as poles, showing samples from the distal (U1417) and proximal (U1418) sites and reference data from literature; sample names indicate the position of the sample in the core (m below sea floor (CCSF-B)). (A) Reference data from literature; (B) 17Mi642; (C)17Mi603, (D) 17Pi400; (E)17Pe234; (F) 17Pe87; (G)18EPe939; (H) 18MPe280; (I) 18MPe170. Grains that have been assigned to be sourced from igneous rocks are marked with gray filled symbols.

2.7 Results

2.7.1 Heavy mineral spectra

Amphibole, epidote, garnet and pyroxene dominate the heavy mineral assemblages (fig. 4A, B). Relatively unaltered, angular amphibole is one of the dominant heavy minerals in all samples. At the distal site, sediment composition changes upwards from unit VI to unit V sediments (figs. 2, 4A). Unit VI sediments contain mostly biotite, opaque oxides and coal fragments while sediments from units V upwards are dominated by rock fragments as well as quartz and feldspar and a heavy mineral fraction consisting of amphibole, epidote, garnet, pyroxene and some biotite. As there are few amphiboles and no garnet grains in the unit VI sediments, they have not been considered for this study.

The abundance of biotite decreases up-core to the Miocene/Pliocene transition while the amphibole and epidote concentrations increase. The amount of opaque grains (oxides) of the Pleistocene sample is relatively high at a level comparable to the oldest Miocene sample. The Pleistocene samples in general contain a similar mineral spectrum as the Pliocene sample but the mica content decreases upsection while the epidote content increases.

At the proximal site, the mineral spectrum is similar to the sediments at the distal site (fig. 4B). Amphibole, epidote, garnet and pyroxene are the dominant heavy minerals but the pyroxene content tends to be higher and the epidote content lower than at the distal site at the same time of deposition.

When assigning the heavy mineral suites of the analyzed samples into the groups A (amphibole), P + O + S (pyroxene + olivine + spinel) and &tHM (other transparent heavy minerals) we obtain sample compositions ranging between $A_{10}P+ O+ S_0$&tHM_{90} and $A_{46}P+O + S_5$&tHM_{49} at the distal site. This relatively limited range corresponds to the Axial-Belt Provenance dominated by “greenschist-facies covers” and “amphibolite-facies metapelites” but also corresponds to the “clastic wedge” provenance of Garzanti et al. (2007) and reflects the tectonic setting of the orogen and provenance of the sediments rather well. At the proximal site, sample compositions are at ca. $A_{29-32}P+O+ S_{32-40}$&tHM_{23-28}, corresponding mostly to a mixed “magmatic arc”/“axial-belt” provenance (Garzanti et al., 2007).

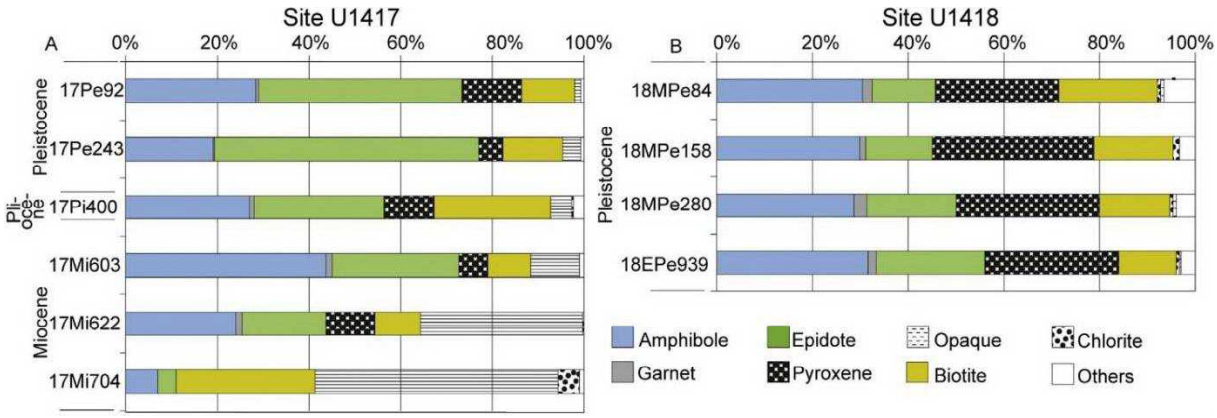

Figure 4: Heavy mineral composition at the distal (A) and proximal (B) sites. X-axis gives percentage of different minerals of the heavy mineral fraction.

2.7.2 Amphibole geochemistry

The amphibole composition at both sites is dominated by magnesiohornblende with a greenish color (fig. 5). SiO_2/TiO_2 diagrams show continuous spectra of increasing Ti with lower Si contents for all samples (fig. 6A, B). Most grains show TiO_2 values of 0.0–1.5 wt%, with some Pleistocene grains showing values up to 6 wt% TiO_2. The number of amphiboles analyzed per sample can be found in table 1.

Figure 5: Amphibole composition at (A) the distal (U1417) and (B) the proximal (U1418) site. Sample names indicate the position of the sample in the core (m below sea floor (CCSF-B)).

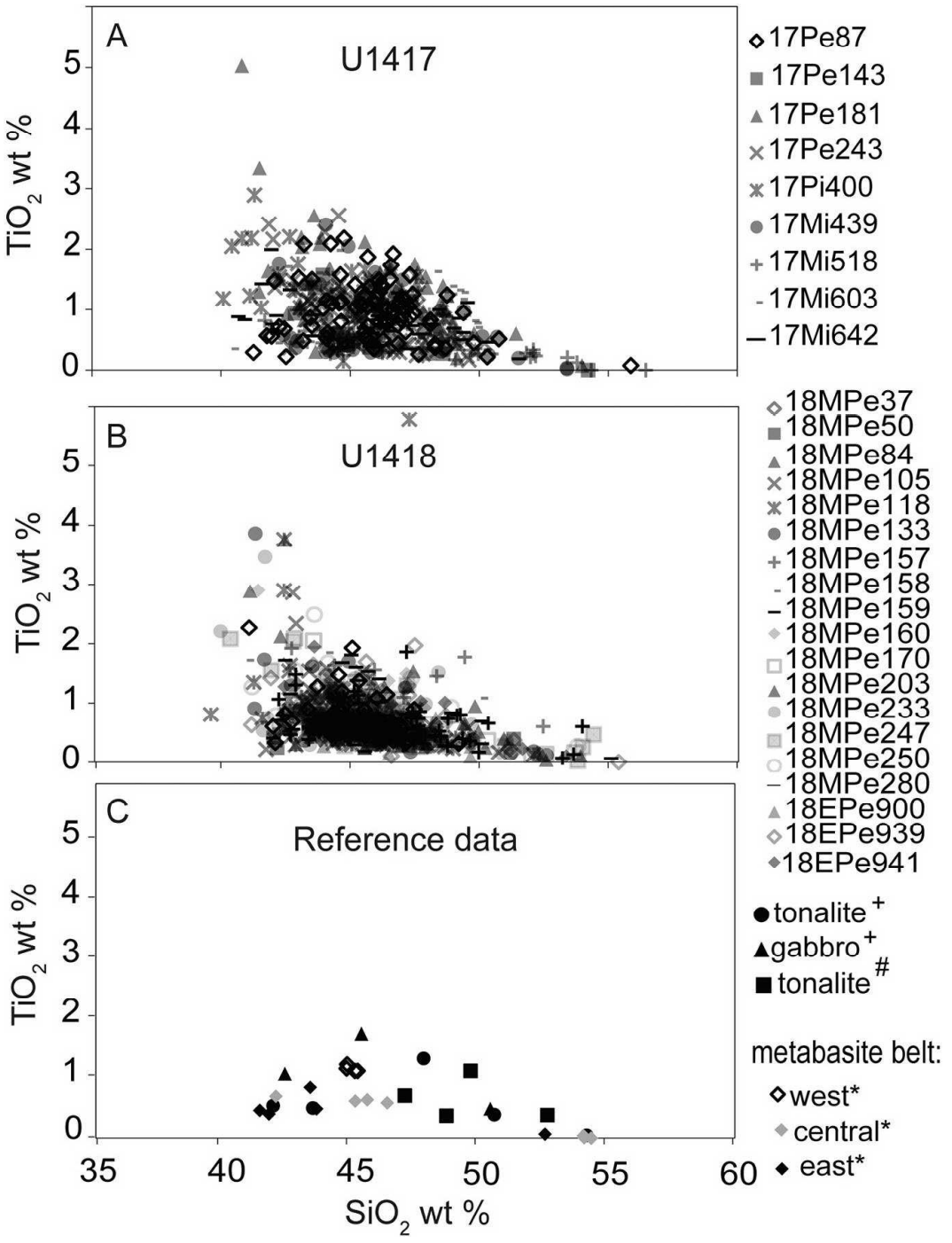

Figure 6: TiO_2/SiO_2 diagram for amphibole for (A) the distal (U1417) and (B) proximal (U1418) sites (this study) and C: representative amphiboles from a metabasite belt (*Bruand et al., 2011) and gabbroid and tonalitic rock from the CMC (#Sisson et al., 1989, +2003). Names of site U1417 and U1418 samples indicate the position of the samples in the core (m below sea floor (CCSF-B)).

2.7.2.1 Site U1417- distal site

The amphiboles of the Miocene samples are mainly magnesiohornblende (up to ca. 81%; fig. 5A). Amphibole discrimination plots (figs. 7A, 8A) display a dominance of grains with Al^{IV}/Al^{VI} ratios of 1.0–3.3 (ca. 50 to 70%), and show a decrease with younger stratigraphic level (fig. 8A). In the Pliocene, the magnesiohornblende component reduces to ca. 50% and a relatively high amount of magnesiohastingsite (ca. 18%) appears. Nearly 90% of the Pliocene

amphiboles have Al^{IV}/Al^{VI} ratios of >3.3 while ratios of 1.0–3.3 reduce to ca. 10%. The Pleistocene samples have amphibole compositions again dominated by magnesiohornblende (ca. 75–85%) and show a relatively high amount of tschermakite (ca. 6–14%; fig. 5A). On average, the amount of magnesiohornblende and grains with Al^{IV}/Al^{VI} ratios of 1.0–3.3 is as high as in the Miocene (figs. 5A, 8A). Only sample 17PI181 shows over 60% of grains with $Al^{IV}/Al^{VI} > 3.3$.

2.7.2.2 Site U1418-proximal site

All of the Pleistocene to Holocene sediments are dominated by magnesiohornblende (60–90%) with some sediments showing up to 24% tschermakite (fig. 5B). Other components that contribute with at least 5% to some of the samples are actinolite, edenite, ferrohornblede, ferropargasite, ferrotschermakite and magnesiohastingsite. All samples provide mainly amphiboles with Al^{IV}/Al^{VI} ratios of 1.0–3.3 (ca. 60–90%) (figs. 7B, 8B). The mass transport deposit and the Early Pleistocene mud (unit III) contain at least 74% magnesiohornblende and up to 18% tschermakite (fig. 5B). There is no general trend of changing composition for the Pleistocene sediments. Some samples show nearly the same characteristics as the adjacent ones, while others show stronger differences to their vertically neighbouring samples.

Table 1: Numbers of amphibole and garnet grains analyzed per sample.

sample name	number of amphiboles analyzed	number of garnets analyzed
Site U1417		
17Pe87	88	20
17Pe143	34	-
17Pe181	54	-
17Pe243	47	37
17Pi400	51	48
17Mi439	49	-
17Mi518	52	-
17Mi603	90	96
17Mi642	39	53
Site U1418		
18MPe37	51	-
18MPe50	38	-
18MPe84	52	-
18MPe105	56	-
18MPe118	54	-
18MPe119	45	-
18MPe133	46	-
18MPe157	58	-
18MPe158	60	-
18MPe159	47	-
18MPe160	38	-
18MPe164	47	-
18MPe170	52	35
18MPe203	21	-
18MPe233	55	-
18MPe247	43	-
18MPe250	49	-
18MPe280	52	38
18EPe900	55	-
18EPe939	51	70
18EPe941	53	-

2.7.3 Garnet geochemistry

Garnets are less abundant in all sediments than amphibole and many samples are devoid of garnet (fig. 4A, B). The number of garnets analyzed per sample can be found in table 1. All are light rose colored and slightly rounded and most are free of inclusions while some have quartz and TiO_2 rich inclusions. Most garnets show a compositionally homogeneous cross-sectional profile without zoning, with almandine as the dominant endmember (ca. 60–70%) followed by spessartine and pyrope (fig. 3B–I). Most of them have been found to be sourced from amphibolite facies metamorphic source rocks and some from igneous sources (table 2). Using the 32 garnet profiles that we measured, we can identify four main groups. Most grains belong to groups (1) and (2) which show no to minor zoning and a dominance of almandine (ca. 60–70%) with the next most abundant component being (1) spessartine (ca. 5-20%) or (2) pyrope (ca. 10–20%; fig. 9A, B). Some grains are richer in grossular (ca. 20%), with spessartine and almandine making up ca. 10% each, while others have only cores enriched in grossular (group 3; fig. 9C) and also show relatively high amounts of spessartine (ca. 2%; group 4; fig. 9D). Garnet zoning with different core and rim compositions are found in group (4). Therefore, we propose that the composition of the core reflects the general composition of most of the grains. When the grossular content is very high, a zonation typical for group (4) may develop.

2.7.3.1 Site U1417- distal site

All samples show a dominance of grains that are assigned to an amphibolite facies source using the multivariate discrimination scheme (table 2). The oldest Miocene sample (17Mi642, depositional age of ca. 11.5 ± 1.5 Ma) and the youngest Middle Pleistocene sample (depositional age of ca. 0.50-0.75 Ma) show only grains of this type while the later Miocene (depositional age of ca. 7.9 ± 0.4 Ma), the Pliocene (depositional age of ca. 4-5 Ma) and the Early Pleistocene sample (depositional age of ca. 2.0–2.8 Ma) also provide grains of igneous or granulite sources (table 2).

The oldest sample (17Mi642) is dominated by almandine rich garnet with variable amounts of spessartine and pyrope and only a small grossular component, leading to over 90% of the grains being type Bi garnets (fig. 3B). From 17Mi642 (ca. 11.5 ± 1.5 Ma) to sample 17Mi603 (ca. 7.9 ± 0.4 Ma) there is a clear change in garnet composition. Sample 17Mi603 provides a larger range of garnet compositions. The grossular containing garnet suite increases and the amount of “Bi-type” grains decreases to ca. 53% while “B-type” garnets make up ca. 30% (fig. 3C). In addition, some grains appear that very likely have an igneous source (table 2). All younger samples show similar amounts of Bi- and B- type grains (fig. 3C–F). Only the amount of “C-” and “A-type” grains varies, with “C-type” grains being relatively abundant in the Pliocene sample and missing in the oldest Pleistocene sample (fig. 3B–F).

2.7.3.2 Site U1418-proximal site

All the Pleistocene samples from this site are dominated by garnet derived from amphibolite facies metamorphic source rocks (ca. 88%-95%; table 2). All grains have almandine as the main component. Most grains in the two oldest samples (depositional age of ca. 1.2 Ma and 0.16–0.3 Ma; fig. 3G, H) are “Bi-type” grains (72%; 74%), the remaining grains belong to “type-A” and “-B”. The youngest sample (depositional age of ca. 0.075–0.175 Ma) shows fewer “Bi-type” grains (44%) but more “B-type” grains (29%; fig. 3I). “A-type” garnets (15%) are less abundant while 12% “Ci-type” garnets appear.

Table 2: Percentage of garnets assigned to the certain facies groups using the multivariate discrimination scheme of Tolosana-Delgado et al. (in press).

sample name	amphibolite facies	granulite facies	ultra-mafic	igneous	eclogite facies	number of grains analyzed
	(%)	(%)	(%)	(%)	(%)	
Site U1417						
17Pe87	100	0	0	0	0	20
17Pe243	92	3	0	5	0	37
17Pi400	85	8	0	6	0	48
17Mi603	81	12	0	8	0	96
17Mi642	100	0	0	0	0	53
Site U1418						
18MPe119	88	3	0	12	0	35
18MPe280	95	3	0	3	0	38
18EPe939	94	4	0	1	0	70

2.7.4 $^{40}Ar/^{39}Ar$ dating

Small grain sizes resulted in only very few grains being suitable for $^{40}Ar/^{39}Ar$ dating. In total, five $^{40}Ar/^{39}Ar$ cooling ages of amphibole grains and three of biotite grains from 7 different samples from Pleistocene sediments could be determined (table 3). Two biotite and two amphibole cooling ages of ca. 40–50 Ma were measured for grains of the Mass Transport Deposit (unit IV) and the mud deposit (unit I, middle Pleistocene) at the proximal site (U1418). Three ages between ca. 130 and 150 Ma were measured for two amphibole grains from the Mass Transport Deposit (proximal site, U1418) and one from the unit IB sediments (middle Pleistocene) from the distal site (U1417). One biotite grain from the proximal site (unit I) showed an age of 17.8 ± 0.2 Ma.

One amphibole grain from sample 18MPe105 was large enough (7.3 mg) to perform a step heating experiment. The age and K/Ca spectra and the inverse isochrone diagram are shown in Appendix E. The age spectrum provides a weighted mean age of 48.9 ± 0.9 Ma from 99.5% of the ^{39}Ar released. Overall, the low temperature steps yield slightly younger ages than the high temperature steps. This might be either caused by intergrown biotite having a lower closure temperature than hornblende (~300–350 °C vs. ~500–580 °C; Harrison, 1981; Harrison et al., 1985), or by a K-rich rim, possibly due to K uptake during postmagmatic overprinting. Decreasing K/Ca ratios are consistent with both assumptions.

2.7.5 Statistical tests

To evaluate the similarity of and differences between our samples we apply three way Multidimensional-Scaling (MDS) using the “provenance” software package (Vermeesch et al., 2016). We compare our dataset on amphibole composition with a second dataset of Al^{IV}/Al^{VI} values of amphiboles where we differentiate three groups (Al^{IV}/Al^{VI}>3.3, Al^{IV}/Al^{VI} = 3.3-2.0, Al^{IV}/Al^{VI} = 2–1; fig. 10A). The plot confirms increasing statistical difference between the samples from the Miocene to the Pliocene (samples 17Mi642 to 17Mi400; fig. 10A). The Pleistocene samples and the oldest Miocene samples form a single cloud and are considered to be similar. Only sample 17Pe143 is different to the other samples in the cloud (fig. 10A).

The comparison of the garnet data, using two datasets, one with information on the attribution of each grain to the different fields in the triangular diagram and the second with information on the source rock type from the multivariate discrimination scheme, shows that the biggest difference can be found between sample 17Mi642 (Miocene) and 17Pi400 (Pliocene) (fig. 10B). In contrast to the amphibole data, sample 17Pe143 does not diverge from the other Pleistocene sample, suggesting the difference in amphibole composition to be an outlier.

We also compare similar datasets for site U1418. The amphibole data form one big cloud, supporting the idea that there is no significant difference between all the Pleistocene samples from the proximal site (fig. 10C). The garnet data indicate that there is a small difference between the youngest middle Pleistocene sample and the older ones (fig. 10D). A comparison of samples for which we have garnet and amphibole data from both sites (fig. 10E) indicates that the sites are different concerning their amphibole and garnet geochemistry. However, the difference between samples 17Mi642 and 17Pi400 and the other samples from site U1417 is larger than the difference between those samples and the samples from site U1418.

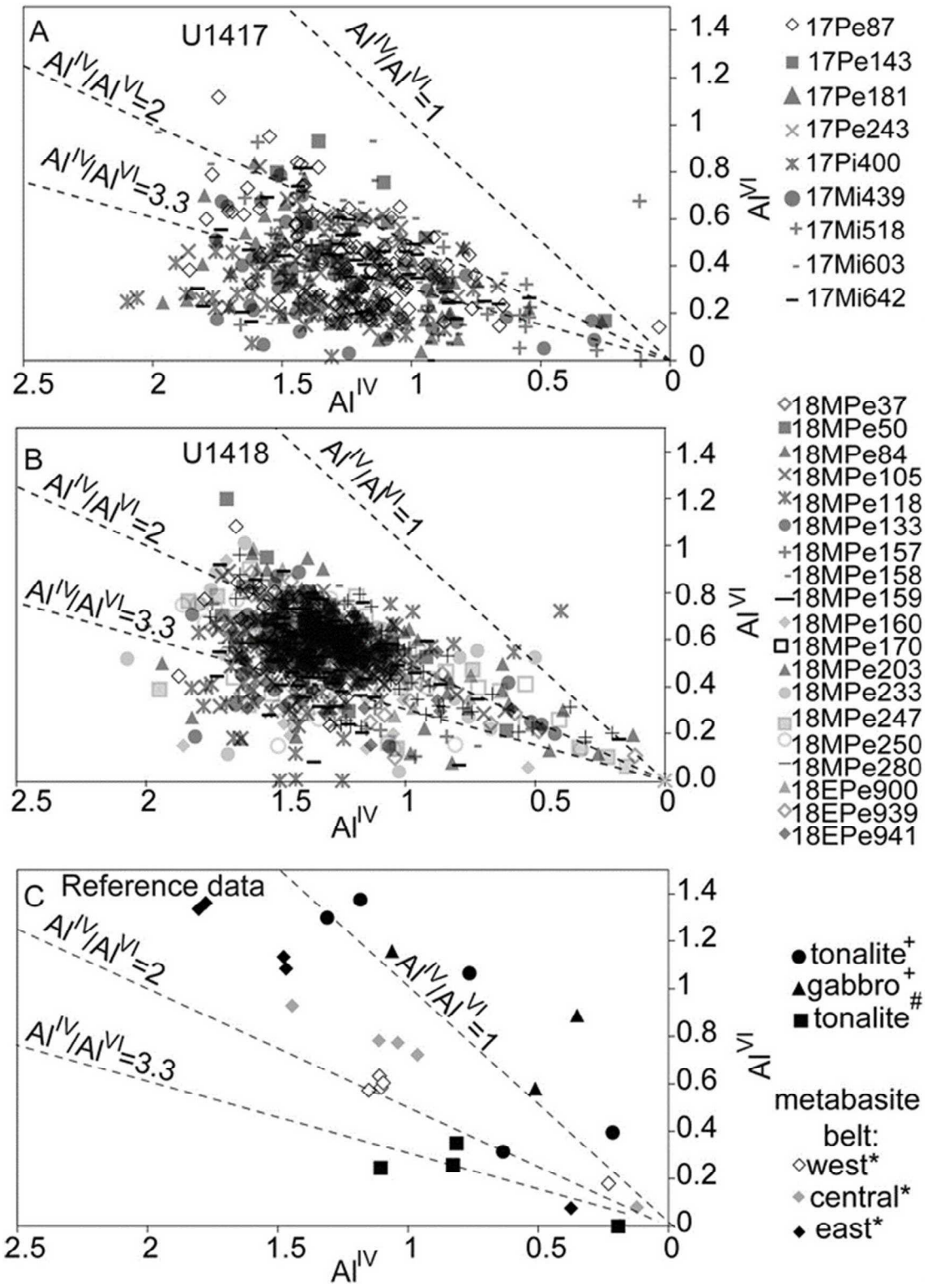

Figure 7: Al^{IV}/Al^{VI} diagrams after Li et al. (2015) for amphiboles from: (A) the distal (U1417) and (B) the proximal (U1418) sites (this study) and (C) representative amphiboles from a metabasite belt (*Bruand et al., 2011) and gabbroid and tonalitic rock from the CMC (#Sisson et al., 1989, +2003). Names of site U1417 and U1418 samples indicate the position of the samples in the core (m below sea floor (CCSF-B)). Al^{IV}/Al^{VI} > 3.3: igneous or greenschist facies metamorphic conditions; Al^{IV}/Al^{VI} = 3.3 to 1.0: amphibolite facies conditions with 3.3 to 2.0 = low P and 2.0 to 1.0 = high P conditions.

2.8 Source characteristics

Regarding the northwestward transport of the Pacific Plate since the late Miocene (Bruns, 1983; Plafker, 1987; Plafker et al., 1994; Perry et al., 2009), and thereby of the sampling sites, input to sites U1417 and U1418 could have been supplied from the Chugach-Prince-William and Yakutat terranes as well as from the Coast Plutonic Complex (fig. 11). Much of the material of the Chugach flysch might have been fed by the Coast Plutonic Complex due to the plate tectonic configuration (Garver and Davidson, 2015). The Yakutat Group is considered to be a displaced fragment of the Chugach terrane (Plafker et al., 1994). Olistostromal blocks with a likely Wrangellia terrane origin have been found in the Yakutat Group on Queen Charlotte Island (Plafker, 1987). Sediments on the Yakutat terrane might also have experienced input from the Coast Plutonic Complex (Meigs et al., 2008; Perry et al., 2009). Around 65-70% of the onland Yakataga Formation is sourced by the CMC and plutons of the Sanak-Baranof Plutonic Belt in the Chugach and Prince William terranes and ca. 30-35% by reworking of the Kulthieth and Poul Creek Formations (Enkelmann et al., 2008; Perry et al., 2009). This illustrates how similar parent sources for different sedimentary deposits along the southern Alaska continental margin complicate the provenance interpretation as many potential source areas might provide similar minerals. Still, it is possible to constrain the provenance as wide parts of the St. Elias Mountains underwent different grades of metamorphism leaving specific imprints on their mineralogy, particularly in garnet and amphibole (Wright, 1938; Hudson and Plafker, 1982; Sisson et al., 1989; Teraoka et al., 1997, 1998; Mange and Morton, 2007; Bruand et al., 2011, 2014; Andò et al., 2014; Tolosana-Delgado et al., in press).

The most common garnet and amphibole in our samples at both sites are almandine and magnesiohornblende. Their densities are 4.1 g cm^{-3} and 3.2 g cm^{-3}, respectively. If sorting processes between the two sites were a major factor, garnet should be more abundant at the proximal site, which it is not. Enrichment of specific minerals also depends on the selected grain size window (Garzanti et al., 2009). In our study, we use a broader size range to minimize the bias in our data.

2.8.1 Amphibole geochemistry of the potential source rocks

The SiO_2/TiO_2 contents of the amphiboles from sites U1417 and U1418 (fig. 6A, B) imply a source region covering the complete range of non-metamorphic or low grade to higher amphibolite facies metamorphic rocks, with a dominance of the latter. Amphibolite facies rocks are dominant in the CMC while lower metamorphic grades are more typical for the west and south-west Chugach, Prince William and Yakutat terrane and igneous rocks are hosted by the Sanak-Baranof Plutonic Belt (Hudson and Plafker, 1982; Sisson et al., 1989). Lithologies with up to 70% amphibole are reported for the metabasite belt at the southern flank of the CMC (Bruand et al., 2011). Within the Coast Plutonic Complex, metamorphic grades range from non-metamorphic and low metamorphic to upper amphibolite to lower granulite in the central part (Crawford et al., 1987).

Single grain geochemical data of amphiboles are available for different parts of the metabasite belt (Bruand et al., 2011) and from tonalitic and gabbroic intrusives within the CMC (Sisson et al., 1989, 2003). Data for comparison from the non-metamorphic or low grade metamorphic areas and many intrusions of the Sanak-Baranof Plutonic Belt as well as from the other amphibolite facies rocks within the CMC and from the Coast Plutonic Complex are not available. (Magnesio-)Hornblende and minor amounts of actinolite and tschermakite, which are the most abundant amphibole types in the sediments from site U1417 and U1418, are also the main amphibole types of the metabasites and the tonalitic intrusions (Sisson et al., 1989, 2003; Bruand et al., 2011). In the TiO_2 vs. SiO_2 diagrams (fig. 6C), amphiboles from the metabasite belt and the gabbroic and tonalitic intrusions from within the CMC plot in the same area as many of the amphiboles from sites U1417 and U1418 but do not provide the whole spectrum found in the sediments (fig. 6C). Most of the compositions plot in the field of 3.3-1 in the Al^{IV}/Al^{VI} diagrams (fig. 7C), typical for amphibolite facies conditions. Some grains plot in the igneous/greenschist facies field close to the amphibolite facies field. We conclude that most

amphiboles from within the CMC, including tonalitic and gabbroic rocks, tend to plot in the amphibolite facies field of 1.0–3.3.

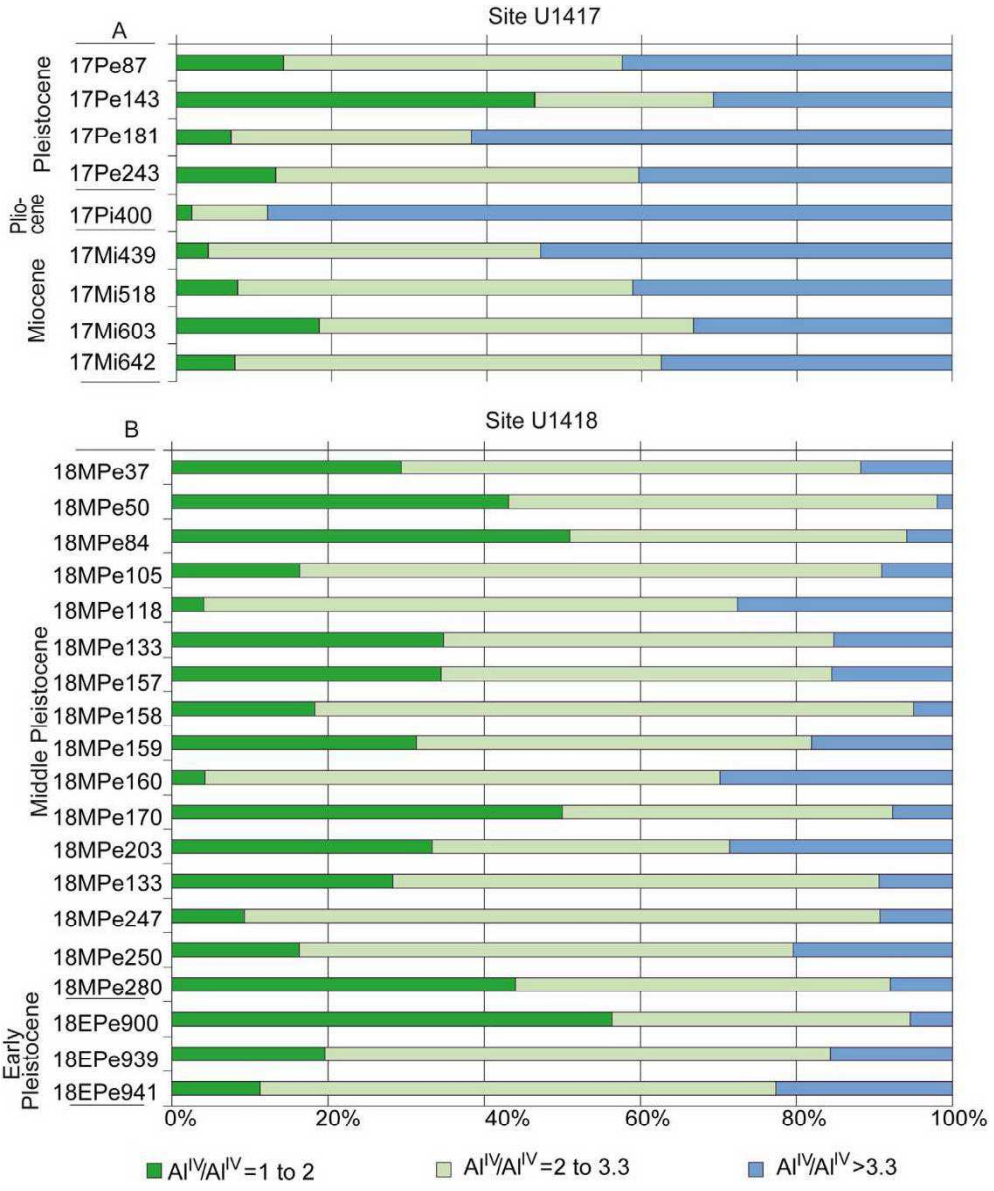

Figure 8: Percentage of Al^{IV}/Al^{VI} values of 1.0–2.0, 2–0-3.3 and >3.3 of amphibole at (A) the distal (U1417) and (B) the proximal (U1418) site. Sample names indicate the position of the sample in the core (m below sea floor (CCSF-B)).

A relevant fraction of amphiboles from the sediments from sites U1417 and U1418 plots in the field of Al^{IV}/Al^{VI} > 3.3 typical for greenschist facies metamorphic and igneous grains. We infer these grains to be sourced from the area surrounding the CMC (igneous, non-metamorphic to greenschist facies conditions) for which we have no source data for verification. Consequently, we interpret the amphibole suite which has an Al^{IV}/Al^{VI} of 1.0–3.3 to be indicative of a general CMC provenance, and assign amphiboles with an Al^{IV}/Al^{VI} > 3.3 to the low grade metamorphic areas surrounding the CMC.

2.8.2 Garnet geochemistry of the potential source rocks

Several garnet-bearing lithologies crop out along the southern Alaska continental margin: the plutons of the Sanak-Baranof Plutonic Belt, the amphibolite facies metamorphic rocks of the

CMC, the (meta-) sedimentary rocks of the surrounding Chugach, Wrangellia and Yakutat terranes and metamorphic rocks of the Coast Plutonic Complex (Dumoulin, 1987; Pell, 1987; Sisson et al., 1989); McClelland et al., 1991; Stowell and Goldberg, 1997; Kusky et al., 2003; Zumsteg et al., 2003; Himmelberg et al., 2004; Bruand et al., 2011, 2014; Clift et al., 2012).

Garnets from the CMC and the metabasite belt show regional differences (Sisson et al., 1989; Bruand et al., 2011, 2014). Grains with composition and zoning resembling type (1) and (2) garnets identified in the sediments from site U1417 and U1418 have been found in the metamorphic rocks of the west and central part of the CMC (Sisson et al., 1989; Bruand et al., 2014). The slight zoning at the rims of the grains reported by Sisson et al. (1989) is only partly present in the grains from sites U1417 and U1418, which might be the result of abrasion. Garnets from the eastern part of the CMC show stronger zoning between core and rim with cores enriched in Ca (grossular-endmember; (Sisson et al., 1989; Bruand et al., 2011, 2014). No garnets are reported from the western part of the metabasite belt (Bruand et al., 2011) (fig. 3A). Therefore groups 1 and 2 garnets may have been fed from the central and western CMC while groups 3 and 4 garnets may have been sourced by the eastern part of the CMC and the eastern part of the metabasite belt. Garnets from within the western and central CMC plot in field Bi in the triangular diagram, while garnets from the eastern CMC plot on the line between fields B and Bi; garnets from the eastern part of the metabasite belt plot in the “B-type” field.

Garnets from metamorphic rocks of the accretionary complex on Baranof Island, associated with the most eastern termination of the Sanak-Baranof Plutonic Belt, have a similar metamorphic grade and composition as within the interior of the CMC (Zumsteg et al., 2003), also plotting in field Bi (fig. 3A). Grains show zoning patterns similar to groups (1) and (2) with some grains having a more pronounced zonation (Zumsteg et al., 2003). Thus, the presence of “B-type” garnets in our samples implies input from the eastern part of the CMC and metabasite belt while “Bi-type” garnets are more typical for sources restricted to the central and western CMC or to the eastern termination of the Sanak-Baranof Plutonic Belt. Accordingly, compositions falling in fields B and Bi gain a regional significance.

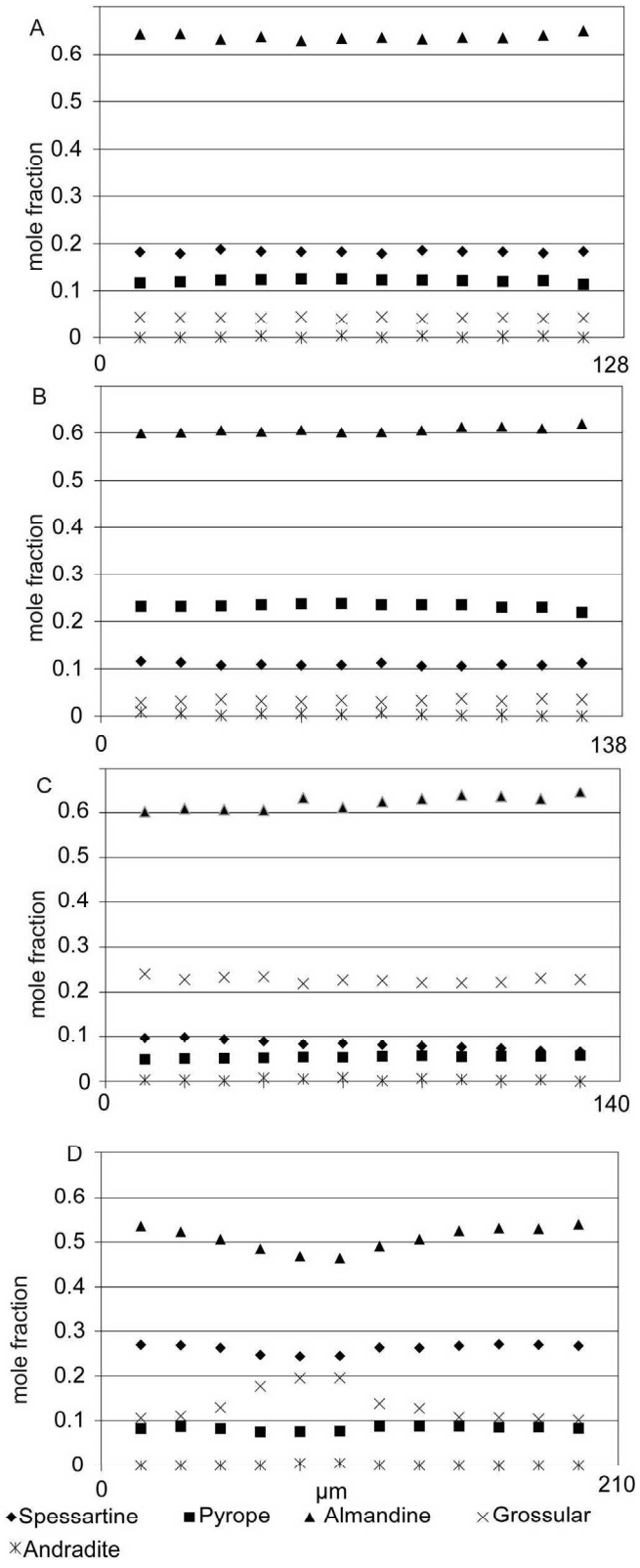

Figure 9: Geochemistry of garnets measured along lines from rim to rim across four representative garnet grains from site U1417 and U1418 sediments.

Garnets are present in the plutons of the Sanak-Baranof Plutonic Belt on Kodiak Island (Kusky et al., 2003) but only a single detailed geochemical garnet analysis is available from Granite Creek (Sisson et al., 1989). In the triangular diagram, it plots in the outer left corner of field Bi (fig. 3A). There is no information on zoning dismissing zonation as discriminating feature. Garnets from site U1417 and U1418, which are assigned to have an igneous provenance using the multivariate discrimination scheme of Tolosana-Delgado et al. (in press), plot in fields Bi and in field A. In field Bi, all igneous grains except one plot in the outer left corner, like the one igneous grain from literature. Field Bi is supposed to represent felsic igneous rocks, but according to Krippner et al. (2014), this field can also host grains from amphibolite facies metamorphic rocks, which is most probable in this case. We conclude that grains plotting in the outer left corner of field Bi and in field A are very likely derived from the Sanak-Baranof Plutonic Belt while garnets that plot in the rest of field Bi are sourced most likely by the CMC.

Garnets are present in low abundances in the non-metamorphic or low-grade metamorphic rocks of the Orca and Valdez Groups in the Prince William Sound areas but only three garnet analyses are available (Dumoulin, 1987; Clift et al., 2012). The grains are very rich in pyrope- or grossular (Type Ci, Cii or D) (fig. 3A). Grains of type Ci that occur in the samples from sites U1417 and U1418 have smaller pyrope components while D-type garnets are absent, indicating the Valdez Group not to be a major garnet source. As these rocks have very low garnet abundances (Dumoulin, 1987) we expect them to have little influence on our data and interpretations.

Garnets form metamorphic rocks from the Coast Plutonic Complex are also dominated by almandine and plot in fields B, Bi, A and Ci overlapping with grains from the metabasite belt and the CMC (Pell, 1987; McClelland et al., 1991; Stowell and Goldberg, 1997; Himmelberg et al., 2004) (fig. 3A). Their composition is much more complex and diverse than found in the garnets from sites U1417 and U1418 (McClelland et al., 1991; Himmelberg et al., 2004). We cannot exclude that garnets from this region found their way into the Surveyor fan. We would expect a higher diversity of garnet composition, zoning and habitus, however, if there was a major input from this region.

2.8.3 Provenance significance of the Ar-Ar data

Our $^{40}Ar/^{39}Ar$ ages support input in the Pleistocene mainly from the Chugach-Prince William and the southern Wrangellia terrane. The Eocene $^{40}Ar/^{39}Ar$ cooling ages are typical for the plutons and the metamorphic rocks in the Chugach and Prince William terrane, supporting our earlier inferences that this area was a main source of these sediments (Dodds and Campbell, 1988; Falkowski et al., 2016). The Jurassic/Cretaceous ages are typical for the Wrangellia terrane (Dodds and Campbell, 1988; Plafker et al., 1994). Main plutonic intrusions crop out at the Wrangellia margin to the Chugach terrane (Dodds and Campbell, 1988). The Miocene cooling age of ca. 18 Ma can be connected to similar ages reported from the Chugach terrane in the area close to the Nunatak Fjord (fig. 1B) and from cobbles from the Malaspina glacier moraines with a most likely Chugach terrane origin (Sisson et al., 2003; Gasser et al., 2011; Falkowski et al., 2016).

2.9 Provenance implications of the data

2.9.1 Provenance of site U1417 sediments

The high biotite content and presence of coal supports derivation of the sediments below unit VG from the Kulthieth and Poul Creek Formations on the Yakutat terrane that contain high amounts of coal and volcanic material (Plafker, 1987) (fig. 11). The reduction of mica and coal content and the increase in quartz, feldspar, amphibole, pyroxene, epidote and garnet in the younger Miocene samples (above ca. 650 m CCSF-B) supports a general change in provenance in the Miocene, predating the onset of glaciation. We conclude that this change is therefore driven by tectonic processes, changes in sediment transport or exposure of new lithologies as a result of ongoing exhumation.

Sample 17Mi642 (depositional age of ca. 11.5 ± 1.5 Ma) still shows a relatively high amount of mica, indicating input from the Kulthieth and Poul Creek Formations or reworking of the older sediments to carry over. The homogeneous garnet geochemistry of this sample, with all grains referred to amphibolite facies metamorphic source rocks (table 2) imply a restricted, homogeneous amphibolite facies metamorphic source area. This is also supported by the amphibole geochemistry (figs. 7A, 8A). Today, a narrow zone of epidote and amphibolite facies rock crops out on the Yakutat terrane east of Yakutat Bay separated from lower grade metamorphic rocks by the Fairweather fault in the northeast and another fault in the southwest (Dusel-Bacon et al., 1993; Dusel-Bacon et al., 1996). These rocks contain abundant biotite and also provide garnet and hornblende (Dusel-Bacon et al., 1996). The change in provenance could therefore still record erosion on the Yakutat terrane. However, we cannot test this hypothesis because of the absence of single grain geochemical data allowing validation. Alternatively, our data may record the beginning of input from the exhuming CMC. The high amounts of amphiboles with an amphibolite facies source (ca. 60%) in the Miocene samples match the CMC as the main provenance. Furthermore, the garnet geochemistry is in line with the homogeneous geochemistry of the central and western CMC, suggesting this area as an important source at this time (fig. 11). The homogeneity of the garnet compositions favors a higher grade metamorphic source area which makes input from the low grade metamorphic sediments of the rest of the Yakutat terrane unlikely. Input from the Coast Plutonic Complex cannot be excluded but the literature data indicate garnets from that region to have a more variable geochemistry.

The change in garnet geochemistry from sample 17Mi642 (depositional age of ca. 11.5 ± 1.5 Ma) to sample 17Mi603 (depositional age of ca. 7.9 ± 0.4 Ma) indicates a change in erosion patterns to integrate over a wider range of source rock types. According to the literature, this change might have been caused by increasing input from the metabasite belt at the southern flank of the CMC and to the eastern part of the CMC, providing “B-type” garnets. This would mark an extension of the source area from the central CMC to the outer reaches of the orogen closer to the coast or a complete change in provenance from mainly Yakutat to Chugach sources (fig. 11). “C-type” garnets are not mentioned in the literature. Their presence supports a widening of the source area that provides a more variable garnet spectrum. “Type-C” garnets might be stored in the sedimentary deposits of the Valdez and Orca Groups, Kulthieth, Poul Creek and Yakataga Formations that crop out south and westward of the CMC. Input from the Coast Plutonic Complex cannot be excluded but northwestward drift of the Yakutat terrane makes increasing input from eastward sources unlikely.

Approaching the Miocene/Pliocene boundary, the amount of amphibole grains with Al^{IV}/Al^{VI} ratios >3.3 increases, also suggesting rising input from the low grade metamorphic or non-metamorphic areas outside the CMC between ~11 and 4 Ma (fig. 8A). This trend is even stronger in the Pliocene where more than ca. 90% of the amphibole grains were sourced from non-amphibolite facies sources. The reduction of the amount of amphibole in the Pliocene sample and the relatively high amount of opaque grains supports a change in provenance to higher input from low grade metamorphic or non-metamorphic sources on the Yakutat terrane.

During the Pleistocene, the number of amphiboles from an amphibolite facies source is comparable to the Miocene (ca. 60–70%) indicating a similar provenance with higher input from the CMC than during the Pliocene. Only one sample (17Pe181) seems to have a lower input from the amphibolitic source area (ca. 40%) but the general amphibole geochemistry remains the same. In contrast, the composition of the Pliocene and Pleistocene garnets implies a similar provenance. High numbers of garnets in the metabasite belt, compared to lower garnet abundance in the low grade metamorphic units on the Yakutat terrane, might lead to garnets only recording changes in erosion within the CMC and of the metabasite belt but to give only minor information on input from the Yakutat terrane. In contrast, the amphibole data might be strongly influenced by input from the lower grade metamorphic areas of the Yakutat terrane because of higher amphibole yield. We suggest erosion to have been focused in the CMC or increasing exposure of lithologies of higher metamorphic grade due to ongoing exhumation to cause the changing provenance signal (fig. 11). The very high epidote content in the Pleistocene samples and the decreasing mica content suggest a very epidote rich area to have increasingly contributed material to the samples. There is no implication for a general change in provenance at the mid-Pleistocene transition in the amphibole and garnet data.

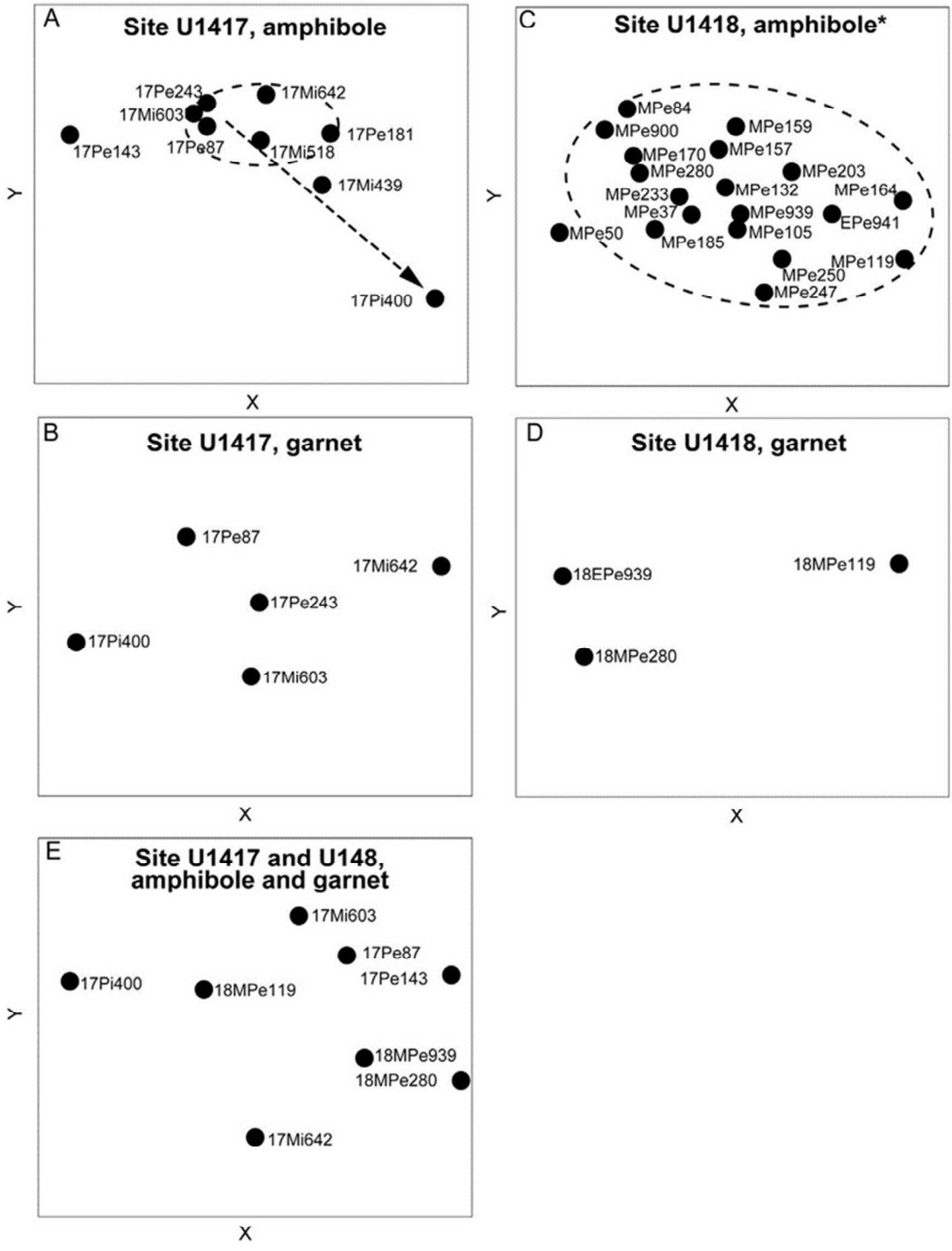

Figure 10: Three-way MDS (Multidimensional scaling) plots comparing the similarity of the samples. (A) Site U1417, amphibole data; (B) Site U1417, garnet data; (C) Site U1418, amphibole data; (D) Site U1418, garnet data; (E) site U1417 and U1418, amphibole and garnet data. Dashed ellipsoids mark samples grouping together. Dashed line indicates increasing difference of samples with younger depositional age.

Table 3: $^{40}Ar/^{39}Ar$ ages from Pleistocene biotites and amphiboles from the distal (U1417) and proximal (U1418) sites.

site	sample name	Mineral type	Lith. Unit	$^{40}Ar/^{39}Ar$ age	Error 1σ	measuring method
				(Ma)	(Ma)	
U1417	17Pe92	amphibole	IB	146.3	17.83	Single grain total fusion
U1418	18MPe37	amphibole	I	36.8	2.60	Single grain total fusion
U1418	18MPe105	amphibole	I	48.9	0.87	Step heating experiment
U1418	18MPe170	biotite	I	54.5	9.91	Single grain total fusion
U1418	18MPe250	biotite	I	17.8	0.21	Single grain total fusion
U1418	18EPe939	biotite	IV	43.8	5.30	Single grain total fusion
U1418	18EPe941	amphibole	IV	143.9	20.16	Single grain total fusion
U1418	18EPe941	amphibole	IV	133.3	17.51	Single grain total fusion

2.9.2 Provenance of site U1418 sediments

The Pleistocene samples from the proximal site show a relatively similar heavy mineral spectrum as the Pliocene samples at the distal site, but provide less epidote and more pyroxene pointing to a similar but not identical source area. Both the relatively uniform composition of abundant magnesiohornblende and tschermakite (fig. 5B) and the dominance of amphibole and garnet grains with an amphibolite facies origin imply a CMC source for all samples (fig. 8B). The amount of amphibole grains interpreted to have a CMC source is higher than in equivalent samples from the distal site. This indicates that the two sites to experience input from different parts of the orogen and through different sediment routing systems, influencing the provenance signal.

The amphibole data from the Early Pleistocene Mass Transport Deposit is very similar to that of the Middle Pleistocene sediments. The Mass Transport Deposit represents a massive slope failure (Expedition 341 Scientists, 2014). Therefore, the Mass Transport Deposit samples cannot be used to directly constrain onshore exhumation centers. Still, they imply that the material shed onto the continental slope before had a similar provenance.

The dominance of “Bi-type” garnet and the amphibole geochemistry support high input from the west and central CMC. “B-type” grains are present, implying some input from the metabasite belt, but are less abundant than in the Pleistocene samples from the distal site. The older Middle Pleistocene sediments show a similar geochemistry and provenance, which is more homogeneous with a stronger focus on the central CMC than in the Pleistocene samples at the distal site. Rising amounts of “B-type” and “C-type” and igneous garnets in the late Middle Pleistocene (ca. 0.175–0.075 Ma), indicate a decrease of input from the western and central CMC and an increasing supply from the metabasite belt and from the non-metamorphic or low grade lithologies of the Valdez and Orca Groups, and the Poul Creek, Kulthieth and Yakataga formations. This change in provenance cannot be recovered in the amphibole data.

2.10 Discussion

In our study, we evaluate the relative contributions of climate and tectonics on exhumation of St. Elias Mountains and the resulting mass transfer to the Surveyor fan on the Gulf of Alaska abyssal plain. A number of processes influence the provenance signal displayed by our data. They include (i) exhumation and denudation, (ii) sediment evacuation, transport and dispersal, (iii) reworking of sediments, and (iv) the delay between erosion and transfer into the offshore sedimentary record.

Glacial cover and erosive potential of the glaciers are considered to vary strongly in the possible source areas in time and space (Péwé, 1975; Lagoe et al., 1993; Mann and Hamilton, 1995; Lagoe and Zellers, 1996; Berger et al., 2008a; Worthington et al., 2010; Headley et al.,

2013; Expedition 341 Scientists, 2014). Different degrees of glaciation result in significant erosional mass flux variabilities between unglaciated and highly glaciated regions and glacial and interglacial periods (Headley et al., 2013; Headley and Ehlers, 2015). The sediments drilled by IODP Expedition 341 represent material deposited over the whole glacial cycle, and include potentially reworked sediments deposited during interglacial cycles. Input to the Surveyor fan system is periodic and enhanced during glacial periods and evacuation mechanism vary for the different glacial systems (Reece et al., 2011; Headley et al., 2013). While today's subglacial drainage system of the Seward-Malaspina glacial system effectively evacuates material out of the orogen, glacial surges have been suggested to be the major mechanism for sediment evacuation from the Bering-Bagley system (Headley et al., 2013).

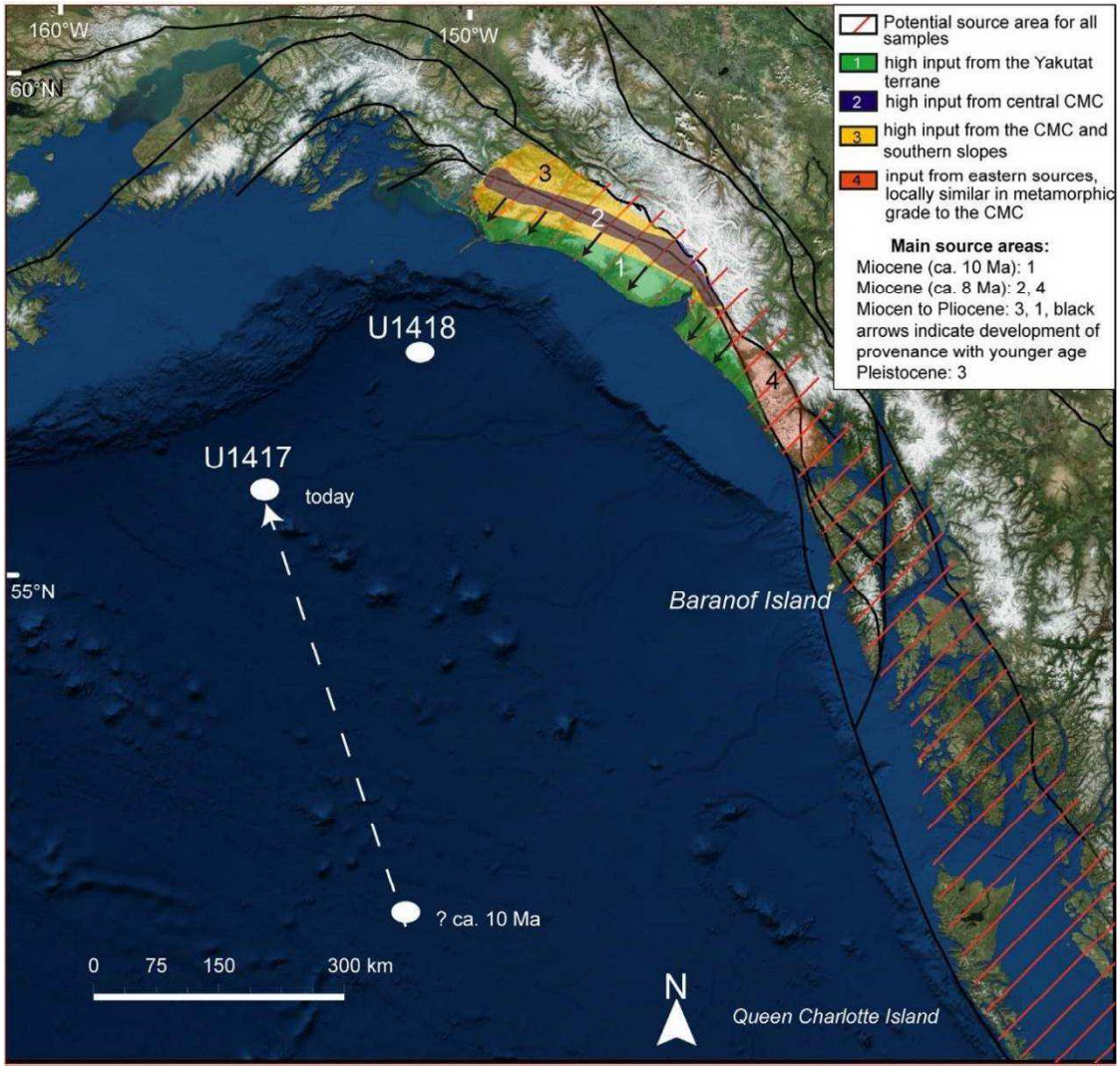

Figure 11: Map showing a schematic summary of the inferred provenance areas of site U1417 and U1418 sediments from Miocene to Pleistocene. Base map from Esri DigitalGlobe (2018).

The large glaciers contributed most of the material to the Surveyor fan (e.g., Carlson et al., 1996; Jaeger et al., 1998; Expedition 341 Scientists, 2014). The Icy and Alsek leg of the Surveyor fan may have received input form the Copper and Alsek River, respectively, which are the two main rivers draining into the Gulf of Alaska today (fig. 1B). The Bering-Bagley glacial system ultimately drains northward into the Copper River, draining the area north of the drainage divide (Dunn et al., 2017). Thermochronologic data from Copper River mouth revealed material mostly from the southern side of the orogen, similar to material accumulated under the Bering Glacier and in the western fold-and-thrust belt (Dunn et al., 2017). Significantly higher erosion

rates in the southern coastal regions dilute the input from the dry northern side (Dunn et al., 2017).

The Alsek River transports material from the Wrangellia terrane north of the drainage divide upstream of the Alsek lake (Falkowski and Enkelmann, 2016; Dunn et al., 2017). The Alsek River has been blocked several times by advancing glaciers that extended eastward from Mt. St. Elias (Bevington and Copland, 2014). There are no provenance data on the sediment load downstream of Alsek Lake, which is the terminus of the Alsek glacier (Molina, 2008). It is therefore unknown if these sediments have a Wrangell signature when reaching the Gulf of Alaska.

Erosion and transport from the St. Elias orogen into the Gulf of Alaska have been assumed to be geologically instantaneous because of the proximity of source and sink (Dunn et al., 2017). The time lag between cooling of thermochronologic systems through closure temperature and exposure of respective grains to erosion (dead zone signal, Garver et al., 1999) delays the transfer into the sedimentary record of signals of erosion and exhumation stored in thermochronological data (Dunn et al., 2017). In contrast, petrography and geochemistry of single grain data should shift directly, given that the source rocks show detectable differences.

2.10.1 Miocene provenance changes before the onset of glaciation

Predating the onset of glaciation, the first notable change in sediment composition occurred in the Miocene and coincides with the final collision of the Yakutat terrane with the North American continent. Collision initiated increased exhumation of the central part of the Chugach Mountains at ca. 11 ± 2 Ma (Enkelmann et al., 2008). Starting from a likely Yakutat terrane-Kulthieth Formation provenance, erosion centers changed to a source area composed mainly of amphibolite facies metamorphic rocks. This source may have been an exhuming sliver of the Yakutat terrane or may represent interior parts of the CMC. Enkelmann et al. (2015b) found fault initiation and associated rock exhumation on the Yakutat terrane migrating to the southwest, eventually due to progressive initiation of thrusting, but could not define the onset of exhumation east of Yakutat Bay. Future data constraining the onset of exhumation in this area will show if input from east of Yakutat bay to the Miocene Surveyor fan is likely.

Zircon U-Pb and Hf-isotopic data from the distal site support input from the CMC since ca. 11.5 ± 1.5 Ma (Huber et al., unpublished manuscript). Zircons from the coeval Yakataga Formation onshore also point to increased input from the CMC during the Miocene (Perry et al., 2009). Thermochronologic data from site U1417 for a sample deposited at ca. 8 Ma signal input from the fast exhuming Syntaxis area (Dunn et al., 2017). The tectonic driver for input of CMC material to the late Miocene Surveyor fan was the actual collision of the Yakutat terrane with the North American continent (Spotila and Berger, 2010; Falkowski et al., 2014, 2016; Enkelmann et al., 2017). Onset of deep seated and rapid exhumation in the Syntaxis is considered to have started between ca. ~11-8 Ma as a result of coupling between erosion and active tectonic rock uplift (Enkelmann et al., 2009; Falkowski et al., 2016; Dunn et al., 2017). This supports our inference of significant input from the CMC by the Miocene (fig. 11). It requires effective fluvial transport to the Surveyor fan from sources relatively far to the northwest. Concerning Miocene transport into the fan, Stevenson and Embley (1987) suggested a now subducted system of channels to have supplied material from northern sources including the CMC.

2.10.2 Transition from mountain to tidewater glaciation at the Miocene/Pliocene boundary

Garnet and amphibole representing non-metamorphic to low grade source rocks trace a progressive migration of provenance to areas west- and southward of the CMC at the transition from the Miocene to the Pliocene (fig. 11). A change in provenance has also been revealed by low temperature thermochronological data from the same site (U1417) by two samples dated at 8 and 3 Ma (Dunn et al., 2017). The older sample records input from areas with high exhumation rates, very likely from the Syntaxis area, while the younger sample records input from an area where exhumation is slower, having been suggested to record erosion of a dead

zone signal after a shift of the center of exhumation (Dunn et al., 2017). The Syntaxis area has been found to have been moving to the southeast from north of the active plate boundary to south of it (Enkelmann et al., 2015a; Falkowski and Enkelmann, 2016). This change may have facilitated the incorporation of low grade metamorphic areas located in the center of the exhuming area. However, in view of high exhumation and rock uplift rates, and of the position of the Syntaxis in the CMC area, we would expect the progressive exhumation of rocks with higher metamorphic grade. The progressively decreasing input of such detritus from the Miocene to the Pliocene informs us that additional processes must have driven the shift to erosion of low grade metamorphic material.

The respective changes coincide with the intensification of glaciation resulting in the onset of tidewater glaciation at the Miocene/Pliocene boundary (Reece et al., 2011). Exhumation has been found to be stronger in the low elevation areas close to the coast, correlating with the southward advance of orographic precipitation patterns and the position of the glacier equilibrium line altitude (Spotila et al., 2004). This is in line with the sediments of the Surveyor fan experiencing increasing input from the low-grade or non-metamorphic sources closer to the coast across the Miocene to Pliocene transition. We infer the erosive power of the glaciers to have triggered increasing erosion in the low-elevation areas with increasing glaciation. Enkelmann et al. (2015a) inferred a similar scenario with increasing glaciation, shifting erosion centers to lower altitudes during the Pleistocene. Furthermore, the final collision of the Yakutat terrane led to the reactivation of the Contact fault at ca. 6–5 Ma and a southward shift of the backstop (Enkelmann et al., 2008). Dextral transpression associated with lens-like pop-up structures is suggested to have resulted in locally very rapid exhumation along the Contact fault and in the accretionary wedge (Enkelmann et al., 2008). These tectonic drivers might have also funneled input from the areas closer to the coast. A combination of glacial and tectonic processes likely triggered incorporation of sources south- and westward of the CMC at lower elevations and closer to the coast, augmenting the changing provenance signal (fig. 11).

2.10.3 The Early Pleistocene and the mid-Pleistocene transition

Site U1417 and U148 record increasing sedimentation rates caused by more intense erosion in the Pliocene and Pleistocene and especially following the mid-Pleistocene transition (Gulick et al., 2015). Tectonic material transport changed from net influx to the orogen during the Early Pleistocene to net efflux since the mid-Pleistocene transition (Gulick et al., 2015). While the Miocene/Pliocene transition can only be studied at site U1417, the Pleistocene is resolved at both sites (Expedition 341 Scientists, 2014).

The geographical position of the proximal site and the geochemical characteristics of amphibole and garnet imply input mainly from the western part of the CMC. This is in line with limited sediment mixing and input mainly from the western part of the wet southern side of the orogen (Dunn et al., 2017). Provenance signals therefore likely reflect local changes linked to the dynamics of the Bering Bagley-glacier system rather than large scale changes affecting the entire orogen as seen in input from channels connecting directly to the Bering glacier (Expedition 341 Scientists, 2014) (fig. 1A). Some input from sources farther east could have been supplied by the westward-flowing coastparallel Alaska current that crosses the site (Stabeno et al., 2004; Expedition 341 Scientists, 2014). In contrast, the distal site experienced input from a way larger source area, integrating sediments spurred by the Alsek, Yakutat and Icy legs, integrating material from the Syntaxis, the wet southern side and also from the dry northern side (Dunn et al., 2017) (fig. 1A). Furthermore, the westward termination of the Syntaxis area has been found not to reach into the catchment of the Bering-Bagley glacial system (Enkelmann et al., 2015a; Dunn et al., 2017), resulting in both sites recording information on different parts of the St. Elias orogen. The composition of the heavy mineral spectrum of both sites is also different. Thus, the provenance evolution at the distal site is not simply an extension of that of the proximal site, and special caution is required when drawing conclusions on the evolution of the orogen from the sediments at the proximal site.

Different scenarios have been suggested for the impact of glaciation on the St. Elias orogen during the Pleistocene: (i) increased exhumation since the mid-Pleistocene transition resulting in

a structural reorganization of the orogen (Berger et al., 2008a; Berger et al., 2008b; Pavlis et al., 2012); (ii) changes in faulting in the Pamplona zone following an increase in sediment accumulation rates in the Bering valley after the mid-Pleistocene transition (Worthington et al., 2018), or (iii) a structural shift after the Plio-Pleistocene transition in response to the high sedimentation rates on the Yakutat shelf (Enkelmann et al., 2015a). The latter has been proposed to have triggered a southward shift of deformation and the development of high relief, focusing precipitation in the lower elevation areas in the south and a shift of the Syntaxis in similar direction after 2.6 Ma (Enkelmann et al., 2015a).

Our data imply a change in erosion centers already in the Early Pleistocene, with increasing erosion in the CMC compared to erosion in the low grade metamorphic areas close to the coast. This change was potentially triggered by the northern hemisphere glaciation and/or increasing exhumation of higher grade metamorphic material. The relatively high input from the CMC also to the distal site suggests these changes to have had strong impact on the area of maximum sediment export from the orogen. Erosion under the Bagley Ice field, which covers wide parts of the CMC, may have provided an essential part of this input to the proximal site. Dextral strike-slip motions along the Bagley fault (continuation of the Contact fault under the Bagley Ice Field) have been suggested to have been enhanced during the last 5 Ma (Bruhn et al., 2012). The increased uplift and the intensification of glaciation and glacial erosion in the Pleistocene are both probable triggers for the high CMC input.

The more intensive and widespread glaciation since the mid-Pleistocene transition may have again accelerated erosion in the higher relief areas (Gulick et al., 2015). However, changes may not be detectable by the methods used in this study due to the uniformity of rocks within the CMC and the response time of the orogen to changes after the mid-Pleistocene transition. Alternatively, the respective compositional changes may have been diluted in the sediments at the distal site by processes like downslope reworking of sediments. Still, the amphibole compositions in the two youngest samples from the distal site are more homogeneous than the older sediments, supporting a focusing of the source area after the mid-Pleistocene transition. As we only have Early Pleistocene sediments of the Mass Transport Deposit from the proximal site, comparison of provenance before and after the mid-Pleistocene transition is not straight forward, inhibiting confirmation of changes at the mid-Pleistocene transition with the data from this site. The provenance inferred by us, however, is in line with erosion of material essentially from the CMC.

2.11 Conclusions

The single grain geochemical heavy mineral data on garnet and amphibole presented here indicate that the Miocene to Pleistocene Surveyor fan sediments, drilled during IODP Expedition 341 at sites U1417 and U1418, were almost exclusively derived from persistent sources on the Chugach, Prince William and Yakutat terranes. Input from the Coast Plutonic Complex seems to have been minor which has already been indicated by previous studies (Perry et al., 2009).

Our data are in line with tectonics to be the prevalent factor in determining the main erosion centers. The area of the CMC supplied material to the Surveyor fan by ca. 11.5 ± 1.4 Ma. The extension of the glacial coverage to the tidewater line at the Miocene-Pliocene boundary caused strong interaction with tectonics in determining erosion centers. The onset of glaciation itself has been proposed to have resulted from the interaction of tectonic uplift and erosion, resulting in the formation of high mountains triggering alpine glaciation even though climatic conditions were probably warmer than today (Enkelmann et al., 2017). In turn, effective erosion in the Syntaxis area was caused by the onset of glaciation (Enkelmann et al., 2010), underlining the strong interaction of climate and tectonics.

The provenance affiliations of the Surveyor fan sediments imply changes associated with the northern hemisphere glaciation at the Plio-Pleistocene transition. Increasing glaciation at the mid-Pleistocene transition did not result in a significant change in the provenance, implying the drainage area and glaciers to have been nested in their topographically defined positions throughout, as assumed by Gulick et al. (2015).

Our data demonstrate that the sediments on the distal fan (site U1417) rather integrate the input from exhumation centers along the South Alaska continental margin. Contrastingly, the sediments at the proximal site (site U1418) are more indicative of local supply via the Bering glacier system (Expedition 341 Scientists, 2014; Dunn et al., 2017). Garnet and amphibole data show slight differences in timing of provenance change, likely caused by their fertility in different rock types. This emphasizes the necessity to study several different heavy minerals to facilitate a more complete reconstruction of provenance.

2.12 Acknowledgement

This study was funded by German Research Foundation (DFG) grant BA 1011/43-1 and -2. We thank M. Dröllner, Münster, for helping to process the samples and J. Berndt and B. Schmitte, Münster, for assistance with acquiring the microprobe data. Blanka Sperner is thanked for sharing expertise during Ar-Ar work in Freiberg. We thank S. Andò and two anonymous reviewers for their constructive reviews, and J. Knight for editorial guidance.

2.13 References

Adlakha, V., Patel, R.C., Lal, N., Mehta, Y.P., Jain, A.K., Kumar, A., 2013. Tectonics and climate interplay: exhumation patterns of the Dhauladhar Range, Northwest Himalaya. Curr. Sci. 104, 1551–1559.

Aliazi, A., Clift, P., Still, J., 2016. Indus Basin sediment provenance constrained using garnet geochemistry. J. Asian Earth Sci. 126, 29–57.

Andò, S., Morton, A., Garzanti, E., 2014. Metamorphic grade of source rocks revealed by chemical fingerprints of detrital amphibole and garnet. In: Scott, R.A., Smyth, H.R., Morton, A.C., Richardson, N. (Eds.), Sediment Provenance Studies in Hydrocarbon Exploration and Production. 386. Geol. Soc. London, Spec. Publ., pp. 351–371.

Berger, A.L., Gulick, S.P.S., Spotila, J.A., Upton, P., Jaeger, J.M., Chapman, J.B., Worthington, L. A., Pavlis, T.L., Ridgway, K.D., Willems, B.A., McAleer, R.J., 2008a. Quaternary tectonic response to intensified glacial erosion in an orogenic wedge. Nature Geosci. 1, 793–799.

Berger, A.L., Spotila, J.A., 2008. Denudation and deformation in a glaciated orogenic wedge: the St. Elias orogen, Alaska. Geology 36, 523–526.

Berger, A.L., Spotila, J.A., Chapman, J.B., Pavlis, T.L., Enkelmann, E., Ruppert, N.A., Buscher, J. T., 2008b. Architecture, kinematics, and exhumation of a convergent orogenic wedge: a thermochronological investigation of tectonic–climatic interactions within the central St. Elias orogen, Alaska. Earth Planetary Sci. Lett. 270, 13–24.

Bevington, A., Copland, L., 2014. Characteristics of the last five surges of Lowell Glacier, Canada, since 1948. Yukon. J. Glaciol. 60, 113–123.

Bruand, E., Gasser, D., Bonnand, P., Stüwe, K., 2011. The petrology and geochemistry of a metabasite belt along the southern margin of Alaska. Lithos 127, 282–297.

Bruand, E., Gasser, D., Stüwe, K., 2014. Metamorphic P–T conditions across the Chugach metamorphic complex (Alaska)—a record of focussed exhumation during transpression. Lithos 190–191, 292–312.

Bruhn, R.L., Pavlis, T.L., Plafker, G., Serpa, L., 2004. Deformation during terrane accretion in the Saint Elias orogen, Alaska. Geol. Soci. Am. Bull. 116, 771–787.

Bruhn, R.L., Sauber, J., Cotton, M.M., Pavlis, T.L., Burgess, E., Ruppert, N., Forster, R.R., 2012. Plate margin deformation and active tectonics along the northern edge of the Yakutat Terrane in the Saint Elias Orogen, Alaska, and Yukon, Canada. Geosphere 8, 1384–1407.

Bruns, T.R., 1983. Model for the origin of the Yakutat terrane, an accreting terrane in the northern Gulf of Alaska. Geology 11, 718–721.

Carlson, P.R., Stevenson, A.J., Bruns, T.R., Mann, D.M., Huggett, Q., 1996. Sediment pathways in the Gulf of Alaska from beach to abyssal plain. In: Gardner, J.V., Field,

M.E., Twichell, D.C. (Eds.), Geology of the United States' Seafloor: The View from GLORIA. Cambridge University Press, Cambridge, pp. 255–278.
Chapman, J.B., Pavlis, T.L., Gulick, S., Berger, A., Lowe, L., Spotila, J., Bruhn, R., Vorkink, M., Koons, P., Barker, A., Picornell, C., Ridgway, K., Hallet, B., Jaeger, J., Mccalpin, J., 2013. Neotectonics of the Yakutat collision: changes in deformation driven by mass redistribution. In: Freymueller, J.T., Haeussler, P.J., Wesson, R.L., Ekström, G. (Eds.), Active Tectonics and Seismic Potential of Alaska. Geoph. Monog. 179. American Geophysical Union, Washington DC, pp. 65–81.
Clift, P.D., 2006. Controls on the erosion of Cenozoic Asia and the flux of clastic sediment to the ocean. Earth Planet. Sci. Lett. 241, 571–580.
Clift, P.D., Hodges, K.V., Heslop, D., Hannigan, R., Van Long, H., Calves, G., 2008. Correlation of Himalayan exhumation rates and Asian monsoon intensity. Nature Geosci. 1, 875–880.
Clift, P.D., Wares, N.M., Amato, J.M., Pavlis, T.L., Hole, M.J., Worthman, C., Day, E., 2012. Evolving heavy mineral assemblages reveal changing exhumation and trench tectonics in the Mesozoic Chugach accretionary complex, south-central Alaska. Geol. Soci. Am. Bull. 124, 989–1006.
Colpron, M., Nelson, J.L., 2011. A digital atlas of terranes for the Northern Cordillera. Accessed online from Yukon Geological Survey. www.geology.gov.yk.ca, Accesse date: 25 July 2017.
Crawford, M.L., Hollister, L.S., Woodsworth, G.J., 1987. Crustal deformation and regional metamorphism across a terrane boundary, coast plutonic complex, British Columbia. Tectonics 6, 343–361.
Cui, Y., Miller, D., Nixon, G., Nelson, J., 2015. British Columbia digital geology. British Columbia Geological Survey. http://www.empr.gov.bc.ca/mining/geoscience/bedrockmapping/pages/bcgeomap.aspx, Accessed date: 24 July 2017.
Dobson, M.R., O'Leary, D., Veart, M., 1998. Sediment delivery to the Gulf of Alaska: source mechanisms along a glaciated transform margin. In: Stocker, M.S., Evans, D., CCramp, A. (Eds.), Geological processes on continental margins: sedimentation, mass-wasting and stability. Geological Society of London, Special Publication 129, pp. 43–66.
Dodds, C.J., Campbell, P.B., 1988. Potassium-argon ages of mainly intrusive rocks in the Saint Elias Mountains, Yukon and British Columbia. Geol. Surv. Can. Paper 87-16 (43 pp.).
Dumoulin, J., 1987. Sandstone composition of the Valdez and Orca groups, Prince William Sound, Alaska. U.S. Geological Survey Bulletin 1774 (37 pp.).
Dunn, C.A., Enkelmann, E., Ridgway, K.D., Allen, W.A., 2017. Source to sink evaluation of sediment routing in the Gulf of Alaska and Southeast Alaska: a thermochronometric perspective. J. Geophys. Res. 122, 711–734.
Dusel-Bacon, C., Csejtey Jr., B., Foster, H.L., Doyle, E.O., Nokleberg, W.J., Plafker, G., 1993. Distribution, facies, ages, and proposed tectonic associations of regionally metamor- phosed rocks in east- and south-central Alaska. U.S. Geological Survey Professional Paper 1479 (73 pp.).
Dusel-Bacon, C., Brew, D.A., Douglass, S.L., 1996. Metamorphic facies map of Southeastern Alaska-distribution, facies, and ages of regionally metamorphosed rocks. U.S. Geological Survey Professional Paper 1497-D,48 pp.
Elliott, J.L., Larsen, C.F., Freymueller, J.T., Motyka, R.J., 2010. Tectonic block motion and glacial isostatic adjustment in southeast Alaska and adjacent Canada constrained by GPS measurements. J. Geophys. Res. https://doi.org/10.1029/ 2009JB007139.
Enkelmann, E., Garver, J.I., Pavlis, T.L., 2008. Rapid exhumation of ice-covered rocks of the Chugach–St. Elias orogen, Southeast Alaska. Geology 36, 915–918.
Enkelmann, E., Zeitler, P.K., Pavlis, T.L., Garver, J.I., Ridgway, K.D., 2009. Intense localized rock uplift and erosion in the St. Elias orogen of Alaska. Nature Geosci. 2, 360–363.
Enkelmann, E., Zeitler, P.K., Garver, J.I., Pavlis, T.L., Hooks, B.P., 2010. The thermochronological record of tectonic and surface process interaction at the Yakutat-North American collision zone in Southeast Alaska. Am. J. Sci. 310, 231–260.

Enkelmann, E., Koons, P.O., Pavlis, T.L., Hallet, B., Barker, A., Elliott, J., Garver, J.I., Gulick, S.P. S., Headley, R.M., Pavlis, G.L., Ridgway, K.D., Ruppert, N., van Avendonk, H., 2015a. Cooperation of tectonic and surface processes produces Earth's highest coastal mountains. Geophys. Res. Lett. 42, 5838–5846.

Enkelmann, E., Valla, P.G., Champagnac, J.-D., 2015b. Low-temperature thermochronology of the Yakutat Plate corner, St. Elias Range (Alaska): bridging short-term and long- term deformation. Quat. Sci. Rev. 113, 23–38.

Enkelmann, E., Piestrzeniewicz, A., Falkowski, S., Stübner, K., Ehlers, T.A., 2017. Thermochronology in Southeast Alaska and Southwest Yukon: implications for North American plate response to terrane accretion. Earth Planet. Sci. Lett. 457, 348–358.

Esri, 2018. DigitalGlobe, GeoEye, Earthstar Geographics, CNES/Airbus DS, USDA, USGS, AeroGrid, IGN, and the GIS user Community.

Expedition 341 Scientists, 2014. Southern Alaska Margin: Interactions of Tectonics, Climate, and Sedimentation. IODP Preliminary Report 341 (http://publications.iodp. org/preliminary_report/341/341_2.htm (last accessed on 7 Mai 2018)). https://doi. org/10.2204/iodp.pr.341.2014.

Falkowski, S., Enkelmann, E., Ehlers, T.A., 2014. Constraining the area of rapid and deep-seated exhumation at the St. Elias syntaxis, Southeast Alaska, with detrital zircon fission-track analysis. Tectonics 33, 597–616.

Falkowski, S., Enkelmann, E., 2016. Upper-crustal cooling of the Wrangellia composite terrane in the northern St. Elias Mountains, western Canada. Lithosphere 8, 359–378.

Falkowski, S., Enkelmann, E., Drost, K., Pfänder, J.A., Stübner, K., Ehlers, T.A., 2016. Cooling history of the St. Elias syntaxis, Southeast Alaska, revealed by geochronology and thermochronology of cobble-sized glacial detritus. Tectonics 35, 447–468.

Finzel, E.S., Trop, J.M., Ridgway, K.D., Enkelmann, E., 2011. Upper plate proxies for flat-slab subduction processes in southern Alaska. Earth Planet. Sci. Lett. 303, 348–360.

Finzel, E.S., Flesch, L.M., Ridgway, K.D., Holt, W.E., Ghosh, A., 2015. Surface motions and intraplate continental deformation in Alaska driven by mantle flow. Geophys. Res. Lett. 42, 4350–4358.

Fleet, M.E., Barnett, R.L., 1978. Al^{IV}/Al^{VI} partitioning in calciferous amphiboles from the Frood mine Sudbury, Ontario. Can Mineral. 16, 527–532.

Garver, J.I., Brandon, M.T., Roden-Tice, M., Kamp, P.J.J., 1999. Exhumation history of orogenic highlands determined by detrital fission-track thermochronology. In: Ring, U., Brandon, M.T., Lister, G.S., Willet, S.D. (Eds.), Exhumation Processes: Normal Faulting, Ductile Flow and Erosion. Geol. Soc. London, Spec. Publ. 154, pp. 283–304.

Garver, J.I., Davidson, C.M., 2015. Southwestern Laurentian zircons in Upper Cretaceous flysch of the Chugach-Prince William terrane in Alaska. Am. J. Sci. 315, 537–556.

Garzanti, E., Doglioni, C., Andò, S., Vezzoli, G., 2007. Orogenic belts and orogenic sediment provenance. J. Geology 115, 315–334.

Garzanti, E., Andò, S., Vezzoli, G., 2008. Settling-equivalence of detrital minerals and grain-size dependence of sediment composition. Earth Planet. Sci. Lett. 273, 138–151.

Garzanti, E., Andò, S., Vezzoli, G., 2009. Grain size dependence of sediment composition and environmental bias in provenance studies. Earth Planet. Sci. Lett. 277, 422–432.

Garzanti, E., 2016. From static to dynamic provenance analysis-sedimentary petrology upgraded. Sed. Geol. 336, 3–13.

Gasser, D., Bruand, E., Stüwe, K., Foster, D.A., Schuster, R., Fügenschuh, B., Pavlis, T.L., 2011. Formation of a metamorphic complex along an oblique convergent margin: structural and thermochronological evolution of the Chugach Metamorphic Complex, southern Alaska. Tectonics 30, TC2012. https://doi.org/10.1029/2010TC002776.

Gasser, D., Rubatto, D., Bruand, E., Stüwe, K., 2012. Large-scale, short-lived metamorphism, deformation, and magmatism in the Chugach metamorphic complex, southern Alaska: a SHRIMP U-Pb study of zircons. GSA Bulletin 124, 886–905.

Gehrels, G.E., Berg, H.C., 1994. Geology of Southeastern Alaska. In: Plafker, G., Berg, H.C. (Eds.), The Geology of North America, Volume G. The Geology of Alaska. Geological Society of America, Boulder, Colorado, pp. 451–467.

Gulick, S.P.S., Jaeger, J.M., Mix, A.C., Asahi, H., Bahlburg, H., Belanger, C.L., Berbel, G.B.B., Childress, L., Cowan, E., Drab, L., Forwick, M., Fukumura, A., Ge, S., Gupta, S., Kioka, A., Konno, S., LeVay, L.J., März, C., Matsuzaki, K.M., McClymont, E.L., Moy, C., Müller, J., Nakamura, A., Ojima, T., Ribeiro, F.R., Ridgway, K.D., Romero, O.E., Slagle, A.L., Stoner, J.S., St-Onge, G., Suto, I., Walczak, M.D., Worthington, L.L., Bailey, I., Enkelmann, E., Reece, R., Swartz, J.M., 2015. Mid-Pleistocene climate transition drives net mass loss from rapidly uplifting St. Elias Mountains, Alaska. Proceedings of the National Academy of Sciences of the United States of America 112, 15042–15047.

Harrison, T.M., 1981. Diffusion of 40Ar in hornblende. Contrib. Mineral. Petr. 78, 324–331.

Harrison, T.M., Duncan, I., McDougall, I., 1985. Diffusion of 40Ar in biotite: temperature, pressure and compositional effects. Geochim. Cosmochim. Ac. 49, 2461–2468.

Headley, R., Hallet, B., Roe, G., Waddington, E.D., Rignot, E., 2012. Spatial distribution of glacial erosion rates in the St. Elias range, Alaska, inferred from a realistic model of glacier dynamics. J. Geophys. Res. 117, F03027. https://doi.org/10.1029/2011JF002291.

Headley, R.M., Enkelmann, E., Hallet, B., 2013. Examination of the interplay between glacial processes and exhumation in the Saint Elias Mountains, Alaska. Geosphere 9, 229–241.

Headley, R.M., Ehlers, T.A., 2015. Ice flow models and glacial erosion over multiple glacial–interglacial cycles. Earth Surf. Dyn. 3, 153–170.

Hillhouse, J.W., 1977. Paleomagnetism of the Triassic Nikolai Greenstone, McCarthy Quadrangle, Alaska. Can. J. Earth Sci. 14, 2578–2592.

Himmelberg, G.R., Haeussler, P.J., Brew, D.A., 2004. Emplacement, rapid burial, and exhumation of 90-Ma plutons in southeastern Alaska. Can. J. Earth Sci. 41, 87–102.

Hogan, L.G., Scheidegger, K.F., Kulm, L.D., Dymond, J., Mikkelsen, N., 1978. Biostratigraphic and tectonic implications of ^{40}Ar-^{39}Ar dates of ash layers from the northeast Gulf of Alaska. Geol. Soci. Am. Bull. 89, 1259–1264.

Huber B., Bahlburg H., Berndt J., Dunkl I. and Gerdes A., Multi-method provenance analysis of zircons from the Surveyor fan: implications on climate induced modification of erosion centers in the evolving Chugach-St. Elias mountain belt, The Journal of Geology 2018, (under revision, unpublished manuscript).

Hudson, T., Plafker, G., 1982. Paleogene metamorphism of an accretionary flysch terrane, eastern Gulf of Alaska. Geol. Soci. Am. Bull. 93, 1280–1290.

Huntington, K.W., Blythe, A.E., Hodges, K.V., 2006. Climate change and Late Pliocene acceleration of erosion in the Himalaya. Earth and Planetary Science Letters 252, 107–118. Jaeger, J.M., Nittrouer, C.A., Scott, N.D., Milliman, J.D., 1998. Sediment accumulation along a glacially impacted mountainous coastline: north-east Gulf of Alaska. Basin Res. 10, 155–173.

Jaeger, J.M., Gulick, S., LeVay, L.J., Asahi, H., Bahlburg, H., Belanger, C.L., Berbel, G., Childress, L.B., Cowan, E.A., Drab, L., Forwick, M., Fukumura, A., Ge, S., Gupta, S.M., Kioka, A., Konno, S., März, C.E., Matsuzaki, K.M., McClymont, E.L., Mix, A.C., Moy, C. M., Müller, J., Nakamura, A., Ojima, T., Ridgway, K.D., Rodrigues Ribeiro, F., Romero, O.E., Slagle, A.L., Stoner, J.S., St-Onge, G., Suto, I., Walczak, M.H., Worthington, L.L., 2014. Methods. In: Jaeger, J.M., Gulick, S., LeVay, L.J., Expedition 341 Scientists (Eds.), Proceedings of the Integrated Ocean Drilling Program. 341. (Integrated Ocean Drilling Program), College Station, TX (58 pp.).

Krippner, A., Meinhold, G., Morton, A.C., von Eynatten, H., 2014. Evaluation of garnet discrimination diagrams using geochemical data of garnets derived from various host rocks. Sed. Geol. 306, 36–52.

Krippner, A., Meinhold, G., Morton, A.C., Russell, E., von Eynatten, H., 2015. Grain-size dependence of garnet composition revealed by provenance signatures of modern stream sediments from the western Hohe Tauern (Austria). Sed. Geol. 321, 25–38.

Kusky, T.M., Bradley, D.C., Donely, D.T., Rowley, D., Haeussler, P.J., 2003. Controls on intrusion of neartrench magmas of the Sanak-Baranof Belt, Alaska, during Paleogene ridge subduction, and consequences for forearc evolution. In: Sisson, V.B., Roeske, S. M., Pavlis, T.L. (Eds.), Geology of a Transpressional Orogen Developed during Ridge-

trench Interaction along the North Pacific Margin. 371. Geol. Soci. Am., Boulder, Colorado, pp. 269–292.
Lagoe, M.B., Eyles, C.H., Eyles, N., Hale, C., 1993. Timing of late Cenozoic tidewater glaciation in the far North Pacific. Geological Society of America Bulletin 105, 1542–1560. Leake, B.E., 1965. The relationship between composition of calciferous amphibole and grade of metamorphism. In: Pitcher, W.S., Flinn, G.W. (Eds.), Controls of Metamorphism. Oliver and Boyd, Edinburgh, pp. 299–318.
Lagoe, M.B., Zellers, S.D., 1996. Climates and climate variability of the Pliocene depositional and microfaunal response to Pliocene climate change and tectonics in the eastern Gulf of Alaska. Marine Micropaleontol. 27, 121–140.
Leake, B.E., 1978. Nomenclature of amphiboles. American Mineralogist 63, 1023–1052. Leake, B.E., Woolley, A.R., Birch, W.D., Burke, E.A., Ferraris, G., Grice, J.D., Hawthorne, F.C., Kisch, H.J., Krivovichev, V.G., Schumacher, J.C., Stephenson, N.C.N., Whitaker, E.J.W., 2004. Nomenclature of amphiboles: additions and revisions to the international mineralogical Association's amphibole nomenclature. Mineral. Mag. 68, 209–215.
Li, G., Yan, W., Zhong, L., Xia, Z., Wang, S., 2015. Provenance of heavy mineral deposits on the northwestern shelf of the South China Sea, evidence from single-mineral chemistry. Mar. Geol. 363, 112–124.
Lipovsky, P.S., Bond, J.D., 2014. Yukon digital surficial geology compilation, digital release 1, 8 April 2014, Bedrock Geology Dataset. Yukon Geological Survey. http://data.geology.gov.yk.ca/Compilation/3, Accessed date: 2 August 2017 (compilers).
Mange, M.A., Maurer, H.F.W., 1992. Heavy Minerals in Colour. Chapman & Hall, London (147 pp.).
Mange, M.A., Morton, A.C., 2007. Chapter 13, Geochemistry of Heavy Minerals. In: Mange, M.A., Wright, D.K. (Eds.), Heavy Minerals in Use. Developments in Sedimentology. Elsevier, Amsterdam, pp. 345–391.
Manley, W.F., Kaufman, D.S., 2002. Alaska PaleoGlacier Atlas. Institute of Arctic and Alpine Research (INSTAAR), University of Colorado http://instaar.colorado.edu/QGISL/ak_paleoglacier_atlas.
Mann, D.H., Hamilton, T.D., 1995. Late Pleistocene and Holocene paleoenvironments of the North Pacific coast. Quat. Sci. Rev. 14, 449–471.
McAleer, R.J., Spotila, J.A., Enkelmann, E., Berger, A.L., 2009. Exhumation along the Fairweather fault, southeastern Alaska, based on low-temperature thermochronometry. Tectonics 28, TC1007. https://doi.org/10.1029/2007TC002240.
McClelland, W.C., Anovitz, L.M., Gehrels, G.E., 1991. Thermobarometric constraints on the structural evolution of the Coast Mountains batholith, central southeastern Alaska. Can. J. Earth Sci. 28, 912–928.
Meigs, A., Sauber, J., 2000. Southern Alaska as an example of the long-term consequences of mountain building under the influence of glaciers. Quat. Sci. Rev. 19, 1543–1562.
Meigs, A., Johnston, S., Garver, J., Spotila, J., 2008. Crustal-scale structural architecture, shortening, and exhumation of an active, eroding orogenic wedge (Chugach/St Elias Range, southern Alaska). Tectonics 27, TC4003. https://doi.org/10.1029/2007TC002168.
Molina, B.F., 2008. Glaciers of North America–glaciers of Alaska. In: Williams Jr., R.S., Ferrigno, J.G. (Eds.), Satellite Image Atlas of Glaciers of the World. U.S. Geological Survey Professional Paper 1386-K (750 pp.).
Molnar, P., 2004. Late Cenozoic increase in accumulation rates of terrestrial sediment: how might climate change have affected erosion rates? Annu. Rev. Earth Planet. Sci. 32, 67–89.
Molnar, P., England, P., 1990. Late Cenozoic uplift of mountain ranges and global climate change: chicken or egg? Nature 346, 29–34.
Morton, A.C., 1984. Stability of detrital heavy minerals in tertiary sandstones from the North Sea basin. Clay Minerals 19, 287–308.
Ness, G.E., Kulm, L.D., 1973. Origin and development of surveyor deep-sea channel. Geol. Soc. Am. Bull. 84, 3339–3354.

Nokleberg, W.J., Plafker, G., Wilson, F.H., 1994. Geology of south-central Alaska. In: Plafker, G., Berg, H.C. (Eds.), The Geology of Alaska. The Geology of North America G1. Geological Society of America, Boulder, Colorado, pp. 311–366.
Pandey, D.K., Clift, P.D., Kulhanek, D.K., Expedition 355 Scientists, 2016. In: Pandey, D.K., Clift, P.D., Kulhanek, D.K., Expedition 355 Scientists (Eds.), Expedition 355 summary 355. (International Ocean Discovery Program), College Station, TX (32 pp.).
Pavlis, T.L., Chapman, J.B., Bruhn, R.L., Ridgway, K., Worthington, L.L., Gulick, S.P.S., Spotila, J., 2012. Structure of the actively deforming fold-thrust belt of the St. Elias orogen with implications for glacial exhumation and three-dimensional tectonic processes. Geosphere 8, 991–1019.
Peizhen, Z., Molnar, P., Downs, W.R., 2001. Increased sedimentation rates and grain sizes 2 ±4 Myr ago due to the influence of climate change on erosion rates. Nature 410, 891–897.
Pell, J., 1987. Industrial mineral potential of kyanite and garnet in British Columbia (NTS 92H/7, 10). British Columbia Ministry of Energy, Mines and Petroleum Resources, Geological Open File, Fieldwork Paper 1988-1, pp. 421–424.
Perry, S.E., Garver, J.I., Ridgway, K.D., 2009. Transport of the Yakutat terrane, southern Alaska: evidence from sediment petrology and detrital zircon fission-track and U/Pb double dating. J. Geol. 117, 156–173.
Péwé, T.L., 1975. Quaternary Geology of Alaska. U.S. Geological Survey Professional Paper 835 (145 pp.).
Plafker, G., 1987. Regional geology and petroleum potential of the Northern Gulf of Alaska continental margin. In: Scholl, D.W., Grantz, A., Vedder, J.G. (Eds.), Petroleum Geology Potential of the Continental Margin of Western North America and Adjacent Ocean Basins. Circum-Pacific Council for Energy and Mineral Resources, Earth Science Series 6, pp. 229–268. Plafker, G., Winkler, G.R., Coonrad, W.L., Claypool, G.E., 1980. Preliminary report on the geology of the continental slope adjacent to OCS lease sale 55, eastern Gulf of Alaska, petroleum resource implications. U.S. Geological Survey Open-File Report 80-1089 (103 pp.).
Plafker, G., Nokleberg, W.J., Lull, J.S., 1989. Bedrock geology and tectonic evolution of the Wrangellia, Peninsular, and Chugach terranes along the Trans-Alaska Crustal Transect in the Chugach Mountains and southern Copper River basin, Alaska. J. Geophys. Res. 94, 4255–4295.
Plafker, G., Moore, J.C., Winkler, G.R., 1994. Geology of the southern Alaska margin. In: Plafker, G., Berg, H.C. (Eds.), The Geology of Alaska. Geology of North America, G-1. Geological Society of America, Boulder, Colorado, pp. 389–450.
Post, A., 1972. Periodic surge origin of folded medial moraines on Bering Piedmont glacier, Alaska. J. Glaciol. 11 (62), 219–226.
Raymo, M.E., Ruddiman, W.F., 1992. Tectonic forcing of late Cenozoic climate. Nature 359, 117–122.
Rea, D.K., Snoeckx, H., 1995. Sediment Fluxes in the Gulf of Alaska: Paleoceanographic Record from Site 887 on the Patton-Murray Seamount Platform. In: Rea, D.K., Basov, I.A., Scholl, D.W., Allan, J.F. (Eds.), Proceedings of the Ocean Drilling Program: Scientific Results. 145. (Ocean Drilling Program), College Station, Texas, pp. 247–256.
Reece, R.S., Gulick, S.P.S., Horton, B.K., Christeson, G.L., Worthington, L.L., 2011. Tectonic and climatic influence on the evolution of the Surveyor fan and channel system, Gulf of Alaska. Geosphere 7, 830–844.
Sisson, V.B., Hollister, L.S., Onstott, T.C., 1989. Petrologic and age constraints on the origin of a low-pressure/high-temperature metamorphic complex, southern Alaska. J. Geophys. Res. 94, 4392–4410.
Sisson, V.B., Poole, A.R., Harris, N.R., Cooper Bruner, H., Pavlis, T.L., Copeland, P., Donelick, R.A., McClelland, W.C., 2003. Geochemical and geochronologic constraints for genesis of a tonalite-trondhjemite suite and associated mafic intrusive rocks in the eastern Chugach Mountains, Alaska: A record of ridge-transform subduction. In: Sisson, V. B., Roeske, S.M., Pavlis, T.L. (Eds.), Geology of a Transpressional Orogen

Developed during Ridge-trench Interaction along the North-Pacific Margin. 371. Geol. Soc. Am. Spec. Pap., Boulder, Colorado, pp. 293–326.
Spotila, J.A., Berger, A.L., 2010. Exhumation at orogenic indentor cornders under long-term glacial conditions: example of the St. Elias Orogen, Southern Alaska. Tectonophysics 490, 241–256.
Spotila, J.A., Buscher, J.T., Meigs, A.J., Reiners, P.W., 2004. Long-term glacial erosion of active mountain belts: example of the Chugach–St. Elias Range, Alaska. Geology 32, 501–504.
Stabeno, P.J., Bond, N.A., Hermann, A.J., Kachel, N.B., Mordy, C.W., Overland, J.E., 2004. Meteorology and oceanography of the Northern Gulf of Alaska. Cont. Shelf Res. 24, 859–897.
Stevenson, A.J., Embley, R., 1987. Deep-sea fan bodies, terrigenous turbidite sedimentation and petroleum geology, Gulf of Alaska. In: Scholl, D.W., Grantz, A., Vedder, J.G. (Eds.), Geology and Resource Potential of the Continental Margin of Western North America and Adjacent Ocean Basins—Beaufort Sea to Baja California. Earth Science Series. Circum-Pacific Council for Energy and Mineral Resources, Houston, pp. 503–522.
Stowell, H.H., Goldberg, S.A., 1997. Sm–Nd garnet dating of polyphase metamorphism: northern Coast Mountains, south-eastern Alaska, USA. J. Metamorph. Geol. 15, 439–450.
Stowell, H.H., Green, L.N., Hooper, R.J., 2002. Geochemistry and tectonic wetting of basaltic volcanism, northern Coast Mountains, southeastern Alaska. In: Stowell, H.H., McCelland, W.C. (Eds.), Tectonics of the Coast Mountains, Southeastern Alaska and British Columbia. Geological Society of America, Special Paper 343, Boulder, Colorado, pp. 235–256.
Teraoka, Y., Suzuki, M., Hayashi, T., Kawakami, K., 1997. Detrital garnets from Paleozoic and Mesozoic sandstones in the Onogawa area, East Kyushu, Southwest Japan. Bulletin of the Faculty of School Education, Hiroshima University, Part II. 19, pp. 87–101 (in Japanese with English abstract).
Teraoka, Y., Suzuki, M., Kawakami, K., 1998. Provenance of cretaceous and paleogene sediments in the median zone of Southwest Japan. Bull. Geol. Soc. Japan 49, 395–411 (in Japanese with English abstract).
Tolosana-Delgado, R., Eynatten, H., Krippner, A., Meinhold, G., 2018. A multivariate discrimination scheme of detrital garnet chemistry for use in sedimentary provenance analysis. Sedimentary Geology https://doi.org/10.1016/j.sedgeo.2017.11.003 (in press).
Trop, J.M., Ridgway, K.D., Manuszak, J.D., Layer, P., 2002. Mesozoic sedimentary-basin development on the allochthonous Wrangellia composite terrane, Wrangell Mountains basin, Alaska: a long-term record of terrane migration and arc construction. Geol. Soc. Am. Bull. 114, 693–717.
Usman, M.O., Massago, H., Winkler, W., Strasser, M., 2014. Mid-quaternary decoupling of sediment routing in the Nankai Forearc revealed by provenance analysis of turbiditic sands. Int. J. Earth Sci. 103, 1141–1161.
Vermeesch, P., Resentini, A., Garzanti, E., 2016. An R package for statistical provenance analysis. Sed. Geol. 336, 14–25.
Wilson, F.H., Hults, C.P., Mull, C.G., Karl, S.M., 2015. Geologic Map of Alaska: U.S. Geological Survey Scientific Investigations Map 3340. U.S. Geological Survey. https://doi.org/ 10.3133/sim3340.
Worthington, L.L., Gulick, S.P.S., Pavlis, T.L., 2010. Coupled stratigraphic and structural evolution of a glaciated orogenic wedge, offshore St. Elias orogen, Alaska. Tectonics 29, TC6013–TC6039. https://doi.org/10.1029/2010TC002723.
Worthington, L.L., Van Avendonk, H.J.A., Gulick, S.P.S., Christeson, G.L., Pavlis, T.L., 2012. Crustal structure of the Yakutat terrane and the evolution of subduction and collision in southern Alaska. J. Geophys. Res., Solid Earth 117, B01102. https://doi.org/10.1029/2011JB008493.
Worthington, L.L., Daigle, H., Clary, W.A., Gulick, S.P.S., Montelli, A., 2018. High sedimentation rates and thrust fault modulation: insights from ocean drilling offshore the St. Elias Mountains, southern Alaska. Earth Planet. Sci. Lett. 483, 1–12.

Wright, W., 1938. The composition and occurrence of garnets. Am. Mineral. 23, 436–499.
Zumsteg, C.L., Himmelberg, G.R., Karl, S.M., Haeussler, P.J., 2003. Metamorphism within the Chugach accretionary complex on southern Baranof Island, southeastern Alaska, Geology of a transpressional orogen developed during ridge-trench interaction along the North Pacific margin. In: Sisson, V.B., Roeske, S.M., Pavlis, T.L. (Eds.), Geology of a Transpressional Orogen Developed during Ridge-Trench Interaction along the North Pacific Margin. Geol. Soc. Am. Spec. Pap. 371, pp. 253–267.

3 Provenance of the Surveyor Fan and precursor sediments in the Gulf of Alaska – implications of a combined U-Pb, (U-Th)/He, Hf and REE study of detrital zircons

This chapter has been published as Huber, B., Bahlburg, H., Berndt, J., Dunkl, I., Gerdes, A., 2018. Provenance of the Surveyor Fan and precursor sediments in the Gulf of Alaska – implications of a combined U-Pb, (U-Th)/He, Hf and REE study of detrital zircons. The Journal of Geology 12, 577-600. https://doi.org/10.1086/699740

Abstract

The history of exhumation and denudation of the Cenozoic St. Elias orogen is stored in the sediments of the Miocene to Holocene Surveyor Fan, Gulf of Alaska. The orogeny of the mountain belt coincides with major climatic events leading to varying degrees of glaciation that are considered to have strongly interacted with mountain building processes. In order to assess the relative influence of climate and tectonics on erosion patterns and reconstructing sediment routing to the ocean we combine zircon U-Pb dating and (U-Th)/He thermochronology with the analysis of rare earth elements and Hf-isotopes of zircons of sands and silts from IODP expedition 341 sites U1417 and U1418 drilled in the Surveyor Fan.

All Miocene to Pleistocene sediments show similar U-Pb age spectra indicating the main source areas to have remained the same during different stages of glaciation. A prominent age component at 50-60 Ma can be linked to the Chugach Metamorphic Complex and Sanak-Baranof Plutonic belt in the mountain range. Older grains can be referred to low grade metamorphic sources within the Chugach, Prince William and Yakutat terranes. A decrease in 50-60 Ma old igneous and metamorphic zircons implies a reduction of input from the Chugach Metamorphic Complex and the Sanak Baranof Plutonic belt. This indicates that the southward advance of glaciers towards the ocean together with tectonic changes from the Miocene to the Pliocene have triggered a higher contribution from the newly glaciated areas. During times of increased glaciation in the Pleistocene, glaciers appear to have been nested in the same area as before. Our data do not give evidence of a general change in the drainage systems or the tectonic setting during the Pleistocene but also do not prove absence of such.

3.1 Introduction

Erosional mass transfer intimately links the evolution of orogenic topography to the deposition in periorogenic basins. In the case of the Neogene to Quaternary St. Elias orogen at the southern Alaska margin, tectonically induced exhumation is modulated by climate processes triggering varying degrees and styles of glaciation (e.g., Berger et al., 2008a, 2008b; Enkelmann et al., 2008, 2010, 2017; Gulick et al. 2015; Falkowski and Enkelmann, 2016; Worthington et al., 2018). The formation of the St. Elias orogen is caused by northwestward movement of the Yakutat terrane along the Fairweather strike-slip fault toward the Pamplona Zone and the Aleutian Trench and collision along the Chugach–St. Elias fault (fig. 1). Exhumation in the orogen has been found to vary in time and space. An area of extremely rapid exhumation has been identified (the St. Elias syntaxis) that has been moving to the south since ca. 10 Ma (late Miocene), and different exhumation scenarios have been suggested for the Pleistocene (e.g., Berger et al., 2008a; Enkelmann et al., 2008, 2009, 2010, 2015, 2017; Spotila and Berger 2010; Falkowski et al., 2014; Worthington et al., 2018).

In the course of the St. Elias orogeny, alpine glaciation began at the southern Alaska continental margin in the late Miocene (ca. 7 Ma) and increased to tidewater glaciation at the Miocene/Pliocene boundary (ca. 6.7–5.0 Ma; glacial interval A in fig. 3; Lagoe et al., 1993). After a warm period in the middle Pliocene (glacial interval B; Lagoe et al., 1993), glaciers returned during the Pleistocene. This coincided with a change in global glacial-interglacial climate cycles from 40 to 100 ka at the mid-Pleistocene transition (MPT; ca. 0.7–1 Ma), which caused an increase in glaciation and the establishment of highly erosive ice streams (glacial interval C; Lagoe and Zellers 1996). The impact of these changes in glacial intensity on and their interaction with ongoing tectonic processes are still poorly understood, partly because glaciers still cover wide parts of the orogen (e.g., Spotila et al., 2004; Berger et al., 2008a; Berger and Spotila, 2008; Meigs et al., 2008; Enkelmann et al., 2010, 2015, 2017; Spotila and Berger, 2010; Worthington et al., 2010, 2018; Expedition 341 Scientists, 2014; Gulick et al., 2015).

As the windward side of the orogen faces the Gulf of Alaska, the major part of the detrital mass export from the orogen to the ocean ends up as deep-sea sediments on the Gulf of Alaska abyssal plain, in particular in the Surveyor deep-sea fan (Stevenson and Embley, 1987; Berger et al., 2008a, 2008b; Reece et al. 2011; Gulick et al., 2015). Sediments on the Gulf of Alaska abyssal plain range in age from early Miocene to Holocene. They record the exhumation of the St. Elias Mountains and reflect the interaction of tectonic and climatic processes governing the terrigenous mass transfer to the abyssal plain (Ingle, 1973; Plafker, 1987; Plafker et al., 1994; Reece et al., 2011; Jaeger et al., 2014; Gulick et al., 2015; Montelli et al., 2017).

Previous studies of zircon and apatite U-Pb and fission-track (FT) double-dating and heavy-mineral analysis of sediments from the Surveyor Fan and precursor sediments revealed the usefulness of these sediments to constrain information on onshore exhumation rates during the Miocene to Pliocene and provenance (Dunn et al., 2017; Huber et al. 2018). In this contribution, we present new detrital zircon data on the geochemical composition, U-Pb age distributions, Hf isotope patterns, and (U-Th)/He thermochronological data of Miocene through Pleistocene sediments from two sites drilled by Integrated Ocean Drilling Program (IODP) Expedition 341 on the distal and proximal Surveyor Fan (sites U147 and U1418, respectively; fig. 1A). Each detrital zircon grain stores a variety of information on the temporal evolution and geochemistry of its source rock (Gehrels et al., 2014), which is conducive to constraining the catchment of the recovered sediments.

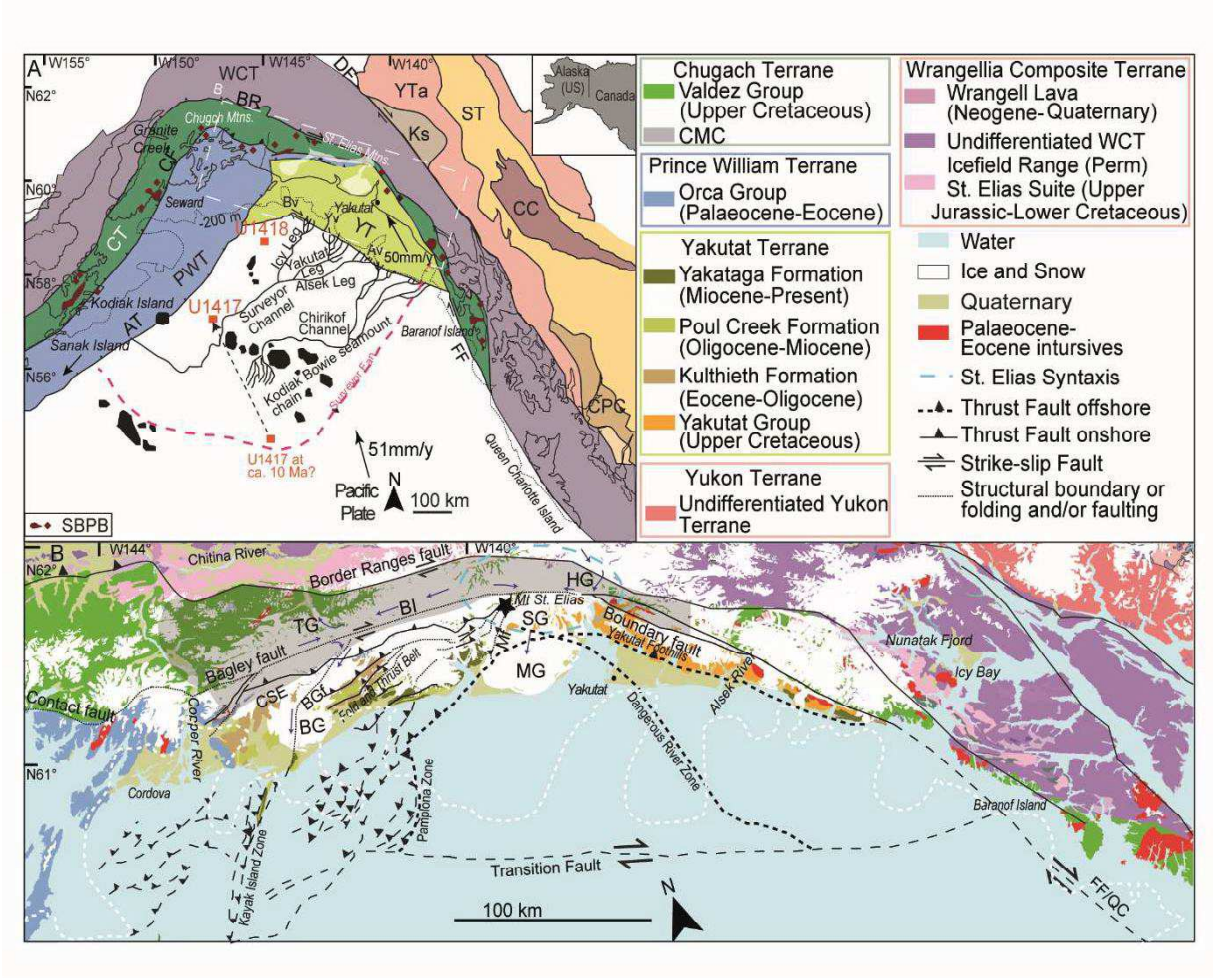

Figure 1: A, Terrane map of the southern Alaska continental margin. Squares mark the distal (U1417) and proximal (U1418) sites of Integrated Ocean Drilling Program (IODP) Expedition 341. The dashed arrow indicates the roughly estimated position of sampling site U1417 at ca. 10 Ma and its movement to its present position. AT=Aleutian Trench; Av=Alsek valley; BR=Border Ranges fault; Bv=Bering valley; CC=Cache Creek terrane; CF=Contact fault; CPC=Coast Plutonic Complex; CT=Chugach terrane; KS=Kluane schist; FF=Fairweather fault; PWT=Prince William terrane; SBPB=Sanak-Baranof plutonic belt; ST=Stikinia terrane; WCT=Wrangellia composite terrane; YT=Yakutat terrane; YTa=Yukon-Tana terrane; Yv=Yakutat valley. B, Simplified geological map of the southern Alaska continental margin. Arrows indicate glacial flow directions, after Post (1972). Glacier extent during the Last Glacial Maximum, after Manley and Kaufman (2002), is marked with a dashed white line. The extent of the Chugach Metamorphic Complex (CMC) is marked by the gray shaded area south of the Border Ranges fault. Modified after Huber et al. (2018) and references therein. BG=Bering glacier; BGf=Bering glacier fault; BI=Bagley icefield; CSE=Chugach–St. Elias fault; FF/QC=Queen Charlotte–Fairweather fault system; HG=Hubbard glacier; Mf=Malaspina fault; MG=Malaspina glacier; SG=Seward glacier; TG=Tana glacier.

3.2 Background

3.2.1 Geology

The southernmost part of the southern Alaska margin formed through accretion of several terranes against the Yukon composite terrane (Yukon-Tanana, Stikine, and Cache Creek terranes). These are, from north to south, the Wrangellia composite terrane, the Chugach–Prince William terrane, and the Yakutat terrane (fig. 1A; Plafker, 1987). The Wrangellia composite terrane was emplaced against the continental margin in mid-Cretaceous time and consists of Paleozoic and Mesozoic magmatic-arc assemblages (Plafker et al. 1994). The

Chugach and Prince William terranes were accreted during the Middle to Late Cretaceous and host a complex deformed accretionary belt (Plafker, 1987; Plafker et al., 1994). Wide parts are made up of the flysch of the Upper Cretaceous Valdez Group (depositional age of 99–60 Ma), while the Orca Group (depositional age 69 to ~35 Ma) makes up most of the Prince William terrane (fig. 1B; Mendenhall, 1905; Dumoulin, 1987; Plafker et al., 1994). The partially ice-covered Contact fault separates the two terranes. Eocene ridge subduction resulted in the emplacement of plutons of the Sanak-Baranof plutonic belt (SBPB), a 2100-km-long belt of granodioritic and granitic plutons that intruded into the active accretionary prism between Sanak and Baranof Islands (intrusion ages of ca. 61 Ma in the west and ca. 50 Ma in the east; fig. 2), and formation of the Chugach Metamorphic Complex (CMC; Sisson et al., 1989, 2003; Bradley et al., 1993, 2003; Plafker et al., 1994; Pavlis and Sisson, 1995; Haeussler et al., 2003; Farris and Paterson 2009). The CMC is a metamorphic complex of up to amphibolite facies metamorphic grade that spans a distance of ca. 350 km along strike of the orogen (Hudson and Plafker, 1982; Bruand et al. 2011; Gasser et al., 2011).

The currently accreting and subducting Yakutat terrane is bordered by the Kayak Island Zone in the west and by the Chugach–St. Elias and Fairweather–Queen Charlotte faults in the north and east. The Transition fault separates it from the Pacific plate in the south. Northwestward movement of the Yakutat terrane along the dextral Fairweather–Queen Charlotte transform fault system started at ca. 30 Ma (Plafker, 1987). Two different scenarios have been suggested for the transport history of the Yakutat terrane. The far-traveled option suggests an origin close to northern California or southern Oregon in the Eocene (~45 Ma; Bruns, 1983; Plafker et al., 1994), requiring ca. 1500–2000 km, or ca. 24°, of northward transport (Perry et al., 2009; White et al., 2017). The short-traveled option suggests transport over a relatively short distance, starting ca. 600 km to the southeast (near Prince Rupert; Plafker, 1987; Plafker et al., 1994; Perry et al., 2009). Since ca. 6 Ma, the Yakutat terrane and the Pacific plate have both moved in a northwestward direction at ca. 50 mm/y relative to the North American plate (Elliott et al., 2010; Gulick et al., 2015).

Flat-slab subduction of the Yakutat terrane since the Oligocene and collision with the North American plate along the Chugach–Saint Elias fault system since the Miocene resulted in the formation of the St. Elias Mountains (Plafker et al., 1994; Enkelmann et al., 2008, 2015; Finzel et al., 2011; Arkle et al., 2013; Falkowski et al., 2014). About 600 km of the Yakutat terrane has already been subducted (fig. 1A; Plafker et al., 1994; Eberhart-Phillips et al., 2006; Fuis et al., 2008; Finzel et al., 2011; Worthington et al., 2012). Very high exhumation rates have been found in the area of the St. Elias syntaxis at the Yakutat plate corner, where transform motion along Fairweather fault changes to flat-slab subduction (Enkelmann et al., 2009, 2010, 2015; Falkowski et al., 2014; Falkowski and Enkelmann, 2016; Dunn et al., 2017). Imbricated Eocene to Holocene sediments of the preorogenic Kulthieth (middle Eocene) and Poul Creek (lower Oligocene to lower Miocene) Formations and the synorogenic Yakataga (Miocene through Holocene) Formation form a fold-and-thrust belt up to 15 km thick overlying the western part of the Yakutat terrane (Plafker, 1987; Plafker et al. 1994; Worthington et al., 2010; Enkelmann et al., 2015). The eastern part consists of the Yakutat Group, part of the Chugach flysch and mélange (Plafker, 1987; Plafker et al., 1994).

To the northeast follow the Jurassic to Tertiary plutonic (ca. 45–190 Ma) and associated metamorphic rocks of the Coast Plutonic Complex (CPC) that extend from Washington State to southwest Yukon (fig. 1A; Gehrels et al., 2009; Mahoney et al., 2009). They separate the Wrangellia terrane from the Stikine terrane in the east.

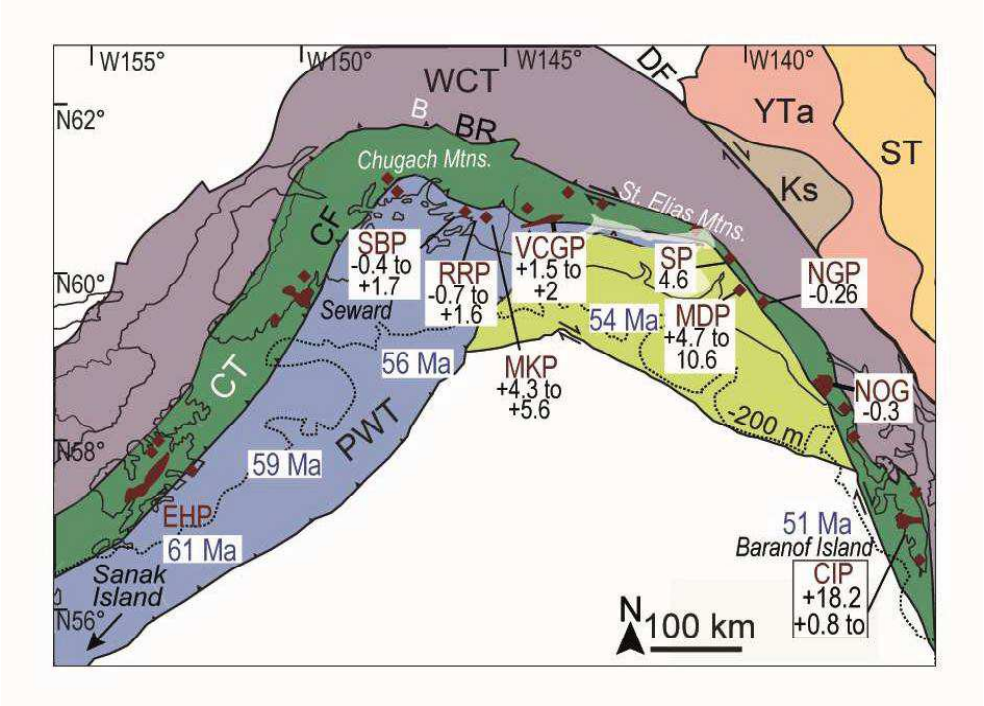

Figure 2: Simplified terrane map of southern Alaska, modified after Carlson et al. (1996), Colpron et al. (2007), Colpron and Nelson (2011), and Grabowski et al. (2013), with U-Pb ages of the intrusions from the Sanak-Baranof plutonic belt (SBPB) showing the eastward younging of the plutons (after Farris and Paterson 2009). Numbers other than ages are ε(Hf)t values of plutons of the SBPB from Roig (2014) and Arntson et al. (2017) and recalculated values from Barker et al. (1992) and Sisson et al. (2003); see Appendix F. AT=Aleutian Trench; CT=Chugach terrane; PWT=Prince William terrane; WCT=Wrangellia composite terrane; YT=Yakutat terrane. CIP=Crawfish Inlet pluton; EHP=Eagle Harbor pluton; MDP=Mount Draper pluton; MK= McKinley pluton; NOG=Novatak glacier pluton; NGP=Nunatak glacier pluton; RRP=Rude River pluton; SBP=Sheep Bay pluton; SP=Mt. Stamy pluton; VCGP=Van Cleve glacier pluton.

3.2.2 The Surveyor Fan system

The Surveyor Fan can be divided into two depositional sequences based on seismic data (Stevenson and Embley, 1987). The older sequence represents turbiditic deposition since ca. 9.7 Ma, in the Miocene (Stevenson and Embley,1987; Rea and Snoeckx, 1995). In view of the absence of a major channel system, it is undecided whether sediment transport in the older sequences of the fan occurred without development of a main channel system or whether a channel system was originally present in the north and has already been subducted into the Aleutian Trench (Stevenson and Embley, 1987). Since the beginning of deposition, northwestward movement of the Pacific plate, including a component of that motion of the Yakutat terrane, has been accommodated by dextral transform movement along the North American plate margin (Stevenson and Embley, 1987; Plafker et al., 1994; Reece et al., 2011). This consequently led to potentially significant changes in the provenance of the deposits with time.

Deposition of the younger sequence has lasted from ca. 5 Ma to the present (Hogan et al., 1978; Reece et al., 2011; Gulick et al., 2015). A noteworthy characteristic of the Surveyor Channel is that it is not linked to a major fluvial system (Ness and Kulm, 1973; Carlson et al., 1996; Reece et al., 2011). Today, glaciers are the main sediment suppliers, and sediment routing into the ocean is accomplished through several shelf-crossing gullies that merge to form three main channels that join ca. 150 km from the continental margin to form the Surveyor Channel (the Icy, Yakutat, and Alsek legs; fig. 1A). The Surveyor Channel has been the main sediment-routing system since at least ca. 2.7 Ma (Gulick et al., 2015). The Alsek leg might have existed since the Miocene-Pliocene boundary and the onset of glaciation at that time (Reece et al. 2011). The Bering, Malaspina, and Hubbard glaciers (fig. 1B) form the biggest

glaciers in the Gulf of Alaska region today (Molnia 2008). The Bagley icefield and the adjacent Bering glacier drain the orogen to the southwest. Ice flow of the Seward-Malaspina glacial system, draining to the southeast, is separated from the Bering glacier (Bruhn et al. 2012). The Seward glacier is funneled through the Seward Throat before flowing into the Malaspina piedmont glacier (Bruhn et al. 2012; Headley et al. 2013), delivering material into the Yakutat and Alsek legs, the two main tributaries of the Surveyor channel. The Hubbard glacier and the Alsek glacial system also feed material into these tributaries (Reece et al. 2011). The Yakutat leg experienced ca. 35 km of lateral relocation to the southeast because of its proximity to a basement high and an overlying sediment wedge that grew to the southeast (Reece et al. 2011). The other legs did not experience lateral movement (Reece et al. 2011). The Icy leg connected to now partially buried sea valleys and had received input from the Bering glacier before it was shut off after the onset of glacial interval C (fig. 3; Reece 2011). The Surveyor Channel discharges into the Aleutian Trench ca. 700 km from the continental margin (Stevenson and Embley 1987; Carlson et al. 1996; Dobson et al. 1998; Reece et al. 2011).

Sedimentation rates on the distal fan started at ~30–70 m/My between 5.2 and 2.8 Ma and doubled to peak values of 120±20 m/My between 2.4 and 2.0 Ma in response to the expansion of Northern Hemisphere glaciation at the Plio-Pleistocene boundary (Gulick et al. 2015). In distal locations of the Surveyor Fan, ca. 460 km southwest of the present shoreline, the first glacial diamicts appear at ca. 2.6 Ma, after the mid-Pliocene warm interval (Rea and Snoeckx 1995; Jaeger et al. 2014). Reduced sedimentation rates of ~60 m/My from 1.6 to 1.2 Ma indicate an apparent reduction of regional glacial erosion (Gulick et al. 2015). Coinciding with the MPT, sedimentation rates rose to peaks of ~140 m/My by 0.8 Ma and even higher at more proximal sites (80 cm/ka at site U1418, 130 cm/ka on the shelf, and up to 300 cm/ka on the slope; Gulick et al. 2015). Since ca. 2.5 Ma, glaciers have reached the edge of the continental shelf several times during glacial maxima; the glacial extent during the Last Glacial Maximum has been mapped in figure 1B (Mann and Hamilton, 1995; Berger et al., 2008a).

3.3 Sampling

Sampling was performed on fine sand and silt intervals from sites U1417 and U1418 drilled during IODP Expedition 341 in the distal and proximal Surveyor Fan, respectively (Expedition 341 Scientists, 2014). Depths are reported in meters as core composite depth below seafloor (m CCSF-B; Jaeger et al., 2014).

Site U1417 is situated in the distal Surveyor Fan ca. 60 km west of today's Surveyor Channel (fig. 1A), receiving input from the Alsek, Yakutat, and Icy legs (Expedition 341 Scientists, 2014; Dunn et al., 2017). It recovered Miocene (ca. 10 Ma) to Holocene sediments from a maximum depth of ca. 700 m (CCSF-B; fig. 3). Lithostratigraphic units I–V are in line with hemipelagic/pelagic rainout and overbank levee deposition from turbidity currents (Expedition 341 Scientists 2014; fig. 3).

Site U1418 is situated between an active channel and an abandoned channel-like structure (Bering Channel), both with an Aleutian Trench terminus, originating seaward of the continental shelf break between the Bering Trough and the Pamplona Zone (fig. 1A; Expedition 341 Scientists, 2014). It recovered early Pleistocene to Holocene sediments from a maximum depth of ca. 950 m. The lowermost lithostratigraphic unit is interpreted as a mass transport deposit (MTD) recording early Pleistocene massive slope failure (unit IV; fig. 3; Reece et al., 2011; Expedition 341 scientists, 2014). The upper units are inferred to have formed through hemipelagic settling and gravity flows from the neighboring channels (Reece et al., 2011; Expedition 341 Scientists 2014). Units II and I are considered to correlate with units II and I at the distal site (fig. 3; Expedition 341 Scientist, 2014). Sediments are unconsolidated and consist mostly of muddy and silty material, with some contribution of fine sand and thick intervals of diamict.

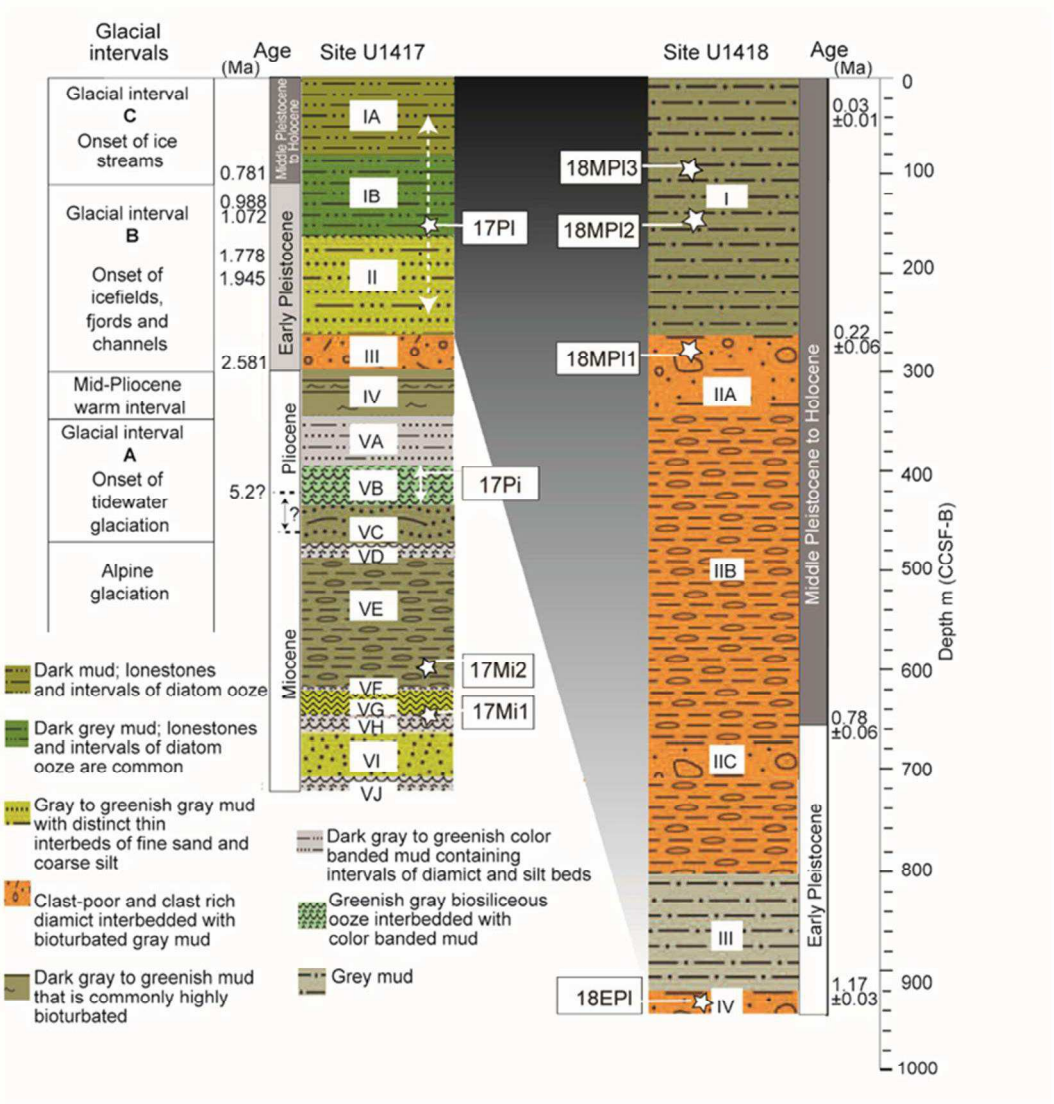

Figure 3: Lithostratigraphy of Integrated Ocean Drilling Program Expedition 341 sites U1417 (distal site) and U1418 (proximal site) and climatic events in southern Alaska. Sample positions are marked with white stars. Modified after Lagoe et al. (1993) and Expedition 341 Scientists (2014).

We sampled four intervals at each site, covering material from the Miocene (turbidite sequence), the Miocene-Pliocene boundary (beginning of Surveyor Channel transport and intensification of glaciation), and the early and middle Pleistocene (intensification of glaciation at the MPT; fig. 3). Sample names start with the abbreviated name of the site from which they were chosen (17 and 18 for U1417 and U1418, respectively), followed by the abbreviated name of the stratigraphic interval (Mi for Miocene, Pi for Pliocene, EPe for early Pleistocene, MPe for middle Pleistocene, and Pe for Pleistocene). If more than one sample was processed for one interval, a number is attached, starting with 1 for the stratigraphically oldest sample. Some samples are composite samples (see the appendix). Time of deposition was deduced from bio- and magnetostratigraphic reconstructions (Jaeger et al., 2014; Gulick et al., 2015).

3.4 Methods

Samples were wet-sieved to remove mud. Zircons were selected from the size fractions 0.063–0.25 mm by density separation and magnetic sorting with a Frantz magnetic separator followed by handpicking under a binocular microscope.

3.4.1 U/Pb dating

Grains were randomly handpicked and mounted on 1-inch epoxy mounts. For most samples, all zircons available in each fraction were picked to get the highest possible number of zircon grains out of the limited sample volume. No selection was made regarding grain size, shape, or color. The grains were embedded into epoxy pucks and polished for cathodoluminescence (CL) analysis performed with a JEOL 6610 scanning electron microprobe. All mounted grains were dated to minimize operator influence. The grains were analyzed by laser ablation (LA) ICP-MS at the Institute for Mineralogy at the University of Münster. Laser spots were set in the cores and rims of the grains if possible (two spots per grain) with a diameter of 25 or 35 µm, depending on the size of the zircon zonations. Some grains were too small to measure core and rim (for details of analytical methods, see the appendix). Age data were processed for visualization with DensityPlotter (Vermeesch 2012), showing normalized kernel density estimation. The bandwidth of the kernel density estimations was calculated by an algorithm implemented in the program on the basis of the diffusion equation (Botev et al., 2010; Vermeesch, 2012).

3.4.2 Hf-isotopes

Analyses of Lu–Hf isotope systems were carried out by laser ablation inductively coupled plasma mass spectrometry (LA-ICP-MS) at the Goethe University of Frankfurt. A subset of grains representing all U-Pb age Groups was selected for measuring (for analytical details see Appendix A). Round Lu-Hf spots of 43 µm were placed on top of or next to the previously measured U–Pb age spots. Hf-isotope data of zircon are usually reported in the epsilon notation $\varepsilon(Hf)_t$ where the measured $^{176}Hf/^{177}Hf$ is normalized to the $^{176}Hf/^{177}Hf$ of the undifferentiated mantle (chondritic uniform reservoir [CHUR]) with positive $\varepsilon(Hf)_t$ values representing input from a mantel source that experienced earlier depletion while negative $\varepsilon(Hf)_t$ values suggest incorporation of a pre-existing crustal component into the evolving magma (Siebel and Van den haute 2009). $\varepsilon(Hf)_t$ values were calculated using the apparent U-Pb age determined by LA-ICP-MS dating.

3.4.3 Rare earth elements

Rare earth elements (REEs) were measured for selected grains that were previously dated by U-Pb. Measurement was performed by LA-ICP-MS at the Institute for Mineralogy at the University of Münster. Laser spots with a diameter of 35 µm were set in the cores of the grains, avoiding impurities and cracks (for analytical details, see the appendix).

3.4.4 (U-Th)/He dating

(U-Th)/He dating was applied to Miocene to Pliocene samples from site U1417. From sample 17Mi1,-2 and sample 17Pi 70 zircons (37 and 33 zircons, respectively) were selected for (U-Th)/He analysis performed at the GÖochron Laboratories of Geozentrum, University of Göttingen (for analytical details see Appendix A). Component identification was performed by two methods using PopShare (Dunkl and Székely, 2002) and DensityPlotter (Vermeesch, 2012) softwares.

3.5 Results

The sample volume was restricted because of the limited amount of material present in the drill core half supplied for sampling (6.2 cm in diameter) and the small grain size of the samples (mostly muddy to silty, with local fine sand layers). Zircon yield was very small and for some samples was nearly zero. All Pleistocene sediments at site U1417 were very muddy, and heavy-mineral content was low. These samples supplied very few to no zircons.

All zircons are euhedral to subrounded, 70–250 µm in length, and all have a short-prismatic to long-prismatic shape. Color ranges from colorless to slightly pinkish. The CL pictures show a large variety of zonations (fig. 4): oscillatory-growth zoning, banded zoning, complex patchy cores, linear-growth zoning, and sector zoning. Many grains have a pitted surface, with cavities truncating the core. Some show dark or bright rims. Some grains did not allow analysis of a core and a rim spot for U-Pb dating because of small grain size. Inclusions, high common-lead contents, or a short analytical signal represented obstacles to meaningful age determination.

3.5.1 U-Pb dating

A total of 1127 U-Pb ages from 651 zircon grains were measured (fig. 5; Appendix B). U-Pb ages of zircon record the crystallization time or resetting during a high-temperature metamorphic event (Cherniak and Watson, 2001; Rahl et al., 2003). Combining U-Pb dating and CL-imaging gives information on crystallization ages of different domains of each crystal revealing detailed information on its growth history (Koschek, 1993). The Southern Alaska margin comprises a mixed magmatic and metasedimentary source area (Plafker, 1987; Plafker et al., 1994). Especially with metamorphic peak conditions in the CMC allowing formation of metamorphic zircon rims that overlap in age with the emplacement of intrusions of the SBPB (e.g., Gasser et al., 2012), detailed analyses of zircon CI-images and dating of cores as well as rims are crucial to discriminate the different source rocks (Moecher and Samson, 2006).

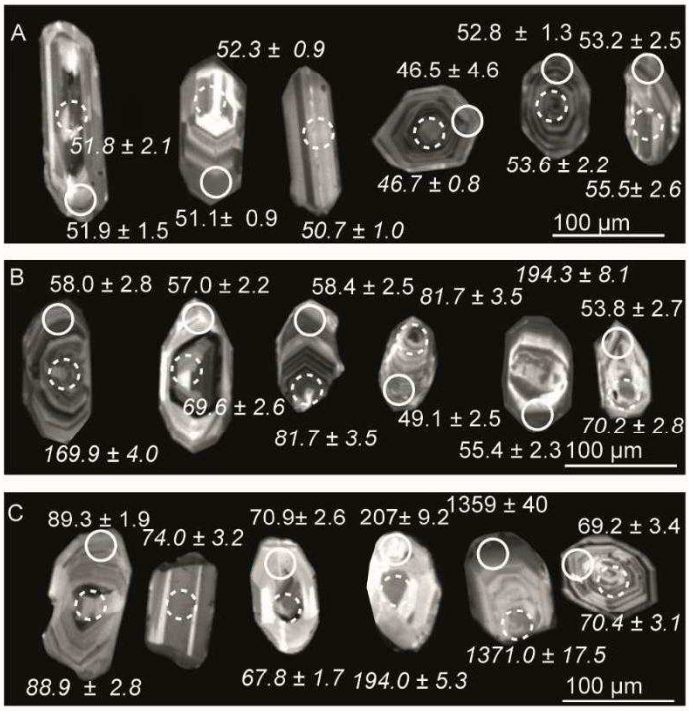

Figure 4: Representative cathodoluminescence images of zircons from site U1417 and U1418 sediments and associated U-Pb ages. Dashed circles mark the positions of core analyses; solid circles mark the positions of rim analyses. Rim ages are in italics. A, Zircons showing overlapping core and rim ages of ca. 50–60 Ma (group 1); B, grains with a rim of ca. 50–60 Ma and an inherited (xenocrystic) older core (group 2); C, zircons showing overlapping core and rim ages of 163 Ma (group 3).

All samples show Paleogene to Precambrian ages (fig. 5; table 1). Only sample 18EPI shows a limited age range with an oldest detrital zircon age at 264 ±4 Ma. The majority of grains in all samples are < ca. 340 Ma. All samples have a main age component of ca 50-55 Ma. Most samples have a second age component at ca. 70 Ma, only samples 18EPI and 18MPI2 show a second age component of 97 and 90 Ma, respectively. All samples show grains with inherited cores and younger rims. Most rim ages are ca. 40-50 Ma while core ages range from ca. 62 to 1244 Ma. Details of analyzed grains, youngest and oldest grains per sample, age components and numbers of grains with inheritance are given in table 1 and Appendix B. Based on the U-Pb age spectra (fig. 5) and the comparison of core and rim ages of each zircon we identify three main groups of zircons that are present in all samples. These are (1) zircons of ca. 50-60 Ma with overlapping core and rim ages (fig. 4A); (2) xenocrystic zircons with rims of ca. 50-60 Ma and inherited older cores ranging from 62 to 1244 Ma (fig. 4B); (3) zircons > 63 Ma that lack a metamorphic rim (fig. 4C).

To account for the information stored in the core and rim data we evaluate the number of grains which can be assigned to groups 1-3 (fig. 9). We give a range for the number of grains which belong to each group. Here, the minimum number represents the amount of grains which can be assigned to a specific group unambiguously. The maximum number includes the

zircons that could also belong to another group because of the lack of a core or rim age data. The sediments from Site U1417 show a decrease of group 1 (21-38%) and 2 (4-15%) and an increase of group 3 (29-58%) zircons from Miocene to Pleistocene. Only the number of group 2 zircons in the Pleistocene sample diverges from this pattern, being similar to the Pliocene sample. Still the range of the number of group 2 zircons is large, especially for the Pleistocene sample, lowering its significance.

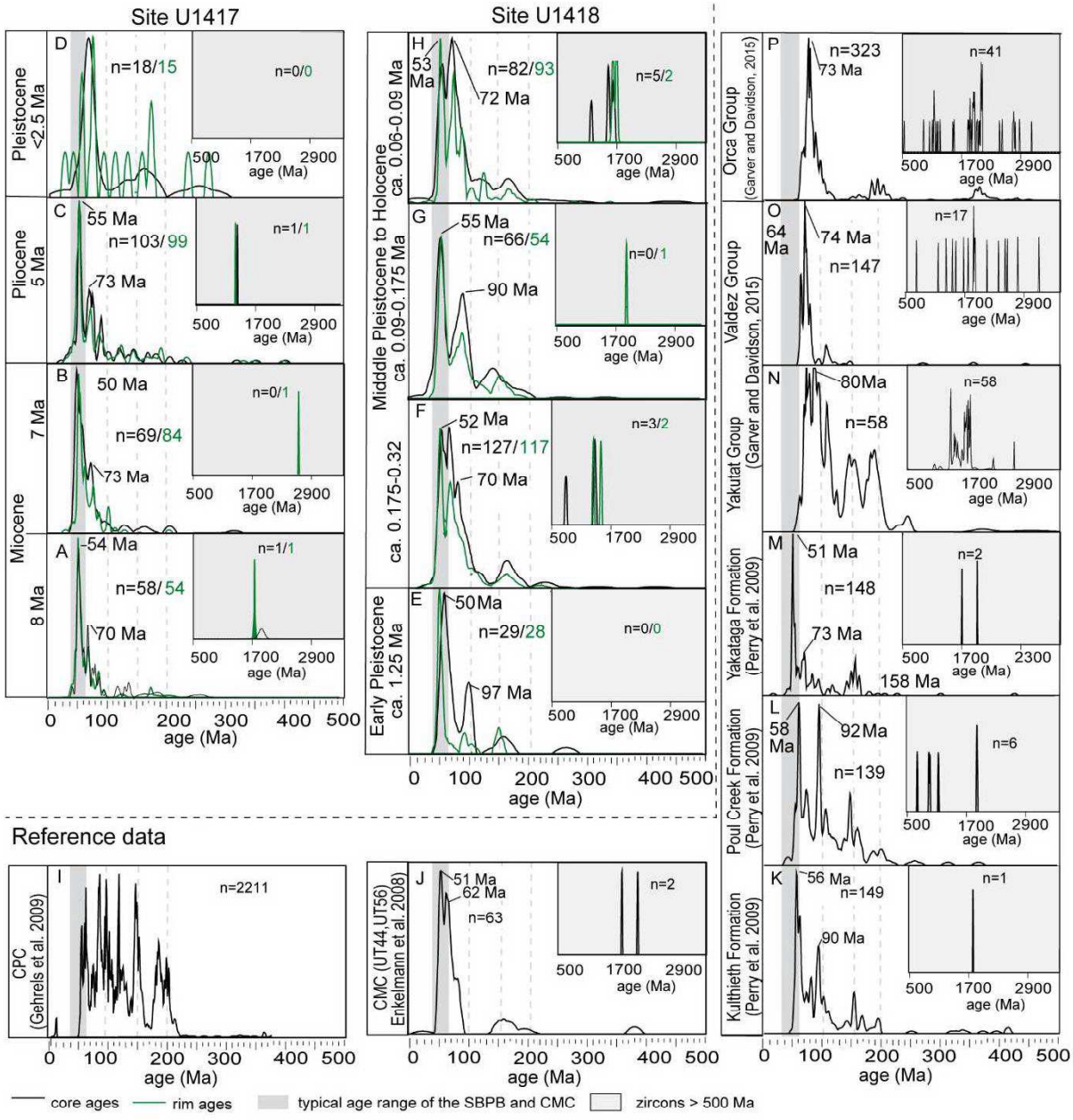

Figure 5: Normalized kernel density estimate distributions of U-Pb laser ablation ICP-MS ages of zircon cores and rims of sediments from Integrated Ocean Drilling Program sites U1417 (distal site; A–D) and U1418 (proximal site; E–H; this study) and of zircon core U-Pb ages from the Valdez, Orca, and Yakutat Groups; the Kulthieth, Poul Creek, and Yakataga Formations; the Coast Plutonic Complex (CPC) and the Chugach Metamorphic Complex (CMC; I–P; from Enkelmann et al. 2008;Gehrels et al. 2009; Perry et al. 2009; Garver and Davidson 2015). Sample names are 17Mi1 (A), 17Mi2 (B); 17Pi (C); 17PI (D); 18EPI (E), 18MPI1 (F); 18MPI2 (G), and 18MPI3 (H). SBPB=Sanak-Baranof plutonic belt.

The samples from site U1418 all show relatively high numbers of group 3 zircons (46-62%). The number of group 2 zircons slightly increases with younger depositional age (8-12%) even though the range between the minimum and maximum number of grains belonging to each group somewhat limits the discriminative power of the data. Group 1 zircons contribute 19 - 34% to the sediments, not showing a continuous trend. Only sample 18EPI diverges from this pattern, showing higher numbers of group 1 (38%) and 2 (31%) zircons and lower numbers of group 3 zircons.

3.5.2 Statistics

We compared the Surveyor Fan zircon age spectra to literature data (reference materials) from the Yakataga, Kulthieth, and Poul Creek Formations and the Yakutat, Orca, and Valdez Groups (fig. 5I–5N), a representative sample from the CPC, and two plutons of the SBPB for which we could find a large set of U-Pb ages (Sheep Bay and McKinley plutons), using a multidimensional scaling (MDS) analysis plot generated with the "provenance" algorithm (fig. 10; Vermeesch et al., 2016). All middle Pleistocene samples from site U1418 and the Pliocene sample from site U1417 form a dense cloud with the Yakataga Formation, supporting similar sources. Furthermore, they plot in the middle of all reference samples, indicating that they are a mixture of all. The Miocene samples from site U1417 plot closer to the pluton samples, indicating that they record higher input from the SBPB. Only the Pleistocene sample from site U1417 plots close to the CPC and the Poul Creek Formation, but the low grain number lowers the significance.

Table 1: Numbers of Zircon Grains from Sites U1417 and U1418 Dated by U-Pb, with U-Pb Age Ranges and Time of Deposition for Each Sample

Sample	Sample depth (m CCSF-B)	Sediment-ation age (Ma)	n	U-Pb ages (Ma)		Most ages (Ma)	Main age components		Double dated grains	Grains with inherited cores
				Minimum	Maximum		1	2		
U1417:										
17Pl	40-243	<2.5	23*	32±5	281±10	-	-	-	12	1
17Pi	400-438	4-5	118	24±1	1317±22		55	73	86	5
17Mi2	604	7.4-8	86	28±2	2666±26	<318	50	73	68	10
17Mi1	632-642	10-13	65	39±2	1907±43	<270	54	70	49	12
U1418:										
18MPl3	97-119	0.06-0.09	112	2.5±0.5	1788±32	<332	53	72	82	11
18MPl2	140-170	0.09-0.175	73	35±2	1730±5	<340	55	90	48	7
18MPl1	280	0.3-0.175	143	32±2	1475±64	<250	52	70	106	21
18EPl	939	1-1.5 Ma	143	44±2	264±4	<264	50	97	23	6

Note. CCSFB=core composite depth below sea floor
*We prepared 14 Pleistocene samples; only 3 provided some zircons that are summarized in this sample. Therefore, we have only 19 grains dated from the Pleistocene unit I and 4 from unit II.

3.5.3 Hf isotope systematics

Our dataset provides 468 age corrected $\varepsilon(Hf)_t$ values for zircons from the Surveyor Fan dated by U-Pb (fig. 6; Appendix C). All samples have grains with the same $\varepsilon(Hf)_t$ characteristics. Most grains younger 70 Ma give $\varepsilon(Hf)_t$ values of -5 to +5, with some grains having values within the range of -7 and +15. Zircons with ages > 70 Ma have $\varepsilon(Hf)_t$ values that vary from -23 to +13 with most grains between +4 and +13. The Precambrian grains show $\varepsilon(Hf)_t$ values of, -0.4 to +4.5, which would provide as a source for 70 Ma granites a calculated $\varepsilon(Hf)_t$ of -37 to -28.

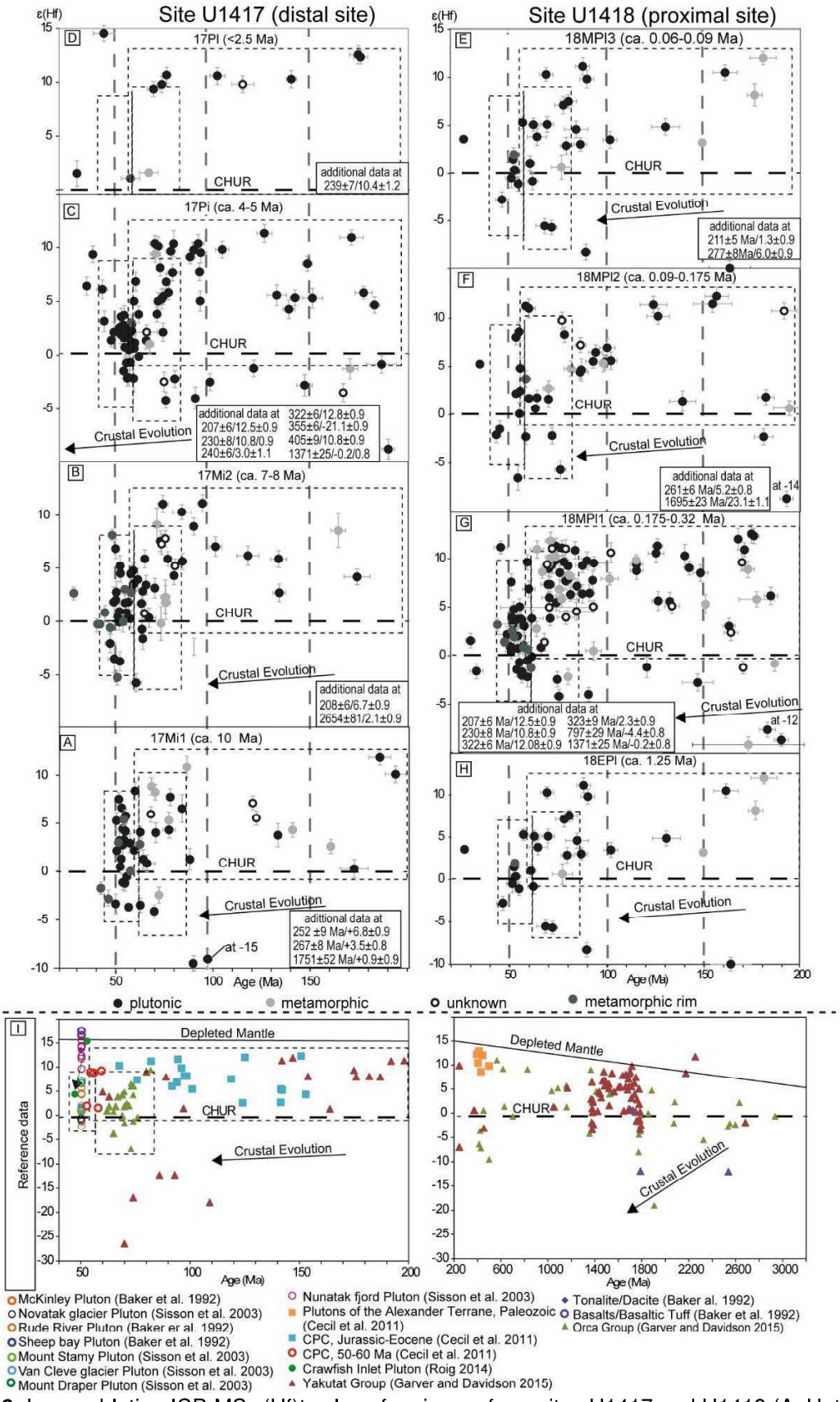

Figure 6: Laser ablation ICP-MS ε(Hf)t values for zircons from sites U1417 and U1418 (A–H; this study) and onshore reference samples (I; Barker et al. 1992; Sisson et al. 2003; Perry et al. 2009; Cecil et al. 2011; Roig 2014; Garver and Davidson 2015). Sample names are 17Mi1 (A); 17Mi2 (B), 17Pi (C), 17PI (D), 18EPI (E), 18MPI1 (F), 18MPI2 (G), and 18MPI3 (H). CHUR = chondritic uniform reservoir.

3.5.4 REEs

Ninety-four REE spectra were measured for the whole age range present in the samples 17Mi, 17Pi and 18MPI1, -2, -3 (Appendix D). Most grains show moderate to pronounced negative Eu and positive Ce anomalies (fig. 7A-C). Some show very low Ce and low to medium Eu anomalies. Grain age and scale of Ce and Eu anomalies do not correlate and are also independent of deposition age.

3.5.5 (U-Th)/He dating

The 37 (U-Th)/He ages measured for sample 17Mi1,-2 range from 6.9 ±0.7 Ma to 114.1 ±10 Ma (Appendix E; fig. 8). Sample 17Pi provided 40 ages from 12.4±0.8 Ma to 136.3 ±12 Ma. The cumulative plot (fig. 8) shows that the majority of the zircons in both samples are Eocene and younger in age. Both methods applied for component identification yielded essentially similar results. In both samples there are three age components, namely Late Cretaceous (rather diffuse), Eocene and Late Oligocene (table 2). Their mean values are similar to identical. The (U-Th)/He zircon (ZHe) ages in sample 17Pi have a wider spread than in sample 17Mi1,-2. The sample contains also a Miocene age component and some weak indications of the presence of Early Cretaceous ages.

Table 2: Age components identified by Simplex algorithm (Dunkl and Székely, 2002) in the zircon (U-Th)/He single-crystals ages obtained on samples 17Pi and 17Mi1, -2.

	17Pi		17Mi1,-2	
Component	Mean ± SD (Ma)	Approximate proportion (%)	Mean ± SD (Ma)	Approximate proportion (%)
Miocene	14 ± 2	12		
Late Oligocene	25 ± 3	13	24 ± 8	70
Eocene	44 ± 6	55	47 ± 3	21
Late Cretaceous	77 ± 8	14	86 ± 13	9
Early Cretaceous	~132* ± 2	6		

*: only indication, represented by 2 data.

3.6 Derivation of the sediments

The composition of sediment generated by weathering and erosion strongly depends on the respective mineral fertilities of the involved source-rock types. Caution is therefore advised when drawing conclusions on quantitative input from available source rocks. Considering zircon age distributions, lithologies with low zircon fertilities result in these source rocks and areas being underrepresented in zircon populations (Moecher and Samson, 2006; O'Sullivan et al., 2016). At the southern Alaska continental margin, a great variety of rock types crop out (e.g., Plafker et al., 1994). Twenty-four of 79 cobbles of fine-grained metasediments and mafic rocks around the Malaspina glacier have already been found to lack any zircon (Grabowski et al., 2013), supporting that zircon fertility markedly influences quantitative provenance information. To account for the information lost through variable zircon fertilities, additional single-grain geochemical analyses of other heavy minerals have been performed (Huber et al. 2018). Still, intersample comparison of the abundances of zircon from different source areas supplies insight into changing input from all zircon-bearing source rocks. A higher concentration of material from one source relative to other sources can always be caused by an increase of input from this source as well as a decrease of input from the other sources. Therefore, the zircon abundances can be interpreted only as relative changes.

3.6.1 U-Pb age provenance of detrital zircons

We can assign each of the three groups of zircons identified to certain source areas in southern Alaska. Group 1 has a ca. 50–60 Ma age maximum and overlapping core and rim ages (fig. 4A). Potential source rocks are the ca. 50–60 Ma intrusions of the SBPB and the CPC (figs. 1, 2). The zircon age range of the SBPB varies from ca. 60 Ma in the west to ca. 50 Ma in the east (fig. 2; Bradley et al., 1993, 2003; Farris et al., 2006; Gasser et al., 2012). In the Yakutat segment of the belt, between Prince William Sound and the Nunatak Fjord, main crystallization ages are 55–52 Ma (fig. 2; Gasser et al., 2012), matching one of the main age components found in the samples (fig. 5A–5H).

The CPC crops out farther to the east (fig. 1A). The igneous rocks in that area are mostly tonalitic and show ages of 50–160 Ma (Gehrels et al., 2009). Especially for the late Miocene sediments, it is a realistic source, considering the northwest-directed movement of the Yakutat and Pacific plates (fig. 1A). The CPC has been inferred to have abundantly contributed material to the sediments of the Poul Creek and Kulthieth Formations on the Yakutat terrane (Perry et al., 2009), but input from the CPC decreases strongly in the Yakataga Formation (Perry et al. 2009), which was deposited at the same time as the Surveyor Fan sediments. Westward transport by the Alaska Current and/or reworking of the Poul Creek and Kulthieth Formations might still have fed some material from the CPC into the fan deposits. Comparison of the amount of 50–60 Ma zircons in the sediments from sites U1417 and U1418 with their abundances in the Poul Creek and Kulthieth Formations, however, supports strong input from an additional source that provides a large number of ca. 50–60 Ma zircons (fig. 5J, 5I). Therefore, we favor the plutons of the SBPB as the main source for most of these zircons, but direct or indirect (reworking of sediments) contribution of material from the CPC is possible.

Group 2 has rims of ca. 50–60 Ma and inherited xenocrystic older cores ranging from ca. 62 to 1244 Ma. At ca. 750°C (Bruand et al., 2014), the highest metamorphic temperatures in the potential source area were reached within the CMC. This was not high enough to reset zircon U-Pb ages (Bruand et al., 2014). Still, zircons from this complex show metamorphic rims and inherited cores; the rims very likely formed during partial melting at the metamorphic peak (Gasser et al., 2011). Zircon rim ages in the CMC were found to be 53–54 Ma; inherited core ages range between 61 and 247 Ma (Gasser et al., 2012). Core and rim ages found for the xenocrystic zircons from sites U1417 and U1418 match ages that support that these zircons are sourced from the metamorphic rocks of the CMC. Another source for this kind of zircon are the plutons of the SBPB. A small number of inherited cores have been found within zircons from the Hive Island pluton (Davidson and Garver, 2017). There is no information on other plutons of the SBPB with inherited zircons, indicating that inherited zircons make up only a minor part of their zircon yield. Some zircons with ca. 50–60 Ma rims and inherited older cores have been reported from the CPC at the latitude of the southern end of Queen Charlotte Island, while zircons from farther north in the complex have thus far not been found to be characterized by inheritance (Gehrels et al., 2009; Cecil et al., 2011). Therefore, some of the zircons might have a CPC origin, but a CMC origin appears more likely.

Group 3, zircons older than 63 Ma, have no discernible metamorphic rim (fig. 4C). The age distributions older than 63 Ma of sites U1417 and U1418 are similar to the age spectra of the low-grade metamorphic areas of the flysch of the Orca and Valdez Groups in the fold-and-thrust belt; the Kulthieth, Poul Creek, and Yakataga Formations; and the rocks of the Yakutat Group south and west of the CMC (fig. 5). These (meta-)sediments store the entire age spectrum of their ancestral source rocks. The Orca, Valdez, and Yakutat Groups are dominated by Jurassic–Cretaceous grains derived from magmatic-arc rocks in the CPC (Garver and Davidson 2015). In addition, these rock units contain up to 10% Precambrian grains (Garver and Davidson, 2015). Single Precambrian grains are also present in our Surveyor Fan samples.

Another source might be the CPC, providing grains of mostly Jurassic through Tertiary age, or the Wrangellia composite terrane that feeds mostly zircons of Early Cretaceous and older age (e.g., Dodds and Campbell, 1988; Plafker et al., 1994; O'Sullivan and Currie, 1996; Enkelmann et al., 2010; Garver and Davidson, 2015). Plutonic activity between 110 and 90 Ma

and between 70 and 80 Ma in the CPC (Armstrong, 1988) matches important age peaks of the sediments from sites U1417 and U1418. With the Orca, Valdez, and Yakutat Groups having been most likely fed by the CPC (Garver and Davidson, 2015), direct input from the CPC and reworking of these coast-proximal sources can provide similar age spectra. Still, the low congruence with the CPC reference samples (figs. 5A–5E, 10) suggests that the CPC was a minor source at best.

The Wrangellia composite terrane comprises rocks that are mostly Early Cretaceous/Jurassic in age and older, together with some younger material of the Wrangell plutonic suite and lava (mid- to late Miocene; Plafker, 1987; Dodds and Campbell, 1988). Upper Jurassic plutonic rocks are widespread in the St. Elias Mountains north of the Border Ranges fault, extending into today's Seward-Malaspina and Hubbard glacier catchments (Armstrong, 1988; Dodds and Campbell, 1988; Falkowski et al., 2016). With most of the zircons of group 3 being ca. 60–100 Ma in age, the Wrangellia composite terrane seems to have been a minor source at best.

3.6.2 Provenance affiliations of low-temperature thermochronology

We use the Hf isotopes of the zircons dated by the U-Pb method to further constrain their provenance. The Hf-isotope systematics of zircons gives information on the crustal evolution of their source rock (Amelin et al., 2000; Kinny, 2003). Because of the scarcity of published Hf isotope data from the source area, we also use $\varepsilon(Hf)_t$ values recalculated from $\varepsilon(Nd)$ values using the equation for the crustal array of Vervoort et al. (1999) (fig. 2; Appendix F).

Most of the zircons of group 1 (plutonic source; SBPB or CPC provenance) have $\varepsilon(Hf)_t$ values of -5 to +5 (fig. 6 A-H) similar to the $\varepsilon(Hf)_t$ values of the intrusions of the SBPB cropping out from Baranof island to Cordova (fig. 2)., supporting the source affiliations indicated by U-Pb dating. The plutons of the SBPB formed as near-trench fore-arc plutons connected to subduction of a spreading ridge, and have a mixed source of melted greywacke and argillite from the accretionary prism (up to 65-90%) and variable amounts of more mafic mantle-derived components, such as MORB, causing varying $\varepsilon(Hf)_t$ values throughout the belt (Moore et al., 1983; Barker et al., 1992; Bradley et al., 1993, 2003; Harris et al., 1996; Cowan 2003; Haeussler et al., 2003; Sisson et al., 2003; Farris et al., 2006; Madsen et al., 2006; Farris and Paterson, 2009; Arntson et al., 2017). Melts in the western part of the belt assimilated larger amounts of sedimentary country rock compared to the eastern part which experienced higher amounts of mantle input (Farris and Paterson, 2009). Locally the contribution of the two sources varies from pluton to pluton and even within individual plutons where $\varepsilon(Hf)_t$ values can vary because of a variable mantel contribution during emplacement (see Crawfish Inlet Pluton; figs. 5I, 2; Farris and Paterson, 2009; Roig, 2014). This inhibits association of certain $\varepsilon(Hf)t$ values to different sections of the SBPB. The 50-60 Ma old zircons from the CPC show $\varepsilon(Hf)_t$ values of ca.+ 9 to +10 and +1 to +2 (Cecil et al., 2011) also overlapping with the values found within the group 1 zircons but don't provide the complete range observed. At present, the CPC cannot be ruled out as source for zircons of group 1 but is less likely than the SBPB.

Most $\varepsilon(Hf)_t$ values of zircons from group 2 (metamorphic rim) range between ca. -5 to +7, matching the values found to be typical for the SBPB (fig. 6). The inherited cores give a wide range of $\varepsilon(Hf)_t$ values of -10 to and +15 similar to values for the Orca and Yakutat Groups (fig. 6). This supports these grains to be sourced by the CMC which provided metamorphically overprinted material from the Orca and Valdez Groups that formed simultaneous to the SBPB.

The $\varepsilon(Hf)_t$ values of group 3 (> 60 Ma) overlap in age and $\varepsilon(Hf)_t$ with the Orca and Yakutat Groups and the CPC (fig. 6A-I; Garver and Davidson 2015), supporting the provenance already indicated by the U-Pb age spectra. Parts of the Orca Group have been deposited shortly before, during, or after the emplacement of the SBPB (< 70 Ma) and show similar $\varepsilon(Hf)_t$ values like the plutons of the SBPB. This causes some overlap of $\varepsilon(Hf)_t$ values and U/Pb ages of both groups. The absence of $\varepsilon(Hf)_t$ data for the Poul Creek, Kulthieth and Yakataga Formation and Valdez Group preclude comparison with these sources.

3.6.3 Provenance affiliations of REEs

The REE spectra of zircons have been found to be not directly indicative for provenance (Hoskin, 2003). Still, certain shapes and slopes of chondrite-normalized REE patterns are characteristic for certain rock types and can help to link detrital grains to certain source lithologies (Rowley et al., 1997; Belousova et al. 2002; Hoskin 2003; Grimes et al. 2007; Rubatto 2017). Inherited cores like those found in zircons of the CMC give information on ancestral sources (Belousova et al., 2002).

The REE spectra of zircons from site U1417 and U1418 samples with different depositional ages show similar patterns (fig. 7). Therefore, a contribution of all zircons from a provenance with similar lithologies is likely. There is no correlation between zircon ages and REE spectra. Zircon REE literature data from the possible source areas are rare. There is one data set from Gasser et al. (2012) that provides REE spectra of zircons from a granodiorite within the CMC that strongly resemble the majority of REE spectra found in our samples in shape and element concentrations. This agrees with a contribution of most of the ca. 50–60 Ma zircons from the granodiorites of the SBPB within the Chugach/Yakutat area. Some grains have a very low Ce anomaly and low to pronounced Eu anomalies and do not match this pattern. They may have a more granitic source, according to Belousova et al. (2002). For the older grains, a granodioritic to granitic source is in line with the proposed source of the flysch sediments in the CPC (Perry et al., 2009).

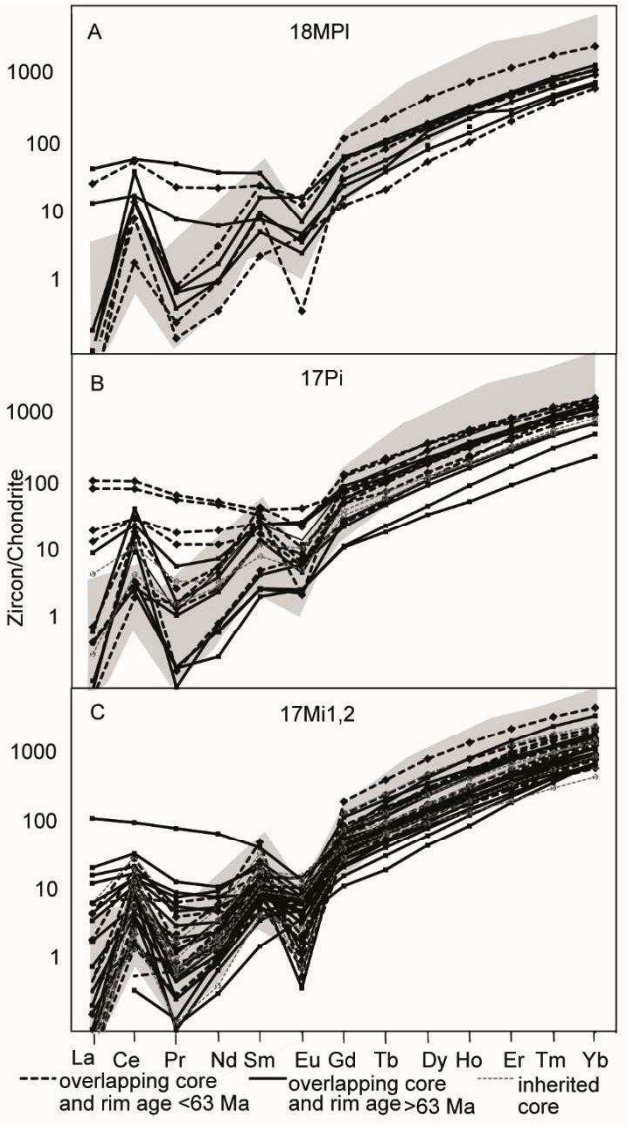

Figure 7: Chondrite normalized REE patterns of representative zircons from site U1417 and U1418. Shaded area shows range of REE spectra from zircons of a metaigneous gneiss from the CMC (Gasser et al. 2012).

3.6.4 Provenance affiliations of the (U-Th)/He data

Fission-track and (U-Th)/He dating provides information on cooling histories of zircons (Hurford and Carter 1991; Reiners 2005). Both methods have been widely used to unravel the orogenic history of southern Alaska (Berger et al., 2008a, 2008b; Berger and Spotila, 2008; Enkelmann et al., 2008, 2010, 2015, 2017; Falkowski et al. 2014, 2016; Dunn et al., 2017). Wide parts of the southern Alaska margin underwent different events of metamorphism that resulted in diverse degrees of heating, causing varying degrees of resetting of the low-temperature thermochronological system (Plafker, 1987; Plafker et al., 1994; Berger et al., 2008b; Berger and Spotila, 2008; Enkelmann et al., 2010; Gasser et al., 2011; Carlson, 2012). All the different signals (reset, unreset, partial reset) that are stored in the source rocks are mixed in the site U1417 and U1418 sediments and complicate the interpretation of the thermochronological data. Because of the close range of zircon FT (ZFT) and ZHe closure temperatures (ca. 190°–270°C and 130°–260°C, respectively; Reiners, 2005), these

thermochronometers yield similar age components. We compare the main age components registered in our samples with the respective literature data obtained for the source rocks onshore: the Orca and Valdez Groups, the Poul Creek and Kulthieth Formations, and the SBPB and CMC, as well as the coeval Yakataga Formation.

Zircon (U-Th)/He cooling ages of ca. 3–154 Ma have been found in the Chugach–Prince William terrane. Three thermal events have been identified for the western Orca and Valdez Groups: a ~50 Ma event caused by the intrusions of the SBPB, a second phase of plutonism at ~38 Ma, and a 25–30 Ma cooling event that is considered to have been caused by the collision of the Yakutat microplate and subsequent exhumation in the evolving mountain belt (Carlson, 2012). Within the Orca Group, these events caused different histories of heating, leading to locally varying degrees of resetting of geochronological systems (Carlson, 2012). Within the CMC, temperatures were high enough to reset all low-temperature thermochronological systems (Gasser et al. 2011, 2012). The western and central parts of the CMC cooled relatively rapidly from 55 to 52 Ma, at rates of 29°–180°C/My (Gasser et al., 2011). This was followed by further rapid cooling to nearly surface temperatures in the Eocene. Contrastingly, in areas to the south, temperatures remained at ca. 300°–400°C for 15–20 My and cooled through FT closure temperature at ca. 30–25 Ma (Gasser et al. 2011). In the eastern part of the CMC, cooling was slow and reached 200°–300°C at ca. 5 Ma (Gasser et al., 2011). Cooling rates increased again during the past ~5 My to rates of 20°–40°C/My (Gasser et al., 2011).

The Poul Creek and Kulthieth Formations might have locally experienced resetting of apatite (U-Th-Sm)/He, ZHe, apatite FT, and ZFT ages (Perry et al., 2009). Main ZFT age components have been found at 29 Ma (37%), 41 Ma (52%), and 63 Ma (11%) for the Poul Creek Formation and at 28 Ma (27%), 39 Ma (65%), and 78 Ma (8%) for the Kulthieth Formation (Perry et al., 2009).

The (U-Th)/He cooling ages of the plutons of the SBPB also decrease from west to east, starting with 37 Ma for the Sanak Island pluton, ~33 Ma for the Eagle Harbor pluton on Kodiak Island, ~29 Ma for the Aialik pluton near Seward, and ~16 Ma for the Crawfish Inlet pluton on Baranof Island (Schneider et al., 2015).

Comparison with our data shows that cooling ages of roughly ~50–96, ~33–45, and ~25–30 Ma in the Orca and Valdez Groups and the Kulthieth and Poul Creek Formations cover the main age components found within the site U1417 and U1418 sediments (table 2). They also overlap the ZHe ages of ca. 36–65 Ma found north of the Border Ranges fault (Enkelmann et al. 2017). The cooling ages of the plutons of the SBPB and the cooling histories of the western and central CMC match the two most prominent age components in the site U1417 samples, at ca. 24 and 44 Ma. This complicates the discrimination of different sources.

A detailed study of the Yakataga Formation, deposited at the same time as the Surveyor Fan sediments, showed four main FT age components, at ca. ~8 Ma (~5%), ~15–17 Ma (~40%), ~21–35 Ma (~30%–50%), and 68–77 Ma (11%–30%; Perry et al., 2009). Excepting the 15–17 Ma population, all the older components were found to be statistically identical to the age components found within the underlying Poul Creek and Kulthieth Formations (Perry et al. 2009). This implies that the Yakataga sediments consist of reworked material from the Poul Creek and Kulthieth Formations and an additional source, delivering mainly 17 and 25 Ma cooling-age components, that is very likely the Chugach terrane (Perry et al., 2009). Perry et al. (2009) found 65% of the Yakutat Formation to be sourced by the CMC and SBPB, while about 35% could be ascribed to recycling of the Poul Creek and Kulthieth Formations. The youngest age component, 24±8 Ma (ca. 70%), of the Miocene site U1417 sediments covers the range of the two youngest age components of the Yakataga Formation, indicating similar sources. The proportions of the different age components have to be interpreted carefully, because they are strongly affected by counting statistics. However, the agreement between our (U-Th)/He age spectra and those from the Yakataga Formation support evidence that the (U-Th)/He data are, in turn, compatible with our U-Pb age data.

Together with the U-Pb ages that imply ca. 60% input from the CMC and SBPB for sample 17Mi1, the provenance of these sediments and the Yakataga Formation is very likely the same. The large fraction of zircons sourced by the CMC and SBPB in samples 17Mi1 and 17Mi2

implies high erosion rates in these areas in the Miocene (ca. 7–10 Ma), compared to the surrounding areas. The Pliocene sample shows fewer grains of the two young populations (ca. 2%). The analysis of the U-Pb ages indicates a reduced transfer of material from the CMC and the SBPB (44%), mainly because less material was provided by the CMC. This implies a change in provenance to more input from the low- and nonmetamorphic parts outside the CMC area.

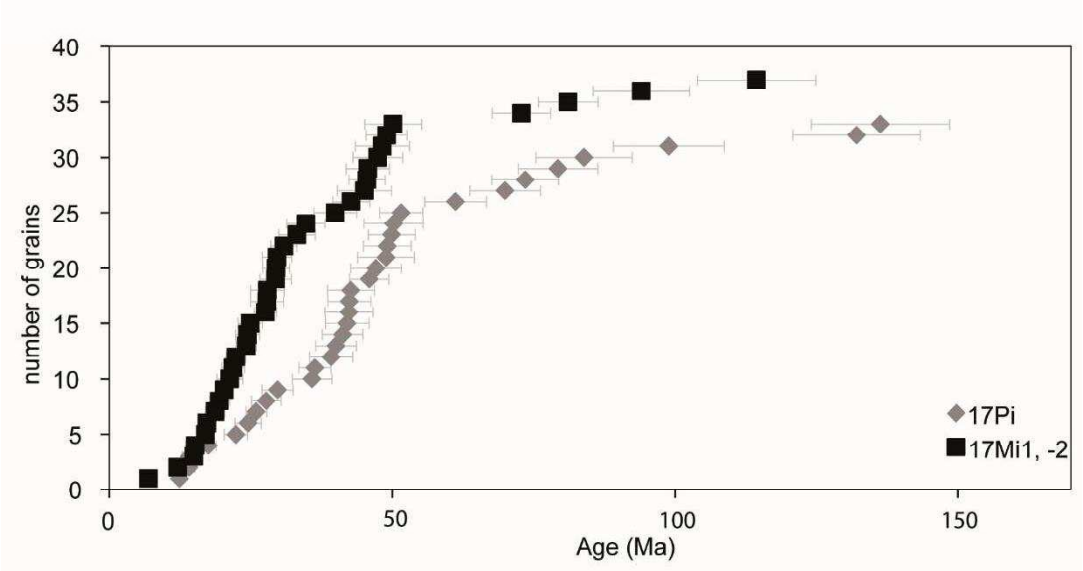

Figure 8: (U-Th)/He age distribution of zircons from samples 17-Mi1, -2 and 17Pi.

3.7 Provenance implications of the data

Our U-Pb age data (fig. 5A–5H) do not show the limited range of ages identified by Dunn et al. (2017). These authors found only a limited range of ages between 85 and 50 Ma in samples from 617 m CCSF-B at site U1417. We conclude that the major sediment sources remained the same throughout the Miocene, albeit with changes in relative contribution. In the MDS plot (fig. 10), the Miocene samples from site U1417 plot closer to the reference data from the plutons than all other samples. They also plot very close to sample UT46 (CMC) and have relatively high fractions of group 2 zircons, indicating that they experienced higher input from the SBPB and the CMC than all other samples. With younger depositional age, both the similarity to the reference samples from the SBPB and the CMC and the fraction of group 1 and 2 zircons decrease (figs. 9, 10). We interpret this as a decrease in the input from the CPC and the CMC. This, in turn, implies rising input from the low- or unmetamorphosed lithologies exposed on the seaward slopes of the mountain range.

From the Pleistocene onward, the input from non-CMC/SBPB grains seems to be relatively constant (figs. 9, 10). The Pliocene sample from site U1417 and all middle Pleistocene samples from site U1418 form a dense cloud in the MDS plot, together with the Yakataga Formation, supporting their similarity. Furthermore, they plot in the middle of all reference samples, indicating them to be a mixture of all. The Pleistocene sample from site U1417 plots close to the CPC and the Poul Creek Formation, but the low grain number lowers the significance. The middle Pleistocene sediments from site U1418 show high fractions of group 3 zircons, implying high input from sources close to the coast.

Sample 18EPI (MTD) differs from the other Pleistocene samples (figs. 9, 10). In the MDS plot, it plots close to samples from the Yakutat terrane that were taken close to the Bering glacier (fig. 10). These samples have a drainage area underlain by the Yakataga and Poul Creek Formations (Enkelmann et al, 2008). They are suggested to have been fed by rapidly exhuming ice-covered rocks (Bagley icefield and Seward glacier) ca. ~50–200 km east of the syntaxis region (Enkelmann et al., 2008). We therefore suggest this sample to have been fed

nearly exclusively through the Bering glacier supplying high amounts of material from the CMC, which is also supported by the absence of grains older than 264±4 Ma.

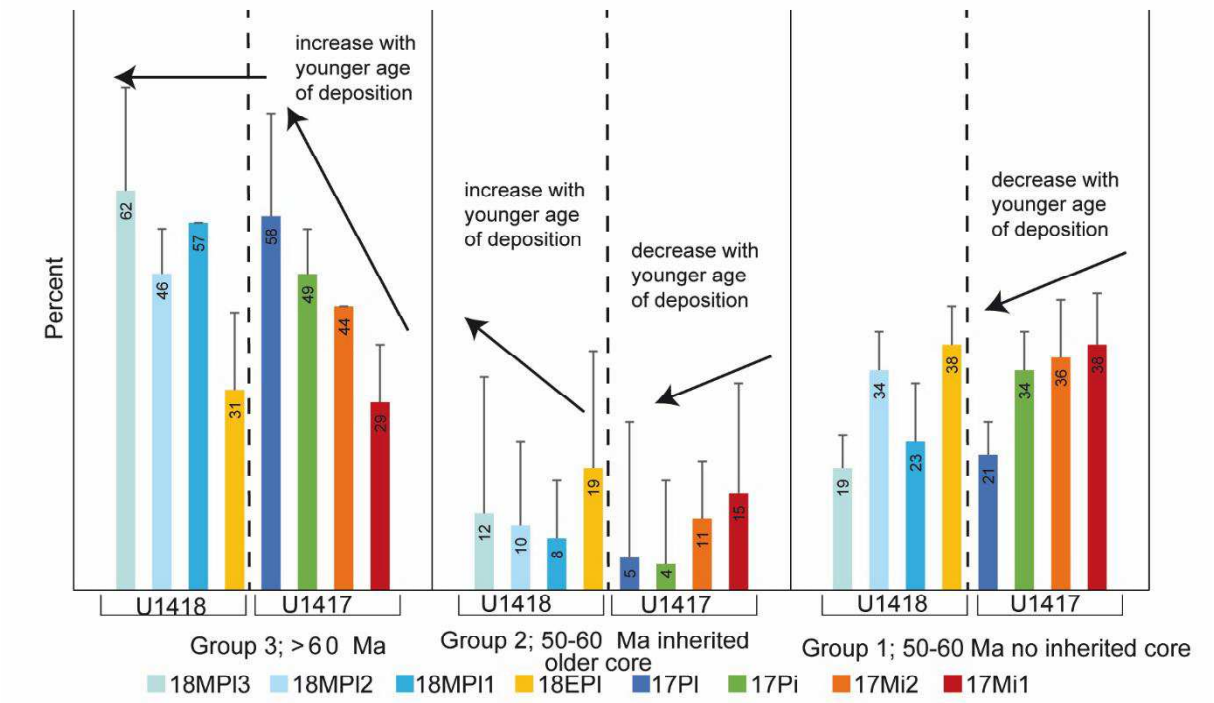

Figure 9: Relative abundances of zircons from Miocene to Pleistocene sediments from sites U1417 and U1418 of U-Pb age groups 1 to 3.

3.8 Exhumation rates

Rising exhumation rates during the Miocene have been deduced from site U1417 sediments on the basis of ZFT data from two samples from ca. 617 m CCSF-B (the same depth interval where we took sample 17Mi2; 603 m CCSF-B) and 700 m CCSF-B (Dunn et al. 2017). The samples were inferred to have depositional ages of 8 and 10 Ma, respectively (Dunn et al. 2017). They calculated an exhumation rate of 2.8±1.0 km/My (lag time of 1.6±0.2 My) for the sample from ca. 617 m CCSF-B (Dunn et al. 2017). We found a (U-Th)/He zircon aged 6.9±0.7 Ma in sample 17Mi2 that has a depositional age of ca. 7.4–8 Ma, according to Expedition 341 Scientists (2014). This indicates that this sediment is not older than 7.6 Ma but very likely younger. When the exhumation rates are recalculated with a deposition age of 7 Ma (resulting in a lag time of ca. 2.6±0.2 My) and the same one-dimensional steady-state thermal model used by Dunn et al. (2017; also see Campbell et al., 2005; Reiners and Brandon, 2006), exhumation appears to have been slower, at ca. 2.1 km/My. Regarding the high uncertainty of the depositional age of the sample, which Dunn et al. (2017) supposed to be 10 Ma but, according to Expedition 341 Scientists (2014), might be as high as 13 Ma, exhumation rates at that time could theoretically be as high as ca. 5 km/My. Considering the whole range of possible exhumation rates for the two Miocene samples, the error on the exhumation rates caused by the analytical error of age determination and the error on the depositional age is too large to support the suggested increase in exhumation rates in the Miocene.

3.9 Discussion

3.9.1 Miocene

The presence of grains in the Miocene sediments that can be attributed to the CMC suggest sediment transport from sources as far northwestward as the position of the CMC to the

Surveyor Fan in the Miocene. Transport of the orogenic detritus into the fan can be inferred to be geologically instantaneous because of the short transport distance (Dunn et al., 2017). Exhumation in the area of the CMC has been going on since the Oligocene to mid-Miocene as a result of transpressive strike-slip movement of the Yakutat terrane, followed by its collision with the North American continent since the mid-Miocene (Spotila and Berger, 2010; Falkowski et al., 2014, 2016; Enkelmann et al. 2017). The depositional age of the oldest sample corresponds to an exhumation phase of the Chugach terrane at ca. 11±2 Ma, caused by changes in plate motion and subduction style and the final collision of the Yakutat terrane (Enkelmann et al. 2008). Furthermore, deep-seated and rapid exhumation of the St. Elias syntaxis started at ca. ~11–8 Ma, and thermochronologic data imply input from there to the distal site at 8 Ma (Dunn et al., 2017). The deep-seated erosion is considered to result from coupling between erosion and active tectonic rock uplift (Enkelmann et al. 2009, 2017; Falkowski et al., 2016; Dunn et al. 2017). Enkelmann et al. (2017) suggest that a fluvial system existed, allowing tectonics and erosion to cause rapid exhumation even before the onset of glaciation. A hypothetical channel system delivering material from northward sources is favored by southward thinning of seismic reflectors within the Miocene precursor of the Surveyor Fan (Stevenson and Embley, 1987). These channels might have drained the hypothetical onshore fluvial system, delivering material from the CMC into the Gulf of Alaska and to the Miocene Surveyor Fan.

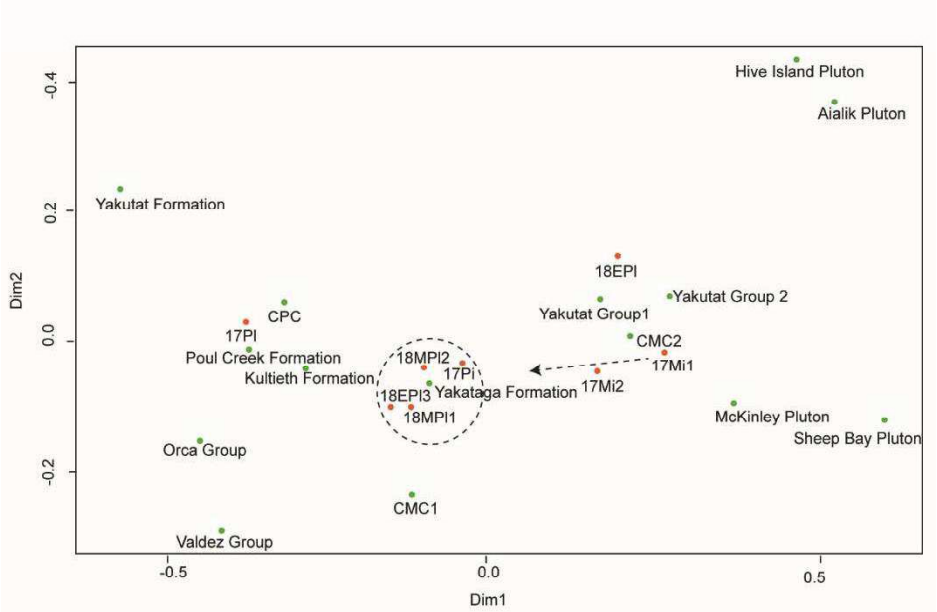

Figure 10: Multidimensional scaling plot for the samples of this study (names beginning with 17 or 18) and from the Valdez, Orca, and Yakutat Groups; the Kulthieth, Poul Creek, and Yakataga Formations; the Coast Plutonic Complex (CPC); and the Chugach Metamorphic Complex (CMC; from Enkelmann et al. 2008; Gehrels et al. 2009; Perry et al. 2009; Garver and Davidson 2015). The dashed circle highlights grouping of samples from site U1418 and sample 17Pi. The dashed arrow highlights increasing similarity of samples from site U1417 with younger depositional age.

3.9.2 Miocene to Pliocene

Our data imply increasing erosion in the low-grade metamorphic areas closer to the coast during the Miocene and Pliocene. This is also supported by single-grain heavy-mineral provenance analysis (Huber et al., 2018). Three main areas of erosion have been identified at the southern Alaska continental margin: (1) the syntaxis area, especially under the Seward glacier, (2) along the Fairweather fault, and (3) in the fold-and-thrust belt (Enkelmann et al., 2009, 2010). The high rates of exhumation found for the St. Elias syntaxis (fig. 1B) are interpreted to be the result of effective coupling of glacial erosion and uplift through tectonic processes at the plate corner (Spotila and Berger, 2010; Enkelmann et al., 2015).

The impact of climate versus tectonic factors on exhumation at the southern Alaska continental margin is a subject of the ongoing research (e.g., Berger et al., 2008a, 2008b; Berger and Spotila, 2008; Enkelmann et al., 2009, 2010, 2015, 2017; Headley et al., 2012, 2013; Pavlis et al., 2012; Gulick et al., 2015). Some authors emphasize the impact of the glacial system (Berger et al., 2008a, 2008b; Pavlis et al., 2012; Gulick et al., 2015); others highlight the interaction of the two (Spotila et al., 2004; Meigs et al., 2008; Enkelmann et al., 2009, 2017; Headley et al., 2012, 2013) or the limited impact of the glaciation (Enkelmann et al. 2010). Reactivation of the Contact fault at ca. 6–5 Ma, caused by the final collision of the Yakutat terrane and dextral transpression associated with lens-like pop-up structures, is suggested to have resulted in locally very rapid exhumation along that fault and in the accretionary wedge (Enkelmann et al., 2008). Bedrock apatite ages are very young (4–0.5 Ma) in the fold-and-thrust belt and the Yakutat Foothills and along the Fairweather fault and show Pliocene ZHe and ZFT ages (Enkelmann et al., 2010). In addition, the decreasing input from the CMC from the Miocene to the Pliocene correlates with the southward progress of glaciers from the interior of the evolving mountain belt toward the ocean. Having started in the Miocene, this trend is even stronger at the transition from the Miocene to the Pliocene, with the onset of tidewater glaciation. Strong glacial erosion since the end of the Miocene is considered to have led to erosion focusing on windward positions, correlating with the equilibrium line altitude (Spotila et al., 2004; Berger et al., 2008a, 2008b; Meigs et al., 2008). This is in line with erosion increasing in the areas closer to the coast. This implies that glacial erosion and sediment evacuation are much more efficient in the areas close to the coast than in the interior parts of the orogen (e.g., Berger et al., 2008a, 2008b; Spotila and Berger, 2010). Glaciation and tectonic processes seem to have interacted in determining the changing provenance signal connected to the evolving main erosion centers, which is also inferred from single-grain heavy-mineral analysis (Huber et al., 2018). However, our data set does not allow for differentiation of the relative contributions of tectonics and climate.

3.9.3 Pleistocene

Low numbers of zircons in the Pleistocene samples at the distal site (U1417) and the different geographic position of the proximal site (U1418) on the upper Surveyor Fan and away from the Surveyor channel complicate the comparison to the Miocene and Pliocene deposits of site U1417. Previous studies have revealed that the Bering-Bagley glacial system and the Malaspina glacier drain different catchments, with only the former delivering material from the syntaxis (Enkelmann et al., 2009; Dunn et al., 2017). Parallel transport paths of sediments below the Malaspina glacier prevent mixing and result in variations in the FT age spectra within the Malaspina lobe (Enkelmann et al., 2009). This emphasizes the strong impact of glacial sediment routing on provenance.

The proximal site U1418 very likely experienced input directly from the Bering-Bagley glacial system, while the distal site U1417 was fed by a much wider part of the continental margin through the Surveyor Channel and its tributaries. Accordingly, the proximal site records more-local processes affecting its catchment (Expedition 341 Scientists, 2014; Dunn et al., 2017; Huber et al., 2018). The early Pleistocene sample from site U1418, which differs from the other Pleistocene samples, represents MTDs very likely connected to a major slope failure (Reece et al., 2011). Of all samples, this one shows the highest amount of material sourced by the CMC. This rather reflects a single extreme event and is not the result of changing erosion patterns.

Before the MPT, denudation rates in the subaerial parts of the orogenic wedge are supposed to have been relatively low (35 km^2/My unit flux; Berger et al., 2008a). During the Pleistocene and especially after the MPT, denudation increased strongly, resulting in denudation rates of ca. 190 km^2/My unit flux (Berger et al., 2008a). At the same time, sedimentation rates of the Surveyor Fan increased markedly (Gulick et al., 2015).

The scarcity of zircons in the Pleistocene sediments at the distal site limits a detailed evaluation of the provenance evolution. Still, the middle Pleistocene sediments from the proximal site have a provenance similar to that of the Pliocene/late Miocene samples from the

distal site, irrespective of the different locations of the sites. As the proximal site did not receive input from the syntaxis (Dunn et al., 2017), we cannot provide information on how the syntaxis might have been affected by changes at the MPT. However, the increased glaciation since the MPT has been found to have not affected tectonic processes within the syntaxis area (Enkelmann et al., 2010).

Our data from the distal site suggest that high erosion rates in the fold-and-thrust belt were not initiated during the MPT. They had already started to develop during the Miocene-Pliocene transition at a time of increasing glaciation. The findings of this study combine well with several aspects of climate-tectonic interactions concurring in the Chugach–St. Elias orogeny. These are (1) the strong correlation of rising sedimentation rates in the Surveyor Fan and increasing glaciation of the southern Alaska continental margin (Gulick et al., 2015) and (2) enhanced erosion at the windward side of the orogen (e.g., Pewé 1975; Berger et al. 2008a), denudation patterns being strongly influenced by the location of glaciers (Spotila et al., 2004). We conclude that climate and glacial erosion have strongly affected erosion patterns in the Chugach–St. Elias orogen since the onset and intensification of glaciation at the Miocene-Pliocene boundary.

Our data from the proximal site do not evince a general change in the tectonic pattern after the MPT. This may be an effect of the methods applied and may not necessarily be suggestive of the absence of such a change. As the response time of orogens to changing climatic and tectonic forces varies strongly (Tomkin and Roe, 2007), changes since the MPT might be too recent to be effectively detected in the Surveyor Fan sediments. Determination of exhumation rates for the Pleistocene through low-temperature thermochronology of the Surveyor Fan sediments is not possible for the Chugach–St. Elias orogen because of a lag time of several million years (Dunn et al., 2017). At present, it cannot be decided whether the observed changes reflect variations in the rates of sediment removal or exhumation.

3.10 Conclusion

Our multimethod zircon data identify the main sediment sources of the Surveyor Fan to be located on the Chugach and Yakutat terranes since the Miocene. Additional input from the CPC cannot be ruled out. Even during enhanced glaciation in the Pleistocene, glaciers seem to have been nested in the same area as before, providing zircons with similar characteristics. Our data favor sediment input from the CMC to the Surveyor Fan during Miocene time (ca. 11 Ma). Transport during the Miocene to the Surveyor Fan may have occurred via a channel system that has already been subducted in the Aleutian Trench (Stevenson and Embley, 1987). Thermochronological data support that exhumation rates in the Miocene were more or less constant; the large errors on the depositional ages and the thermochronological data might mask small variations.

From the Miocene-Pliocene boundary onward, the advance of glaciers toward the Gulf of Alaska, as well as tectonics, has focused erosion along the spine of the orogen. The absence of zircons in the Pleistocene sediments at the distal site U1417 hampers a comparison of the provenance of the Miocene-Pliocene and Pleistocene sediments. Still, our data from the proximal site imply a constant sediment provenance over the MPT, indicating that the main erosion centers have remained the same. The similarity of age distributions and geochemical compositions of zircons from different source areas along the Gulf of Alaska, as well as the transfer times of tectonic events recorded in the Surveyor Fan sediments, may mask local changes in the Pleistocene.

ACKNOWLEDGMENTS

This study was funded by German Research Foundation (DFG) grants BA 1011/43-1 and 43-2. We thank M. Dröllner, Münster, for helping to process the samples and B. Schmitte, Münster, for assistance with acquiring the microprobe and La-ICP-MS data. We thank P. Wilde, Berkeley, for revising the language of the English text. We than E. Enkelmann and an anonymous reveiewer fro constructive and for constructive reviews, and D. Rowley for editorial guidance.

3.11 References cited

Amelin, Y., Lee, D.C., Halliday, A.N., 2000. Early-middle archaean crustal evolution deduced from Lu-Hf and U-Pb isotopic studies of single zircon grains. Geochim. Cosmochim. Acta 64, 4205–4225.

Arkle, J.C., Armstrong, P.A., Haeussler, P.J., Prior, M.G., Hartman, S., Sendziak, K.L., Brush, J.A. 2013. Focused exhumation in the syntaxis of the western Chugach Mountains and Prince William Sound, Alaska. Geol. Soc. America Bull. 125, 776–793.

Armstrong, R.L., 1988. Mesozoic and Early Cenozoic magmatic evolution of the Canadian Cordillera. Geol. Soc. Am. Spec. Pap. 218, 55–92.

Arntson, E., Olson, H., Davidson, C., Garver, J., 2017. Geochemistry, U-Pb ages, and Hf isotopes of the Mt. Draper and Mt. Stamy Plutons, Nunatak fjord, Alaska: Implications for the Sanak-Baranof Plutonic Belt. Geol. Soc. Am. Abstr. Program 49(4).

Barker, F., Farmer, G.L., Ayuso, R.A., Plafker, G., Lull, J.S. 1992. The 50 Ma granodiorite of the eastern Gulf of Alaska: Melting in an accretionary prism in the forearc. J. Geophys. Res. 97, 6757-6778.

Belousova, E., Griffin, W., O'Reilly, S.Y., Fisher, N., 2002. Igneous zircon: Trace element composition as an indicator of source rock type. Contrib. Min. Petrol. 14, 602–622.

Berger, A.L., Gulick, S.P.S., Spotila, J.A., Upton, P., Jaeger, J.M., Chapman, J.B., Worthington, L.A., Pavlis, T.L., Ridgway, K.D., Willems, B.A., McAleer, R.J., 2008a. Quaternary tectonic response to intensified glacial erosion in an orogenic wedge. Nature Geosci. 1, 793–799.

Berger, A.L., Spotila, J.A., 2008. Denudation and deformation in a glaciated orogenic wedge: The St. Elias orogen, Alaska. Geology 36, 523-526.

Berger, A.L., Spotila, J.A., Chapman, J.B., Pavlis, T.L., Enkelmann, E., Ruppert, N.A., Buscher, J.T., 2008b. Architecture, kinematics, and exhumation of a convergent orogenic wedge: A thermochronological investigation of tectonic–climatic interactions within the central St. Elias orogen, Alaska. Earth Planet. Sci. Lett. 270, 13–24.

Botev, Z.I., Grotowski, J.F., Kroese, D.P., 2010. Kernel density estimation via diffusion. Ann. Statist. 38, 2916–2957.

Bradley, D.C., Haeussler, P.J., Kusky, T.M., 1993. Timing of early Tertiary ridge subduction in southern Alaska. In: Dusel-Bacon, C., Till, A.B. (Eds.). Geologic studies in Alaska by the U.S. Geological Survey. U.S. Geol. Surv. Bull. 2068, 163-177.

Bradley, D.C., Kusky, T.M., Haeussler, P.J., Goldfarb, R.J., Miller, M.L., Dumoulin, J.A., Nelson, S.W., Karl, S.M., 2003. Geologic signature of early Tertiary ridge subduction in Alaska. *In* Sisson, V.B., Roeske, S.M., Pavlis, T.L. (Eds.). Geology of a transpressional orogen developed during ridge-trench interaction along the North Pacific margin, vol. 371. Geol. Soc. Am., Boulder, Colo., p. 19–49.

Bruhn, R.L., Sauber, J., Cotton, M.M., Pavlis, T.L., Burgess, E., Ruppert, N., Forster, R.R., 2012. Plate margin deformation and active tectonics along the northern edge of the Yakutat Terrane in the Saint Elias Orogen, Alaska, and Yukon, Canada: Geosphere 8, 1384–1407.

Bruns, T.R., 1983. Model for the origin of the Yakutat terrane, an accreting terrane in the northern Gulf of Alaska. Geology 11, 718–721.

Bruand, E., Gasser, D., Bonnand, P., Stuewe, K., 2011. The petrology and geochemistry of a metabasite belt along the southern margin of Alaska, Lithos 127, 282-297.

Bruand, E., Gasser, D., Stüwe, K., 2014. Metamorphic P–T conditions across the Chugach Metamorphic Complex (Alaska)—A record of focused exhumation during transpression. Lithos 190-191, 292–312.

Campbell, I.H., Reiners, P.W., Allen, C.M., Nicolescu, S., Upadhyay, R., 2005. He–Pb double dating of detrital zircons from the Ganges and Indus Rivers: Implication for quantifying sediment recycling and provenance studies. Earth Planet. Sci. Lett. 237, 402–432.

Carlson, P.R., Stevenson, A.J., Bruns, T.R., Mann, D.M., Huggett, Q., 1996. Sediment Pathways in Gulf of Alaska from Beach to Abyssal Plain. In: Gardner, J.V., Field, M.E.,

Twichell, D.C. (Eds.). Geology of the United States Seafloor. Cambridge University Press, Cambridge, p. 255–278.
Carlson, B.M., 2012. Analysis of detrital zircon fission track ages of the Upper Cretaceous Valdez Group and Paleogene Orca Group in western Prince William Sound, Alaska. In Varga, R.J., ed. Keck Geology Consortium Undergraduate Research Symposium, 25th (Amherst, MA, 2012), Proc., p. 8–16.
Cecil, M.R., Gehrels, G., Ducea, M.N., Patchett, P.J., 2011. U-Pb-Hf characterization of the central Coast Mountains batholith: Implications for petrogenesis and crustal architecture. Lithosphere 3, 247–260.
Cherniak, D.J., Watson, E.B., 2001. Pb diffusion in zircon. Chem. Geol. 172, 5–24.
Cowan, D.S., 2003. Revisiting the Baranof–Leech River hypothesis for early Tertiary coastwise transport of the Chugach–Prince William terrane. Earth Planet. Sci. Lett. 213, 463–475.
Colpron, M., Nelson, J.L., 2011. A Digital Atlas of Terranes for the Northern Cordillera. Yukon Geological Survey. Accessed online from www.geology.gov.yk.ca, 15.03.2018.
Colpron, M., Nelson, J.L., Murphy, D.C., 2007. Northern Cordilleran terranes and their interactions through time. GSA Today 17, 4-10.
Davidson, C., Garver, J.I., 2017. Age and Origin of the Resurrection Ophiolite and Associated Turbidites of the Chugach–Prince William Terrane, Kenai Peninsula, Alaska. J. Geol. 125, 681-700.
Dobson, M.R., O'Leary, D., Veart, M., 1998. Sediment delivery to the Gulf of Alaska: Source mechanisms along a glaciated transform margin. Geol. Soc. London Spec. Publ. 129, 43–66.
Dodds, C. J., Campbell, P.B., 1988. Potassium-argon ages of mainly intrusive rocks in the Saint Elias Mountains, Yukon and British Columbia. Geol. Surv. Canada paper 87-16, 43 p.
Dumoulin, J., 1987. Sandstone composition of the Valdez and Orca groups, Prince William Sound, Alaska. U.S. Geol. Surv. Bull. 1774, 37 pp.
Dunkl, I., Székely B., 2002. Component analysis with visualization of fitting-PopShare, a Windows program for data analysis. Goldschmidt Conference Abstracts 2002, Geochim. Cosmochim. Ac. 66/15A, 201.
Dunn, C.A., Enkelmann, E., Ridgway, K.D., Allen, W.K., 2017. Source to sink evaluation of sediment routing in the Gulf of Alaska and Southeast Alaska: A thermochronometric perspective. J. Geophys. Res. Earth Surf. 122, 711–734.
Eberhart-Phillips, D., Christensen, D.H., Brocher, T.M., Hansen, R., Ruppert, N.A., Haeussler, P.J., Abers, G.A., 2006. Imaging the transition from Aleutian subduction to Yakutat collision in central Alaska, with local earthquakes and active source data. J. Geophys. Res. 111, B1130. doi:10.1029/2005JB004240.
Elliott, J.L., Larsen, C.F., Freymueller, J.T., Motyka, R.J., 2010. Tectonic block motion and glacial isostatic adjustment in southeast Alaska and adjacent Canada constrained by GPS measurements. J. Geophys. Res. 11, B09407. doi:10.1029/2009JB007139.
Enkelmann, E., Garver, J.I., Pavlis, T.L., 2008. Rapid exhumation of ice-covered rocks of the Chugach–St. Elias orogen, Southeast Alaska. Geology 36, 915-918.
Enkelmann, E., Zeitler, P.K., Pavlis, T.L., Garver, J.I., Ridgway, K.D., 2009. Intense localized rock uplift and erosion in the St Elias orogen of Alaska. Nat. Geosci. 2, 360–363.
Enkelmann, E., Zeitler, P.K., Garver, J.I., Pavlis, T.L., Hooks, B.P., 2010. The thermochronological record of tectonic and surface process interaction at the Yakutat-North American collision zone in southeast Alaska. Am. J. Sci. 310, 231–260.
Enkelmann, E., Koons, P.O., Pavlis, T.L., Hallet, B., Barker, A., Elliott, J., Garver, J.I., Gulick, S.P.S., Headley, R.M., Pavlis, G.L., Ridgway, K.D., Ruppert, N., van Avendonk, H.J.A., 2015. Cooperation among tectonic and surface processes in the St. Elias Range, Earth's highest coastal mountains. Geophys. Res. Lett. 42, 5838–5846.
Enkelmann, E., Piestrzeniewicz, A., Falkowski, S., Stübner, K., Ehlers, T.A., 2017. Thermochronology in southeast Alaska and southwest Yukon: Implications for North American Plate Response to Terrane Accretion. Earth Planet. Sci. Lett. 457, 348–358.

Expedition 341 Scientists, 2014. Southern Alaska Margin: interactions of tectonics, climate, and sedimentation. IODP Prel. Rep. 341. doi:10.2204/iodp.pr.341.2014.
Falkowski, S., Enkelmann, E., Ehlers, T.A., 2014. Constraining the area of rapid and deep-seated exhumation at the St. Elias syntaxis, Southeast Alaska, with detrital zircon fission-track analysis. Tectonics 33, 597–616.
Falkowski, S., Enkelmann, E., 2016. Upper-crustal cooling of the Wrangellia composite terrane in the northern St. Elias Mountains, western Canada. Litosphere 8, 359-378.
Falkowski, S., Enkelmann, E., Drost, K., Pfänder, J.A., Stübner, K., Ehlers, T.A., 2016. Cooling history of the St. Elias syntaxis, southeast Alaska, revealed by geochronology and thermochronology of cobble-sized glacial detritus. Tectonics 35, 447–468.
Farris, D.W., Haeussler, P., Friedman, R., Paterson, S.R., Saltus, R.W., Ayuso, R., 2006. Emplacement of the Kodiak batholith and slab-window migration. Geol. Soc. Am. Bull. 118, 1360–1376.
Farris, D.W., Paterson, S.R., 2009. Subduction of a segmented ridge along a curved continental margin: Variations between the western and eastern Sanak–Baranof belt, southern Alaska. Tectonophysics 464, 100–117.
Finzel, E.S., Trop, J.M., Ridgway, K.D., Enkelmann, E., 2011. Upper plate proxies for flat-slab subduction processes in southern Alaska. Earth Planet. Sci. Lett., 303, 348-360.
Fuis, G.S., Moore, T.E., Plafker, G., Brocher, T.M., Fisher, M.A., Mooney, W.D., Nokleberg, W.J., Page, R.A., Beaudoin, B.C., Christensen, N.I., Levander, A.R., Lutter, W.J., Saltus, R.W., Ruppert, N.A., 2008. Trans-Alaska Crustal Transect and continental evolution involving subduction underplating and synchronous foreland thrusting. Geology 36, 267-270.
Garver, J.I., Davidson, C.M., 2015. Southwestern Laurentian zircons in Upper Cretaceous flysch of the Chugach-Prince William terrane in Alaska. Am. J. of Sci. 315, 537–556.
Gasser, D., Bruand, E., Stüwe, K., Foster, D.A., Schuster, R., Fügenschuh, B., Pavlis, T., 2011. Formation of a metamorphic complex along an obliquely convergent margin: Structural and thermochronological evolution of the Chugach Metamorphic Complex, southern Alaska. Tectonics 30, TC2012. doi:10.1029/2010TC002776.
Gasser, D., Rubatto, D., Bruand, E., Stuwe, K., 2012. Large-scale, short-lived metamorphism, deformation, and magmatism in the Chugach metamorphic complex, southern Alaska: A SHRIMP U-Pb study of zircons. Geol. Soc. Am. Bull. 124, 886–905.
Gehrels, G., Rusmore, M., Woodsworth, G., Crawford, M., Andronicos, C., Hollister, L., Patchett, J., Ducea, M., Butler, R., Klepeis, K., Davidson, C., Friedman, R., Haggart, J., Mahoney, B., Crawford, W., Pearson, D., Girardi, J., 2009. U-Th-Pb geochronology of the Coast Mountains batholith in north-coastal British Columbia: Constraints on age and tectonic evolution. Geol. Soc. Am. Bull. 121, 1341–1361.
Gehrels, G.E., 2014. Detrital Zircon U-Pb Geochronology Applied to Tectonics. Ann. Rev. of Earth Planet. Sci. 42, 127-149.
Grabowski, D.M., Enkelmann, E., Ehlers, T.A., 2013. Spatial extent of rapid denudation in the glaciated St. Elias syntaxis region, SE Alaska. J. Geophys. Res. Earth Surf. 118, 1921–1938.
Grimes, C.B., John, B.E., Kelemen, P.B., Mazdab, F.K., Wooden, J.L., Cheadle, M.J., Hanghøj, K., Schwartz, J.J., 2007. Trace element chemistry of zircons from oceanic crust. A method for distinguishing detrital zircon provenance. Geology 35, 643-646.
Gulick, S.P.S., Jaeger, J.M., Mix, A.C., Asahi, H., Bahlburg, H., Belanger, C.L., Berbel, G.B.B., Childress, L., Cowan, E., Drab, L., Forwick, M., Fukumura, A., Ge, S., Gupta, S., Kioka, A., Konno, S., LeVay, L.J., März, C., Matsuzaki, K.M., McClymont, E.L., Moy, C., Müller, J., Nakamura, A., Ojima, T., Ribeiro, F.R., Ridgway, K.D., Romero, O.E., Slagle, A.L., Stoner, J.S., St-Onge, G., Suto, I., Walczak, M.D., Worthington, L.L., Bailey, I., Enkelmann, E., Reece, R., Swartz, J.M., 2015. Mid-Pleistocene climate transition drives net mass loss from rapidly uplifting St. Elias Mountains, Alaska. P. Natl. Acad. Sci. USA 112, 15042–15047.
Haeussler, P.J., Bradley, D.C., Wells, R.E., Miller, M.L., 2003. Life and death of the Resurrection plate: Evidence for its existence and subduction in the northeastern Pacific in Paleocene–Eocene time. Geol. Soc. Am. Bull. 115, 867-880.

Harris, N.R., Sisson, V.B., Wright, J.E., Pavlis, T.L., 1996. Evidence for Eocene mafic underplating during fore-arc intrusive activity, eastern Chugach Mountains, Alaska. Geology 24, 263-266.
Headley, R., Hallet, B., Roe, G., Waddington, E.D., Rignot, E., 2012. Spatial distribution of glacial erosion rates in the St. Elias range, Alaska, inferred from a realistic model of glacier dynamics: J. Geophys. Res. 117, F03027. doi:10.1029/2011JF002291.
Headley, R.M., Enkelmann, E. Hallet, B., 2013. Examination of the interplay between glacial processes and exhumation in the Saint Elias Mountains, Alaska. Geosphere 9, 229-241.
Hogan, L.G., Scheidegger, K.F., Kulm, L.D., Dymond. J., Mikkelsehn, N., 1978. Biostratigraphic and tectonic implications of ^{40}Ar-^{39}Ar dates of ash layers from the northeast Gulf of Alaska. Geol. Soci.Am. Bull. 89, 1259-1264.
Hoskin, P.W.O., 2003. The Composition of Zircon and Igneous and Metamorphic Petrogenesis. Rev. Min. Geochem. 53, 27–62.
Huber, B., Bahlburg, H., Pfänder, J.A. 2018. Single grain heavy mineral provenance of garnet and amphibole in the Surveyor Fan and precursor sediments on the Gulf of Alaska abyssal plain - Implications for climate-tectonic interactions in the St. Elias orogen. Sediment. Geol. 372, 173-192.
Hudson, T., Plafker, G., 1982. Paleogene metamorphism of an accretionary flysch terrane, eastern Gulf of Alaska. Geological Society of America Bulletin 93, 1280-1290.
Hurford, A.J., Carter, A., 1991. The role of fission track dating in discrimination of provenance. In: Developments in sedimentary provenance studies. Morton, A.C., Todd, S.P., Haughton, P.D.W. (Eds.). Geol. Soc. Spec. Publ. 57, 67-78.
Ingle, J.C., 1973. Summary comments on Neogene biostratigraphy, physical stratigraphy, and paleo-oceanography in the marginal northeastern Pacific Ocean Deep Sea Drilling Project, Leg 18. *In* Kulm, L.D., et al. Initial Reports of the Deep Sea Drilling Project. Volume 18, Washington (U.S. Government Printing Office), p. 949-960.
Jaeger, J.M., Gulick, S., LeVay, L.J., Asahi, H., Bahlburg, H., Belanger, C.L., Berbel, G., Childress, L.B., Cowan, E.A., Drab, L., Forwick, M., Fukumura, A., Ge, S., Gupta, S.M., Kioka, A., Konno, S., März, C.E., Matsuzaki, K.M., McClymont, E.L., Mix, A.C., Moy, C.M., Müller, J., Nakamura, A., Ojima, T., Ridgway, K.D., Rodrigues Ribeiro, F., Romero, O.E., Slagle, A.L., Stoner, J.S., St-Onge, G., Suto, I., Walczak, M.H., Worthington, L.L., 2014. Methods. In: Jaeger, J.M., Gulick, S., LeVay, L.J., and the Expedition 341 Scientists (Eds.). Proc. IODP, 341. College Station, TX (IODP).
Kinny, P.D., 2003. Lu-Hf and Sm-Nd isotope systems in zircon. Rev. Min. Geochem. 53, 327–341.
Koschek, G., 1993. Origin and significance of the SEM cathodoluminescence from zircon. J. Microscopy 171, 223–232.
Lagoe, M.B., Eyles, C.H., Eyles, N., Hale, C., 1993. Timing of late Cenozoic tidewater glaciation in the far North Pacific. Geol. Soci. Am. Bull. 105, 1542–1560.
Lagoe, M.B., Zellers, S.D., 1996. Depositional and microfaunal response to Pliocene climate change and tectonics in the eastern Gulf of Alaska. Mar. Micropalentol. 27, 121–140.
Madsen, J.K., Thorkelson, D.J., Friedman, R.M., Marshall, D.D., 2006. Cenozoic to Recent plate configurations in the Pacific Basin: Ridge subduction and slab window magmatism in western North America. Geosphere 2, 11-34.
Mahoney J.B., Gordee, S.M., Haggart, J.W., Friedman, R.M., Diakow, L.J., Woodsworth, G.J., 2009. Magmatic evolution of the eastern Coast Plutonic Complex, Bella Coola region, west-central British Columbia. GSA Bulletin 121, 1362–1380.
Manley, W. F., and Kaufman, D. S. 2002. Alaska Paleo-Glacier Atlas. Institute of Arctic and Alpine Research (INSTAAR), University of Colorado. http://instaar.coloradoq25 .edu/QGISL/ak_paleoglacier_atlas.
Mann, D.H., Hamilton, T.D., 1995. Late Pleistocene and Holocene paleoenvironments of the North Pacific coast. Quaternary Sci. Rev. 14, 449–471.
Meigs, A., Johnston, S., Garver, J., Spotila, J., 2008. Crustal-scale structural architecture, shortening, and exhumation of an active, eroding orogenic wedge (Chugach/St Elias Range, southern Alaska). Tectonics 27, TC4003. doi:10.1029/2007TC002168.

Mendenhall, W.C., 1905. Geology of the central Copper River region, Alaska. Professional Paper 41, 170 p.
Moecher, D.P., Samson, S.D., 2006. Differential zircon fertility of source terranes and natural bias in the detrital zircon record: Implications for sedimentary provenance analysis. Earth Planet. Sci. Lett. 247, 252–266.
Molnia, B., 2008. Glaciers of North America—Survey Professional Paper 1386-K. In: Williams, R.S., Jr., Ferrigno, J.G. (Eds.). Satellite image atlas of glaciers of the world, Geol. Surv. Prof. Paper 1386-K, 525 p.
Montelli, A., Gulick, S.P.S., Worthington, L.L., Mix, A., Davies-Walczak, M., Zellers, S.D., Jaeger, J.M., 2017. Late Quaternary glacial dynamics and sedimentation variability in the Bering Trough, Gulf of Alaska. Geology 45, 251-254.
Moore, J.C., Byrne, T., Plumley, P.W., Reid, M., Gibbons, H., Coe, R.S., 1983. Paleogene evolution of the Kodiak Islands, Alaska: Consequences of ridge-trench interaction in a more southerly latitude. Tectonics 2, 265–293.
Ness, G.E., Kulm, L.D. 1973. Origin and Development of Surveyor Deep-Sea Channel. Geol. Soc. Am. Bull. 84, 3339-3354.
O'Sullivan, P. B., and Currie, L. D. 1996. Thermotectonic history of Mt Logan, Yukon Territory, Canada: implications of multiple episodes of Middle to Late Cenozoic denudation. Earth Planet. Sci. Lett. 144, 251–261.
O'Sullivan, G.J., Chew, D.M., Samson, S.D., 2016. Detecting magma-poor orogens in the detrital record. Geology 44, 871–874.
Pavlis, T. L., Sisson, V. B. 1995. Structural history of the Chugach metamorphic complex in the Tana River region, eastern Alaska: A record of Eocene ridge subduction. Geol. Soc. Am. Bull. 107, 1333-1355.
Pavlis, T.L., Chapman, J.B., Bruhn, R.L., Ridgway, K., Worthington, L.L., Gulick, S.P.S., Spotila, J. 2012. Structure of the actively deforming fold-thrust belt of the St. Elias orogen with implications for glacial exhumation and three-dimensional tectonic processes. Geosphere 8, 991–1019.
Perry, S.E., Garver, J.I., Ridgway, K.D., 2009. Transport of the Yakutat Terrane, Southern Alaska: Evidence from Sediment Petrology and Detrital Zircon Fission-Track and U/Pb Double Dating. J. Geol. 117, 156–173.
Pewé, T.L., 1975. Quaternary geology of Alaska. U.S. geol. Surv. Prof. Pap. 835, 145 p.
Plafker, G., 1987. Regional Geology and Petroleum Potential of the Reginal Geology and Petroleum Potential of the Northern Gulf of Alaska Continental Margin. In: Scholl, D.W., Grantz, A., Vedder, J.G. (Eds.). Geology and Resource Potential of the Continental Margin of Western North America and Adjacent Ocean Basins—Beaufort Sea to Baja California. Circum-Pacific Council for Energy and Mineral Resources; AAPG Bookstore Houston, Tex., U.S.A., Tulsa, Okla., U.S.A., p. 229–268.
Plafker, G., Moore, J.C., Winkler, G.R., 1994. Geology of the southern Alaska margin. In: Plafker, G., Berg, H.C. (Eds.). The geology of North America (Vol. G): The Geology of Alaska. Boulder, Co., Geological Society of America, p. 389–449.
Post, A. 1972. Periodic surge origin of folded medial moraines on Bering piedmont glacier, Alaska. J. Glaciol. 11, 219–226.
Rahl, J.M., Reiners, P.W., Campbell, I.H., Nicolescu, S., Allen, C.M., 2003. Combined single-grain (U-Th)/He and U/Pb dating of detrital zircons from the Navajo Sandstone, Utah. Geology 31, 761-764.
Rea, D.K., Snoeckx, H., 1995. Sediment fluxes in the Gulf of Alaska: paleoceanographic record from Site 887 on the Patton-Murray Seamount platform. In: Rea, D.K., Basov, I.A., Scholl, D.W., Allan, J.F. (Eds.). Proc. ODP, Sci. Results, 145: College Station, Texas (ODP), p. 247–256. doi:10.2973/odp.proc.sr.145.122.1995.
Reece, R.S., Gulick, S.P.S., Horton, B.K., Christeson, G.L., Worthington, L.L., 2011. Tectonic and climatic influence on the evolution of the Surveyor Fan and Channel system, Gulf of Alaska. Geosphere 7, 830–844.
Reiners, P.W., 2005. Zircon (U-Th)/He Thermochronometry. Rev. Min. Geochem. 58, 151–179.

Reiners, P.W., Brandon, M.T., 2006. Using Thermochronology to understand Orogenic Erosion. Annu. Rev. Earth Planet. Sci. 34, 419–466.
Roig, C., 2014. Oxygen and hafnium isotope geochemistry of zircon, quartz, and garnet from the Crawfish Inlet and Krestof plutons, Baranof Island, Alaska. *In* Varga, R. J., ed. Keck Geology Consortium Undergraduate Research Symposium, 27th (South Hadley, MA), Proc., 6 p.
Rowley, D.B., Xue, F., Tucker, R.D., Peng, Z.X., Baker, J., Davis, A.M., 1997, Ages of Ultrahigh Pressure Metamorphism and Protolith Orthogneisses from the Eastern Dabie Shan: U/Pb Zircon Geochronology. Earth Planet. Sci. Lett. 151 (3), 191-203.
Rubatto, D. 2017. Zircon: The Metamorphic Mineral. Rev. Min. Geochem. 9, 261–295.
Schneider, E., Garver, J.I., Davidson, C., 2015. Cooling History of the Sanak-Baranof Plutons, Alaska, using Zircon and Apatite (U-Th)/He Thermochronology. Geol. Soc. Am. Abstr. Program 47, 58.
Siebel, W., Van den haute, P., 2009. Radiometric Dating and Tracing. *In* Sandor Nagy ed. Radiochemistry and Nuclear Chemistry. EOLSS, Oxford, UK.
Sisson, V.B., Hollister, L.S., Onstott, T.C., 1989. Petrologic and age constraints on the origin of a low-pressure/high-temperature metamorphic complex, southern Alaska. J. Geophys. Res. 94, 4392–4410.
Sisson, V.B., Poole, A.R., Harris, N.R., Burner, H.C., Pavlis, T.L., Copeland, P., Donelick, R.A., McLelland, W.C., 2003. Geochemical and geochronologic constraints for genesis of a tonalitetrondjemite suite and associated mafic intrusive rocks in the eastern Chugach Mountains, Alaska: A record of ridge-transform subduction. In: Sisson, V. B., Roeske, S. M., Pavlis, T. L. (Eds.). Geology of a transpressional orogen developed during ridge-trench interaction along the North Pacific margin. Geol. Soci. Am. 371, 293–326.
Spotila, J.A., Buscher, J.T., Meigs, A.J., Reiners, P.W., 2004. Long-term glacial erosion of active mountain belts: Example of the Chugach–St. Elias Range, Alaska. Geology 32, 501-504.
Spotila, J.A., Berger, A.L., 2010. Exhumation at orogenic indentor corners under long-term glacial conditions: Example of the St. Elias orogen, Southern Alaska. Tectonophysics 490, 241–256.
Stevenson, A., J., Embley, R., 1987. Deep-sea fan bodies, terrigenous turbidite sedimentation and petroleum geology, Gulf of Alaska. In: Scholl, D.W., Grantz, A., Vedder, J.G. (Eds.). Geology and Resource Potential of the Continental Margin of Western North America and Adjacent Ocean Basins—Beaufort Sea to Baja California. Circum-Pacific Council for Energy and Mineral Resources; AAPG Bookstore, Houston, Tex., Tulsa, Okla., p. 503–522.
Tomkin, J.H., Roe, G.H., 2007. Climate and tectonic controls on glaciated critical-taper orogens. Earth and Planetary Science Letters 262, 385–397.
Vermeesch, P., 2012. On the visualisation of detrital age distributions. Chem. Geol. 312-313, 190–194.
Vermeesch, P., Resentini, A., Garzanti, E., 2016. An R package for statistical provenance analysis. Sedimentary Geology 336, 14-25.
Vervoort, J.D., Patchett, P., Blichert-Toft, J., Albarède, F., 1999. Relationships between Lu–Hf and Sm–Nd isotopic systems in the global sedimentary system. Earth Planet. Sci. Lett. 168, 79–99.
White, T., Bradley, D., Haeussler, P., Rowley, D.B., 2017. Late Paleocene–Early Eocene Paleosols and a New Measure of the Transport Distance of Alaska's Yakutat Terrane. J. Geol. 125(2), 113-123.
Worthington, L.L., Gulick, S.P.S., Pavlis, T.L., 2010. Coupled stratigraphic and structural evolution of a glaciated orogenic wedge, offshore St. Elias orogen, Alaska. Tectonics 29, TC6013. doi:10.1029/2010TC002723.
Worthington, L.L., Van Avendonk, H.J.A., Gulick, S.P S., Christeson, G.L., Pavlis, T.L., 2012. Crustal structure of the Yakutat terrane and the evolution of subduction and collision in southern Alaska. J. Geophys. Res. 117, B01102. doi:10.1029/2011JB008493.

Worthington, L.L., Daigle, H., Clary, W.A., Gulick, S.P.S., Montelli, A., 2018. High sedimentation rates and thrust fault modulation: Insights from ocean drilling offshore the St. Elias Mountains, southern Alaska. Earth. Planet. Sci. Lett., 483, 1-12.

4 Framework petrography of sediments from IODP 341 sites U1417 and U1418

This chapter will be submitted to the International Journal of Earth Sciences as Huber, B. and Bahlburg, H., Framework petrography of IODP 341 sites U1417 and U1418.

4.1 Abstract

The Miocene to Holocene sediments of the Surveyor Fan, Gulf of Alaska, store material shed from the adjacent southern Alaska continental margin during the formation of the St. Elias mountains. The orogen formed in the crossfire of tectonic processes related to subduction and accretion of the Yakutat terrane and changes in climatic conditions with a strong intensification of glaciation. These sediments were drilled during IODP expedition 341. The recovered material is used to constrain information on changes in erosion centers during the last 10 Ma to study the impact of climatic and tectonic forces on orogen formation. Point counting of light minerals and analysis of epidote and pyroxene geochemistry is applied to reveal changes in sedimentary provenance of two sites in the distal and proximal Surveyor Fan (site U1417 and U1418, respectively).

Epidote and pyroxene compositions are very homogenous and show no change with time of deposition. Associations of epidote and pyroxene with albite, titanite and pumpellyite are in line with near shore sources in the metabasite belt at the southern border of the Chugach metamorphic complex and on the Yakutat terrane, respectively. Rock fragments indicate high input from a metamorphic source area during the Miocene and Pliocene and slightly higher input from low grade metamorphic and sedimentary rocks in the Pleistocene which is also supported by the abundance of epidote and pyroxene. This implies increasing erosion of the nearshore areas with advance of glaciers to the shore since the Miocene, being enhanced by the onset of the Northern Hemisphere glaciation at the beginning of the Pleistocene. The light minerals suggest slightly different source areas for the proximal and the distal sites but show no systematical changes with time of deposition. No changes could be found for the mid-Pleistocene transition. Glaciers seem to have remained in their topographically predefined positions, feeding material with the same characteristics into the fan as before.

4.2 Introduction

The southern Alaska continental margin hosts the highest coastal mountain range on earth, the St. Elias Mountains, that formed through accretion and subduction during concomitant glaciation in the course of the last ca. 8 Ma (Plafker et al., 1994; Bruhn et al., 2004; Enkelmann et al., 2008, 2015; Finzel et al., 2011, 2015; Pavlis et al., 2012; Falkowski et al., 2014). This makes the St. Elias mountain range a key location to study climate-tectonic interactions during mountain building. Several questions concerning sediment transport from the onshore sources into the adjacent Surveyor Fan, terrane transport/accretion and centers of erosion and uplift in the interplay of active tectonics and changing glacial conditions at the southern continental margin are in the focus of current research (Spotila et al., 2004; Berger et al., 2008a, b; Berger and Spotila, 2008; Meigs et al., 2008; Enkelmann et al., 2010, 2015, 2017; Spotila and Berger, 2010; Worthington et al., 2010, 2018; Expedition 341 Scientists 2014; Gulick et al., 2015; Dunn et al., 2017; Huber et al., 2018a, b).

The Miocene to Pleistocene Surveyor Fan and precursor sediments in the Gulf of Alaska serve as a sedimentary archive storing material eroded from the evolving St. Elias orogen (Expedition 341 Scientists, 2014; Dunn et al., 2017; Huber et al., 2018a, b). During IODP Expedition 341 this record was drilled recovering Miocene to Pleistocene sediments (fig. 1A). Unraveling the history of orogen formation and climate tectonic interaction at the southern Alaska continental margin by performing heavy mineral analysis and zircon and apatite thermochronology of the material recovered by IODP expedition 341 has already revealed information on changing erosion centers and exhumation rates (Dunn et al., 2017; Huber et al., 2018a, b). The complex geology of the source area, recycling of onshore sedimentary units and homogenous mineral characteristics in areas that might have experienced variable histories of erosion and exhumation challenge the study of how climate change at the mid-Pleistocene transition impacted the orogen (Huber et al., 2018a, b).

Here, we describe the light mineral petrography and the single grain geochemistry of pyroxene and epidote of samples taken from two sites on the distal and proximal Fan (sites U1417 and U1418, respectively; fig. 1A) to further constrain the provenance of the sediments. Combining several provenance tools gives a variety of options to extract different information on provenance (von Eynatten et al, 2003; Weltje and von Eynatten, 2004; von Eynatten and Dunkl, 2012; Reimann et al., 2015, Garzanti, 2016). Sandstone petrography is one of the most traditional (Weltje and von Eynatten, 2004). Evaluation of the light mineral framework of a sedimentary deposit permits an initial discrimination of provenance (e.g., Dickinson and Suczek, 1979; von Eynatten et al., 2003) and allows for a general insight into the nature of the sediment (Pettijohn et al., 1987). Together with rock fragments they can unravel information on source rock lithology and mixing of material supplied from different endmember sources (e.g., Dickinson, 1988; Garzanti, 2016). Pyroxene geochemistry reveals information on the source rock type and its plate tectonic setting (Cawood, 1983; Nechaev and Isphording, 1993). Epidote analysis is a less valuable tool in provenance (Mange and Morton, 2007), its geochemistry, however, has the potential to release provenance information as shown in some cases (e.g., Cawood, 1983; Krawinkel et al., 1999; Caracciolo et al., 2016).

4.3 Geological background

The southern Alaska continental margin formed through successive accretion of several allochthonous terranes against the North American continent (Plafker et al., 1994). South of the Border Ranges fault, the accreted terranes form one big accretionary complex that developed in relation to subduction, creating the Southern Margin composite terrane (Wrangellia composite terrane, Chugach terrane, Prince William terrane, Yakutat terrane; fig. 1A; Plafker et al., 1994). The Wrangellia terrane accreted during Middle Jurassic-Late Cretaceous (Trop et al., 2002). The Wrangellia, Alexander and Peninsular terranes form the Wrangellia composite terrane. The Early Mississippian to Permian Wrangellia and Peninsular

terranes consist of intraoceanic andesitic arc rocks, carbonates, meta-sediments, mafic and ultramafic plutonic material covered by Triassic and Jurassic sedimentary, volcanic and magmatic rocks (Plafker et al., 1994). The Alexander Terrane consists of Late Proterozoic to Triassic strata and intrusives (Jones et al., 1986). The Chugach terrane accreted during the middle to latest Cretaceous along the Border Ranges Fault, consisting mostly of the upper Cretaceous rocks of the Valdez Group (Mendenhall 1905; Dumoulin 1987; Plafker, 1987; Plafker and Berg, 1994) (fig. 1B). The sedimentary and volcanic material of the Orca Group (Prince William terrane) accreted between ca. 52 and 62 Ma along the contact fault (Plafker, 1987). In the course of these developments western Alaska experienced counterclockwise rotation (Plafker, 1987).

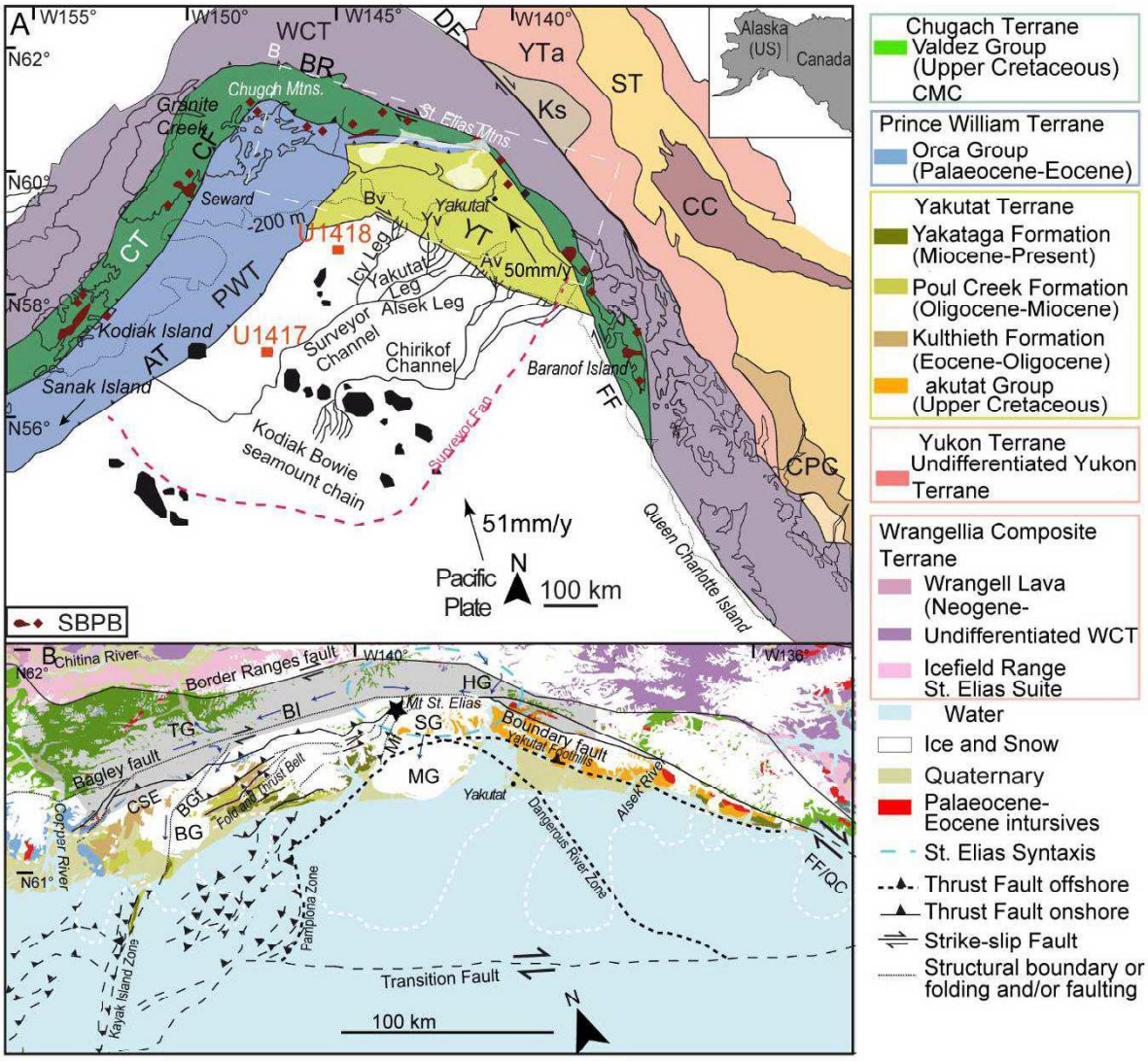

Figure 1: (A) Terrane map of the southern Alaska continental margin. AT=Aleutian trench; Av=Alsek valley; BR=Border Ranges fault; Bv=Bering valley; CC=Cache Creek terrane; CF=Contact fault; CPC=Coast Plutonic Complex; CT=Chugach terrane; KS=Kluane Schist; FF=Fairweather Fault; PWT= Prince William terrane; SBPB=Sanak Baranof Plutonic Belt; ST=Stikinia terrane; WCT=Wrangellia composite terrane; YT=Yakutat terrane, YTa=Yukon-Tana terrane; Yv=Yakutat valley. Orange squares mark the distal (U1417) and proximal (U1418) sites of IODP Expedition 341. (B) Simplified geological map of the southern Alaska continental margin. BG=Bering Glacier, BGf=Bering Glacier fault, BI=Bagley Icefield, FF/QC= Queen Charlotte - Fairweather Fault System; CSE=Chugach-St. Elias Fault, HG=Hubbard Glacier, Mf=Malaspina fault, MG=Malaspina Glacier, SG=Seward Glacier, TG=Tana Glacier. Blue arrows indicate glacial flow directions after Post (1972). Glacier extent during LGM (Last Glacial Maximum) after Manley and Kaufman (2002) is marked with a white dashed line. The extent of the Chugach metamorphic complex (CMC) is marked by the gray shaded area. Modified after Huber et al. (2018b) and references therein.

Between ca. 50 and 60 Ma, the plutons of the Sanak-Baranof Plutonic Belt (SBPB) intruded into the accretionary prism of the Chugach and Prince William terrane for 2100 km along strike of the terranes, leading to the formation of the Chugach metamorphic complex (Sisson et al., 1989; Bradley et al., 1993, 2003; Plafker et al., 1994; Pavlis and Sisson, 1995; Haeussler et al., 2003; Sisson et al., 2003; Farris and Paterson, 2009). The ca. 350 km long Chugach metamorphic complex consist of rocks of up to amphibolite facies conditions (Hudson and Plafker 1982; Bruand et al., 2011; Gasser et al., 2011). A metabasite belt of ampibolite facies metamorphic overprinted rocks is juxaposed against the CMC along the Contact fault and Fairweather Fault system facing lower grade metamorphic rocks to the south (Bruand et al., 2011; Gasser et al., 2011).

The most outboard terrane, the Yakutat terrane, is tied to the movement of the Pacific plate and is the latest terrane accreting to the southern Alaska margin (Plafker and Berg, 1994). Northwestward transport of the Yakutat terrane along the dextral Fairweather-Queen Charlotte transform fault system since ca. 30 Ma led to subduction of the Yakutat slab and accretion of the Yakutat terrane along the Chugach-St. Elias Fault since the Miocene driving the formation of the St. Elias Mountains (Plafker, 1987; Plafker et al., 1994; Bruhn et al., 2004; Enkelmann et al., 2008, 2015; Finzel et al., 2011; Arkle et al., 2013; Falkowski et al., 2014). Strong uplift and erosion characterize the orogeny during the last ca. 10 Ma, especially at the Yakutat plate corner (Syntaxis) where transform motions along Fairweather fault change to flat-slab subduction (Pavlis et al., 2012; Enkelmann et al., 2009, 2010, 2015, 2017; Falkowski et al., 2014; Dunn et al., 2017).

The origin and transport history of the Yakutat terrane are under debate. One option favors short transport (ca. 600 km) with origin of the terrane near Prince Rupert (Plafker 1987; Plafker et al., 1994; Perry et al., 2009) while the far travelled history suggests an origin at ~44° paleonorth or close to northern California or southern Oregon in the Eocene (~45 Ma; Bruns, 1983; Plafker et al., 1994; Perry et al., 2009; White et al, 2017). The western part of the terrane is characterized by a fold and thrust belt that formed during the accretion, consisting of imbricated sediments of the pre-orogenic Kulthieth (Middle Eocene), Poul Creek (Lower Oligocene to Lower Miocene) and the syn-orogenic Yakataga (Miocene through Holocene) Formations (Plafker, 1987; Plafker et al., 1994; Worthington et al., 2010; Enkelmann et al., 2015). The eastern part is covered by the Yakutat Group which is part of the Chugach flysch and mélange (Plafker, 1987; Plafker et al., 1994).

Alpine glaciation at the Southern Alaska continental margin started in the late Miocene (ca. 7 Ma) shortly after the onset of the formation of the St. Elias orogen and expanded to tidewater glaciation between 6.7 and 5.0 Ma (Lagoe et al., 1993) (fig. 2). After a warm mid-Pliocene period from 4.2 to ca. 3 Ma, the Northern Hemisphere glaciation started at ca. 2.5 Ma with an intensification of glaciation especially when global glacial-interglacial climate cycles changed from 40 to 100 Kyr at 0.7 to 1 Ma at the mid-Pleistocene transition (Lagoe et al., 1993; Lagoe and Zellers, 1996). Glaciation reached onto the shelf during phases of strong glaciation; today, the Bering, Malaspina and Hubbard glaciers are the largest glaciers at the Gulf of Alaska (Pewé, 1975; Mann and Hamilton, 1995; Berger et al., 2008a; Molina, 2008; Worthington et al., 2010; Headley et al., 2013; Expedition 341 Scientists, 2014) (fig. 1B). These glacial systems directly feed orogenic detritus into today's Surveyor fan through the Surveyor Channel system. Several small shelf-crossing gullies merge to three channels (Icy, Yakutat and Alsek Leg) joining to form the main Surveyor channel system ca. 150 km from the continental margin integrating input from the Malaspina and Hubbard Glaciers (Yakutat Leg and Yakutat Sea Valley), the Alsek glacial system (Alsek Leg, Alsek Sea Valley) and the Bering glacier (Icy Leg). The Icy Leg was shut after the onset of glacial interval C (figs. 1A and 2) (Reece et al., 2011). The main channel feeds into the Aleutian trench ca. 600 km from the continental shelf (Ness and Kulm, 1973; Stevenson and Embley, 1987; Dobson et al., 1998; Carlson et al., 1996; Reece et al., 2011) (fig. 1A). The initiation of this transport system is discussed to have started at the Miocene/Pliocene transition at ca. 5 Ma (Hogan et al., 1978, Reece et al., 2011) or at ca. 2.7 Ma (Gulick et al., 2015). The precursor of today's Surveyor Fan is active since ca. 9.7 Ma; moving to the northwest with the Pacific Plate since onset of deposition (Stevenson and Embeley, 1987; Rea and Snoeckx, 1995; Reece et al., 2011). How sediment transport into

the precursor of today's Surveyor fan worked during the early stages of deposition is not resolved so far but absence of a glacial transport system as well as implications from heavy mineral and zircon data and seismic reflection data of the early fan sediments imply the presence of a fluvial tributary system before the onset of glaciation in the late Miocene, funneling material from sources in the North (Stevenson and Embley, 1987; Huber et al., 2018 a, b).

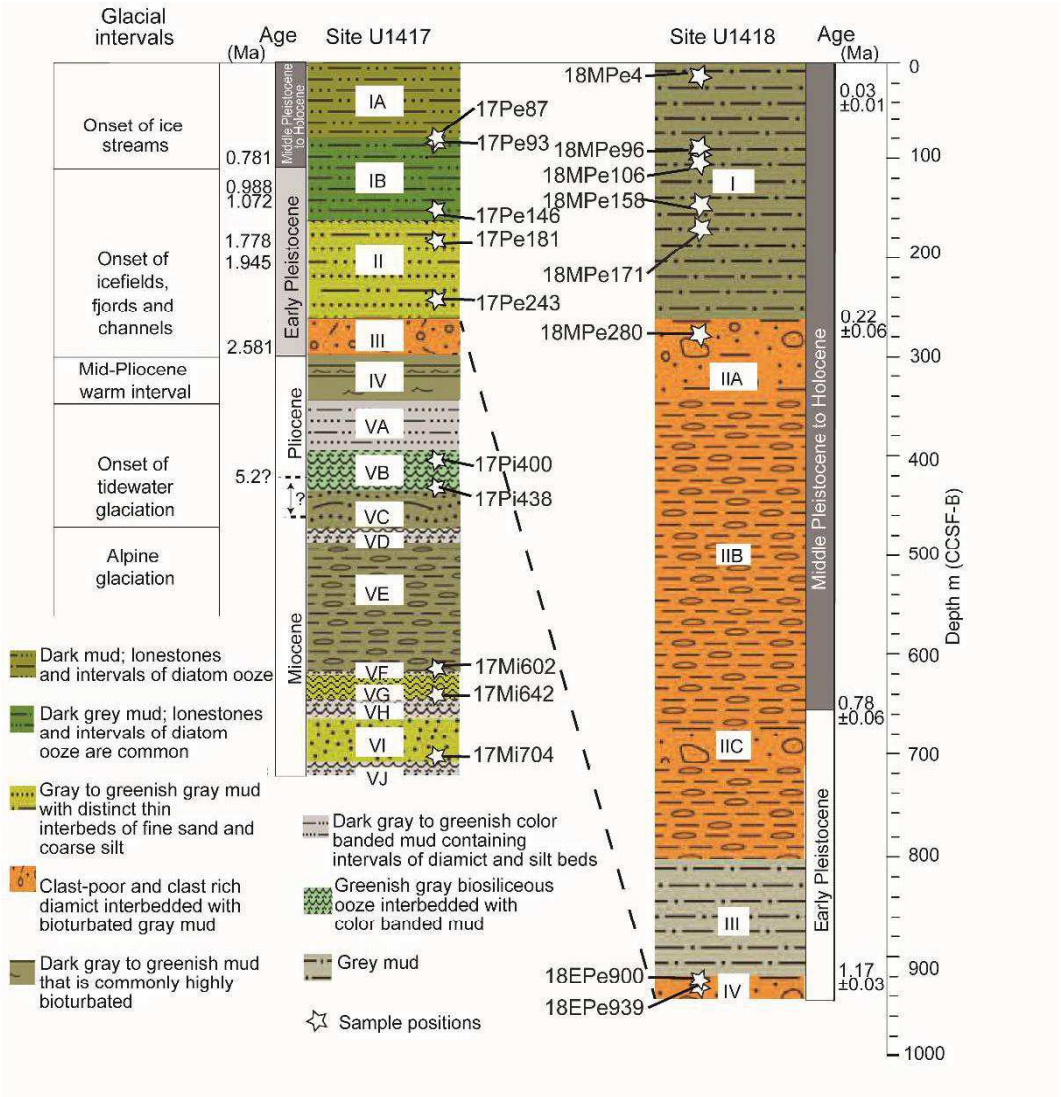

Figure 2: Lithostratigraphy of IODP 341 sites U1417 (distal site) and U1418 (proximal site) and climatic events in southern Alaska. Sample positions are marked with white stars. Modified after Lagoe et al. (1993) and Expedition 341 Scientists (2014).

4.4 Sampling

Samples were taken from sands and silts of IODP Expedition 341 sites U1417 and U1418. Site U1417 was drilled ca. 60 km west of today's Surveyor Channel in the distal Surveyor Fan, today being fed by the Alsek, Yakutat and Icy legs through hemipelagic/pelagic rainout and overbank levee deposition from turbidity currents (Expedition 341 Scientists, 2014; Dunn et al., 2017) (fig. 1A). Sediments from a maximum depth of ca. 700 m below sea floor of Miocene (ca. 10 Ma) to Holocene age were recovered (fig. 2). Site U1418 recovered ca. 950 m of Early Pleistocene to Holocene sediments from the proximal Surveyor Fan (Expedition 341 Scientists, 2014) (fig. 2). The lowermost lithostratigraphic unit IV formed through an Early Pleistocene massive slope failure (mass transport deposit) (Reece et al., 2011; Expedition 341 Scientists, 2014). All younger units were deposited through hemipelagic settling and gravity flows from

nearby channels (Reece et al., 2011; Expedition 341 Scientists, 2014). Sample names start with the abbreviated name of the site (17 for U1417 or 18 for U1418) followed by the abbreviated name of the stratigraphic interval (Mi=Miocene, Pi=Pliocene, Pe=Pleistocene, EPe=Early Pleistocene, MPe=Middle Pleistocene) and the sampling depth in m core composite depth below seafloor (m CCSF-B) (fig. 2). The IODP code of each sample can be found in Appendix A. Deposition ages were deduced from bio- and magnetostratigraphic reconstructions and the resulting age model (Expedition 341 Scientists, 2014; Jaeger et al., 2014; Gulick et al., 2015) (fig. 2). The sample volume is limited by the amount of material recovered in the sediment core half provided for sampling.

4.5 Methods

Samples were wet sieved to remove grains <63 µm. Bulk samples >63 µm were investigated under a binocular microscope. Light and heavy minerals were separated using sodium polytungstate at 2.95 g/cm^3 by density separation. The fraction 250-63 µm was mounted on microscopy slides in epoxy and grinded to ca. 35 µm. On each slide 300 grains were point counted after the Gazzi-Dickinson point counting method (Ingersoll et al., 1984; Dickinson 1985, 1988) using a polarization microscope equipped with a Petrog SteppingStage. Grains >250 µm were rare and examined under a binocular microscope and exemplary grains of the most common rock fragments were mounted in epoxy and prepared to be examined with a microscope. For pyroxene and epidote analysis, grains were handpicked under a binocular microscope from fractions of heavy mineral separates used in Huber et al. (2018a, b). Pyroxene and epidote major element geochemistry was measured using a microprobe at the University of Münster. Minerals intergrown with the pyroxenes and epidotes were measured alongside. Acceleration voltage was at 15 kV, beam current at 10µA and spot size at 5 µm. Pyroxene end-members were calculated using the WinPyrox software (Yavuz, 2013).

4.6 Results

4.6.1 Framework components

The overall grain spectra of all samples mainly consist of subrounded rock fragments, quartz, feldspar, biotite and some heavy minerals. Only the oldest Miocene samples recovered (unit VI) are primarily made up of coalified organic material, mica and opaque, angular grains (fig. 3). Rock fragments, quartz and feldspar make up less than 5% of these sediments. They are also very rich in biotite; the mica content progressively decreases with younger depositional age.

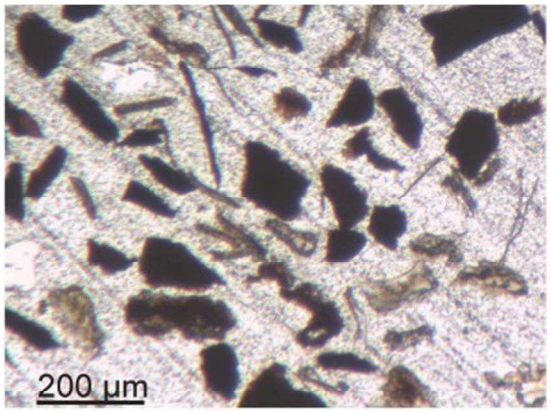

Figure 3: Microphotograph of sediments from Unit VI (oldest Miocene sediments drilled) showing the dominance of coalified organic fragments.

Thin sections of the sand-size fractions reveal this fraction to be dominated by quartz in all units (except unit VI) (fig. 4). Most of the feldspar is plagioclase while K-feldspar is rare to absent. Feldspars are relatively fresh with only minor sericitization (fig. 5). Plagioclase shows polysynthetic twinning. Quartz is present as mono- and polycrystalline variety.

Rock fragments are mainly metamorphic and sedimentary (figs. 4, 5, 6). The most common rock fragments are mostly argillite, sand and siltstones, slaty to schistose grains, gneiss and metasilt- and sandstone. Some of the sedimentary rock fragments show abundant opaque

grains. The framework component spectra of samples from both sites are relatively similar (fig. 7) but show a minor difference in feldspar content with the samples from site U1418 showing slightly higher amounts of feldspar. All samples plot in the field "recycled orogen provenance" in the QFL-diagram. The sample from unit VI (17Mi704) could not be plotted in this diagram because of the lack of grains of the respective groups.

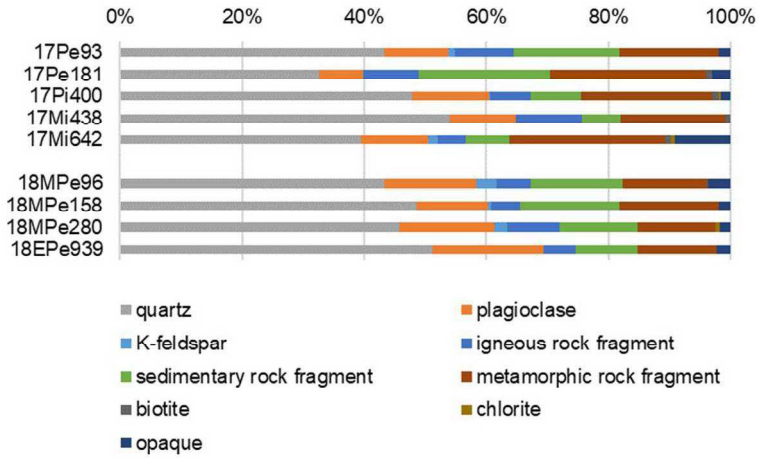

Figure 4: Light mineral spectra of sites U1417 and U1418.

Evaluation of the main rock fragments shows a difference between the samples from sites U1417 and U1418. The Miocene to Pliocene samples from site U1417 give higher numbers of metamorphic grains compared to the Pleistocene samples from site U1417 and site U1418 (fig. 8). This is also confirmed by principal component analysis showing all Pleistocene samples besides sample 17Pe181 to cluster in the topmost right corner of the plot while the Miocene to Pliocene samples plot in the bottom right corner (fig. 9).

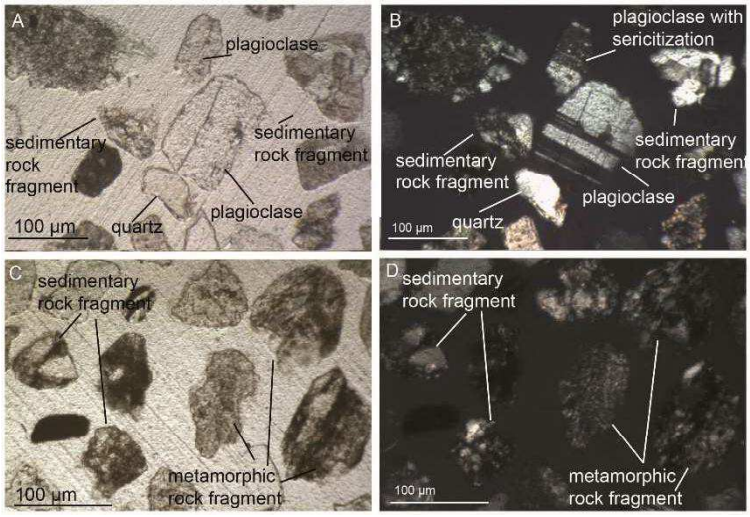

Figure 5: Representative microphotographs of sediments from site U1417 and U1418. A and C PPL, B and D XPL.

Grains >0.25 mm are rare in most samples providing less than 2%. In general, these grains are subangular to subrounded (fig. 10 and 11). Most samples show mainly subrounded quartz, feldspar and fine grained sedimentary and metamorphic rock fragments in this size fraction (fig. 10 and 11). In contrast, the samples from the mass transport deposit at the base of the core retrieved from site U1418 are dominated by black angular grains of iron oxides in this fraction (fig. 11).

Figure 6 (next page): Exemplary microphotographs of the most common rock fragments in the sediments from sites U1417 and U1418. A: PPL (plane-polarized light); very fine-grained silt/mud stone with abundant quartz and feldspar; (B) XPL (cross-polarized light); same as A; (C) PPL; metasedimentary rock fragment showing beginning recrystallization and lineation; (D) XPL; same as C; (E) PPL; medium grained sandstone showing beginning recrystallization; (F) XPL; same as E; (G) PPL; sedimentary rock fragment with abundant opaque grains; (H) XPL; same as G; (I) metabasite showing chlorite formation; (J) XPL; same as I; (K) LPL; metasedimentary grain showing chlorite formation and recrystallization, (L) XPL; same as K; (M) quartzofeldspathic schist showing lineation defined by biotite; (N) same grain as in M but cut and embedded into epoxy; PPL (O) XPL; same as M; (P) greenschist facies metamorphic rock fragment; (Q) same as P but cut and embedded into epoxy; PPL; (R) XPL; same as (Q); (S) mudstone fragment; (T) PPL; rock fragment from R cut and embedded into epoxy; (U) XPL, same as T.

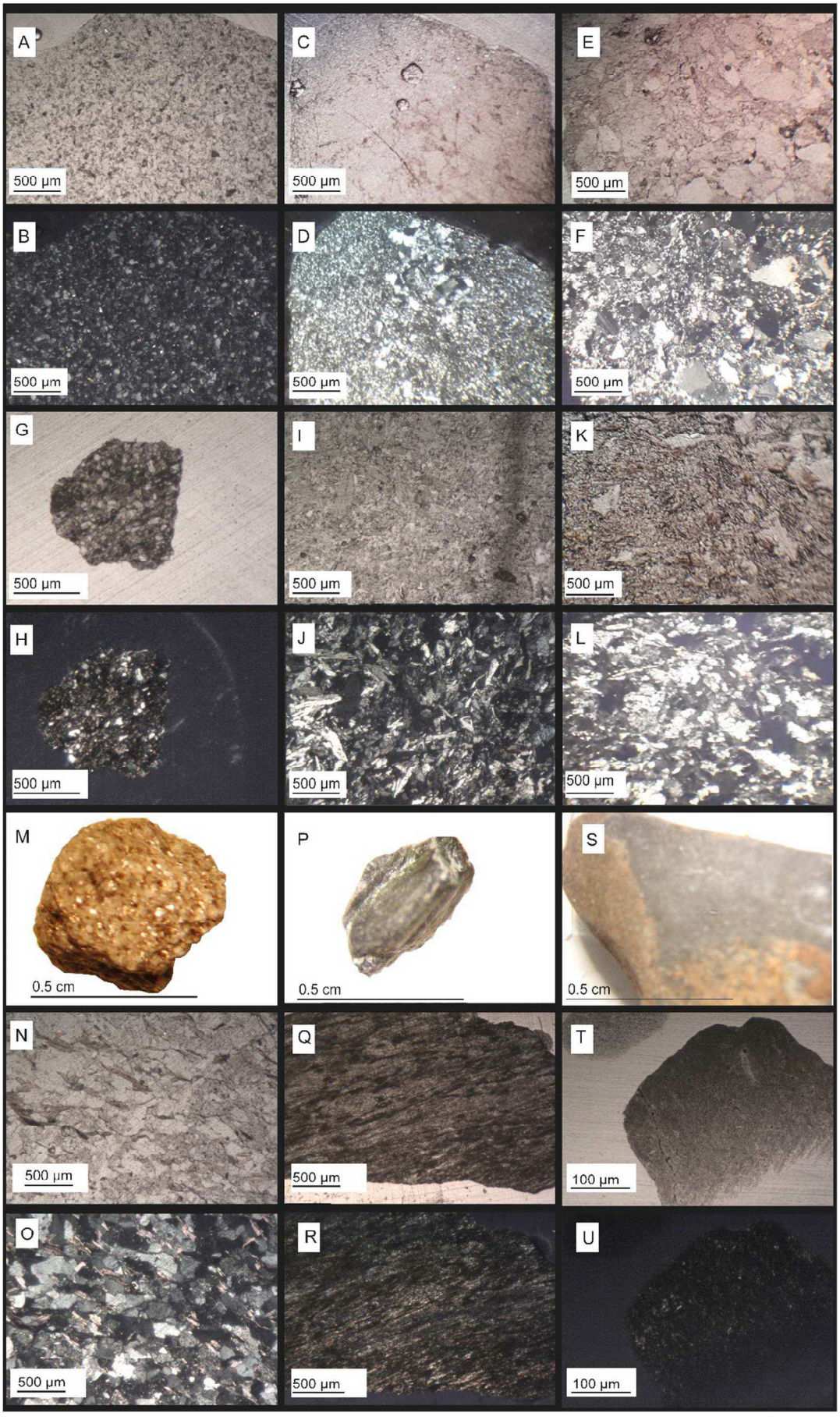
A
500 µm
C
500 µm
E
500 µm
B
500 µm
D
500 µm
F
500 µm
G
500 µm
I
500 µm
K
500 µm
H
500 µm
J
500 µm
L
500 µm
M
0.5 cm
P
0.5 cm
S
0.5 cm
N
500 µm
Q
500 µm
T
100 µm
O
500 µm
R
500 µm
U
100 µm

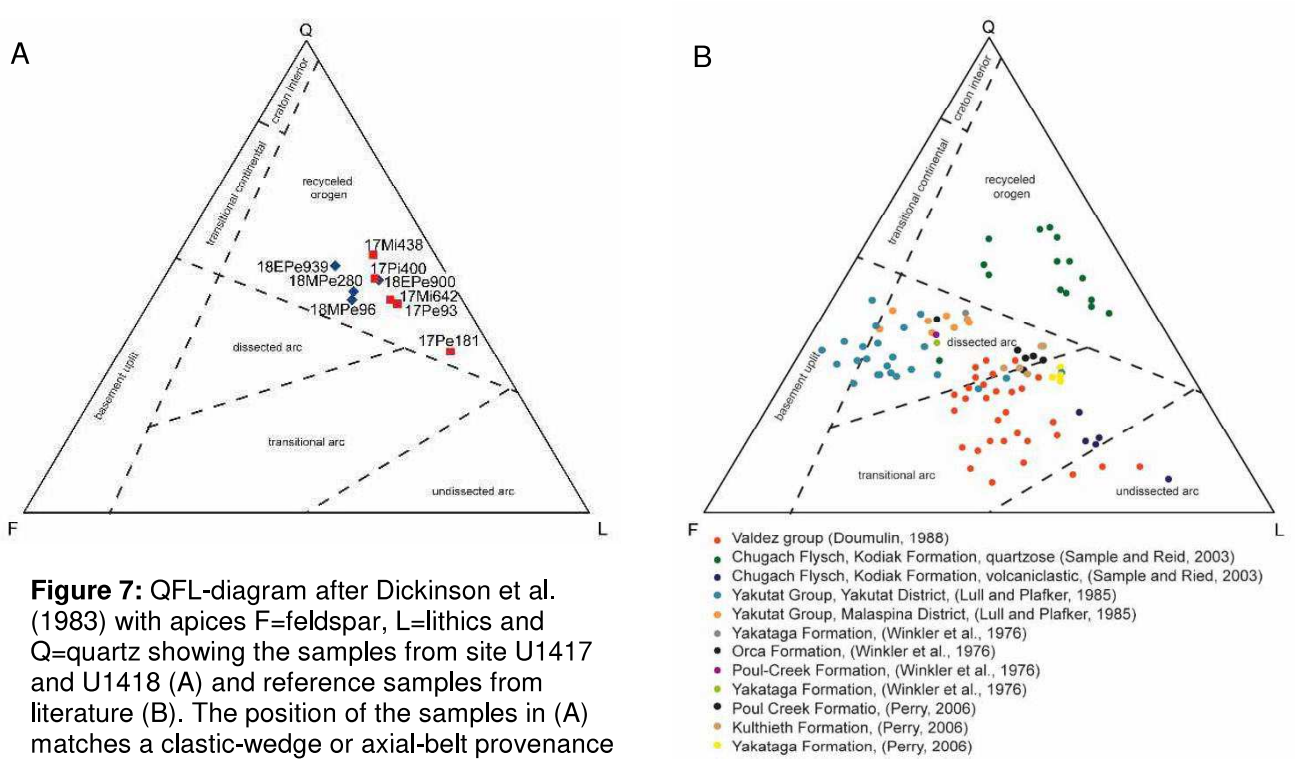

Figure 7: QFL-diagram after Dickinson et al. (1983) with apices F=feldspar, L=lithics and Q=quartz showing the samples from site U1417 and U1418 (A) and reference samples from literature (B). The position of the samples in (A) matches a clastic-wedge or axial-belt provenance after Garzanti et al. (2007).

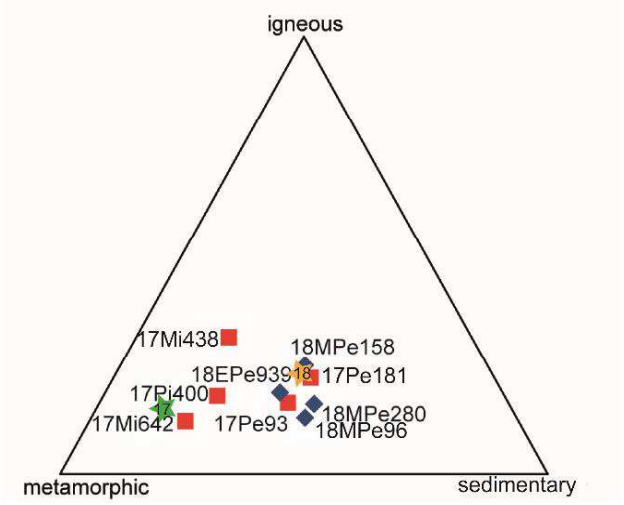

Figure 8: Diagram showing the lithology of the rock fragments in samples from sites U1417 (red squares) and U1418 (blue squares). The green and yellow stars represent the average abundances of the main types of clasts larger than 2 mm in diameter at sites U1417 and U1418, respectively, as determined from IODP Expedition 341 Scientists (2014).

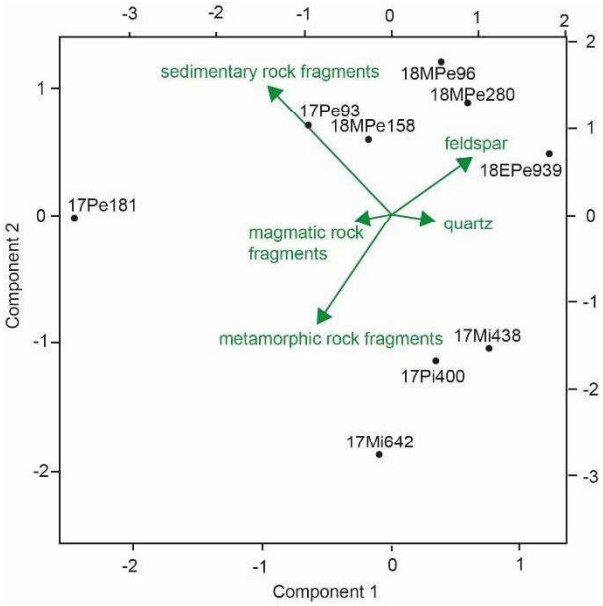

Figure 9: Principal component analysis plot of the main framework components from samples of sites U1417 and U1418. Calculated with the provenance software of Vermeesch et al. (2016).

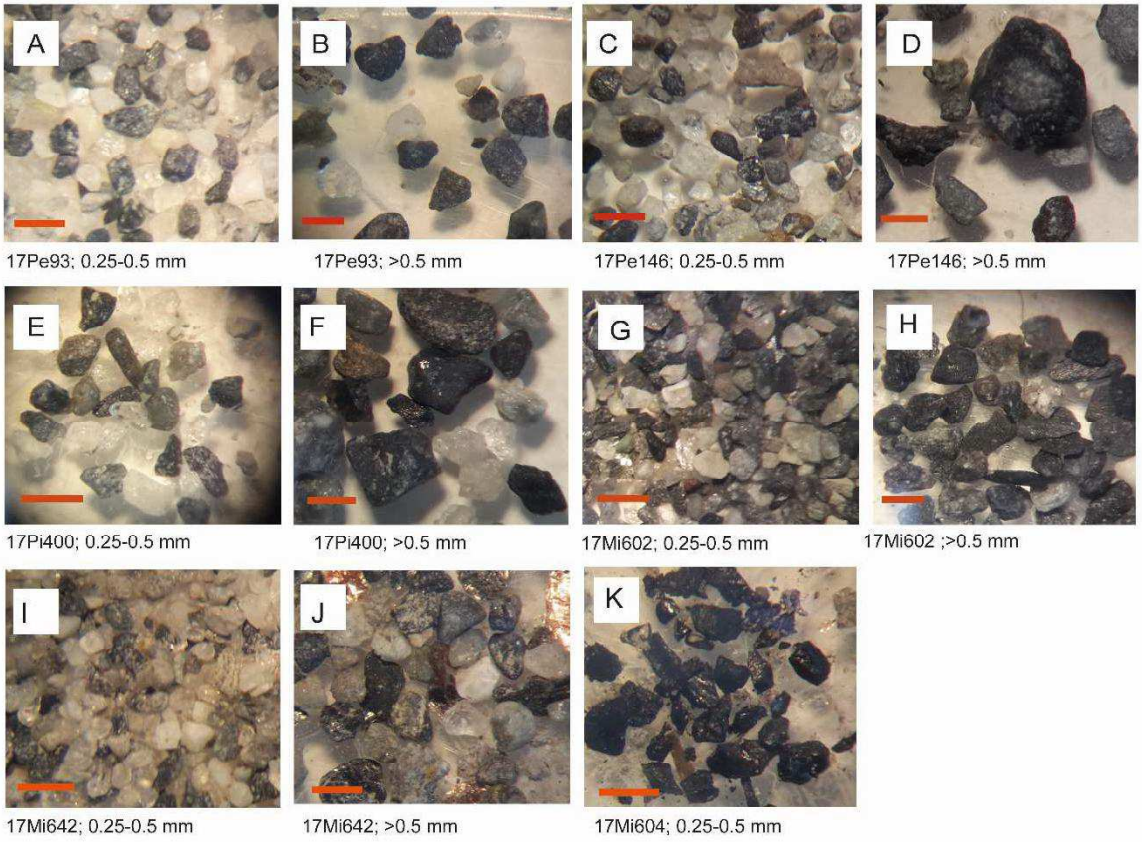

Figure 10: Microphotographs giving an overview over the grain fractions >0.25 mm from site U1417. (A-J) rounded gray to black, fine grained sedimentary and metamorphic rock fragments, feldspar and quartz dominate most samples. K shows the dominace of coalified organic material in sample 17Mi704. Scale bar represents 0.5 mm.

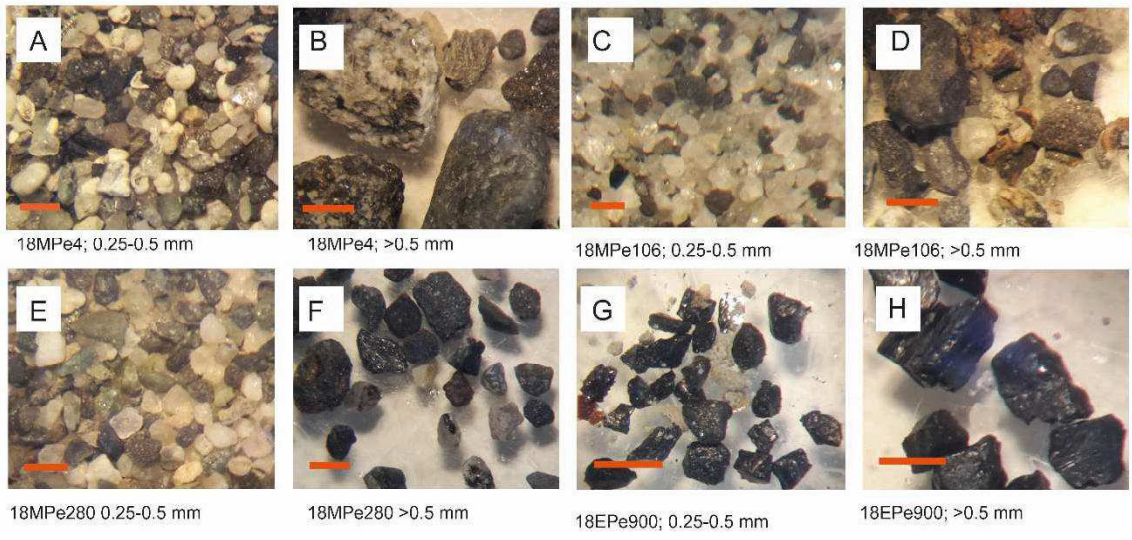

Figure 11: Microphotographs giving an overview of the grain fraction >0.25 mm from site U1418. Most samples are dominated by rounded, black to grey, fine grained sedimentary and metamorphic grains as well as quartz and feldspar (A-F). G and H show the dominance of angular black grains (mainly iron oxides) in sample 18Pe900. Scale bar represents 0.5 mm.

4.6.2 Heavy minerals pyroxene and epidote

Most pyroxene found occurs intergrown with feldspar (mostly albite rich), pumpellyite and titanite as revealed by microprobe imaging (fig. 12A). The most abundant pyroxene endmember at both sites is the clinopyroxene (aegirine-) augite (fig. 13A). All augite is relatively rich in aluminum (Appendix B). There is no systematic variability in pyroxene composition between the two sites and between samples from different stratigraphic intervals (fig. 13A, B).

All grains of the epidote group show a very similar geochemistry (tab. 1). Most are intergrown with albite rich feldspar or quartz (fig. 12B). There is no systematic variability in epidote composition with time of deposition or between sites.

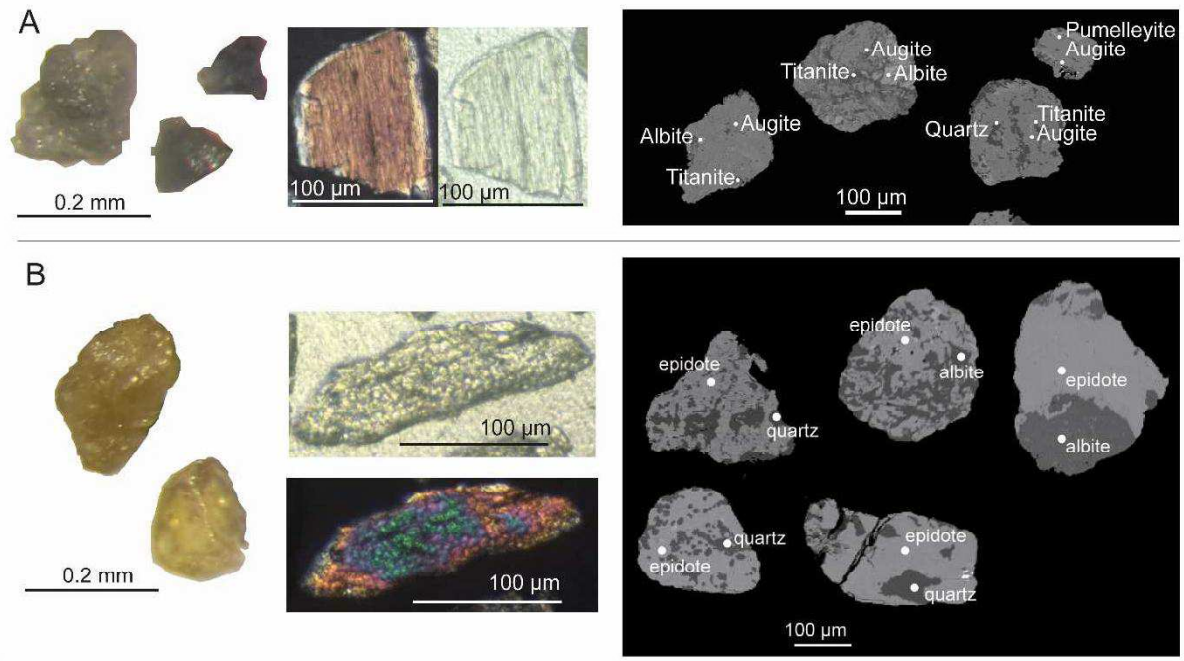

Figure 12: Representative binocular microscope, thin section and microprobe images of (A) pyroxene intergrown with augite, titanite and/or quartz and (B) epidote intergrown with albite, titanite and/or quartz from the site U1417 and U1418 samples.

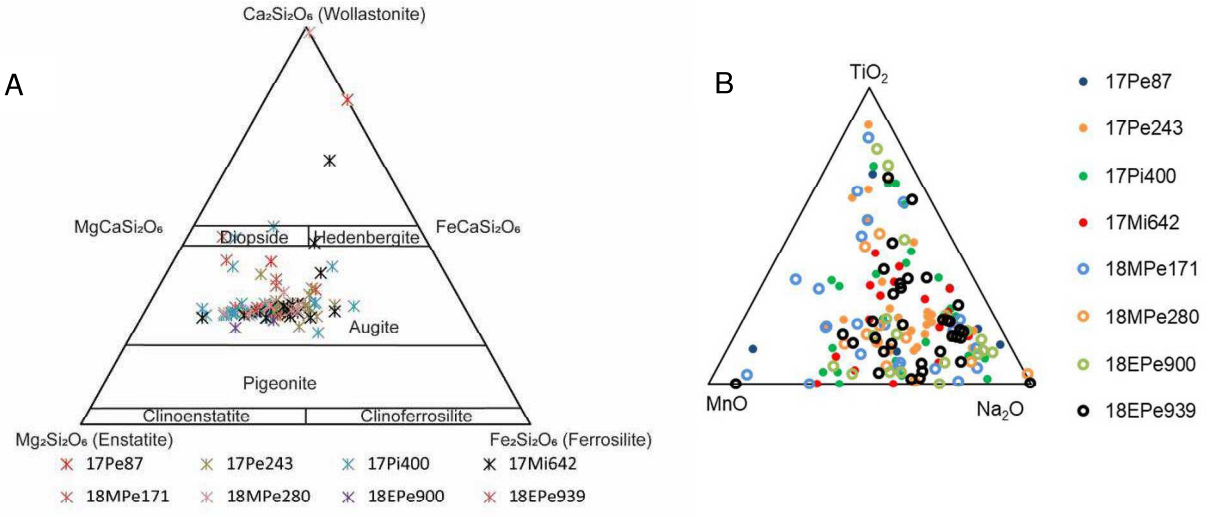

Figure 13: (A) Main element composition of pyroxene from site U1417 and U1418. (B) Minor elements of pyroxene form site U1417 and U1418 showing no trend in correlation to sampling depth.

Table 1: Representative analyses of epidotes from different samples from IODP 341 sites U1417 and U1418 in wt.%.

sample	Na_2O	MgO	SiO_2	Al_2O_3	K_2O	CaO	FeO	TiO_2	Cr_2O_3	MnO	Total
17Mi642	0.02	1.97	36.50	20.96	0.02	21.84	10.02	0.04	0.02	0.06	91.45
17Mi642	0.01	0.02	37.15	20.46	0.00	20.37	14.50	0.08	0.01	0.05	92.66
17Mi642	0.01	0.01	37.16	21.28	0.04	19.17	13.83	0.07	0.02	0.12	91.70
17Mi642	0.00	0.02	37.22	22.02	0.00	22.67	12.84	0.06	0.08	0.17	95.08
17Mi642	0.01	0.02	37.23	21.44	0.00	22.86	13.56	0.10	0.04	0.20	95.46
17Pi400	0.04	0.01	36.84	19.32	0.00	21.58	16.20	0.00	0.01	0.00	94.00
17Pi400	0.03	0.20	37.30	21.33	0.00	22.11	14.04	0.24	0.00	0.11	95.35
17Pi400	0.00	0.11	37.37	21.28	0.01	21.93	13.66	0.08	0.00	0.17	94.61
17Pi400	0.00	0.05	37.40	21.38	0.01	22.15	13.81	0.00	0.01	0.26	95.08
17Pi400	0.03	0.04	37.49	22.61	0.00	20.56	13.03	0.09	0.00	1.05	94.90
17Pe93	0.07	1.98	34.88	23.69	0.03	17.19	14.88	0.00	0.00	0.77	93.50
17Pe93	0.00	0.03	35.34	15.31	0.02	24.08	9.73	10.27	0.02	0.08	94.88
17Pe93	0.00	0.06	36.88	21.26	0.02	22.73	13.03	0.00	0.00	0.27	94.25
17Pe93	0.01	0.01	37.17	21.52	0.00	21.40	13.36	0.08	0.00	0.12	93.67
17Pe93	0.00	0.04	37.18	20.73	0.00	22.64	14.38	0.15	0.00	0.07	95.19
18MPe280	0.00	0.06	36.49	22.28	0.03	23.58	11.41	0.15	0.02	0.28	94.30
18MPe280	0.02	0.09	36.50	18.88	0.01	22.87	12.27	4.29	0.01	0.11	95.05
18MPe280	0.02	0.05	36.81	20.57	0.02	22.64	14.78	0.17	0.00	0.18	95.24
18MPe280	0.04	0.02	36.95	20.72	0.05	22.52	13.94	0.20	0.03	0.13	94.59
18MPe280	0.01	1.93	37.00	22.38	0.00	20.94	12.47	0.25	0.04	0.18	95.19

4.7 Interpretation

The major change in sediment composition in the late Miocene, from mainly coalified organic material and mica to abundant quartz, feldspar and rock fragments, implies a modification of sediment transport mechanism on- and/or offshore, and/or a change in erosion patterns in the potential source areas. As it predates the onset of glaciation (Reece et al., 2011) tectonic processes are most likely to have triggered the change in sediment composition by changes in the center of erosion and sediment dispersal. The high abundance of coalified organic material in Unit VI implies a coal bearing horizon to have fed most of these deposits. Jaeger et al. (2014) suggest the Kulthieth Formation on the Yakutat terrane as main source. The Eocene (56 to 33.9 Ma) Kulthieth Formation mostly consists of fluvial, lacustrine, shallow marine and local debris flow deposits, coal bearing arkosic sandstones rich in mica and feldspar up to 1.5 km thick, carbonaceous siltstone shale and coal, commonly intensively deformed sedimentary deposits, and some shallow marine sediments with up to 3 m thick coal layers (Winkler and Plafker, 1993; Plafker et al, 1994). Today, this formation is exposed in eastern Prince William Sound. Due to the northwestward movement of the Yakutat terrane since 10 Ma, these rocks must have been located further southeast during deposition of the site U1417 sediments. Geochemical and biomarker analysis of the coals from the Kulthieth Formation and the site U1417 sediments are being carried out to confirm the origin of the material (Childress et al., 2013). The Yakataga, Poul Creek and Kulthieth Formation have been found to differ in the biomarkers of their organic carbon (Childress and Ridgway, 2014). For now, the source region of these sediments cannot be further specified but a Yakutat terrane source is likely. The Yakataga Formation that has been deposited coevally with the Surveyor Fan sediments has itself been suggested to be sourced by two or more sources, most likely the Chugach-Prince William terrane and the Poul Creek and Kulthieth formation (Plafker et al.,

1994; Enkelmann et al., 2008; Perry et al., 2009). This is in line with erosion and transport of material from the Kulthieth Formation via the Yakataga Formation or directly into the precursor of today's Surveyor Fan at ca. 11 Ma.

The first increase in sediment accumulation in the Gulf of Alaska occurred between 9.87 and 9.47 Ma with deposition of the first turbidites which initiated the formation of the Surveyor Fan (Rea and Snoeckx, 1995). At the same time, deposition of unit VG from where sample 17Mi642 was taken started (ca. 8.5-9.5 Ma). This unit has been found to be very likely sourced by the CMC (Huber et al., 2018a, b). The high amount of metamorphic rock fragments (sample 17Mi642) supports this finding. The Chugach metamorphic complex is mainly made up of green to amphibolite facies schistose rocks (Plafker et al., 1994). Because of the Miocene position of site U1417 further to the southwest, an efficient transport system is required to feed material into the site U1417 region. Seismic data suggest transport of material from sources to the north into the precursor of the Surveyor Fan (Stevenson and Embley, 1987). Exhumation of the northeastern side of the St. Elias Syntaxis was extremely high at ca. 10 Ma and a fluvial system is considered to have existed, effectively eroding and exporting the material out of the orogen (Enkelmann et al., 2017). A link between these two inferred fluvial systems might explain the early input from the St. Elias orogen into the Surveyor Fan precursor. The change in sediment composition from mica and organic rich material to higher amounts of heavier minerals and rock fragments also implies changes in the transport regime to higher energy deposition.

While detailed analysis of heavy minerals from the Miocene to Pleistocene sediments from sites U1417 and U1418 show changes with depositional age (Huber et al, 2018b), the light mineral composition is very constant from late Miocene onwards for site U1417 and for the entire Pleistocene at the proximal site (U1418). This is not surprising as light mineral analysis has already been found to be less discriminative for provenance in general than heavy mineral analysis (von Eynatten et al., 2003) and many lithologies at the southern Alaska continental margin provide high amounts of quartz and feldspar (Bruand et al., 2014, Hudson and Plafker, 1982). Biotite, quartz and plagioclase have been found to make up 90% of the central part of the schist zone of the CMC. The lower grade metamorphic parts of the CMC show abundant recrystallization, and all contain quartz, plagioclase and biotite (Hudson and Plafker, 1982).

Still, the framework grains of the sediments give a general impression on the kind of sediment. Dickinson and Suzeck (1979) introduced the QFL-diagram to connect plate tectonic setting and sedimentary provenance. The relative amounts of quartz, feldspar and lithics are displayed, giving information on grain stability and thereby on weathering, relief of the source area, transport mechanisms and source rock type. The authors differentiate three types of sources: continental block, magmatic arc and recycled orogen (Dickinson and Suzeck, 1979; modified by Dickinson et al., 1983) (fig. 7). Garzanti et al. (2007) extended this concept and developed a conceptual provenance model for prediction of evolutionary trends of detrital modes and heavy-mineral assemblages of the detritus produced from various types of orogenic belts. They identified five main types of orogenic domains of which composite orogens are formed: magmatic arcs, obducted or accreted ophiolites, neo-metamorphic axial belts, accreted paleomargin remnants and accreted orogenic clastic wedges. Each of these domains has a corresponding sediment provenance type: "Magmatic Arc", "Ophiolite", "Axial-Belt", "Continental-Block", and "Clastic-Wedge" provenance. These different domains and their conjoined provenance types are combined to describe complex mixtures of detritus from orogens. The concept can be used to describe how detrital modes and heavy-mineral assemblages change during uplift and unroofing (Garzanti et al., 2007). These unroofing trends show wide overlap in sediment composition for different primary sediment sources (Garzanti, 2016). Therefore, QFL-plots cannot be used alone to unambiguously constrain the tectonic provenance of a sedimentary deposit but serve as an initial graphical classification tool (Garzanti, 2016).

We use the QFL-diagram to evaluate differences in the light mineral spectra with time of deposition and between the site U1417 and U1418 sediments. According to the classification of Dickinson and Suzeck (1979) all samples from site U1417 and U1418 imply a recycled orogen source matching an origin of the sediments in the Chugach, Prince-William and Yakutat

terranes. The slightly higher feldspar content of site U1418 sediments compared to site U1417 sediments might result from the position of site U1418 in relation to the tributary system of the Surveyor Fan. Plutons along the southern Alaska continental margin in the eastern and central CMC show granitoid to tonalitic compositions, while plutons in the east tend to have less quartz and more plagioclase, showing less granitic but more gabbroic composition (Bradley et al., 1993). Site U1418 sediments have been found to be sourced through the Bering-Bagley glacial system while site U1417 are sourced from a much wider part of the orogen (Dunn et al., 2017; Huber et al., 2018a, b), being in line with the difference in feldspar occurrence. K-feldspar is only present in very small amounts in all samples (0-3%). In the potential source region, K-feldspar has only been found in relevant amounts in the sedimentary units of the cretaceous Chugach terrane units in the Yakutat area (Zuffa et al., 1980). On average they show 5% K-feldspar with minimum values of 0.65 and maximum values of 14.5% (Zuffa et al., 1980). K-feldspar is absent in the amphibolite facies schists of the CMC while it is present in the migmatites in the central parts of the CMC (Hudson and Plafker, 1982). Therefore, the small amount of K-feldspar matches a Chugach and Yakutat terrane provenance but cannot be used to further define the provenance of the sediments.

The differences in the amount of the various types of rock fragments present in the samples, showing slightly decreasing amounts of metamorphic grains from the Miocene to the Pliocene and even lower numbers of metamorphic grains in all Pleistocene samples from both sites, support increasing derivation of material from the lower grade metamorphic or non-metamorphic units of the near shore on the Yakutat terrane in the Pliocene. Metapelites and metagraywacke are the main lithology of the Chugach metamorphic complex (Bruand et al., 2014). Greenschist facies phyllites occur outside the Chugach metamorphic complex while schist and migmatite are present within (Bruand et al., 2014). The phyllites have a monotonous petrography of chlorite, epidote, muscovite, plagioclase, quartz and biotite (Bruand et al., 2014).

The trend of increasing input from the areas closer to the coast with younger depositional age and increasing glaciation has also been indicated by zircon U/Pb age data (Huber et al., 2018a). Still, the position of the site very likely influences the sediment composition as the overall trend to higher amounts of metamorphic rock fragments found for site U1417 compared to site U1418 is also present in the average abundance of rock fragments in the fraction > 2mm as reported in IODP 341 Scientists (2014) (fig. 8).

Samples from site U1417 and U1418 plot in the same part of the QFL-diagram as quartzose samples from the Chugach flysch but are both different from refence data from the Poul Creek, Yakataga, Yakutat and Kulthieth formation and the Orca and Valdez group in the Prince William Sound area (fig. 7A, B). This supports substantial input from the Chugach area to all samples. Input from the other formations is also likely but appears to be diminished by the input form the Chugach area.

The high amount of iron-oxides in the coarser fractions of the mass transport deposit from site U1418 emphasize these sediments to have formed through different processes compared to the other sediments. Placer deposits rich in iron-oxides (e.g., ilmenite) make up many black beach sands along todays southern Alaska coast (Foley et al., 1995). The material of the mass transport deposit might be strongly influenced through reworking and sorting by nearshore processes. Consequently, these sediments cannot be used unambiguously to define an early Pleistocene baseline for comparison with the sediments deposited after the mid-Pleistocene transition.

In contrast, the suites of transparent heavy minerals of both sites show stronger differences (fig. 14). While the site U1417 sediments are rich in amphibole, plotting in the typical area for a clastic wedge or greenschist facies to amphibolite facies axial-belt provenance according to Garzanti et al. (2007). The site U1418 sediments show higher amounts of epidote, placing them in the middle of the unroofing trend typical for undissected arc settings Garzanti et al. (2007). This underlines the difference in provenance of the two sites being fed by different glacial system and different parts of the orogen.

Pyroxene is the most abundant ferromagnesian mineral, occurring in most igneous and metamorphic rocks. Pyroxene is used less frequently in provenance studies because it is less stable than other minerals (Mange and Morton, 2007). Still, when preserved, they can be very useful in provenance analysis (e.g., Cawood, 1983; Krawinkel et al., 1999; Caracciolo et al., 2016). In the site U1417 and U1418 samples pyroxene is well preserved. Augite appears together with pumpellyite, titanite, albite and quartz which is typical for the pumpellyite facies (Coombs, 1989) supporting input from the low-grade metamorphic areas close to the coast to all samples. The homogenous pyroxene composition points to a relatively constant source area with time. The higher amount of pyroxene present in the sediments at the proximal sites is in line with high input from the low-grade metamorphic rocks from the near shore areas on the Yakutat terrane.

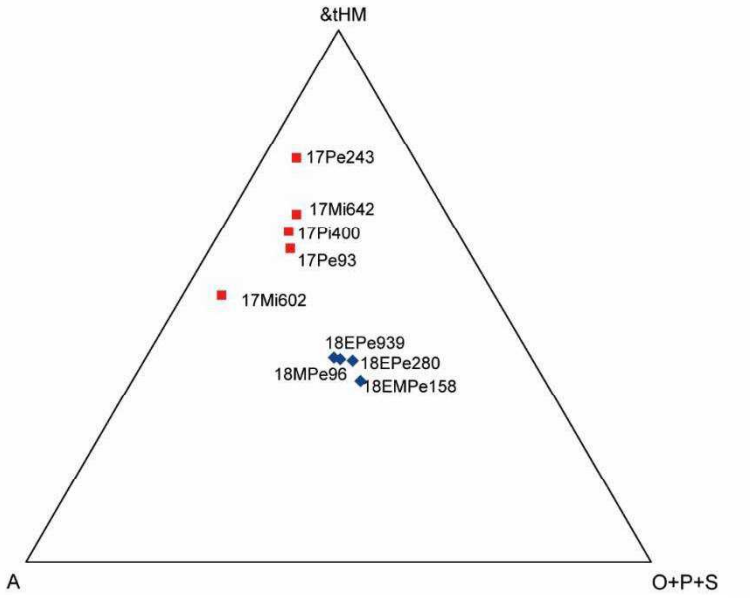

Figure 14: Triangular diagram after Garzanti et al., 2007 showing the heavy mineral composition of site U1417 and U1418 sediments. A = amphibole, &tHM = other transparent heavy minerals, O+P+S=olivine + pyroxene + spinel. Data from Huber et al, 2018b.

Epidote occurs in a large variety of rocks (Mange and Morton, 2007). Similar epidote compositions have been found for different rock types, prohibiting identification of their source rocks when mixed in a sedimentary deposit (Mange and Morton, 2007). Still, epidote makes up a large fraction of the heavy mineral spectra of site U1417 and U1418. The amount of epidote varies between the two sites. At the distal site, the epidote content rises from ca. 16% in the Miocene to 58% of the heavy mineral fraction of the Pleistocene sediments (Huber et al., 2018b). Within the Pleistocene samples from the proximal site (U1418), epidote content is relatively constant at ca. 22% to ca. 18% age (Huber et al., 2018b). Epidote together with quartz and albite has been described in the metabasalt belt cropping out along the southern border of the Chugach metamorphic complex (Lull and Plafker, 1989; Bruand et al., 2011). The rising amount of pyroxene present at the distal site from Miocene to Pliocene and especially in the Pleistocene is in line with an increasing input from this part of the orogen. Compared to the lower pyroxene abundance in the Pleistocene at the proximal site, the distal site receives much more input from this part of the metabasite belt. This again highlights the geographic position of the two sites relative to the continental margin and the tributary system of the Surveyor Fan to impact the mineral spectra as also indicated by pyroxene being less abundant at the distal site. Still, the mineral associations found for epidote and pyroxene all match a strong input from the lower grade metamorphic rocks on the Yakutat terrane to the proximal site and from the southern side of the Chugach metamorphic complex to the distal site during the Pleistocene being in line with high erosion rates in the nearshore areas funnelled by advancing glaciers.

A general change in provenance in response to the intensification of glaciation at the mid-Pleistocene transition could not be found in our data. The proximal site supplies mostly sediments of mid-Pleistocene or younger age with the only early Pleistocene sediments having been fed by a mass transport event, making different transport mechanisms very likely to have impacted the sediment composition as also indicated by the high amount of opaque oxide grains present in the mass transport deposit. This lowers the significance of the direct comparison of the early and middle Pleistocene sediments. Still, the framework compositions are similar indicating no major changes in sediment sources. Heavy mineral spectra, the

composition of amphibole and garnet as well as the zircon age data and the framework petrography are also homogeneous throughout the Pleistocene sediments (Huber et al., 2018 a, b). This implies that climatic changes at the mid-Pleistocene transition did not cause significant changes in the main area under erosion with glaciers eroding most of the material in their topographically predefined positions (Gulick et al., 2015). Similar results of homogenous heavy mineral spectra and amphibole and garnet geochemistry have been found for the middle Pleistocene to Holocene sediments from site U1419 and U1420 (Drewer, 2016). Examination of the silt sized fraction (15-63 µm) of surficial sediments collected throughout the Gulf of Alaska and of mid-Pleistocene sediments of IODP Expedition 341 sites are also in line with steady erosion centres determined by the strong interaction of the glacial coverage and tectonics at least since the mid-Pleistocene transition (Jaeger et al., 2017; Penkrot et al., 2017, 2018). Since the MPT at ca. 0.7 Ma, sediment sources are inferred to have been situated within a narrow band of ~200-1500 m elevation that coincides with the modern proposed last glacial maximum equilibrium-line altitude (ELA) range during the mid-late Pleistocene (<0.7 Ma), feeding sediments of relatively homogenous composition into the Gulf of Alaska through the Bering-Bagley and Malaspina glacial systems (Jaeger et al., 2017; Penkrot et al., 2017). Recent studies on glacimarine sediments from the Gulf of Alaska indicate a homogenous provenance for the past 50 kyr suggesting the position of the ELA to be not the main factor controlling glacial erosion centers, leaving tectonic forces as the more important determinant. Should the mass redistribution after the mid-Pleistocene transition have affected the stress regime of the orogen, this is not deducible with the applied methods from the offshore sedimentary record drilled.

4.8 Conclusion

Pyroxene and epidote geochemistry are very homogenous for all Miocene to Pleistocene samples thus indicating the absence of a general change of provenance regarding their source lithologies. Detailed analyses of pyroxene and epidote grains imply the metabasite belt at the southern border of the Chugach metamorphic complex as main source for the pyroxene and the low grade metamorphic rocks on the Yakutat terrane as sources for the epidotes. Rising amounts of epidote from Miocene to Pliocene and especially in the Pleistocene at the distal site are in line with increasing input from the metabasite belt at the southern edge of the Chugach metamorphic complex. This supports a general shift in erosion from the central part of the Chugach metamorphic complex to the southern flanks of the orogen with increasing glaciation. The higher amount of epidote in the Pleistocene sediments from the proximal site compared to the distal site are in line with higher contribution from the nearshore Yakutat terrane formations. The different positions of the sites in relation to the Surveyor Fan tributary system very likely caused different parts of the orogen to contribute variable amounts of material from different source rocks. This has also been found in zircon and heavy mineral data (Dunn et al., 2017; Huber et al., 2018a, b). In general, pyroxene and epidote data as well as the abundance of different rock fragments are in line with high contribution from relatively nearshore sources in the Pleistocene. This concurs with the increasing glaciation since the Miocene to shift erosion to the coast, which is enhanced by the onset of Northern Hemisphere glaciation in the Pleistocene.

ACKNOWLEDGEMENT

This study was funded by German Research Foundation (DFG) grant BA 1011/43-1 and -2. We thank M. Dröllner, Münster, for helping to process the samples and J. Berndt and B. Schmitte, Münster, for assistance with acquiring the microprobe data.

4.9 References cited

Arkle, J.C., Armstrong, P.A., Haeussler, P.J., Prior, M.G., Hartman, S., Sendziak, K.L., Brush, J.A., 2013. Focused exhumation in the syntaxis of the western Chugach Mountains and Prince William Sound, Alaska. Geol. Soc. America Bull. 125, 776–793.

Berger, A.L., Gulick, S.P.S., Spotila, J.A., Upton, P., Jaeger, J.M., Chapman, J.B., Worthington, L.A., Pavlis, T.L., Ridgway, K.D., Willems, B.A., McAleer, R.J., 2008a. Quaternary tectonic response to intensified glacial erosion in an orogenic wedge. Nature Geosci. 1, 793–799.

Berger, A.L., Spotila, J.A., 2008. Denudation and deformation in a glaciated orogenic wedge: The St. Elias orogen, Alaska. Geology 36, 523-526.

Berger, A.L., Spotila, J.A., Chapman, J.B., Pavlis, T.L., Enkelmann, E., Ruppert, N.A., Buscher, J.T., 2008b. Architecture, kinematics, and exhumation of a convergent orogenic wedge: A thermochronological investigation of tectonic–climatic interactions within the central St. Elias orogen, Alaska. Earth Planet. Sci. Lett. 270, 13–24.

Bradley, D.C., Haeussler, P.J., and Kusky, T.M. 1993. Timing of early Tertiary ridge subduction in southern Alaska. In: Dusel-Bacon, C., Till, A.B. (Eds.). Geologic studies in Alaska by the U.S. Geological Survey. U.S. Geol. Surv. Bull. 2068, 163-177.

Bradley, D.C., Kusky, T.M., Haeussler, P.J., Goldfarb, R.J., Miller, M.L., Dumoulin, J.A., Nelson, S.W., and Karl, S.M. 2003. Geologic signature of early Tertiary ridge subduction in Alaska. In: Sisson, V.B., Roeske, S.M., and Pavlis, T.L., (Eds.). Geology of a transpressional orogen developed during ridge-trench interaction along the North Pacific margin, vol. 371. Geol. Soc. Am., Boulder, Colo., p. 19–49.

Bruand, E., Gasser, D., Bonnand, P., Stuewe, K., 2011. The petrology and geochemistry of a metabasite belt along the southern margin of Alaska, Lithos 127, 282-297.

Bruand, E., Gasser, D., Stüwe, K., 2014. Metamorphic P–T conditions across the Chugach Metamorphic Complex (Alaska)—A record of focussed exhumation during transpression. Lithos 190-191, 292-312.

Bruhn, R.L., Pavlis, T.L., Plafker, G., Serpa, L., 2004. Deformation during terrane accretion in the Saint Elias orogen, Alaska, Geol. Soc. Am. Bull. 116, 771–787.

Bruns, T.R. 1983. Model for the origin of the Yakutat terrane, an accreting terrane in the northern Gulf of Alaska. Geology 11, 718–721.

Caracciolo, L., Orlando, A., Marchev, P., Critelli, S., Manetti, P., Raycheva, R., Riley, D., 2016. Provenance of Tertiary volcanoclastic sediment in NW Thrace (Bulgaria): Evidence from detrital amphibole and pyroxene geochemistry. Sed. Geology 336, 120-137.

Carlson, P.R., Stevenson, A.J., Bruns, T.R., Mann, D.M., Huggett, Q., 1996. Sediment pathways in the Gulf of Alaska from beach to abyssal plain. In: Gardner, J.V., Field, M.E., Twichell, D.C. (Eds.), Geology of the United States' Seafloor: The View from GLORIA. Cambridge University press, Cambridge, pp. 255-278.

Cawood, P.A., 1983. Modal Composition of detrital clinopyroxene geochemistry of lithic sandstones from New England Fold and Belt (east Australia): a Paleozoic terrane forearc. Geol. Soc. Am. Bull. 94, 199-1214.

Childress, L.B, Ridgway, K.D., 2014. Glacial and tectonic influence on terrestrial organic carbon delivery to high latitude deep marine systems: IODP Site U1417, Surveyor Fan, Gulf of Alaska. AGU Fall Meeting 2014, abstract id. PP23D-05

Childress, L B., Ridgway, K.D., Blair, N.E., Bahlburg, H., Berbel, G., Cowan, E.A., Forwick, M., Gulick, S.P., Jaeger, J.M., Maerz, C., McClymont, E., Moy, C.M., Müller, J., Nakamura, A., Ribeiro, F., 2013. Potential links between onshore tectonics and terrestrial organic carbon delivery to distal submarine fan environments: IODP Site U1417, Surveyor Fan, Gulf of Alaska. AGU Fall Meeting, abstract id. T23D-2624.

Coombs, D.S., 1989. Prehnite–pumpellyite facies. In: Petrology. Encyclopedia of Earth Science. Springer, Boston, MA.

Dickinson, W.R., 1988. Provenance and sediment dispersal in relation to Platetectonics and Paleogeography of sedimentary basins. In: Keinsphen, K.L. and Paola, C., (Eds.) New perspectives in basin analysis. Berlin, Heidelberg, NY, Springer, p. 3-27.

Dickinson, W.R., Beard, L.S., Brakenridge, G.R., Erjavec, J.L., Ferguson, R.C., Inman, K.F., Knepp, R.A., Lindberg, F.A., Ryberg, P.T., 1983. Provenance of North American Phanerozoic sandstones in relation to tectonic setting. Geological Society of America Bulletin 94, 222-235.

Dickinson, W.R., Suzeck, C.A., 1979. Plate tectonics and sandstone compositions. Am. Assoc. Petroleum Geologists Bull. 63, 2164-2182.

Dobson, M.R., O´Leary, D., Veart, M., 1998. Sediment delivery to the Gulf of Alaska: source mechanisms along a glaciated transform margin. In: Stocker, M.S., Evans, D., Cramp, A. (Eds.), Geological Processes on Continental Margins: Sedimentation, Mass-Wasting and Stability. Geol. Soci. London, Special Publication 129, pp. 43-66.

Drewer, C. 2016. Provenanzanalyse an den Proben der Sites U1419 und U1420 der IODP Expedition 341 im Golf von Alaska. M.Sc. Thesis, WWU Münster, 134 p.

Dumoulin, J.A., 1987. Sandstone Composition of the Valdez and Orca Groups, Prince William Sound, Alaska. U.S. Geol. Surv. Bull. 1774.

Dunn, C.A., Enkelmann, E., Ridgway, K.D., Allen, W.K., 2017. Source to sink evaluation of sediment routing in the Gulf of Alaska and Southeast Alaska: A thermochronometric perspective. J. Geophys. Res. Earth Surf. 122, 711–734.

Enkelmann, E., Garver, J.I., Pavlis, T.L., 2008. Rapid exhumation of ice-covered rocks of the Chugach–St. Elias orogen, Southeast Alaska. Geology 36, 915–918.

Enkelmann, E., Koons, P.O., Pavlis, T.L., Hallet, B., Barker, A., Elliott, J., Garver, J.I., Gulick, S.P.S., Headley, R.M., Pavlis, G.L., Ridgway, K.D., Ruppert, N., van Avendonk, H.J.A., 2015. Cooperation among tectonic and surface processes in the St. Elias Range, Earth's highest coastal mountains. Geophys. Res. Lett. 42, 5838–5846.

Enkelmann, E., Piestrzeniewicz, A., Falkowski, S., Stübner, K., Ehlers, T.A., 2017. Thermochronology in southeast Alaska and southwest Yukon: Implications for North American Plate Response to Terrane Accretion. Earth Planet. Sci. Lett. 457, 348–358.

Enkelmann, E., Zeitler, P.K., Garver, J.I., Pavlis, T.L., Hooks, B.P., 2010. The thermochronological record of tectonic and surface process interaction at the Yakutat-North American collision zone in southeast Alaska. Am. J. Sci. 310, 231–260.

Enkelmann, E., Zeitler, P.K., Pavlis, T.L., Garver, J.I., Ridgway, K.D. 2009. Intense localized rock uplift and erosion in the St Elias orogen of Alaska. Nat. Geosci. 2, 360–363.

Expedition 341 Scientists, 2014. Southern Alaska Margin: interactions of tectonics, climate, and sedimentation. IODP Prel. Rep. 341. doi:10.2204/iodp.pr.341.2014.

Falkowski, S., Enkelmann, E., Ehlers, T.A., 2014. Constraining the area of rapid and deep-seated exhumation at the St. Elias syntaxis, Southeast Alaska, with detrital zircon fission-track analysis. Tectonics 33, 597–616.

Farris, D.W., Paterson, S.R., 2009. Subduction of a segmented ridge along a curved continental margin: Variations between the western and eastern Sanak–Baranof belt, southern Alaska. Tectonophysics 464, 100–117.

Finzel, E.S., Flesch, L.M., Ridgway, K.D., Holt, W.E., Ghosh, A., 2015. Surface motions and intraplate continental deformation in Alaska driven by mantle flow. Geophys. Res. Lett. 42, 4350-4358.

Finzel, E.S., Trop, J.M., Ridgway, K.D., Enkelmann, E., 2011. Upper plate proxies for flat-slab subduction processes in southern Alaska. Earth Planet. Sci. Lett., 303, 348-360.

Foley, J.Y., LaBerge, R.D., Grosz, A.E., Oliver, F.S., Hirt, W.C., 1995. Onshore Titanium and Related Heavy-Mineral Investigations in the Eastern Gulf of Alaska Region, Southern Alaska. United States department of the interior, U.S. Bureau of mines, Open File Report 10-95, 125 p.

Gasser, D., Bruand, E., Stüwe, K., Foster, D.A., Schuster, R., Fügenschuh, B., Pavlis, T., 2011. Formation of a metamorphic complex along an obliquely convergent margin: Structural and thermochronological evolution of the Chugach Metamorphic Complex, southern Alaska. Tectonics 30, TC2012. doi:10.1029/2010TC002776.

Garzanti, E., 2016. From static to dynamic provenance analysis—Sedimentary petrology upgraded. Sed. Geol. 336, 3-13.
Garzanti, E., Doglioni, C., Vezzoli, G., and Andò, S., 2007. Orogenic Belts and Orogenic Sediment Provenance. J. Geol. 115, 315-334.
Gulick, S.P.S., Jaeger, J.M., Mix, A.C., Asahi, H., Bahlburg, H., Belanger, C.L., Berbel, G.B.B., Childress, L., Cowan, E., Drab, L., Forwick, M., Fukumura, A., Ge, S., Gupta, S., Kioka, A., Konno, S., LeVay, L.J., März, C., Matsuzaki, K.M., McClymont, E.L., Moy, C., Müller, J., Nakamura, A., Ojima, T., Ribeiro, F.R., Ridgway, K.D., Romero, O.E., Slagle, A.L., Stoner, J.S., St-Onge, G., Suto, I., Walczak, M.D., Worthington, L.L., Bailey, I., Enkelmann, E., Reece, R., Swartz, J.M., 2015. Mid-Pleistocene climate transition drives net mass loss from rapidly uplifting St. Elias Mountains, Alaska. P. Natl. Acad. Sci. USA 112, 15042–15047.
Haeussler, P.J., Bradley, D.C., Wells, R.E., Miller, M.L. 2003. Life and death of the Resurrection plate: Evidence for its existence and subduction in the northeastern Pacific in Paleocene–Eocene time. Geol. Soc. Am. Bull. 115, 867-880.
Headley, R.M., Enkelmann, E., Hallet, B., 2013. Examination of the interplay between glacial processes and exhumation in the Saint Elias Mountains, Alaska. Geosphere 9, 229-241.
Hogan, L.G., Scheidegger, K.F., Kulm, L.D., Dymond, J., Mikkelsen, N., 1978. Biostratigraphic and tectonic implications of ^{40}Ar-^{39}Ar dates of ash layers from the northeast Gulf of Alaska. Geol. Soc. Am. Bull. 89, 1259-1264.
Hudson, T., Plafker, G., 1982. Paleogene metamorphism of an accretionary flysch terrane, eastern Gulf of Alaska. Geol. Soc. Am. Bull. 93, 1280-1290.
Huber, B., Bahlburg, H., Berndt, J., Dunkl, I., Gerdes, A., 2018a. Provenance of the Surveyor Fan and Precursor Sediments in the Gulf of Alaska—Implications of a Combined U-Pb, (U-Th)/He, Hf, and Rare Earth Element Study of Detrital Zircons. J. Geol. 126, 577-600.
Huber, B., Bahlburg, H., Pfänder, J.A., 2018b. Single grain heavy mineral provenance of garnet and amphibole in the Surveyor Fan and precursor sediments on the Gulf of Alaska abyssal plain - Implications for climate-tectonic interactions in the St. Elias orogen. Sed. Geol. 372, 173-192.
Ingersoll, R.V., Bullard, T.F., Ford, R.L., Grimm, J.P., Pickle, J.D., Sares, S.W., 1984. The effect of grain size on detrital modes: a test of the Gazzi-Dickinson point-counting method. J. Sed. Res. 54, 103–116.
Jaeger, J.M., Gulick, S.P.S., LeVay, L.J., Asahi, H., Bahlburg, H., Belanger, C.L., Berbel, G.B.B., Childress, L.B., Cowan, E.A., Drab, L., Forwick, M., Fukumura, A., Ge, S., Gupta, S.M., Kioka, A., Konno, S., März, C.E., Matsuzaki, K.M., McClymont, E.L., Mix, A.C., Moy, C.M., Müller, J., Nakamura, A., Ojima, T., Ridgway, K.D., Rodrigues Ribeiro, F., Romero, O.E., Slagle, A.L.,Stoner, J.S., St-Onge, G., Suto, I., Walczak, M.H., Worthington, L.L., 2014. Site U1417. In Jaeger, J.M., Gulick, S.P.S., LeVay, L.J., and the Expedition 341 Scientists, Proc. IODP, 341: College Station, TX (Integrated Ocean Drilling Program). doi:10.2204/iodp.proc.341.103.2014.
Jaeger, J.M., Salinas, J.K., Penkrot, M.L., Bruand, M., 2017. Persistence of the Pleistocene glacial buzzsaw in the St. Elias Mountains, Alaska. Geological Society of America Abstracts with Programs 49. doi:10.1130/abs/2017AM-303894.
Jones, D.L., Silberling, N. J., Coney, P. J., 1986. Collision tectonics in the Cordillera of western N America: examples from Alaska. Geol. Soc. London, Special Publications 19, 367-387.
Krawinkel, H., Wozazek, S., Krawinkel, J., Hellmann, W., 1999. Heavy-mineral analysis and clinopyroxene geochemistry applied to provenance analysis of lithic sandstones from the Azuero–Soná Complex (NW Panama). Sed. Geol. 24, Issues 1–4, 149-168.
Lagoe, M.B., Eyles, C.H., Eyles, N., Hale, C., 1993. Timing of late Cenozoic tidewater glaciation in the far North Pacific. Geol. Soc. Am. Bull. 105, 1542-1560.
Lagoe, M.B., Zellers, S.D., 1996. Climates and Climate Variability of the Pliocene Depositional and microfaunal response to Pliocene climate change and tectonics in the eastern Gulf of Alaska. Marine Micropaleontology 27, 121-140.

Lull, S., Plafker, G., 1985. Petrography of sandstone from the Yakutat Group, Malaspina District, Southern Alaska. In: Bartsch-Winkler, S., Reed, K.M., (Eds.). U.S. Geol. Surv. in Alaska: Accomplishments during 1983, pp. 73-77.

Mange, M.A., Morton, A.C., 2007. Chapter 13 Geochemistry of Heavy Minerals. In: Mange, M.A., Wright, D.T., (Eds.). Developments in Sedimentology, Elsevier, 58, pp. 345-391.

Manley, W. F., and Kaufman, D. S. 2002. Alaska Paleo-Glacier Atlas. Institute of Arctic and Alpine Research (INSTAAR), University of Colorado. http://instaar.coloradoq25 .edu/QGISL/ak_paleoglacier_atlas.

Mann, D.H., Hamilton, T.D., 1995. Late Pleistocene and Holocene paleoenvironments of the North Pacific coast. Quaternary Science Reviews 14, 449-47.

Meigs, A., Johnston, S., Garver, J., Spotila, J. 2008. Crustal-scale structural architecture, shortening, and exhumation of an active, eroding orogenic wedge (Chugach/St Elias Range, southern Alaska). Tectonics 27, TC4003. doi:10.1029/2007TC002168.

Mendenhall, W.C. 1905. Geology of the central Copper River region, Alaska. USGS Professional Paper 41, 133 p.

Molnia, B.F., 2008. Sattelite images atlas of glaciers of the world. Glacier of North America-Glaciers of Alaska. U.S. Geol. Surv. Professional Paper 1386, 525 p.

Nechaev, V. P., Isphording, W.C., 1993, Heavy-mineral assemblages of continental margins as indicators of plate-tectonic environments. Jour. Sed. Petrol. 63, 1110-1117.

Ness, G.E., Kulm, L.D., 1973. Origin and Development of Surveyor Deep-Sea Channel. Geol. Soc. Am. Bull. 84, 3339-335.

Pavlis, T.L., Chapman, J.B., Bruhn, R.L., Ridgway, K., Worthington, L.L., Gulick, S.P.S., Spotila, J., 2012. Structure of the actively deforming fold-thrust belt of the St. Elias orogen with implications for glacial exhumation and three-dimensional tectonic processes. Geosphere 8, 991–1019.

Pavlis, T.L., Sisson, V.B., 1995. Structural history of the Chugach metamorphic complex in the Tana River region, eastern Alaska: A record of Eocene ridge subduction. Geol. Soc. Am. Bull. 107, 1333-1355.

Penkrot, M.L., Jaeger, J.M., Cowan, E.A., Walczak, M.H., Mix, A.C., LeVay, L., 2018. Tectonic and Climate Influences on Spatial and Temporal Variations of Subglacial Erosion; Bering Glacier, Alaska. AGU Fall meeting, abstract id. C51E-1119.

Penkrot, M., Jaeger, J.M., Loss, D.P., Bruand, E., 2017. Persistence of the Pleistocene glacial buzzsaw in the St. Elias Mountains, Alaska. Geological Society of America Abstracts with Programs 49. doi:10.1130/abs/2017AM-303894.

Perry, S., Garver, J., Ridgway, K., 2009. Transport of the Yakutat Terrane, southern Alaska: evidence from sediment petrology and detrital zircon fission-track and U/Pb double dating. J. Geol. 117, 156–173.

Péwé, T.L., 1975. Quaternary Geology of Alaska. U.S. Geological Survey Professional Paper 835 (145 pp.).

Pettijohn, F.J., Potter, P. E., Siever, R., 1987. Sand and sandstones. Springer, New York, Berlin, Heidelberg, London, Paris, Tokyo, 2nd ed., 553 p.

Plafker, G., 1987. Regional geology and petroleum potential of the northern Gulf of Alaska continental margin. In: Scholl, D.W., Grantz, A., Vedder, J.G. (Eds.). Geology and resource potential of the continental margin of western North America and adjacent ocean basins—Beaufort Sea to Baja California. Circum-Pacific Council for Energy and Mineral Resources, Earth Sci. Ser. 6, 229–268.

Plafker, G., Moore, J., Winkler, G., 1994. Geology of the southern Alaska margin. In: Plafker, G., Berg, H. (Eds.). The geology of Alaska (Geology of North America, Vol. G-1). Boulder, CO, Geol. Soc. Am., p. 389–449.

Post, A. 1972. Periodic surge origin of folded medial moraines on Bering piedmont glacier, Alaska. J. Glaciol. 11, 219–226.

Rea, D.K., Snockx, H., 1995. Sediment Fluxes in the Gulf of Alaska: Paleoceanographic Record from Site 887 on the Patton-Murray Seamount Platform. In: Rea, D.K., Basov, I.A., Scholl, D.W., Allan, J.F. (Eds.). Proceedings of the Ocean Drilling Program: Scientific Results 145. doi:10.2973/odp.proc.sr.145.122.1995

Reece, R.S., Gulick, S.P.S., Horton, B.K., Christeson, G.L., Worthington, L.L., 2011. Tectonic and climatic influence on the evolution of the Surveyor fan and channel system, Gulf of Alaska. Geosphere 7, 830-844.

Reimann Zumsprekel C., Bahlburg H., Carlotto V., Boekhout F., Berndt J., Lopez S., 2015. Multi-method provenance model for early Paleozoic sedimentary basins of southern Peru and northern Bolivia (13°-18°S). J. S. Am. Earth Sci. 64, p. 94-115.

Sisson, V.B., Hollister, L.S., Onstott, T.C., 1989. Petrologic and age constraints on the origin of a low-pressure/high-temperature metamorphic complex, southern Alaska. J. Geophys. Res. 94, 4392-4410.

Sisson, V.B., Poole, A.R., Harris, N.R., Cooper Bruner, H., Pavlis, T.L., Copeland, P., Donelick, R.A., McClelland, W.C., 2003. Geochemical and geochronologic constraints for genesis of a tonalite-trondhjemite suite and associated mafic intrusive rocks in the eastern Chugach Mountains, Alaska: A record of ridge-transform subduction. In: Sisson, V.B., Roeske, S.M., Pavlis, T.L. (Eds.), Geology of a transpressional orogen developed during ridge-trench interaction along the North-Pacific margin. Geol. Soc. Spec. Pa. 371, Boulder, Colorado, pp. 293-326.

Spotila, J.A., Berger, A.L., 2010. Exhumation at orogenic indentor corners under long-term glacial conditions: Example of the St. Elias orogen, Southern Alaska. Tectonophysics 490, 241–256.

Spotila, J.A., Buscher, J.T., Meigs, A.J., Reiners, P.W., 2004. Long-term glacial erosion of active mountain belts: Example of the Chugach–St. Elias Range, Alaska. Geology 32, 501-504.

Stevenson, A.J., Embley, R., 1987. Deep-sea fan bodies, terrigenous turbidite sedimentation and petroleum geology, Gulf of Alaska. In: Scholl, D.W., Grantz, A., Vedder, J.G. (Eds.). Geology and Resource Potential of the Continental Margin of Western North America and Adjacent Ocean Basins—Beaufort Sea to Baja California. Circum-Pacific Council for Energy and Mineral Resources, AAPG Bookstore, Houston, Tex., Tulsa, Okla., p. 503–522.

Trop, J.M., Ridgway, K.D., Manuszak, J.D., Layer, P., 2002. Mesozoic sedimentary-basin development on the allochthonous Wrangellia composite terrane, Wrangell Mountains basin, Alaska: a long-term record of terrane migration and arc construction. Geol. Soc. Am. Bull. 114, 693-717.

Vermeesch, P., Resentini, A., Garzanti, E., 2016. An R package for statistical provenance analysis. Sedimentary Geology. doi:10.1016/j.sedgeo.2016.01.009.

von Eynatten, H., Barceló-Vidal, C., Pawlowski-Glahn, V., 2003. Composition and discrimination of sandstones: a statistical evaluation of different analytical methods. J. Sed. Res. 73, 47-57.

von Eynatten, H., Dunkl, I., 2012. Assessing the sediment factory: The role of single grain analysis. Earth-Science Reviews, 115, 97-120.

Weltje, G.J., von Eynatten, H., 2004. Quantitative provenance analysis of sediments: review and outlook. Sed. Geol., 171, 1-11.

White, T., Bradley, D., Haeussler, P., Rowley, D.B., 2017. Late Paleocene–Early Eocene Paleosols and a New Measure of the Transport Distance of Alaska's Yakutat Terrane. J. Geol. 125, 113-123.

Winkler, G.R., Plafker, G., 1993. Geologic map of the Cordova and Middleton Island quadrangles, southern Alaska: U.S. Geological Survey Miscellaneous Investigations Map I-1984, 1 sheet, scale 1:250,000.

Worthington, L.L., Daigle, H., Clary, W.A., Gulick, S.P.S., Montelli, A., 2018. High sedimentation rates and thrust fault modulation: Insights from ocean drilling offshore the St. Elias Mountains, southern Alaska. Earth. Planet. Sci. Lett., 483, 1-12.

Worthington, L.L., Gulick, S.P.S., Pavlis, T.L. 2010. Coupled stratigraphic and structural evolution of a glaciated orogenic wedge, offshore, St. Elias orogen, Alaska. Tectonics 29, TC6013. doi:10.1029/2010TC002723.

Yavuz, F. 2013. WinPyrox: A Windows program for pyroxene calculation classification and thermobarometry. American Mineralogist 98, 1338-1359.

Zuffa, G.G., Nilsen, T.H., Winkler, G.R., 1980. Rock-fragment petrography of the Upper Cretaceous Chugach terrane, southern Alaska: U.S. Geological Survey Open-File Report 80-713, 28 p.

5 Summary and Outlook

This study is part of an ongoing interdisciplinary approach carried out in the aftermath of IODP expedition 341 that involves several working groups working on different aspects in the fields of biogeochemistry, structural geology, thermochronology and sedimentology (e.g., Belanger et al., 2016; Gulick et al., 2015; Dunn et al., 2017; Montelli et al., 2017; Swayer et al., 2017; Müller et al., 2018; Worthington et al., 2018; Zirndorf et al., submitted). Detailed provenance analysis of Miocene to Pleistocene sediments from IODP expedition 341 sites U1417 and U1418 in the Gulf of Alaska was performed to unravel changes in provenance with time of deposition. These data were interpreted in the context of climate and tectonic events at the southern Alaska continental margin since the Miocene. Small sample volume, limited by the drill core diameter, small grain size, and missing high resolution geochemical, isotopic and petrographic data for the source rocks challenge the interpretation of the data. Ongoing studies of onshore material (e.g., Arntson et al., 2017; Dolcimascolo et al., 2017; Olson et al., 2017; Sophis et al., 2017) will help to build a more comprehensive database for comparison with the offshore data discussed in the present study.

The results of this work significantly further the understanding of the interplay of climate, tectonic and oceanographic events and processes during mountain building at the southern Alaska continental margin since the end of the Miocene. Our data are in line with tectonics as prevalent factor in determining the main erosion centers being modified through the changing glacial cover since the end of the Miocene. The study elucidates how changing degrees of glaciation modified the main centers of erosion and how the position of the study sites in relation to the tributary system impacts the obtained information.

(1) The single grain geochemical heavy mineral data on garnet and amphibole and multi-method zircon data imply all the recovered Miocene to Pleistocene sediments, from sites U1417 and U1418, to have been almost exclusively fed from persistent sources on the Chugach, Prince William and Yakutat terranes. Additional input from the Coast Plutonic Complex cannot be excluded but seems to have been minor as indicated also by previous studies (Perry et al., 2009). Glaciers continuously occupied the same areas during times of variable and overall increasing degree of glaciation in the Pleistocene feeding material with the same characteristics into the fan.

(2) The oldest sediments drilled, being of Miocene age, show high amounts of coalified organic material and are very likely related to the erosion of the Kulthieth formation on the Yakutat terrane. Analysis of the organic material from the oldest sediments found will show if these sediments were fed from the Kulthieth formation on the Yakutat terrane or from another source (Childress et al., 2013; 2014).

(3) Changing sediment composition indicates a shift in sedimentary provenance from a very likely Yakutat terrane, Kulthieth formation source for the oldest deposits in the Miocene to high input from the Chugach metamorphic complex supported by single grain geochemical and zircon data at ca. 11 Ma. This change predates the onset of glaciation in southern Alaska, leaving tectonic forces as the most likely cause. It coincided with the collision of the Yakutat terrane against the southern Alaska margin and reflects the onset of exhumation and erosion of the evolving St. Elias mountain belt. Erosion was focused in the Chugach metamorphic complex. Input into the precursor of the Surveyor Fan from the Chugach terrane in the late Miocene implies the existence of an effective transport system from the mountain range into the Gulf of Alaska. Drainage was oriented towards the southeast, as the position of today's IODP site U1417 had been situated further to the southeast at that time. The details of this sediment routing system could not be revealed in this study. Seismic data imply a channel system to have existed that today has already been subducted into the Aleutian trench (Stevenson and Embley, 1987). Unraveling the details of this source to sink connection is

difficult as onshore traces are most likely eroded or buried under the thick glacial cover and most of the offshore part of the hypothetical transport system has very likely already been subducted.

(4) Single grain geochemical analysis of heavy minerals and the geochronology of zircon age spectra indicate a progressive change in provenance from Miocene to Pliocene to sources closer to the coast, very likely caused by the increasing glaciation and erosion of the nearshore Yakutat terrane areas. This implies the increasing glaciation to have enhanced erosion in the newly glaciated areas in the spine of the orogen.

(5) Exhumation rates during the Miocene were at ca. 2.1 to 2.8 km/My but the large errors on the depositional ages and the thermochronological data do not allow a more precise determination. Small changes might be masked by these errors.

(6) Rock-fragments indicate a high input from non- and low-grade metamorphic sedimentary sources during the Pleistocene to both sites which is also implied by the low abundance of zircons that can be addressed to a source within the Chugach metamorphic complex as well as epidote and pyroxene data. Therefore, the enhanced glaciation since the beginning of Northern Hemisphere glaciation at the Plio-Pleistocene transition seems to have again intensified erosion in the nearshore areas. High abundances of amphibole in the Chugach metamorphic complex in comparison to the near shore areas and progressive exhumation of higher grade metamorphic rocks in that parts of the Chugach metamorphic complex that progressively came in the focus of erosion from Miocene to Pliocene, removing their lower grade metamorphic cover, might cause the amphibole data to imply higher contribution form the mostly amphibolite facies rocks in the Chugach metamorphic complex during the Pleistocene.

(7) Heavy mineral and zircon data as well as rock fragments show differences between sites U1417 and U1418. This is very likely the result of the position of site U1418 being situated adjacent to the Bering trough, funneling direct input from the Bering glacier and Bagley ice field, while the distal site (U1417) is fed by a wider part of the southern Alaska continental margin (Expedition 341 Scientists, 2014; Dunn et al., 2017). This hampers direct correlation and complementation of the datasets from the two sites.

(8) At both sites, heavy mineral spectra, the composition of amphibole and garnet as well as the zircon age data and the framework petrography are homogeneous throughout the Pleistocene. This implies that climatic changes at the mid-Pleistocene transition did not cause significant changes in the main area under erosion. The drainage area and glaciers seem to have remained in their topographically defined positions throughout, as assumed by Gulick et al. (2015). Low-temperature chronology studies of the same sediments could not reveal information on exhumation rates for this time frame as the transfer time of these signals is too long to have already arrived in the sedimentary record (Dunn et al., 2017). Similar results of homogenous heavy mineral spectra and amphibole and garnet geochemistry have been found for the middle Pleistocene to Holocene from site U1419 and U1420 (Drewer, 2016). If mass redistribution after the mid-Pleistocene transition affected the stress regime of the orogen, this is not deducible with the applied methods from the offshore sedimentary record drilled. Erosion might shift within an area of similar rocks cropping out, making these changes undistinguishable by sedimentary provenance analysis.

5.1 References Cited

Arntson, E., Olson, H., Davidson, C.M., Garver, J.I., 2017. Geochemistry, U-Pb ages, and Hf isotopes of the Mt Draper and Mt Stamy Plutons, Nunatak Fjord, Alaska: Implications for the Sanak-Baranof Belt. Geological Society of America Abstracts with Programs 49, No. 4 Honolulu, HI, doi: 10.1130/abs/2017CD-292866.

Belanger, C.L., Orhun, O.G., Schiller, C.M., 2016. Benthic foraminiferal faunas reveal transport dynamics and no-analog environments on a glaciated margin (Gulf of Alaska). Palaeogeography, Palaeoclimatology, Palaeoecology, 454, 54–64.

Childress, L., Ridgway, K.D., 2014. Glacial and tectonic influence on terrestrial organic carbon delivery to high latitude deep marine systems: IODP Site U1417, Surveyor Fan, Gulf of Alaska. AGU Fall Meeting 2014, San Francisco, abstract id. PP23D-05.

Childress, L B., Ridgway, K.D., Blair, N.E., Bahlburg, H., Berbel, G., Cowan, E.A., Forwick, M., Gulick, S.P., Jaeger, J.M., Maerz, C., McClymont, E., Moy, C.M., Müller, J., Nakamura, A., Ribeiro, F., 2013. Potential links between onshore tectonics and terrestrial organic carbon delivery to distal submarine fan environments: IODP Site U1417, Surveyor Fan, Gulf of Alaska. AGU Fall Meeting, abstract id. T23D-2624.

Dolcimascolo, A., Davidson, C., Garver, J.I., Sophis, J., 2017. Provenance and age of Granitoid and sandstone clasts in conglomerates of the Paleocene to Upper Cretaceous Yakutat Group, Russell Fjord, Alaska. Geological Society of America Abstracts with Programs. Vol. 49, No. 4, Honolulu, HI doi:10.1130/abs/2017CD-292921.

Drewer, C. 2016. Provenanzanalyse an den Proben der Sites U1419 und U1420 der IODP Expedition 341 im Golf von Alaska. M.Sc. Thesis, WWU Münster, 134 p.

Dunn, C.A.; Enkelmann, E.; Ridgway, K.D.; Allen, W.K., 2017. Source to sink evaluation of sediment routing in the Gulf of Alaska and Southeast Alaska: A thermochronometric perspective. J. Geophys. Res. Earth Surf. 122, 711–734.

Expedition 341 Scientists, 2014. Southern Alaska Margin: interactions of tectonics, climate, and sedimentation. IODP Prel. Rep. 341. doi:10.2204/iodp.pr.341.2014.

Gulick, S.P.S., Jaeger, J.M., Mix, A.C., Asahi, H., Bahlburg, H., Belanger, C.L., Berbel, G.B.B., Childress, L., Cowan, E., Drab, L., Forwick, M., Fukumura, A., Ge, S., Gupta, S., Kioka, A., Konno, S., LeVay, L.J., März, C., Matsuzaki, K.M., McClymont, E.L., Moy, C., Müller, J., Nakamura, A., Ojima, T., Ribeiro, F.R., Ridgway, K.D., Romero, O.E., Slagle, A.L., Stoner, J.S., St-Onge, G., Suto, I., Walczak, M.D., Worthington, L.L., Bailey, I., Enkelmann, E., Reece, R., Swartz, J.M. 2015. Mid-Pleistocene climate transition drives net mass loss from rapidly uplifting St. Elias Mountains, Alaska. P. Natl. Acad. Sci. USA 112, 15042–15047.

Jaeger, J.M., Salinas, J.K., Penkrot, M.L., Bruand, M., 2017. Persistence of the Pleistocene glacial buzzsaw in the St. Elias Mountains, Alaska. Geological Society of America Abstracts with Programs 49. doi:10.1130/abs/2017AM-303894.

Montelli, A., Gulick, S.P.S., Worthington, L.L., Mix, A., Davies-Walczak, M., Zellers, S.D., and Jaeger, J.M., 2017. Late Quaternary glacial dynamics and sedimentation variability in the Bering Trough, Gulf of Alaska. Geology 45, 251–254.

Müller, J., Romero, O., Cowan, E.A., McClymont, E.L., Forwick, M., Asahi, H., März, C., et al., 2018. Cordilleran ice-sheet growth fueled primary productivity in the Gulf of Alaska, northeast Pacific Ocean. Geology 46, 307–310.

Olson, H., Sophis, J., Davidson, C, and Garver, JI, 2017. Detrital zircon from the Yakutat terrane: differentiating the Yakutat Group and the Schist of Nunatak Fjord. Geological Society of America Abstracts with Programs. 49, No. 4, Honolulu, HI doi: 10.1130/abs/2017CD-292889.

Perry, S., Garver, J., Ridgway, K., 2009. Transport of the Yakutat Terrane, southern Alaska: evidence from sediment petrology and detrital zircon fission-track and U/Pb double dating. J. Geol. 117, 156–173.

Sawyer, D.E., Reece, R.S., Gulick, S.P.S., and Lenz, B.L., 2017. Submarine landslide and tsunami hazards offshore southern Alaska: seismic strengthening versus rapid sedimentation. Geophys. Res. Lett., 44(16), 8435–8442.

Sophis, J.M., Garver, J.I., Davidson, C.M., Dolcimascolo, A., and Olson, H., 2017. Provenance and age distribution of detrital zircon in the Upper Cretaceous-Paleocene flysch and mélange of the Yakutat Group, Yakutat Bay and Russell Fjord, Alaska, Geological Society of America Abstracts with Programs 49, No. 4, Honolulu, HI, doi: 10.1130/abs/2017CD-292959.

Stevenson, A., J., Embley, R., 1987. Deep-sea fan bodies, terrigenous turbidite sedimentation and petroleum geology, Gulf of Alaska. In: Scholl, D.W., Grantz, A., Vedder, J.G. (Eds.). Geology and Resource Potential of the Continental Margin of Western North America and Adjacent Ocean Basins—Beaufort Sea to Baja California. Circum-Pacific Council for Energy and Mineral Resources, AAPG Bookstore, Houston, Tex., Tulsa, Okla., p. 503–522.

Worthington, L.L., Daigle, H., Clary, W.A., Gulick, S.P.S., and Montelli, A., 2018. High sedimentation rates and thrust fault modulation: insights from ocean drilling offshore the St. Elias Mountains, southern Alaska. Earth Planet. Sci. Lett., 483, 1–12.

Zindorf, M., März, C., Wagner, T., Gulick, S.P.S., Strauss, H., Benowitz, J., Jaeger, J., Schnetger, B., Childress, L., Land, C.v.d., La Rosa, M., and LeVay, L., submitted. Deep sulphate-methane-transition and sediment diagenesis in the Gulf of Alaska (IODP Site U1417). Geochim. Cosmochim Ac.

6 Acknowledgements

During the last four years many different people supported and encouraged me in many ways, I am very thankful for each one. First, I want to thank the people that made this work possible. Special thanks go to Prof. Dr. Heinrich Bahlburg who gave me the opportunity to do this PhD thesis and supervised this work. I am thankful for all the discussions, encouragement and trust you had in me. I also thank István Dunkel for being the second reviewer and for helping with the (U-Th)/He dating. I thank the IODP for providing the samples for my studies and the Deutsche Forschungsgemeinschaft for financial support of my research work.

Many different people helped me with the preparation of the samples and all the different measuring methods used, sharing their knowledge with me. I thank Maximilian Dröllner for all the help with lab work. It was great to know that my samples are in good hands when you were working with them. I thank Beate Schmitte and Jasper Berndt Gerdes for all the help and support with the microprobe and laser measurements. I always enjoyed working with you. I want to thank Maik Trogisch, Gerd Schreiber and the members of the geological preparation workshop for help with the preparation of thinsections and mineral mounts. I thank Jörg Pfänder, Freiberg for Ar/Ar dating. I thank Axel Gerdes for help with the Hf-isotope measurements.

I thank Vanessa Nentwig, Elke Hahnenkamp, Reinhard Wolf, Flora Bokhout, Vanessa Fichtner, Franziska Nenning, Katharina Siedenberg, Daniela Oberleitner, Caroline Heineke and Paula Castillo for all the nice lunch times, talks on the corridor and fruitful discussions and advices. Special thanks go to Flora Boukout and Vanessa Nentwig for always being a friend when I needed one. I always enjoyed our talks and appreciate your help and availability for all kind of questions. I thank Julian Hülscher for sharing an office with me and folding a big pile of sampling bags while sitting in an airplane. I thank all my friends from the chemistry department for the Wednesday lunches, encouraging talks and funny evenings we had allowing me to sometimes forget about work. I also thank all my other friends for being a mental support and all the times when you lightened up my day. I also want to thank my oldest friend which will not be able to read this as horses can’t read but I hope that the big pile of carrots I bring you will at least help to let you partly understand how much the time we spent together almost every day enriches my life and helped me to finish this thesis. Big thanks go to my family that always supported and believed in me and red through parts of this work.

7 Curriculum Vitae

8 Appendix

8.1 Appendix for Huber et al., 2018; Sedimentary Geology

8.1.1 Appendix A: Sample names and IODP codes

sample name	IODP label identifier
17Pe87	341-U1417C-11H-2-W 70/72-BAHL
17Pe92	341-U1417C-11H-6-W 18/21-BAHL
17Pe143	341-U1417D-17H-4-W 104/105-BAHL
17Pe181	341-U1417D-25H-1-W 148/150-BAHL
17Pe243	341-U1417D-40X-1-W 52/54-BAHL
17Pi400	341-U1417E-7R-2-W 15/24-BAHL
17Mi439	341-U1417E-11R-CC-W 0/14-BAHL
17Mi603	341-U1417E-28R-2-W 0/13-BAHL
17Mi622	341-U1417E-30R-1-W 4/5-BAHL
17Mi642	341-U1417E-32R-1-W 113/120-BAHL
17Mi704	341-U1417E-39R-4-W 144/149-BAHL
18MPe37	341-U1418C-5H-1-W 69/76-BAHL
18MPe50	341-U1418D-6H-7-W 48/51-BAHL
18MPe84	341-U1418C-12H-2-W 94/96-BAHL
18MPe105	341-U1418D-12H-CC-W 6/8-BAHL
18MPe118	341-U1418A-14H-1-W 34/37-BAHL
18MPe119	341-U1418D-14H-4-W 56/60-BAHL
18MPe133	341-U1418C-21H-4-W 62/64-BAHL
18MPe157	341-U1418E-11H-3-W 81/83-BAHL
18MPe158	341-U1418D-18H-5-W 115/118-BAHL
18MPe159	341-U1418C-24H-3-W 99/101-BAHL
18MPe160	341-U1418E-11H-4-W 146/147-BAHL
18MPe164	341-U1418D-19H-3-W 17/20-BAHL
18MPe170	341-U1418A-25H-1-W 87/91-BAHL
18MPe203	341-U1418A-32H-1-W 14/16-BAHL
18MPe233	341-U1418D-27H-3-W 7/10-BAHL
18MPe247	341-U1418D-30H-3-W 28/30-BAHL
18MPe250	341-U1418D-31H-2-W 36/37-BAHL
18MPe280	341-U1418D-35X-3-W 53/58-BAHL
18EPe900	341-U1418F-68R-1-W 27/33-BAHL
18EPe939	341-U1418F-72R-1-W 1/19-BAHL
18EPe941	341-U1418F-72R-2-W 67/73-BAHL

8.1.2 Appendix B: Analytical details

Sample preparation and analytical methods

The samples were wet sieved to remove grains smaller 63 µm. The grain size fraction 63-250 µm was chosen for analyses. Small amounts of the heavy mineral fraction were mounted on microscopy slides using epoxy and grinded to ca. 30 µm. On each slide, 300 grains were point counted under a microscope using the Gazzi-Dickinson point counting method (Gazzi, 1966; Dickinson, 1970). For analysis of garnet and amphibole geochemistry, the heavy mineral fractions were separated using Na-Polytungstate with a density of 2.95 g/cm^3 and divided according to magnetic properties using a Frantz magnetic separator. Ca. 50 amphiboles (some samples did provide less material) and all garnet available were hand-picked from the heavy mineral separates under a binocular, mounted in epoxy, grinded to expose the central part of the grains and were polished. Major element geochemistry was measured using a JEOL JXA 8900 Microprobe at the Institute of Mineralogie at the University of Münster. Measurement conditions were at 15 kV acceleration potential, 15nA beam current and a spot size of 5 µm. All analyses were carried out close to the mineral cores to get a general impression on mineral geochemistry, avoiding inclusions and zones of structural damage. For evaluation of garnet zoning patterns, lines with 12 measuring points from rim to rim and per grain across 32 garnet grains were measured. The amphibole data were processed with the software WinAmphcal (Yavuz, 2007) and classified according to the rules of the International Mineralogical Association (IMA) from 2004 (Appendix C). Garnet data were processed using an Excel spreadsheet after Locock (2008). The spreadsheet calculates Fe^{2+} and Fe^{3+} based on stoichiometry (Locock, 2008; Appendix D).

For $^{40}Ar/^{39}Ar$ single grain dating, the largest biotite and amphibole grains available were chosen under a binocular and cleaned by washing with distilled water in an ultrasonic bath. Single grain total fusion was performed at Argonlab Freiberg (ALF), TU Freiberg, Germany. Individual grains were packed onto an Al disc for neutron irradiation, which was done for 3h at the LVR-15 research reactor of the Nuclear Research Institute in Řež, Czech Republic. The thermal neutron flux was ~8×1013 n/cm2s at a thermal to fast neutron ratio of ~1.1. After irradiation, individual grains were loaded onto an oxygen-free copper disc, and fused using a power-controlled floating 30W New Wave CO_2 laser system with a defocused beam having a diameter between 1.0 and 1.5 mm. Laser degassing time was 5 min per step. One large amphibole grain (7.3 mg) was analyzed by step-heating using a Createc HTC (details are given in Pfänder et al., 2014). Argon isotope compositions were measured in static mode on a GV Instruments ARGUS noble gas mass spectrometer. Data reduction and age calculation was done applying an in-house developed Matlab® toolbox, reported errors are 1σ, the external reproducibility is in the order of ± 1-2%. Ages were calculated relative to an age of 25.682 ± 0.030 Ma of our in-house sanidine fluence monitor DRF1 (calibrated against Fish Canyon Tuff sanidine using 28.305 ± 0.036 Ma; Renne at al., 2010). Decay constants used are from Renne et al. (2010). Atmospheric correction was achieved using $^{40}Ar/^{36}Ar$ = 298.6 ± 0.3 (Lee et al., 2006). Corrections for interfering Ar isotope abundances were done using $(^{36}Ar/^{37}Ar)_{Ca}$ = 0.000227 ± 0.000002, $(^{39}Ar/^{37}Ar)Ca$ = 0.000602 ± 0.000006, $(^{38}Ar/^{39}Ar)_K$ = 0.01211 ± 0.00061, $(^{40}Ar/^{39}Ar)_K$ = 0.00183 ± 0.00009. Results are reported in Appendix E.

8.1.2.1 References

Dickinson, W.R., 1970. Interpreting detrital modes of graywacke and arkose. J. Sed. Petrol. 40, 695-707.

Gazzi, P., 1966. Le arenarie del flysch sopracretaceo dell`Appennino modenese; correlazioni con il flysch di Monghidoro. Mineralogica e Petrografica Acta 12, 69-97.

Lee, JY, Marti, K., Severinghaus, J.P., Kawamura, K., Yoo, H.S., Lee, J.B., Kim, J.S., 2006. A redetermination of the isotopic abundances of atmospheric Ar. Geochim. Cosmochim Ac. 70, 4507-4512.

Locock, A.J., 2008. An Excel spreadsheet to recast analyses of garnet into end-member components, and a synopsis of the crystal chemistry of natural silicate garnets. Comput. Geosci. 34, 1769-1780.

Pfänder, J. A., Sperner, B., Ratschbacher, L., Fischer, A., Meyer, M., Leistner, M., Schaeben, H., 2014. High-resolution $^{40}Ar/^{39}Ar$ dating using a mechanical sample transfer system combined with a high-temperature cell for step heating experiments and a multicollector ARGUS noble gas mass spectrometer. Geochem. Geophys., Geosy. 15, 2713-2726.

Renne, P.R., Mundil, R., Balco, G., Kyoungwon Min, and Ludwig, K.R., 2010. Joint determination of ^{40}K decay constants and $^{40}Ar/^{40}K$ for the Fish Canyon sanidine standard, and improved accuracy for $^{40}Ar/^{39}Ar$ geochronology. Geochim. Cosmochim. Ac. 74, 5349-5367.

Yavuz, F., 2007. WinAmphcal. A Windows program for the IMA-04 amphibole classification. Geochem. Geophys. Geosys. 8. doi:10.1029/2006GC001391.

8.1.1 Appendix C: Geochemical data of amphiboles from site U1417 and U1418

COMPOSITION OF AMPHIBOLE FROM SITE U1417, DISTAL SITE																	
	Analysis (wt%)																
sample name	Na_2O	MgO	SiO_2	Al_2O_3	K_2O	CaO	FeO	TiO_2	Cr_2O_3	MnO	Total	Al(T)	Ti(T)	[Al(C)	Ti(C)	Groups	Names
17Pe87	1.03	10.21	45.59	9.33	0.82	11.51	16.56	1.25	0.00	0.42	96.72	1.18	0.00	0.46	0.14	Calcic amphibole	Magnesiohornblende
17Pe87	1.74	13.96	44.62	10.31	0.54	11.01	12.43	1.57	0.11	0.23	96.53	1.52	0.00	0.25	0.17	Calcic amphibole	Tschermakite
17Pe87	1.11	11.40	46.42	7.95	0.81	10.76	17.15	0.77	0.03	0.48	96.88	1.15	0.00	0.23	0.09	Calcic amphibole	Magnesiohornblende
17Pe87	0.94	12.90	46.93	7.69	0.74	11.82	14.24	1.14	0.02	0.45	96.86	1.10	0.00	0.24	0.13	Calcic amphibole	Magnesiohornblende
17Pe87	0.94	11.81	47.66	8.18	0.16	11.40	15.36	0.26	0.01	0.83	96.60	0.91	0.00	0.52	0.03	Calcic amphibole	Magnesiohornblende
17Pe87	2.25	11.73	42.07	13.76	0.09	11.85	13.08	1.47	0.09	0.26	96.65	1.79	0.00	0.60	0.16	Calcic amphibole	Pargasite
17Pe87	0.88	11.58	46.41	8.06	0.72	11.41	15.34	0.83	0.00	1.28	96.52	1.12	0.00	0.29	0.09	Calcic amphibole	Magnesiohornblende
17Pe87	1.72	12.64	45.55	12.65	0.15	11.24	11.81	0.62	0.08	0.22	96.68	1.41	0.00	0.74	0.07	Calcic amphibole	Magnesiohornblende
17Pe87	1.02	11.86	46.96	7.59	0.71	11.78	15.73	1.10	0.02	0.45	97.23	1.06	0.00	0.26	0.12	Calcic amphibole	Magnesiohornblende
17Pe87	0.85	14.41	50.76	4.73	0.35	11.78	13.36	0.51	0.01	0.61	97.38	0.66	0.00	0.15	0.06	Calcic amphibole	Magnesiohornblende
17Pe87	1.02	11.89	46.10	7.75	0.89	11.89	15.94	1.28	0.01	0.45	97.21	1.16	0.00	0.19	0.14	Calcic amphibole	Magnesiohornblende
17Pe87	1.42	12.62	44.65	13.17	0.36	11.30	12.55	0.81	0.16	0.34	97.36	1.59	0.00	0.64	0.09	Calcic amphibole	Tschermakite
17Pe87	1.62	13.05	45.75	10.29	0.30	11.55	12.78	1.37	0.32	0.09	97.12	1.35	0.00	0.42	0.15	Calcic amphibole	Magnesiohornblende
17Pe87	0.96	11.63	46.85	6.98	0.78	11.57	16.03	1.05	0.01	0.62	96.49	1.01	0.00	0.22	0.12	Calcic amphibole	Magnesiohornblende
17Pe87	1.22	14.22	47.00	8.69	0.19	10.22	13.63	1.21	0.02	0.51	96.91	1.10	0.00	0.41	0.13	Calcic amphibole	Magnesiohornblende
17Pe87	1.01	10.91	47.31	7.62	0.78	10.96	16.78	1.57	0.05	0.41	97.40	1.02	0.00	0.30	0.17	Calcic amphibole	Magnesiohornblende
17Pe87	1.07	12.02	46.12	8.66	0.69	11.58	15.42	0.67	0.05	0.45	96.72	1.19	0.00	0.32	0.07	Calcic amphibole	Magnesiohornblende
17Pe87	0.96	10.17	43.45	11.07	0.94	11.56	17.05	0.87	0.00	0.45	96.51	1.44	0.00	0.53	0.10	Calcic amphibole	Magnesiohornblende
17Pe87	1.20	14.87	46.67	8.27	0.56	11.02	11.55	1.92	0.00	0.29	96.35	1.25	0.00	0.16	0.21	Calcic amphibole	Magnesiohornblende
17Pe87	1.72	12.45	43.52	11.26	0.58	10.77	14.26	1.50	0.03	0.29	96.37	1.62	0.00	0.33	0.17	Calcic amphibole	Tschermakite
17Pe87	1.24	11.40	45.69	7.95	0.83	10.93	15.70	1.87	0.00	0.63	96.24	1.18	0.00	0.22	0.21	Calcic amphibole	Magnesiohornblende
17Pe87	1.11	14.76	48.11	7.21	0.23	10.41	12.63	0.83	0.01	0.67	95.97	0.89	0.00	0.36	0.09	Calcic amphibole	Magnesiohornblende
17Pe87	1.03	12.09	46.23	8.62	0.62	11.02	15.00	1.37	0.00	0.29	96.27	1.19	0.00	0.31	0.15	Calcic amphibole	Magnesiohornblende
17Pe87	1.14	11.46	44.57	8.62	1.05	11.76	15.89	1.11	0.02	0.48	96.10	1.29	0.00	0.24	0.13	Calcic amphibole	Magnesiohornblende
17Pe87	1.29	14.40	46.68	8.90	0.23	10.48	13.45	1.00	0.00	0.52	96.95	1.16	0.00	0.38	0.11	Calcic amphibole	Magnesiohornblende
17Pe87	1.39	14.04	45.97	9.49	0.25	10.45	13.87	1.10	0.00	0.52	97.08	1.25	0.00	0.39	0.12	Calcic amphibole	Magnesiohornblende
17Pe87	1.24	14.78	47.46	8.36	0.22	10.37	12.50	0.94	0.02	0.48	96.37	1.02	0.00	0.43	0.10	Calcic amphibole	Magnesiohornblende
17Pe87	1.47	13.28	45.48	10.00	0.30	10.42	13.74	1.08	0.03	0.66	96.46	1.25	0.00	0.50	0.12	Calcic amphibole	Magnesiohornblende
17Pe87	1.12	11.64	46.13	7.44	0.83	10.99	16.25	1.29	0.00	0.63	96.33	1.13	0.00	0.17	0.15	Calcic amphibole	Magnesiohornblende

17Pe87	1.40	13.32	45.68	9.81	0.29	10.47	14.06	1.05	0.00	0.52	96.59	1.24	0.00	0.48	0.12	Calcic amphibole	Magnesiohornblende
17Pe87	1.06	11.53	46.18	7.67	0.90	10.97	16.80	1.41	0.00	0.34	96.86	1.16	0.00	0.18	0.16	Calcic amphibole	Magnesiohornblende
17Pe87	1.60	10.88	43.95	11.52	0.46	11.44	14.86	1.02	0.05	0.22	95.99	1.45	0.00	0.58	0.11	Calcic amphibole	Magnesiohornblende
17Pe87	1.32	14.77	48.10	7.81	0.16	10.42	12.85	0.76	0.00	0.57	96.76	0.95	0.00	0.40	0.08	Calcic amphibole	Magnesiohornblende
17Pe87	0.97	12.16	45.59	9.96	0.51	11.69	14.18	0.54	0.07	0.37	96.03	1.27	0.00	0.46	0.06	Calcic amphibole	Magnesiohornblende
17Pe87	0.83	12.88	47.15	8.64	0.38	11.14	13.98	1.16	0.00	0.47	96.62	1.03	0.00	0.48	0.13	Calcic amphibole	Magnesiohornblende
17Pe87	0.98	10.67	46.37	7.65	0.39	10.65	19.05	0.98	0.07	0.46	97.26	1.03	0.00	0.32	0.11	Calcic amphibole	Magnesiohornblende
17Pe87	1.05	12.07	46.58	7.64	0.86	11.63	14.87	1.73	0.02	0.51	96.96	1.10	0.00	0.23	0.19	Calcic amphibole	Magnesiohornblende
17Pe87	1.06	12.38	46.44	8.15	0.65	11.53	15.30	1.02	0.00	0.55	97.08	1.18	0.00	0.23	0.11	Calcic amphibole	Magnesiohornblende
17Pe87	0.63	11.07	48.75	5.64	0.48	11.85	17.06	1.24	0.01	0.59	97.33	0.77	0.00	0.22	0.14	Calcic amphibole	Magnesiohornblende
17Pe87	1.49	14.09	46.85	9.12	0.11	10.11	13.77	0.74	0.04	0.42	96.74	1.10	0.00	0.48	0.08	Calcic amphibole	Magnesiohornblende
17Pe87	0.91	12.47	46.96	6.99	0.66	11.84	15.10	0.84	0.02	0.85	96.62	1.05	0.00	0.18	0.09	Calcic amphibole	Magnesiohornblende
17Pe87	1.53	12.73	44.08	10.92	0.29	10.33	14.72	1.15	0.00	0.63	96.37	1.43	0.00	0.48	0.13	Calcic amphibole	Magnesiohornblende
17Pe87	1.09	10.81	45.21	8.46	1.02	11.57	17.05	1.04	0.03	0.49	96.76	1.23	0.00	0.27	0.12	Calcic amphibole	Magnesiohornblende
17Pe87	1.40	13.59	46.02	9.73	0.25	10.52	13.63	1.18	0.00	0.47	96.79	1.21	0.00	0.48	0.13	Calcic amphibole	Magnesiohornblende
17Pe87	1.49	13.63	45.92	12.81	0.06	11.91	10.13	0.35	0.65	0.19	97.15	1.42	0.00	0.74	0.04	Calcic amphibole	Magnesiohornblende
17Pe87	2.40	16.59	43.00	13.31	0.19	11.22	7.42	1.53	0.13	0.16	95.94	1.86	0.00	0.38	0.16	Calcic amphibole	Tschermakite
17Pe87	1.23	11.24	44.24	9.66	1.08	11.45	15.64	2.09	0.01	0.36	97.00	1.42	0.00	0.28	0.23	Calcic amphibole	Magnesiohornblende
17Pe87	1.70	9.26	43.51	11.05	0.61	11.62	17.95	0.73	0.06	0.34	96.83	1.44	0.00	0.52	0.08	Calcic amphibole	Magnesiohornblende
17Pe87	1.48	8.21	42.51	16.51	0.25	11.00	16.15	0.22	0.10	0.47	96.90	1.75	0.00	1.12	0.02	Calcic amphibole	Tschermakite
17Pe87	1.68	10.46	44.13	11.55	0.28	11.85	16.19	0.62	0.00	0.23	96.99	1.45	0.00	0.58	0.07	Calcic amphibole	Magnesiohornblende
17Pe87	1.19	13.08	47.00	8.61	0.05	11.81	12.50	1.03	0.72	0.18	96.17	1.10	0.00	0.39	0.11	Calcic amphibole	Magnesiohornblende
17Pe87	0.89	13.34	47.15	9.75	0.23	10.96	12.68	0.63	0.00	0.38	96.01	1.04	0.00	0.65	0.07	Calcic amphibole	Magnesiohornblende
17Pe87	1.03	12.75	47.07	7.80	0.49	11.25	14.68	1.05	0.03	0.58	96.73	1.11	0.00	0.23	0.12	Calcic amphibole	Magnesiohornblende
17Pe87	1.07	12.35	46.55	7.69	0.78	11.73	14.61	1.50	0.00	0.51	96.80	1.11	0.00	0.23	0.17	Calcic amphibole	Magnesiohornblende
17Pe87	0.99	12.61	47.32	7.35	0.41	10.94	15.15	0.88	0.00	0.62	96.27	0.93	0.00	0.37	0.10	Calcic amphibole	Magnesiohornblende
17Pe87	1.55	8.20	42.45	12.85	0.44	10.73	19.26	0.68	0.01	0.50	96.67	1.65	0.00	0.62	0.08	Calcic amphibole	Tschermakite
17Pe87	1.57	8.07	41.77	13.19	0.45	10.64	19.30	0.57	0.04	0.43	96.02	1.71	0.00	0.63	0.06	Calcic amphibole	Tschermakite
17Pe87	1.14	11.99	45.69	8.30	0.96	11.75	15.77	1.05	0.02	0.54	97.21	1.24	0.00	0.21	0.12	Calcic amphibole	Magnesiohornblende
17Pe87	1.11	11.55	45.20	8.42	1.00	11.85	16.06	1.42	0.01	0.50	97.12	1.27	0.00	0.21	0.16	Calcic amphibole	Magnesiohornblende
17Pe87	1.45	9.76	44.35	12.92	0.22	11.59	15.59	0.43	0.03	0.22	96.56	1.43	0.00	0.83	0.05	Calcic amphibole	Magnesiohornblende
17Pe87	1.56	8.21	42.24	13.20	0.42	11.01	19.24	0.71	0.05	0.43	97.07	1.69	0.00	0.63	0.08	Calcic amphibole	Tschermakite
17Pe87	1.02	12.42	46.12	7.80	0.82	11.63	14.77	1.49	0.03	0.54	96.64	1.17	0.00	0.19	0.17	Calcic amphibole	Magnesiohornblende
17Pe87	1.02	11.55	46.17	9.39	0.11	11.32	15.07	0.80	0.06	0.30	95.79	1.18	0.00	0.46	0.09	Calcic amphibole	Magnesiohornblende
17Pe87	1.60	8.03	41.96	13.22	0.42	10.88	18.31	0.56	0.01	0.49	95.48	1.63	0.00	0.73	0.06	Calcic amphibole	Tschermakite
17Pe87	2.08	9.53	44.08	13.01	0.26	11.19	15.64	0.53	0.05	0.28	96.65	1.44	0.00	0.84	0.06	Calcic amphibole	Magnesiohornblende
17Pe87	0.69	11.00	49.39	5.01	0.47	11.59	17.05	0.95	0.03	0.74	96.92	0.65	0.00	0.23	0.11	Calcic amphibole	Magnesiohornblende
17Pe87	1.42	11.72	43.22	11.59	0.35	11.70	13.75	2.08	0.01	0.19	96.03	1.59	0.00	0.44	0.23	Calcic amphibole	Tschermakite
17Pe87	0.12	16.97	55.87	1.09	0.05	12.89	10.13	0.07	0.17	0.18	97.55	0.04	0.00	0.14	0.01	Calcic amphibole	Actinolite

17Pe87	1.30	16.74	49.79	6.14	0.33	11.91	9.73	0.45	0.32	0.15	96.85	0.87	0.00	0.16	0.05	Calcic amphibole	Magnesiohornblende
17Pe87	1.20	10.04	44.30	9.22	1.02	11.61	18.00	1.10	0.02	0.73	97.23	1.35	0.00	0.28	0.12	Calcic amphibole	Magnesiohornblende
17Pe87	1.62	14.61	45.69	12.71	0.11	10.50	10.40	0.73	0.12	0.20	96.69	1.36	0.00	0.82	0.08	Calcic amphibole	Magnesiohornblende
17Pe87	0.66	11.36	48.69	7.00	0.58	11.93	15.54	0.36	0.01	0.57	96.71	0.78	0.00	0.45	0.04	Calcic amphibole	Magnesiohornblende
17Pe87	1.55	7.38	41.25	14.37	0.43	10.95	19.46	0.29	0.00	0.47	96.15	1.77	0.00	0.79	0.03	Calcic amphibole	Tschermakite
17Pe87	1.40	12.35	46.27	10.96	0.08	11.86	12.82	0.50	0.13	0.23	96.60	1.24	0.00	0.65	0.06	Calcic amphibole	Magnesiohornblende
17Pe87	1.22	14.34	47.28	8.59	0.20	10.17	13.10	1.05	0.00	0.52	96.48	1.04	0.00	0.45	0.12	Calcic amphibole	Magnesiohornblende
17Pe87	1.06	11.20	45.43	8.57	0.88	11.63	15.68	1.07	0.04	0.46	96.02	1.18	0.00	0.34	0.12	Calcic amphibole	Magnesiohornblende
17Pe87	1.28	14.49	48.29	9.96	0.07	11.86	10.07	0.37	0.16	0.26	96.82	1.08	0.00	0.61	0.04	Calcic amphibole	Magnesiohornblende
17Pe87	1.43	12.09	46.86	8.91	0.06	11.63	15.03	0.43	0.06	0.26	96.76	1.12	0.00	0.42	0.05	Calcic amphibole	Magnesiohornblende
17Pe87	1.16	13.48	47.03	8.51	0.41	11.09	13.77	1.03	0.05	0.48	97.01	1.07	0.00	0.41	0.11	Calcic amphibole	Magnesiohornblende
17Pe87	1.17	12.74	47.04	8.21	0.52	11.78	13.68	0.92	0.04	0.33	96.43	1.06	0.00	0.36	0.10	Calcic amphibole	Magnesiohornblende
17Pe87	1.34	10.71	44.76	8.40	0.96	10.45	17.16	2.18	0.00	0.40	96.36	1.31	0.00	0.17	0.25	Calcic amphibole	Magnesiohornblende
17Pe87	0.64	11.18	48.28	7.25	0.55	11.85	16.46	0.43	0.01	0.40	97.05	0.86	0.00	0.40	0.05	Calcic amphibole	Magnesiohornblende
17Pe87	1.41	15.42	50.31	6.57	0.19	11.88	10.56	0.22	0.09	0.17	96.81	0.75	0.00	0.36	0.02	Calcic amphibole	Magnesiohornblende
17Pe87	0.84	10.94	44.67	9.14	1.02	12.05	15.56	1.14	0.02	0.47	95.84	1.25	0.00	0.38	0.13	Calcic amphibole	Magnesiohornblende
17Pe87	1.24	13.87	47.43	7.67	0.19	10.64	14.34	1.26	0.00	0.50	97.14	1.02	0.00	0.31	0.14	Calcic amphibole	Magnesiohornblende
17Pe87	1.37	10.17	43.18	14.20	0.29	10.69	15.58	0.48	0.00	0.57	96.54	1.55	0.00	0.95	0.05	Calcic amphibole	Tschermakite
17Pe87	1.25	12.51	45.64	11.74	0.17	11.45	13.07	0.51	0.02	0.21	96.56	1.38	0.00	0.63	0.06	Calcic amphibole	Magnesiohornblende
17Pe87	0.77	11.01	46.44	7.78	0.69	11.64	17.37	0.81	0.00	0.59	97.10	1.04	0.00	0.33	0.09	Calcic amphibole	Magnesiohornblende
17Pe143	0.98	12.46	46.23	8.97	0.81	11.65	14.71	1.06	0.01	0.35	97.23	1.23	0.00	0.32	0.12	Calcic amphibole	Magnesiohornblende
17Pe143	1.12	9.62	42.86	10.48	1.31	11.72	18.22	0.93	0.04	0.46	96.76	1.52	0.00	0.35	0.11	Calcic amphibole	Tschermakite
17Pe143	1.94	12.15	44.58	13.52	0.40	10.81	12.02	0.59	0.07	0.29	96.38	1.52	0.00	0.80	0.07	Calcic amphibole	Tschermakite
17Pe143	1.36	10.79	43.63	10.22	0.91	11.47	16.20	1.36	0.02	0.52	96.49	1.47	0.00	0.34	0.15	Calcic amphibole	Magnesiohornblende
17Pe143	0.75	15.94	54.22	2.49	0.15	11.62	11.66	0.00	0.03	0.34	97.20	0.25	0.00	0.17	0.00	Calcic amphibole	Actinolite
17Pe143	1.27	11.80	43.94	10.58	1.16	11.73	14.28	1.57	0.02	0.31	96.65	1.46	0.00	0.39	0.18	Calcic amphibole	Magnesiohornblende
17Pe143	1.45	14.20	48.04	11.01	0.20	11.72	9.67	0.27	0.00	0.15	96.72	1.11	0.00	0.76	0.03	Calcic amphibole	Magnesiohornblende
17Pe143	1.03	11.18	46.09	10.32	0.15	11.68	14.91	0.62	0.02	0.25	96.25	1.20	0.00	0.60	0.07	Calcic amphibole	Magnesiohornblende
17Pe143	1.58	10.61	44.76	10.32	0.19	11.48	16.70	0.41	0.02	0.30	96.37	1.33	0.00	0.48	0.05	Calcic amphibole	Magnesiohornblende
17Pe143	0.93	12.76	48.60	8.55	0.28	11.85	13.67	0.27	0.00	0.25	97.16	0.95	0.00	0.52	0.03	Calcic amphibole	Magnesiohornblende
17Pe143	1.57	12.69	45.74	13.38	0.14	11.16	10.22	0.37	0.11	0.23	95.61	1.36	0.00	0.93	0.04	Calcic amphibole	Magnesiohornblende
17Pe143	1.58	10.08	44.08	10.42	0.53	11.37	17.26	0.60	0.04	0.36	96.31	1.38	0.00	0.46	0.07	Calcic amphibole	Magnesiohornblende
17Pe143	0.92	10.72	46.76	9.63	0.26	11.66	15.97	0.38	0.00	0.30	96.61	1.09	0.00	0.59	0.04	Calcic amphibole	Magnesiohornblende
17Pe143	1.11	9.49	45.26	10.09	0.30	11.55	18.10	0.88	0.00	0.27	97.05	1.26	0.00	0.51	0.10	Calcic amphibole	Magnesiohornblende
17Pe143	1.61	9.44	43.02	13.95	0.11	11.53	15.83	0.55	0.06	0.27	96.37	1.61	0.00	0.84	0.06	Calcic amphibole	Tschermakite
17Pe143	0.95	11.73	46.05	8.65	0.55	11.33	15.33	1.05	0.01	0.68	96.32	1.19	0.00	0.32	0.12	Calcic amphibole	Magnesiohornblende
17Pe143	0.83	14.38	48.98	6.23	0.40	11.61	12.90	0.79	0.02	0.33	96.47	0.88	0.00	0.19	0.09	Calcic amphibole	Magnesiohornblende
17Pe143	1.01	12.95	48.71	5.25	0.55	11.35	15.16	0.98	0.00	0.68	96.63	0.82	0.00	0.09	0.11	Calcic amphibole	Magnesiohornblende
17Pe143	0.69	14.76	49.15	7.77	0.48	12.46	11.20	0.19	0.16	0.21	97.07	0.91	0.00	0.41	0.02	Calcic amphibole	Magnesiohornblende

17Pe143	1.15	11.18	46.99	8.54	0.46	10.84	16.55	1.28	0.02	0.39	97.38	1.13	0.00	0.35	0.14	Calcic amphibole	Magnesiohornblende
17Pe143	1.20	10.70	43.51	10.20	1.23	11.73	16.39	1.27	0.03	0.35	96.61	1.46	0.00	0.35	0.14	Calcic amphibole	Magnesiohornblende
17Pe143	1.18	15.10	48.64	8.37	0.50	12.22	10.30	0.59	0.00	0.23	97.13	1.00	0.00	0.43	0.06	Calcic amphibole	Magnesiohornblende
17Pe143	0.96	10.69	47.83	5.96	0.60	11.08	17.87	0.98	0.00	0.57	96.54	0.85	0.00	0.20	0.11	Calcic amphibole	Magnesiohornblende
17Pe143	1.13	9.14	42.55	11.10	1.48	11.74	18.63	0.92	0.02	0.49	97.20	1.57	0.00	0.41	0.11	Calcic amphibole	Magnesiohastingsite
17Pe143	1.07	9.65	43.08	10.08	1.29	11.94	18.45	1.09	0.02	0.41	97.08	1.49	0.00	0.31	0.12	Calcic amphibole	Magnesiohornblende
17Pe143	1.33	9.09	44.20	12.44	0.49	11.65	16.87	0.63	0.07	0.22	96.99	1.41	0.00	0.77	0.07	Calcic amphibole	Magnesiohornblende
17Pe143	0.74	12.65	47.50	7.47	0.27	10.88	14.80	1.75	0.00	0.44	96.50	0.94	0.00	0.37	0.20	Calcic amphibole	Magnesiohornblende
17Pe143	0.38	13.94	51.42	4.49	0.20	11.78	13.54	0.60	0.07	0.44	96.87	0.55	0.00	0.22	0.07	Calcic amphibole	Magnesiohornblende
17Pe143	1.05	15.57	49.06	7.17	0.10	11.67	11.32	0.43	0.01	0.30	96.68	0.87	0.00	0.35	0.05	Calcic amphibole	Magnesiohornblende
17Pe143	1.59	15.72	47.61	7.14	0.32	10.88	10.75	1.61	0.02	0.43	96.07	1.13	0.00	0.09	0.18	Calcic amphibole	Magnesiohornblende
17Pe181	1.14	12.05	46.18	8.70	0.55	11.43	15.12	0.96	0.03	0.49	96.66	1.19	0.00	0.32	0.11	Calcic amphibole	Magnesiohornblende
17Pe181	1.48	10.95	45.05	10.16	0.36	11.60	16.19	0.59	0.03	0.27	96.69	1.31	0.00	0.46	0.07	Calcic amphibole	Magnesiohornblende
17Pe181	1.01	12.19	46.52	7.52	0.72	11.64	14.76	1.62	0.02	0.56	96.56	1.10	0.00	0.22	0.18	Calcic amphibole	Magnesiohornblende
17Pe181	0.92	10.62	47.69	6.93	0.65	11.08	17.61	0.89	0.03	0.54	96.96	0.92	0.00	0.29	0.10	Calcic amphibole	Magnesiohornblende
17Pe181	0.32	16.22	53.98	2.52	0.12	12.39	11.01	0.07	0.03	0.33	97.00	0.26	0.00	0.16	0.01	Calcic amphibole	Actinolite
17Pe181	1.04	12.07	47.89	9.21	0.14	12.03	14.54	0.44	0.04	0.29	97.70	1.05	0.00	0.53	0.05	Calcic amphibole	Magnesiohornblende
17Pe181	1.34	14.10	47.93	7.06	0.15	10.68	13.64	1.54	0.02	0.37	96.83	1.09	0.00	0.11	0.17	Calcic amphibole	Magnesiohornblende
17Pe181	2.13	12.55	43.11	11.22	0.45	10.90	14.26	2.19	0.09	0.32	97.22	1.70	0.00	0.23	0.24	Calcic amphibole	Tschermakite
17Pe181	1.15	12.12	46.06	8.86	0.61	11.71	14.99	1.00	0.01	0.34	96.85	1.21	0.00	0.33	0.11	Calcic amphibole	Magnesiohornblende
17Pe181	1.20	13.40	47.00	8.11	0.44	11.48	14.03	1.33	0.00	0.29	97.29	1.17	0.00	0.21	0.15	Calcic amphibole	Magnesiohornblende
17Pe181	0.67	11.91	47.97	6.66	0.62	12.43	15.78	1.37	0.00	0.42	97.83	0.93	0.00	0.23	0.15	Calcic amphibole	Magnesiohornblende
17Pe181	0.73	12.78	49.80	6.32	0.30	11.65	14.65	0.60	0.01	0.29	97.13	0.75	0.00	0.34	0.07	Calcic amphibole	Magnesiohornblende
17Pe181	2.40	11.04	40.80	11.99	1.04	11.63	13.26	5.03	0.04	0.24	97.47	1.87	0.00	0.26	0.57	Calcic amphibole	Kaersutite
17Pe181	1.07	14.63	48.76	5.88	0.41	11.41	13.49	1.24	0.02	0.40	97.31	0.96	0.00	0.04	0.13	Calcic amphibole	Magnesiohornblende
17Pe181	1.14	13.49	46.57	7.83	0.84	11.47	12.98	1.76	0.00	0.44	96.52	1.16	0.00	0.20	0.20	Calcic amphibole	Magnesiohornblende
17Pe181	0.96	11.82	46.27	8.17	0.86	11.74	15.35	1.18	0.00	0.47	96.81	1.14	0.00	0.29	0.13	Calcic amphibole	Magnesiohornblende
17Pe181	1.13	14.07	48.60	5.92	0.34	11.10	13.60	1.39	0.03	0.31	96.49	0.92	0.00	0.10	0.15	Calcic amphibole	Magnesiohornblende
17Pe181	1.89	13.12	43.50	12.66	0.34	11.81	11.64	1.45	0.00	0.16	96.58	1.64	0.00	0.54	0.16	Calcic amphibole	Tschermakite
17Pe181	2.45	15.12	41.49	12.86	0.50	12.12	8.96	3.34	0.07	0.08	96.99	1.96	0.00	0.25	0.37	Calcic amphibole	Magnesiohastingsite
17Pe181	1.27	9.05	43.04	12.09	1.58	11.68	16.71	1.02	0.02	0.47	96.94	1.49	0.00	0.67	0.12	Calcic amphibole	Edenite
17Pe181	2.18	14.43	46.86	8.39	0.29	10.47	12.97	1.39	0.00	0.37	97.35	1.27	0.00	0.16	0.15	Calcic amphibole	Magnesiohornblende
17Pe181	1.43	15.10	47.48	7.96	0.29	10.01	12.71	1.15	0.00	0.37	96.50	1.01	0.00	0.37	0.13	Calcic amphibole	Magnesiohornblende
17Pe181	1.67	14.78	46.85	8.97	0.22	10.14	12.97	1.02	0.02	0.43	97.07	1.13	0.00	0.42	0.11	Calcic amphibole	Edenite
17Pe181	2.02	12.95	43.14	12.04	0.35	11.48	12.73	2.04	0.02	0.15	96.93	1.70	0.00	0.38	0.22	Calcic amphibole	Tschermakite
17Pe181	0.87	12.03	46.51	7.53	0.88	11.73	15.38	1.68	0.00	0.45	97.07	1.12	0.00	0.20	0.19	Calcic amphibole	Magnesiohornblende
17Pe181	1.50	9.44	41.47	14.20	0.66	11.70	16.07	1.30	0.00	0.30	96.64	1.80	0.00	0.70	0.15	Calcic amphibole	Tschermakite
17Pe181	1.28	10.61	43.50	9.53	1.32	11.31	16.86	1.50	0.04	0.40	96.35	1.44	0.00	0.26	0.17	Calcic amphibole	Magnesiohornblende
17Pe181	0.94	11.40	45.44	8.35	0.90	11.82	16.26	0.95	0.03	0.50	96.58	1.21	0.00	0.26	0.11	Calcic amphibole	Magnesiohornblende

17Pe181	0.92	14.53	48.61	6.59	0.37	11.13	13.39	1.02	0.00	0.39	96.95	0.87	0.00	0.27	0.11	Calcic amphibole	Magnesiohornblende
17Pe181	1.17	9.84	43.21	11.55	0.76	11.80	16.88	0.83	0.04	0.31	96.39	1.51	0.00	0.54	0.09	Calcic amphibole	Tschermakite
17Pe181	1.23	10.49	44.67	8.33	1.08	11.57	17.65	1.37	0.00	0.47	96.85	1.27	0.00	0.21	0.16	Calcic amphibole	Magnesiohornblende
17Pe181	1.28	13.49	46.58	7.54	0.69	11.50	13.21	1.68	0.00	0.47	96.44	1.14	0.00	0.17	0.19	Calcic amphibole	Magnesiohornblende
17Pe181	1.28	13.25	46.31	9.62	0.49	11.58	12.62	1.18	0.00	0.33	96.66	1.25	0.00	0.41	0.13	Calcic amphibole	Magnesiohornblende
17Pe181	2.27	13.03	42.23	12.82	0.43	11.18	12.71	1.51	0.01	0.13	96.33	1.81	0.00	0.41	0.17	Calcic amphibole	Tschermakite
17Pe181	1.15	15.98	48.82	6.74	0.18	10.12	11.23	0.87	0.03	0.83	95.95	0.84	0.00	0.33	0.10	Calcic amphibole	Magnesiohornblende
17Pe181	0.89	8.87	43.66	9.96	0.67	12.16	19.43	0.30	0.56	0.33	96.83	1.38	0.00	0.41	0.03	Calcic amphibole	Ferrohornblende
17Pe181	1.53	14.71	45.57	10.16	0.62	11.98	10.06	2.12	0.06	0.15	96.96	1.39	0.00	0.34	0.23	Calcic amphibole	Magnesiohornblende
17Pe181	1.04	10.96	46.17	9.36	0.65	11.62	15.22	1.61	0.09	0.35	97.07	1.17	0.00	0.47	0.18	Calcic amphibole	Magnesiohornblende
17Pe181	1.11	14.21	48.48	6.51	0.49	11.61	12.86	0.99	0.01	0.59	96.87	0.95	0.00	0.17	0.11	Calcic amphibole	Magnesiohornblende
17Pe181	0.67	13.16	47.57	7.35	0.78	11.52	14.06	1.41	0.00	0.36	96.90	1.05	0.00	0.22	0.16	Calcic amphibole	Magnesiohornblende
17Pe181	1.06	13.52	48.48	6.06	0.51	11.62	13.57	0.55	0.03	0.76	96.17	0.86	0.00	0.20	0.06	Calcic amphibole	Magnesiohornblende
17Pe181	1.11	12.09	44.21	11.46	0.44	11.60	13.18	1.68	0.00	0.29	96.07	1.49	0.00	0.50	0.19	Calcic amphibole	Magnesiohornblende
17Pe181	1.82	13.83	43.82	12.21	0.60	11.49	10.01	2.09	0.18	0.15	96.20	1.60	0.00	0.50	0.23	Calcic amphibole	Tschermakite
17Pe181	1.88	12.65	43.88	12.63	0.97	11.70	11.03	2.19	0.03	0.18	97.15	1.57	0.00	0.62	0.24	Calcic amphibole	Pargasite
17Pe181	0.77	15.69	49.85	7.49	0.13	11.17	10.98	0.33	0.12	0.28	96.82	0.80	0.00	0.48	0.04	Calcic amphibole	Magnesiohornblende
17Pe181	1.15	14.69	48.56	7.09	0.28	10.91	12.33	1.17	0.00	0.53	96.71	1.02	0.00	0.18	0.13	Calcic amphibole	Magnesiohornblende
17Pe181	1.80	10.49	41.82	12.81	0.96	11.26	15.44	1.63	0.00	0.35	96.56	1.75	0.00	0.51	0.18	Calcic amphibole	Magnesiohastingsite
17Pe181	1.03	11.45	45.32	8.89	0.79	11.68	16.22	1.08	0.00	0.37	96.84	1.27	0.00	0.29	0.12	Calcic amphibole	Magnesiohornblende
17Pe181	2.38	16.65	43.33	12.81	0.08	11.00	8.00	1.43	0.67	0.12	96.46	1.85	0.00	0.29	0.15	Calcic amphibole	Tschermakite
17Pe181	1.42	9.35	43.01	10.59	1.06	10.83	18.31	1.10	0.02	0.47	96.17	1.50	0.00	0.39	0.13	Calcic amphibole	Magnesiohornblende
17Pe181	0.88	11.11	46.58	8.35	0.41	10.36	16.03	1.21	0.04	0.40	95.37	1.09	0.00	0.37	0.14	Calcic amphibole	Magnesiohornblende
17Pe181	2.05	11.95	43.60	9.54	0.92	10.71	14.64	2.55	0.00	0.36	96.32	1.49	0.00	0.18	0.29	Calcic amphibole	Magnesiohornblende
17Pe181	0.80	10.26	45.13	8.31	0.58	11.66	17.81	0.53	0.04	0.35	95.46	1.12	0.00	0.38	0.06	Calcic amphibole	Magnesiohornblende
17Pe181	1.17	11.29	45.00	8.37	0.98	11.09	16.26	0.97	0.01	0.55	95.69	1.24	0.00	0.25	0.11	Calcic amphibole	Magnesiohornblende
17Pe243	1.59	14.94	44.55	10.30	0.15	11.05	12.22	1.39	0.00	0.26	96.46	1.47	0.00	0.31	0.15	Calcic amphibole	Magnesiohornblende
17Pe243	0.98	11.81	47.57	9.31	0.11	12.02	14.38	0.24	0.35	0.27	97.05	1.04	0.00	0.56	0.03	Calcic amphibole	Magnesiohornblende
17Pe243	1.13	12.25	45.84	8.67	0.53	11.70	15.18	0.98	0.00	0.49	96.76	1.24	0.00	0.27	0.11	Calcic amphibole	Magnesiohornblende
17Pe243	1.12	11.27	45.20	9.76	0.53	11.65	15.58	0.86	0.02	0.39	96.38	1.29	0.00	0.42	0.10	Calcic amphibole	Magnesiohornblende
17Pe243	1.26	11.53	45.78	10.85	0.15	11.58	14.78	0.49	0.07	0.22	96.72	1.29	0.00	0.58	0.05	Calcic amphibole	Magnesiohornblende
17Pe243	1.26	11.83	46.76	10.06	0.08	11.95	14.26	0.35	0.07	0.24	96.85	1.15	0.00	0.59	0.04	Calcic amphibole	Magnesiohornblende
17Pe243	1.07	7.18	42.01	10.81	1.31	11.96	20.09	2.16	0.05	0.32	96.96	1.51	0.00	0.45	0.25	Calcic amphibole	Ferropargasite
17Pe243	1.28	10.32	45.28	10.86	0.08	11.58	16.17	0.39	0.07	0.27	96.30	1.28	0.00	0.62	0.04	Calcic amphibole	Magnesiohornblende
17Pe243	1.12	11.91	46.91	9.05	0.17	11.72	15.15	0.29	0.21	0.34	96.87	1.12	0.00	0.44	0.03	Calcic amphibole	Magnesiohornblende
17Pe243	1.11	10.81	46.35	9.11	0.17	11.83	16.32	0.34	0.01	0.29	96.34	1.10	0.00	0.50	0.04	Calcic amphibole	Magnesiohornblende
17Pe243	1.12	10.61	43.48	10.22	0.87	11.38	16.77	1.10	0.01	0.45	96.01	1.47	0.00	0.34	0.12	Calcic amphibole	Magnesiohornblende
17Pe243	1.58	9.93	44.06	10.55	0.01	11.11	18.28	0.51	0.06	0.32	96.42	1.34	0.00	0.54	0.06	Calcic amphibole	Magnesiohornblende
17Pe243	1.16	11.48	44.55	9.45	0.79	11.44	15.06	2.55	0.10	0.25	96.83	1.39	0.00	0.26	0.29	Calcic amphibole	Magnesiohornblende

17Pe243	1.25	10.89	44.68	8.58	1.09	11.55	16.83	1.26	0.03	0.39	96.54	1.28	0.00	0.24	0.14	Calcic amphibole	Magnesiohornblende
17Pe243	2.11	14.89	41.85	13.44	0.03	11.05	10.21	2.41	0.02	0.21	96.22	1.86	0.00	0.46	0.27	Calcic amphibole	Pargasite
17Pe243	1.42	12.23	45.34	11.25	0.16	11.58	14.56	0.57	0.00	0.26	97.37	1.34	0.00	0.61	0.06	Calcic amphibole	Magnesiohornblende
17Pe243	0.85	10.72	44.52	8.65	1.08	11.46	17.77	1.20	0.03	0.44	96.72	1.26	0.00	0.28	0.14	Calcic amphibole	Magnesiohornblende
17Pe243	1.15	12.83	45.82	8.73	0.56	11.86	13.84	1.24	0.05	0.29	96.37	1.23	0.00	0.29	0.14	Calcic amphibole	Magnesiohornblende
17Pe243	1.13	11.36	47.27	8.94	0.09	11.82	15.63	0.42	0.02	0.28	96.95	1.05	0.00	0.50	0.05	Calcic amphibole	Magnesiohornblende
17Pe243	1.77	11.41	44.15	11.18	0.42	11.63	15.10	0.72	0.05	0.34	96.76	1.47	0.00	0.49	0.08	Calcic amphibole	Magnesiohornblende
17Pe243	1.78	11.68	45.13	10.25	0.26	11.39	15.41	0.53	0.05	0.29	96.78	1.35	0.00	0.43	0.06	Calcic amphibole	Magnesiohornblende
17Pe243	1.08	12.95	45.82	8.64	0.51	11.21	14.45	1.38	0.03	0.47	96.55	1.19	0.00	0.33	0.16	Calcic amphibole	Magnesiohornblende
17Pe243	1.40	12.08	45.22	9.94	0.15	11.82	15.00	0.77	0.08	0.34	96.79	1.35	0.00	0.37	0.09	Calcic amphibole	Magnesiohornblende
17Pe243	1.11	11.08	43.35	10.50	1.53	12.00	15.04	1.16	0.03	0.33	96.13	1.45	0.00	0.42	0.13	Calcic amphibole	Edenite
17Pe243	0.82	11.40	47.80	7.80	0.66	11.65	16.26	0.54	0.05	0.47	97.46	0.97	0.00	0.38	0.06	Calcic amphibole	Magnesiohornblende
17Pe243	0.96	11.64	47.82	8.41	0.08	11.84	15.53	0.26	0.03	0.30	96.87	0.98	0.00	0.48	0.03	Calcic amphibole	Magnesiohornblende
17Pe243	1.08	12.76	45.98	10.36	0.32	11.93	12.71	0.41	0.15	0.22	95.93	1.24	0.00	0.55	0.05	Calcic amphibole	Magnesiohornblende
17Pe243	1.23	11.75	46.68	10.44	0.09	11.91	14.30	0.30	0.08	0.29	97.07	1.18	0.00	0.62	0.03	Calcic amphibole	Magnesiohornblende
17Pe243	1.22	10.22	44.02	12.09	0.53	11.86	15.78	0.47	0.01	0.27	96.48	1.44	0.00	0.68	0.05	Calcic amphibole	Magnesiohornblende
17Pe243	0.94	15.75	50.20	6.48	0.17	11.77	10.78	0.44	0.02	0.27	96.83	0.82	0.00	0.27	0.05	Calcic amphibole	Magnesiohornblende
17Pe243	1.22	11.48	44.47	12.53	0.49	12.04	14.22	0.34	0.03	0.18	97.00	1.48	0.00	0.69	0.04	Calcic amphibole	Magnesiohornblende
17Pe243	1.31	11.61	44.70	8.80	1.04	11.57	15.84	1.33	0.02	0.41	96.63	1.32	0.00	0.23	0.15	Calcic amphibole	Magnesiohornblende
17Pe243	1.15	11.28	45.76	7.35	0.86	11.46	17.03	1.51	0.03	0.39	96.82	1.16	0.00	0.14	0.17	Calcic amphibole	Magnesiohornblende
17Pe243	1.07	12.05	47.17	10.04	0.06	12.11	13.66	0.42	0.10	0.25	96.94	1.11	0.00	0.62	0.05	Calcic amphibole	Magnesiohornblende
17Pe243	1.69	10.02	44.02	9.26	0.80	10.77	17.66	2.28	0.01	0.34	96.85	1.40	0.00	0.24	0.26	Calcic amphibole	Magnesiohornblende
17Pe243	1.38	14.65	47.90	9.41	0.20	11.35	10.78	0.77	0.03	0.26	96.73	1.13	0.00	0.46	0.08	Calcic amphibole	Magnesiohornblende
17Pe243	1.85	15.07	47.77	9.53	0.08	11.67	10.06	0.41	0.25	0.21	96.90	1.14	0.00	0.47	0.04	Calcic amphibole	Magnesiohornblende
17Pe243	1.18	11.33	44.09	9.65	1.16	11.64	15.88	1.23	0.03	0.41	96.60	1.41	0.00	0.30	0.14	Calcic amphibole	Magnesiohornblende
17Pe243	0.99	14.10	49.52	7.41	0.06	11.25	12.84	0.23	0.30	0.19	96.88	0.89	0.00	0.36	0.03	Calcic amphibole	Magnesiohornblende
17Pe243	1.16	10.18	43.40	10.67	1.10	11.64	17.24	1.16	0.00	0.51	97.07	1.51	0.00	0.38	0.13	Calcic amphibole	Tschermakite
17Pe243	1.72	9.28	43.79	10.61	0.01	11.31	18.72	0.68	0.01	0.29	96.42	1.42	0.00	0.46	0.08	Calcic amphibole	Magnesiohornblende
17Pe243	1.34	7.93	42.25	10.93	1.20	11.47	20.06	1.54	0.00	0.42	97.13	1.56	0.00	0.41	0.18	Calcic amphibole	Hastingsite
17Pe243	0.94	9.88	42.09	10.91	1.42	11.75	17.66	1.37	0.00	0.46	96.48	1.63	0.00	0.32	0.16	Calcic amphibole	Tschermakite
17Pe243	0.91	13.08	48.37	8.49	0.05	11.81	14.05	0.32	0.02	0.26	97.37	0.94	0.00	0.52	0.04	Calcic amphibole	Magnesiohornblende
17Pe243	1.41	10.29	44.40	10.88	0.09	11.20	15.82	0.42	0.12	0.30	94.93	1.32	0.00	0.60	0.05	Calcic amphibole	Magnesiohornblende
17Pe243	0.70	11.46	49.60	5.63	0.11	11.26	16.98	0.17	0.00	0.32	96.22	0.67	0.00	0.32	0.02	Calcic amphibole	Magnesiohornblende
17Pe243	1.72	12.12	44.24	14.10	0.22	11.38	12.38	0.38	0.00	0.13	96.68	1.59	0.00	0.82	0.04	Calcic amphibole	Tschermakite
17Pi400	1.27	10.18	42.80	11.17	1.07	11.34	18.50	1.48	0.00	0.45	98.25	1.60	0.00	0.37	0.17	Calcic amphibole	Pargasite
17Pi400	1.26	10.36	42.82	10.98	1.08	11.37	18.48	1.34	0.01	0.48	98.18	1.59	0.00	0.34	0.15	Calcic amphibole	Magnesiohastingsite
17Pi400	1.48	10.71	42.90	10.86	0.94	11.60	18.31	1.32	0.00	0.44	98.56	1.61	0.00	0.29	0.15	Calcic amphibole	Magnesiohastingsite
17Pi400	1.43	12.16	46.48	7.88	0.24	11.65	17.22	0.91	0.05	0.31	98.32	1.15	0.00	0.22	0.10	Calcic amphibole	Magnesiohornblende
17Pi400	1.28	10.94	44.26	9.43	1.05	11.56	18.75	1.26	0.01	0.42	98.96	1.43	0.00	0.22	0.14	Calcic amphibole	Edenite

17Pi400	1.44	8.72	43.54	8.73	1.15	11.13	22.41	1.02	0.04	0.95	99.13	1.41	0.00	0.15	0.12	Calcic amphibole	Ferro-edenite
17Pi400	0.65	13.95	49.00	5.84	0.41	11.78	15.32	0.58	0.02	0.65	98.20	0.87	0.00	0.13	0.06	Calcic amphibole	Magnesiohornblende
17Pi400	0.76	11.82	49.17	6.11	0.36	10.71	18.41	0.44	0.02	0.79	98.59	0.76	0.00	0.30	0.05	Calcic amphibole	Magnesiohornblende
17Pi400	1.45	11.29	45.57	7.65	0.83	10.99	18.46	1.66	0.00	0.49	98.40	1.31	0.00	0.02	0.18	Calcic amphibole	Magnesiohornblende
17Pi400	0.94	13.23	47.56	6.75	0.36	10.85	16.18	1.54	0.00	0.67	98.08	1.01	0.00	0.15	0.17	Calcic amphibole	Magnesiohornblende
17Pi400	1.29	15.47	48.07	7.24	0.27	10.55	14.11	0.91	0.00	0.40	98.31	1.05	0.00	0.18	0.10	Calcic amphibole	Magnesiohornblende
17Pi400	2.09	12.41	42.66	12.07	0.73	11.27	14.78	2.20	0.00	0.19	98.41	1.81	0.00	0.26	0.24	Calcic amphibole	Tschermakite
17Pi400	1.05	10.81	46.94	8.00	0.24	11.67	18.85	0.48	0.02	0.34	98.40	1.06	0.00	0.34	0.05	Calcic amphibole	Magnesiohornblende
17Pi400	1.03	10.52	46.45	8.55	0.67	11.61	18.63	1.08	0.01	0.24	98.80	1.20	0.00	0.27	0.12	Calcic amphibole	Magnesiohornblende
17Pi400	1.79	13.73	44.33	11.62	0.08	11.09	13.28	1.51	0.00	0.27	97.70	1.54	0.00	0.46	0.17	Calcic amphibole	Pargasite
17Pi400	1.37	9.36	42.26	11.74	0.98	11.18	20.42	1.48	0.03	0.44	99.26	1.70	0.00	0.36	0.17	Calcic amphibole	Hastingsite
17Pi400	0.88	12.48	49.50	7.40	0.17	11.35	16.16	0.51	0.02	0.26	98.74	0.80	0.00	0.47	0.06	Calcic amphibole	Magnesiohornblende
17Pi400	0.71	12.83	48.84	7.26	0.02	11.66	16.01	0.54	0.06	0.33	98.26	0.90	0.00	0.35	0.06	Calcic amphibole	Magnesiohornblende
17Pi400	1.10	10.95	45.27	9.21	0.96	11.64	18.91	1.20	0.06	0.40	99.70	1.34	0.00	0.25	0.13	Calcic amphibole	Magnesiohornblende
17Pi400	1.06	11.45	45.01	8.96	0.77	11.93	17.85	1.12	0.00	0.46	98.61	1.35	0.00	0.21	0.13	Calcic amphibole	Magnesiohornblende
17Pi400	1.47	14.85	49.05	8.19	0.20	10.96	12.88	0.48	0.07	0.55	98.69	1.11	0.00	0.25	0.05	Calcic amphibole	Magnesiohornblende
17Pi400	1.42	8.09	40.08	12.98	1.57	11.33	21.43	1.18	0.00	0.41	98.49	1.91	0.00	0.41	0.14	Calcic amphibole	Hastingsite
17Pi400	1.23	9.15	41.55	11.20	1.26	11.79	21.13	1.03	0.00	0.46	98.80	1.76	0.00	0.22	0.12	Calcic amphibole	Magnesiohastingsite
17Pi400	2.19	14.71	40.81	13.76	0.72	11.84	11.01	2.17	0.03	0.08	97.31	2.10	0.00	0.25	0.24	Calcic amphibole	Magnesiohastingsite
17Pi400	1.31	9.69	42.19	11.07	1.30	11.33	19.84	1.59	0.00	0.50	98.81	1.67	0.00	0.28	0.18	Calcic amphibole	Magnesiohastingsite
17Pi400	0.78	11.22	47.63	7.06	0.71	11.83	18.18	1.27	0.00	0.38	99.07	1.06	0.00	0.16	0.14	Calcic amphibole	Magnesiohornblende
17Pi400	1.09	9.61	43.25	10.22	1.12	11.97	20.48	1.00	0.02	0.43	99.19	1.56	0.00	0.24	0.11	Calcic amphibole	Magnesiohastingsite
17Pi400	1.08	13.27	46.97	7.95	0.67	11.50	15.69	0.85	0.00	0.56	98.55	1.14	0.00	0.23	0.09	Calcic amphibole	Magnesiohornblende
17Pi400	1.15	12.98	47.35	7.89	0.39	11.24	16.59	1.09	0.03	0.43	99.14	1.11	0.00	0.24	0.12	Calcic amphibole	Magnesiohornblende
17Pi400	1.98	8.03	42.67	12.33	0.58	10.43	21.73	0.37	0.00	0.36	98.48	1.69	0.00	0.46	0.04	Calcic amphibole	Tschermakite
17Pi400	1.49	8.55	41.95	10.92	1.34	11.92	22.32	0.70	0.00	0.53	99.72	1.71	0.00	0.23	0.08	Calcic amphibole	Hastingsite
17Pi400	0.70	14.39	48.65	6.62	0.60	12.13	13.78	0.85	0.00	0.30	98.01	0.94	0.00	0.20	0.09	Calcic amphibole	Magnesiohornblende
17Pi400	1.10	9.50	43.07	9.63	1.06	11.57	20.56	1.03	0.03	0.72	98.27	1.51	0.00	0.20	0.12	Calcic amphibole	Magnesiohastingsite
17Pi400	1.21	11.77	45.06	8.37	0.98	11.39	17.30	1.63	0.00	0.79	98.48	1.31	0.00	0.16	0.18	Calcic amphibole	Edenite
17Pi400	1.05	11.29	45.52	8.28	1.01	11.67	18.68	1.07	0.05	0.59	99.21	1.28	0.00	0.16	0.12	Calcic amphibole	Magnesiohornblende
17Pi400	1.56	14.30	45.85	10.05	0.47	11.73	12.23	1.46	0.04	0.12	97.81	1.41	0.00	0.29	0.16	Calcic amphibole	Magnesiohornblende
17Pi400	1.30	8.05	44.73	9.19	0.42	11.28	23.32	0.14	0.04	0.46	98.93	1.27	0.00	0.36	0.02	Calcic amphibole	Ferrohornblende
17Pi400	1.16	8.61	41.12	11.39	1.62	11.41	21.45	1.23	0.00	0.58	98.57	1.77	0.00	0.27	0.14	Calcic amphibole	Hastingsite
17Pi400	1.42	11.05	42.98	9.65	1.25	11.46	17.99	1.76	0.04	0.37	97.97	1.62	0.00	0.07	0.20	Calcic amphibole	Tschermakite
17Pi400	1.44	10.51	43.31	11.67	0.32	11.07	19.05	0.83	0.01	0.30	98.50	1.59	0.00	0.44	0.09	Calcic amphibole	Tschermakite
17Pi400	1.16	13.36	47.42	6.95	0.66	11.59	15.75	1.21	0.02	0.79	98.90	1.07	0.00	0.12	0.13	Calcic amphibole	Magnesiohornblende
17Pi400	2.50	14.45	41.18	13.68	0.60	11.66	11.39	2.18	0.03	0.13	97.80	2.06	0.00	0.26	0.24	Calcic amphibole	Magnesiohastingsite
17Pi400	1.05	10.62	45.18	8.32	0.96	11.47	19.92	1.16	0.00	0.57	99.26	1.30	0.00	0.16	0.13	Calcic amphibole	Magnesiohornblende
17Pi400	1.04	11.03	45.54	7.87	0.98	11.38	18.44	1.29	0.00	0.63	98.20	1.20	0.00	0.19	0.15	Calcic amphibole	Magnesiohornblende

17Pi400	1.10	9.50	44.30	8.95	1.06	11.68	21.28	0.99	0.01	0.43	99.29	1.38	0.00	0.19	0.11	Calcic amphibole	Ferro-edenite
17Pi400	0.88	13.49	47.58	6.53	0.49	11.44	15.80	1.04	0.00	0.76	98.01	1.02	0.00	0.11	0.12	Calcic amphibole	Magnesiohornblende
17Pi400	0.82	9.44	45.44	8.45	0.88	11.42	18.26	0.84	0.07	0.51	96.15	1.12	0.00	0.39	0.10	Calcic amphibole	Magnesiohornblende
17Pi400	1.25	10.76	43.83	9.11	0.71	11.20	16.69	1.08	0.00	0.52	95.14	1.36	0.00	0.27	0.12	Calcic amphibole	Magnesiohornblende
17Pi400	1.91	12.92	41.29	12.31	0.85	11.40	12.04	2.89	0.07	0.26	95.94	1.87	0.00	0.28	0.32	Calcic amphibole	Magnesiohastingsite
17Pi400	1.24	14.50	46.91	8.13	0.29	10.31	13.24	1.20	0.03	0.47	96.32	1.07	0.00	0.34	0.13	Calcic amphibole	Magnesiohornblende
17Pi400	1.39	8.49	40.42	12.17	1.66	11.27	17.77	2.05	0.00	0.39	95.61	1.76	0.00	0.46	0.24	Calcic amphibole	Pargasite
17Mi439	1.20	14.55	48.49	6.12	0.26	10.36	15.72	0.99	0.00	0.38	98.06	0.92	0.00	0.14	0.11	Calcic amphibole	Magnesiohornblende
17Mi439	1.88	10.91	44.37	11.53	0.27	11.05	17.42	0.29	0.00	0.30	98.03	1.54	0.00	0.44	0.03	Calcic amphibole	Tschermakite
17Mi439	0.80	13.07	47.86	8.35	0.22	11.58	15.22	0.62	0.00	0.21	97.93	1.03	0.00	0.41	0.07	Calcic amphibole	Magnesiohornblende
17Mi439	1.29	12.13	45.74	8.25	0.62	11.42	17.16	1.39	0.00	0.66	98.66	1.26	0.00	0.18	0.15	Calcic amphibole	Magnesiohornblende
17Mi439	1.17	11.58	45.44	9.36	0.61	11.35	16.61	1.21	0.00	0.59	97.92	1.26	0.00	0.37	0.14	Calcic amphibole	Magnesiohornblende
17Mi439	1.74	9.18	42.41	11.66	0.15	11.32	20.95	0.58	0.00	0.38	98.37	1.65	0.00	0.40	0.07	Calcic amphibole	Magnesiohastingsite
17Mi439	1.88	11.81	44.47	12.08	0.43	11.15	16.20	0.62	0.05	0.20	98.90	1.62	0.00	0.43	0.07	Calcic amphibole	Tschermakite
17Mi439	0.84	14.81	50.69	6.85	0.05	11.30	14.09	0.55	0.06	0.30	99.53	0.79	0.00	0.36	0.06	Calcic amphibole	Magnesiohornblende
17Mi439	1.27	11.83	46.16	10.29	0.26	11.75	15.96	0.30	0.02	0.22	98.05	1.23	0.00	0.55	0.03	Calcic amphibole	Magnesiohornblende
17Mi439	0.18	13.58	53.40	2.23	0.13	12.39	16.54	0.02	0.00	0.64	99.11	0.29	0.00	0.09	0.00	Calcic amphibole	Actinolite
17Mi439	1.66	11.47	42.95	14.00	0.30	11.89	15.44	0.48	0.02	0.26	98.47	1.73	0.00	0.68	0.05	Calcic amphibole	Pargasite
17Mi439	1.02	11.87	48.52	7.22	0.00	11.81	18.24	0.31	0.00	0.26	99.25	0.94	0.00	0.30	0.03	Calcic amphibole	Magnesiohornblende
17Mi439	2.41	13.18	44.07	13.58	0.16	10.51	13.38	0.85	0.10	0.12	98.36	1.76	0.00	0.51	0.09	Calcic amphibole	Tschermakite
17Mi439	0.88	11.83	48.68	6.87	0.03	11.59	18.21	0.33	0.00	0.28	98.70	0.88	0.00	0.31	0.04	Calcic amphibole	Magnesiohornblende
17Mi439	1.60	11.66	42.90	13.69	0.25	11.56	15.55	0.37	0.01	0.27	97.85	1.71	0.00	0.66	0.04	Calcic amphibole	Pargasite
17Mi439	1.00	11.72	48.35	7.29	0.02	11.40	17.77	0.72	0.03	0.29	98.60	0.91	0.00	0.35	0.08	Calcic amphibole	Magnesiohornblende
17Mi439	0.95	12.44	45.88	9.66	0.90	12.11	15.58	0.47	0.05	0.56	98.61	1.30	0.00	0.37	0.05	Calcic amphibole	Magnesiohornblende
17Mi439	0.52	12.99	51.52	3.13	0.18	10.91	18.81	0.20	0.06	0.80	99.11	0.49	0.00	0.05	0.02	Calcic amphibole	Actinolite
17Mi439	1.20	9.69	42.70	11.43	0.80	11.56	19.24	0.53	0.00	0.47	97.62	1.59	0.00	0.44	0.06	Calcic amphibole	Magnesiohastingsite
17Mi439	1.36	9.48	44.17	12.09	0.30	11.55	18.28	0.32	0.00	0.29	97.84	1.42	0.00	0.70	0.04	Calcic amphibole	Magnesiohornblende
17Mi439	1.20	11.34	44.10	9.40	1.12	11.73	17.75	1.34	0.03	0.45	98.46	1.45	0.00	0.20	0.15	Calcic amphibole	Edenite
17Mi439	0.80	12.41	50.12	4.71	0.26	11.10	18.08	0.55	0.00	0.53	98.57	0.63	0.00	0.18	0.06	Calcic amphibole	Magnesiohornblende
17Mi439	1.34	11.91	45.10	11.49	0.27	11.88	15.53	0.34	0.04	0.26	98.16	1.41	0.00	0.57	0.04	Calcic amphibole	Magnesiohornblende
17Mi439	1.35	13.37	45.41	11.99	0.42	11.69	12.92	0.89	0.00	0.16	98.20	1.43	0.00	0.62	0.10	Calcic amphibole	Magnesiohornblende
17Mi439	1.77	14.84	44.93	9.71	0.51	11.27	12.77	2.05	0.03	0.15	98.02	1.57	0.00	0.07	0.22	Calcic amphibole	Tschermakite
17Mi439	1.23	9.84	45.50	9.70	0.25	11.88	19.62	0.43	0.01	0.31	98.77	1.27	0.00	0.43	0.05	Calcic amphibole	Magnesiohornblende
17Mi439	1.09	11.27	47.04	6.87	0.67	11.43	18.13	1.49	0.02	0.41	98.42	1.10	0.00	0.09	0.17	Calcic amphibole	Magnesiohornblende
17Mi439	1.39	10.65	44.86	10.29	0.50	11.78	18.41	0.41	0.04	0.60	98.93	1.39	0.00	0.40	0.05	Calcic amphibole	Magnesiohornblende
17Mi439	1.34	11.18	44.06	13.20	0.13	10.52	16.46	0.30	0.00	0.29	97.47	1.51	0.00	0.79	0.03	Calcic amphibole	Tschermakite
17Mi439	0.86	11.74	48.30	7.78	0.03	11.42	17.38	0.66	0.12	0.26	98.56	0.94	0.00	0.41	0.07	Calcic amphibole	Magnesiohornblende
17Mi439	1.77	11.41	44.40	13.23	0.19	11.62	14.52	0.62	0.06	0.29	98.11	1.58	0.00	0.68	0.07	Calcic amphibole	Tschermakite
17Mi439	1.32	10.11	43.31	10.49	1.10	11.50	19.06	1.43	0.02	0.42	98.76	1.61	0.00	0.21	0.16	Calcic amphibole	Tschermakite

17Mi439	1.40	12.71	46.60	9.21	0.19	11.28	15.34	0.60	0.04	0.25	97.62	1.15	0.00	0.45	0.07	Calcic amphibole	Magnesiohornblende
17Mi439	0.18	13.54	53.39	2.76	0.04	13.04	15.55	0.03	0.00	0.35	98.89	0.30	0.00	0.17	0.00	Calcic amphibole	Actinolite
17Mi439	1.19	11.54	45.43	10.00	0.50	10.75	17.57	1.19	0.06	0.41	98.65	1.31	0.00	0.42	0.13	Calcic amphibole	Magnesiohornblende
17Mi439	1.12	12.54	45.83	11.52	0.49	12.09	13.60	0.45	0.08	0.20	97.91	1.38	0.00	0.58	0.05	Calcic amphibole	Magnesiohornblende
17Mi439	1.20	11.18	45.80	9.87	0.13	11.80	17.98	0.29	0.04	0.34	98.63	1.29	0.00	0.42	0.03	Calcic amphibole	Magnesiohornblende
17Mi439	1.16	11.46	44.05	9.15	1.09	11.50	17.47	1.16	0.00	0.42	97.47	1.40	0.00	0.22	0.13	Calcic amphibole	Edenite
17Mi439	1.29	9.82	44.91	11.53	0.14	11.72	18.98	0.40	0.12	0.29	99.21	1.41	0.00	0.58	0.05	Calcic amphibole	Magnesiohornblende
17Mi439	1.41	10.56	44.06	10.49	1.25	11.20	16.69	2.40	0.05	0.39	98.50	1.51	0.00	0.31	0.27	Calcic amphibole	Tschermakite
17Mi439	1.71	15.19	45.96	9.21	0.42	11.01	12.13	1.61	0.05	0.12	97.41	1.43	0.00	0.12	0.17	Calcic amphibole	Magnesiohornblende
17Mi439	1.40	10.01	42.24	11.05	1.41	11.54	19.11	1.76	0.01	0.47	98.99	1.75	0.00	0.17	0.20	Calcic amphibole	Tschermakite
17Mi439	1.51	11.76	44.76	12.07	0.10	11.14	16.53	0.55	0.02	0.39	98.83	1.48	0.00	0.59	0.06	Calcic amphibole	Magnesiohornblende
17Mi439	1.28	14.48	49.40	5.75	0.25	10.25	16.11	0.99	0.01	0.35	98.87	0.82	0.00	0.16	0.11	Calcic amphibole	Magnesiohornblende
17Mi439	1.27	12.93	46.66	7.45	0.79	11.63	16.26	1.30	0.01	0.52	98.84	1.24	0.00	0.03	0.14	Calcic amphibole	Magnesiohornblende
17Mi439	1.66	12.16	43.81	10.82	0.65	11.43	15.90	1.42	0.00	0.30	98.15	1.62	0.00	0.23	0.16	Calcic amphibole	Tschermakite
17Mi439	1.20	15.31	50.37	7.10	0.06	11.54	11.73	0.24	0.02	0.15	97.73	0.86	0.00	0.33	0.03	Calcic amphibole	Magnesiohornblende
17Mi439	1.13	11.68	45.79	8.73	0.78	11.74	17.54	1.07	0.05	0.43	98.94	1.26	0.00	0.25	0.12	Calcic amphibole	Magnesiohornblende
17Mi439	1.11	11.75	46.01	8.79	0.81	12.24	17.00	0.32	0.05	0.35	98.42	1.22	0.00	0.31	0.04	Calcic amphibole	Magnesiohornblende
17Mi518	0.73	11.19	49.08	5.15	0.41	10.54	19.70	0.64	0.05	0.97	98.45	0.71	0.00	0.20	0.07	Calcic amphibole	Magnesiohornblende
17Mi518	2.12	9.47	44.52	14.86	0.45	9.95	16.49	0.34	0.02	0.17	98.38	1.59	0.00	0.93	0.04	Calcic amphibole	Tschermakite
17Mi518	1.37	12.37	44.96	11.96	0.41	11.63	14.37	0.60	0.03	0.26	97.96	1.43	0.00	0.63	0.07	Calcic amphibole	Magnesiohornblende
17Mi518	1.15	12.25	46.18	7.84	0.64	11.49	16.91	1.29	0.00	0.83	98.58	1.20	0.00	0.17	0.14	Calcic amphibole	Magnesiohornblende
17Mi518	1.90	12.55	46.14	9.71	0.16	11.17	16.26	0.46	0.00	0.30	98.64	1.37	0.00	0.27	0.05	Calcic amphibole	Magnesiohornblende
17Mi518	1.21	11.39	46.49	9.13	0.06	11.62	18.16	0.32	0.03	0.10	98.52	1.18	0.00	0.40	0.04	Calcic amphibole	Magnesiohornblende
17Mi518	1.19	12.08	46.13	8.39	0.58	11.62	16.81	1.13	0.02	0.66	98.61	1.21	0.00	0.24	0.13	Calcic amphibole	Magnesiohornblende
17Mi518	1.27	11.20	44.84	10.78	0.23	11.66	17.19	0.46	0.03	0.26	97.92	1.39	0.00	0.49	0.05	Calcic amphibole	Magnesiohornblende
17Mi518	1.72	12.14	45.90	11.02	0.03	11.15	15.48	0.37	0.01	0.39	98.21	1.28	0.00	0.62	0.04	Calcic amphibole	Magnesiohornblende
17Mi518	1.14	11.43	46.31	8.82	0.05	11.87	17.50	0.65	0.00	0.26	98.03	1.18	0.00	0.36	0.07	Calcic amphibole	Magnesiohornblende
17Mi518	0.91	11.79	45.81	9.64	0.35	11.71	16.71	0.69	0.00	0.83	98.44	1.30	0.00	0.37	0.08	Calcic amphibole	Magnesiohornblende
17Mi518	1.20	11.92	45.81	9.20	0.03	11.44	16.87	0.68	0.01	0.30	97.45	1.23	0.00	0.37	0.08	Calcic amphibole	Magnesiohornblende
17Mi518	1.37	10.94	44.06	9.67	1.19	11.61	19.07	1.12	0.01	0.55	99.58	1.49	0.00	0.20	0.13	Calcic amphibole	Edenite
17Mi518	0.87	12.90	48.57	5.81	0.55	11.93	17.10	0.52	0.01	0.49	98.75	0.90	0.00	0.11	0.06	Calcic amphibole	Magnesiohornblende
17Mi518	1.25	10.52	44.23	10.24	0.41	11.35	18.64	0.27	0.04	0.34	97.28	1.38	0.00	0.42	0.03	Calcic amphibole	Magnesiohornblende
17Mi518	0.79	11.87	48.59	6.81	0.00	11.61	18.36	0.91	0.04	0.41	99.40	0.94	0.00	0.23	0.10	Calcic amphibole	Magnesiohornblende
17Mi518	1.60	10.81	44.73	10.49	0.17	11.19	18.57	0.24	0.01	0.34	98.16	1.37	0.00	0.46	0.03	Calcic amphibole	Magnesiohornblende
17Mi518	1.53	10.67	44.73	10.32	0.10	11.60	19.03	0.54	0.00	0.37	98.88	1.41	0.00	0.38	0.06	Calcic amphibole	Magnesiohornblende
17Mi518	1.42	11.33	45.14	10.29	0.29	11.54	17.02	0.38	0.04	0.24	97.69	1.31	0.00	0.48	0.04	Calcic amphibole	Magnesiohornblende
17Mi518	0.37	15.74	53.79	1.93	0.09	12.00	13.99	0.12	0.02	0.43	98.47	0.28	0.00	0.04	0.01	Calcic amphibole	Actinolite
17Mi518	0.59	16.09	51.98	5.20	0.06	11.90	11.39	0.22	0.05	0.18	97.66	0.56	0.00	0.32	0.02	Calcic amphibole	Magnesiohornblende
17Mi518	1.01	13.40	49.08	7.91	0.06	11.62	14.51	0.17	0.01	0.28	98.04	0.88	0.00	0.48	0.02	Calcic amphibole	Magnesiohornblende

17Mi518	0.66	15.67	52.18	4.55	0.09	12.11	12.76	0.23	0.00	0.25	98.50	0.54	0.00	0.23	0.03	Calcic amphibole	Magnesiohornblende
17Mi518	1.51	12.61	46.25	10.32	0.15	10.94	15.71	0.29	0.05	0.29	98.11	1.24	0.00	0.54	0.03	Calcic amphibole	Magnesiohornblende
17Mi518	0.60	15.96	52.10	4.31	0.08	12.26	12.28	0.27	0.02	0.27	98.16	0.55	0.00	0.18	0.03	Calcic amphibole	Magnesiohornblende
17Mi518	1.64	10.45	43.34	12.98	0.09	11.60	16.74	0.47	0.00	0.31	97.63	1.58	0.00	0.69	0.05	Calcic amphibole	Tschermakite
17Mi518	1.27	10.75	45.56	9.46	0.15	11.95	18.36	0.52	0.11	0.34	98.47	1.28	0.00	0.37	0.06	Calcic amphibole	Magnesiohornblende
17Mi518	1.48	6.81	41.69	10.10	1.48	11.11	24.59	0.82	0.04	0.63	98.75	1.66	0.00	0.15	0.09	Calcic amphibole	Hastingsite
17Mi518	0.58	15.58	51.83	4.57	0.11	12.16	13.05	0.28	0.01	0.20	98.38	0.58	0.00	0.19	0.03	Calcic amphibole	Magnesiohornblende
17Mi518	1.16	12.05	46.22	8.04	0.83	11.69	17.61	0.95	0.01	0.57	99.12	1.21	0.00	0.18	0.11	Calcic amphibole	Magnesiohornblende
17Mi518	1.32	12.08	45.63	10.48	0.31	10.82	16.48	0.83	0.02	0.29	98.26	1.31	0.00	0.51	0.09	Calcic amphibole	Magnesiohornblende
17Mi518	0.43	16.26	52.10	4.16	0.22	12.58	11.66	0.33	0.04	0.31	98.10	0.56	0.00	0.14	0.04	Calcic amphibole	Magnesiohornblende
17Mi518	1.30	15.33	49.66	7.03	0.12	11.43	12.58	0.33	0.02	0.27	98.07	0.84	0.00	0.35	0.04	Calcic amphibole	Magnesiohornblende
17Mi518	1.12	11.74	44.88	11.63	0.24	11.57	15.15	0.48	0.02	0.26	97.08	1.38	0.00	0.64	0.05	Calcic amphibole	Magnesiohornblende
17Mi518	1.44	11.43	45.15	10.44	0.09	11.77	16.92	0.43	0.01	0.20	97.87	1.34	0.00	0.47	0.05	Calcic amphibole	Magnesiohornblende
17Mi518	1.32	9.92	44.35	12.18	0.26	11.34	17.58	0.50	0.01	0.36	97.82	1.42	0.00	0.72	0.06	Calcic amphibole	Magnesiohornblende
17Mi518	1.34	11.34	44.79	8.58	0.95	11.60	18.50	0.87	0.01	0.46	98.45	1.33	0.00	0.17	0.10	Calcic amphibole	Edenite
17Mi518	1.30	10.62	43.63	9.46	1.12	11.48	18.70	0.89	0.00	0.56	97.76	1.44	0.00	0.24	0.10	Calcic amphibole	Edenite
17Mi518	1.61	9.90	44.54	11.46	0.19	11.43	17.92	0.37	0.01	0.23	97.66	1.44	0.00	0.55	0.04	Calcic amphibole	Magnesiohornblende
17Mi518	1.49	9.97	44.33	11.24	0.24	11.38	18.89	0.58	0.02	0.27	98.41	1.42	0.00	0.54	0.07	Calcic amphibole	Magnesiohornblende
17Mi518	1.51	11.14	44.90	10.77	0.11	11.61	17.33	0.54	0.04	0.31	98.25	1.39	0.00	0.48	0.06	Calcic amphibole	Magnesiohornblende
17Mi518	1.35	11.08	44.68	11.13	0.07	11.59	17.63	0.36	0.00	0.30	98.20	1.43	0.00	0.50	0.04	Calcic amphibole	Magnesiohornblende
17Mi518	1.55	11.68	44.12	12.06	0.15	12.07	15.72	0.50	0.08	0.27	98.19	1.54	0.00	0.54	0.06	Calcic amphibole	Tschermakite
17Mi518	1.68	19.70	53.41	3.87	0.32	11.19	6.91	0.20	0.14	0.25	97.68	0.58	0.00	0.05	0.02	Calcic amphibole	Magnesiohornblende
17Mi518	1.79	12.61	44.94	11.86	0.22	11.31	13.86	0.70	0.05	0.34	97.69	1.52	0.00	0.50	0.08	Calcic amphibole	Tschermakite
17Mi518	0.77	14.43	49.96	5.77	0.18	11.73	14.14	0.27	0.00	0.46	97.71	0.74	0.00	0.25	0.03	Calcic amphibole	Magnesiohornblende
17Mi518	0.59	18.18	56.45	0.69	0.08	12.09	10.16	0.00	0.03	0.19	98.45	0.11	0.00	0.00	0.00	Calcic amphibole	Actinolite
17Mi518	1.47	11.78	44.91	12.12	0.35	11.15	14.88	1.00	0.08	0.21	97.95	1.53	0.00	0.53	0.11	Calcic amphibole	Tschermakite
17Mi518	1.60	12.09	45.09	11.77	0.37	11.24	14.79	1.00	0.07	0.20	98.21	1.51	0.00	0.49	0.11	Calcic amphibole	Tschermakite
17Mi518	1.54	9.20	43.24	13.47	0.36	11.82	17.77	0.65	0.06	0.25	98.36	1.64	0.00	0.69	0.07	Calcic amphibole	Tschermakite
17Mi518	2.15	13.39	54.34	4.65	0.10	10.68	11.51	0.00	0.02	0.24	97.08	0.12	0.00	0.68	0.00	Calcic amphibole	Actinolite
17Mi518	1.15	10.62	45.91	9.64	0.13	11.53	18.19	0.97	0.04	0.23	98.41	1.22	0.00	0.45	0.11	Calcic amphibole	Magnesiohornblende
17Mi603	0.94	13.97	47.99	8.27	0.17	10.88	15.09	0.57	0.04	0.45	98.36	1.06	0.00	0.35	0.06	Calcic amphibole	Magnesiohornblende
17Mi603	0.92	14.40	48.22	8.33	0.17	11.19	13.62	0.60	0.03	0.38	97.85	1.02	0.00	0.40	0.07	Calcic amphibole	Magnesiohornblende
17Mi603	0.70	13.09	50.16	5.90	0.27	11.09	16.39	0.34	0.00	0.65	98.58	0.70	0.00	0.32	0.04	Calcic amphibole	Magnesiohornblende
17Mi603	1.63	9.60	43.33	11.24	0.24	11.24	20.13	0.81	0.00	0.51	98.73	1.55	0.00	0.42	0.09	Calcic amphibole	Magnesiohastingsite
17Mi603	1.43	15.55	49.28	5.48	0.41	10.59	13.87	1.17	0.03	0.38	98.19	0.83	0.00	0.11	0.13	Calcic amphibole	Magnesiohornblende
17Mi603	0.97	16.50	49.73	8.67	0.29	11.54	9.49	0.81	0.20	0.19	98.39	0.95	0.00	0.50	0.09	Calcic amphibole	Magnesiohornblende
17Mi603	1.47	10.92	43.30	10.17	1.21	11.60	18.94	1.44	0.01	0.45	99.51	1.59	0.00	0.19	0.16	Calcic amphibole	Magnesiohastingsite
17Mi603	1.47	9.49	43.56	10.60	0.26	11.64	20.75	0.80	0.03	0.40	99.00	1.53	0.00	0.33	0.09	Calcic amphibole	Tschermakite
17Mi603	1.75	12.78	46.44	12.30	0.25	10.72	13.46	0.29	0.17	0.27	98.43	1.43	0.00	0.63	0.03	Calcic amphibole	Magnesiohornblende

17Mi603	1.33	13.60	47.26	9.20	0.02	11.29	14.45	0.68	0.11	0.28	98.22	1.14	0.00	0.43	0.07	Calcic amphibole	Magnesiohornblende
17Mi603	1.07	10.55	44.41	9.99	0.75	11.42	18.88	1.06	0.00	0.39	98.50	1.41	0.00	0.34	0.12	Calcic amphibole	Magnesiohornblende
17Mi603	1.46	15.09	48.28	5.94	0.32	10.73	14.10	1.63	0.02	0.41	97.97	0.95	0.00	0.08	0.18	Calcic amphibole	Magnesiohornblende
17Mi603	1.13	11.19	45.61	8.61	0.86	11.77	18.04	0.97	0.02	0.52	98.72	1.25	0.00	0.25	0.11	Calcic amphibole	Magnesiohornblende
17Mi603	1.20	11.52	45.88	9.50	0.59	11.82	17.23	0.72	0.05	0.28	98.79	1.26	0.00	0.38	0.08	Calcic amphibole	Magnesiohornblende
17Mi603	1.37	11.07	43.87	13.14	0.27	11.41	15.47	0.49	0.06	0.22	97.38	1.53	0.00	0.76	0.06	Calcic amphibole	Tschermakite
17Mi603	1.40	8.48	44.44	10.54	0.02	11.21	21.64	0.86	0.04	0.26	98.88	1.37	0.00	0.49	0.10	Calcic amphibole	Ferrohornblende
17Mi603	0.85	11.04	47.60	9.61	0.29	11.47	16.97	0.55	0.03	0.48	98.90	1.05	0.00	0.61	0.06	Calcic amphibole	Magnesiohornblende
17Mi603	1.40	10.69	43.89	11.99	0.06	11.76	17.29	0.43	0.02	0.32	97.84	1.52	0.00	0.56	0.05	Calcic amphibole	Tschermakite
17Mi603	0.83	12.67	48.70	7.76	0.09	10.75	16.54	0.90	0.02	0.29	98.54	0.91	0.00	0.42	0.10	Calcic amphibole	Magnesiohornblende
17Mi603	1.01	10.86	46.53	9.30	0.01	12.11	17.85	0.66	0.02	0.29	98.64	1.18	0.00	0.43	0.07	Calcic amphibole	Magnesiohornblende
17Mi603	1.17	9.86	43.01	9.78	1.32	11.32	20.03	1.33	0.00	0.62	98.44	1.53	0.00	0.21	0.15	Calcic amphibole	Magnesiohastingsite
17Mi603	1.08	10.25	46.08	9.64	0.00	12.02	17.98	0.71	0.02	0.29	98.07	1.19	0.00	0.50	0.08	Calcic amphibole	Magnesiohornblende
17Mi603	1.81	9.00	43.30	13.21	0.29	10.27	19.43	0.80	0.06	0.45	98.62	1.54	0.00	0.78	0.09	Calcic amphibole	Ferropargasite
17Mi603	0.94	12.28	49.82	5.35	0.23	10.68	18.64	0.78	0.02	0.42	99.16	0.70	0.00	0.22	0.09	Calcic amphibole	Magnesiohornblende
17Mi603	0.63	12.24	49.85	6.16	0.00	11.80	17.41	0.35	0.00	0.27	98.71	0.74	0.00	0.31	0.04	Calcic amphibole	Magnesiohornblende
17Mi603	1.08	13.46	47.31	6.96	0.63	11.66	14.59	1.23	0.01	0.47	97.40	1.10	0.00	0.10	0.14	Calcic amphibole	Magnesiohornblende
17Mi603	1.16	12.47	46.38	9.99	0.47	11.46	14.74	0.44	0.02	0.27	97.40	1.28	0.00	0.43	0.05	Calcic amphibole	Magnesiohornblende
17Mi603	1.40	15.37	48.88	5.47	0.46	10.68	13.95	1.39	0.01	0.44	98.04	0.87	0.00	0.08	0.15	Calcic amphibole	Magnesiohornblende
17Mi603	1.11	11.23	44.48	9.04	0.91	11.52	17.57	1.98	0.00	0.41	98.26	1.38	0.00	0.21	0.22	Calcic amphibole	Magnesiohornblende
17Mi603	1.39	10.59	44.47	11.90	0.31	11.54	17.79	0.42	0.03	0.29	98.73	1.47	0.00	0.59	0.05	Calcic amphibole	Magnesiohornblende
17Mi603	1.45	15.11	49.32	5.57	0.33	10.60	13.90	1.29	0.01	0.31	97.90	0.94	0.04	0.00	0.10	Calcic amphibole	Magnesiohornblende
17Mi603	1.03	10.60	44.52	10.15	0.75	11.55	18.85	0.87	0.00	0.44	98.77	1.42	0.00	0.35	0.10	Calcic amphibole	Magnesiohornblende
17Mi603	1.32	13.63	47.17	9.32	0.03	11.17	14.65	0.67	0.11	0.26	98.34	1.16	0.00	0.43	0.07	Calcic amphibole	Magnesiohornblende
17Mi603	1.19	11.64	47.67	12.37	1.79	9.13	12.54	0.27	0.14	0.25	96.99	1.16	0.00	0.93	0.03	Calcic amphibole	Magnesiohornblende
17Mi603	1.37	9.53	43.86	10.62	0.26	11.38	21.18	0.84	0.02	0.38	99.44	1.52	0.00	0.34	0.09	Calcic amphibole	Tschermakite
17Mi603	1.23	10.61	43.69	9.89	1.31	11.59	18.47	1.60	0.01	0.48	98.89	1.56	0.00	0.16	0.18	Calcic amphibole	Tschermakite
17Mi603	1.42	10.46	44.90	10.84	0.28	11.26	18.17	0.79	0.03	0.31	98.46	1.36	0.00	0.53	0.09	Calcic amphibole	Magnesiohornblende
17Mi603	1.23	10.39	44.43	10.65	0.27	11.73	18.93	0.69	0.01	0.28	98.61	1.44	0.00	0.41	0.08	Calcic amphibole	Magnesiohornblende
17Mi603	0.85	16.35	49.87	8.45	0.29	11.38	9.41	0.70	0.26	0.14	97.70	0.88	0.00	0.54	0.08	Calcic amphibole	Magnesiohornblende
17Mi603	1.44	15.55	49.15	5.45	0.40	10.56	14.25	1.32	0.00	0.40	98.52	0.86	0.00	0.07	0.15	Calcic amphibole	Magnesiohornblende
17Mi603	1.66	9.58	43.56	11.13	0.33	11.43	20.00	0.67	0.03	0.62	99.00	1.53	0.00	0.42	0.08	Calcic amphibole	Pargasite
17Mi603	0.78	13.02	50.47	5.95	0.28	10.96	16.22	0.26	0.05	0.70	98.69	0.65	0.00	0.37	0.03	Calcic amphibole	Magnesiohornblende
17Mi603	1.50	9.17	41.53	14.86	0.61	10.98	16.16	0.57	0.03	0.29	95.69	1.79	0.00	0.83	0.06	Calcic amphibole	Tschermakite
17Mi603	1.31	12.77	45.46	10.25	0.00	10.69	14.07	0.58	0.00	0.24	95.37	1.21	0.00	0.59	0.07	Calcic amphibole	Magnesiohornblende
17Mi603	0.93	12.07	46.73	9.68	0.01	11.40	13.61	0.68	0.07	0.24	95.42	1.12	0.00	0.56	0.08	Calcic amphibole	Magnesiohornblende
17Mi603	1.25	7.32	42.11	12.51	0.82	11.36	19.04	0.45	0.01	0.29	95.16	1.51	0.00	0.77	0.05	Calcic amphibole	Ferrotschermakite
17Mi603	1.35	11.29	45.62	10.84	0.01	10.36	15.20	0.62	0.00	0.41	95.70	1.32	0.00	0.55	0.07	Calcic amphibole	Magnesiohornblende
17Mi603	0.82	11.18	48.24	6.60	0.41	10.07	16.97	0.75	0.03	0.87	95.94	0.89	0.00	0.26	0.08	Calcic amphibole	Magnesiohornblende

17Mi603	1.16	11.67	46.53	8.72	0.03	11.15	15.91	0.74	0.00	0.37	96.29	1.04	0.00	0.49	0.08	Calcic amphibole	Magnesiohornblende
17Mi603	0.84	11.19	47.63	6.89	0.58	10.77	16.47	0.53	0.02	0.75	95.68	0.90	0.00	0.31	0.06	Calcic amphibole	Magnesiohornblende
17Mi603	1.07	12.04	45.42	11.21	0.02	10.32	15.53	0.62	0.05	0.22	96.50	1.28	0.00	0.68	0.07	Calcic amphibole	Magnesiohornblende
17Mi603	1.10	14.38	48.10	8.41	0.01	10.62	12.15	0.55	0.20	0.30	95.83	0.91	0.00	0.55	0.06	Calcic amphibole	Magnesiohornblende
17Mi603	1.33	11.19	45.13	10.58	0.03	10.55	16.03	0.57	0.03	0.24	95.67	1.21	0.00	0.67	0.07	Calcic amphibole	Magnesiohornblende
17Mi603	0.93	12.68	47.38	9.17	0.02	11.64	13.61	0.37	0.04	0.25	96.10	1.00	0.00	0.60	0.04	Calcic amphibole	Magnesiohornblende
17Mi603	1.27	12.39	45.70	10.74	0.27	11.84	13.35	0.61	0.04	0.33	96.54	1.31	0.00	0.55	0.07	Calcic amphibole	Magnesiohornblende
17Mi603	1.30	12.22	46.08	10.95	0.00	10.49	14.19	0.47	0.01	0.35	96.06	1.15	0.00	0.76	0.05	Calcic amphibole	Magnesiohornblende
17Mi603	1.36	9.88	43.50	12.15	0.47	10.96	16.64	0.78	0.00	0.49	96.22	1.53	0.00	0.59	0.09	Calcic amphibole	Tschermakite
17Mi603	1.55	12.32	45.32	12.95	0.20	11.22	12.64	0.49	0.01	0.23	96.93	1.46	0.00	0.74	0.05	Calcic amphibole	Magnesiohornblende
17Mi603	1.38	10.25	43.85	12.20	0.35	11.46	15.87	0.30	0.08	0.33	96.06	1.47	0.00	0.67	0.03	Calcic amphibole	Magnesiohornblende
17Mi603	1.55	8.89	44.15	10.41	0.18	9.85	20.95	0.66	0.00	0.46	97.10	1.29	0.00	0.58	0.08	Calcic amphibole	Ferrohornblende
17Mi603	1.18	13.14	46.99	9.42	0.02	11.43	13.90	0.70	0.02	0.32	97.12	1.11	0.00	0.51	0.08	Calcic amphibole	Magnesiohornblende
17Mi603	1.36	12.27	46.24	9.99	0.00	11.26	14.46	0.60	0.01	0.36	96.56	1.26	0.00	0.46	0.07	Calcic amphibole	Magnesiohornblende
17Mi603	1.44	10.27	44.53	10.27	0.42	11.59	17.07	0.53	0.00	0.38	96.49	1.34	0.00	0.47	0.06	Calcic amphibole	Magnesiohornblende
17Mi603	1.19	11.39	45.73	10.59	0.19	11.82	14.80	0.50	0.08	0.22	96.51	1.26	0.00	0.58	0.06	Calcic amphibole	Magnesiohornblende
17Mi603	2.11	10.06	43.03	13.85	0.23	10.16	15.27	0.40	0.11	0.24	95.46	1.62	0.00	0.80	0.04	Calcic amphibole	Tschermakite
17Mi603	1.32	11.90	45.41	8.52	0.96	11.43	15.21	1.52	0.02	0.43	96.72	1.25	0.00	0.25	0.17	Calcic amphibole	Magnesiohornblende
17Mi603	1.39	15.44	48.88	5.52	0.41	10.64	12.57	1.26	0.00	0.41	96.52	0.94	0.02	0.00	0.12	Calcic amphibole	Magnesiohornblende
17Mi603	0.94	11.21	47.96	7.62	0.03	11.46	17.01	0.90	0.03	0.31	97.47	0.98	0.00	0.33	0.10	Calcic amphibole	Magnesiohornblende
17Mi603	2.03	9.41	40.41	16.90	0.32	11.46	14.89	0.35	0.07	0.37	96.21	1.99	0.00	0.97	0.04	Calcic amphibole	Tschermakite
17Mi603	0.93	10.91	46.51	9.13	0.03	11.51	15.84	0.64	0.05	0.36	95.92	1.10	0.00	0.50	0.07	Calcic amphibole	Magnesiohornblende
17Mi603	1.24	11.64	45.97	9.88	0.03	11.50	15.15	0.56	0.07	0.29	96.31	1.24	0.00	0.48	0.06	Calcic amphibole	Magnesiohornblende
17Mi603	1.27	12.67	46.61	7.83	0.75	11.27	15.11	1.14	0.06	0.41	97.12	1.16	0.00	0.19	0.13	Calcic amphibole	Magnesiohornblende
17Mi603	1.08	11.38	46.31	10.00	0.02	11.84	15.44	0.52	0.00	0.31	96.90	1.14	0.00	0.60	0.06	Calcic amphibole	Magnesiohornblende
17Mi603	1.28	11.91	47.13	8.46	0.00	11.78	14.90	0.82	0.07	0.31	96.66	1.06	0.00	0.41	0.09	Calcic amphibole	Magnesiohornblende
17Mi603	1.24	9.77	42.65	10.66	1.05	11.68	17.55	0.99	0.00	0.32	95.91	1.51	0.00	0.40	0.11	Calcic amphibole	Tschermakite
17Mi603	1.46	13.85	47.08	7.95	0.38	10.48	14.23	0.91	0.00	0.46	96.80	1.03	0.00	0.36	0.10	Calcic amphibole	Magnesiohornblende
17Mi603	1.50	9.87	43.89	12.42	0.29	11.23	16.19	0.54	0.01	0.19	96.13	1.47	0.00	0.71	0.06	Calcic amphibole	Magnesiohornblende
17Mi603	1.46	10.37	44.59	12.84	0.12	11.94	15.05	0.35	0.01	0.31	97.04	1.44	0.00	0.79	0.04	Calcic amphibole	Magnesiohornblende
17Mi603	0.98	10.56	46.90	8.32	0.02	11.41	17.17	0.92	0.03	0.27	96.57	1.05	0.00	0.40	0.10	Calcic amphibole	Magnesiohornblende
17Mi603	1.37	11.90	46.30	7.97	0.81	11.44	15.42	1.12	0.00	0.65	96.99	1.14	0.00	0.25	0.13	Calcic amphibole	Magnesiohornblende
17Mi603	1.21	10.18	44.66	8.79	1.06	11.61	17.55	1.10	0.00	0.73	96.89	1.27	0.00	0.29	0.12	Calcic amphibole	Magnesiohornblende
17Mi603	1.65	8.40	43.65	11.08	0.46	11.51	19.44	0.45	0.01	0.31	96.96	1.41	0.00	0.56	0.05	Calcic amphibole	Ferrohornblende
17Mi603	1.21	10.70	45.11	11.00	0.42	11.74	15.82	0.58	0.10	0.32	97.00	1.34	0.00	0.58	0.06	Calcic amphibole	Magnesiohornblende
17Mi603	1.28	10.02	43.78	11.30	0.79	11.21	17.07	1.08	0.02	0.45	96.99	1.50	0.00	0.48	0.12	Calcic amphibole	Magnesiohornblende
17Mi603	1.22	13.05	46.70	7.87	0.72	11.70	13.95	1.11	0.00	0.54	96.86	1.13	0.00	0.23	0.12	Calcic amphibole	Magnesiohornblende
17Mi603	1.04	9.33	44.19	10.26	1.10	11.95	18.07	1.33	0.06	0.49	97.82	1.38	0.00	0.43	0.15	Calcic amphibole	Magnesiohornblende
17Mi603	0.90	13.38	48.71	6.99	0.37	10.99	14.56	1.15	0.00	0.27	97.33	0.98	0.00	0.21	0.13	Calcic amphibole	Magnesiohornblende

17Mi603	1.31	11.76	44.68	10.46	0.44	11.80	15.17	0.83	0.01	0.48	96.94	1.42	0.00	0.40	0.09	Calcic amphibole	Magnesiohornblende
17Mi603	1.05	7.44	42.49	10.55	1.34	11.49	20.63	1.71	0.02	0.44	97.16	1.50	0.00	0.41	0.20	Calcic amphibole	Ferrohornblende
17Mi603	1.04	14.25	49.41	5.61	0.49	11.53	13.12	0.90	0.05	0.49	96.89	0.81	0.00	0.15	0.10	Calcic amphibole	Magnesiohornblende
17Mi642	1.11	12.80	46.46	10.22	0.31	11.24	14.68	0.84	0.10	0.24	97.99	1.22	0.00	0.54	0.09	Calcic amphibole	Magnesiohornblende
17Mi642	1.53	11.41	41.95	11.69	0.89	11.67	16.08	1.99	0.01	0.39	97.61	1.80	0.00	0.23	0.22	Calcic amphibole	Tschermakite
17Mi642	1.19	12.14	45.33	13.15	0.29	11.57	13.79	0.54	0.02	0.27	98.29	1.43	0.00	0.82	0.06	Calcic amphibole	Magnesiohornblende
17Mi642	0.55	13.72	49.23	6.29	0.39	10.25	16.72	0.86	0.05	0.37	98.42	0.83	0.00	0.25	0.09	Calcic amphibole	Magnesiohornblende
17Mi642	1.16	10.04	45.53	10.28	0.37	11.40	18.28	0.69	0.09	0.23	98.07	1.33	0.00	0.45	0.08	Calcic amphibole	Magnesiohornblende
17Mi642	1.04	13.14	48.58	8.37	0.00	11.88	14.85	0.46	0.03	0.26	98.62	0.98	0.00	0.45	0.05	Calcic amphibole	Magnesiohornblende
17Mi642	0.82	11.20	47.89	8.61	0.01	10.91	18.39	0.60	0.06	0.27	98.76	0.99	0.00	0.49	0.07	Calcic amphibole	Magnesiohornblende
17Mi642	1.32	10.61	42.67	10.12	1.28	11.64	19.09	1.33	0.05	0.50	98.61	1.62	0.00	0.16	0.15	Calcic amphibole	Magnesiohastingsite
17Mi642	1.04	11.68	47.68	8.60	0.04	10.88	17.88	0.59	0.00	0.25	98.64	1.02	0.00	0.46	0.07	Calcic amphibole	Magnesiohornblende
17Mi642	0.69	11.10	48.45	6.32	0.39	10.80	19.76	1.00	0.05	0.45	99.01	0.86	0.00	0.24	0.11	Calcic amphibole	Magnesiohornblende
17Mi642	1.49	10.33	41.57	12.17	1.39	11.40	17.69	1.42	0.01	0.40	97.87	1.83	0.00	0.31	0.16	Calcic amphibole	Magnesiohastingsite
17Mi642	0.98	12.51	46.27	9.47	0.34	10.91	16.31	0.73	0.00	0.35	97.87	1.21	0.00	0.43	0.08	Calcic amphibole	Magnesiohornblende
17Mi642	0.67	14.87	50.39	5.67	0.25	12.11	13.00	0.46	0.01	0.39	97.82	0.72	0.00	0.25	0.05	Calcic amphibole	Magnesiohornblende
17Mi642	0.77	11.92	49.03	6.73	0.02	11.76	17.95	0.69	0.03	0.23	99.13	0.87	0.00	0.29	0.08	Calcic amphibole	Magnesiohornblende
17Mi642	1.46	12.57	45.78	10.89	0.00	10.77	15.22	0.39	0.00	0.29	97.37	1.28	0.00	0.61	0.04	Calcic amphibole	Magnesiohornblende
17Mi642	0.95	11.99	47.88	7.99	0.00	11.69	17.02	0.76	0.01	0.26	98.55	1.01	0.00	0.37	0.08	Calcic amphibole	Magnesiohornblende
17Mi642	0.66	13.29	49.40	6.45	0.01	11.98	15.94	0.62	0.00	0.28	98.64	0.85	0.00	0.25	0.07	Calcic amphibole	Magnesiohornblende
17Mi642	1.45	12.61	46.15	10.15	0.00	10.89	16.35	0.76	0.06	0.39	98.82	1.29	0.00	0.45	0.08	Calcic amphibole	Magnesiohornblende
17Mi642	1.36	12.70	46.86	8.79	0.01	11.69	15.72	0.80	0.20	0.26	98.38	1.16	0.00	0.35	0.09	Calcic amphibole	Magnesiohornblende
17Mi642	1.10	12.50	47.43	8.80	0.02	11.35	16.37	0.73	0.06	0.34	98.69	1.10	0.00	0.40	0.08	Calcic amphibole	Magnesiohornblende
17Mi642	1.21	8.87	41.99	10.42	1.21	11.45	22.04	0.76	0.03	0.51	98.49	1.65	0.00	0.20	0.09	Calcic amphibole	Hastingsite
17Mi642	1.23	11.90	44.89	12.63	0.06	10.64	15.70	0.38	0.00	0.33	97.76	1.44	0.00	0.74	0.04	Calcic amphibole	Magnesiohornblende
17Mi642	1.72	4.35	40.92	12.66	0.32	10.36	28.57	0.83	0.02	0.38	100.14	1.76	0.00	0.52	0.10	Calcic amphibole	Ferropargasite
17Mi642	1.63	4.16	40.67	12.62	0.31	10.27	28.22	0.88	0.01	0.44	99.21	1.74	0.00	0.56	0.10	Calcic amphibole	Ferropargasite
17Mi642	0.69	11.11	49.38	5.14	0.45	10.83	19.49	0.50	0.00	0.77	98.36	0.66	0.00	0.24	0.06	Calcic amphibole	Magnesiohornblende
17Mi642	1.54	9.52	43.52	11.00	0.42	11.50	19.94	0.56	0.01	0.30	98.31	1.50	0.00	0.44	0.06	Calcic amphibole	Edenite
17Mi642	0.97	12.45	46.07	8.02	0.86	11.66	16.55	0.90	0.01	0.46	97.95	1.19	0.00	0.21	0.10	Calcic amphibole	Magnesiohornblende
17Mi642	0.74	14.17	51.54	4.74	0.08	12.01	14.60	0.18	0.04	0.23	98.33	0.54	0.00	0.26	0.02	Calcic amphibole	Magnesiohornblende
17Mi642	0.90	12.92	46.86	8.26	0.80	12.31	15.18	1.27	0.00	0.29	98.79	1.21	0.00	0.20	0.14	Calcic amphibole	Magnesiohornblende
17Mi642	1.58	12.70	46.22	10.48	0.02	10.85	15.90	0.41	0.03	0.26	98.45	1.27	0.00	0.53	0.05	Calcic amphibole	Magnesiohornblende
17Mi642	0.91	11.35	48.13	7.70	0.04	11.76	18.21	0.76	0.02	0.27	99.15	0.98	0.00	0.35	0.08	Calcic amphibole	Magnesiohornblende
17Mi642	1.38	13.33	47.28	9.12	0.16	11.72	14.29	0.35	0.01	0.24	97.87	1.11	0.00	0.46	0.04	Calcic amphibole	Magnesiohornblende
17Mi642	0.86	14.86	49.55	5.86	0.24	11.14	14.20	1.12	0.04	0.34	98.21	0.83	0.00	0.18	0.12	Calcic amphibole	Magnesiohornblende
17Mi642	1.65	14.34	45.61	13.04	0.22	9.92	12.01	0.61	0.07	0.26	97.73	1.41	0.00	0.82	0.07	Calcic amphibole	Edenite
17Mi642	1.25	12.21	46.68	9.24	0.10	11.17	16.90	0.64	0.02	0.42	98.62	1.18	0.00	0.41	0.07	Calcic amphibole	Magnesiohornblende
17Mi642	1.36	12.71	46.08	9.21	0.20	11.36	15.87	0.82	0.04	0.30	97.95	1.24	0.00	0.35	0.09	Calcic amphibole	Magnesiohornblende

17Mi642	1.51	6.97	42.14	11.76	0.40	10.93	24.05	0.90	0.04	0.33	99.04	1.63	0.00	0.47	0.10	Calcic amphibole	Ferropargasite
17Mi642	1.20	12.89	46.35	10.70	0.18	10.48	15.03	0.75	0.02	0.37	97.97	1.24	0.00	0.60	0.08	Calcic amphibole	Magnesiohornblende
17Mi642	1.37	12.57	45.87	10.28	0.02	11.16	15.52	0.61	0.09	0.27	97.76	1.28	0.00	0.49	0.07	Calcic amphibole	Magnesiohornblende

COMPOSITION OF AMPHIBOLE FROM SITE U1418, PROXIMAL SITE

	Analysis wt%																
sample name	Na_2O	MgO	SiO_2	Al_2O_3	K_2O	CaO	FeO	TiO_2	Cr_2O_3	MnO	Total	Al(T)	Ti(T)	[Al(C)	Ti(C)	Groups	Names
18MPe37	1.10	13.72	46.87	11.50	0.10	11.68	10.77	0.61	0.05	0.20	96.60	1.27	0.00	0.68	0.07	Calcic amphibole	Magnesiohornblende
18MPe37	1.58	13.87	45.47	12.50	0.14	11.12	10.73	0.89	0.41	0.19	96.90	1.51	0.00	0.60	0.10	Calcic amphibole	Tschermakite
18MPe37	1.62	9.83	41.92	14.55	0.64	11.67	15.64	0.60	0.02	0.32	96.81	1.78	0.00	0.77	0.07	Calcic amphibole	Tschermakite
18MPe37	1.87	8.12	40.99	13.17	0.10	9.50	19.57	2.27	0.00	0.34	95.93	1.87	0.00	0.45	0.26	Calcic amphibole	Tschermakite
18MPe37	1.31	11.23	45.44	10.42	0.22	11.82	15.01	0.48	0.11	0.32	96.36	1.27	0.00	0.55	0.05	Calcic amphibole	Magnesiohornblende
18MPe37	1.85	12.32	44.26	14.15	0.13	11.51	11.66	0.83	0.06	0.24	97.00	1.60	0.00	0.81	0.09	Calcic amphibole	Tschermakite
18MPe37	1.56	10.84	43.63	13.12	0.22	11.45	14.15	0.68	0.04	0.32	96.01	1.55	0.00	0.74	0.08	Calcic amphibole	Tschermakite
18MPe37	1.59	9.91	44.38	10.41	0.25	11.05	17.58	0.79	0.01	0.22	96.18	1.36	0.00	0.47	0.09	Calcic amphibole	Magnesiohornblende
18MPe37	1.34	12.38	46.03	10.21	0.19	11.58	13.76	0.55	0.12	0.26	96.43	1.26	0.00	0.50	0.06	Calcic amphibole	Magnesiohornblende
18MPe37	1.73	15.63	44.60	12.30	0.38	11.15	9.44	1.20	0.00	0.24	96.67	1.53	0.00	0.58	0.13	Calcic amphibole	Pargasite
18MPe37	1.07	15.84	49.13	8.83	0.22	11.24	9.50	0.32	0.13	0.33	96.61	1.04	0.00	0.44	0.03	Calcic amphibole	Magnesiohornblende
18MPe37	1.50	11.21	44.89	12.68	0.11	11.63	13.65	0.56	0.02	0.21	96.45	1.41	0.00	0.78	0.06	Calcic amphibole	Magnesiohornblende
18MPe37	1.58	9.87	44.64	10.73	0.14	11.64	17.24	0.94	0.00	0.25	97.03	1.36	0.00	0.53	0.11	Calcic amphibole	Magnesiohornblende
18MPe37	1.25	10.51	44.19	13.34	0.14	11.67	14.68	0.46	0.05	0.23	96.52	1.50	0.00	0.81	0.05	Calcic amphibole	Tschermakite
18MPe37	1.64	8.20	43.64	10.95	0.48	11.53	20.00	1.28	0.03	0.30	98.05	1.46	0.00	0.48	0.14	Calcic amphibole	Ferrohornblende
18MPe37	2.12	14.70	47.08	10.51	0.12	11.33	9.59	0.33	0.17	0.25	96.20	1.20	0.00	0.59	0.04	Calcic amphibole	Magnesiohornblende
18MPe37	0.94	13.58	47.41	9.84	0.02	12.04	11.93	0.89	0.10	0.32	97.06	1.17	0.00	0.50	0.10	Calcic amphibole	Magnesiohornblende
18MPe37	1.30	14.00	46.56	12.19	0.10	11.74	10.19	0.66	0.15	0.22	97.12	1.36	0.00	0.69	0.07	Calcic amphibole	Magnesiohornblende
18MPe37	1.30	7.22	42.01	15.36	0.45	11.53	17.42	0.33	0.06	0.36	96.05	1.65	0.00	1.08	0.04	Calcic amphibole	Ferrotschermakite
18MPe37	1.41	12.57	46.49	10.81	0.00	12.01	13.16	0.60	0.00	0.26	97.31	1.26	0.00	0.59	0.07	Calcic amphibole	Magnesiohornblende
18MPe37	1.51	11.71	45.59	11.98	0.22	11.39	13.61	0.58	0.12	0.23	96.95	1.36	0.00	0.69	0.06	Calcic amphibole	Magnesiohornblende
18MPe37	1.32	11.17	46.13	10.94	0.10	11.78	14.42	0.47	0.03	0.21	96.57	1.21	0.00	0.69	0.05	Calcic amphibole	Magnesiohornblende
18MPe37	2.39	13.62	45.91	11.95	0.07	11.39	10.33	0.54	0.21	0.20	96.61	1.35	0.00	0.70	0.06	Calcic amphibole	Magnesiohornblende
18MPe37	1.90	9.91	43.85	11.30	0.16	11.32	17.09	0.71	0.05	0.30	96.59	1.45	0.00	0.54	0.08	Calcic amphibole	Magnesiohornblende
18MPe37	1.09	11.18	46.03	10.25	0.24	11.87	15.03	0.39	0.00	0.34	96.42	1.19	0.00	0.59	0.04	Calcic amphibole	Magnesiohornblende
18MPe37	1.28	12.15	46.30	10.57	0.13	11.81	13.43	0.59	0.07	0.24	96.58	1.22	0.00	0.60	0.07	Calcic amphibole	Magnesiohornblende
18MPe37	1.36	12.20	46.34	9.39	0.07	11.20	14.60	1.15	0.07	0.27	96.65	1.23	0.00	0.39	0.13	Calcic amphibole	Magnesiohornblende
18MPe37	1.13	11.41	46.65	9.16	0.10	12.04	15.55	0.54	0.05	0.25	96.88	1.12	0.00	0.48	0.06	Calcic amphibole	Magnesiohornblende
18MPe37	1.37	12.47	46.01	12.16	0.22	12.03	12.01	0.55	0.02	0.20	97.05	1.32	0.00	0.76	0.06	Calcic amphibole	Magnesiohornblende
18MPe37	1.33	13.40	46.33	9.20	0.49	12.03	13.39	0.43	0.10	0.22	96.92	1.23	0.00	0.36	0.05	Calcic amphibole	Magnesiohornblende

18MPe37	1.91	8.18	42.39	12.84	0.16	11.13	18.71	0.82	0.00	0.28	96.42	1.61	0.00	0.67	0.09	Calcic amphibole	Tschermakite
18MPe37	0.80	11.45	46.06	8.60	0.33	11.05	16.14	0.69	0.00	0.41	95.52	1.05	0.00	0.48	0.08	Calcic amphibole	Magnesiohornblende
18MPe37	1.45	9.06	44.14	10.86	0.18	11.69	18.03	0.70	0.02	0.34	96.46	1.36	0.00	0.57	0.08	Calcic amphibole	Magnesiohornblende
18MPe37	1.31	10.93	44.75	11.46	0.19	11.94	14.71	0.50	0.06	0.21	96.06	1.35	0.00	0.66	0.06	Calcic amphibole	Magnesiohornblende
18MPe37	1.66	13.05	44.48	13.76	0.11	11.04	11.52	0.88	0.27	0.21	96.97	1.63	0.00	0.69	0.09	Calcic amphibole	Tschermakite
18MPe37	1.47	11.32	46.91	8.93	0.11	11.25	15.79	0.57	0.09	0.35	96.79	1.10	0.00	0.45	0.06	Calcic amphibole	Magnesiohornblende
18MPe37	1.32	9.72	44.42	11.45	0.35	11.50	16.32	0.77	0.02	0.27	96.14	1.35	0.00	0.67	0.09	Calcic amphibole	Magnesiohornblende
18MPe37	1.08	11.52	45.00	8.67	0.87	11.40	15.52	1.93	0.00	0.42	96.41	1.29	0.00	0.23	0.22	Calcic amphibole	Magnesiohornblende
18MPe37	1.60	12.64	45.26	11.65	0.09	11.27	13.01	1.37	0.06	0.23	97.19	1.46	0.00	0.52	0.15	Calcic amphibole	Magnesiohornblende
18MPe37	1.12	11.65	44.47	10.45	0.77	11.74	14.52	1.47	0.01	0.38	96.57	1.41	0.00	0.42	0.16	Calcic amphibole	Magnesiohornblende
18MPe37	1.63	11.16	44.74	12.90	0.09	11.10	13.66	0.64	0.10	0.30	96.32	1.45	0.00	0.77	0.07	Calcic amphibole	Magnesiohornblende
18MPe37	1.94	13.24	44.57	13.99	0.16	11.63	10.03	0.86	0.00	0.18	96.60	1.56	0.00	0.82	0.09	Calcic amphibole	Tschermakite
18MPe37	2.27	8.29	42.66	11.42	0.69	9.74	19.87	0.68	0.00	0.56	96.18	1.56	0.00	0.48	0.08	Calcic amphibole	Tschermakite
18MPe37	1.15	13.17	46.46	10.51	0.15	11.86	12.03	0.55	0.09	0.30	96.27	1.24	0.00	0.57	0.06	Calcic amphibole	Magnesiohornblende
18MPe37	1.46	11.39	43.27	14.40	0.22	11.78	12.44	0.90	0.03	0.25	96.14	1.65	0.00	0.85	0.10	Calcic amphibole	Tschermakite
18MPe37	1.31	11.58	46.59	9.45	0.11	11.57	14.81	0.36	0.07	0.23	96.08	1.11	0.00	0.54	0.04	Calcic amphibole	Magnesiohornblende
18MPe37	1.75	10.02	44.69	10.95	0.21	11.57	17.25	0.58	0.00	0.32	97.34	1.37	0.00	0.54	0.07	Calcic amphibole	Magnesiohornblende
18MPe37	1.59	15.12	45.96	11.13	0.08	11.58	10.02	1.08	0.09	0.20	96.85	1.44	0.00	0.44	0.12	Calcic amphibole	Magnesiohornblende
18MPe37	1.89	9.31	43.98	12.30	0.16	11.18	16.21	0.65	0.07	0.30	96.05	1.41	0.00	0.77	0.07	Calcic amphibole	Magnesiohornblende
18MPe37	1.60	11.36	45.80	11.17	0.16	11.47	14.49	0.59	0.04	0.30	96.97	1.29	0.00	0.64	0.07	Calcic amphibole	Magnesiohornblende
18MPe37	1.10	13.62	46.46	11.72	0.12	11.92	10.78	0.61	0.13	0.25	96.71	1.32	0.00	0.67	0.07	Calcic amphibole	Magnesiohornblende
18MPe50	1.31	12.32	47.10	10.47	0.06	11.76	13.10	0.49	0.07	0.28	96.96	1.15	0.00	0.64	0.05	Calcic amphibole	Magnesiohornblende
18MPe50	1.05	12.15	46.41	9.81	0.11	11.91	14.65	0.57	0.08	0.24	96.97	1.16	0.00	0.54	0.06	Calcic amphibole	Magnesiohornblende
18MPe50	1.44	10.85	45.55	10.48	0.08	11.67	15.46	0.39	0.01	0.29	96.22	1.24	0.00	0.60	0.04	Calcic amphibole	Magnesiohornblende
18MPe50	1.52	9.80	44.14	10.98	0.34	11.20	16.98	1.20	0.10	0.27	96.52	1.41	0.00	0.52	0.13	Calcic amphibole	Magnesiohornblende
18MPe50	1.34	14.50	47.31	10.98	0.05	11.54	9.92	0.49	0.18	0.22	96.53	1.23	0.00	0.62	0.05	Calcic amphibole	Magnesiohornblende
18MPe50	2.21	9.90	41.94	13.64	0.37	11.67	15.96	0.42	0.02	0.24	96.37	1.71	0.00	0.70	0.05	Calcic amphibole	Pargasite
18MPe50	1.56	11.03	45.74	10.92	0.16	11.35	14.87	0.37	0.35	0.17	96.53	1.26	0.00	0.64	0.04	Calcic amphibole	Magnesiohornblende
18MPe50	1.20	10.95	45.61	11.19	0.19	11.99	14.92	0.60	0.00	0.29	96.94	1.29	0.00	0.66	0.07	Calcic amphibole	Magnesiohornblende
18MPe50	1.93	10.40	43.67	12.50	0.21	11.26	15.53	0.74	0.02	0.24	96.50	1.52	0.00	0.66	0.08	Calcic amphibole	Tschermakite
18MPe50	1.37	8.24	44.73	10.12	0.13	11.43	19.24	0.48	0.00	0.36	96.10	1.22	0.00	0.60	0.06	Calcic amphibole	Ferrohornblende
18MPe50	1.30	10.09	43.95	11.60	0.28	11.60	16.96	0.59	0.00	0.24	96.60	1.47	0.00	0.56	0.07	Calcic amphibole	Magnesiohornblende
18MPe50	0.99	12.21	45.87	8.70	0.74	11.71	14.95	1.04	0.03	0.37	96.60	1.22	0.00	0.30	0.12	Calcic amphibole	Magnesiohornblende
18MPe50	1.28	8.92	42.08	16.33	0.25	10.91	15.81	0.24	0.00	0.35	96.16	1.69	0.00	1.20	0.03	Calcic amphibole	Tschermakite
18MPe50	1.15	11.69	45.95	10.55	0.08	12.00	14.39	0.48	0.00	0.32	96.61	1.25	0.00	0.58	0.05	Calcic amphibole	Magnesiohornblende
18MPe50	1.32	11.71	45.54	11.74	0.18	11.57	13.80	0.60	0.00	0.23	96.68	1.35	0.00	0.67	0.07	Calcic amphibole	Magnesiohornblende
18MPe50	1.20	12.08	46.80	9.69	0.14	11.90	13.71	0.39	0.04	0.30	96.25	1.11	0.00	0.57	0.04	Calcic amphibole	Magnesiohornblende
18MPe50	1.42	11.07	45.85	10.37	0.16	11.65	15.14	0.65	0.03	0.23	96.57	1.22	0.00	0.59	0.07	Calcic amphibole	Magnesiohornblende
18MPe50	1.63	11.14	42.98	12.95	0.45	10.39	14.59	0.87	0.02	0.33	95.34	1.65	0.00	0.61	0.10	Calcic amphibole	Tschermakite

18MPe50	1.13	11.36	45.94	10.55	0.12	11.68	14.72	0.43	0.04	0.26	96.22	1.23	0.00	0.61	0.05	Calcic amphibole	Magnesiohornblende
18MPe50	1.09	13.72	46.57	11.31	0.12	11.92	11.00	0.60	0.20	0.21	96.74	1.30	0.00	0.62	0.07	Calcic amphibole	Magnesiohornblende
18MPe50	1.97	12.38	44.32	12.14	0.22	11.38	12.81	1.11	0.18	0.14	96.65	1.52	0.00	0.57	0.12	Calcic amphibole	Tschermakite
18MPe50	1.38	12.86	46.23	11.06	0.20	11.50	12.37	0.61	0.06	0.15	96.42	1.28	0.00	0.62	0.07	Calcic amphibole	Magnesiohornblende
18MPe50	1.62	13.71	45.66	13.24	0.05	11.57	10.03	0.55	0.05	0.18	96.66	1.46	0.00	0.78	0.06	Calcic amphibole	Magnesiohornblende
18MPe50	1.39	10.20	44.43	11.51	0.21	11.62	16.21	0.38	0.07	0.21	96.23	1.38	0.00	0.64	0.04	Calcic amphibole	Magnesiohornblende
18MPe50	1.95	8.20	42.46	11.30	0.32	10.92	19.57	0.81	0.03	0.41	95.97	1.53	0.00	0.50	0.09	Calcic amphibole	Tschermakite
18MPe50	1.63	10.72	44.48	11.54	0.20	11.41	15.43	0.60	0.00	0.27	96.28	1.40	0.00	0.62	0.07	Calcic amphibole	Magnesiohornblende
18MPe50	1.36	11.88	45.39	10.70	0.03	11.63	14.44	0.74	0.08	0.28	96.53	1.34	0.00	0.51	0.08	Calcic amphibole	Magnesiohornblende
18MPe50	1.38	10.28	44.69	12.45	0.22	11.22	14.69	0.49	0.11	0.26	95.79	1.37	0.00	0.81	0.05	Calcic amphibole	Magnesiohornblende
18MPe50	1.44	9.52	43.56	12.59	0.18	11.42	16.74	0.78	0.00	0.28	96.52	1.52	0.00	0.68	0.09	Calcic amphibole	Tschermakite
18MPe50	2.74	12.07	44.75	14.59	0.23	10.26	11.09	0.58	0.06	0.32	96.69	1.53	0.00	0.95	0.06	Calcic amphibole	Tschermakite
18MPe50	1.26	12.63	48.43	8.39	0.10	11.75	13.45	0.36	0.02	0.29	96.68	0.92	0.00	0.53	0.04	Calcic amphibole	Magnesiohornblende
18MPe50	2.18	12.60	44.00	14.36	0.28	11.13	11.12	0.65	0.11	0.17	96.60	1.63	0.00	0.83	0.07	Calcic amphibole	Tschermakite
18MPe50	1.88	9.36	43.30	12.80	0.22	11.35	17.20	0.58	0.02	0.32	97.03	1.56	0.00	0.68	0.07	Calcic amphibole	Tschermakite
18MPe50	1.36	10.96	45.35	11.72	0.21	11.53	14.10	0.41	0.11	0.25	96.01	1.29	0.00	0.75	0.05	Calcic amphibole	Magnesiohornblende
18MPe50	1.32	10.91	45.75	11.44	0.07	11.59	14.76	0.49	0.04	0.26	96.63	1.28	0.00	0.71	0.06	Calcic amphibole	Magnesiohornblende
18MPe50	1.48	8.90	43.72	11.65	0.08	11.99	18.14	0.82	0.03	0.28	97.08	1.45	0.00	0.61	0.09	Calcic amphibole	Magnesiohornblende
18MPe50	1.25	11.81	46.53	10.48	0.10	11.64	13.69	0.57	0.06	0.23	96.36	1.17	0.00	0.64	0.06	Calcic amphibole	Magnesiohornblende
18MPe50	0.63	14.89	51.27	4.84	0.13	11.58	12.52	0.39	0.03	0.29	96.57	0.61	0.00	0.21	0.04	Calcic amphibole	Magnesiohornblende
18MPe84	1.53	11.09	44.93	12.88	0.12	11.57	13.97	0.99	0.07	0.38	97.52	1.47	0.00	0.74	0.11	Calcic amphibole	Magnesiohornblende
18MPe84	1.63	11.10	43.89	14.87	0.24	11.86	12.44	0.56	0.04	0.24	96.88	1.59	0.00	0.97	0.06	Calcic amphibole	Tschermakite
18MPe84	1.31	10.22	46.09	9.21	0.12	11.60	17.82	0.65	0.02	0.28	97.33	1.18	0.00	0.43	0.07	Calcic amphibole	Magnesiohornblende
18MPe84	1.29	11.46	45.23	12.46	0.39	11.46	13.48	0.52	0.02	0.22	96.52	1.38	0.00	0.77	0.06	Calcic amphibole	Magnesiohornblende
18MPe84	1.52	11.26	46.04	10.19	0.09	11.71	14.78	0.51	0.06	0.31	96.47	1.19	0.00	0.59	0.06	Calcic amphibole	Magnesiohornblende
18MPe84	1.66	13.23	45.24	13.47	0.03	12.36	10.08	1.07	0.13	0.17	97.42	1.49	0.00	0.80	0.12	Calcic amphibole	Magnesiohornblende
18MPe84	1.23	11.53	46.22	11.12	0.15	11.98	13.56	0.41	0.02	0.26	96.48	1.20	0.00	0.72	0.05	Calcic amphibole	Magnesiohornblende
18MPe84	1.36	10.83	46.07	9.68	0.06	11.75	15.82	0.54	0.01	0.25	96.37	1.15	0.00	0.54	0.06	Calcic amphibole	Magnesiohornblende
18MPe84	1.37	10.37	45.62	10.24	0.13	11.68	16.03	0.58	0.00	0.26	96.29	1.20	0.00	0.60	0.07	Calcic amphibole	Magnesiohornblende
18MPe84	0.51	14.28	52.37	4.05	0.07	12.11	12.79	0.13	0.00	0.32	96.62	0.39	0.00	0.30	0.01	Calcic amphibole	Actinolite
18MPe84	1.54	13.29	46.35	12.35	0.07	11.18	10.60	0.53	0.13	0.15	96.18	1.32	0.00	0.78	0.06	Calcic amphibole	Magnesiohornblende
18MPe84	2.02	13.43	46.14	12.04	0.10	11.72	10.26	0.42	0.14	0.18	96.45	1.30	0.00	0.76	0.05	Calcic amphibole	Magnesiohornblende
18MPe84	1.60	12.44	46.24	9.96	0.19	10.86	13.82	1.28	0.13	0.21	96.73	1.27	0.00	0.44	0.14	Calcic amphibole	Magnesiohornblende
18MPe84	1.44	11.81	45.96	11.64	0.20	11.81	13.33	0.42	0.04	0.29	96.94	1.29	0.00	0.71	0.05	Calcic amphibole	Magnesiohornblende
18MPe84	0.51	11.58	52.53	2.14	0.17	11.99	18.58	0.04	0.05	0.32	97.91	0.26	0.00	0.12	0.00	Calcic amphibole	Actinolite
18MPe84	1.71	12.80	45.41	13.31	0.08	11.66	10.92	0.72	0.09	0.22	96.93	1.45	0.00	0.81	0.08	Calcic amphibole	Magnesiohornblende
18MPe84	1.16	8.66	45.87	9.01	0.22	11.49	19.13	1.14	0.00	0.31	97.00	1.11	0.00	0.49	0.13	Calcic amphibole	Ferrohornblende
18MPe84	1.84	9.54	43.34	12.48	0.45	11.13	16.08	0.56	0.03	0.20	95.66	1.47	0.00	0.74	0.06	Calcic amphibole	Magnesiohornblende
18MPe84	1.83	9.87	45.48	9.70	0.23	11.30	17.68	0.25	0.01	0.29	96.64	1.19	0.00	0.52	0.03	Calcic amphibole	Magnesiohornblende

18MPe84	1.79	13.20	45.27	12.36	0.07	10.72	11.77	1.25	0.10	0.17	96.70	1.50	0.00	0.59	0.14	Calcic amphibole	Magnesiohornblende
18MPe84	0.22	13.90	53.86	1.83	0.05	11.49	15.45	0.10	0.00	0.59	97.49	0.12	0.00	0.19	0.01	Calcic amphibole	Actinolite
18MPe84	1.49	9.66	44.14	10.95	0.36	11.29	17.09	0.67	0.01	0.28	95.94	1.37	0.00	0.57	0.08	Calcic amphibole	Magnesiohornblende
18MPe84	1.38	9.57	44.32	10.88	0.39	11.15	17.04	0.69	0.08	0.26	95.76	1.34	0.00	0.59	0.08	Calcic amphibole	Magnesiohornblende
18MPe84	0.96	15.41	49.76	5.28	0.56	11.86	11.92	0.95	0.01	0.54	97.25	0.82	0.00	0.08	0.10	Calcic amphibole	Magnesiohornblende
18MPe84	1.82	12.45	45.10	12.87	0.17	12.01	11.06	0.50	0.24	0.23	96.44	1.40	0.00	0.82	0.06	Calcic amphibole	Magnesiohornblende
18MPe84	1.19	9.61	45.54	9.50	0.25	11.92	17.93	0.48	0.00	0.31	96.72	1.17	0.00	0.51	0.05	Calcic amphibole	Magnesiohornblende
18MPe84	1.47	11.53	45.24	11.46	0.12	11.63	13.86	0.66	0.07	0.25	96.29	1.34	0.00	0.65	0.07	Calcic amphibole	Magnesiohornblende
18MPe84	1.12	8.98	45.61	10.87	0.23	11.96	17.35	0.54	0.09	0.39	97.14	1.19	0.00	0.72	0.06	Calcic amphibole	Ferrohornblende
18MPe84	1.28	12.08	46.61	9.56	0.11	11.96	14.35	0.59	0.09	0.22	96.85	1.16	0.00	0.49	0.07	Calcic amphibole	Magnesiohornblende
18MPe84	1.57	13.39	47.22	9.52	0.30	11.83	11.72	0.28	0.21	0.22	96.25	1.08	0.00	0.56	0.03	Calcic amphibole	Magnesiohornblende
18MPe84	1.16	11.68	46.02	10.43	0.06	11.92	14.40	0.53	0.06	0.28	96.55	1.24	0.00	0.57	0.06	Calcic amphibole	Magnesiohornblende
18MPe84	1.31	9.09	43.95	11.85	0.63	11.77	16.87	0.89	0.08	0.30	96.74	1.40	0.00	0.70	0.10	Calcic amphibole	Magnesiohornblende
18MPe84	0.58	8.45	47.82	5.97	0.29	11.58	21.34	0.26	0.00	0.40	96.69	0.76	0.00	0.31	0.03	Calcic amphibole	Ferrohornblende
18MPe84	1.40	11.52	46.77	10.46	0.13	11.68	14.53	0.28	0.07	0.33	97.17	1.17	0.00	0.64	0.03	Calcic amphibole	Magnesiohornblende
18MPe84	1.46	17.10	47.12	11.45	0.08	11.85	6.70	0.63	0.19	0.10	96.68	1.37	0.00	0.53	0.07	Calcic amphibole	Magnesiohornblende
18MPe84	1.21	7.41	42.82	13.66	0.34	11.34	18.69	0.31	0.03	0.26	96.07	1.53	0.00	0.90	0.04	Calcic amphibole	Ferrotschermakite
18MPe84	1.01	9.71	47.01	8.91	0.04	11.53	17.34	0.77	0.06	0.34	96.72	1.01	0.00	0.55	0.09	Calcic amphibole	Magnesiohornblende
18MPe84	1.05	11.76	46.93	10.82	0.13	11.85	13.90	0.29	0.04	0.21	96.98	1.17	0.00	0.69	0.03	Calcic amphibole	Magnesiohornblende
18MPe84	1.06	10.43	46.40	9.16	0.10	9.98	17.71	0.91	0.03	0.33	96.10	0.99	0.00	0.65	0.10	Calcic amphibole	Magnesiohornblende
18MPe84	1.34	11.37	46.64	9.50	0.15	11.92	15.40	0.47	0.00	0.31	97.09	1.13	0.00	0.52	0.05	Calcic amphibole	Magnesiohornblende
18MPe84	1.60	12.86	45.42	12.23	0.13	11.60	11.22	0.65	0.02	0.22	95.96	1.37	0.00	0.73	0.07	Calcic amphibole	Magnesiohornblende
18MPe84	0.72	14.35	50.89	5.94	0.45	11.76	11.72	0.40	0.16	0.27	96.66	0.63	0.00	0.39	0.04	Calcic amphibole	Magnesiohornblende
18MPe84	0.79	11.97	49.39	7.29	0.26	11.25	15.21	0.65	0.07	0.49	97.37	0.83	0.00	0.42	0.07	Calcic amphibole	Magnesiohornblende
18MPe84	1.49	10.69	46.44	10.37	0.09	11.51	15.84	0.54	0.05	0.31	97.33	1.18	0.00	0.61	0.06	Calcic amphibole	Magnesiohornblende
18MPe84	1.16	11.79	47.90	8.95	0.02	11.75	14.15	0.32	0.06	0.24	96.34	0.95	0.00	0.60	0.04	Calcic amphibole	Magnesiohornblende
18MPe84	1.26	9.53	45.63	8.85	0.32	11.54	17.93	1.07	0.00	0.32	96.46	1.13	0.00	0.44	0.12	Calcic amphibole	Magnesiohornblende
18MPe84	1.70	9.33	43.61	12.75	0.14	11.43	16.28	0.56	0.03	0.32	96.15	1.47	0.00	0.77	0.06	Calcic amphibole	Magnesiohornblende
18MPe84	1.57	10.61	44.94	10.92	0.27	11.89	15.67	0.48	0.04	0.24	96.63	1.31	0.00	0.61	0.05	Calcic amphibole	Magnesiohornblende
18MPe84	1.16	11.20	47.14	6.25	0.66	11.13	17.71	1.29	0.00	0.36	96.90	0.98	0.00	0.12	0.14	Calcic amphibole	Magnesiohornblende
18MPe84	0.76	14.94	52.17	3.36	0.05	11.46	13.00	0.17	0.02	0.41	96.34	0.45	0.00	0.13	0.02	Calcic amphibole	Actinolite
18MPe84	1.42	11.97	45.83	10.24	0.07	11.26	13.49	1.34	0.12	0.23	95.97	1.25	0.00	0.52	0.15	Calcic amphibole	Magnesiohornblende
18MPe84	1.28	10.79	45.49	12.83	0.21	11.66	13.62	0.24	0.02	0.25	96.40	1.32	0.00	0.90	0.03	Calcic amphibole	Magnesiohornblende
18MPe105	1.72	9.57	42.69	10.31	0.39	10.39	18.74	2.86	0.00	0.30	96.96	1.63	0.00	0.18	0.32	Calcic amphibole	Tschermakite
18MPe105	1.44	11.45	45.85	10.31	0.22	12.03	14.79	0.50	0.05	0.22	96.87	1.23	0.00	0.56	0.06	Calcic amphibole	Magnesiohornblende
18MPe105	0.65	12.21	49.49	5.20	0.33	10.59	17.20	0.57	0.01	0.63	96.89	0.62	0.00	0.30	0.06	Calcic amphibole	Magnesiohornblende
18MPe105	2.18	14.78	44.27	14.13	0.05	11.28	9.89	0.32	0.04	0.19	97.13	1.72	0.00	0.64	0.03	Calcic amphibole	Tschermakite
18MPe105	1.66	8.27	43.10	11.61	0.02	11.67	19.63	1.03	0.00	0.32	97.31	1.53	0.00	0.53	0.12	Calcic amphibole	Ferrotschermakite
18MPe105	1.64	15.97	45.44	12.61	0.09	11.18	8.77	0.72	0.20	0.14	96.76	1.46	0.00	0.68	0.08	Calcic amphibole	Magnesiohornblende

18MPe105	1.42	11.81	45.50	12.02	0.10	11.82	13.34	0.57	0.06	0.24	96.87	1.36	0.00	0.71	0.06	Calcic amphibole	Magnesiohornblende
18MPe105	1.81	8.96	43.57	11.52	0.09	11.26	18.39	0.45	0.02	0.37	96.45	1.46	0.00	0.58	0.05	Calcic amphibole	Magnesiohornblende
18MPe105	1.10	8.19	42.45	14.67	0.44	11.45	17.60	0.56	0.00	0.31	96.76	1.68	0.00	0.89	0.06	Calcic amphibole	Tschermakite
18MPe105	1.88	13.87	45.67	12.57	0.17	10.94	10.75	0.67	0.15	0.21	96.88	1.47	0.00	0.65	0.07	Calcic amphibole	Magnesiohornblende
18MPe105	1.65	9.09	43.48	11.66	0.34	11.25	17.88	1.09	0.00	0.27	96.71	1.49	0.00	0.57	0.12	Calcic amphibole	Magnesiohornblende
18MPe105	1.03	14.54	48.03	9.29	0.08	11.64	10.93	0.63	0.09	0.19	96.44	1.10	0.00	0.47	0.07	Calcic amphibole	Magnesiohornblende
18MPe105	1.89	14.82	45.90	12.86	0.06	10.61	9.75	0.68	0.36	0.13	97.07	1.53	0.00	0.61	0.07	Calcic amphibole	Tschermakite
18MPe105	1.63	14.09	45.95	12.19	0.25	11.60	10.38	0.70	0.12	0.24	97.15	1.42	0.00	0.63	0.08	Calcic amphibole	Magnesiohornblende
18MPe105	1.10	8.41	41.65	14.49	0.34	11.25	18.49	0.22	0.02	0.36	96.33	1.71	0.00	0.87	0.03	Calcic amphibole	Ferrotschermakite
18MPe105	1.35	10.54	45.61	8.94	0.25	9.45	19.41	0.81	0.02	0.30	96.68	1.10	0.00	0.50	0.09	Calcic amphibole	Ferrohornblende
18MPe105	1.46	9.81	43.69	12.67	0.46	11.43	16.22	0.95	0.03	0.21	96.93	1.53	0.00	0.69	0.11	Calcic amphibole	Tschermakite
18MPe105	1.20	12.47	45.42	11.55	0.47	11.81	12.67	0.77	0.01	0.22	96.59	1.37	0.00	0.62	0.09	Calcic amphibole	Magnesiohornblende
18MPe105	1.84	16.51	46.81	11.32	0.13	10.16	8.64	0.48	0.40	0.14	96.43	1.44	0.00	0.43	0.05	Calcic amphibole	Magnesiohornblende
18MPe105	1.48	15.72	46.11	11.81	0.06	11.52	9.11	0.38	0.14	0.15	96.49	1.35	0.00	0.66	0.04	Calcic amphibole	Magnesiohornblende
18MPe105	1.40	14.61	46.96	10.36	0.06	10.81	11.49	0.76	0.09	0.23	96.77	1.16	0.00	0.62	0.08	Calcic amphibole	Magnesiohornblende
18MPe105	1.02	13.09	48.32	9.01	0.16	12.08	13.09	0.33	0.04	0.25	97.40	1.01	0.00	0.52	0.04	Calcic amphibole	Magnesiohornblende
18MPe105	1.03	11.95	46.94	8.92	0.12	12.29	14.85	0.47	0.08	0.29	96.93	1.09	0.00	0.45	0.05	Calcic amphibole	Magnesiohornblende
18MPe105	1.80	15.58	46.41	11.42	0.12	10.93	9.80	0.43	0.29	0.15	96.93	1.44	0.00	0.46	0.05	Calcic amphibole	Magnesiohornblende
18MPe105	1.37	9.51	44.78	10.82	0.06	11.65	18.10	0.72	0.03	0.27	97.31	1.36	0.00	0.53	0.08	Calcic amphibole	Magnesiohornblende
18MPe105	1.69	12.62	44.93	12.00	0.06	11.60	12.65	1.04	0.11	0.24	96.94	1.48	0.00	0.58	0.11	Calcic amphibole	Magnesiohornblende
18MPe105	1.10	12.21	47.29	9.68	0.09	11.92	13.75	0.44	0.03	0.23	96.74	1.09	0.00	0.58	0.05	Calcic amphibole	Magnesiohornblende
18MPe105	1.67	10.88	43.34	13.66	0.05	11.38	14.69	1.24	0.01	0.21	97.13	1.67	0.00	0.68	0.14	Calcic amphibole	Tschermakite
18MPe105	1.37	10.74	45.59	10.53	0.13	11.70	16.11	0.48	0.02	0.26	96.92	1.27	0.00	0.56	0.05	Calcic amphibole	Magnesiohornblende
18MPe105	1.90	12.81	42.82	11.74	0.44	11.20	12.94	2.34	0.01	0.25	96.45	1.71	0.00	0.32	0.26	Calcic amphibole	Tschermakite
18MPe105	1.43	13.31	46.19	12.30	0.18	11.30	11.28	0.70	0.15	0.22	97.06	1.39	0.00	0.69	0.08	Calcic amphibole	Magnesiohornblende
18MPe105	1.29	11.61	46.69	9.37	0.07	11.78	15.45	0.48	0.10	0.27	97.11	1.15	0.00	0.47	0.05	Calcic amphibole	Magnesiohornblende
18MPe105	1.17	12.97	46.85	9.96	0.18	11.89	12.89	0.50	0.10	0.25	96.75	1.19	0.00	0.52	0.05	Calcic amphibole	Magnesiohornblende
18MPe105	1.38	9.96	44.16	11.40	0.28	11.75	17.09	0.61	0.04	0.36	97.03	1.44	0.00	0.55	0.07	Calcic amphibole	Magnesiohornblende
18MPe105	1.36	10.42	44.59	11.38	0.32	11.54	16.32	0.73	0.04	0.22	96.93	1.41	0.00	0.57	0.08	Calcic amphibole	Magnesiohornblende
18MPe105	1.18	11.73	46.41	10.02	0.07	11.87	14.85	0.45	0.02	0.29	96.90	1.20	0.00	0.53	0.05	Calcic amphibole	Magnesiohornblende
18MPe105	1.48	11.77	45.84	10.72	0.15	11.55	14.05	0.55	0.09	0.23	96.44	1.26	0.00	0.59	0.06	Calcic amphibole	Magnesiohornblende
18MPe105	1.36	11.82	45.40	9.97	0.09	11.76	14.04	1.52	0.07	0.24	96.27	1.29	0.00	0.45	0.17	Calcic amphibole	Magnesiohornblende
18MPe105	0.55	11.66	48.60	6.70	0.51	12.13	15.78	0.26	0.00	0.59	96.79	0.80	0.00	0.37	0.03	Calcic amphibole	Magnesiohornblende
18MPe105	1.91	11.13	43.32	12.14	0.10	11.41	14.90	1.54	0.05	0.28	96.78	1.61	0.00	0.50	0.17	Calcic amphibole	Tschermakite
18MPe105	1.40	13.04	45.59	11.33	0.06	11.77	12.22	0.72	0.24	0.24	96.62	1.38	0.00	0.56	0.08	Calcic amphibole	Magnesiohornblende
18MPe105	0.92	13.77	48.20	8.51	0.26	12.22	11.74	0.35	0.04	0.24	96.25	0.97	0.00	0.50	0.04	Calcic amphibole	Magnesiohornblende
18MPe105	1.32	11.72	45.56	10.36	0.12	12.00	14.52	0.52	0.13	0.19	96.44	1.27	0.00	0.53	0.06	Calcic amphibole	Magnesiohornblende
18MPe105	1.40	11.14	44.69	11.45	0.43	11.64	14.34	0.65	0.14	0.16	96.04	1.36	0.00	0.64	0.07	Calcic amphibole	Magnesiohornblende
18MPe105	1.41	10.72	44.75	11.01	0.07	11.97	15.26	0.78	0.05	0.23	96.26	1.34	0.00	0.60	0.09	Calcic amphibole	Magnesiohornblende

18MPe105	1.51	15.71	48.61	8.91	0.05	11.36	9.77	0.37	0.19	0.25	96.72	1.08	0.00	0.41	0.04	Calcic amphibole	Magnesiohornblende
18MPe105	1.90	17.11	46.21	11.76	0.05	10.87	8.22	0.31	0.17	0.16	96.76	1.37	0.00	0.61	0.03	Calcic amphibole	Edenite
18MPe105	0.61	13.92	50.69	5.79	0.42	11.12	13.80	0.17	0.02	0.36	96.89	0.70	0.00	0.29	0.02	Calcic amphibole	Magnesiohornblende
18MPe105	1.92	15.34	45.68	13.15	0.12	10.50	9.13	0.78	0.19	0.13	96.94	1.58	0.00	0.60	0.08	Calcic amphibole	Tschermakite
18MPe105	1.16	12.48	45.46	11.64	0.17	11.66	12.74	0.50	0.08	0.25	96.14	1.37	0.00	0.64	0.06	Calcic amphibole	Magnesiohornblende
18MPe105	1.34	13.06	45.55	13.01	0.07	11.41	11.56	0.73	0.09	0.20	97.02	1.48	0.00	0.72	0.08	Calcic amphibole	Magnesiohornblende
18MPe105	1.73	15.56	45.81	12.48	0.09	10.33	9.53	0.71	0.22	0.20	96.66	1.37	0.00	0.76	0.08	Calcic amphibole	Edenite
18MPe105	0.92	9.54	44.00	9.99	1.80	9.76	18.73	1.59	0.00	0.38	96.71	1.44	0.00	0.32	0.18	Calcic amphibole	Magnesiohornblende
18MPe105	1.77	14.65	45.74	12.33	0.12	9.86	10.95	0.67	0.15	0.21	96.44	1.32	0.00	0.81	0.07	Calcic amphibole	Edenite
18MPe105	1.27	11.73	46.32	9.81	0.09	12.04	14.72	0.55	0.07	0.25	96.84	1.19	0.00	0.52	0.06	Calcic amphibole	Magnesiohornblende
18MPe105	1.36	11.19	45.09	10.77	0.19	12.13	15.04	0.55	0.01	0.23	96.55	1.31	0.00	0.57	0.06	Calcic amphibole	Magnesiohornblende
18MPe118	1.60	8.11	43.42	12.55	0.13	11.55	21.36	0.60	0.06	0.36	99.74	1.57	0.00	0.62	0.07	Calcic amphibole	Ferrotschermakite
18MPe118	1.82	14.32	45.43	12.56	0.13	10.51	12.09	0.92	0.16	0.20	98.14	1.44	0.00	0.69	0.10	Calcic amphibole	Edenite
18MPe118	1.13	10.17	46.02	9.96	0.18	11.83	18.33	0.44	0.04	0.29	98.39	1.20	0.00	0.53	0.05	Calcic amphibole	Magnesiohornblende
18MPe118	1.79	9.19	42.55	11.46	0.05	11.12	20.53	1.54	0.00	0.31	98.54	1.63	0.00	0.39	0.17	Calcic amphibole	Ferropargasite
18MPe118	1.66	10.50	43.75	12.00	0.31	11.71	17.17	0.72	0.05	0.22	98.09	1.59	0.00	0.49	0.08	Calcic amphibole	Tschermakite
18MPe118	1.69	8.67	42.32	13.76	0.29	10.86	19.76	0.57	0.00	0.33	98.25	1.67	0.00	0.75	0.06	Calcic amphibole	Ferropargasite
18MPe118	1.09	10.74	47.41	8.12	0.03	11.53	19.35	0.89	0.01	0.29	99.46	1.06	0.00	0.34	0.10	Calcic amphibole	Magnesiohornblende
18MPe118	1.15	11.69	47.53	9.65	0.06	11.90	16.24	0.40	0.04	0.27	98.92	1.09	0.00	0.56	0.04	Calcic amphibole	Magnesiohornblende
18MPe118	1.99	14.75	46.12	13.11	0.14	11.04	10.16	0.61	0.17	0.12	98.20	1.54	0.00	0.63	0.06	Calcic amphibole	Tschermakite
18MPe118	1.83	10.71	42.35	11.44	0.52	11.15	17.40	2.90	0.04	0.23	98.57	1.80	0.00	0.18	0.32	Calcic amphibole	Tschermakite
18MPe118	1.40	11.19	46.05	9.94	0.10	11.67	17.34	0.55	0.05	0.29	98.59	1.24	0.00	0.48	0.06	Calcic amphibole	Magnesiohornblende
18MPe118	1.27	12.49	46.46	11.44	0.12	12.02	13.97	0.55	0.04	0.28	98.63	1.36	0.00	0.57	0.06	Calcic amphibole	Magnesiohornblende
18MPe118	1.23	13.61	48.91	7.09	0.11	11.69	15.31	0.23	0.01	0.33	98.52	0.90	0.00	0.31	0.03	Calcic amphibole	Magnesiohornblende
18MPe118	1.39	12.90	46.95	10.00	0.18	11.34	14.46	0.75	0.15	0.26	98.37	1.29	0.00	0.40	0.08	Calcic amphibole	Magnesiohornblende
18MPe118	2.00	13.08	42.35	10.65	1.06	11.71	13.99	3.76	0.02	0.24	98.86	1.82	0.00	0.01	0.41	Calcic amphibole	Magnesiohastingsite
18MPe118	1.48	10.55	44.94	11.81	0.19	11.74	17.42	0.67	0.03	0.28	99.11	1.42	0.00	0.61	0.07	Calcic amphibole	Magnesiohornblende
18MPe118	1.36	10.11	42.58	10.27	1.43	11.55	19.25	1.64	0.02	0.57	98.78	1.68	0.00	0.12	0.18	Calcic amphibole	Tschermakite
18MPe118	1.25	11.38	44.26	9.53	1.17	11.47	18.01	1.07	0.00	0.41	98.55	1.42	0.00	0.25	0.12	Calcic amphibole	Edenite
18MPe118	1.43	11.25	45.78	10.12	0.23	11.72	17.29	0.45	0.06	0.24	98.57	1.27	0.00	0.48	0.05	Calcic amphibole	Magnesiohornblende
18MPe118	1.72	11.58	46.20	11.24	0.11	11.43	15.45	0.65	0.07	0.26	98.71	1.36	0.00	0.55	0.07	Calcic amphibole	Magnesiohornblende
18MPe118	1.45	10.86	45.89	10.39	0.15	11.81	18.08	0.53	0.07	0.26	99.50	1.30	0.00	0.49	0.06	Calcic amphibole	Magnesiohornblende
18MPe118	1.24	9.66	44.20	10.24	1.05	11.67	19.36	1.29	0.00	0.39	99.10	1.48	0.00	0.30	0.14	Calcic amphibole	Magnesiohornblende
18MPe118	1.79	13.94	45.52	11.86	0.10	11.39	11.78	1.13	0.18	0.17	97.87	1.52	0.00	0.47	0.12	Calcic amphibole	Tschermakite
18MPe118	1.48	11.39	46.25	10.99	0.35	11.55	16.54	0.39	0.00	0.23	99.17	1.36	0.00	0.50	0.04	Calcic amphibole	Magnesiohornblende
18MPe118	1.27	11.19	45.29	11.04	0.10	11.86	17.00	0.47	0.00	0.31	98.52	1.37	0.00	0.53	0.05	Calcic amphibole	Magnesiohornblende
18MPe118	1.98	14.49	45.25	12.27	0.03	11.05	12.48	0.42	0.22	0.19	98.38	1.49	0.00	0.59	0.05	Calcic amphibole	Edenite
18MPe118	1.47	9.65	44.05	13.03	0.23	11.63	17.36	0.58	0.09	0.31	98.39	1.57	0.00	0.67	0.06	Calcic amphibole	Tschermakite
18MPe118	1.43	13.00	45.48	11.71	0.07	10.99	13.99	0.81	0.17	0.29	97.94	1.39	0.00	0.62	0.09	Calcic amphibole	Magnesiohornblende

18MPe118	1.58	9.34	43.46	11.54	0.31	11.25	19.32	0.43	0.00	0.35	97.58	1.47	0.00	0.58	0.05	Calcic amphibole	Ferro-edenite
18MPe118	1.31	10.36	45.52	10.68	0.10	11.77	17.44	0.50	0.03	0.27	97.98	1.33	0.00	0.51	0.06	Calcic amphibole	Magnesiohornblende
18MPe118	1.15	11.67	46.47	9.76	0.34	11.85	16.63	0.34	0.06	0.28	98.55	1.20	0.00	0.48	0.04	Calcic amphibole	Magnesiohornblende
18MPe118	1.41	12.44	46.24	10.22	0.34	11.97	15.45	0.57	0.05	0.27	98.95	1.35	0.00	0.38	0.06	Calcic amphibole	Magnesiohornblende
18MPe118	1.48	10.07	44.98	10.77	0.32	11.35	18.72	0.30	0.13	0.26	98.39	1.32	0.00	0.56	0.03	Calcic amphibole	Magnesiohornblende
18MPe118	1.59	11.83	45.46	12.62	0.22	11.27	14.69	0.62	0.09	0.27	98.65	1.51	0.00	0.62	0.07	Calcic amphibole	Tschermakite
18MPe118	1.22	12.03	46.06	10.59	0.20	11.76	15.71	0.55	0.10	0.30	98.52	1.29	0.00	0.53	0.06	Calcic amphibole	Magnesiohornblende
18MPe118	1.59	13.09	46.15	11.21	0.28	11.73	13.82	0.30	0.00	0.23	98.40	1.40	0.00	0.49	0.03	Calcic amphibole	Magnesiohornblende
18MPe118	1.88	12.69	46.05	11.66	0.11	11.01	14.12	0.33	0.04	0.22	98.10	1.42	0.00	0.54	0.04	Calcic amphibole	Magnesiohornblende
18MPe118	1.69	12.61	45.59	13.33	0.12	11.70	12.51	0.53	0.07	0.26	98.40	1.50	0.00	0.74	0.06	Calcic amphibole	Tschermakite
18MPe118	1.34	11.88	45.99	10.64	0.23	11.71	15.72	0.56	0.06	0.27	98.39	1.28	0.00	0.56	0.06	Calcic amphibole	Magnesiohornblende
18MPe118	1.50	10.12	44.55	11.10	0.24	11.47	18.15	1.25	0.01	0.24	98.62	1.50	0.00	0.41	0.14	Calcic amphibole	Magnesiohornblende
18MPe118	1.40	16.73	48.25	10.86	0.08	11.34	8.30	0.49	0.21	0.19	97.84	1.16	0.00	0.66	0.05	Calcic amphibole	Magnesiohornblende
18MPe118	1.83	15.56	49.01	8.20	0.13	11.66	10.88	0.41	0.06	0.19	97.93	1.04	0.00	0.34	0.04	Calcic amphibole	Magnesiohornblende
18MPe118	1.42	9.63	43.22	12.26	0.70	11.47	18.93	0.96	0.02	0.28	98.89	1.59	0.00	0.55	0.11	Calcic amphibole	Pargasite
18MPe118	1.33	8.57	44.00	11.87	0.31	11.28	20.56	0.38	0.00	0.40	98.69	1.44	0.00	0.64	0.04	Calcic amphibole	Ferrohornblende
18MPe118	1.38	9.92	44.09	12.24	0.26	11.57	18.06	0.71	0.04	0.29	98.55	1.49	0.00	0.64	0.08	Calcic amphibole	Magnesiohornblende
18MPe118	1.35	12.11	46.01	9.99	0.14	12.19	16.40	0.45	0.03	0.25	98.91	1.31	0.00	0.40	0.05	Calcic amphibole	Magnesiohornblende
18MPe118	2.10	7.36	41.51	11.31	1.29	10.71	23.74	0.74	0.00	0.45	99.21	1.77	0.00	0.23	0.08	Calcic amphibole	Hastingsite
18MPe118	1.33	7.43	43.88	10.76	0.48	11.16	23.24	0.75	0.02	0.37	99.42	1.41	0.00	0.49	0.08	Calcic amphibole	Ferrohornblende
18MPe118	1.45	10.55	44.47	12.33	0.34	11.14	17.41	0.74	0.00	0.28	98.72	1.46	0.00	0.68	0.08	Calcic amphibole	Magnesiohornblende
18MPe118	1.75	13.85	45.52	11.68	0.04	10.73	13.47	0.47	0.06	0.25	97.82	1.39	0.00	0.61	0.05	Calcic amphibole	Magnesiohornblende
18MPe118	1.46	10.90	45.20	11.54	0.12	11.84	16.79	0.47	0.09	0.26	98.67	1.38	0.00	0.61	0.05	Calcic amphibole	Magnesiohornblende
18MPe118	1.55	12.85	45.61	10.08	0.11	11.21	15.34	1.41	0.10	0.22	98.48	1.35	0.00	0.39	0.15	Calcic amphibole	Magnesiohornblende
18MPe118	1.61	13.46	45.53	10.90	0.41	10.68	14.84	0.54	0.03	0.35	98.34	1.37	0.00	0.50	0.06	Calcic amphibole	Edenite
18MPe118	1.70	11.27	44.85	10.99	0.08	11.75	16.72	0.66	0.09	0.23	98.35	1.48	0.00	0.41	0.07	Calcic amphibole	Magnesiohornblende
18MPe119*	1.09	10.92	47.10	9.10	0.18	11.91	17.64	0.41	0.03	0.23	98.60	1.08	0.00	0.49	0.05	Calcic amphibole	Magnesiohornblende
18MPe119*	1.09	11.90	47.67	8.75	0.05	12.05	16.22	0.37	0.06	0.23	98.39	1.04	0.00	0.47	0.04	Calcic amphibole	Magnesiohornblende
18MPe119*	1.47	10.19	45.07	11.09	0.39	11.32	17.86	0.70	0.06	0.20	98.35	1.42	0.00	0.49	0.08	Calcic amphibole	Magnesiohornblende
18MPe119*	1.12	11.18	44.35	9.44	1.10	12.11	17.54	1.24	0.06	0.43	98.57	1.46	0.00	0.18	0.14	Calcic amphibole	Magnesiohornblende
18MPe119*	1.40	9.48	42.64	13.42	0.39	11.39	17.08	0.44	0.02	0.29	96.55	1.66	0.00	0.69	0.05	Calcic amphibole	Tschermakite
18MPe119*	1.20	10.23	43.18	11.11	0.76	11.80	18.57	1.02	0.00	0.35	98.22	1.57	0.00	0.38	0.11	Calcic amphibole	Tschermakite
18MPe119*	1.14	10.49	44.05	9.72	0.79	11.42	18.81	1.20	0.00	0.54	98.15	1.42	0.00	0.29	0.13	Calcic amphibole	Magnesiohornblende
18MPe119*	1.32	12.43	46.05	11.56	0.17	11.61	13.51	0.84	0.15	0.17	97.81	1.38	0.00	0.58	0.09	Calcic amphibole	Magnesiohornblende
18MPe119*	0.47	9.62	47.21	4.64	0.12	15.19	15.40	5.78	0.01	0.27	98.72	0.81	0.16	0.00	0.49	Calcic amphibole	Magnesiohornblende
18MPe119*	1.13	9.32	44.21	12.26	0.39	11.46	17.93	0.58	0.01	0.27	97.56	1.49	0.00	0.64	0.06	Calcic amphibole	Magnesiohornblende
18MPe119*	1.79	8.88	42.56	12.25	0.09	11.43	19.77	1.06	0.02	0.26	98.11	1.62	0.00	0.55	0.12	Calcic amphibole	Ferropargasite
18MPe119*	0.49	8.93	45.06	5.53	0.53	11.38	15.66	0.76	0.01	0.48	88.83	0.58	0.00	0.49	0.09	Calcic amphibole	Magnesiohornblende
18MPe119*	1.17	11.24	46.32	10.34	0.08	11.87	16.63	0.55	0.03	0.26	98.49	1.23	0.00	0.56	0.06	Calcic amphibole	Magnesiohornblende

18MPe119*	1.47	10.77	44.67	11.69	0.16	11.62	16.95	0.54	0.06	0.26	98.18	1.42	0.00	0.61	0.06	Calcic amphibole	Magnesiohornblende
18MPe119*	1.69	10.96	44.45	10.62	0.12	11.65	17.65	1.03	0.00	0.18	98.35	1.43	0.00	0.42	0.11	Calcic amphibole	Edenite
18MPe119*	1.38	9.70	44.15	12.58	0.37	11.62	17.30	0.50	0.06	0.17	97.83	1.51	0.00	0.67	0.06	Calcic amphibole	Tschermakite
18MPe119*	1.53	8.40	42.60	13.26	0.55	11.32	20.01	0.88	0.00	0.24	98.79	1.73	0.00	0.57	0.10	Calcic amphibole	Tschermakite
18MPe119*	1.14	12.62	46.52	11.77	0.03	11.81	13.59	0.58	0.00	0.23	98.29	1.28	0.00	0.72	0.06	Calcic amphibole	Magnesiohornblende
18MPe119*	0.90	11.42	52.04	2.34	0.19	11.24	20.42	0.13	0.00	0.51	99.19	0.40	0.01	0.00	0.00	Calcic amphibole	Actinolite
18MPe119*	1.17	11.54	46.59	10.45	0.10	11.89	16.72	0.43	0.07	0.25	99.21	1.24	0.00	0.54	0.05	Calcic amphibole	Magnesiohornblende
18MPe119*	0.87	13.67	47.58	7.86	0.55	11.96	14.41	0.52	0.00	0.29	97.71	1.05	0.00	0.30	0.06	Calcic amphibole	Magnesiohornblende
18MPe119*	1.24	10.37	44.49	11.92	0.21	11.70	17.43	0.64	0.04	0.28	98.31	1.45	0.00	0.62	0.07	Calcic amphibole	Magnesiohornblende
18MPe119*	1.56	10.60	44.45	11.06	0.18	11.56	18.59	0.96	0.02	0.33	99.32	1.48	0.00	0.43	0.11	Calcic amphibole	Magnesiohornblende
18MPe119*	1.74	10.54	44.01	13.04	0.48	11.50	15.95	0.54	0.04	0.24	98.08	1.58	0.00	0.67	0.06	Calcic amphibole	Tschermakite
18MPe119*	1.02	11.87	47.46	8.17	0.04	11.34	17.35	0.88	0.02	0.34	98.48	1.05	0.00	0.36	0.10	Calcic amphibole	Magnesiohornblende
18MPe119*	1.32	10.07	45.18	11.03	0.20	11.63	18.54	0.70	0.07	0.36	99.11	1.36	0.00	0.55	0.08	Calcic amphibole	Magnesiohornblende
18MPe119*	1.40	12.73	46.14	10.44	0.29	11.16	14.88	0.80	0.04	0.30	98.18	1.26	0.00	0.54	0.09	Calcic amphibole	Magnesiohornblende
18MPe119*	1.35	14.64	47.40	8.63	0.21	10.44	14.54	0.69	0.06	0.42	98.39	1.14	0.00	0.33	0.08	Calcic amphibole	Magnesiohornblende
18MPe119*	2.05	7.92	39.51	11.18	0.18	10.62	20.57	0.80	0.00	0.29	93.13	1.69	0.00	0.41	0.10	Calcic amphibole	Ferropargasite
18MPe119*	2.42	12.19	44.47	14.24	0.26	10.58	12.86	0.37	0.02	0.26	97.67	1.63	0.00	0.78	0.04	Calcic amphibole	Tschermakite
18MPe119*	2.41	14.22	46.59	11.01	0.09	11.67	11.23	0.57	0.38	0.27	98.44	1.35	0.00	0.50	0.06	Calcic amphibole	Magnesiohornblende
18MPe119*	1.71	14.96	45.79	12.22	0.08	10.51	11.43	0.63	0.11	0.19	97.63	1.40	0.00	0.68	0.07	Calcic amphibole	Magnesiohornblende
18MPe119*	1.68	14.66	45.99	12.24	0.09	10.73	10.62	0.44	0.16	0.13	96.74	1.48	0.00	0.56	0.05	Calcic amphibole	Magnesiohornblende
18MPe119*	1.12	9.37	46.23	9.82	0.16	11.60	19.80	0.46	0.05	0.24	98.85	1.16	0.00	0.56	0.05	Calcic amphibole	Ferrohornblende
18MPe119*	1.33	11.77	46.63	9.52	0.11	11.84	15.94	0.45	0.05	0.24	97.88	1.21	0.00	0.42	0.05	Calcic amphibole	Magnesiohornblende
18MPe119*	1.29	12.36	46.56	9.94	0.03	11.81	15.00	0.48	0.07	0.25	97.79	1.19	0.00	0.53	0.05	Calcic amphibole	Magnesiohornblende
18MPe119*	2.03	8.99	42.80	12.84	0.29	11.10	19.02	0.29	0.03	0.22	97.61	1.65	0.00	0.59	0.03	Calcic amphibole	Tschermakite
18MPe119*	1.17	11.05	44.64	9.74	0.81	11.71	17.85	1.21	0.00	0.28	98.46	1.38	0.00	0.32	0.14	Calcic amphibole	Magnesiohornblende
18MPe119*	1.45	6.00	41.18	12.30	0.94	11.30	24.04	1.35	0.05	0.31	98.92	1.78	0.00	0.41	0.15	Calcic amphibole	Ferrotschermakite
18MPe119*	1.52	8.69	41.99	14.06	0.50	11.52	19.25	0.38	0.05	0.55	98.50	1.75	0.00	0.72	0.04	Calcic amphibole	Ferropargasite
18MPe119*	1.65	16.02	49.52	7.49	0.13	12.01	10.37	0.41	0.28	0.20	98.09	0.97	0.00	0.28	0.04	Calcic amphibole	Magnesiohornblende
18MPe119*	1.54	9.97	44.43	10.54	0.06	11.37	19.81	0.89	0.00	0.34	98.96	1.43	0.00	0.41	0.10	Calcic amphibole	Magnesiohornblende
18MPe119*	1.45	11.43	45.18	12.52	0.19	11.54	15.08	0.63	0.08	0.30	98.40	1.50	0.00	0.62	0.07	Calcic amphibole	Tschermakite
18MPe119*	2.21	14.76	46.27	11.80	0.17	11.26	9.92	0.49	0.23	0.21	97.32	1.41	0.00	0.58	0.05	Calcic amphibole	Magnesiohornblende
18MPe119*	2.07	12.51	44.54	12.72	0.08	11.32	14.16	0.84	0.06	0.23	98.53	1.63	0.00	0.51	0.09	Calcic amphibole	Tschermakite
18MPe133	1.17	13.55	47.89	8.99	0.10	11.77	12.50	0.47	0.11	0.26	96.81	1.07	0.00	0.47	0.05	Calcic amphibole	Magnesiohornblende
18MPe133	0.63	11.46	51.15	4.12	0.06	11.73	17.80	0.15	0.02	0.32	97.43	0.48	0.00	0.24	0.02	Calcic amphibole	Actinolite
18MPe133	1.69	12.64	44.75	13.09	0.07	11.35	11.11	1.01	0.18	0.20	96.10	1.49	0.00	0.75	0.11	Calcic amphibole	Magnesiohornblende
18MPe133	1.15	13.87	47.50	9.93	0.14	12.02	11.56	0.64	0.08	0.21	97.10	1.16	0.00	0.53	0.07	Calcic amphibole	Magnesiohornblende
18MPe133	1.68	12.70	46.20	9.89	0.09	11.45	13.88	0.52	0.07	0.26	96.74	1.26	0.00	0.45	0.06	Calcic amphibole	Magnesiohornblende
18MPe133	1.49	11.19	42.62	12.22	1.58	11.62	14.06	1.30	0.07	0.58	96.73	1.63	0.00	0.52	0.15	Calcic amphibole	Pargasite
18MPe133	0.96	12.41	47.06	6.96	0.74	11.68	15.60	1.26	0.01	0.51	97.19	1.06	0.00	0.15	0.14	Calcic amphibole	Magnesiohornblende

18MPe133	1.40	11.53	45.54	9.67	0.25	11.62	15.69	0.48	0.01	0.28	96.47	1.26	0.00	0.43	0.05	Calcic amphibole	Magnesiohornblende
18MPe133	1.42	11.18	44.87	10.87	0.22	11.60	15.55	0.74	0.00	0.21	96.67	1.38	0.00	0.51	0.08	Calcic amphibole	Magnesiohornblende
18MPe133	1.15	11.22	43.45	10.73	0.99	11.67	14.99	1.61	0.00	0.46	96.27	1.51	0.00	0.39	0.18	Calcic amphibole	Tschermakite
18MPe133	2.02	9.82	43.36	12.46	0.27	11.26	17.22	0.71	0.00	0.30	97.43	1.59	0.00	0.59	0.08	Calcic amphibole	Tschermakite
18MPe133	1.54	9.54	44.52	9.65	0.24	11.86	18.50	0.54	0.01	0.32	96.72	1.29	0.00	0.42	0.06	Calcic amphibole	Magnesiohornblende
18MPe133	1.15	10.25	44.77	11.32	0.11	11.70	15.97	0.63	0.03	0.32	96.26	1.35	0.00	0.63	0.07	Calcic amphibole	Magnesiohornblende
18MPe133	1.25	10.10	46.67	9.22	0.17	11.37	16.58	0.40	0.39	0.35	96.50	1.06	0.00	0.56	0.05	Calcic amphibole	Magnesiohornblende
18MPe133	1.37	10.90	47.26	9.20	0.19	11.44	15.93	0.17	0.36	0.31	97.14	1.05	0.00	0.55	0.02	Calcic amphibole	Magnesiohornblende
18MPe133	1.89	8.11	43.49	10.53	0.13	10.93	20.28	0.64	0.03	0.40	96.43	1.41	0.00	0.47	0.07	Calcic amphibole	Ferrohornblende
18MPe133	1.49	12.87	45.99	11.37	0.09	11.46	11.58	0.75	0.10	0.24	95.94	1.29	0.00	0.67	0.08	Calcic amphibole	Magnesiohornblende
18MPe133	1.61	13.43	44.85	10.49	0.72	11.78	11.41	1.70	0.01	0.23	96.23	1.39	0.00	0.43	0.19	Calcic amphibole	Magnesiohornblende
18MPe133	1.74	9.71	41.21	14.31	1.06	11.36	15.81	0.91	0.02	0.29	96.42	1.82	0.00	0.71	0.10	Calcic amphibole	Pargasite
18MPe133	1.51	10.81	44.65	12.04	0.17	11.59	14.93	0.60	0.07	0.29	96.67	1.42	0.00	0.67	0.07	Calcic amphibole	Magnesiohornblende
18MPe133	1.66	7.71	43.15	13.32	0.08	11.75	18.29	0.36	0.01	0.36	96.68	1.49	0.00	0.87	0.04	Calcic amphibole	Ferrohornblende
18MPe133	1.52	11.75	44.50	13.63	0.18	11.64	12.37	0.60	0.01	0.21	96.41	1.50	0.00	0.84	0.07	Calcic amphibole	Tschermakite
18MPe133	1.37	12.15	45.45	12.85	0.07	11.59	12.17	0.74	0.02	0.28	96.69	1.41	0.00	0.78	0.08	Calcic amphibole	Magnesiohornblende
18MPe133	0.44	12.88	52.04	3.63	0.18	11.80	15.68	0.19	0.00	0.62	97.47	0.42	0.00	0.20	0.02	Calcic amphibole	Actinolite
18MPe133	1.67	9.35	42.99	12.94	0.42	11.48	16.95	0.91	0.03	0.25	96.99	1.60	0.00	0.68	0.10	Calcic amphibole	Tschermakite
18MPe133	1.14	14.07	48.08	9.83	0.09	11.98	10.66	0.46	0.42	0.24	96.98	1.09	0.00	0.58	0.05	Calcic amphibole	Magnesiohornblende
18MPe133	1.06	13.57	46.70	10.26	0.28	10.75	12.95	0.77	0.03	0.34	96.71	1.15	0.00	0.62	0.09	Calcic amphibole	Magnesiohornblende
18MPe133	1.95	9.90	42.38	11.78	0.45	11.46	17.60	0.61	0.09	0.29	96.51	1.63	0.00	0.45	0.07	Calcic amphibole	Magnesiohastingsite
18MPe133	1.13	11.76	45.90	10.14	0.06	11.94	14.82	0.57	0.01	0.21	96.54	1.25	0.00	0.51	0.06	Calcic amphibole	Magnesiohornblende
18MPe133	1.14	9.33	44.73	10.18	0.21	11.59	18.66	0.63	0.05	0.31	96.82	1.25	0.00	0.56	0.07	Calcic amphibole	Ferrohornblende
18MPe133	1.25	12.59	45.98	11.29	0.09	12.05	12.65	0.39	0.08	0.22	96.59	1.30	0.00	0.64	0.04	Calcic amphibole	Magnesiohornblende
18MPe133	1.69	12.65	45.80	11.58	0.14	11.36	12.83	0.47	0.05	0.26	96.84	1.36	0.00	0.62	0.05	Calcic amphibole	Magnesiohornblende
18MPe133	0.62	12.34	49.67	5.82	0.29	10.47	16.30	0.38	0.06	0.73	96.68	0.60	0.00	0.42	0.04	Calcic amphibole	Magnesiohornblende
18MPe133	1.05	13.69	47.72	9.70	0.28	12.34	10.92	0.47	0.11	0.16	96.44	1.05	0.00	0.61	0.05	Calcic amphibole	Magnesiohornblende
18MPe133	1.40	12.40	45.47	12.38	0.25	11.46	11.98	0.65	0.00	0.31	96.30	1.38	0.00	0.74	0.07	Calcic amphibole	Magnesiohornblende
18MPe133	1.28	9.34	41.59	11.00	1.62	11.51	17.56	1.73	0.00	0.88	96.51	1.66	0.00	0.32	0.20	Calcic amphibole	Magnesiohastingsite
18MPe133	0.56	17.11	52.55	4.57	0.18	12.81	8.94	0.12	0.06	0.27	97.16	0.52	0.00	0.25	0.01	Calcic amphibole	Magnesiohornblende
18MPe133	1.23	11.18	44.75	11.98	0.18	11.97	14.31	0.43	0.01	0.20	96.24	1.39	0.00	0.70	0.05	Calcic amphibole	Magnesiohornblende
18MPe133	1.46	11.21	45.48	10.93	0.20	11.71	15.21	0.73	0.12	0.33	97.38	1.34	0.00	0.55	0.08	Calcic amphibole	Magnesiohornblende
18MPe133	1.93	8.25	43.14	12.11	0.23	11.09	19.28	0.82	0.02	0.30	97.17	1.53	0.00	0.61	0.09	Calcic amphibole	Ferrotschermakite
18MPe133	1.26	11.27	45.56	10.63	0.13	11.62	15.13	0.59	0.03	0.20	96.42	1.28	0.00	0.56	0.07	Calcic amphibole	Magnesiohornblende
18MPe133	1.22	11.14	44.24	9.89	0.85	11.66	16.06	0.96	0.02	0.51	96.55	1.40	0.00	0.34	0.11	Calcic amphibole	Magnesiohornblende
18MPe133	1.97	13.16	46.05	13.64	0.11	10.81	10.15	0.50	0.10	0.20	96.69	1.41	0.00	0.89	0.05	Calcic amphibole	Magnesiohornblende
18MPe133	2.11	12.07	41.24	11.30	1.31	11.57	13.06	3.86	0.00	0.30	96.82	1.81	0.00	0.19	0.44	Calcic amphibole	Pargasite
18MPe133	1.18	11.00	45.88	10.83	0.12	11.82	14.97	0.65	0.02	0.23	96.70	1.24	0.00	0.64	0.07	Calcic amphibole	Magnesiohornblende
18MPe133	1.67	9.45	42.79	13.15	0.36	10.91	16.53	0.75	0.01	0.29	95.91	1.61	0.00	0.71	0.08	Calcic amphibole	Tschermakite

18MPe157	1.04	10.97	45.26	8.42	0.98	11.69	16.98	0.99	0.05	0.45	96.82	1.23	0.00	0.26	0.11	Calcic amphibole	Magnesiohornblende
18MPe157	1.35	11.95	45.40	11.53	0.24	11.79	13.46	0.77	0.10	0.18	96.78	1.36	0.00	0.63	0.09	Calcic amphibole	Magnesiohornblende
18MPe157	1.53	11.50	45.74	10.50	0.15	11.16	13.92	0.44	0.08	0.66	95.68	1.23	0.00	0.60	0.05	Calcic amphibole	Magnesiohornblende
18MPe157	1.18	9.95	45.64	10.57	0.23	11.62	16.33	0.50	0.03	0.22	96.28	1.19	0.00	0.66	0.06	Calcic amphibole	Magnesiohornblende
18MPe157	1.66	10.76	44.82	10.22	0.47	11.33	16.08	0.60	0.05	0.39	96.38	1.32	0.00	0.48	0.07	Calcic amphibole	Magnesiohornblende
18MPe157	0.92	14.21	49.37	6.02	0.21	11.45	12.09	1.77	0.22	0.46	96.72	0.84	0.00	0.19	0.19	Calcic amphibole	Magnesiohornblende
18MPe157	1.44	11.75	46.78	10.39	0.09	11.60	13.78	0.51	0.05	0.29	96.67	1.15	0.00	0.65	0.06	Calcic amphibole	Magnesiohornblende
18MPe157	1.73	8.69	43.54	11.28	0.33	11.11	18.93	0.63	0.00	0.33	96.58	1.45	0.00	0.55	0.07	Calcic amphibole	Magnesiohornblende
18MPe157	1.49	10.90	45.13	12.45	0.01	11.39	14.19	0.45	0.06	0.32	96.38	1.38	0.00	0.78	0.05	Calcic amphibole	Magnesiohornblende
18MPe157	1.30	10.86	44.36	14.07	0.32	11.32	14.13	0.42	0.03	0.20	97.02	1.55	0.00	0.86	0.05	Calcic amphibole	Tschermakite
18MPe157	1.57	10.95	46.04	10.74	0.14	11.77	15.09	0.51	0.05	0.23	97.08	1.22	0.00	0.65	0.06	Calcic amphibole	Magnesiohornblende
18MPe157	1.07	12.83	47.00	7.56	0.80	11.72	14.66	1.10	0.04	0.41	97.19	1.10	0.00	0.21	0.12	Calcic amphibole	Magnesiohornblende
18MPe157	1.54	9.34	43.03	11.22	0.82	11.26	17.38	1.10	0.04	0.37	96.09	1.49	0.00	0.52	0.13	Calcic amphibole	Magnesiohornblende
18MPe157	1.38	9.53	44.23	11.38	0.26	11.33	16.69	0.59	0.00	0.30	95.69	1.35	0.00	0.66	0.07	Calcic amphibole	Magnesiohornblende
18MPe157	1.33	9.99	44.68	10.82	0.28	11.65	16.41	0.64	0.08	0.29	96.18	1.31	0.00	0.60	0.07	Calcic amphibole	Magnesiohornblende
18MPe157	1.64	11.65	45.99	11.12	0.23	11.36	13.37	0.77	0.05	0.29	96.47	1.25	0.00	0.68	0.09	Calcic amphibole	Magnesiohornblende
18MPe157	1.78	8.30	43.44	11.71	0.15	11.25	18.92	0.51	0.06	0.38	96.51	1.45	0.00	0.63	0.06	Calcic amphibole	Ferrohornblende
18MPe157	1.76	13.80	45.08	12.77	0.07	10.57	10.33	0.84	0.14	0.15	95.50	1.50	0.00	0.67	0.09	Calcic amphibole	Tschermakite
18MPe157	1.42	10.43	44.79	11.16	0.09	11.68	16.16	0.79	0.02	0.24	96.77	1.37	0.00	0.58	0.09	Calcic amphibole	Magnesiohornblende
18MPe157	1.25	11.20	45.95	10.43	0.10	11.97	14.81	0.51	0.01	0.22	96.44	1.20	0.00	0.61	0.06	Calcic amphibole	Magnesiohornblende
18MPe157	1.42	10.29	44.48	10.11	0.16	11.60	17.28	1.07	0.12	0.28	96.81	1.38	0.00	0.40	0.12	Calcic amphibole	Magnesiohornblende
18MPe157	1.85	8.96	42.57	13.90	0.17	11.36	16.69	0.52	0.02	0.34	96.37	1.64	0.00	0.81	0.06	Calcic amphibole	Tschermakite
18MPe157	1.12	12.27	47.03	9.66	0.13	12.03	13.95	0.40	0.04	0.23	96.87	1.12	0.00	0.54	0.04	Calcic amphibole	Magnesiohornblende
18MPe157	1.15	11.11	46.64	9.77	0.06	11.77	15.45	0.53	0.09	0.23	96.80	1.13	0.00	0.56	0.06	Calcic amphibole	Magnesiohornblende
18MPe157	1.62	10.47	44.71	11.74	0.23	11.43	15.51	0.64	0.06	0.21	96.62	1.38	0.00	0.67	0.07	Calcic amphibole	Magnesiohornblende
18MPe157	1.68	12.27	45.84	11.80	0.29	11.58	12.34	0.58	0.09	0.27	96.74	1.31	0.00	0.72	0.06	Calcic amphibole	Magnesiohornblende
18MPe157	1.89	10.69	43.09	14.60	0.18	9.77	15.07	0.64	0.01	0.28	96.22	1.75	0.00	0.75	0.07	Calcic amphibole	Tschermakite
18MPe157	1.15	10.08	46.31	9.55	0.33	11.79	16.59	0.61	0.05	0.23	96.70	1.09	0.00	0.59	0.07	Calcic amphibole	Magnesiohornblende
18MPe157	2.00	13.58	46.39	10.77	0.16	11.44	10.51	0.53	0.54	0.15	96.07	1.23	0.00	0.62	0.06	Calcic amphibole	Magnesiohornblende
18MPe157	1.40	11.05	46.14	10.10	0.18	11.63	15.02	0.41	0.02	0.24	96.19	1.15	0.00	0.61	0.05	Calcic amphibole	Magnesiohornblende
18MPe157	1.32	11.47	44.88	11.72	0.25	11.77	13.60	0.56	0.07	0.21	95.85	1.36	0.00	0.69	0.06	Calcic amphibole	Magnesiohornblende
18MPe157	1.55	9.90	44.96	10.05	0.19	11.04	17.25	0.49	0.02	0.33	95.78	1.26	0.00	0.52	0.06	Calcic amphibole	Magnesiohornblende
18MPe157	1.52	10.25	45.56	10.57	0.10	11.81	15.84	0.56	0.07	0.29	96.56	1.21	0.00	0.64	0.06	Calcic amphibole	Magnesiohornblende
18MPe157	0.97	11.87	46.91	9.90	0.06	12.16	13.73	0.42	0.07	0.27	96.36	1.10	0.00	0.62	0.05	Calcic amphibole	Magnesiohornblende
18MPe157	1.74	9.20	43.73	11.51	0.24	11.15	17.68	0.51	0.05	0.33	96.14	1.43	0.00	0.61	0.06	Calcic amphibole	Magnesiohornblende
18MPe157	1.20	11.80	45.86	7.77	1.01	11.45	15.24	1.56	0.02	0.59	96.50	1.15	0.00	0.22	0.18	Calcic amphibole	Magnesiohornblende
18MPe157	1.37	13.65	48.28	6.20	0.33	11.16	14.14	1.46	0.01	0.38	96.97	0.96	0.00	0.10	0.16	Calcic amphibole	Magnesiohornblende
18MPe157	0.95	12.65	48.03	8.42	0.21	12.13	13.53	0.51	0.24	0.26	96.93	0.98	0.00	0.47	0.06	Calcic amphibole	Magnesiohornblende
18MPe157	1.58	9.55	45.10	10.63	0.11	11.43	16.92	0.48	0.26	0.34	96.40	1.25	0.00	0.62	0.05	Calcic amphibole	Magnesiohornblende

18MPe157	1.46	9.39	43.53	11.37	0.42	11.26	17.62	0.79	0.02	0.28	96.14	1.46	0.00	0.56	0.09	Calcic amphibole	Magnesiohornblende
18MPe157	1.81	10.69	44.31	10.86	0.10	10.93	16.47	1.63	0.07	0.22	97.10	1.48	0.00	0.41	0.18	Calcic amphibole	Magnesiohornblende
18MPe157	1.65	11.79	42.64	11.38	0.93	12.21	14.33	1.92	0.00	0.16	97.01	1.64	0.00	0.36	0.22	Calcic amphibole	Pargasite
18MPe157	1.97	9.32	43.36	11.61	0.13	10.92	17.28	0.89	0.00	0.30	95.78	1.47	0.00	0.59	0.10	Calcic amphibole	Magnesiohornblende
18MPe157	1.46	11.23	46.15	10.10	0.22	11.66	14.88	0.50	0.02	0.30	96.52	1.17	0.00	0.59	0.06	Calcic amphibole	Magnesiohornblende
18MPe157	1.74	12.52	44.43	12.91	0.12	11.45	11.56	1.03	0.13	0.22	96.11	1.51	0.00	0.71	0.11	Calcic amphibole	Tschermakite
18MPe157	1.08	11.86	47.06	10.13	0.11	11.96	13.97	0.36	0.00	0.32	96.85	1.12	0.00	0.63	0.04	Calcic amphibole	Magnesiohornblende
18MPe157	1.08	10.25	46.52	9.16	0.54	10.95	16.34	0.56	0.00	0.78	96.18	1.08	0.00	0.53	0.06	Calcic amphibole	Magnesiohornblende
18MPe157	1.19	12.04	45.25	12.05	0.28	11.92	12.50	0.43	0.14	0.32	96.11	1.36	0.00	0.73	0.05	Calcic amphibole	Magnesiohornblende
18MPe157	1.34	10.77	46.31	9.45	0.19	11.69	15.31	0.76	0.13	0.28	96.23	1.10	0.00	0.56	0.09	Calcic amphibole	Magnesiohornblende
18MPe157	1.34	10.40	44.48	11.51	0.22	11.33	15.72	0.74	0.11	0.26	96.11	1.40	0.00	0.62	0.08	Calcic amphibole	Magnesiohornblende
18MPe157	1.23	10.28	43.77	11.29	0.31	11.50	16.45	0.70	0.03	0.29	95.84	1.46	0.00	0.53	0.08	Calcic amphibole	Magnesiohornblende
18MPe157	1.50	11.24	46.64	9.21	0.18	11.45	15.17	0.45	0.12	0.31	96.27	1.08	0.00	0.53	0.05	Calcic amphibole	Magnesiohornblende
18MPe157	1.53	12.63	45.99	11.43	0.12	11.34	12.36	0.82	0.16	0.25	96.64	1.33	0.00	0.63	0.09	Calcic amphibole	Magnesiohornblende
18MPe157	1.28	8.13	43.31	11.98	0.32	11.56	18.89	0.80	0.01	0.29	96.57	1.47	0.00	0.66	0.09	Calcic amphibole	Ferrohornblende
18MPe157	1.31	11.99	46.46	8.16	0.63	11.61	15.31	0.65	0.02	0.58	96.71	1.12	0.00	0.31	0.07	Calcic amphibole	Magnesiohornblende
18MPe157	0.54	15.21	52.41	4.32	0.08	12.03	11.88	0.60	0.27	0.21	97.55	0.51	0.00	0.22	0.06	Calcic amphibole	Magnesiohornblende
18MPe157	1.49	9.83	45.37	10.52	0.21	11.84	16.86	0.52	0.04	0.23	96.91	1.23	0.00	0.62	0.06	Calcic amphibole	Magnesiohornblende
18MPe157	0.91	10.04	45.66	11.38	0.24	11.83	15.79	0.26	0.01	0.34	96.46	1.23	0.00	0.75	0.03	Calcic amphibole	Magnesiohornblende
18MPe158	1.77	10.30	44.12	10.63	0.17	11.56	17.01	0.63	0.02	0.30	96.50	1.41	0.00	0.47	0.07	Calcic amphibole	Magnesiohornblende
18MPe158	1.44	13.91	47.18	10.55	0.12	11.12	11.43	0.46	0.11	0.20	96.52	1.22	0.00	0.56	0.05	Calcic amphibole	Magnesiohornblende
18MPe158	1.52	12.06	45.67	12.07	0.26	11.23	11.63	0.43	0.01	0.30	95.18	1.27	0.00	0.83	0.05	Calcic amphibole	Magnesiohornblende
18MPe158	1.68	7.50	41.42	12.92	0.44	10.97	20.55	0.67	0.00	0.32	96.46	1.72	0.00	0.59	0.08	Calcic amphibole	Ferrotschermakite
18MPe158	1.71	13.93	44.97	14.39	0.15	10.51	9.99	0.59	0.07	0.21	96.51	1.63	0.00	0.78	0.06	Calcic amphibole	Tschermakite
18MPe158	1.16	11.17	47.36	8.03	0.05	11.88	16.86	0.27	0.03	0.28	97.09	1.01	0.00	0.39	0.03	Calcic amphibole	Magnesiohornblende
18MPe158	1.47	12.10	46.31	10.93	0.07	11.32	13.50	0.64	0.13	0.18	96.66	1.26	0.00	0.62	0.07	Calcic amphibole	Magnesiohornblende
18MPe158	1.72	8.45	41.91	13.16	0.70	11.27	18.43	0.56	0.02	0.26	96.47	1.67	0.00	0.67	0.06	Calcic amphibole	Tschermakite
18MPe158	1.21	13.33	46.73	10.27	0.13	11.95	12.17	0.51	0.08	0.20	96.59	1.21	0.00	0.55	0.06	Calcic amphibole	Magnesiohornblende
18MPe158	1.21	12.11	45.66	11.28	0.05	11.37	13.50	0.78	0.06	0.30	96.32	1.34	0.00	0.59	0.09	Calcic amphibole	Magnesiohornblende
18MPe158	1.63	15.00	45.75	12.71	0.08	10.26	10.17	0.86	0.09	0.18	96.73	1.37	0.00	0.81	0.09	Calcic amphibole	Magnesiohornblende
18MPe158	1.24	12.15	46.29	10.45	0.21	12.18	14.02	0.42	0.00	0.25	97.21	1.24	0.00	0.56	0.05	Calcic amphibole	Magnesiohornblende
18MPe158	1.46	15.81	49.44	7.60	0.18	11.60	9.67	0.35	0.42	0.15	96.69	0.92	0.00	0.36	0.04	Calcic amphibole	Magnesiohornblende
18MPe158	1.20	12.15	46.11	10.22	0.06	11.64	14.53	0.47	0.00	0.32	96.71	1.19	0.00	0.59	0.05	Calcic amphibole	Magnesiohornblende
18MPe158	1.58	9.48	43.64	12.51	0.13	11.42	16.93	0.51	0.04	0.25	96.49	1.50	0.00	0.69	0.06	Calcic amphibole	Tschermakite
18MPe158	0.90	15.56	48.37	8.78	0.28	11.04	10.55	0.41	0.25	0.28	96.42	0.98	0.00	0.53	0.05	Calcic amphibole	Magnesiohornblende
18MPe158	1.24	10.58	44.88	10.35	0.78	11.86	15.83	0.49	0.17	0.33	96.51	1.28	0.00	0.54	0.06	Calcic amphibole	Magnesiohornblende
18MPe158	1.13	12.88	46.32	10.29	0.09	12.03	13.11	0.52	0.02	0.20	96.59	1.25	0.00	0.52	0.06	Calcic amphibole	Magnesiohornblende
18MPe158	1.33	9.33	43.07	13.24	0.48	11.57	17.01	1.06	0.01	0.34	97.44	1.63	0.00	0.68	0.12	Calcic amphibole	Tschermakite
18MPe158	1.72	9.11	43.09	12.16	0.14	11.42	17.25	0.69	0.02	0.32	95.93	1.50	0.00	0.66	0.08	Calcic amphibole	Tschermakite

18MPe158	1.09	16.31	50.00	5.14	0.38	11.03	11.85	1.08	0.03	0.33	97.25	0.73	0.00	0.15	0.12	Calcic amphibole	Magnesiohornblende
18MPe158	1.41	11.79	47.20	9.78	0.05	11.73	14.03	0.48	0.00	0.27	96.73	1.08	0.00	0.62	0.05	Calcic amphibole	Magnesiohornblende
18MPe158	1.46	10.89	45.97	10.11	0.11	11.74	15.90	0.41	0.05	0.25	96.89	1.21	0.00	0.55	0.05	Calcic amphibole	Magnesiohornblende
18MPe158	1.83	13.91	45.50	12.78	0.09	10.48	10.56	0.65	0.10	0.17	96.07	1.49	0.00	0.67	0.07	Calcic amphibole	Magnesiohornblende
18MPe158	1.05	11.41	46.73	9.31	0.10	11.76	15.34	0.43	0.10	0.26	96.48	1.11	0.00	0.51	0.05	Calcic amphibole	Magnesiohornblende
18MPe158	1.46	12.25	45.55	11.87	0.26	11.55	12.74	0.59	0.04	0.30	96.61	1.36	0.00	0.68	0.07	Calcic amphibole	Magnesiohornblende
18MPe158	1.66	13.53	45.42	12.89	0.16	11.53	10.92	0.70	0.04	0.21	97.06	1.49	0.00	0.69	0.08	Calcic amphibole	Magnesiohornblende
18MPe158	2.01	12.92	46.01	12.01	0.13	10.43	12.52	0.57	0.13	0.32	97.05	1.41	0.00	0.62	0.06	Calcic amphibole	Magnesiohornblende
18MPe158	1.16	11.24	44.66	13.27	0.23	11.37	13.66	0.75	0.01	0.39	96.74	1.50	0.00	0.77	0.08	Calcic amphibole	Tschermakite
18MPe158	0.90	11.73	47.55	8.76	0.37	11.16	15.12	0.71	0.01	0.55	96.86	1.06	0.00	0.45	0.08	Calcic amphibole	Magnesiohornblende
18MPe158	1.06	12.43	46.99	9.36	0.01	12.06	13.53	0.42	0.12	0.24	96.23	1.10	0.00	0.53	0.05	Calcic amphibole	Magnesiohornblende
18MPe158	1.05	12.40	46.01	10.93	0.23	11.87	13.08	0.62	0.10	0.32	96.62	1.29	0.00	0.59	0.07	Calcic amphibole	Magnesiohornblende
18MPe158	0.44	13.48	52.92	2.77	0.12	12.10	15.37	0.04	0.01	0.34	97.60	0.31	0.00	0.16	0.01	Calcic amphibole	Actinolite
18MPe158	1.71	11.36	44.73	11.10	0.26	11.55	15.04	0.65	0.00	0.31	96.71	1.40	0.00	0.53	0.07	Calcic amphibole	Magnesiohornblende
18MPe158	1.31	15.42	45.98	9.27	0.12	10.59	11.36	0.28	0.09	0.19	94.60	1.18	0.00	0.44	0.03	Calcic amphibole	Magnesiohornblende
18MPe158	1.10	11.76	46.50	10.56	0.05	11.79	14.00	0.46	0.04	0.29	96.55	1.19	0.00	0.63	0.05	Calcic amphibole	Magnesiohornblende
18MPe158	1.90	13.53	45.97	12.52	0.12	11.39	10.74	0.45	0.12	0.27	97.02	1.40	0.00	0.72	0.05	Calcic amphibole	Magnesiohornblende
18MPe158	1.79	17.33	45.96	11.67	0.03	11.17	7.57	0.76	0.30	0.15	96.73	1.42	0.00	0.55	0.08	Calcic amphibole	Edenite
18MPe158	1.47	10.61	44.59	11.57	0.25	11.56	15.73	0.54	0.00	0.26	96.58	1.40	0.00	0.62	0.06	Calcic amphibole	Magnesiohornblende
18MPe158	1.39	12.69	45.82	12.04	0.16	10.73	12.75	0.83	0.00	0.21	96.63	1.41	0.00	0.63	0.09	Calcic amphibole	Magnesiohornblende
18MPe158	1.20	10.60	45.05	11.47	0.31	11.67	15.80	0.79	0.05	0.22	97.17	1.38	0.00	0.61	0.09	Calcic amphibole	Magnesiohornblende
18MPe158	2.42	12.02	40.91	15.42	0.35	11.43	12.36	1.72	0.00	0.11	96.74	2.01	0.00	0.66	0.19	Calcic amphibole	Pargasite
18MPe158	1.69	11.49	45.40	11.94	0.21	11.46	13.47	0.74	0.06	0.30	96.76	1.35	0.00	0.71	0.08	Calcic amphibole	Magnesiohornblende
18MPe158	1.60	11.28	45.26	10.11	0.21	11.75	15.60	0.41	0.10	0.36	96.67	1.29	0.00	0.47	0.05	Calcic amphibole	Magnesiohornblende
18MPe158	1.74	9.39	43.16	10.96	0.06	10.90	18.42	1.58	0.00	0.32	96.53	1.55	0.00	0.39	0.18	Calcic amphibole	Tschermakite
18MPe158	2.43	14.18	45.13	12.88	0.08	10.43	10.03	0.53	0.18	0.16	96.03	1.52	0.00	0.66	0.06	Calcic amphibole	Tschermakite
18MPe158	1.32	11.83	45.42	10.59	0.36	11.95	14.67	0.67	0.08	0.24	97.15	1.33	0.00	0.50	0.07	Calcic amphibole	Magnesiohornblende
18MPe158	1.09	12.26	46.34	9.71	0.10	12.04	13.85	0.44	0.03	0.23	96.09	1.17	0.00	0.52	0.05	Calcic amphibole	Magnesiohornblende
18MPe158	1.69	12.70	45.17	11.72	0.20	11.26	12.28	0.65	0.10	0.31	96.09	1.40	0.00	0.61	0.07	Calcic amphibole	Magnesiohornblende
18MPe158	1.77	11.92	43.99	10.94	0.41	11.24	13.87	1.85	0.06	0.29	96.35	1.50	0.00	0.41	0.21	Calcic amphibole	Magnesiohornblende
18MPe158	1.33	12.54	46.50	10.87	0.10	11.84	12.91	0.72	0.10	0.25	97.15	1.26	0.00	0.60	0.08	Calcic amphibole	Magnesiohornblende
18MPe158	1.83	16.39	45.13	12.41	0.01	11.19	8.23	0.54	0.23	0.20	96.17	1.48	0.00	0.63	0.06	Calcic amphibole	Edenite
18MPe158	1.13	11.85	46.16	10.35	0.16	11.93	14.05	0.48	0.06	0.25	96.43	1.21	0.00	0.58	0.05	Calcic amphibole	Magnesiohornblende
18MPe158	1.68	12.16	44.46	12.72	0.12	11.06	13.52	0.98	0.07	0.24	97.03	1.57	0.00	0.60	0.11	Calcic amphibole	Tschermakite
18MPe158	1.71	14.66	46.28	11.85	0.11	10.92	10.64	0.42	0.06	0.20	96.84	1.43	0.00	0.56	0.05	Calcic amphibole	Magnesiohornblende
18MPe158	1.74	13.98	45.15	11.76	0.09	10.97	11.40	0.98	0.17	0.15	96.39	1.51	0.00	0.49	0.11	Calcic amphibole	Tschermakite
18MPe158	1.79	10.91	45.21	12.11	0.03	11.47	14.69	0.55	0.09	0.28	97.13	1.38	0.00	0.71	0.06	Calcic amphibole	Magnesiohornblende
18MPe158	1.40	12.12	46.61	10.51	0.09	11.86	13.37	0.51	0.05	0.28	96.80	1.18	0.00	0.63	0.06	Calcic amphibole	Magnesiohornblende
18MPe158	1.34	10.61	44.87	11.21	0.17	11.74	15.91	0.73	0.04	0.29	96.92	1.37	0.00	0.58	0.08	Calcic amphibole	Magnesiohornblende

18MPe158	1.85	11.84	44.04	12.76	0.07	11.54	12.97	0.72	0.05	0.27	96.12	1.52	0.00	0.69	0.08	Calcic amphibole	Tschermakite
18MPe159	1.36	12.25	46.31	11.36	0.15	11.77	12.94	0.54	0.03	0.25	96.97	1.27	0.00	0.68	0.06	Calcic amphibole	Magnesiohornblende
18MPe159	1.84	12.49	45.15	10.59	0.10	11.01	13.66	1.60	0.05	0.25	96.74	1.42	0.00	0.41	0.18	Calcic amphibole	Magnesiohornblende
18MPe159	1.08	12.68	47.10	9.27	0.06	11.69	13.90	0.81	0.05	0.30	96.94	1.16	0.00	0.43	0.09	Calcic amphibole	Magnesiohornblende
18MPe159	1.30	12.97	47.27	11.28	0.12	11.82	11.30	0.42	0.03	0.24	96.74	1.16	0.00	0.76	0.05	Calcic amphibole	Magnesiohornblende
18MPe159	1.42	11.48	45.37	12.24	0.08	11.63	13.22	0.60	0.00	0.22	96.26	1.34	0.00	0.77	0.07	Calcic amphibole	Magnesiohornblende
18MPe159	1.51	12.52	45.49	11.73	0.28	12.10	12.19	0.19	0.23	0.21	96.44	1.33	0.00	0.70	0.02	Calcic amphibole	Magnesiohornblende
18MPe159	1.68	10.35	44.58	11.80	0.34	11.33	15.16	0.44	0.04	0.33	96.06	1.36	0.00	0.72	0.05	Calcic amphibole	Magnesiohornblende
18MPe159	2.18	13.21	45.58	12.78	0.20	10.83	11.41	0.70	0.21	0.18	97.28	1.47	0.00	0.69	0.08	Calcic amphibole	Magnesiohornblende
18MPe159	1.39	10.35	44.57	11.98	0.47	11.16	15.99	0.83	0.00	0.28	97.02	1.44	0.00	0.64	0.09	Calcic amphibole	Magnesiohornblende
18MPe159	0.94	11.06	44.68	9.55	0.67	11.91	16.27	0.72	0.00	0.45	96.25	1.28	0.00	0.42	0.08	Calcic amphibole	Magnesiohornblende
18MPe159	1.32	10.29	43.31	12.21	0.44	11.69	16.04	0.59	0.00	0.45	96.34	1.55	0.00	0.59	0.07	Calcic amphibole	Tschermakite
18MPe159	1.90	13.93	45.76	12.16	0.03	11.51	10.57	0.79	0.15	0.23	97.04	1.44	0.00	0.62	0.09	Calcic amphibole	Magnesiohornblende
18MPe159	1.64	10.66	45.72	10.86	0.18	11.53	15.46	0.55	0.02	0.25	96.87	1.24	0.00	0.65	0.06	Calcic amphibole	Magnesiohornblende
18MPe159	2.39	13.58	45.33	13.91	0.10	11.20	9.00	0.53	0.24	0.17	96.45	1.47	0.00	0.89	0.06	Calcic amphibole	Magnesiohornblende
18MPe159	1.22	11.17	46.94	9.37	0.16	11.74	15.07	0.43	0.08	0.24	96.43	1.05	0.00	0.58	0.05	Calcic amphibole	Magnesiohornblende
18MPe159	0.74	12.54	48.85	4.95	0.52	14.15	14.55	0.83	0.01	0.40	97.54	0.79	0.00	0.07	0.09	Calcic amphibole	Magnesiohornblende
18MPe159	1.49	10.84	45.51	10.70	0.16	11.22	15.38	0.67	0.02	0.21	96.20	1.27	0.00	0.60	0.08	Calcic amphibole	Magnesiohornblende
18MPe159	0.78	14.38	50.04	6.23	0.59	12.02	11.74	0.69	0.06	0.21	96.73	0.72	0.00	0.35	0.08	Calcic amphibole	Magnesiohornblende
18MPe159	1.14	12.35	47.77	8.84	0.03	12.12	14.10	0.31	0.30	0.27	97.23	1.03	0.00	0.49	0.03	Calcic amphibole	Magnesiohornblende
18MPe159	1.42	9.42	42.40	10.04	1.34	11.02	17.55	1.72	0.04	1.03	95.98	1.53	0.00	0.28	0.20	Calcic amphibole	Tschermakite
18MPe159	1.41	11.71	47.11	9.69	0.09	11.74	14.50	0.44	0.04	0.26	96.98	1.10	0.00	0.58	0.05	Calcic amphibole	Magnesiohornblende
18MPe159	1.05	12.66	46.50	10.82	0.13	11.92	11.92	0.40	0.44	0.25	96.09	1.20	0.00	0.66	0.04	Calcic amphibole	Magnesiohornblende
18MPe159	1.69	7.48	42.50	12.00	0.33	11.34	20.33	0.77	0.03	0.34	96.81	1.55	0.00	0.59	0.09	Calcic amphibole	Ferrotschermakite
18MPe159	1.21	10.73	44.03	12.22	0.56	11.65	15.03	0.76	0.07	0.24	96.50	1.48	0.00	0.65	0.08	Calcic amphibole	Magnesiohornblende
18MPe159	1.11	12.37	46.03	7.83	0.84	11.53	14.91	1.01	0.02	0.74	96.39	1.17	0.00	0.20	0.11	Calcic amphibole	Magnesiohornblende
18MPe159	1.90	14.77	47.30	10.63	0.15	10.98	9.99	0.56	0.13	0.20	96.62	1.24	0.00	0.56	0.06	Calcic amphibole	Magnesiohornblende
18MPe159	0.13	17.39	55.05	2.10	0.02	12.94	9.31	0.07	0.05	0.18	97.23	0.18	0.00	0.18	0.01	Calcic amphibole	Actinolite
18MPe159	1.21	13.18	46.60	11.12	0.07	11.97	11.48	0.63	0.12	0.23	96.61	1.25	0.00	0.65	0.07	Calcic amphibole	Magnesiohornblende
18MPe159	1.74	12.69	45.77	12.18	0.08	11.46	11.07	0.80	0.11	0.15	96.05	1.32	0.00	0.77	0.09	Calcic amphibole	Magnesiohornblende
18MPe159	1.43	10.76	44.25	12.35	0.34	11.24	14.73	1.09	0.04	0.25	96.48	1.48	0.00	0.67	0.12	Calcic amphibole	Magnesiohornblende
18MPe159	1.86	14.63	47.23	10.00	0.04	12.01	10.13	0.44	0.19	0.22	96.75	1.18	0.00	0.53	0.05	Calcic amphibole	Magnesiohornblende
18MPe159	1.24	12.84	46.28	11.00	0.10	11.34	12.05	0.54	0.12	0.26	95.77	1.25	0.00	0.64	0.06	Calcic amphibole	Magnesiohornblende
18MPe159	1.76	14.92	46.36	12.43	0.11	10.37	9.35	0.79	0.33	0.16	96.58	1.45	0.00	0.62	0.08	Calcic amphibole	Magnesiohornblende
18MPe159	2.38	13.18	44.68	14.38	0.10	10.86	10.19	0.52	0.11	0.21	96.61	1.58	0.00	0.86	0.06	Calcic amphibole	Tschermakite
18MPe159	1.82	12.14	45.45	12.37	0.09	11.80	12.17	0.51	0.04	0.21	96.60	1.35	0.00	0.78	0.06	Calcic amphibole	Magnesiohornblende
18MPe159	1.59	12.00	45.29	12.10	0.24	11.13	12.42	1.00	0.20	0.25	96.23	1.38	0.00	0.70	0.11	Calcic amphibole	Magnesiohornblende
18MPe159	2.10	10.44	42.70	15.19	0.35	11.70	13.51	0.55	0.20	0.34	97.08	1.72	0.00	0.92	0.06	Calcic amphibole	Pargasite
18MPe159	1.18	11.91	45.62	9.30	0.64	11.26	15.08	1.54	0.00	0.46	96.98	1.30	0.00	0.31	0.17	Calcic amphibole	Magnesiohornblende

18MPe159	1.24	10.65	45.80	10.13	0.20	12.00	15.98	0.61	0.04	0.29	96.94	1.21	0.00	0.56	0.07	Calcic amphibole	Magnesiohornblende
18MPe159	2.06	13.32	45.95	11.55	0.09	12.00	11.23	0.39	0.01	0.21	96.82	1.31	0.00	0.67	0.04	Calcic amphibole	Magnesiohornblende
18MPe159	1.73	15.36	45.90	12.66	0.10	10.44	9.56	0.62	0.23	0.18	96.78	1.36	0.00	0.80	0.07	Calcic amphibole	Edenite
18MPe159	1.17	7.88	44.61	8.89	0.58	10.29	21.22	1.68	0.02	0.29	96.63	1.27	0.00	0.32	0.19	Calcic amphibole	Ferrohornblende
18MPe159	1.68	7.93	42.60	11.68	0.21	11.09	19.20	1.15	0.00	0.29	95.83	1.51	0.00	0.59	0.13	Calcic amphibole	Ferrotschermakite
18MPe159	2.07	13.34	45.85	12.73	0.14	10.84	10.95	0.60	0.13	0.18	96.82	1.42	0.00	0.73	0.06	Calcic amphibole	Magnesiohornblende
18MPe159	1.11	10.83	45.18	8.24	0.95	11.48	16.81	1.38	0.00	0.57	96.55	1.22	0.00	0.24	0.16	Calcic amphibole	Magnesiohornblende
18MPe159	1.93	7.49	42.16	12.31	0.11	11.24	20.38	0.70	0.00	0.48	96.80	1.61	0.00	0.59	0.08	Calcic amphibole	Ferrotschermakite
18MPe159	1.05	11.54	47.39	9.44	0.08	12.06	14.79	0.41	0.04	0.27	97.07	1.05	0.00	0.58	0.05	Calcic amphibole	Magnesiohornblende
18MPe160	1.46	11.88	45.09	12.72	0.18	11.78	14.77	0.29	0.00	0.25	98.42	1.45	0.00	0.73	0.03	Calcic amphibole	Magnesiohornblende
18MPe160	1.37	11.38	45.15	11.72	0.29	11.37	16.19	0.58	0.07	0.25	98.37	1.38	0.00	0.64	0.06	Calcic amphibole	Magnesiohornblende
18MPe160	1.30	11.42	45.43	11.31	0.14	11.68	15.95	0.63	0.05	0.26	98.16	1.34	0.00	0.61	0.07	Calcic amphibole	Magnesiohornblende
18MPe160	1.49	15.73	47.56	11.33	0.04	11.44	9.17	0.61	0.29	0.20	97.85	1.34	0.00	0.53	0.06	Calcic amphibole	Magnesiohornblende
18MPe160	1.10	11.72	46.16	9.99	0.22	11.93	16.63	0.41	0.03	0.23	98.40	1.25	0.00	0.47	0.05	Calcic amphibole	Magnesiohornblende
18MPe160	1.61	8.96	43.67	10.73	0.36	11.45	21.29	0.55	0.04	0.30	98.96	1.48	0.00	0.41	0.06	Calcic amphibole	Ferro-edenite
18MPe160	1.95	8.42	43.36	11.48	0.13	10.94	21.95	0.57	0.04	0.36	99.20	1.51	0.00	0.51	0.06	Calcic amphibole	Ferropargasite
18MPe160	1.35	13.02	45.83	12.45	0.09	11.67	13.03	0.59	0.00	0.21	98.24	1.39	0.00	0.73	0.06	Calcic amphibole	Magnesiohornblende
18MPe160	1.25	12.32	46.23	10.79	0.10	11.75	14.33	0.51	0.03	0.20	97.50	1.31	0.00	0.53	0.06	Calcic amphibole	Magnesiohornblende
18MPe160	1.35	12.00	46.60	11.27	0.06	11.69	14.43	0.57	0.07	0.27	98.30	1.31	0.00	0.60	0.06	Calcic amphibole	Magnesiohornblende
18MPe160	1.22	11.06	46.62	10.09	0.12	11.85	16.46	0.41	0.00	0.32	98.15	1.22	0.00	0.51	0.04	Calcic amphibole	Magnesiohornblende
18MPe160	1.68	11.79	44.63	11.64	0.45	11.52	14.56	0.87	0.11	0.27	97.52	1.49	0.00	0.52	0.10	Calcic amphibole	Magnesiohornblende
18MPe160	0.95	13.79	48.95	8.39	0.05	11.84	13.58	0.27	0.62	0.24	98.67	0.96	0.00	0.46	0.03	Calcic amphibole	Magnesiohornblende
18MPe160	1.31	10.27	44.97	11.72	0.26	11.38	17.03	0.52	0.09	0.27	97.82	1.43	0.00	0.58	0.06	Calcic amphibole	Magnesiohornblende
18MPe160	1.04	9.71	45.56	9.31	0.21	11.98	19.81	0.73	0.00	0.26	98.61	1.25	0.00	0.38	0.08	Calcic amphibole	Magnesiohornblende
18MPe160	1.54	12.67	45.75	10.67	0.17	11.69	14.20	0.50	0.17	0.28	97.62	1.38	0.00	0.44	0.05	Calcic amphibole	Magnesiohornblende
18MPe160	1.69	9.24	44.73	10.01	0.14	11.62	20.35	0.48	0.00	0.31	98.57	1.39	0.00	0.36	0.05	Calcic amphibole	Magnesiohornblende
18MPe160	1.76	12.42	45.54	12.09	0.12	11.66	13.46	0.50	0.05	0.25	97.85	1.44	0.00	0.62	0.05	Calcic amphibole	Magnesiohornblende
18MPe160	0.93	15.52	50.03	7.59	0.08	12.24	11.23	0.31	0.18	0.22	98.32	0.87	0.00	0.41	0.03	Calcic amphibole	Magnesiohornblende
18MPe160	1.11	11.52	44.96	8.22	0.87	12.00	18.06	1.81	0.00	0.37	98.92	1.35	0.00	0.08	0.20	Calcic amphibole	Magnesiohornblende
18MPe160	1.30	9.70	44.59	11.87	0.20	11.93	18.55	0.54	0.03	0.27	98.99	1.44	0.00	0.62	0.06	Calcic amphibole	Magnesiohornblende
18MPe160	1.15	10.31	46.04	8.80	0.15	11.40	18.98	1.41	0.01	0.28	98.52	1.17	0.00	0.36	0.16	Calcic amphibole	Magnesiohornblende
18MPe160	1.16	11.18	45.83	11.58	0.42	11.79	15.52	0.43	0.03	0.35	98.28	1.36	0.00	0.61	0.05	Calcic amphibole	Magnesiohornblende
18MPe160	1.47	10.19	45.65	10.14	0.09	11.60	19.36	0.46	0.06	0.37	99.40	1.30	0.00	0.46	0.05	Calcic amphibole	Magnesiohornblende
18MPe160	1.31	12.24	46.58	10.48	0.08	11.64	15.68	0.51	0.10	0.29	98.91	1.25	0.00	0.54	0.06	Calcic amphibole	Magnesiohornblende
18MPe160	1.44	10.92	45.09	11.11	0.10	11.54	17.29	0.52	0.10	0.28	98.39	1.37	0.00	0.56	0.06	Calcic amphibole	Magnesiohornblende
18MPe160	1.25	9.20	41.93	12.31	1.32	11.82	19.79	0.41	0.00	0.67	98.70	1.73	0.00	0.45	0.05	Calcic amphibole	Magnesiohastingsite
18MPe160	1.47	9.88	44.35	10.87	0.09	11.82	19.11	0.75	0.00	0.27	98.62	1.44	0.00	0.46	0.08	Calcic amphibole	Magnesiohornblende
18MPe160	1.71	10.37	44.96	10.53	0.18	11.51	18.25	0.55	0.00	0.25	98.31	1.41	0.00	0.41	0.06	Calcic amphibole	Magnesiohornblende
18MPe160	1.52	10.59	45.23	9.50	0.33	11.66	18.34	0.45	0.02	0.36	97.99	1.33	0.00	0.32	0.05	Calcic amphibole	Magnesiohornblende

18MPe160	1.17	14.81	47.56	8.66	0.08	11.08	13.26	0.73	0.13	0.30	97.77	1.12	0.00	0.36	0.08	Calcic amphibole	Magnesiohornblende
18MPe160	1.59	10.87	44.99	11.10	0.24	11.64	17.57	0.63	0.03	0.22	98.88	1.39	0.00	0.53	0.07	Calcic amphibole	Magnesiohornblende
18MPe160	1.47	11.62	45.78	10.29	0.21	11.92	17.05	0.64	0.01	0.22	99.20	1.33	0.00	0.44	0.07	Calcic amphibole	Magnesiohornblende
18MPe160	1.95	10.54	43.41	13.27	0.46	10.66	17.03	0.71	0.00	0.33	98.36	1.72	0.00	0.55	0.08	Calcic amphibole	Tschermakite
18MPe160	1.12	10.62	48.60	8.79	0.06	11.34	16.62	0.27	0.04	0.31	97.77	0.92	0.00	0.59	0.03	Calcic amphibole	Magnesiohornblende
18MPe160	1.25	12.55	46.54	11.46	0.11	11.56	14.52	0.58	0.04	0.26	98.87	1.29	0.00	0.66	0.06	Calcic amphibole	Magnesiohornblende
18MPe160	1.43	11.01	45.26	11.07	0.10	11.65	16.12	0.65	0.06	0.26	97.61	1.39	0.00	0.52	0.07	Calcic amphibole	Magnesiohornblende
18MPe160	1.40	11.27	46.79	10.25	0.07	11.52	16.32	0.47	0.03	0.30	98.43	1.24	0.00	0.51	0.05	Calcic amphibole	Magnesiohornblende
18MPe164**	1.30	10.82	46.49	8.62	0.01	12.06	18.31	0.78	0.00	0.24	98.63	1.15	0.00	0.35	0.09	Calcic amphibole	Magnesiohornblende
18MPe164**	1.64	10.72	45.41	11.23	0.32	11.61	16.76	0.38	0.00	0.24	98.30	1.38	0.00	0.55	0.04	Calcic amphibole	Magnesiohornblende
18MPe164**	1.82	12.80	44.96	13.28	0.07	11.49	12.59	0.54	0.17	0.22	97.94	1.57	0.00	0.66	0.06	Calcic amphibole	Tschermakite
18MPe164**	1.33	12.93	45.96	11.22	0.32	11.69	13.15	0.87	0.05	0.26	97.79	1.39	0.00	0.51	0.09	Calcic amphibole	Magnesiohornblende
18MPe164**	1.80	7.00	42.32	12.06	0.29	11.08	23.70	0.76	0.00	0.40	99.41	1.63	0.00	0.52	0.09	Calcic amphibole	Ferropargasite
18MPe164**	1.86	8.60	43.34	11.38	0.14	11.48	21.43	1.07	0.00	0.25	99.55	1.55	0.00	0.45	0.12	Calcic amphibole	Ferropargasite
18MPe164**	1.37	11.81	45.48	11.54	0.04	11.71	15.68	0.58	0.11	0.20	98.52	1.38	0.00	0.60	0.06	Calcic amphibole	Magnesiohornblende
18MPe164**	1.65	13.05	45.90	11.93	0.22	11.49	12.96	0.59	0.12	0.20	98.11	1.44	0.00	0.57	0.06	Calcic amphibole	Magnesiohornblende
18MPe164**	1.38	10.78	42.93	11.23	0.96	11.52	17.64	1.16	0.00	0.43	98.02	1.60	0.00	0.38	0.13	Calcic amphibole	Magnesiohastingsite
18MPe164**	1.52	11.87	45.53	11.25	0.05	11.71	15.98	0.62	0.10	0.19	98.82	1.38	0.00	0.55	0.07	Calcic amphibole	Magnesiohornblende
18MPe164**	1.62	7.05	42.28	12.02	0.27	11.31	23.38	0.76	0.02	0.35	99.05	1.63	0.00	0.51	0.09	Calcic amphibole	Ferropargasite
18MPe164**	1.94	9.32	43.25	11.27	0.09	11.12	20.44	0.54	0.00	0.32	98.30	1.52	0.00	0.47	0.06	Calcic amphibole	Ferropargasite
18MPe164**	1.25	12.13	46.41	10.08	0.16	11.87	15.42	0.46	0.10	0.26	98.14	1.22	0.00	0.52	0.05	Calcic amphibole	Magnesiohornblende
18MPe164**	1.35	9.35	44.23	10.18	0.02	11.34	21.28	0.86	0.00	0.33	98.94	1.43	0.00	0.35	0.10	Calcic amphibole	Ferrohornblende
18MPe164**	1.45	11.09	43.84	11.89	0.57	11.66	16.88	0.66	0.04	0.28	98.35	1.54	0.00	0.53	0.07	Calcic amphibole	Pargasite
18MPe164**	1.34	12.13	46.66	9.95	0.11	11.92	15.16	0.44	0.05	0.26	98.03	1.24	0.00	0.46	0.05	Calcic amphibole	Magnesiohornblende
18MPe164**	1.90	9.17	42.62	12.90	0.49	10.93	19.07	0.51	0.00	0.27	97.86	1.71	0.00	0.54	0.06	Calcic amphibole	Tschermakite
18MPe164**	1.51	9.89	43.81	11.15	0.30	11.42	19.02	0.48	0.07	0.30	97.95	1.46	0.00	0.50	0.05	Calcic amphibole	Magnesiohornblende
18MPe164**	0.95	11.08	47.80	8.29	0.04	11.85	17.51	0.92	0.03	0.32	98.78	1.00	0.00	0.43	0.10	Calcic amphibole	Magnesiohornblende
18MPe164**	1.75	8.34	44.27	9.18	0.42	10.60	22.82	0.86	0.01	0.42	98.67	1.29	0.00	0.35	0.10	Calcic amphibole	Ferro-edenite
18MPe164**	1.56	14.49	45.75	7.51	0.12	10.98	9.96	0.31	0.20	0.18	91.06	1.01	0.00	0.34	0.04	Calcic amphibole	Magnesiohornblende
18MPe164**	0.85	11.64	47.11	7.15	0.53	10.46	19.18	1.49	0.04	0.40	98.86	1.05	0.00	0.20	0.17	Calcic amphibole	Magnesiohornblende
18MPe164**	1.29	12.10	46.73	10.55	0.13	11.82	14.78	0.32	0.02	0.25	97.99	1.25	0.00	0.54	0.04	Calcic amphibole	Magnesiohornblende
18MPe164**	1.56	10.65	44.94	10.84	0.18	11.56	17.79	0.55	0.02	0.20	98.29	1.36	0.00	0.53	0.06	Calcic amphibole	Magnesiohornblende
18MPe164**	1.10	12.00	47.30	9.74	0.33	10.53	16.44	0.75	0.00	0.56	98.75	1.09	0.00	0.58	0.08	Calcic amphibole	Magnesiohornblende
18MPe164**	1.62	10.55	44.91	10.91	0.21	11.20	18.35	0.78	0.00	0.22	98.75	1.37	0.00	0.53	0.09	Calcic amphibole	Edenite
18MPe164**	0.54	10.49	50.72	3.36	0.11	11.80	22.01	0.14	0.02	0.38	99.57	0.53	0.00	0.06	0.02	Calcic amphibole	Ferrohornblende
18MPe164**	1.08	12.10	48.02	8.82	0.14	12.01	16.25	0.49	0.05	0.30	99.26	1.05	0.00	0.46	0.05	Calcic amphibole	Magnesiohornblende
18MPe164**	1.57	12.73	46.64	9.34	0.25	11.63	15.65	0.50	0.01	0.41	98.73	1.20	0.00	0.40	0.06	Calcic amphibole	Magnesiohornblende
18MPe164**	1.41	13.49	46.40	10.94	0.06	11.65	12.57	1.00	0.06	0.23	97.80	1.36	0.00	0.48	0.11	Calcic amphibole	Magnesiohornblende
18MPe164**	1.44	10.91	45.43	10.56	0.23	11.40	17.11	0.59	0.08	0.22	97.97	1.38	0.00	0.44	0.07	Calcic amphibole	Magnesiohornblende

18MPe164**	1.61	9.43	42.56	12.69	0.49	11.07	19.59	0.47	0.00	0.30	98.22	1.64	0.00	0.59	0.05	Calcic amphibole	Pargasite
18MPe164**	1.29	9.55	43.52	9.67	1.01	11.37	20.39	1.20	0.00	0.76	98.77	1.47	0.00	0.24	0.14	Calcic amphibole	Ferro-edenite
18MPe164**	1.26	9.80	43.70	9.25	0.95	11.36	20.44	0.99	0.02	0.89	98.66	1.44	0.00	0.19	0.11	Calcic amphibole	Edenite
18MPe164**	1.58	15.14	41.34	11.45	0.78	11.79	10.13	2.90	0.03	0.26	95.40	1.86	0.00	0.15	0.32	Calcic amphibole	Magnesiohastingsite
18MPe164**	1.48	8.05	43.40	11.25	0.26	11.61	21.57	0.61	0.03	0.30	98.55	1.48	0.00	0.51	0.07	Calcic amphibole	Ferrohornblende
18MPe164**	1.27	11.28	46.40	9.58	0.08	11.89	17.30	0.53	0.00	0.26	98.57	1.20	0.00	0.46	0.06	Calcic amphibole	Magnesiohornblende
18MPe164**	2.18	14.86	45.93	12.58	0.15	11.09	10.41	0.77	0.29	0.17	98.43	1.55	0.00	0.53	0.08	Calcic amphibole	Tschermakite
18MPe164**	1.36	9.25	42.74	15.10	0.26	11.38	17.45	0.38	0.02	0.22	98.16	1.69	0.00	0.94	0.04	Calcic amphibole	Tschermakite
18MPe164**	1.39	10.26	45.70	11.28	0.10	11.72	17.03	0.28	0.02	0.25	98.03	1.32	0.00	0.62	0.03	Calcic amphibole	Magnesiohornblende
18MPe164**	1.06	13.78	46.41	7.40	0.73	11.19	14.94	1.37	0.01	0.51	97.40	1.15	0.00	0.14	0.15	Calcic amphibole	Magnesiohornblende
18MPe164**	1.92	13.98	46.82	11.66	0.10	11.03	11.35	0.61	0.20	0.20	97.88	1.36	0.00	0.59	0.07	Calcic amphibole	Magnesiohornblende
18MPe164**	1.28	11.81	46.76	9.11	0.25	11.62	16.66	0.90	0.07	0.22	98.68	1.24	0.00	0.31	0.10	Calcic amphibole	Magnesiohornblende
18MPe164**	1.39	12.29	46.39	10.84	0.08	11.96	14.28	0.64	0.13	0.20	98.20	1.31	0.00	0.53	0.07	Calcic amphibole	Magnesiohornblende
18MPe164**	1.43	14.48	47.12	9.22	0.11	10.77	13.51	0.88	0.19	0.19	97.90	1.16	0.00	0.41	0.10	Calcic amphibole	Magnesiohornblende
18MPe164**	1.35	10.60	43.77	12.52	0.27	11.29	16.81	0.36	0.06	0.32	97.35	1.50	0.00	0.69	0.04	Calcic amphibole	Tschermakite
18MPe164**	1.95	10.59	43.83	11.81	0.08	11.13	16.61	1.45	0.10	0.22	97.77	1.58	0.00	0.46	0.16	Calcic amphibole	Tschermakite
18MPe170	1.10	16.63	52.51	4.63	0.13	11.81	9.98	0.14	0.10	0.18	97.21	0.54	0.00	0.24	0.02	Calcic amphibole	Magnesiohornblende
18MPe170	1.48	11.56	46.26	10.70	0.11	11.53	14.31	0.81	0.14	0.25	97.15	1.24	0.00	0.60	0.09	Calcic amphibole	Magnesiohornblende
18MPe170	1.52	12.41	45.76	12.17	0.23	11.64	12.26	0.52	0.11	0.24	96.85	1.36	0.00	0.73	0.06	Calcic amphibole	Magnesiohornblende
18MPe170	1.19	10.88	45.57	11.03	0.19	11.71	15.09	0.46	0.08	0.44	96.64	1.28	0.00	0.63	0.05	Calcic amphibole	Magnesiohornblende
18MPe170	1.94	14.43	48.06	9.60	0.13	11.71	10.20	0.30	0.20	0.20	96.78	1.06	0.00	0.58	0.03	Calcic amphibole	Magnesiohornblende
18MPe170	1.63	10.81	45.79	10.60	0.14	11.62	15.38	0.48	0.03	0.29	96.77	1.23	0.00	0.62	0.05	Calcic amphibole	Magnesiohornblende
18MPe170	1.73	9.91	44.11	10.70	0.24	11.11	17.66	0.55	0.06	0.29	96.36	1.41	0.00	0.48	0.06	Calcic amphibole	Magnesiohornblende
18MPe170	1.28	11.84	46.48	10.58	0.17	11.71	13.44	0.52	0.03	0.26	96.31	1.17	0.00	0.66	0.06	Calcic amphibole	Magnesiohornblende
18MPe170	1.17	9.25	46.20	9.58	0.50	10.53	17.91	1.08	0.00	0.46	96.67	1.13	0.00	0.55	0.12	Calcic amphibole	Magnesiohornblende
18MPe170	2.00	11.91	42.76	12.03	0.86	11.45	13.40	2.09	0.00	0.26	96.76	1.66	0.00	0.44	0.23	Calcic amphibole	Pargasite
18MPe170	1.46	13.87	48.42	9.01	0.10	11.78	11.34	0.63	0.08	0.33	97.02	1.01	0.00	0.53	0.07	Calcic amphibole	Magnesiohornblende
18MPe170	0.54	15.29	51.98	5.61	0.07	12.48	10.51	0.12	0.12	0.22	96.95	0.54	0.00	0.41	0.01	Calcic amphibole	Magnesiohornblende
18MPe170	1.03	12.90	47.78	9.79	0.10	11.92	13.11	0.64	0.14	0.24	97.66	1.12	0.00	0.54	0.07	Calcic amphibole	Magnesiohornblende
18MPe170	1.18	9.18	45.31	10.81	0.66	10.93	17.60	0.94	0.05	0.61	97.27	1.29	0.00	0.60	0.11	Calcic amphibole	Magnesiohornblende
18MPe170	1.00	13.35	48.40	7.79	0.05	12.01	12.95	0.31	0.01	0.27	96.14	0.91	0.00	0.43	0.04	Calcic amphibole	Magnesiohornblende
18MPe170	1.60	11.21	43.87	14.53	0.01	11.85	12.94	0.47	0.03	0.22	96.73	1.60	0.00	0.90	0.05	Calcic amphibole	Tschermakite
18MPe170	1.44	11.96	46.25	11.31	0.17	11.23	13.12	0.89	0.05	0.17	96.58	1.26	0.00	0.68	0.10	Calcic amphibole	Magnesiohornblende
18MPe170	1.58	11.73	43.50	10.73	0.83	11.41	14.01	2.05	0.00	0.37	96.21	1.52	0.00	0.37	0.23	Calcic amphibole	Tschermakite
18MPe170	2.24	14.09	45.70	12.76	0.11	10.74	10.10	0.77	0.14	0.25	96.90	1.48	0.00	0.67	0.08	Calcic amphibole	Magnesiohornblende
18MPe170	1.35	11.19	46.60	9.64	0.09	11.77	15.09	0.46	0.00	0.27	96.46	1.10	0.00	0.58	0.05	Calcic amphibole	Magnesiohornblende
18MPe170	1.32	9.11	44.24	11.10	0.29	11.43	17.90	0.50	0.00	0.32	96.21	1.35	0.00	0.61	0.06	Calcic amphibole	Magnesiohornblende
18MPe170	1.55	14.54	45.42	10.49	0.30	10.11	12.36	1.41	0.00	0.30	96.49	1.32	0.00	0.50	0.16	Calcic amphibole	Magnesiohornblende
18MPe170	1.30	11.74	47.18	9.37	0.32	11.77	14.92	0.40	0.01	0.25	97.27	1.09	0.00	0.53	0.04	Calcic amphibole	Magnesiohornblende

18MPe170	1.14	12.47	46.60	10.95	0.10	11.69	12.60	0.47	0.07	0.26	96.35	1.21	0.00	0.67	0.05	Calcic amphibole	Magnesiohornblende
18MPe170	0.87	16.97	53.64	3.99	0.09	11.92	9.35	0.16	0.08	0.23	97.30	0.41	0.00	0.26	0.02	Calcic amphibole	Actinolite
18MPe170	1.47	9.67	44.41	12.14	0.25	11.50	16.06	0.42	0.00	0.29	96.21	1.37	0.00	0.76	0.05	Calcic amphibole	Magnesiohornblende
18MPe170	1.31	8.96	47.65	7.39	0.14	11.35	19.54	0.27	0.00	0.36	96.96	0.84	0.00	0.46	0.03	Calcic amphibole	Ferrohornblende
18MPe170	1.54	10.42	44.43	11.74	0.40	11.36	15.27	0.48	0.11	0.30	96.04	1.38	0.00	0.68	0.05	Calcic amphibole	Magnesiohornblende
18MPe170	1.94	14.64	45.30	13.26	0.15	10.13	9.69	0.77	0.12	0.18	96.18	1.58	0.00	0.64	0.08	Calcic amphibole	Tschermakite
18MPe170	0.49	11.73	50.25	5.89	0.01	11.90	15.93	0.37	0.03	0.48	97.08	0.64	0.00	0.38	0.04	Calcic amphibole	Magnesiohornblende
18MPe170	0.94	13.02	49.01	6.37	0.08	11.02	14.96	0.55	0.06	0.30	96.31	0.72	0.00	0.40	0.06	Calcic amphibole	Magnesiohornblende
18MPe170	0.98	9.61	45.37	10.43	0.29	9.76	18.85	1.12	0.02	0.42	96.84	1.16	0.00	0.70	0.13	Calcic amphibole	Ferrohornblende
18MPe170	1.45	11.52	46.10	10.90	0.07	11.57	13.84	0.38	0.12	0.32	96.28	1.22	0.00	0.67	0.04	Calcic amphibole	Magnesiohornblende
18MPe170	1.36	9.75	44.30	12.10	0.25	11.77	15.87	0.63	0.07	0.31	96.40	1.39	0.00	0.74	0.07	Calcic amphibole	Magnesiohornblende
18MPe170	1.64	13.14	45.68	12.68	0.10	11.75	10.35	0.73	0.12	0.18	96.37	1.38	0.00	0.79	0.08	Calcic amphibole	Magnesiohornblende
18MPe170	1.52	15.58	45.41	12.59	0.08	10.63	9.74	0.73	0.19	0.12	96.59	1.44	0.00	0.71	0.08	Calcic amphibole	Magnesiohornblende
18MPe170	2.10	13.34	44.94	13.58	0.14	10.65	10.23	0.69	0.50	0.19	96.36	1.54	0.00	0.76	0.08	Calcic amphibole	Tschermakite
18MPe170	2.38	13.16	44.64	12.96	0.10	11.74	10.66	0.49	0.10	0.17	96.41	1.48	0.00	0.75	0.05	Calcic amphibole	Edenite
18MPe170	1.15	9.42	44.34	9.99	0.97	11.50	17.69	1.16	0.04	0.64	96.91	1.33	0.00	0.44	0.13	Calcic amphibole	Magnesiohornblende
18MPe170	1.60	11.93	46.20	10.14	0.32	11.53	14.38	0.56	0.02	0.34	97.02	1.23	0.00	0.52	0.06	Calcic amphibole	Magnesiohornblende
18MPe170	1.24	11.49	44.96	9.76	0.82	10.63	15.84	1.35	0.03	0.49	96.61	1.38	0.00	0.31	0.15	Calcic amphibole	Magnesiohornblende
18MPe170	0.93	12.41	48.32	8.80	0.07	12.10	13.55	0.40	0.09	0.27	96.93	0.95	0.00	0.56	0.04	Calcic amphibole	Magnesiohornblende
18MPe170	1.19	12.64	46.82	11.51	0.01	11.92	11.27	0.65	0.06	0.23	96.29	1.19	0.00	0.78	0.07	Calcic amphibole	Magnesiohornblende
18MPe170	1.24	11.09	44.02	9.49	1.11	11.49	15.94	1.45	0.00	0.56	96.40	1.40	0.00	0.28	0.16	Calcic amphibole	Magnesiohornblende
18MPe170	1.41	11.17	45.91	10.39	0.24	11.87	14.87	0.53	0.02	0.25	96.65	1.21	0.00	0.61	0.06	Calcic amphibole	Magnesiohornblende
18MPe170	1.66	11.05	44.77	12.88	0.09	11.54	13.61	0.71	0.07	0.25	96.62	1.43	0.00	0.80	0.08	Calcic amphibole	Magnesiohornblende
18MPe170	1.48	10.56	45.12	11.02	0.05	11.57	15.71	0.85	0.04	0.24	96.64	1.32	0.00	0.60	0.09	Calcic amphibole	Magnesiohornblende
18MPe170	1.74	12.77	46.01	11.03	0.20	11.74	11.93	0.57	0.07	0.26	96.32	1.26	0.00	0.65	0.06	Calcic amphibole	Magnesiohornblende
18MPe170	1.55	15.28	49.32	8.88	0.11	11.69	9.09	0.36	0.15	0.20	96.64	0.93	0.00	0.57	0.04	Calcic amphibole	Magnesiohornblende
18MPe170	1.41	13.54	46.36	9.84	0.45	11.75	11.57	1.00	0.17	0.20	96.29	1.22	0.00	0.48	0.11	Calcic amphibole	Magnesiohornblende
18MPe170	1.47	12.01	45.87	10.37	0.18	11.76	13.77	0.64	0.07	0.31	96.46	1.25	0.00	0.55	0.07	Calcic amphibole	Magnesiohornblende
18MPe170	1.55	10.11	44.96	9.76	0.09	11.63	16.80	0.51	0.06	0.30	95.76	1.22	0.00	0.51	0.06	Calcic amphibole	Magnesiohornblende
18MPe203	1.40	10.99	44.97	12.02	0.21	11.21	14.57	0.83	0.03	0.19	96.43	1.40	0.00	0.69	0.09	Calcic amphibole	Magnesiohornblende
18MPe203	1.61	11.71	45.04	12.53	0.17	11.87	13.20	0.68	0.17	0.23	97.20	1.43	0.00	0.72	0.07	Calcic amphibole	Magnesiohornblende
18MPe203	1.68	12.15	45.51	11.44	0.21	11.74	13.22	0.80	0.08	0.28	97.11	1.36	0.00	0.61	0.09	Calcic amphibole	Magnesiohornblende
18MPe203	0.45	11.92	49.90	5.31	0.41	11.86	15.38	0.51	0.03	0.56	96.34	0.60	0.00	0.33	0.06	Calcic amphibole	Magnesiohornblende
18MPe203	1.19	8.65	43.71	11.68	0.50	10.81	19.11	1.09	0.01	0.55	97.30	1.52	0.00	0.53	0.12	Calcic amphibole	Tschermakite
18MPe203	0.61	11.66	50.16	6.47	0.11	11.66	15.23	0.25	0.13	0.26	96.54	0.63	0.00	0.50	0.03	Calcic amphibole	Magnesiohornblende
18MPe203	0.76	12.23	49.32	7.09	0.08	11.35	15.23	0.65	0.06	0.42	97.19	0.84	0.00	0.37	0.07	Calcic amphibole	Magnesiohornblende
18MPe203	0.68	10.97	47.37	6.52	0.95	11.46	17.00	1.53	0.02	0.31	96.82	0.93	0.00	0.22	0.17	Calcic amphibole	Magnesiohornblende
18MPe203	1.56	10.74	45.31	11.32	0.09	11.36	15.28	0.69	0.03	0.31	96.69	1.33	0.00	0.64	0.08	Calcic amphibole	Magnesiohornblende
18MPe203	1.43	13.85	45.47	13.55	0.22	9.88	11.49	0.67	0.02	0.22	96.81	1.38	0.00	0.95	0.07	Calcic amphibole	Magnesiohornblende

18MPe203	2.21	14.21	42.22	12.13	0.39	11.63	11.18	2.12	0.00	0.25	96.33	1.82	0.00	0.27	0.23	Calcic amphibole	Magnesiohastingsite
18MPe203	1.15	12.73	47.82	10.05	0.16	11.57	12.42	0.32	0.01	0.28	96.51	1.06	0.00	0.67	0.04	Calcic amphibole	Magnesiohornblende
18MPe203	1.26	11.54	47.60	9.46	0.06	11.73	14.35	0.33	0.05	0.25	96.64	1.00	0.00	0.63	0.04	Calcic amphibole	Magnesiohornblende
18MPe203	1.38	10.53	44.13	9.16	0.95	11.48	17.75	1.18	0.04	0.98	97.58	1.42	0.00	0.19	0.13	Calcic amphibole	Magnesiohornblende
18MPe203	1.50	10.36	44.25	11.41	0.30	11.41	16.00	0.91	0.00	0.25	96.40	1.42	0.00	0.58	0.10	Calcic amphibole	Magnesiohornblende
18MPe203	2.14	12.23	42.39	10.24	0.97	11.25	12.94	3.75	0.04	0.24	96.19	1.63	0.00	0.18	0.42	Calcic amphibole	Pargasite
18MPe203	1.37	12.02	45.46	11.14	0.10	11.78	13.41	0.85	0.03	0.26	96.43	1.33	0.00	0.60	0.09	Calcic amphibole	Magnesiohornblende
18MPe203	2.94	11.48	41.03	14.00	0.06	11.13	13.16	2.89	0.03	0.17	96.89	1.94	0.00	0.50	0.32	Calcic amphibole	Pargasite
18MPe203	0.86	11.43	45.07	9.14	0.89	11.74	15.87	1.18	0.00	0.40	96.58	1.30	0.00	0.31	0.13	Calcic amphibole	Magnesiohornblende
18MPe203	1.88	12.15	44.06	14.17	0.19	11.03	11.47	0.66	0.28	0.20	96.09	1.59	0.00	0.84	0.07	Calcic amphibole	Tschermakite
18MPe203	1.82	10.81	44.49	11.16	0.18	11.36	15.54	0.59	0.09	0.28	96.31	1.39	0.00	0.56	0.07	Calcic amphibole	Magnesiohornblende
18MPe233	1.75	15.34	48.67	8.84	0.15	11.86	9.92	0.34	0.28	0.16	97.32	1.04	0.00	0.45	0.04	Calcic amphibole	Magnesiohornblende
18MPe233	0.78	14.07	48.79	6.67	0.24	11.38	13.08	0.74	0.02	0.54	96.31	0.81	0.00	0.35	0.08	Calcic amphibole	Magnesiohornblende
18MPe233	1.31	14.16	48.35	6.25	0.32	10.85	14.10	1.52	0.00	0.41	97.28	1.03	0.00	0.04	0.17	Calcic amphibole	Magnesiohornblende
18MPe233	1.42	12.82	47.24	9.69	0.08	11.88	13.09	0.24	0.03	0.28	96.76	1.11	0.00	0.55	0.03	Calcic amphibole	Magnesiohornblende
18MPe233	1.42	11.58	45.26	10.21	0.04	11.18	15.85	0.68	0.05	0.29	96.56	1.25	0.00	0.54	0.08	Calcic amphibole	Magnesiohornblende
18MPe233	2.14	14.47	46.25	11.84	0.08	10.54	10.03	0.55	0.24	0.21	96.36	1.39	0.00	0.61	0.06	Calcic amphibole	Magnesiohornblende
18MPe233	1.03	8.62	44.17	11.50	0.59	11.57	17.37	0.54	0.00	0.52	95.91	1.32	0.00	0.73	0.06	Calcic amphibole	Magnesiohornblende
18MPe233	1.64	12.41	46.65	9.44	0.05	11.34	13.92	0.38	0.04	0.31	96.17	1.15	0.00	0.49	0.04	Calcic amphibole	Magnesiohornblende
18MPe233	1.37	9.86	44.49	11.23	0.20	11.38	16.24	0.66	0.03	0.29	95.74	1.33	0.00	0.65	0.08	Calcic amphibole	Magnesiohornblende
18MPe233	2.23	12.55	44.73	11.82	0.17	10.88	12.99	0.68	0.05	0.27	96.38	1.47	0.00	0.57	0.08	Calcic amphibole	Magnesiohornblende
18MPe233	1.73	12.80	39.89	14.80	1.28	11.97	11.16	2.21	0.00	0.11	95.95	2.07	0.00	0.52	0.25	Calcic amphibole	Pargasite
18MPe233	1.18	9.98	43.71	9.38	1.04	11.50	18.30	1.10	0.04	0.78	97.01	1.43	0.00	0.23	0.12	Calcic amphibole	Magnesiohornblende
18MPe233	1.28	11.02	45.30	10.68	0.16	11.61	15.27	0.45	0.07	0.27	96.11	1.29	0.00	0.58	0.05	Calcic amphibole	Magnesiohornblende
18MPe233	2.04	13.35	44.00	13.08	0.13	10.80	11.48	1.31	0.12	0.18	96.49	1.66	0.00	0.57	0.14	Calcic amphibole	Tschermakite
18MPe233	2.09	11.29	43.35	15.09	0.18	10.15	14.08	0.30	0.00	0.24	96.77	1.75	0.00	0.81	0.03	Calcic amphibole	Tschermakite
18MPe233	2.03	12.70	39.90	14.80	1.47	11.81	11.41	1.42	0.00	0.13	95.67	2.04	0.00	0.57	0.16	Calcic amphibole	Pargasite
18MPe233	0.72	14.23	49.64	5.97	0.51	12.08	12.30	0.64	0.10	0.41	96.60	0.76	0.00	0.27	0.07	Calcic amphibole	Magnesiohornblende
18MPe233	1.20	13.29	46.79	9.17	0.08	10.90	14.14	0.64	0.01	0.26	96.48	1.09	0.00	0.50	0.07	Calcic amphibole	Magnesiohornblende
18MPe233	1.34	10.99	45.57	9.52	0.19	11.19	16.57	0.86	0.04	0.27	96.53	1.26	0.00	0.40	0.10	Calcic amphibole	Magnesiohornblende
18MPe233	1.16	11.65	45.35	11.46	0.37	11.91	13.74	0.51	0.06	0.26	96.46	1.33	0.00	0.66	0.06	Calcic amphibole	Magnesiohornblende
18MPe233	1.61	15.11	47.37	10.17	0.14	11.32	9.98	0.48	0.04	0.16	96.37	1.21	0.00	0.50	0.05	Calcic amphibole	Magnesiohornblende
18MPe233	1.39	11.07	44.95	11.71	0.21	11.58	14.33	0.49	0.11	0.20	96.04	1.35	0.00	0.69	0.06	Calcic amphibole	Magnesiohornblende
18MPe233	1.36	10.99	44.55	12.34	0.40	11.35	14.42	0.82	0.13	0.27	96.63	1.46	0.00	0.68	0.09	Calcic amphibole	Magnesiohornblende
18MPe233	1.62	12.66	45.78	12.30	0.11	11.49	12.05	0.63	0.08	0.29	97.02	1.39	0.00	0.71	0.07	Calcic amphibole	Magnesiohornblende
18MPe233	1.37	9.05	41.54	14.71	0.51	11.17	16.90	0.53	0.00	0.60	96.40	1.73	0.00	0.89	0.06	Calcic amphibole	Tschermakite
18MPe233	1.86	10.77	43.07	11.71	0.36	10.67	16.18	0.76	0.00	0.40	95.78	1.59	0.00	0.46	0.09	Calcic amphibole	Tschermakite
18MPe233	1.88	9.30	43.92	10.67	0.23	11.08	18.39	0.71	0.00	0.31	96.49	1.40	0.00	0.49	0.08	Calcic amphibole	Magnesiohornblende
18MPe233	1.54	8.99	41.70	14.48	0.63	10.85	17.04	0.75	0.00	0.35	96.33	1.79	0.00	0.75	0.08	Calcic amphibole	Tschermakite

18MPe233	1.28	10.31	44.91	10.96	0.43	11.78	16.04	0.59	0.04	0.28	96.63	1.31	0.00	0.61	0.07	Calcic amphibole	Magnesiohornblende
18MPe233	1.18	12.24	46.20	10.49	0.09	12.03	14.31	0.51	0.03	0.23	97.29	1.28	0.00	0.52	0.06	Calcic amphibole	Magnesiohornblende
18MPe233	1.62	13.19	45.42	11.89	0.09	11.06	11.58	1.04	0.14	0.19	96.22	1.43	0.00	0.60	0.11	Calcic amphibole	Magnesiohornblende
18MPe233	1.26	11.29	44.98	11.28	0.14	11.68	15.33	0.47	0.00	0.29	96.72	1.32	0.00	0.65	0.05	Calcic amphibole	Magnesiohornblende
18MPe233	1.53	13.01	46.04	12.11	0.08	12.24	10.46	0.43	1.07	0.20	97.18	1.34	0.00	0.73	0.05	Calcic amphibole	Magnesiohornblende
18MPe233	1.12	13.83	48.22	9.69	0.04	11.63	11.16	0.56	0.16	0.25	96.66	1.06	0.00	0.58	0.06	Calcic amphibole	Magnesiohornblende
18MPe233	1.56	12.56	45.08	12.82	0.06	11.00	12.62	0.81	0.14	0.19	96.85	1.51	0.00	0.66	0.09	Calcic amphibole	Tschermakite
18MPe233	0.67	11.56	48.68	7.54	0.50	12.25	14.92	0.24	0.00	0.40	96.75	0.79	0.00	0.52	0.03	Calcic amphibole	Magnesiohornblende
18MPe233	1.32	11.60	46.79	9.96	0.04	11.59	13.86	0.40	0.09	0.26	95.91	1.09	0.00	0.65	0.05	Calcic amphibole	Magnesiohornblende
18MPe233	1.31	7.51	44.26	9.59	0.12	11.49	21.65	0.45	0.00	0.37	96.75	1.27	0.00	0.45	0.05	Calcic amphibole	Ferrohornblende
18MPe233	1.21	12.08	46.55	10.05	0.10	11.60	14.06	0.77	0.05	0.20	96.67	1.20	0.00	0.53	0.09	Calcic amphibole	Magnesiohornblende
18MPe233	1.09	11.55	46.62	10.22	0.36	10.51	15.20	0.76	0.06	0.47	96.84	1.24	0.00	0.51	0.08	Calcic amphibole	Magnesiohornblende
18MPe233	1.54	11.38	45.09	10.48	0.04	10.79	14.93	1.42	0.08	0.19	95.95	1.35	0.00	0.47	0.16	Calcic amphibole	Magnesiohornblende
18MPe233	1.36	12.00	46.52	10.41	0.05	11.81	13.59	0.45	0.07	0.28	96.53	1.18	0.00	0.62	0.05	Calcic amphibole	Magnesiohornblende
18MPe233	1.47	12.06	43.60	13.57	0.52	10.12	14.43	0.98	0.00	0.47	97.22	1.56	0.00	0.80	0.11	Calcic amphibole	Pargasite
18MPe233	1.42	8.16	43.33	12.18	0.34	11.32	18.73	0.61	0.03	0.34	96.47	1.47	0.00	0.69	0.07	Calcic amphibole	Ferrohornblende
18MPe233	1.04	11.73	47.02	10.20	0.07	11.74	13.92	0.36	0.08	0.25	96.42	1.11	0.00	0.65	0.04	Calcic amphibole	Magnesiohornblende
18MPe233	0.52	12.80	49.54	5.11	0.34	11.79	14.91	0.34	0.00	0.61	95.96	0.67	0.00	0.22	0.04	Calcic amphibole	Magnesiohornblende
18MPe233	1.54	16.57	47.62	10.22	0.06	11.20	8.42	0.46	0.17	0.22	96.48	1.28	0.00	0.43	0.05	Calcic amphibole	Magnesiohornblende
18MPe233	1.85	10.78	41.61	10.05	1.16	11.76	15.86	3.46	0.00	0.31	96.84	1.69	0.00	0.11	0.40	Calcic amphibole	Magnesiohastingsite
18MPe233	0.54	11.73	50.99	5.91	0.55	11.54	14.55	0.36	0.02	0.59	96.78	0.50	0.00	0.52	0.04	Calcic amphibole	Magnesiohornblende
18MPe233	0.87	10.82	47.84	8.22	0.00	11.52	16.78	0.98	0.06	0.30	97.39	0.99	0.00	0.43	0.11	Calcic amphibole	Magnesiohornblende
18MPe233	1.80	12.10	44.14	15.45	0.13	11.54	10.65	0.51	0.03	0.29	96.64	1.62	0.00	1.01	0.06	Calcic amphibole	Tschermakite
18MPe233	1.11	12.99	46.33	11.82	0.08	11.41	11.31	0.48	0.08	0.22	95.83	1.29	0.00	0.73	0.05	Calcic amphibole	Magnesiohornblende
18MPe233	1.43	12.17	45.62	11.82	0.12	11.16	12.57	0.98	0.07	0.21	96.14	1.35	0.00	0.68	0.11	Calcic amphibole	Magnesiohornblende
18MPe233	0.69	11.83	48.63	7.23	0.22	10.45	15.74	0.67	0.01	0.69	96.16	0.72	0.00	0.55	0.08	Calcic amphibole	Magnesiohornblende
18MPe233	1.35	7.36	43.43	10.54	0.10	11.07	20.82	1.17	0.00	0.32	96.16	1.39	0.00	0.50	0.13	Calcic amphibole	Ferrohornblende
18MPe247	1.33	12.78	46.69	10.35	0.22	11.89	12.57	0.44	0.11	0.30	96.68	1.19	0.00	0.59	0.05	Calcic amphibole	Magnesiohornblende
18MPe247	1.82	11.95	45.20	10.85	0.32	11.87	14.55	0.77	0.05	0.29	97.67	1.39	0.00	0.49	0.09	Calcic amphibole	Magnesiohornblende
18MPe247	1.44	9.73	43.48	12.83	0.10	11.85	16.21	0.48	0.01	0.22	96.35	1.52	0.00	0.74	0.05	Calcic amphibole	Tschermakite
18MPe247	1.44	10.24	43.73	13.53	0.35	11.63	14.40	0.66	0.64	0.25	96.86	1.55	0.00	0.80	0.07	Calcic amphibole	Tschermakite
18MPe247	2.14	10.21	42.44	14.41	0.17	11.44	14.75	0.88	0.11	0.24	96.78	1.73	0.00	0.79	0.10	Calcic amphibole	Tschermakite
18MPe247	2.08	13.95	44.67	13.94	0.12	10.88	10.47	1.03	0.07	0.19	97.41	1.66	0.00	0.67	0.11	Calcic amphibole	Tschermakite
18MPe247	1.04	12.37	46.70	10.53	0.13	11.93	13.55	0.57	0.05	0.22	97.09	1.22	0.00	0.58	0.06	Calcic amphibole	Magnesiohornblende
18MPe247	1.35	12.37	46.24	9.94	0.09	11.83	13.59	0.90	0.11	0.25	96.67	1.23	0.00	0.49	0.10	Calcic amphibole	Magnesiohornblende
18MPe247	1.34	10.94	45.68	10.72	0.14	11.63	15.59	0.32	0.00	0.24	96.59	1.26	0.00	0.60	0.04	Calcic amphibole	Magnesiohornblende
18MPe247	1.05	10.48	46.32	8.42	0.02	11.18	17.67	1.05	0.00	0.34	96.53	1.03	0.00	0.46	0.12	Calcic amphibole	Magnesiohornblende
18MPe247	1.44	12.32	46.39	9.27	0.34	11.26	14.35	0.67	0.03	0.19	96.26	1.18	0.00	0.43	0.07	Calcic amphibole	Magnesiohornblende
18MPe247	0.47	16.91	53.75	2.80	0.01	12.48	10.17	0.02	0.09	0.30	96.99	0.33	0.00	0.14	0.00	Calcic amphibole	Actinolite

18MPe247	1.45	9.73	43.49	12.10	0.20	11.38	16.92	0.78	0.08	0.27	96.40	1.52	0.00	0.60	0.09	Calcic amphibole	Tschermakite
18MPe247	1.70	8.78	42.16	13.24	0.38	10.96	17.70	0.59	0.02	0.27	95.80	1.65	0.00	0.70	0.07	Calcic amphibole	Tschermakite
18MPe247	0.96	13.22	47.13	7.08	0.71	11.88	14.14	1.30	0.05	0.42	96.89	1.07	0.00	0.16	0.14	Calcic amphibole	Magnesiohornblende
18MPe247	1.30	12.49	45.85	11.96	0.10	11.61	12.55	0.69	0.12	0.23	96.91	1.37	0.00	0.67	0.08	Calcic amphibole	Magnesiohornblende
18MPe247	1.21	12.48	46.11	10.76	0.09	12.00	13.64	0.46	0.00	0.19	96.95	1.29	0.00	0.56	0.05	Calcic amphibole	Magnesiohornblende
18MPe247	2.41	15.17	41.86	13.71	0.35	11.67	9.55	1.55	0.04	0.11	96.43	1.95	0.00	0.39	0.17	Calcic amphibole	Magnesiohastingsite
18MPe247	1.36	14.60	46.84	9.40	0.21	9.88	13.62	1.08	0.02	0.38	97.39	1.17	0.00	0.45	0.12	Calcic amphibole	Magnesiohornblende
18MPe247	1.13	11.92	46.04	10.41	0.08	12.04	14.24	0.47	0.06	0.29	96.68	1.25	0.00	0.55	0.05	Calcic amphibole	Magnesiohornblende
18MPe247	0.96	9.90	46.55	8.91	0.07	11.88	17.76	0.74	0.03	0.32	97.12	1.09	0.00	0.47	0.08	Calcic amphibole	Magnesiohornblende
18MPe247	1.55	12.83	45.83	11.46	0.15	11.56	12.52	0.71	0.05	0.22	96.88	1.36	0.00	0.60	0.08	Calcic amphibole	Magnesiohornblende
18MPe247	1.07	7.24	45.61	6.50	0.71	10.33	23.38	1.21	0.04	0.65	96.73	1.03	0.00	0.14	0.14	Calcic amphibole	Ferrohornblende
18MPe247	1.66	11.29	44.48	12.95	0.09	11.69	13.25	0.55	0.02	0.26	96.24	1.45	0.00	0.80	0.06	Calcic amphibole	Magnesiohornblende
18MPe247	1.26	10.59	44.71	11.23	0.09	11.74	15.12	0.28	0.42	0.23	95.67	1.33	0.00	0.65	0.03	Calcic amphibole	Magnesiohornblende
18MPe247	2.18	7.13	40.27	14.42	1.37	11.04	18.23	2.08	0.00	0.28	97.00	1.84	0.00	0.76	0.24	Calcic amphibole	Ferropargasite
18MPe247	1.40	12.43	45.93	11.16	0.07	11.78	12.89	0.69	0.12	0.25	96.72	1.31	0.00	0.61	0.08	Calcic amphibole	Magnesiohornblende
18MPe247	1.72	11.89	44.11	11.72	0.18	11.99	14.02	0.65	0.11	0.25	96.64	1.50	0.00	0.54	0.07	Calcic amphibole	Magnesiohornblende
18MPe247	1.08	13.73	46.85	11.26	0.11	11.73	11.36	0.38	0.02	0.21	96.73	1.28	0.00	0.63	0.04	Calcic amphibole	Magnesiohornblende
18MPe247	1.46	15.23	47.94	9.87	0.05	11.49	9.85	0.47	0.24	0.21	96.81	1.17	0.00	0.49	0.05	Calcic amphibole	Magnesiohornblende
18MPe247	1.65	12.36	44.89	12.95	0.23	11.60	12.78	0.93	0.01	0.11	97.52	1.52	0.00	0.68	0.10	Calcic amphibole	Tschermakite
18MPe247	0.15	15.38	53.95	1.89	0.00	12.67	12.99	0.26	0.06	0.28	97.63	0.22	0.00	0.10	0.03	Calcic amphibole	Actinolite
18MPe247	1.50	11.27	45.66	10.85	0.09	11.62	14.63	0.65	0.09	0.26	96.62	1.28	0.00	0.61	0.07	Calcic amphibole	Magnesiohornblende
18MPe247	1.07	11.11	47.51	8.76	0.32	11.21	15.87	0.57	0.03	0.60	97.06	1.03	0.00	0.48	0.06	Calcic amphibole	Magnesiohornblende
18MPe247	0.80	11.96	47.13	8.09	0.86	12.20	14.65	0.88	0.01	0.37	96.96	1.02	0.00	0.40	0.10	Calcic amphibole	Magnesiohornblende
18MPe247	0.80	15.32	50.94	7.22	0.01	12.14	10.04	0.27	0.20	0.21	97.16	0.74	0.00	0.47	0.03	Calcic amphibole	Magnesiohornblende
18MPe247	0.32	15.16	54.36	1.22	0.11	12.60	13.08	0.46	0.02	0.34	97.67	0.15	0.00	0.06	0.05	Calcic amphibole	Actinolite
18MPe247	1.50	11.60	44.74	10.89	0.26	11.90	14.81	0.69	0.10	0.23	96.72	1.39	0.00	0.50	0.08	Calcic amphibole	Magnesiohornblende
18MPe247	1.33	10.97	42.71	10.91	1.19	12.00	15.63	2.04	0.04	0.29	97.11	1.60	0.00	0.32	0.23	Calcic amphibole	Magnesiohastingsite
18MPe247	1.16	12.69	46.07	11.77	0.10	11.92	11.71	0.42	0.07	0.20	96.11	1.29	0.00	0.74	0.05	Calcic amphibole	Magnesiohornblende
18MPe247	1.40	11.37	45.73	11.10	0.10	11.53	14.42	0.54	0.08	0.26	96.53	1.28	0.00	0.64	0.06	Calcic amphibole	Magnesiohornblende
18MPe247	2.07	8.88	42.96	11.29	0.47	10.82	18.77	0.80	0.00	0.32	96.38	1.51	0.00	0.50	0.09	Calcic amphibole	Tschermakite
18MPe247	1.34	11.92	43.51	12.80	0.48	11.51	13.55	0.61	0.04	0.27	96.05	1.60	0.00	0.62	0.07	Calcic amphibole	Tschermakite
18MPe250	2.08	13.46	44.93	13.56	0.17	10.32	11.28	0.94	0.11	0.21	97.06	1.61	0.00	0.67	0.10	Calcic amphibole	Tschermakite
18MPe250	1.60	9.20	44.01	10.56	0.25	10.47	19.39	0.69	0.03	0.35	96.56	1.44	0.00	0.41	0.08	Calcic amphibole	Magnesiohornblende
18MPe250	1.43	11.22	44.36	12.55	0.21	11.19	13.72	0.47	0.04	0.28	95.47	1.45	0.00	0.74	0.05	Calcic amphibole	Magnesiohornblende
18MPe250	1.57	10.43	44.06	10.65	0.96	11.35	15.29	1.68	0.00	0.39	96.39	1.38	0.00	0.50	0.19	Calcic amphibole	Magnesiohornblende
18MPe250	1.48	9.74	44.23	12.15	0.31	11.50	16.49	0.37	0.03	0.31	96.61	1.42	0.00	0.71	0.04	Calcic amphibole	Magnesiohornblende
18MPe250	1.45	13.41	47.29	6.80	0.38	10.74	13.89	1.42	0.00	0.48	95.86	1.05	0.00	0.13	0.16	Calcic amphibole	Magnesiohornblende
18MPe250	1.24	12.14	45.26	10.77	0.32	11.24	14.45	0.79	0.01	0.33	96.55	1.28	0.00	0.60	0.09	Calcic amphibole	Magnesiohornblende
18MPe250	1.99	11.37	43.44	14.53	0.21	9.75	14.35	0.63	0.00	0.18	96.46	1.74	0.00	0.73	0.07	Calcic amphibole	Tschermakite

18MPe250	2.05	11.23	43.88	14.19	0.19	9.67	14.20	0.59	0.02	0.18	96.20	1.65	0.00	0.77	0.06	Sodic-calcic amphibole	Tschermakite
18MPe250	1.99	11.44	43.34	14.44	0.20	9.61	14.81	0.69	0.00	0.18	96.70	1.77	0.00	0.67	0.07	Sodic-calcic amphibole	Tschermakite
18MPe250	1.39	12.68	46.96	10.37	0.07	11.84	12.82	0.49	0.07	0.25	96.94	1.17	0.00	0.60	0.05	Calcic amphibole	Magnesiohornblende
18MPe250	1.14	8.62	42.76	10.05	1.19	11.68	19.43	1.56	0.01	0.62	97.06	1.49	0.00	0.31	0.18	Calcic amphibole	Ferrohornblende
18MPe250	1.88	10.83	43.01	15.03	0.28	9.56	14.99	0.60	0.03	0.38	96.59	1.80	0.00	0.75	0.07	Sodic-calcic amphibole	Ferrohornblende
18MPe250	1.26	11.54	44.28	11.29	0.60	11.51	15.01	0.67	0.00	0.27	96.43	1.46	0.00	0.50	0.08	Calcic amphibole	Magnesiohornblende
18MPe250	1.56	12.06	44.51	12.53	0.28	11.13	12.82	0.73	0.09	0.28	95.99	1.49	0.00	0.68	0.08	Calcic amphibole	Magnesiohornblende
18MPe250	1.14	11.86	45.79	11.76	0.42	11.59	13.67	0.49	0.00	0.33	97.04	1.34	0.00	0.67	0.05	Calcic amphibole	Magnesiohornblende
18MPe250	1.82	10.04	44.73	9.64	0.11	10.69	18.06	0.61	0.00	0.49	96.19	1.32	0.00	0.38	0.07	Calcic amphibole	Magnesiohornblende
18MPe250	1.21	9.85	44.93	10.88	0.09	11.42	16.96	0.78	0.09	0.33	96.54	1.33	0.00	0.58	0.09	Calcic amphibole	Magnesiohornblende
18MPe250	1.28	11.55	45.73	10.50	0.03	11.91	14.13	0.54	0.06	0.29	96.01	1.23	0.00	0.60	0.06	Calcic amphibole	Magnesiohornblende
18MPe250	1.84	14.62	45.44	13.37	0.15	10.05	9.90	0.84	0.18	0.13	96.53	1.59	0.00	0.63	0.09	Calcic amphibole	Tschermakite
18MPe250	1.88	15.30	45.36	12.84	0.09	10.02	9.14	1.07	0.14	0.14	95.97	1.59	0.00	0.55	0.11	Calcic amphibole	Tschermakite
18MPe250	1.29	12.65	45.85	9.15	0.61	11.57	14.04	1.05	0.02	0.35	96.56	1.25	0.00	0.34	0.12	Calcic amphibole	Magnesiohornblende
18MPe250	1.75	8.53	42.91	12.00	0.29	11.21	18.36	1.03	0.00	0.29	96.37	1.52	0.00	0.61	0.12	Calcic amphibole	Tschermakite
18MPe250	0.89	12.05	47.47	7.48	0.08	12.01	15.35	0.40	0.00	0.30	96.02	0.92	0.00	0.40	0.05	Calcic amphibole	Magnesiohornblende
18MPe250	1.17	9.83	44.30	12.37	0.35	11.84	15.57	0.72	0.03	0.26	96.44	1.41	0.00	0.76	0.08	Calcic amphibole	Magnesiohornblende
18MPe250	1.36	10.92	46.28	9.26	0.11	11.87	16.31	0.38	0.03	0.30	96.82	1.14	0.00	0.48	0.04	Calcic amphibole	Magnesiohornblende
18MPe250	2.33	12.14	43.53	9.30	0.61	10.48	14.71	2.49	0.00	0.21	95.80	1.49	0.00	0.15	0.28	Calcic amphibole	Magnesiohornblende
18MPe250	1.39	11.23	46.09	10.25	0.14	11.89	15.17	0.51	0.04	0.22	96.93	1.21	0.00	0.57	0.06	Calcic amphibole	Magnesiohornblende
18MPe250	1.54	9.47	43.96	11.82	0.27	11.39	17.41	0.68	0.03	0.30	96.87	1.46	0.00	0.62	0.08	Calcic amphibole	Magnesiohornblende
18MPe250	0.30	14.64	53.75	2.71	0.19	12.05	13.69	0.27	0.03	0.68	98.31	0.32	0.00	0.13	0.03	Calcic amphibole	Actinolite
18MPe250	0.84	11.56	46.69	10.81	0.44	11.74	13.86	0.39	0.04	0.52	96.90	1.18	0.00	0.68	0.04	Calcic amphibole	Magnesiohornblende
18MPe250	2.02	8.97	41.11	14.80	0.56	11.55	16.66	1.27	0.05	0.19	97.18	1.86	0.00	0.75	0.14	Calcic amphibole	Pargasite
18MPe250	1.26	10.61	45.83	9.77	0.06	11.86	16.13	0.71	0.00	0.24	96.47	1.18	0.00	0.53	0.08	Calcic amphibole	Magnesiohornblende
18MPe250	1.74	9.17	42.52	11.97	0.49	11.35	18.35	0.85	0.01	0.40	96.85	1.62	0.00	0.50	0.10	Calcic amphibole	Tschermakite
18MPe250	0.66	13.92	48.84	5.54	0.54	12.04	14.01	0.93	0.00	0.50	96.99	0.81	0.00	0.15	0.10	Calcic amphibole	Magnesiohornblende
18MPe250	1.34	11.48	44.96	9.00	0.82	11.52	15.68	1.11	0.04	0.34	96.28	1.28	0.00	0.31	0.13	Calcic amphibole	Magnesiohornblende
18MPe250	1.05	13.60	47.64	10.02	0.16	12.11	11.73	0.46	0.10	0.23	97.10	1.13	0.00	0.57	0.05	Calcic amphibole	Magnesiohornblende
18MPe250	1.97	12.34	44.16	12.35	0.08	11.96	12.95	1.25	0.06	0.21	97.34	1.56	0.00	0.57	0.14	Calcic amphibole	Tschermakite
18MPe250	1.59	10.05	43.91	12.34	0.24	11.47	15.97	0.70	0.04	0.29	96.60	1.48	0.00	0.68	0.08	Calcic amphibole	Magnesiohornblende
18MPe250	1.71	10.16	44.47	10.51	0.48	11.70	17.30	0.58	0.03	0.36	97.30	1.37	0.00	0.47	0.07	Calcic amphibole	Magnesiohornblende
18MPe250	1.23	9.59	43.37	12.35	0.40	11.48	16.51	0.72	0.02	0.30	95.97	1.51	0.00	0.67	0.08	Calcic amphibole	Tschermakite
18MPe250	1.77	15.94	45.21	12.66	0.13	10.80	9.18	0.68	0.11	0.17	96.65	1.47	0.00	0.68	0.07	Calcic amphibole	Edenite
18MPe250	1.75	15.28	46.13	12.04	0.12	9.65	10.50	0.83	0.06	0.27	96.63	1.29	0.00	0.77	0.09	Calcic amphibole	Edenite
18MPe250	1.83	8.37	42.03	12.21	0.67	10.92	19.25	0.79	0.07	0.30	96.44	1.64	0.00	0.54	0.09	Calcic amphibole	Tschermakite
18MPe250	1.21	13.28	46.99	9.78	0.09	11.63	12.46	0.59	0.05	0.24	96.33	1.17	0.00	0.51	0.06	Calcic amphibole	Magnesiohornblende

18MPe250	1.11	10.63	43.98	8.93	1.09	11.61	16.91	1.18	0.03	0.44	95.92	1.33	0.00	0.26	0.14	Calcic amphibole	Magnesiohornblende
18MPe250	1.47	10.61	45.03	11.26	0.15	11.43	15.65	0.63	0.04	0.26	96.53	1.34	0.00	0.62	0.07	Calcic amphibole	Magnesiohornblende
18MPe250	1.39	11.49	44.87	12.60	0.22	11.90	13.40	0.66	0.06	0.21	96.80	1.43	0.00	0.75	0.07	Calcic amphibole	Magnesiohornblende
18MPe250	1.93	13.45	46.33	11.51	0.13	11.44	11.68	0.39	0.10	0.18	97.13	1.33	0.00	0.63	0.04	Calcic amphibole	Magnesiohornblende
18MPe280	1.35	9.75	42.15	12.70	1.11	11.60	16.61	1.06	0.01	0.39	96.73	1.68	0.00	0.57	0.12	Calcic amphibole	Tschermakite
18MPe280	1.06	11.47	47.64	6.87	0.00	11.66	16.54	0.55	0.19	0.30	96.28	0.92	0.00	0.28	0.06	Calcic amphibole	Magnesiohornblende
18MPe280	1.37	11.61	46.25	10.09	0.15	11.74	14.43	0.49	0.04	0.30	96.46	1.18	0.00	0.57	0.06	Calcic amphibole	Magnesiohornblende
18MPe280	1.28	10.00	45.16	10.64	0.21	11.23	16.37	0.68	0.43	0.26	96.26	1.28	0.00	0.59	0.08	Calcic amphibole	Magnesiohornblende
18MPe280	1.32	12.68	47.29	11.59	0.15	11.60	11.32	0.74	0.07	0.19	96.95	1.18	0.00	0.79	0.08	Calcic amphibole	Magnesiohornblende
18MPe280	1.22	11.32	46.97	10.86	0.20	11.76	14.12	0.29	0.01	0.25	96.99	1.13	0.00	0.74	0.03	Calcic amphibole	Magnesiohornblende
18MPe280	2.24	13.35	45.07	12.88	0.20	11.34	11.07	0.50	0.07	0.22	96.95	1.49	0.00	0.70	0.05	Calcic amphibole	Magnesiohornblende
18MPe280	0.00	0.09	42.80	21.12	0.01	26.31	2.18	1.30	0.02	0.02	93.85	1.51	0.00	2.27	0.15	Calcic amphibole	Cannilloite
18MPe280	1.42	11.33	45.64	10.44	0.14	11.42	14.66	0.80	0.08	0.27	96.20	1.26	0.00	0.56	0.09	Calcic amphibole	Magnesiohornblende
18MPe280	2.14	12.26	42.81	14.23	0.09	11.67	11.81	1.48	0.13	0.15	96.78	1.75	0.00	0.70	0.16	Calcic amphibole	Tschermakite
18MPe280	0.90	10.68	47.50	7.43	0.00	11.59	17.53	0.74	0.00	0.29	96.66	0.95	0.00	0.35	0.08	Calcic amphibole	Magnesiohornblende
18MPe280	0.85	13.49	49.29	6.84	0.06	11.83	13.83	0.40	0.14	0.28	97.01	0.85	0.00	0.31	0.04	Calcic amphibole	Magnesiohornblende
18MPe280	1.43	15.45	49.57	8.04	0.10	12.06	8.93	0.36	0.06	0.13	96.13	0.84	0.00	0.53	0.04	Calcic amphibole	Magnesiohornblende
18MPe280	1.61	8.94	43.31	12.28	0.58	11.76	17.14	0.38	0.04	0.30	96.33	1.45	0.00	0.73	0.04	Calcic amphibole	Magnesiohornblende
18MPe280	2.34	13.90	46.07	12.16	0.09	11.00	10.25	0.74	0.15	0.24	96.94	1.39	0.00	0.67	0.08	Calcic amphibole	Magnesiohornblende
18MPe280	1.20	10.68	45.52	11.08	0.30	11.54	15.54	0.49	0.05	0.27	96.67	1.29	0.00	0.64	0.05	Calcic amphibole	Magnesiohornblende
18MPe280	1.09	11.82	47.82	9.05	0.08	11.89	14.56	0.43	0.02	0.29	97.04	1.00	0.00	0.56	0.05	Calcic amphibole	Magnesiohornblende
18MPe280	1.21	9.55	46.18	9.79	0.16	11.86	17.06	0.51	0.03	0.31	96.65	1.09	0.00	0.64	0.06	Calcic amphibole	Magnesiohornblende
18MPe280	0.21	15.31	53.94	2.37	0.00	12.31	11.67	0.60	0.00	0.20	96.61	0.20	0.00	0.20	0.07	Calcic amphibole	Actinolite
18MPe280	1.12	9.06	46.77	9.11	0.03	11.61	18.44	0.63	0.01	0.33	97.12	1.03	0.00	0.57	0.07	Calcic amphibole	Ferrohornblende
18MPe280	0.71	11.74	47.68	7.49	0.29	11.65	16.45	0.43	0.02	0.29	96.74	0.91	0.00	0.41	0.05	Calcic amphibole	Magnesiohornblende
18MPe280	0.37	15.57	53.60	2.90	0.08	12.52	11.59	0.13	0.49	0.19	97.45	0.31	0.00	0.18	0.01	Calcic amphibole	Actinolite
18MPe280	1.35	8.62	42.60	14.78	0.91	11.20	16.25	0.46	0.02	0.28	96.47	1.64	0.00	0.96	0.05	Calcic amphibole	Tschermakite
18MPe280	1.31	9.93	44.73	11.67	0.36	11.66	16.69	0.45	0.00	0.29	97.08	1.38	0.00	0.66	0.05	Calcic amphibole	Magnesiohornblende
18MPe280	1.10	14.41	48.21	8.30	0.42	11.53	11.56	0.45	0.01	0.42	96.42	1.02	0.00	0.39	0.05	Calcic amphibole	Magnesiohornblende
18MPe280	0.97	12.69	47.40	9.44	0.07	11.69	13.18	0.38	0.04	0.23	96.08	1.08	0.00	0.55	0.04	Calcic amphibole	Magnesiohornblende
18MPe280	1.38	14.98	48.70	9.13	0.15	11.93	9.66	0.28	0.06	0.15	96.42	0.99	0.00	0.56	0.03	Calcic amphibole	Magnesiohornblende
18MPe280	1.72	9.61	44.18	12.05	0.11	11.04	16.26	0.44	0.05	0.29	95.75	1.39	0.00	0.73	0.05	Calcic amphibole	Magnesiohornblende
18MPe280		0.59	11.44	0.03	12.80	0.22	12.30	11.75	1.22	0.08	98.47	1.12	0.00	0.57	0.04	Calcic amphibole	Magnesiohornblende
18MPe280	1.84	9.10	42.30	13.73	0.57	11.03	16.41	0.79	0.01	0.31	96.09	1.65	0.00	0.78	0.09	Calcic amphibole	Tschermakite
18MPe280	1.28	11.39	46.22	10.63	0.09	11.45	14.17	0.70	0.10	0.24	96.27	1.20	0.00	0.64	0.08	Calcic amphibole	Magnesiohornblende
18MPe280	1.03	11.77	47.62	8.64	0.32	11.27	15.43	0.85	0.03	0.27	97.23	1.06	0.00	0.43	0.09	Calcic amphibole	Magnesiohornblende
18MPe280	1.45	11.46	45.42	11.77	0.14	11.56	13.84	0.58	0.07	0.22	96.51	1.34	0.00	0.70	0.06	Calcic amphibole	Magnesiohornblende
18MPe280	1.51	11.93	46.19	11.49	0.17	11.93	12.48	0.53	0.06	0.22	96.51	1.22	0.00	0.77	0.06	Calcic amphibole	Magnesiohornblende
18MPe280	1.55	11.65	45.24	8.42	0.53	10.86	15.74	1.13	0.05	0.61	95.78	1.25	0.00	0.23	0.13	Calcic amphibole	Magnesiohornblende

18MPe280	0.92	13.51	48.43	8.10	0.61	11.87	12.40	0.43	0.02	0.26	96.56	0.93	0.00	0.46	0.05	Calcic amphibole	Magnesiohornblende
18MPe280	0.93	11.56	48.37	6.85	0.03	11.61	16.61	0.52	0.02	0.26	96.77	0.87	0.00	0.32	0.06	Calcic amphibole	Magnesiohornblende
18MPe280	0.68	14.64	50.28	6.01	0.06	11.30	12.83	0.65	0.05	0.31	96.82	0.67	0.00	0.37	0.07	Calcic amphibole	Magnesiohornblende
18MPe280	0.91	11.14	49.91	4.38	0.09	11.32	18.04	0.17	0.04	0.39	96.39	0.56	0.00	0.21	0.02	Calcic amphibole	Magnesiohornblende
18MPe280	1.19	15.13	49.19	5.96	0.20	9.32	14.21	0.80	0.01	0.51	96.52	0.74	0.00	0.29	0.09	Na-Ca-Mg-Fe-Mn-Li amphibole	Magnesiohornblende
18MPe280	1.31	14.60	49.07	6.26	0.32	10.19	14.11	0.79	0.02	0.44	97.10	0.78	0.00	0.31	0.09	Calcic amphibole	Magnesiohornblende
18MPe280	0.93	12.02	48.72	6.58	0.04	11.27	16.24	0.73	0.02	0.25	96.80	0.86	0.00	0.27	0.08	Calcic amphibole	Magnesiohornblende
18MPe280	0.97	10.37	47.34	7.96	0.06	11.51	17.38	0.83	0.00	0.31	96.72	0.98	0.00	0.42	0.09	Calcic amphibole	Magnesiohornblende
18MPe280	1.34	10.49	44.93	12.03	0.21	11.68	14.69	0.39	0.10	0.26	96.12	1.33	0.00	0.77	0.04	Calcic amphibole	Magnesiohornblende
18MPe280	1.42	11.04	44.82	12.98	0.06	11.13	14.26	0.40	0.10	0.27	96.48	1.46	0.00	0.77	0.04	Calcic amphibole	Magnesiohornblende
18MPe280	0.55	14.82	53.16	4.01	0.07	12.15	12.17	0.07	0.14	0.23	97.36	0.37	0.00	0.31	0.01	Calcic amphibole	Actinolite
18MPe280	2.16	11.36	43.71	14.66	0.15	10.41	12.90	0.50	0.03	0.22	96.11	1.64	0.00	0.88	0.06	Calcic amphibole	Tschermakite
18MPe280	1.22	14.18	47.11	8.20	0.08	11.46	12.11	1.86	0.02	0.26	96.49	1.17	0.00	0.23	0.20	Calcic amphibole	Magnesiohornblende
18MPe280	1.84	12.82	45.83	11.61	0.21	10.93	11.97	0.70	0.17	0.22	96.29	1.34	0.00	0.65	0.08	Calcic amphibole	Magnesiohornblende
18MPe280	1.69	12.68	43.89	13.99	0.14	11.91	10.74	0.66	0.04	0.23	95.97	1.59	0.00	0.82	0.07	Calcic amphibole	Tschermakite
18MPe280	1.10	10.80	44.67	8.08	1.05	11.70	16.47	1.10	0.02	0.74	95.72	1.21	0.00	0.24	0.13	Calcic amphibole	Magnesiohornblende
18MPe280	1.27	11.54	45.08	9.95	0.47	10.93	14.80	1.20	0.00	0.42	95.65	1.31	0.00	0.43	0.13	Calcic amphibole	Magnesiohornblende
18EPe900	1.75	15.89	51.01	6.62	0.07	11.17	10.08	0.30	0.21	0.22	97.32	0.75	0.00	0.36	0.03	Calcic amphibole	Magnesiohornblende
18EPe900	1.22	12.30	45.98	11.44	0.08	11.75	12.80	0.59	0.03	0.22	96.42	1.30	0.00	0.67	0.07	Calcic amphibole	Magnesiohornblende
18EPe900	1.17	12.20	46.20	11.56	0.10	11.91	12.73	0.53	0.05	0.26	96.71	1.28	0.00	0.71	0.06	Calcic amphibole	Magnesiohornblende
18EPe900	2.16	13.23	44.29	12.75	0.26	11.97	11.17	0.72	0.31	0.21	97.07	1.56	0.00	0.63	0.08	Calcic amphibole	Pargasite
18EPe900	1.25	11.78	45.55	8.91	0.91	11.90	15.24	0.95	0.01	0.44	96.94	1.23	0.00	0.33	0.11	Calcic amphibole	Magnesiohornblende
18EPe900	1.84	9.54	43.54	14.22	0.05	11.49	15.40	0.55	0.02	0.27	96.92	1.57	0.00	0.90	0.06	Calcic amphibole	Tschermakite
18EPe900	0.92	13.22	47.36	7.61	0.64	12.07	13.71	0.85	0.00	0.41	96.79	1.04	0.00	0.28	0.09	Calcic amphibole	Magnesiohornblende
18EPe900	1.37	10.65	46.35	9.62	0.13	11.94	15.73	0.54	0.05	0.31	96.70	1.11	0.00	0.58	0.06	Calcic amphibole	Magnesiohornblende
18EPe900	1.42	10.80	45.31	11.73	0.15	11.72	14.81	0.57	0.00	0.29	96.80	1.33	0.00	0.71	0.06	Calcic amphibole	Magnesiohornblende
18EPe900	1.67	10.55	44.31	12.73	0.05	11.49	14.50	0.51	0.12	0.28	96.22	1.45	0.00	0.77	0.06	Calcic amphibole	Magnesiohornblende
18EPe900	1.91	14.39	45.64	12.99	0.17	9.57	10.68	0.69	0.07	0.20	96.31	1.56	0.00	0.61	0.07	Sodic-calcic amphibole	Magnesiohornblende
18EPe900	1.11	11.56	47.48	9.38	0.09	11.95	14.55	0.46	0.07	0.32	96.97	1.03	0.00	0.59	0.05	Calcic amphibole	Magnesiohornblende
18EPe900	1.23	12.69	47.00	9.75	0.16	11.43	13.04	0.84	0.11	0.37	96.63	1.16	0.00	0.51	0.09	Calcic amphibole	Magnesiohornblende
18EPe900	1.59	10.83	45.19	11.41	0.15	11.64	14.64	0.56	0.05	0.26	96.31	1.30	0.00	0.69	0.06	Calcic amphibole	Magnesiohornblende
18EPe900	1.58	10.45	45.45	11.29	0.19	11.90	15.31	0.46	0.05	0.26	96.93	1.27	0.00	0.71	0.05	Calcic amphibole	Magnesiohornblende
18EPe900	1.36	10.47	45.54	10.73	0.13	11.86	15.71	0.44	0.00	0.26	96.50	1.23	0.00	0.65	0.05	Calcic amphibole	Magnesiohornblende
18EPe900	1.76	14.88	46.71	11.47	0.07	11.31	9.02	0.44	0.19	0.16	96.02	1.30	0.00	0.64	0.05	Calcic amphibole	Magnesiohornblende
18EPe900	1.32	10.43	44.72	12.39	0.26	11.72	14.54	0.39	0.00	0.21	95.99	1.36	0.00	0.81	0.04	Calcic amphibole	Magnesiohornblende
18EPe900	1.63	7.74	43.89	11.24	0.46	11.31	19.55	0.28	0.12	0.31	96.53	1.33	0.00	0.68	0.03	Calcic amphibole	Ferrohornblende
18EPe900	1.51	9.48	44.48	11.43	0.14	11.67	17.04	0.49	0.00	0.26	96.50	1.35	0.00	0.67	0.06	Calcic amphibole	Magnesiohornblende

18EPe900	1.31	12.58	45.06	11.12	0.29	10.05	14.37	0.78	0.22	0.40	96.19	1.30	0.00	0.66	0.09	Calcic amphibole	Magnesiohornblende
18EPe900	1.60	11.96	44.93	12.57	0.22	10.03	14.10	0.54	0.05	0.30	96.30	1.52	0.00	0.62	0.06	Calcic amphibole	Tschermakite
18EPe900	1.24	13.19	46.71	11.02	0.12	11.52	11.75	0.92	0.05	0.20	96.72	1.26	0.00	0.62	0.10	Calcic amphibole	Magnesiohornblende
18EPe900	1.33	13.93	46.43	12.77	0.08	12.17	9.89	0.14	0.00	0.19	96.94	1.35	0.00	0.80	0.02	Calcic amphibole	Magnesiohornblende
18EPe900	1.41	12.31	46.90	10.91	0.09	11.58	12.74	0.51	0.00	0.32	96.77	1.18	0.00	0.69	0.06	Calcic amphibole	Magnesiohornblende
18EPe900	1.22	8.95	44.67	10.57	0.59	10.78	17.95	1.25	0.03	0.40	96.41	1.31	0.00	0.56	0.14	Calcic amphibole	Magnesiohornblende
18EPe900	1.37	11.94	47.27	9.51	0.21	11.30	14.17	0.79	0.04	0.26	96.87	1.09	0.00	0.54	0.09	Calcic amphibole	Magnesiohornblende
18EPe900	1.22	12.86	45.53	10.72	0.33	11.91	12.10	0.47	0.90	0.24	96.29	1.33	0.00	0.52	0.05	Calcic amphibole	Magnesiohornblende
18EPe900	1.25	11.82	45.70	12.45	0.21	11.11	13.00	0.46	0.17	0.24	96.41	1.37	0.00	0.77	0.05	Calcic amphibole	Magnesiohornblende
18EPe900	1.21	13.65	47.52	10.32	0.15	11.98	11.07	0.42	0.03	0.26	96.61	1.13	0.00	0.64	0.05	Calcic amphibole	Magnesiohornblende
18EPe900	1.32	12.35	46.38	11.01	0.08	11.84	12.79	0.46	0.04	0.23	96.50	1.23	0.00	0.67	0.05	Calcic amphibole	Magnesiohornblende
18EPe900	1.32	11.04	45.59	11.63	0.07	11.60	14.14	0.68	0.05	0.25	96.37	1.29	0.00	0.73	0.08	Calcic amphibole	Magnesiohornblende
18EPe900	1.44	10.83	46.12	10.58	0.12	11.64	15.28	0.31	0.00	0.22	96.53	1.18	0.00	0.66	0.03	Calcic amphibole	Magnesiohornblende
18EPe900	1.85	10.27	44.06	10.48	0.12	11.35	17.34	0.64	0.02	0.28	96.41	1.41	0.00	0.43	0.07	Calcic amphibole	Magnesiohornblende
18EPe900	1.24	12.49	46.52	11.01	0.06	11.70	12.60	0.62	0.05	0.22	96.50	1.23	0.00	0.66	0.07	Calcic amphibole	Magnesiohornblende
18EPe900	0.81	14.90	49.61	7.49	0.53	11.67	10.60	0.27	0.18	0.24	96.29	0.84	0.00	0.44	0.03	Calcic amphibole	Magnesiohornblende
18EPe900	1.23	12.39	46.70	10.41	0.14	11.86	12.97	0.49	0.02	0.23	96.45	1.17	0.00	0.63	0.05	Calcic amphibole	Magnesiohornblende
18EPe900	1.35	11.61	46.09	10.16	0.07	11.84	14.72	0.46	0.03	0.21	96.55	1.21	0.00	0.56	0.05	Calcic amphibole	Magnesiohornblende
18EPe900	1.54	9.19	44.79	10.71	0.08	11.47	17.36	0.72	0.01	0.39	96.26	1.27	0.00	0.63	0.08	Calcic amphibole	Magnesiohornblende
18EPe900	1.19	13.95	48.49	7.50	0.30	11.67	13.11	0.45	0.02	0.27	96.95	0.97	0.00	0.31	0.05	Calcic amphibole	Magnesiohornblende
18EPe900	1.38	14.76	48.24	8.90	0.16	9.89	11.22	0.74	0.10	0.31	95.71	1.11	0.00	0.39	0.08	Calcic amphibole	Magnesiohornblende
18EPe900	1.45	8.91	43.39	14.78	0.12	10.92	15.85	0.43	0.02	0.31	96.18	1.59	0.00	0.99	0.05	Calcic amphibole	Tschermakite
18EPe900	1.58	11.13	45.73	10.59	0.07	11.75	14.77	0.80	0.08	0.30	96.80	1.25	0.00	0.59	0.09	Calcic amphibole	Magnesiohornblende
18EPe900	1.16	11.30	46.63	9.54	0.14	11.74	15.73	0.58	0.05	0.22	97.10	1.15	0.00	0.50	0.06	Calcic amphibole	Magnesiohornblende
18EPe900	1.07	11.51	46.83	9.22	0.16	12.28	15.09	0.36	0.06	0.21	96.79	1.08	0.00	0.53	0.04	Calcic amphibole	Magnesiohornblende
18EPe900	1.59	9.18	44.93	10.61	0.14	11.73	17.58	0.46	0.02	0.31	96.54	1.24	0.00	0.64	0.05	Calcic amphibole	Magnesiohornblende
18EPe900	1.60	13.73	45.74	14.13	0.13	10.71	9.23	0.30	0.21	0.17	95.96	1.47	0.00	0.90	0.03	Calcic amphibole	Magnesiohornblende
18EPe900	2.14	15.57	47.56	9.63	0.09	11.47	9.65	0.32	0.21	0.18	96.81	1.19	0.00	0.44	0.04	Calcic amphibole	Magnesiohornblende
18EPe900	1.34	11.74	45.98	11.69	0.14	11.85	13.22	0.42	0.07	0.23	96.68	1.28	0.00	0.74	0.05	Calcic amphibole	Magnesiohornblende
18EPe900	1.18	10.62	46.24	10.41	0.05	11.58	15.25	0.40	0.05	0.34	96.12	1.15	0.00	0.67	0.04	Calcic amphibole	Magnesiohornblende
18EPe900	0.85	13.43	49.59	6.95	0.22	11.95	12.35	0.10	0.58	0.28	96.29	0.75	0.00	0.45	0.01	Calcic amphibole	Magnesiohornblende
18EPe900	1.20	11.36	46.17	9.24	0.05	11.58	15.96	0.74	0.02	0.27	96.58	1.19	0.00	0.42	0.08	Calcic amphibole	Magnesiohornblende
18EPe900	1.97	12.85	44.82	13.46	0.11	10.38	11.15	0.67	0.06	0.16	95.63	1.52	0.00	0.78	0.07	Calcic amphibole	Tschermakite
18EPe900	1.23	11.64	46.08	10.64	0.08	11.42	13.98	0.49	0.05	0.27	95.87	1.22	0.00	0.63	0.05	Calcic amphibole	Magnesiohornblende
18EPe900	1.46	10.89	45.19	10.38	0.05	11.35	16.17	0.55	0.05	0.29	96.37	1.32	0.00	0.50	0.06	Calcic amphibole	Magnesiohornblende
18EPe939	1.18	11.27	45.72	9.87	0.19	11.83	15.84	0.41	0.00	0.32	96.63	1.24	0.00	0.48	0.05	Calcic amphibole	Magnesiohornblende
18EPe939	1.37	11.68	45.69	9.73	0.15	11.87	15.67	0.38	0.00	0.27	96.81	1.27	0.00	0.43	0.04	Calcic amphibole	Magnesiohornblende
18EPe939	1.18	10.94	45.13	11.78	0.27	11.86	14.86	0.31	0.00	0.25	96.59	1.35	0.00	0.70	0.04	Calcic amphibole	Magnesiohornblende
18EPe939	1.11	11.73	46.89	9.38	0.12	11.88	15.24	0.44	0.11	0.30	97.20	1.14	0.00	0.48	0.05	Calcic amphibole	Magnesiohornblende

18EPe939	2.05	14.56	43.59	14.18	0.23	11.99	9.17	1.03	0.07	0.13	97.00	1.75	0.00	0.65	0.11	Calcic amphibole	Tschermakite
18EPe939	1.02	12.30	48.16	8.44	0.08	11.93	14.41	0.29	0.06	0.26	96.95	0.96	0.00	0.49	0.03	Calcic amphibole	Magnesiohornblende
18EPe939	1.50	10.61	43.57	12.76	0.11	11.31	15.05	0.53	0.05	0.28	95.77	1.54	0.00	0.69	0.06	Calcic amphibole	Tschermakite
18EPe939	0.93	11.54	47.16	7.86	0.49	10.77	16.23	1.29	0.04	0.47	96.78	1.08	0.00	0.28	0.14	Calcic amphibole	Magnesiohornblende
18EPe939	0.48	12.29	51.11	4.01	0.29	11.77	16.20	0.23	0.01	0.62	97.01	0.49	0.00	0.21	0.03	Calcic amphibole	Actinolite
18EPe939	1.46	11.73	45.19	10.41	0.23	11.60	15.14	0.56	0.00	0.28	96.61	1.35	0.00	0.46	0.06	Calcic amphibole	Magnesiohornblende
18EPe939	1.63	10.84	43.78	12.20	0.62	11.00	15.08	0.82	0.04	0.28	96.28	1.52	0.00	0.61	0.09	Calcic amphibole	Tschermakite
18EPe939	0.74	14.81	49.61	7.73	0.06	12.00	12.05	0.30	0.00	0.25	97.56	0.86	0.00	0.46	0.03	Calcic amphibole	Magnesiohornblende
18EPe939	1.14	12.01	46.14	10.07	0.41	10.70	14.47	1.20	0.04	0.22	96.38	1.27	0.00	0.46	0.13	Calcic amphibole	Magnesiohornblende
18EPe939	1.85	13.10	43.80	12.92	0.12	12.00	12.40	0.77	0.01	0.18	97.15	1.65	0.00	0.56	0.08	Calcic amphibole	Tschermakite
18EPe939	1.31	10.12	43.85	11.24	0.80	11.50	16.88	0.82	0.09	0.27	96.88	1.46	0.00	0.51	0.09	Calcic amphibole	Magnesiohornblende
18EPe939	1.34	12.88	46.53	11.07	0.05	12.24	12.07	0.62	0.17	0.24	97.20	1.25	0.00	0.64	0.07	Calcic amphibole	Magnesiohornblende
18EPe939	0.17	17.75	55.34	1.31	0.00	12.26	10.18	0.00	0.00	0.33	97.34	0.12	0.00	0.11	0.00	Calcic amphibole	Actinolite
18EPe939	1.35	15.59	49.63	8.09	0.05	11.61	10.23	0.35	0.04	0.20	97.14	0.94	0.00	0.41	0.04	Calcic amphibole	Magnesiohornblende
18EPe939	1.13	11.24	45.54	9.15	0.26	11.12	16.56	1.69	0.01	0.23	96.93	1.30	0.00	0.28	0.19	Calcic amphibole	Magnesiohornblende
18EPe939	1.64	8.42	41.09	11.74	0.22	10.54	16.30	0.63	0.00	0.36	90.94	1.48	0.00	0.72	0.08	Calcic amphibole	Magnesiohornblende
18EPe939	1.30	9.64	45.63	9.80	0.11	11.74	18.30	0.53	0.04	0.31	97.40	1.22	0.00	0.49	0.06	Calcic amphibole	Magnesiohornblende
18EPe939	1.69	9.74	43.32	13.12	0.61	11.78	15.88	0.43	0.10	0.22	96.88	1.54	0.00	0.77	0.05	Calcic amphibole	Tschermakite
18EPe939	0.87	11.37	47.18	6.55	0.72	11.59	17.82	1.13	0.01	0.61	97.84	1.04	0.00	0.10	0.13	Calcic amphibole	Magnesiohornblende
18EPe939	1.49	11.42	45.99	10.66	0.14	11.47	14.64	0.69	0.04	0.27	96.80	1.25	0.00	0.59	0.08	Calcic amphibole	Magnesiohornblende
18EPe939	1.25	12.77	45.26	10.35	0.79	12.18	12.60	1.11	0.00	0.18	96.50	1.32	0.00	0.49	0.12	Calcic amphibole	Magnesiohornblende
18EPe939	1.42	8.38	41.84	11.17	1.46	11.64	19.62	1.42	0.01	0.51	97.47	1.63	0.00	0.37	0.16	Calcic amphibole	Hastingsite
18EPe939	0.50	14.57	51.24	5.07	0.20	12.46	12.48	0.18	0.02	0.26	96.98	0.58	0.00	0.29	0.02	Calcic amphibole	Magnesiohornblende
18EPe939	1.49	10.84	44.60	11.28	0.11	11.86	16.03	0.32	0.04	0.26	96.83	1.41	0.00	0.56	0.04	Calcic amphibole	Magnesiohornblende
18EPe939	1.25	9.63	44.22	10.80	0.42	11.72	17.38	0.98	0.00	0.29	96.69	1.38	0.00	0.53	0.11	Calcic amphibole	Magnesiohornblende
18EPe939	1.55	12.83	43.63	13.78	1.15	12.37	10.46	0.60	0.30	0.11	96.78	1.59	0.00	0.79	0.07	Calcic amphibole	Pargasite
18EPe939	1.20	11.08	44.21	10.18	0.79	11.06	16.08	1.36	0.07	0.44	96.47	1.44	0.00	0.34	0.15	Calcic amphibole	Magnesiohornblende
18EPe939	2.10	13.21	43.49	12.90	0.07	11.35	11.28	1.64	0.14	0.17	96.35	1.67	0.00	0.54	0.18	Calcic amphibole	Tschermakite
18EPe939	1.30	11.04	43.62	13.07	0.47	11.67	14.27	0.64	0.07	0.21	96.36	1.57	0.00	0.71	0.07	Calcic amphibole	Tschermakite
18EPe939	1.46	11.85	45.25	11.41	0.12	11.60	13.60	0.47	0.15	0.25	96.16	1.35	0.00	0.63	0.05	Calcic amphibole	Magnesiohornblende
18EPe939	1.22	13.63	47.65	8.83	0.08	11.90	12.33	0.31	0.44	0.26	96.64	1.08	0.00	0.43	0.03	Calcic amphibole	Magnesiohornblende
18EPe939	1.45	11.90	45.23	12.70	0.11	11.66	12.31	0.44	0.10	0.28	96.17	1.38	0.00	0.81	0.05	Calcic amphibole	Magnesiohornblende
18EPe939	0.83	13.38	47.43	8.12	0.22	11.66	13.29	1.97	0.00	0.34	97.24	1.14	0.00	0.25	0.21	Calcic amphibole	Magnesiohornblende
18EPe939	1.63	13.18	46.69	9.36	0.22	10.47	14.25	0.57	0.04	0.29	96.70	1.26	0.00	0.34	0.06	Calcic amphibole	Magnesiohornblende
18EPe939	1.43	12.16	44.48	13.78	0.01	11.85	12.12	0.73	0.07	0.18	96.81	1.56	0.00	0.80	0.08	Calcic amphibole	Tschermakite
18EPe939	1.37	9.60	43.97	11.29	0.17	11.39	17.79	0.49	0.04	0.25	96.36	1.44	0.00	0.55	0.06	Calcic amphibole	Magnesiohornblende
18EPe939	1.47	14.50	45.60	12.16	0.10	11.40	10.27	0.80	0.07	0.17	96.54	1.48	0.00	0.57	0.09	Calcic amphibole	Magnesiohornblende
18EPe939	1.42	13.46	46.51	11.70	0.07	11.96	12.08	0.11	0.02	0.20	97.53	1.34	0.00	0.64	0.01	Calcic amphibole	Magnesiohornblende
18EPe939	0.91	9.93	47.10	7.52	0.74	11.56	18.45	0.62	0.06	0.61	97.51	0.98	0.00	0.34	0.07	Calcic amphibole	Magnesiohornblende

18EPe939	1.46	10.66	43.94	14.43	0.05	11.06	13.99	0.45	0.05	0.27	96.36	1.59	0.00	0.89	0.05	Calcic amphibole	Tschermakite
18EPe939	1.42	14.35	47.17	10.38	0.14	10.80	10.37	0.35	0.27	0.24	95.49	1.20	0.00	0.57	0.04	Calcic amphibole	Magnesiohornblende
18EPe939	1.40	10.84	45.86	10.12	0.12	11.49	15.60	0.43	0.03	0.28	96.16	1.19	0.00	0.58	0.05	Calcic amphibole	Magnesiohornblende
18EPe939	1.51	10.32	44.28	13.13	0.27	11.19	14.48	0.43	0.08	0.15	95.84	1.44	0.00	0.85	0.05	Calcic amphibole	Magnesiohornblende
18EPe939	1.26	10.11	44.21	12.68	0.19	11.22	15.00	0.60	0.01	0.27	95.55	1.43	0.00	0.79	0.07	Calcic amphibole	Magnesiohornblende
18EPe939	1.81	8.73	43.07	10.01	0.17	11.03	19.25	1.03	0.00	0.40	95.50	1.42	0.00	0.38	0.12	Calcic amphibole	Magnesiohornblende
18EPe939	1.01	13.24	48.64	7.62	0.17	11.19	12.92	0.78	0.01	0.23	95.82	0.89	0.00	0.42	0.09	Calcic amphibole	Magnesiohornblende
18EPe939	0.61	16.20	51.28	5.42	0.28	12.09	10.35	0.37	0.06	0.19	96.84	0.67	0.00	0.24	0.04	Calcic amphibole	Magnesiohornblende
18EPe941	1.31	10.79	45.26	10.80	0.17	11.47	15.89	0.50	0.02	0.31	96.53	1.32	0.00	0.57	0.06	Calcic amphibole	Magnesiohornblende
18EPe941	1.41	11.08	45.34	10.58	0.14	11.35	15.91	0.50	0.01	0.30	96.62	1.32	0.00	0.51	0.06	Calcic amphibole	Magnesiohornblende
18EPe941	1.20	11.82	46.63	9.64	0.11	12.13	14.23	0.45	0.08	0.24	96.52	1.12	0.00	0.56	0.05	Calcic amphibole	Magnesiohornblende
18EPe941	0.93	13.51	47.39	9.30	0.08	12.16	12.72	0.45	0.08	0.27	96.88	1.08	0.00	0.52	0.05	Calcic amphibole	Magnesiohornblende
18EPe941	1.18	11.82	44.94	9.14	0.74	11.74	15.35	1.04	0.07	0.41	96.44	1.31	0.00	0.29	0.12	Calcic amphibole	Magnesiohornblende
18EPe941	1.33	13.15	46.43	11.06	0.09	11.82	12.13	0.63	0.00	0.22	96.85	1.28	0.00	0.60	0.07	Calcic amphibole	Magnesiohornblende
18EPe941	1.87	9.97	43.44	12.24	0.27	10.41	18.02	0.50	0.03	0.28	97.02	1.61	0.00	0.51	0.06	Calcic amphibole	Tschermakite
18EPe941	1.10	12.77	46.74	8.49	0.46	11.73	14.04	0.64	0.22	0.72	96.92	1.16	0.00	0.31	0.07	Calcic amphibole	Magnesiohornblende
18EPe941	2.26	13.31	44.13	12.16	0.05	10.75	11.96	1.48	0.17	0.24	96.50	1.61	0.00	0.47	0.16	Calcic amphibole	Tschermakite
18EPe941	1.73	11.55	44.42	12.21	0.16	10.52	14.76	0.31	0.02	0.29	95.97	1.50	0.00	0.60	0.03	Calcic amphibole	Tschermakite
18EPe941	1.62	11.15	44.35	11.38	0.34	11.66	15.31	0.46	0.10	0.28	96.65	1.44	0.00	0.55	0.05	Calcic amphibole	Magnesiohornblende
18EPe941	1.60	9.43	44.71	9.85	0.37	11.20	18.63	0.80	0.00	0.31	96.90	1.31	0.00	0.43	0.09	Calcic amphibole	Magnesiohornblende
18EPe941	0.86	11.13	48.25	7.00	0.45	11.59	16.69	0.64	0.01	0.60	97.21	0.88	0.00	0.34	0.07	Calcic amphibole	Magnesiohornblende
18EPe941	1.76	10.35	42.87	13.22	0.66	11.12	15.36	1.33	0.00	0.31	96.98	1.67	0.00	0.64	0.15	Calcic amphibole	Tschermakite
18EPe941	1.53	10.63	44.84	10.66	0.21	11.34	16.41	0.64	0.00	0.25	96.51	1.35	0.00	0.51	0.07	Calcic amphibole	Magnesiohornblende
18EPe941	1.34	12.26	46.45	10.15	0.23	11.43	14.04	0.56	0.01	0.27	96.73	1.22	0.00	0.52	0.06	Calcic amphibole	Magnesiohornblende
18EPe941	1.16	13.19	46.37	10.87	0.30	11.82	12.63	0.52	0.13	0.26	97.24	1.31	0.00	0.54	0.06	Calcic amphibole	Magnesiohornblende
18EPe941	1.33	12.21	46.12	9.72	0.12	11.97	14.94	0.31	0.03	0.27	97.02	1.25	0.00	0.43	0.03	Calcic amphibole	Magnesiohornblende
18EPe941	2.46	11.05	43.74	11.51	0.23	10.55	15.88	0.78	0.06	0.31	96.57	1.54	0.00	0.47	0.09	Calcic amphibole	Tschermakite
18EPe941	1.88	11.60	44.27	11.37	0.35	10.32	15.55	1.03	0.01	0.33	96.72	1.54	0.00	0.42	0.11	Calcic amphibole	Tschermakite
18EPe941	1.42	13.38	46.73	10.74	0.13	11.81	11.68	0.37	0.00	0.31	96.57	1.22	0.00	0.61	0.04	Calcic amphibole	Magnesiohornblende
18EPe941	0.63	17.43	53.31	4.17	0.02	12.23	8.99	0.10	0.02	0.31	97.21	0.47	0.00	0.22	0.01	Calcic amphibole	Actinolite
18EPe941	1.71	13.12	43.53	10.99	0.87	12.00	12.25	1.95	0.06	0.21	96.69	1.57	0.00	0.35	0.22	Calcic amphibole	Pargasite
18EPe941	1.33	9.88	44.03	11.58	0.36	11.46	16.75	1.13	0.00	0.29	96.82	1.46	0.00	0.57	0.13	Calcic amphibole	Magnesiohornblende
18EPe941	1.09	12.17	46.53	9.71	0.11	11.88	14.59	0.66	0.06	0.31	97.12	1.21	0.00	0.46	0.07	Calcic amphibole	Magnesiohornblende
18EPe941	1.12	8.23	43.33	12.50	1.05	11.44	17.95	0.55	0.00	0.61	96.77	1.47	0.00	0.75	0.06	Calcic amphibole	Ferrohornblende
18EPe941	1.10	12.35	46.54	9.91	0.12	11.90	13.95	0.42	0.04	0.26	96.59	1.19	0.00	0.52	0.05	Calcic amphibole	Magnesiohornblende
18EPe941	1.68	12.06	45.23	10.79	0.23	10.54	14.60	0.54	0.06	0.28	96.02	1.38	0.00	0.48	0.06	Calcic amphibole	Magnesiohornblende
18EPe941	1.21	11.05	46.09	10.88	0.07	11.84	14.57	0.27	0.00	0.29	96.29	1.19	0.00	0.70	0.03	Calcic amphibole	Magnesiohornblende
18EPe941	1.69	11.78	46.30	10.21	0.21	10.97	15.08	0.37	0.05	0.30	96.96	1.24	0.00	0.51	0.04	Calcic amphibole	Magnesiohornblende
18EPe941	0.90	13.59	48.60	6.72	0.24	11.55	14.24	1.01	0.05	0.39	97.28	0.87	0.00	0.30	0.11	Calcic amphibole	Magnesiohornblende

18EPe941	1.03	13.18	47.91	8.97	0.10	11.91	13.32	0.25	0.00	0.18	96.86	1.05	0.00	0.48	0.03	Calcic amphibole	Magnesiohornblende
18EPe941	1.66	11.04	43.87	12.72	0.19	11.10	14.57	0.74	0.07	0.20	96.15	1.54	0.00	0.67	0.08	Calcic amphibole	Tschermakite
18EPe941	1.41	11.08	43.53	11.10	0.51	11.41	16.13	0.57	0.00	0.31	96.05	1.44	0.00	0.53	0.07	Calcic amphibole	Edenite
18EPe941	1.50	11.55	45.03	9.99	0.30	11.34	15.85	0.75	0.00	0.26	96.57	1.35	0.00	0.39	0.08	Calcic amphibole	Magnesiohornblende
18EPe941	1.29	14.69	47.18	12.10	0.04	11.23	9.46	0.38	0.05	0.16	96.59	1.31	0.00	0.71	0.04	Calcic amphibole	Magnesiohornblende
18EPe941	1.16	13.62	47.35	9.69	0.16	12.07	11.96	0.38	0.06	0.23	96.66	1.13	0.00	0.53	0.04	Calcic amphibole	Magnesiohornblende
18EPe941	1.20	9.95	42.37	10.79	1.41	11.77	17.78	1.28	0.08	0.45	97.07	1.61	0.00	0.31	0.15	Calcic amphibole	Magnesiohastingsite
18EPe941	1.09	12.39	46.34	8.94	0.02	12.23	14.01	0.47	0.04	0.27	95.80	1.13	0.00	0.43	0.05	Calcic amphibole	Magnesiohornblende
18EPe941	1.14	12.59	46.66	9.95	0.09	12.08	13.81	0.50	0.09	0.26	97.16	1.21	0.00	0.49	0.05	Calcic amphibole	Magnesiohornblende
18EPe941	1.02	12.31	47.66	8.09	0.29	9.83	15.64	1.03	0.05	0.48	96.41	0.88	0.00	0.55	0.12	Calcic amphibole	Magnesiohornblende
18EPe941	0.64	15.36	51.61	5.27	0.10	12.41	11.23	0.23	0.06	0.23	97.14	0.59	0.00	0.30	0.03	Calcic amphibole	Magnesiohornblende
18EPe941	1.07	10.53	43.56	10.11	0.99	11.80	17.16	1.16	0.04	0.35	96.76	1.47	0.00	0.32	0.13	Calcic amphibole	Magnesiohornblende
18EPe941	0.97	12.98	46.51	7.38	0.70	11.86	14.81	0.98	0.02	0.41	96.63	1.13	0.00	0.15	0.11	Calcic amphibole	Magnesiohornblende
18EPe941	1.53	11.01	44.60	10.15	0.09	11.40	15.44	0.49	0.24	0.61	95.55	1.33	0.00	0.46	0.06	Calcic amphibole	Magnesiohornblende
18EPe941	1.98	12.78	44.81	11.74	0.13	10.64	13.61	0.53	0.03	0.31	96.55	1.51	0.00	0.49	0.06	Calcic amphibole	Tschermakite
18EPe941	1.65	10.69	44.71	10.19	0.24	10.38	17.32	1.04	0.00	0.42	96.64	1.42	0.00	0.35	0.12	Calcic amphibole	Magnesiohornblende
18EPe941	1.45	12.23	45.05	11.19	0.09	11.70	14.07	0.51	0.01	0.27	96.56	1.41	0.00	0.52	0.06	Calcic amphibole	Magnesiohornblende
18EPe941	1.90	12.79	44.42	13.71	0.13	10.64	12.15	0.71	0.07	0.27	96.78	1.63	0.00	0.69	0.08	Calcic amphibole	Tschermakite
18EPe941	1.17	10.15	45.31	9.42	0.40	11.05	17.85	0.64	0.02	0.49	96.51	1.26	0.00	0.39	0.07	Calcic amphibole	Magnesiohornblende
18EPe941	1.30	12.28	46.82	9.90	0.11	11.86	13.96	0.32	0.05	0.29	96.89	1.16	0.00	0.54	0.04	Calcic amphibole	Magnesiohornblende
18EPe941	1.45	11.58	45.03	11.02	0.29	11.71	14.70	0.61	0.06	0.30	96.75	1.37	0.00	0.54	0.07	Calcic amphibole	Magnesiohornblende
18EPe941	1.30	14.32	47.57	10.49	0.18	10.95	11.01	0.44	0.24	0.11	96.61	1.21	0.00	0.55	0.05	Calcic amphibole	Magnesiohornblende

8.1.2 Appendix D: Geochemical data of garnets from site U1417 and U1418 and of representative garnet profiles

GEOCHEMICAL DATA OF GARNETS FROM SITE U1417, DISTAL SITE

	Analysis (wt%)										Composition				
sample name	MgO	Na_2O	Al_2O_3	SiO2	CaO	MnO	FeO	TiO_2	Cr_2O_3	Total	Spessartine	Pyrope	Almandine	Grossular	Others
17Pe87	1.80	0.01	21.12	37.59	6.80	1.14	30.81	0.03	0.00	99.30	3%	7%	69%	20%	1%
17Pe87	1.58	0.00	21.11	37.80	8.86	5.48	24.48	0.08	0.00	99.39	12%	6%	55%	25%	1%
17Pe87	4.43	0.01	21.46	37.81	2.85	2.02	31.09	0.04	0.01	99.72	5%	18%	69%	8%	1%
17Pe87	3.18	0.00	21.05	37.32	1.76	1.17	34.55	0.05	0.03	99.11	3%	13%	78%	5%	1%
17Pe87	5.24	0.00	21.53	38.10	2.05	4.02	28.56	0.05	0.01	99.57	9%	21%	63%	6%	1%
17Pe87	3.17	0.03	21.17	37.71	6.81	1.42	28.40	0.00	0.04	98.75	3%	13%	64%	19%	1%
17Pe87	1.24	0.00	20.65	37.27	5.33	5.11	29.15	0.14	0.04	98.93	12%	5%	66%	15%	1%
17Pe87	3.99	0.02	21.10	37.62	2.79	1.39	31.52	0.02	0.03	98.48	3%	16%	71%	8%	2%
17Pe87	4.23	0.01	21.16	37.87	4.02	2.03	29.43	0.02	0.00	98.76	5%	17%	66%	11%	1%
17Pe87	2.75	0.04	20.79	37.32	0.72	10.19	27.72	0.21	0.00	99.74	23%	11%	63%	2%	1%
17Pe87	1.95	0.01	21.00	37.79	8.40	4.84	24.93	0.13	0.04	99.10	11%	8%	56%	24%	1%
17Pe87	2.27	0.00	21.13	38.33	13.52	3.30	20.76	0.07	0.14	99.51	7%	9%	46%	36%	2%
17Pe87	3.58	0.01	21.35	37.49	1.39	4.35	31.05	0.00	0.01	99.23	10%	14%	70%	4%	2%
17Pe87	4.21	0.00	21.36	37.84	2.50	1.15	32.03	0.03	0.00	99.13	3%	17%	72%	7%	2%
17Pe87	4.00	0.02	21.26	37.92	1.25	3.54	31.49	0.00	0.03	99.52	8%	16%	70%	3%	2%
17Pe87	1.79	0.02	20.92	37.23	1.55	10.74	27.89	0.03	0.00	100.16	25%	7%	63%	4%	1%
17Pe87	2.91	0.02	20.96	37.25	1.33	8.26	28.84	0.02	0.04	99.64	19%	12%	65%	4%	1%
17Pe87	1.35	0.04	20.82	37.38	4.30	0.18	34.59	0.07	0.00	98.73	0%	5%	79%	13%	3%
17Pe87	3.65	0.01	21.00	37.37	1.56	4.22	31.53	0.00	0.00	99.34	10%	15%	71%	4%	0%
17Pe87	4.44	0.01	21.55	38.29	4.67	1.32	29.29	0.03	0.02	99.62	3%	17%	65%	13%	2%
17Pe243	0.77	0.01	20.83	37.35	8.98	8.63	22.51	0.16	0.01	99.25	20%	3%	51%	26%	1%
17Pe243	2.47	0.04	21.05	37.15	1.98	10.23	26.14	0.05	0.06	99.17	23%	10%	59%	5%	2%
17Pe243	0.55	0.01	20.73	37.15	9.18	15.23	15.94	0.22	0.02	99.02	35%	2%	36%	26%	1%
17Pe243	3.59	0.03	20.91	37.16	2.19	3.76	30.99	0.01	0.03	98.66	9%	14%	70%	6%	1%

17Pe243	5.54	0.02	21.29	37.62	1.22	1.94	30.88	0.07	0.07	98.64	4%	22%	69%	3%	1%
17Pe243	2.42	0.03	20.94	37.04	2.80	9.56	26.21	0.03	0.04	99.07	22%	10%	59%	8%	1%
17Pe243	3.22	0.03	20.81	37.08	2.04	3.45	31.78	0.16	0.00	98.57	8%	13%	72%	6%	1%
17Pe243	3.20	0.01	21.12	37.35	2.07	7.02	28.39	0.00	0.02	99.18	16%	13%	64%	6%	1%
17Pe243	4.55	0.00	21.34	37.59	2.02	3.62	29.97	0.00	0.01	99.10	8%	18%	67%	6%	1%
17Pe243	2.78	0.01	20.90	37.24	2.07	7.07	29.04	0.17	0.00	99.28	16%	11%	66%	6%	1%
17Pe243	3.37	0.00	21.11	37.50	2.45	3.03	31.70	0.00	0.01	99.18	7%	14%	71%	7%	1%
17Pe243	3.78	0.00	21.11	37.53	1.74	3.49	31.79	0.00	0.01	99.45	8%	15%	71%	5%	1%
17Pe243	2.00	0.00	21.41	37.57	7.83	2.22	28.43	0.11	0.03	99.61	5%	8%	63%	22%	1%
17Pe243	2.88	0.02	21.00	37.51	3.00	3.01	32.03	0.07	0.00	99.52	7%	12%	72%	9%	1%
17Pe243	1.36	0.00	20.83	37.37	7.30	3.67	28.18	0.07	0.03	98.81	8%	5%	64%	21%	1%
17Pe243	3.48	0.00	21.30	37.41	2.75	2.54	31.53	0.09	0.00	99.11	6%	14%	71%	8%	2%
17Pe243	3.50	0.02	21.20	37.01	1.16	3.27	32.86	0.14	0.01	99.17	7%	14%	74%	3%	1%
17Pe243	3.65	0.03	21.04	37.36	2.80	2.17	31.92	0.01	0.00	98.98	5%	15%	72%	8%	1%
17Pe243	3.90	0.00	21.01	37.22	1.33	0.66	34.55	0.05	0.00	98.72	2%	16%	78%	4%	1%
17Pe243	3.76	0.02	21.15	37.26	1.23	4.49	30.99	0.03	0.00	98.94	10%	15%	70%	4%	1%
17Pe243	4.86	0.00	21.28	37.81	1.20	1.66	32.37	0.00	0.00	99.18	4%	19%	72%	3%	1%
17Pe243	2.44	0.01	21.11	37.57	4.74	7.63	25.80	0.03	0.02	99.35	17%	10%	58%	14%	1%
17Pe243	1.50	0.02	20.92	36.97	1.59	12.62	25.72	0.00	0.00	99.34	29%	6%	59%	5%	1%
17Pe243	2.66	0.03	21.00	37.21	2.01	6.71	29.41	0.00	0.02	99.05	15%	11%	67%	6%	1%
17Pe243	1.98	0.05	21.05	37.44	6.34	8.44	23.69	0.03	0.00	99.03	19%	8%	53%	18%	1%
17Pe243	3.12	0.00	21.17	37.57	3.66	3.86	29.93	0.01	0.01	99.33	9%	12%	67%	10%	1%
17Pe243	1.38	0.00	20.97	37.39	8.17	6.20	24.69	0.16	0.01	98.97	14%	6%	56%	24%	1%
17Pe243	0.25	0.02	20.71	37.25	11.26	18.98	10.85	0.16	0.03	99.51	43%	1%	23%	30%	2%
17Pe243	3.82	0.00	21.23	37.74	5.22	1.90	28.26	0.04	0.04	98.25	4%	15%	63%	15%	2%
17Pe243	3.14	0.01	21.07	37.25	1.87	2.61	33.03	0.03	0.02	99.03	6%	13%	75%	5%	1%
17Pe243	0.97	0.00	20.66	37.12	4.94	3.67	31.37	0.19	0.00	98.92	8%	4%	72%	14%	2%
17Pe243	5.37	0.00	21.20	37.84	1.29	2.36	30.72	0.04	0.03	98.85	5%	21%	69%	4%	1%
17Pe243	1.06	0.03	20.99	38.14	13.67	6.52	19.08	0.10	0.00	99.58	15%	4%	42%	37%	2%

17Pe243	2.94	0.00	21.26	37.34	1.17	9.31	27.71	0.01	0.00	99.74	21%	12%	62%	3%	1%
17Pe243	2.42	0.00	21.09	38.51	9.21	2.61	25.35	0.04	0.00	99.23	6%	10%	56%	26%	2%
17Pe243	6.20	0.00	21.51	38.41	1.21	0.90	30.83	0.02	0.01	99.10	2%	24%	68%	3%	2%
17Pe243	3.93	0.00	21.20	37.41	1.14	5.10	29.81	0.02	0.02	98.62	12%	16%	67%	3%	2%
17Mi400	3.00	0.00	21.01	37.44	1.54	8.52	28.41	0.00	0.01	99.93	19%	12%	64%	4%	0%
17Mi400	3.52	0.00	20.89	37.40	2.39	4.33	30.46	0.04	0.00	99.03	10%	14%	69%	7%	1%
17Mi400	1.53	0.01	21.47	38.04	10.55	3.36	24.85	0.11	0.01	99.92	8%	6%	55%	30%	1%
17Mi400	3.76	0.02	21.18	37.58	1.76	5.20	29.68	0.04	0.02	99.24	12%	15%	67%	5%	2%
17Mi400	4.12	0.02	21.52	38.14	5.90	1.70	28.25	0.03	0.02	99.70	4%	16%	62%	17%	1%
17Mi400	6.14	0.01	21.58	38.47	2.75	0.95	29.53	0.01	0.00	99.44	2%	24%	65%	8%	1%
17Mi400	10.21	0.03	22.14	39.22	1.64	0.72	25.62	0.01	0.00	99.59	2%	39%	55%	4%	0%
17Mi400	2.17	0.02	21.54	38.23	9.76	3.26	24.85	0.06	0.03	99.93	7%	9%	55%	27%	2%
17Mi400	5.32	0.01	21.75	38.34	4.99	1.31	27.64	0.11	0.00	99.47	3%	21%	61%	14%	2%
17Mi400	2.55	0.02	21.11	36.91	2.20	5.46	30.72	0.01	0.03	99.01	13%	10%	70%	6%	1%
17Mi400	4.89	0.00	21.88	38.55	6.51	1.17	26.98	0.00	0.00	99.98	3%	19%	59%	18%	1%
17Mi400	2.77	0.03	21.05	37.50	1.75	13.16	23.74	0.00	0.01	100.01	30%	11%	53%	5%	1%
17Mi400	2.87	0.00	20.97	37.51	1.84	13.49	23.58	0.03	0.02	100.31	31%	11%	53%	4%	1%
17Mi400	5.04	0.00	21.37	37.97	1.85	0.81	31.95	0.01	0.00	99.00	2%	20%	71%	5%	2%
17Mi400	6.36	0.02	21.42	38.24	5.30	0.89	26.53	0.04	0.05	98.85	2%	25%	58%	14%	1%
17Mi400	2.98	0.00	21.39	38.08	8.64	1.50	26.70	0.02	0.00	99.31	3%	12%	59%	25%	1%
17Mi400	3.06	0.02	20.95	37.21	2.21	4.35	31.18	0.03	0.01	99.03	10%	12%	70%	6%	1%
17Mi400	3.60	0.00	21.21	37.33	2.05	7.01	28.11	0.02	0.00	99.33	16%	14%	63%	6%	1%
17Mi400	3.66	0.02	20.99	37.21	1.19	3.95	31.70	0.01	0.08	98.81	9%	15%	72%	3%	1%
17Mi400	1.10	0.02	20.41	36.39	0.17	7.80	32.85	0.00	0.00	98.74	18%	5%	76%	1%	1%
17Mi400	4.18	0.03	21.14	37.62	4.77	1.93	29.02	0.23	0.00	98.93	4%	17%	65%	14%	1%
17Mi400	4.27	0.01	21.43	37.69	5.59	0.48	29.10	0.06	0.00	98.63	1%	17%	65%	16%	1%
17Mi400	4.22	0.02	21.15	37.59	1.85	6.21	28.03	0.01	0.00	99.08	14%	17%	63%	5%	1%
17Mi400	3.70	0.01	21.10	37.45	2.12	3.24	31.08	0.04	0.01	98.74	7%	15%	70%	6%	2%
17Mi400	2.47	0.01	21.12	37.13	1.71	11.50	25.39	0.00	0.00	99.33	26%	10%	57%	5%	1%

17Mi400	3.38	0.04	21.09	37.50	2.81	6.20	27.83	0.04	0.04	98.93	14%	14%	63%	8%	2%
17Mi400	3.51	0.01	21.14	37.67	1.97	4.28	30.46	0.00	0.02	99.06	10%	14%	69%	6%	2%
17Mi400	3.55	0.03	21.16	37.38	1.37	5.72	29.92	0.12	0.00	99.26	13%	14%	67%	4%	2%
17Mi400	2.89	0.00	21.12	37.69	5.75	2.99	28.25	0.12	0.01	98.81	7%	12%	63%	17%	2%
17Mi400	3.25	0.04	20.96	37.82	4.79	3.69	28.83	0.25	0.01	99.65	8%	13%	64%	13%	1%
17Mi400	5.69	0.00	21.37	38.07	1.93	1.17	30.38	0.03	0.07	98.70	3%	23%	68%	5%	2%
17Mi400	2.57	0.00	20.99	37.10	1.26	6.84	30.08	0.05	0.01	98.89	16%	10%	68%	4%	2%
17Mi400	1.36	0.02	21.26	38.31	15.05	2.74	20.41	0.08	0.02	99.26	6%	5%	45%	42%	1%
17Mi400	3.95	0.00	21.14	37.30	2.10	6.70	28.08	0.03	0.04	99.34	15%	16%	63%	6%	0%
17Mi400	1.52	0.03	20.91	37.49	9.09	0.59	29.46	0.10	0.01	99.20	1%	6%	66%	26%	1%
17Mi400	2.87	0.01	21.22	37.68	3.01	4.41	30.51	0.07	0.01	99.80	10%	11%	68%	9%	2%
17Mi400	3.57	0.02	20.84	37.31	1.19	4.02	31.49	0.02	0.03	98.50	9%	14%	71%	3%	2%
17Mi400	3.27	0.00	21.08	37.41	4.43	2.91	29.67	0.01	0.03	98.81	7%	13%	67%	13%	1%
17Mi400	1.39	0.03	20.83	36.77	0.51	13.63	26.32	0.03	0.00	99.51	32%	6%	60%	1%	1%
17Mi400	0.29	0.02	20.88	37.36	9.72	17.73	13.52	0.19	0.01	99.71	40%	1%	30%	27%	1%
17Mi400	2.37	0.03	20.93	36.85	1.37	9.34	28.55	0.01	0.00	99.45	21%	10%	65%	4%	0%
17Mi400	1.61	0.04	21.06	37.91	15.04	1.53	21.33	0.40	0.01	98.93	3%	6%	47%	42%	1%
17Mi400	4.92	0.02	21.22	37.98	1.59	1.29	32.06	0.00	0.03	99.11	3%	20%	72%	4%	2%
17Mi400	1.91	0.04	20.85	36.96	1.52	2.62	35.28	0.02	0.00	99.20	6%	8%	80%	4%	1%
17Mi400	3.94	0.01	21.12	37.66	3.09	2.63	30.48	0.13	0.01	99.08	6%	16%	68%	9%	1%
17Mi400	1.66	0.01	21.23	37.73	8.68	0.94	28.99	0.10	0.03	99.37	2%	7%	65%	25%	2%
17Mi400	2.96	0.05	20.96	37.29	3.70	4.96	28.84	0.21	0.02	98.98	11%	12%	65%	11%	1%
17Mi400	2.72	0.04	21.18	37.96	8.02	0.99	28.54	0.06	0.00	99.51	2%	11%	63%	23%	1%
17Mi603	4.58	not measured	21.14	37.10	1.27	1.98	34.01	0.00	0.01	100.09	4%	18%	72%	2%	3%
17Mi603	7.85	not measured	21.67	38.42	5.19	0.75	26.20	0.05	0.00	100.13	2%	30%	53%	12%	4%
17Mi603	3.11	not measured	20.75	36.75	3.28	7.40	27.87	0.05	0.06	99.27	17%	12%	59%	9%	2%
17Mi603	3.66	not measured	21.02	37.06	1.98	5.82	30.53	0.04	0.00	100.11	13%	15%	66%	4%	2%
17Mi603	3.74	not measured	20.96	37.00	1.43	4.64	32.35	0.01	0.01	100.14	11%	15%	69%	2%	3%
17Mi603	3.69	not measured	20.98	37.02	1.20	2.68	33.90	0.00	0.00	99.48	6%	15%	75%	3%	1%

17Mi603	3.35	not measured	20.92	36.81	1.77	6.69	30.03	0.03	0.00	99.60	15%	13%	65%	4%	2%
17Mi603	6.59	not measured	21.49	37.77	2.06	1.77	30.78	0.03	0.01	100.50	4%	26%	63%	4%	4%
17Mi603	1.11	not measured	20.79	37.28	11.38	9.17	19.97	0.16	0.02	99.88	21%	4%	42%	30%	3%
17Mi603	2.58	not measured	20.86	37.18	3.67	9.84	26.00	0.03	0.00	100.16	22%	10%	56%	9%	2%
17Mi603	3.43	not measured	20.82	36.85	1.30	6.46	31.02	0.00	0.04	99.93	15%	14%	67%	2%	3%
17Mi603	3.61	not measured	20.95	37.17	3.78	11.21	23.21	0.06	0.03	100.02	25%	14%	49%	9%	3%
17Mi603	3.61	not measured	20.87	37.19	2.14	4.01	32.41	0.00	0.03	100.25	9%	14%	70%	4%	3%
17Mi603	6.56	not measured	21.47	37.25	1.45	1.89	30.78	0.00	0.06	99.46	4%	26%	64%	3%	3%
17Mi603	0.83	not measured	20.76	37.48	15.16	7.02	18.30	0.13	0.00	99.68	16%	3%	37%	39%	4%
17Mi603	3.70	not measured	20.72	36.82	1.41	4.01	32.72	0.05	0.02	99.45	9%	15%	71%	2%	3%
17Mi603	3.52	not measured	20.84	36.78	2.06	5.94	30.84	0.09	0.02	100.09	13%	14%	65%	3%	4%
17Mi603	3.87	not measured	20.95	36.99	1.89	5.26	31.20	0.06	0.00	100.22	12%	15%	66%	3%	3%
17Mi603	6.71	not measured	21.53	37.66	2.17	0.28	31.17	0.10	0.02	99.64	1%	26%	66%	5%	2%
17Mi603	1.87	not measured	20.65	36.65	2.30	1.71	37.18	0.03	0.01	100.40	4%	8%	81%	5%	3%
17Mi603	3.99	not measured	21.14	37.03	1.47	5.01	31.53	0.00	0.05	100.22	11%	16%	67%	3%	3%
17Mi603	1.91	not measured	20.91	36.74	1.70	10.72	28.16	0.05	0.00	100.19	25%	8%	62%	4%	1%
17Mi603	4.32	not measured	21.13	37.39	1.31	6.38	29.79	0.02	0.03	100.37	14%	17%	64%	2%	2%
17Mi603	4.83	not measured	21.00	37.24	1.42	3.42	32.22	0.02	0.02	100.17	8%	19%	68%	2%	3%
17Mi603	3.58	not measured	20.80	36.90	1.55	9.43	28.00	0.07	0.03	100.35	21%	14%	59%	2%	4%
17Mi603	1.40	not measured	21.03	37.13	8.67	0.91	30.79	0.07	0.01	100.01	2%	6%	67%	23%	2%
17Mi603	5.93	not measured	21.28	37.12	1.10	2.04	32.24	0.01	0.04	99.75	5%	23%	67%	2%	4%
17Mi603	5.20	not measured	21.50	38.27	9.37	0.44	25.12	0.12	0.00	100.03	19%	12%	63%	3%	2%
17Mi603	3.66	not measured	21.07	37.12	1.12	4.48	32.61	0.00	0.00	100.06	10%	15%	71%	3%	1%
17Mi603	2.69	not measured	20.79	36.89	1.27	11.11	28.03	0.04	0.01	100.83	25%	11%	59%	1%	4%
17Mi603	4.05	not measured	21.01	37.04	1.83	4.37	31.86	0.00	0.01	100.17	10%	16%	67%	3%	3%
17Mi603	5.04	not measured	21.32	37.22	1.31	4.08	31.47	0.01	0.01	100.46	9%	20%	66%	2%	3%
17Mi603	2.55	not measured	20.59	37.03	4.90	9.30	25.22	0.12	0.03	99.75	21%	10%	54%	11%	3%
17Mi603	4.66	not measured	21.03	37.11	1.17	1.98	34.04	0.02	0.01	100.01	4%	18%	72%	2%	3%
17Mi603	3.43	not measured	21.55	37.81	11.69	0.50	25.04	0.09	0.02	100.14	1%	13%	52%	31%	3%

17Mi603	4.41	not measured	20.94	37.04	1.74	4.04	31.93	0.04	0.00	100.14	9%	17%	67%	3%	4%
17Mi603	1.78	not measured	20.48	36.31	0.83	1.42	38.68	0.04	0.00	99.54	3%	7%	86%	1%	2%
17Mi603	3.23	not measured	20.82	36.79	1.44	9.59	28.10	0.03	0.07	100.07	22%	13%	60%	2%	3%
17Mi603	0.87	not measured	20.27	36.72	5.66	12.27	24.12	0.16	0.00	100.08	28%	4%	52%	13%	4%
17Mi603	2.56	not measured	20.69	36.67	4.13	3.84	31.90	0.27	0.00	100.06	9%	10%	68%	9%	2%
17Mi603	1.05	not measured	20.28	35.94	0.67	0.67	41.07	0.02	0.00	99.70	2%	4%	91%	0%	1%
17Mi603	1.07	not measured	20.31	35.98	0.70	0.65	40.50	0.08	0.02	99.31	2%	4%	91%	0%	1%
17Mi603	8.07	not measured	21.55	38.21	2.07	0.93	28.80	0.03	0.00	99.67	2%	31%	60%	4%	1%
17Mi603	8.12	not measured	21.48	38.26	2.14	1.00	29.04	0.01	0.00	100.05	2%	31%	60%	4%	1%
17Mi603	1.98	not measured	20.72	36.81	6.91	5.47	27.92	0.01	0.00	99.82	12%	8%	58%	17%	1%
17Mi603	2.12	not measured	20.78	37.01	5.92	5.88	28.56	0.01	0.00	100.28	13%	8%	60%	14%	1%
17Mi603	2.46	not measured	21.13	37.08	7.04	0.09	32.28	0.05	0.01	100.13	0%	10%	69%	19%	1%
17Mi603	2.23	not measured	20.78	36.93	8.29	2.01	28.74	0.44	0.00	99.42	5%	9%	62%	21%	2%
17Mi603	3.62	not measured	20.90	36.79	0.74	1.12	36.67	0.01	0.00	99.85	3%	15%	80%	1%	1%
17Mi603	3.68	not measured	20.93	37.01	0.76	1.28	36.58	0.02	0.00	100.25	3%	15%	79%	1%	1%
17Mi603	1.15	not measured	20.71	36.76	9.17	2.88	28.60	0.13	0.01	99.41	7%	5%	62%	24%	1%
17Mi603	1.17	not measured	20.69	37.04	9.30	3.00	28.86	0.19	0.00	100.26	7%	5%	61%	23%	1%
17Mi603	5.55	not measured	20.86	37.01	1.60	1.91	31.70	0.04	0.03	98.70	4%	22%	68%	3%	1%
17Mi603	5.60	not measured	21.28	37.38	1.55	2.03	32.46	0.00	0.03	100.33	5%	22%	67%	3%	2%
17Mi603	0.50	not measured	19.96	35.97	3.18	18.43	20.85	0.05	0.00	98.94	43%	2%	45%	6%	1%
17Mi603	0.44	not measured	20.13	36.32	3.45	19.34	20.08	0.06	0.02	99.85	45%	2%	43%	7%	1%
17Mi603	8.98	not measured	21.91	38.45	3.17	0.49	27.04	0.05	0.09	100.17	1%	34%	54%	7%	2%
17Mi603	9.06	not measured	21.73	37.61	3.25	0.56	26.77	0.02	0.03	99.03	1%	35%	52%	7%	3%
17Mi603	3.34	not measured	20.75	36.92	4.58	4.77	29.60	0.02	0.03	100.01	11%	13%	61%	10%	2%
17Mi603	3.37	not measured	21.14	37.35	4.55	4.20	29.56	0.01	0.00	100.18	6%	15%	72%	5%	1%
17Mi603	3.79	not measured	21.07	37.08	2.10	2.77	33.26	0.00	0.00	100.08	4%	6%	45%	40%	2%
17Mi603	1.48	not measured	20.82	37.57	16.00	2.67	20.67	0.32	0.03	99.56	6%	6%	43%	41%	1%
17Mi603	0.41	not measured	19.96	36.57	8.48	14.28	19.61	0.37	0.04	99.72	33%	2%	41%	19%	2%
17Mi603	1.14	not measured	20.82	37.20	12.49	7.34	20.66	0.00	0.06	99.71	17%	5%	42%	33%	1%

17Mi603	1.58	not measured	20.92	37.00	7.56	8.68	23.99	0.00	0.00	99.73	20%	6%	51%	20%	1%
17Mi603	0.04	not measured	18.30	38.90	35.56	0.47	6.30	0.13	0.02	99.72	1%	0%	1%	79%	1%
17Mi603	0.05	not measured	15.20	37.92	34.63	0.63	9.85	0.60	0.00	98.87	1%	0%	2%	65%	2%
17Mi603	1.15	not measured	19.62	36.24	1.41	19.48	21.76	0.13	0.00	99.79	45%	5%	44%	0%	0%
17Mi603	1.15	not measured	19.41	36.22	1.54	19.62	21.72	0.25	0.00	99.91	45%	5%	42%	0%	0%
17Mi603	3.18	not measured	20.83	37.25	9.97	0.52	27.99	0.17	0.01	99.92	1%	12%	57%	24%	2%
17Mi603	5.44	not measured	21.12	37.24	1.71	2.07	31.96	0.01	0.03	99.57	5%	22%	68%	3%	1%
17Mi603	1.07	not measured	20.85	37.23	9.86	1.66	29.07	0.08	0.00	99.82	4%	4%	63%	26%	1%
17Mi603	0.67	not measured	20.65	37.08	10.93	5.15	24.91	0.05	0.00	99.44	12%	3%	54%	29%	1%
17Mi603	1.19	not measured	20.86	36.99	10.26	3.54	26.30	0.12	0.01	99.28	8%	5%	57%	28%	1%
17Mi603	1.33	not measured	20.99	37.18	10.35	2.75	27.28	0.13	0.00	100.01	6%	5%	58%	27%	1%
17Mi603	1.64	not measured	20.88	37.71	14.26	1.40	23.69	0.43	0.00	100.01	3%	6%	50%	36%	1%
17Mi603	2.01	not measured	20.08	37.29	14.06	1.76	23.09	1.24	0.06	99.59	4%	8%	48%	32%	6%
17Mi603	9.46	not measured	21.79	39.21	6.18	0.73	23.05	0.10	0.02	100.54	2%	36%	45%	13%	1%
17Mi603	9.60	not measured	21.60	38.73	6.19	0.72	23.14	0.03	0.00	100.01	2%	36%	44%	13%	2%
17Mi603	1.84	not measured	20.81	37.35	12.53	5.47	21.00	0.51	0.04	99.54	12%	7%	45%	32%	2%
17Mi603	1.92	not measured	20.87	37.44	11.99	5.33	21.50	0.53	0.00	99.58	12%	8%	46%	31%	2%
17Mi603	2.55	not measured	21.08	37.81	10.06	1.45	27.32	0.06	0.01	100.34	3%	10%	58%	26%	1%
17Mi603	2.53	not measured	21.17	37.72	10.14	1.39	27.58	0.04	0.00	100.57	3%	10%	58%	26%	1%
17Mi603	8.87	not measured	21.99	38.86	3.24	0.58	26.83	0.04	0.01	100.42	1%	34%	55%	8%	1%
17Mi603	9.06	not measured	21.79	38.79	3.27	0.45	27.15	0.01	0.00	100.52	1%	34%	55%	7%	1%
17Mi603	4.41	not measured	21.22	37.65	3.12	5.95	27.69	0.08	0.02	100.15	13%	17%	60%	8%	1%
17Mi603	4.57	not measured	21.20	37.22	3.14	5.63	28.15	0.07	0.01	100.00	13%	18%	59%	7%	2%
17Mi603	4.33	not measured	21.24	37.23	2.87	3.84	30.52	0.02	0.02	100.07	9%	17%	65%	7%	1%
17Mi603	4.17	not measured	21.16	37.07	2.92	3.96	30.22	0.00	0.00	99.50	9%	17%	65%	8%	1%
17Mi603	4.29	not measured	21.14	37.13	2.12	6.95	28.34	0.00	0.03	100.00	16%	17%	60%	5%	1%
17Mi603	4.33	not measured	21.16	37.21	2.22	6.52	28.62	0.04	0.00	100.10	15%	17%	61%	5%	1%
17Mi603	4.92	not measured	21.23	37.20	1.55	1.14	33.86	0.04	0.05	100.00	3%	19%	72%	3%	2%
17Mi603	4.81	not measured	21.28	37.46	1.32	1.16	34.60	0.03	0.03	100.68	3%	19%	74%	2%	1%

17Mi603	3.65	not measured	21.27	37.79	4.93	1.63	31.53	0.02	0.02	100.84	4%	14%	68%	12%	1%
17Mi603	3.70	not measured	21.38	37.50	5.02	1.73	31.42	0.04	0.03	100.82	4%	15%	66%	13%	2%
17Mi603	2.83	not measured	20.96	36.66	0.96	4.21	34.39	0.02	0.03	100.06	10%	11%	75%	2%	1%
17Mi642	2.94	0.04	21.21	37.06	1.72	5.95	30.19	0.04	0.03	99.17	19%	11%	58%	10%	1%
17Mi642	3.10	0.00	20.94	37.30	1.24	6.71	30.38	0.02	0.04	99.72	14%	12%	68%	5%	1%
17Mi642	4.06	0.00	21.11	37.43	1.95	3.95	30.91	0.00	0.03	99.45	15%	12%	68%	3%	0%
17Mi642	4.10	0.00	21.35	37.77	1.47	3.56	31.17	0.03	0.03	99.48	9%	16%	69%	5%	0%
17Mi642	5.56	0.02	21.32	37.84	1.14	2.07	30.96	0.01	0.01	98.93	8%	16%	70%	4%	2%
17Mi642	2.94	0.02	21.18	36.95	2.27	5.89	29.77	0.04	0.01	99.07	5%	22%	69%	3%	1%
17Mi642	3.81	0.01	20.89	37.45	1.93	4.73	29.89	0.04	0.02	98.76	13%	12%	67%	6%	1%
17Mi642	4.69	0.00	21.11	37.46	1.33	2.87	31.64	0.00	0.02	99.12	11%	15%	67%	6%	1%
17Mi642	3.62	0.03	21.12	37.26	0.79	4.07	32.08	0.04	0.00	99.01	7%	19%	71%	4%	0%
17Mi642	3.34	0.02	20.99	37.06	1.94	4.56	30.88	0.04	0.04	98.86	9%	15%	72%	2%	1%
17Mi642	2.73	0.00	21.01	37.05	1.39	9.08	28.07	0.05	0.00	99.38	10%	13%	70%	5%	1%
17Mi642	3.77	0.00	21.14	37.42	1.29	3.67	31.92	0.09	0.02	99.31	21%	11%	64%	4%	1%
17Mi642	3.66	0.02	21.17	37.44	1.52	4.03	31.33	0.02	0.01	99.20	8%	15%	72%	4%	1%
17Mi642	3.46	0.01	21.13	37.34	1.44	4.89	30.65	0.04	0.01	98.98	9%	15%	70%	4%	1%
17Mi642	2.90	0.02	21.06	37.42	1.40	5.77	30.41	0.06	0.03	99.07	11%	14%	69%	4%	2%
17Mi642	4.72	0.00	21.33	37.61	1.52	3.81	30.21	0.00	0.08	99.28	9%	19%	67%	4%	1%
17Mi642	3.78	0.01	21.17	37.41	1.02	3.58	32.19	0.00	0.01	99.17	8%	15%	72%	3%	1%
17Mi642	3.04	0.02	20.86	37.25	1.22	5.46	30.97	0.05	0.00	98.86	13%	12%	70%	3%	1%
17Mi642	4.66	0.00	21.16	37.60	1.73	1.52	32.37	0.05	0.00	99.09	3%	19%	72%	5%	1%
17Mi642	4.81	0.02	21.39	37.53	1.22	3.56	30.78	0.03	0.03	99.37	8%	19%	69%	3%	1%
17Mi642	3.35	0.00	21.03	37.42	1.26	6.16	30.10	0.00	0.03	99.36	14%	13%	68%	4%	1%
17Mi642	3.76	0.02	21.11	37.31	1.16	6.74	29.29	0.02	0.02	99.43	15%	15%	66%	3%	1%
17Mi642	3.51	0.02	21.10	37.49	1.71	4.73	30.62	0.05	0.00	99.23	11%	14%	69%	5%	1%
17Mi642	3.62	0.02	21.14	37.10	1.14	7.01	29.11	0.00	0.00	99.15	16%	15%	66%	3%	1%
17Mi642	3.11	0.01	21.11	37.20	3.05	8.03	26.73	0.00	0.04	99.28	18%	12%	60%	9%	0%
17Mi642	3.93	0.03	21.19	37.48	1.16	4.33	31.05	0.00	0.02	99.19	10%	16%	70%	3%	1%

17Mi642	2.68	0.01	20.88	37.06	2.05	6.54	29.95	0.05	0.00	99.22	15%	11%	68%	6%	0%
17Mi642	4.44	0.01	21.30	37.48	1.04	4.04	31.31	0.00	0.00	99.62	9%	18%	70%	3%	0%
17Mi642	2.70	0.02	20.79	37.27	1.57	11.28	26.13	0.01	0.02	99.80	26%	10%	59%	4%	1%
17Mi642	5.15	0.02	21.32	38.09	3.30	3.21	27.75	0.01	0.13	98.98	7%	20%	62%	9%	2%
17Mi642	3.80	0.04	21.06	37.49	1.96	3.38	31.32	0.07	0.01	99.13	8%	15%	70%	6%	1%
17Mi642	3.02	0.02	21.07	37.34	0.99	5.94	31.17	0.03	0.00	99.58	14%	12%	70%	3%	1%
17Mi642	3.57	0.03	21.18	37.72	1.64	4.61	30.53	0.00	0.02	99.30	10%	14%	69%	5%	2%
17Mi642	2.61	0.01	21.01	37.30	1.78	9.70	27.74	0.04	0.02	100.21	22%	10%	62%	5%	0%
17Mi642	3.84	0.00	21.16	37.54	2.17	5.38	29.07	0.00	0.06	99.23	12%	15%	65%	6%	1%
17Mi642	3.10	0.00	20.89	37.13	0.96	6.22	30.65	0.01	0.03	98.99	14%	13%	70%	3%	1%
17Mi642	3.12	0.03	21.06	37.37	1.52	5.17	31.21	0.01	0.02	99.51	12%	13%	70%	4%	1%
17Mi642	3.78	0.03	21.18	37.53	1.79	3.27	31.57	0.00	0.02	99.17	7%	15%	71%	5%	1%
17Mi642	3.61	0.01	20.92	37.05	1.17	4.14	31.85	0.00	0.01	98.77	9%	15%	72%	3%	0%
17Mi642	2.89	0.01	21.04	37.14	1.37	7.95	29.07	0.02	0.02	99.51	18%	12%	66%	4%	1%
17Mi642	5.55	0.01	21.46	37.72	1.82	1.88	30.53	0.02	0.00	98.99	4%	22%	68%	5%	1%
17Mi642	3.92	0.01	21.11	37.35	1.22	2.71	32.23	0.01	0.01	98.56	6%	16%	73%	3%	2%
17Mi642	3.54	0.00	21.10	37.18	1.30	5.79	30.32	0.02	0.07	99.32	13%	14%	68%	4%	1%
17Mi642	3.53	0.01	21.19	37.25	1.20	7.65	28.25	0.00	0.02	99.10	17%	14%	64%	3%	1%
17Mi642	4.85	0.00	21.07	37.71	2.48	3.19	29.47	0.04	0.00	98.81	7%	19%	66%	7%	1%
17Mi642	4.48	0.02	21.23	37.25	1.28	4.46	30.09	0.01	0.04	98.85	10%	18%	68%	4%	1%
17Mi642	3.20	0.00	20.47	37.22	1.18	5.40	30.97	0.00	0.04	98.48	12%	13%	71%	3%	1%
17Mi642	4.75	0.01	21.38	37.59	4.39	2.67	27.85	0.00	0.07	98.71	6%	19%	62%	12%	1%
17Mi642	3.27	0.00	21.04	37.35	2.20	5.72	29.66	0.06	0.01	99.31	13%	13%	67%	6%	1%
17Mi642	4.38	0.02	21.05	37.58	1.57	2.92	31.30	0.05	0.06	98.93	7%	18%	70%	4%	1%
17Mi642	2.23	0.03	20.99	37.05	1.37	8.37	29.79	0.06	0.01	99.90	19%	9%	67%	4%	1%
17Mi642	2.93	0.04	21.08	37.27	1.67	5.45	30.96	0.06	0.00	99.46	12%	12%	70%	5%	1%
17Mi642	3.61	0.00	20.91	36.95	1.23	6.53	29.66	0.02	0.04	98.94	15%	15%	67%	3%	0%

GEOCHEMICAL DATA OF GARNETS FROM SITE U1418, PROXIMAL SITE

	Analysis (wt%)										Composition				
sample name	MgO	Na_2O	Al_2O_3	SiO_2	CaO	MnO	FeO	TiO_2	Cr_2O_3	Total	Spessartine	Pyrope	Almandine	Grossular	Others
18MPe119*	4.50	not measured	21.18	37.55	5.71	4.83	26.58	0.01	0.00	100.36	11%	18%	54%	13%	4%
18MPe119*	2.11	not measured	20.57	36.64	5.24	4.54	30.35	0.05	0.00	99.50	10%	8%	65%	12%	4%
18MPe119*	0.24	not measured	18.59	35.82	10.92	18.27	14.65	0.43	0.01	98.93	42%	1%	23%	19%	14%
18MPe119*	0.29	not measured	18.85	36.32	11.67	15.99	16.09	0.33	0.01	99.55	37%	1%	27%	22%	13%
18MPe119*	5.80	not measured	21.15	38.10	5.67	2.49	26.80	0.07	0.03	100.12	5%	23%	56%	13%	4%
18MPe119*	4.97	not measured	21.00	37.48	1.68	1.89	32.94	0.02	0.03	100.01	4%	20%	71%	3%	3%
18MPe119*	4.59	not measured	21.14	37.14	1.41	3.39	31.99	0.00	0.01	99.67	8%	18%	69%	3%	2%
18MPe119*	3.48	not measured	20.99	36.89	1.66	4.45	32.50	0.01	0.04	100.03	10%	14%	70%	3%	2%
18MPe119*	4.39	not measured	21.29	37.55	1.72	3.30	32.09	0.05	0.00	100.39	7%	17%	70%	4%	1%
18MPe119*	5.63	not measured	21.30	37.39	1.63	1.68	32.46	0.02	0.00	100.11	4%	22%	68%	3%	3%
18MPe119*	0.85	not measured	20.35	35.71	0.12	21.77	20.84	0.08	0.00	99.72	51%	3%	42%	0%	4%
18MPe119*	0.21	not measured	20.30	35.25	0.10	24.98	18.95	0.09	0.01	99.88	58%	1%	36%	0%	5%
18MPe170	3.66	0.00	21.20	37.80	5.88	2.42	28.21	0.06	0.00	99.24	5%	15%	63%	17%	1%
18MPe170	5.27	0.01	21.51	38.22	3.98	1.75	28.14	0.08	0.02	98.98	4%	21%	62%	11%	2%
18MPe170	1.66	0.01	21.09	37.94	10.70	2.11	25.63	0.14	0.02	99.30	5%	7%	57%	30%	1%
18MPe170	3.68	0.05	21.04	37.97	3.51	0.58	32.15	0.07	0.00	99.04	1%	15%	72%	10%	2%
18MPe170	2.43	0.05	21.03	37.11	2.25	5.65	30.14	0.36	0.00	99.02	13%	10%	68%	6%	2%
18MPe170	1.29	0.00	21.16	37.91	9.45	2.93	26.69	0.14	0.00	99.57	7%	5%	60%	27%	2%
18MPe170	5.26	0.00	21.55	38.25	3.85	1.74	28.54	0.00	0.01	99.20	4%	21%	63%	11%	2%
18MPe170	2.44	0.00	21.28	38.28	9.67	2.97	25.00	0.10	0.01	99.75	7%	10%	55%	27%	1%
18MPe170	4.26	0.03	21.28	38.16	4.40	2.03	29.17	0.05	0.00	99.37	5%	17%	65%	12%	1%
18MPe170	4.50	0.00	21.29	37.94	1.26	4.64	29.91	0.00	0.01	99.55	10%	18%	67%	4%	1%
18MPe170	2.55	0.00	21.12	37.71	5.94	6.90	24.75	0.02	0.02	99.00	16%	10%	56%	17%	2%
18MPe170	2.58	0.03	20.72	36.87	1.41	11.49	25.13	0.01	0.02	98.26	27%	11%	57%	4%	1%
18MPe170	3.93	0.00	21.22	37.75	1.36	6.55	28.49	0.03	0.03	99.35	15%	16%	64%	4%	2%
18MPe170	3.15	0.02	21.08	37.66	2.76	3.08	31.39	0.04	0.03	99.21	7%	13%	71%	8%	2%
18MPe170	2.75	0.01	21.14	37.35	1.74	1.90	34.47	0.01	0.00	99.37	4%	11%	78%	5%	2%
18MPe170	5.68	0.01	21.47	38.09	1.30	1.85	30.84	0.03	0.03	99.30	4%	22%	68%	4%	2%
18MPe170	1.07	0.02	20.94	37.51	7.44	13.99	18.59	0.13	0.00	99.69	32%	4%	42%	21%	1%
18MPe170	3.65	0.00	21.43	38.07	7.22	3.23	25.96	0.05	0.00	99.61	7%	14%	57%	20%	1%
18MPe170	1.90	0.06	20.88	36.90	0.87	11.46	27.00	0.04	0.01	99.12	26%	8%	62%	3%	2%
18MPe170	3.12	0.01	21.10	37.25	1.34	6.17	30.30	0.00	0.03	99.32	14%	13%	68%	4%	1%
18MPe170	2.83	0.00	21.05	37.29	1.59	11.83	24.65	0.03	0.01	99.28	27%	11%	56%	5%	1%
18MPe170	1.68	0.01	21.00	37.38	3.96	10.16	25.23	0.00	0.00	99.42	23%	7%	57%	11%	1%
18MPe170	3.09	0.03	21.06	37.07	1.92	8.33	27.23	0.02	0.00	98.75	19%	12%	62%	6%	1%

18MPe280	4.40	0.05	21.29	37.90	1.36	3.04	31.58	0.00	0.04	99.66	7%	17%	70%	4%	2%
18MPe280	4.57	0.03	21.45	37.87	1.41	2.17	32.02	0.01	0.00	99.53	5%	18%	71%	4%	2%
18MPe280	5.96	0.02	21.73	38.20	1.22	4.88	27.77	0.02	0.03	99.84	11%	23%	61%	3%	1%
18MPe280	3.88	0.00	21.44	37.62	1.37	2.97	32.16	0.00	0.00	99.45	7%	15%	72%	4%	2%
18MPe280	4.48	0.01	20.51	36.35	1.58	2.44	31.41	0.00	0.03	96.81	6%	18%	71%	4%	1%
18MPe280	5.63	0.00	21.37	38.14	0.99	5.00	28.21	0.04	0.00	99.38	11%	22%	63%	3%	1%
18MPe280	5.81	0.01	21.58	38.16	1.09	1.18	31.58	0.01	0.02	99.44	3%	23%	70%	3%	2%
18MPe280	4.32	0.02	21.28	37.90	1.52	3.31	31.49	0.00	0.03	99.87	7%	17%	70%	4%	1%
18MPe280	4.29	0.01	21.05	37.80	1.76	3.75	30.64	0.02	0.02	99.34	8%	17%	69%	5%	1%
18MPe280	3.40	0.00	21.10	37.33	1.77	5.01	30.24	0.04	0.00	98.89	11%	14%	68%	5%	1%
18MPe280	3.71	0.02	21.10	37.47	1.52	1.29	33.51	0.04	0.01	98.67	3%	15%	76%	4%	2%
18MPe280	3.79	0.03	21.28	37.51	1.09	5.80	29.74	0.01	0.00	99.26	13%	15%	67%	3%	2%
18MPe280	4.69	0.01	21.16	37.49	1.00	2.89	31.07	0.04	0.03	98.38	7%	19%	70%	3%	2%
18MPe280	3.84	0.03	21.19	37.70	1.56	4.20	31.01	0.01	0.00	99.54	10%	15%	69%	4%	1%
18MPe280	4.29	0.00	21.35	37.95	2.08	4.60	29.12	0.02	0.02	99.43	10%	17%	65%	6%	2%
18MPe280	3.06	0.04	21.15	37.52	2.72	5.94	28.77	0.00	0.01	99.20	14%	12%	65%	8%	2%
18MPe280	4.04	0.03	21.29	37.62	2.02	4.89	29.36	0.03	0.01	99.29	11%	16%	66%	6%	1%
18MPe280	4.55	0.00	21.18	37.71	1.06	3.60	30.58	0.00	0.03	98.72	8%	18%	69%	3%	2%
18MPe280	5.92	0.00	21.53	38.08	1.08	1.37	30.94	0.02	0.03	98.97	3%	23%	69%	3%	2%
18MPe280	5.16	0.00	21.36	37.76	1.03	2.73	30.97	0.05	0.03	99.08	6%	21%	69%	3%	1%
18MPe280	0.57	0.00	20.56	37.18	6.80	15.39	18.50	0.17	0.02	99.19	35%	2%	42%	19%	1%
18MPe280	5.97	0.02	21.57	37.99	1.25	1.78	30.67	0.01	0.04	99.31	4%	24%	68%	3%	1%
18MPe280	4.52	0.05	21.53	37.86	1.45	2.43	31.76	0.00	0.04	99.63	5%	18%	71%	4%	2%
18MPe280	4.31	0.02	21.40	37.79	1.36	2.85	31.55	0.06	0.00	99.35	6%	17%	71%	4%	2%
18MPe280	4.97	0.01	21.33	38.17	2.33	2.47	30.11	0.03	0.08	99.51	6%	20%	67%	6%	2%
18MPe280	2.98	0.00	20.98	37.05	1.40	5.22	31.31	0.02	0.02	98.97	12%	12%	71%	4%	1%
18MPe280	5.15	0.02	21.32	38.16	1.82	1.85	30.93	0.03	0.00	99.28	4%	20%	69%	5%	2%
18MPe280	4.17	0.01	21.21	37.50	1.36	2.56	32.12	0.02	0.02	98.98	6%	17%	72%	4%	1%
18MPe280	3.13	0.02	21.07	37.38	2.09	8.35	27.54	0.01	0.00	99.59	19%	13%	62%	6%	1%
18MPe280	5.00	0.02	21.38	37.83	1.00	2.60	31.43	0.01	0.00	99.27	6%	20%	70%	3%	1%
18MPe280	5.57	0.02	21.36	38.08	2.17	1.17	30.74	0.05	0.00	99.16	3%	22%	68%	6%	1%
18MPe280	4.28	0.03	21.44	37.85	2.56	3.73	29.80	0.00	0.06	99.74	8%	17%	66%	7%	1%
18MPe280	2.05	0.00	20.95	37.19	4.27	10.60	24.31	0.00	0.01	99.39	24%	8%	55%	12%	0%
18MPe280	3.79	0.03	21.38	37.94	5.12	2.34	29.01	0.04	0.06	99.71	5%	15%	64%	14%	1%
18MPe280	4.30	0.01	21.27	37.81	3.20	1.94	30.51	0.02	0.04	99.10	4%	17%	68%	9%	1%
18MPe280	4.40	0.03	21.41	37.92	3.16	2.15	30.48	0.02	0.03	99.60	5%	17%	68%	9%	1%
18MPe280	4.54	0.00	21.39	37.63	1.30	3.87	30.84	0.00	0.03	99.60	9%	18%	69%	4%	1%
18MPe280	5.66	0.03	21.61	37.99	1.46	2.80	29.92	0.00	0.05	99.52	6%	22%	66%	4%	1%
18EPe939	2.75	0.01	21.16	37.61	5.05	6.61	26.49	0.00	0.02	99.70	15%	11%	59%	14%	1%

18EPe939	1.42	0.02	21.03	37.77	8.74	6.65	23.78	0.16	0.03	99.58	15%	6%	53%	25%	1%
18EPe939	3.49	0.01	21.04	37.37	2.35	2.53	31.76	0.05	0.00	98.61	6%	14%	72%	7%	2%
18EPe939	4.25	0.01	21.30	37.74	1.34	3.33	31.18	0.02	0.03	99.19	8%	17%	70%	4%	2%
18EPe939	7.14	0.00	21.63	38.30	1.41	1.34	29.59	0.00	0.03	99.44	3%	28%	65%	4%	0%
18EPe939	3.97	0.01	21.25	37.77	1.73	1.87	33.05	0.05	0.02	99.72	4%	16%	74%	5%	1%
18EPe939	2.90	0.01	21.08	37.45	3.97	3.33	30.25	0.02	0.01	99.02	8%	12%	68%	11%	1%
18EPe939	2.49	0.01	20.83	37.31	2.50	9.22	26.73	0.12	0.01	99.22	21%	10%	61%	7%	1%
18EPe939	3.38	0.03	20.85	37.64	1.62	3.71	31.82	0.08	0.00	99.13	8%	14%	72%	5%	2%
18EPe939	3.17	0.01	20.83	37.00	2.47	6.49	28.45	0.06	0.00	98.48	15%	13%	65%	7%	1%
18EPe939	4.87	0.01	21.18	37.61	1.47	2.86	31.21	0.06	0.03	99.29	6%	19%	70%	4%	0%
18EPe939	4.33	0.01	21.12	37.58	1.40	2.16	32.24	0.00	0.01	98.85	5%	17%	72%	4%	1%
18EPe939	5.48	0.01	21.26	38.10	1.29	1.83	31.28	0.02	0.00	99.27	4%	22%	69%	4%	1%
18EPe939	2.99	0.03	21.14	37.59	4.01	3.00	30.55	0.05	0.01	99.36	7%	12%	69%	11%	1%
18EPe939	0.13	0.04	20.63	36.61	0.47	5.51	36.29	0.01	0.00	99.69	13%	1%	84%	1%	2%
18EPe939	5.05	0.00	21.23	37.74	1.44	2.30	31.32	0.03	0.02	99.13	5%	20%	70%	4%	1%
18EPe939	4.94	0.00	21.43	38.00	1.30	3.43	30.34	0.00	0.00	99.45	8%	20%	67%	4%	2%
18EPe939	3.97	0.02	21.16	37.41	1.19	4.79	30.51	0.03	0.05	99.13	11%	16%	69%	3%	1%
18EPe939	3.21	0.00	21.08	37.48	1.82	7.15	28.47	0.01	0.01	99.24	16%	13%	64%	5%	1%
18EPe939	4.05	0.03	21.26	37.83	3.22	3.33	29.61	0.05	0.03	99.41	8%	16%	66%	9%	1%
18EPe939	2.03	0.02	20.88	37.00	1.16	7.71	30.59	0.06	0.03	99.48	18%	8%	70%	3%	1%
18EPe939	4.82	0.00	21.45	37.99	1.30	1.93	32.06	0.02	0.03	99.60	4%	19%	71%	4%	2%
18EPe939	4.07	0.00	21.36	37.62	1.22	1.68	33.38	0.02	0.01	99.37	4%	16%	75%	3%	2%
18EPe939	3.24	0.03	21.19	37.60	2.54	6.37	28.52	0.02	0.01	99.51	14%	13%	64%	7%	1%
18EPe939	4.79	0.02	21.43	37.73	0.84	3.02	31.54	0.01	0.00	99.38	7%	19%	70%	2%	1%
18EPe939	3.85	0.01	21.33	37.46	1.30	5.00	30.55	0.03	0.03	99.56	11%	15%	68%	4%	1%
18EPe939	4.86	0.02	21.28	37.92	1.22	3.20	31.01	0.04	0.01	99.56	7%	19%	69%	3%	1%
18EPe939	2.78	0.01	21.07	37.31	1.04	7.81	29.73	0.00	0.00	99.76	18%	11%	67%	3%	1%
18EPe939	3.26	0.02	21.06	37.57	2.49	5.92	29.08	0.05	0.03	99.48	13%	13%	65%	7%	1%
18EPe939	3.38	0.03	21.19	37.49	2.84	3.01	30.99	0.00	0.00	98.93	7%	14%	70%	8%	2%
18EPe939	4.68	0.00	20.95	37.84	1.81	3.50	30.14	0.01	0.05	98.99	8%	19%	67%	5%	1%
18EPe939	4.18	0.01	21.26	37.95	2.58	3.97	29.69	0.02	0.02	99.67	9%	17%	66%	7%	1%
18EPe939	4.64	0.01	21.32	37.79	2.16	2.31	31.25	0.03	0.01	99.53	5%	18%	69%	6%	1%
18EPe939	2.84	0.02	21.01	37.02	1.45	8.26	28.21	0.04	0.01	98.86	19%	11%	64%	4%	1%
18EPe939	3.70	0.02	21.22	37.63	2.88	2.86	31.03	0.00	0.01	99.35	6%	15%	69%	8%	1%
18EPe939	4.58	0.00	21.56	37.81	1.51	3.83	30.80	0.02	0.00	100.11	9%	18%	68%	4%	1%
18EPe939	3.22	0.01	20.98	37.33	1.38	5.31	30.91	0.05	0.03	99.22	12%	13%	70%	4%	1%
18EPe939	1.33	0.03	20.99	37.59	8.30	3.43	27.64	0.11	0.01	99.42	8%	5%	62%	24%	1%
18EPe939	3.65	0.01	21.00	37.50	1.67	6.45	28.92	0.03	0.03	99.26	15%	15%	65%	5%	1%
18EPe939	2.62	0.01	21.03	37.26	1.75	6.78	30.26	0.06	0.04	99.81	15%	11%	68%	5%	1%

18EPe939	4.36	0.01	21.36	37.68	2.71	1.69	31.36	0.03	0.01	99.20	4%	17%	70%	8%	1%
18EPe939	2.73	0.02	21.05	37.31	3.52	5.12	29.62	0.00	0.02	99.40	12%	11%	67%	10%	1%
18EPe939	5.34	0.00	21.54	38.18	1.53	1.65	31.21	0.01	0.01	99.47	4%	21%	69%	4%	2%
18EPe939	2.21	0.03	20.90	37.53	5.59	4.55	28.01	0.06	0.00	98.88	10%	9%	63%	16%	1%
18EPe939	4.32	0.00	21.22	37.58	1.28	2.73	31.77	0.04	0.01	98.95	6%	17%	71%	4%	2%
18EPe939	1.97	0.00	20.80	36.96	1.68	8.96	28.57	0.06	0.01	99.01	21%	8%	65%	5%	1%
18EPe939	2.13	0.01	21.02	37.42	4.43	8.54	25.94	0.03	0.00	99.52	19%	9%	58%	13%	1%
18EPe939	4.15	0.00	21.33	37.60	1.44	4.48	30.29	0.01	0.00	99.30	10%	17%	68%	4%	1%
18EPe939	2.74	0.01	20.86	37.44	4.02	4.67	28.85	0.06	0.04	98.68	11%	11%	65%	12%	1%
18EPe939	6.17	0.00	21.38	37.90	2.30	1.66	29.43	0.05	0.02	98.91	4%	24%	65%	6%	0%
18EPe939	2.16	0.02	20.74	37.22	3.74	7.38	27.56	0.04	0.00	98.86	17%	9%	63%	11%	1%
18EPe939	4.29	0.01	21.21	37.19	1.06	1.29	33.62	0.00	0.01	98.68	3%	17%	76%	3%	1%
18EPe939	4.73	0.00	21.31	37.72	1.50	2.05	32.01	0.03	0.01	99.36	5%	19%	71%	4%	1%
18EPe939	4.86	0.03	21.37	37.94	2.36	3.99	28.54	0.00	0.03	99.12	9%	19%	64%	7%	2%
18EPe939	3.02	0.01	20.97	37.29	1.19	5.86	30.62	0.05	0.01	99.02	13%	12%	69%	3%	2%
18EPe939	6.01	0.00	21.38	38.21	1.99	2.17	29.45	0.04	0.01	99.26	5%	24%	65%	6%	1%
18EPe939	4.96	0.01	21.33	37.82	2.21	2.89	29.77	0.01	0.05	99.05	7%	20%	66%	6%	1%
18EPe939	4.62	0.00	21.14	37.72	1.37	3.26	31.08	0.03	0.01	99.23	7%	18%	69%	4%	1%
18EPe939	4.89	0.02	21.33	37.80	1.31	2.80	31.00	0.04	0.03	99.22	9%	19%	67%	4%	2%
18EPe939	4.23	0.02	21.30	37.67	1.61	3.35	31.34	0.00	0.02	99.54	6%	19%	69%	4%	2%
18EPe939	2.23	0.01	21.17	37.49	4.22	11.75	22.94	0.03	0.00	99.85	27%	9%	51%	12%	1%
18EPe939	4.64	0.00	21.38	37.65	1.37	4.03	29.88	0.01	0.04	99.00	8%	15%	65%	11%	1%
18EPe939	3.63	0.01	21.00	37.73	3.85	3.73	28.72	0.04	0.03	98.74	13%	16%	65%	4%	1%
18EPe939	4.03	0.04	21.27	37.49	1.57	5.80	29.24	0.04	0.07	99.55	4%	20%	71%	4%	1%
18EPe939	4.37	0.03	21.29	37.83	1.27	4.10	30.88	0.02	0.00	99.78	5%	15%	74%	4%	2%
18EPe939	4.95	0.01	21.48	37.86	1.39	1.92	31.79	0.00	0.02	99.41	11%	16%	68%	4%	2%
18EPe939	3.79	0.03	21.40	37.46	1.51	2.05	32.82	0.04	0.01	99.11	9%	19%	67%	5%	1%
18EPe939	4.08	0.01	21.19	37.67	1.34	4.67	30.16	0.00	0.03	99.16	9%	17%	69%	4%	1%
18EPe939	4.68	0.03	21.46	37.67	1.68	3.81	29.96	0.02	0.02	99.33	8%	17%	70%	5%	1%
18EPe939	5.28	0.01	21.46	37.84	1.25	2.63	30.84	0.02	0.04	99.37	6%	21%	68%	3%	1%

*sample 18Mpe119 was merged with sample 18MPe170 to form one composite sample (18MPe119).

Garnet Profiles										
		Analysis (wt%)								
grain name	sample name	MgO	Al2O3	SiO2	CaO	MnO	FeO	Cr2O3	TiO2	Total
G1d40 Line 001	17Mi603	2.26	21.30	36.77	1.97	14.98	23.28	0.01	0.00	100.57
G1d40 Line 002	17Mi603	2.53	21.22	36.85	2.06	13.98	23.72	0.01	0.01	100.38
G1d40 Line 003	17Mi603	2.70	21.35	37.09	1.92	13.55	24.29	0.00	0.00	100.90
G1d40 Line 004	17Mi603	2.73	21.23	36.86	1.89	13.38	24.43	0.03	0.01	100.56
G1d40 Line 005	17Mi603	2.83	20.97	36.87	1.84	13.34	24.69	0.00	0.00	100.54
G1d40 Line 006	17Mi603	2.86	21.22	36.82	1.81	13.27	24.82	0.00	0.00	100.80
G1d40 Line 007	17Mi603	2.81	21.23	37.03	1.95	13.23	24.80	0.00	0.00	101.05
G1d40 Line 008	17Mi603	2.86	21.11	36.95	1.81	13.15	24.88	0.00	0.00	100.77
G1d40 Line 009	17Mi603	2.83	21.09	36.83	1.83	13.68	24.45	0.02	0.00	100.73
G1d40 Line 010	17Mi603	2.73	21.12	36.88	1.91	13.37	24.58	0.00	0.00	100.59
G1d40 Line 011	17Mi603	2.69	21.17	36.94	2.08	13.85	24.14	0.03	0.01	100.90
G1d40 Line 012	17Mi603	2.45	21.05	36.47	1.95	14.56	23.20	0.01	0.00	99.69
G4d35 Line 001	17Pi400	5.56	21.66	37.49	1.92	1.22	32.19	0.06	0.01	100.11
G4d35 Line 002	17Pi400	5.49	21.54	37.51	1.98	1.27	32.25	0.03	0.01	100.07
G4d35 Line 003	17Pi400	5.76	21.52	37.74	1.85	1.28	32.29	0.08	0.05	100.57
G4d35 Line 004	17Pi400	5.79	21.68	37.72	1.96	1.16	31.96	0.08	0.08	100.42
G4d35 Line 005	17Pi400	5.73	21.14	36.85	1.91	1.14	31.63	0.05	1.98	100.43
G4d35 Line 006	17Pi400	5.85	21.49	37.61	2.04	1.10	31.85	0.08	0.08	100.10
G4d35 Line 007	17Pi400	5.86	21.50	37.72	1.98	1.11	31.89	0.06	0.09	100.21
G4d35 Line 008	17Pi400	5.88	21.57	37.82	1.96	1.14	31.75	0.06	0.03	100.21
G4d35 Line 009	17Pi400	5.86	21.68	37.70	2.00	1.22	31.88	0.08	0.06	100.48
G4d35 Line 010	17Pi400	5.70	21.50	37.56	1.94	1.30	31.92	0.06	0.09	100.06
G4d35 Line 011	17Pi400	5.45	21.47	37.63	1.99	1.43	32.02	0.06	0.08	100.13
G4d35 Line 012	17Pi400	5.11	21.72	37.52	1.96	1.65	32.21	0.04	0.12	100.33
G4d44 Line 001	17Pi400	1.40	21.31	36.88	0.47	13.02	28.13	0.01	0.03	101.25
G4d44 Line 002	17Pi400	1.42	21.16	36.44	0.32	13.14	28.23	0.02	0.00	100.74
G4d44 Line 003	17Pi400	1.51	21.20	35.82	0.35	13.54	27.81	0.00	0.06	100.28

G4d44 Line 004	17Pi400	1.50	21.11	36.03	0.39	13.75	27.57	0.00	0.06	100.41
G4d44 Line 005	17Pi400	1.45	21.05	36.38	0.46	13.54	27.24	0.01	0.05	100.18
G4d44 Line 006	17Pi400	1.46	21.11	36.31	0.44	14.02	27.18	0.00	0.08	100.61
G4d44 Line 007	17Pi400	1.46	21.01	36.61	0.48	13.91	27.65	0.00	0.04	101.17
G4d44 Line 008	17Pi400	1.38	20.96	36.52	0.47	13.65	27.41	0.00	0.03	100.43
G4d44 Line 009	17Pi400	1.42	21.00	36.43	0.48	13.86	27.71	0.00	0.02	100.93
G4d44 Line 010	17Pi400	1.44	20.62	36.00	0.51	13.24	27.24	0.02	0.03	99.10
G4d44 Line 011	17Pi400	1.47	20.98	36.37	0.52	13.14	27.95	0.00	0.04	100.46
G4d44 Line 012	17Pi400	1.38	20.91	36.34	0.45	13.29	28.06	0.01	0.00	100.44
G4d47 Line 001	17Pi400	1.39	21.20	37.66	16.07	2.29	20.99	0.00	0.44	100.04
G4d47 Line 002	17Pi400	1.49	21.40	37.92	16.21	2.71	20.61	0.02	0.38	100.74
G4d47 Line 003	17Pi400	1.45	21.53	38.09	15.67	3.08	20.43	0.01	0.32	100.58
G4d47 Line 004	17Pi400	1.60	21.50	38.09	15.39	1.81	21.77	0.00	0.29	100.45
G4d47 Line 005	17Pi400	1.59	21.45	38.07	15.16	1.56	22.54	0.00	0.38	100.74
G4d47 Line 006	17Pi400	1.63	21.31	38.30	15.17	1.57	22.34	0.00	0.41	100.73
G4d47 Line 007	17Pi400	1.53	21.36	38.12	15.13	1.33	22.91	0.01	0.43	100.82
G4d47 Line 008	17Pi400	1.55	21.34	38.01	14.96	1.32	22.84	0.04	0.40	100.45
G4d47 Line 009	17Pi400	1.61	21.51	38.18	15.11	1.43	22.92	0.00	0.39	101.15
G4d47 Line 010	17Pi400	1.43	21.31	38.20	14.97	2.11	22.45	0.00	0.50	100.97
G4d47 Line 011	17Pi400	1.65	21.45	38.08	15.09	1.66	22.03	0.00	0.38	100.34
G4c1Line 001	17Mi643	2.87	21.37	36.58	2.78	8.12	28.24	0.02	0.02	100.00
G4c1Line 002	17Mi643	2.92	21.24	37.25	2.95	8.39	27.87	0.03	0.03	100.68
G4cLine 003	17Mi643	2.87	21.39	37.39	3.58	8.48	27.21	0.01	0.01	100.93
G4c1Line 004	17Mi643	2.75	21.46	37.15	4.12	8.17	26.62	0.02	0.02	100.32
G4c1Line 005	17Mi643	2.81	21.47	37.12	3.46	8.55	26.60	0.02	0.02	100.05
G4c1Line 006	17Mi643	2.81	21.50	37.35	3.42	8.44	27.12	0.02	0.02	100.68
G4c1Line 007	17Mi643	2.85	21.36	37.17	3.49	8.49	26.89	0.00	0.00	100.26
G4c1Line 008	17Mi643	2.77	21.53	37.32	3.96	8.19	26.73	0.01	0.03	100.53
G4c1Line 009	17Mi643	2.74	21.57	37.51	3.83	8.35	26.64	0.01	0.00	100.65
G4c1Line 010	17Mi643	2.79	21.50	37.52	3.58	8.30	27.32	0.04	0.04	101.09

G4c1Line 011	17Mi643	2.87	21.75	37.45	2.96	8.39	27.98	0.03	0.00	101.43
G4 c1 Line 012	17Mi643	2.74	21.69	37.44	2.79	8.24	27.93	0.02	0.03	100.87
G4 c12 Line 001	17Mi643	2.65	21.15	36.55	1.17	9.09	29.24	0.02	0.03	99.90
G4 c12 Line 002	17Mi643	2.70	21.11	36.72	1.15	8.98	29.28	0.00	0.07	100.01
G4 c12 Line 003	17Mi643	2.75	21.10	36.72	1.35	9.00	29.10	0.01	0.14	100.16
G4 c12 Line 004	17Mi643	2.71	21.11	36.88	1.37	8.94	29.30	0.00	0.11	100.42
G4 c12 Line 005	17Mi643	2.83	21.10	36.89	1.43	8.94	28.96	0.03	0.10	100.28
G4 c12 Line 006	17Mi643	2.73	21.31	36.89	1.42	9.09	28.97	0.01	0.11	100.53
G4 c12 Line 007	17Mi643	2.74	21.22	36.88	1.34	8.96	29.13	0.01	0.06	100.34
G4 c12 Line 008	17Mi643	2.72	21.19	37.02	1.33	9.20	29.28	0.00	0.08	100.83
G4 c12 Line 009	17Mi643	2.70	21.45	36.95	1.33	9.10	29.23	0.00	0.07	100.83
G4 c12 Line 010	17Mi643	2.63	21.33	37.21	1.32	9.07	29.40	0.00	0.09	101.05
G4 c12 Line 011	17Mi643	2.64	21.29	37.38	1.23	8.91	29.56	0.00	0.08	101.09
G4 c12 Line 012	17Mi643	2.56	21.66	37.21	1.12	9.05	29.36	0.01	0.03	101.01
G4 c30 Line 001	17Mi643	2.53	21.23	36.73	1.42	10.50	27.71	0.02	0.00	100.14
G4 c30 Line 002	17Mi643	2.53	21.35	36.94	1.86	10.65	27.35	0.00	0.01	100.69
G4 c30 Line 003	17Mi643	2.61	21.12	36.93	2.11	10.81	26.82	0.00	0.06	100.46
G4 c30 Line 004	17Mi643	2.59	21.21	36.91	2.06	11.13	26.94	0.01	0.05	100.91
G4 c30 Line 005	17Mi643	2.56	21.13	37.09	2.21	11.03	26.76	0.02	0.04	100.84
G4 c30 Line 006	17Mi643	2.67	21.15	36.86	1.87	11.26	26.88	0.01	0.03	100.73
G4 c30 Line 007	17Mi643	2.61	21.16	37.07	1.90	11.18	26.99	0.00	0.05	100.96
G4 c30 Line 008	17Mi643	2.69	21.28	37.09	1.54	11.25	27.46	0.00	0.03	101.35
G4 c30 Line 009	17Mi643	2.59	21.21	37.32	1.94	10.79	26.77	0.02	0.04	100.68
G4 c30 Line 010	17Mi643	2.57	21.29	37.06	1.91	10.96	27.26	0.00	0.03	101.08
G4 c30 Line 011	17Mi643	2.47	21.32	37.10	1.80	10.70	27.51	0.00	0.05	100.95
G4 c30 Line 012	17Mi643	2.32	21.32	37.31	1.42	10.53	28.22	0.01	0.00	101.13
G4 c31 Line 001	17Mi643	4.24	21.28	37.19	2.76	4.49	29.94	0.10	0.01	100.01
G4 c31 Line 002	17Mi643	4.97	21.43	37.49	3.54	3.53	28.80	0.09	0.06	99.91
G4 c31 Line 003	17Mi643	5.26	21.54	37.79	3.63	3.08	28.63	0.09	0.03	100.05
G4 c31 Line 004	17Mi643	5.46	21.81	38.29	3.61	2.90	28.77	0.12	0.04	101.01

G4 c31 Line 005	17Mi643	5.54	21.37	37.94	3.73	2.94	28.30	0.14	0.05	100.01
G4 c31 Line 006	17Mi643	5.63	21.68	37.86	3.78	2.79	28.76	0.14	0.05	100.69
G4 c31 Line 007	17Mi643	5.68	21.71	37.97	3.74	2.72	28.49	0.14	0.04	100.48
G4 c31 Line 008	17Mi643	5.40	21.15	37.31	3.57	2.66	28.09	0.12	0.00	98.30
G4 c31 Line 009	17Mi643	5.66	21.81	38.04	3.68	2.83	28.74	0.10	0.05	100.91
G4 c31 Line 010	17Mi643	5.53	21.71	37.99	3.50	2.91	29.03	0.13	0.04	100.84
G4 c31 Line 011	17Mi643	5.26	21.70	37.86	3.34	3.16	29.01	0.09	0.03	100.45
G4 c31 Line 012	17Mi643	5.07	21.89	38.12	3.00	3.48	29.46	0.06	0.03	101.11
G4 c32 Line 001	17Mi643	3.40	21.33	37.24	2.02	3.84	32.54	0.00	0.03	100.40
G4 c32 Line 002	17Mi643	3.57	21.49	37.13	1.87	3.57	32.94	0.02	0.08	100.67
G4 c32 Line 003	17Mi643	3.70	21.45	37.15	1.86	3.56	32.95	0.01	0.06	100.73
G4 c32 Line 004	17Mi643	3.82	21.31	37.30	1.93	3.53	33.06	0.02	0.05	101.02
G4 c32 Line 005	17Mi643	3.79	21.39	37.28	1.92	3.35	32.75	0.04	0.07	100.59
G4 c32 Line 006	17Mi643	3.81	21.34	37.37	1.95	3.48	32.84	0.00	0.06	100.85
G4 c32 Line 007	17Mi643	3.83	21.47	37.30	1.93	3.41	32.65	0.04	0.05	100.68
G4 c32 Line 008	17Mi643	3.84	21.42	37.40	1.89	3.39	32.80	0.00	0.02	100.76
G4 c32 Line 009	17Mi643	3.74	21.47	37.31	1.89	3.37	32.80	0.02	0.04	100.64
G4 c32 Line 010	17Mi643	3.65	21.66	37.27	2.10	3.29	32.69	0.01	0.07	100.73
G4 c32 Line 011	17Mi643	3.58	21.56	37.49	1.99	3.62	32.82	0.00	0.04	101.10
G4 c32 Line 012	17Mi643	3.28	21.54	37.33	1.85	4.18	32.88	0.03	0.03	101.11
G4 b16 Line 001	17Mi643	4.93	21.54	37.39	4.54	2.40	28.84	0.06	0.05	99.75
G4 b16 Line 002	17Mi643	4.89	21.62	37.57	4.53	2.44	28.92	0.13	0.05	100.14
G4 b16 Line 003	17Mi643	4.90	21.48	37.71	4.60	2.54	29.49	0.10	0.02	100.83
G4 b16 Line 004	17Mi643	4.87	21.80	37.80	4.57	2.44	29.12	0.13	0.05	100.78
G4 b16 Line 005	17Mi643	4.90	21.92	37.89	4.53	2.47	28.99	0.12	0.04	100.86
G4 b16 Line 006	17Mi643	4.87	21.69	37.84	4.54	2.45	29.45	0.07	0.04	100.95
G4 b16 Line 007	17Mi643	4.84	21.69	37.86	4.52	2.46	29.09	0.11	0.02	100.59
G4 b16 Line 008	17Mi643	4.92	22.02	37.81	4.43	2.62	29.43	0.08	0.01	101.32
G4 b16 Line 009	17Mi643	4.85	21.74	38.09	4.27	2.56	29.38	0.10	0.06	101.05
G4 b16 Line 010	17Mi643	4.78	21.78	37.94	4.44	2.41	29.32	0.12	0.03	100.82

G4 b16 Line 011	17Mi643	4.81	21.99	38.04	4.52	2.50	29.32	0.08	0.04	101.30
G4 b16 Line 012	17Mi643	4.70	22.15	38.41	4.36	2.49	29.19	0.08	0.01	101.40
G4 e Line 001	18EP939	1.66	21.30	37.10	8.28	7.11	24.69	0.00	0.12	100.26
G4 e Line 002	18EP939	1.61	21.30	37.39	7.41	7.78	24.99	0.00	0.11	100.59
G4 e Line 003	18EP939	1.49	21.19	36.97	8.51	7.27	24.89	0.03	0.19	100.55
G4 e Line 004	18EP939	1.64	21.17	36.97	5.25	6.28	28.59	0.03	0.06	99.99
G4 e Line 005	18EP939	1.83	21.33	36.96	3.75	3.24	33.76	0.00	0.01	100.88
G4 e Line 006	18EP939	1.82	21.30	37.20	3.75	5.67	31.48	0.01	0.04	101.27
G4 e Line 007	18EP939	1.29	21.29	37.45	8.80	7.64	24.16	0.00	0.19	100.81
G4 e Line 008	18EP939	1.46	21.42	37.46	7.98	7.68	24.81	0.00	0.18	100.99
G4 e Line 009	18EP939	1.63	21.54	37.55	7.46	7.60	25.24	0.02	0.16	101.20
G4 e Line 010	18EP939	0.91	12.26	64.78	4.83	4.16	14.73	0.02	0.08	101.76
G4 e Line 011	18EP939	0.79	9.58	71.07	4.45	3.25	12.11	0.00	0.04	101.29
G4 e Line 012	18EP939	1.60	21.61	37.78	9.58	6.07	24.40	0.01	0.13	101.18
G4 e21 Line 001	18EP939	2.41	21.13	37.09	0.82	5.46	33.90	0.00	0.00	100.81
G4 e21 Line 002	18EP939	2.40	21.12	36.77	1.04	5.96	33.38	0.00	0.05	100.72
G4 e21 Line 003	18EP939	2.35	21.27	36.97	1.30	6.53	32.83	0.01	0.05	101.31
G4 e21 Line 004	18EP939	2.21	21.27	36.91	1.24	7.14	32.45	0.02	0.03	101.27
G4 e21 Line 005	18EP939	2.24	21.15	37.04	1.17	7.44	31.96	0.01	0.04	101.05
G4 e21 Line 006	18EP939	2.17	21.31	36.79	1.28	7.65	32.03	0.00	0.07	101.31
G4 e21 Line 007	18EP939	2.11	21.34	36.94	1.20	7.50	31.37	0.00	0.07	100.53
G4 e21 Line 008	18EP939	2.18	21.53	36.84	1.21	7.57	31.89	0.00	0.03	101.25
G4 e21 Line 009	18EP939	2.25	21.29	36.84	1.21	7.21	32.32	0.00	0.04	101.16
G4 e21 Line 010	18EP939	2.25	21.29	36.91	1.20	7.22	32.86	0.00	0.04	101.77
G4 e21 Line 011	18EP939	2.38	21.30	36.84	1.10	6.90	33.04	0.00	0.01	101.57
G4 e21 Line 012	18EP939	3.14	21.05	36.67	0.92	5.61	31.18	0.04	0.19	98.80
G4f6 Line 001	17Pe87	1.22	21.33	37.28	8.68	4.26	27.73	0.00	0.15	100.64
G4f6 Line 002	17Pe87	1.26	21.35	37.18	8.19	4.33	28.29	0.02	0.09	100.71
G4f6 Line 003	17Pe87	1.28	21.43	37.16	8.39	4.13	28.27	0.00	0.14	100.80
G4f6 Line 004	17Pe87	1.32	21.35	37.39	8.64	3.95	28.34	0.01	0.11	101.11

G4f6 Line 005	17Pe87	1.36	21.28	37.44	7.97	3.65	29.07	0.00	0.09	100.85
G4f6 Line 006	17Pe87	1.35	21.47	37.33	8.43	3.76	29.05	0.00	0.12	101.51
G4f6 Line 007	17Pe87	1.39	21.33	37.09	8.06	3.57	28.84	0.01	0.10	100.39
G4f6 Line 008	17Pe87	1.42	21.30	37.50	8.13	3.47	29.08	0.00	0.11	101.01
G4f6 Line 009	17Pe87	1.37	21.36	37.56	8.01	3.36	29.37	0.01	0.09	101.14
G4f6 Line 010	17Pe87	1.42	21.45	37.49	8.04	3.25	29.47	0.02	0.11	101.26
G4f6 Line 011	17Pe87	1.40	21.40	37.38	8.42	3.00	29.24	0.03	0.14	101.01
G4f6 Line 012	17Pe87	1.44	21.37	37.65	8.14	2.90	29.19	0.02	0.08	100.80
G4f18 Line 001	17Pe87	5.15	21.65	37.54	2.40	1.84	31.90	0.03	0.05	100.56
G4f18 Line 002	17Pe87	5.79	21.76	37.76	2.37	1.62	31.31	0.04	0.03	100.69
G4f18 Line 003	17Pe87	5.77	22.07	38.28	2.35	1.69	31.16	0.04	0.03	101.38
G4f18 Line 004	17Pe87	3.08	13.14	24.24	2.49	0.99	18.26	0.01	0.00	62.21
G4f18 Line 005	17Pe87	7.51	22.18	34.80	1.37	1.27	28.47	0.03	0.02	95.65
G4f18 Line 006	17Pe87	6.35	21.75	38.14	2.35	1.48	30.71	0.01	0.07	100.86
G4f18 Line 007	17Pe87	2.37	11.32	21.06	1.60	1.21	21.13	0.01	0.00	58.70
G4f18 Line 008	17Pe87	6.16	21.91	38.07	2.43	1.64	30.94	0.02	0.05	101.21
G4f18 Line 009	17Pe87	6.16	22.05	38.08	2.26	1.67	31.08	0.00	0.01	101.31
G4f18 Line 010	17Pe87	5.95	21.99	38.09	2.36	1.63	31.34	0.02	0.02	101.40
G4f18 Line 011	17Pe87	5.61	22.03	38.13	2.35	1.65	31.47	0.00	0.01	101.25
G4f24 Line 001	17Pe87	5.90	21.98	38.05	2.15	2.11	30.65	0.02	0.03	100.89
G4f24 Line 002	17Pe87	6.04	21.95	38.17	2.18	2.14	30.59	0.03	0.01	101.11
G4f24 Line 003	17Pe87	6.12	21.98	38.28	2.23	2.16	30.70	0.01	0.02	101.50
G4f24 Line 004	17Pe87	3.12	17.38	30.36	1.67	1.48	21.89	0.02	0.00	75.92
G4f24 Line 005	17Pe87	6.18	21.90	38.09	2.22	2.05	30.85	0.02	0.00	101.31
G4f24 Line 006	17Pe87	6.25	21.96	38.01	2.12	2.11	30.69	0.05	0.03	101.21
G4f24 Line 007	17Pe87	6.17	22.01	38.19	2.10	2.00	31.06	0.01	0.03	101.57
G4f24 Line 008	17Pe87	6.18	21.99	38.07	2.09	2.03	30.93	0.04	0.02	101.34
G4f24 Line 009	17Pe87	6.16	22.01	37.97	2.11	2.16	31.19	0.01	0.01	101.62
G4f24 Line 010	17Pe87	5.88	21.82	38.06	2.04	2.07	31.16	0.04	0.01	101.08
G4f24 Line 011	17Pe87	5.90	22.11	37.76	1.82	2.19	31.55	0.03	0.01	101.37

G4f24 Line 012	17Pe87	5.75	21.86	37.82	1.68	2.38	31.87	0.01	0.00	101.37
G4i3 Line 001	18EPe900	2.08	21.61	37.46	3.77	12.01	24.10	0.01	0.05	101.09
G4i3 Line 002	18EPe900	2.20	21.57	37.34	3.94	11.98	24.09	0.03	0.03	101.17
G4i3 Line 003	18EPe900	2.09	21.59	37.16	4.66	11.77	23.97	0.04	0.06	101.33
G4i3 Line 004	18EPe900	1.92	21.78	37.56	6.36	11.14	22.96	0.02	0.03	101.77
G4i3 Line 005	18EPe900	1.93	21.55	37.68	7.15	10.99	22.30	0.02	0.01	101.63
G4i3 Line 006	18EPe900	1.95	21.50	37.52	7.19	11.01	22.10	0.01	0.06	101.33
G4i3 Line 007	18EPe900	2.22	21.65	37.24	4.96	11.84	23.64	0.01	0.04	101.61
G4i3 Line 008	18EPe900	2.23	21.65	37.26	4.51	11.76	23.84	0.02	0.00	101.27
G4i3 Line 009	18EPe900	2.22	21.47	37.13	3.76	11.89	24.36	0.00	0.01	100.84
G4i3 Line 010	18EPe900	2.16	21.51	37.46	3.76	12.09	24.18	0.00	0.02	101.18
G4i3 Line 011	18EPe900	2.16	21.35	37.08	3.68	11.95	24.32	0.03	0.04	100.61
G4i3 Line 012	18EPe900	2.06	21.17	36.71	3.55	11.72	24.14	0.01	0.05	99.41
G4i8 Line 001	18EPe900	4.64	22.22	38.28	2.36	1.77	32.20	0.00	0.00	101.47
G4i8 Line 002	18EPe900	4.93	21.79	37.53	1.57	1.95	33.15	0.00	0.01	100.94
G4i8 Line 003	18EPe900	4.97	21.80	37.56	1.46	1.92	33.28	0.01	0.00	101.00
G4i8 Line 004	18EPe900	4.98	21.93	37.70	1.33	1.94	33.43	0.01	0.03	101.36
G4i8 Line 005	18EPe900	5.05	21.83	37.68	1.27	1.94	33.29	0.01	0.01	101.08
G4i8 Line 006	18EPe900	5.08	21.76	37.52	1.38	1.96	33.24	0.00	0.00	100.95
G4i8 Line 007	18EPe900	4.99	21.80	37.55	1.36	1.92	33.29	0.00	0.04	100.95
G4i8 Line 008	18EPe900	4.92	21.86	37.74	1.33	1.89	33.37	0.00	0.01	101.13
G4i8 Line 009	18EPe900	4.88	21.73	37.66	1.30	2.07	33.65	0.02	0.00	101.31
G4i8 Line 010	18EPe900	4.81	21.78	37.52	1.29	1.88	33.57	0.04	0.00	100.88
G4i8 Line 011	18EPe900	4.77	21.67	37.29	1.31	2.06	33.47	0.02	0.00	100.59
G4i9 Line 001	18EPe900	5.96	21.72	37.73	1.31	5.24	29.09	0.01	0.01	101.07
G4i9 Line 002	18EPe900	5.97	21.76	37.78	1.34	5.16	29.02	0.03	0.03	101.09
G4i9 Line 003	18EPe900	5.97	21.82	37.61	1.27	4.87	29.18	0.01	0.00	100.73
G4i9 Line 004	18EPe900	6.04	21.74	37.64	1.31	4.93	29.01	0.00	0.04	100.72
G4i9 Line 005	18EPe900	6.09	21.74	37.83	1.29	4.87	29.03	0.00	0.04	100.88
G4i9 Line 006	18EPe900	6.12	21.90	37.82	1.29	4.92	29.13	0.00	0.02	101.20

G4i9 Line 007	18EPe900	6.04	21.67	37.76	1.28	5.09	28.90	0.01	0.00	100.75
G4i9 Line 008	18EPe900	6.04	21.76	37.65	1.29	4.79	29.12	0.02	0.02	100.69
G4i9 Line 009	18EPe900	6.06	21.81	38.09	1.32	4.80	28.92	0.00	0.00	101.00
G4i9 Line 010	18EPe900	5.92	21.83	37.99	1.28	4.94	29.32	0.03	0.04	101.35
G4i9 Line 011	18EPe900	5.91	21.99	37.80	1.30	4.88	29.24	0.02	0.00	101.15
G4i9 Line 012	18EPe900	5.66	22.22	37.98	1.23	5.08	29.32	0.02	0.00	101.51
G4j25 Line 001	18MPe280	5.48	21.61	37.54	1.31	1.97	32.62	0.03	0.00	100.56
G4j25 Line 002	18MPe280	5.67	21.80	37.47	1.32	1.89	32.28	0.00	0.03	100.45
G4j25 Line 003	18MPe280	5.78	21.66	37.70	1.39	1.75	31.98	0.04	0.01	100.31
G4j25 Line 004	18MPe280	5.83	21.69	37.82	1.38	1.82	31.62	0.00	0.01	100.17
G4j25 Line 005	18MPe280	5.95	21.81	37.71	1.31	1.85	31.91	0.01	0.01	100.56
G4j25 Line 006	18MPe280	6.02	21.88	37.61	1.30	1.81	32.21	0.01	0.04	100.88
G4j25 Line 007	18MPe280	5.86	21.94	37.67	1.30	1.85	31.97	0.03	0.00	100.62
G4j25 Line 008	18MPe280	5.91	21.82	37.71	1.29	1.78	32.16	0.01	0.03	100.71
G4j25 Line 009	18MPe280	5.83	21.84	37.74	1.25	1.81	32.48	0.05	0.00	100.99
G4j25 Line 010	18MPe280	5.82	21.82	37.78	1.26	1.80	32.68	0.02	0.01	101.19
G4j25 Line 011	18MPe280	5.39	21.63	37.58	1.30	1.89	32.74	0.02	0.00	100.54
G4j25 Line 012	18MPe280	4.83	21.64	37.73	1.26	2.13	32.90	0.00	0.00	100.49
G4j36 Line 001	18MPe280	1.53	21.49	37.03	4.47	12.61	23.67	0.00	0.03	100.83
G4j36 Line 002	18MPe280	1.73	21.53	37.05	4.23	11.98	24.45	0.03	0.00	101.00
G4j36 Line 003	18MPe280	1.89	21.61	37.00	4.19	11.48	25.14	0.01	0.00	101.33
G4j36 Line 004	18MPe280	1.94	21.39	37.08	4.28	11.04	24.99	0.00	0.00	100.72
G4j36 Line 005	18MPe280	2.02	21.31	37.18	4.30	10.89	25.25	0.01	0.02	100.98
G4j36 Line 006	18MPe280	2.02	21.36	37.06	4.41	10.99	25.11	0.00	0.00	100.95
G4j36 Line 007	18MPe280	2.08	21.32	37.14	4.28	10.84	25.12	0.03	0.00	100.81
G4j36 Line 008	18MPe280	2.03	21.40	37.09	4.33	10.67	24.91	0.02	0.02	100.47
G4j36 Line 009	18MPe280	1.97	21.45	37.05	4.30	10.93	25.13	0.02	0.01	100.86
G4j36 Line 010	18MPe280	1.93	21.49	36.84	4.33	11.43	25.21	0.00	0.02	101.25
G4j36 Line 011	18MPe280	1.77	21.42	36.78	4.28	11.76	24.58	0.00	0.01	100.60
G4j36 Line 012	18MPe280	1.55	21.26	36.74	4.50	12.44	23.63	0.02	0.01	100.15

G3d22 Line 001	18MPe170	3.19	21.54	37.27	1.18	4.31	32.60	0.02	0.00	100.12
G3d22 Line 002	18MPe170	3.60	21.45	37.24	1.58	4.28	32.33	0.00	0.04	100.52
G3d22 Line 003	18MPe170	3.81	21.25	37.15	1.43	4.25	32.32	0.00	0.02	100.24
G3d22 Line 004	18MPe170	0.04	0.41	99.17	0.03	0.11	1.06	0.03	0.00	100.86
G3d22 Line 005	18MPe170	3.89	21.62	37.19	1.38	4.12	32.22	0.01	0.03	100.46
G3d22 Line 006	18MPe170	5.50	20.56	36.69	1.09	3.54	30.21	0.05	0.01	97.66
G3d22 Line 007	18MPe170	4.04	21.25	37.14	1.39	4.13	32.28	0.04	0.02	100.29
G3d22 Line 008	18MPe170	4.05	21.49	37.50	1.40	4.18	32.39	0.03	0.01	101.04
G3d22 Line 009	18MPe170	3.93	21.24	37.10	1.36	4.26	32.33	0.01	0.03	100.26
G3d22 Line 010	18MPe170	3.85	21.16	37.05	1.36	4.21	32.28	0.02	0.00	99.93
G3d22 Line 011	18MPe170	3.87	21.19	36.91	1.44	4.25	32.59	0.03	0.00	100.29
G3d22 Line 012	18MPe170	3.72	21.22	36.98	1.42	4.25	32.36	0.02	0.03	100.00
G3d19 Line 001	18MPe170	3.08	21.15	36.87	2.90	3.61	32.05	0.02	0.04	99.72
G3d19 Line 002	18MPe170	3.16	21.24	36.93	2.76	3.51	32.50	0.00	0.05	100.15
G3d19 Line 003	18MPe170	3.14	21.08	37.18	2.93	3.51	32.44	0.02	0.04	100.34
G3d19 Line 004	18MPe170	3.19	21.27	36.98	2.95	3.37	32.74	0.00	0.01	100.51
G3d19 Line 005	18MPe170	3.09	21.35	37.25	3.05	3.26	32.58	0.00	0.04	100.62
G3d19 Line 006	18MPe170	3.22	21.58	37.07	2.88	3.26	32.89	0.02	0.01	100.94
G3d19 Line 007	18MPe170	3.15	21.42	37.19	2.85	3.03	33.15	0.02	0.07	100.88
G3d19 Line 008	18MPe170	3.22	21.44	37.19	2.76	3.01	32.98	0.03	0.03	100.66
G3d19 Line 009	18MPe170	3.22	21.23	37.17	2.64	2.83	33.32	0.00	0.03	100.44
G3d19 Line 010	18MPe170	3.15	21.79	37.55	2.62	2.74	33.25	0.02	0.04	101.16
G3d19 Line 011	18MPe170	3.05	21.85	37.51	2.67	2.64	33.43	0.01	0.00	101.16
G3d19 Line 012	18MPe170	2.93	21.78	37.77	2.51	2.63	33.48	0.00	0.01	101.11
G3d13 Line 001	18MPe170	4.35	21.44	37.20	1.30	4.74	31.77	0.03	0.02	100.85
G3d13 Line 002	18MPe170	4.36	21.61	37.41	1.45	4.62	31.52	0.01	0.01	100.99
G3d13 Line 003	18MPe170	4.45	21.60	37.53	1.31	4.66	31.50	0.01	0.03	101.09
G3d13 Line 004	18MPe170	4.42	21.61	37.59	1.25	4.77	31.60	0.02	0.02	101.28
G3d13 Line 005	18MPe170	4.50	21.74	37.41	1.31	4.73	31.74	0.01	0.00	101.43
G3d13 Line 006	18MPe170	4.58	21.67	37.64	1.22	4.62	31.55	0.01	0.01	101.30

G3d13 Line 007	18MPe170	4.48	21.70	37.19	1.26	4.70	32.17	0.03	0.01	101.53
G3d13 Line 008	18MPe170	4.41	21.62	37.54	1.16	4.64	31.50	0.04	0.00	100.91
G3d13 Line 009	18MPe170	4.45	21.50	37.46	1.19	4.76	31.66	0.02	0.01	101.05
G3d13 Line 010	18MPe170	4.36	21.78	37.55	1.21	4.58	31.89	0.04	0.02	101.43
G3d13 Line 011	18MPe170	4.20	21.69	37.58	1.21	4.76	31.85	0.05	0.00	101.34
G3d13 Line 012	18MPe170	3.91	21.63	37.47	1.26	4.89	31.85	0.03	0.01	101.06
G3d6 Line 001	18MPe170	5.66	21.54	37.66	3.30	1.48	30.70	0.02	0.01	100.38
G3d6 Line 002	18MPe170	5.53	21.79	38.08	3.62	1.56	30.25	0.00	0.06	100.89
G3d6 Line 003	18MPe170	5.46	21.76	37.85	3.78	1.78	29.83	0.03	0.21	100.71
G3d6 Line 004	18MPe170	5.26	21.62	37.74	4.50	1.64	29.80	0.04	0.06	100.65
G3d6 Line 005	18MPe170	5.35	21.76	37.76	4.07	1.74	29.80	0.03	0.07	100.58
G3d6 Line 006	18MPe170	5.46	21.74	37.73	3.50	1.82	30.14	0.04	0.03	100.46
G3d6 Line 007	18MPe170	5.96	21.17	36.55	3.23	1.62	29.84	0.06	1.84	100.27
G3d6 Line 008	18MPe170	5.40	21.92	37.92	4.01	1.64	30.13	0.00	0.07	101.09
G3d6 Line 009	18MPe170	5.43	21.77	38.00	3.84	1.62	29.92	0.04	0.03	100.65
G3d6 Line 010	18MPe170	5.54	21.88	37.94	3.53	1.52	30.63	0.02	0.05	101.11
G3d6 Line 011	18MPe170	5.62	21.88	37.95	2.99	1.40	30.64	0.01	0.02	100.51
G3d6 Line 012	18MPe170	5.03	21.87	38.20	2.60	1.28	32.24	0.04	0.00	101.26
G1 c5 Line 001	18MPe118	5.63	21.96	38.34	5.42	2.56	27.17	0.01	0.02	101.11
G1 c5 Line 002	18MPe119	5.79	22.10	38.24	5.41	2.52	27.44	0.00	0.03	101.53
G1 c5 Line 003	18MPe119	5.74	21.90	38.27	5.72	2.41	27.13	0.00	0.04	101.21
G1 c5 Line 004	18MPe119	5.74	21.92	38.42	5.66	2.44	27.31	0.02	0.03	101.54
G1 c5 Line 005	18MPe119	5.87	21.90	38.27	5.61	2.41	27.04	0.00	0.01	101.11
G1 c5 Line 006	18MPe119	5.92	21.68	38.25	5.36	2.54	27.37	0.00	0.02	101.14
G1 c5 Line 007	18MPe119	5.84	21.99	38.23	5.22	2.55	27.35	0.00	0.01	101.19
G1 c5 Line 008	18MPe119	5.96	21.66	38.12	5.04	2.44	27.28	0.01	0.28	100.79
G1 c5 Line 009	18MPe119	5.89	21.62	38.17	5.02	2.61	27.47	0.00	0.06	100.84
G1 c5 Line 010	18MPe119	5.99	21.85	38.27	4.76	2.65	27.78	0.00	0.00	101.30
G1 c5 Line 011	18MPe119	6.03	21.62	38.25	5.10	2.59	27.48	0.02	0.05	101.14
G1 c5 Line 012	18MPe119	5.85	21.63	37.82	5.30	2.55	27.43	0.00	0.08	100.66

G1 c6 Line 001	18MPe119	1.72	20.95	36.80	0.77	9.69	31.05	0.00	0.04	101.02
G1 c6 Line 002	18MPe119	1.86	20.99	36.60	0.79	8.96	31.22	0.01	0.04	100.48
G1 c6 Line 003	18MPe119	1.96	20.85	36.64	0.88	8.76	31.48	0.01	0.03	100.61
G1 c6 Line 004	18MPe119	1.96	19.94	35.08	0.89	8.31	31.12	0.00	0.06	97.36
G1 c6 Line 005	18MPe119	2.04	20.91	36.77	0.86	8.66	31.66	0.04	0.09	101.04
G1 c6 Line 006	18MPe119	1.98	20.91	37.01	0.84	8.59	32.03	0.00	0.12	101.48
G1 c6 Line 007	18MPe119	1.23	11.91	47.96	0.64	6.32	23.04	0.00	0.01	91.12
G1 c6 Line 008	18MPe119	1.84	20.28	40.74	0.87	8.22	30.20	0.02	0.04	102.21
G1 c6 Line 009	18MPe119	1.98	20.88	36.62	0.88	8.56	31.25	0.01	0.00	100.19
G1 c6 Line 010	18MPe119	1.95	20.97	37.02	0.84	8.94	31.89	0.01	0.00	101.61
G1 c6 Line 011	18MPe119	1.87	20.98	36.85	0.80	8.90	31.34	0.00	0.06	100.80
G1 c6 Line 012	18MPe119	1.70	21.27	36.77	0.76	9.67	30.57	0.00	0.05	100.79
G1 c7 Line 001	18MPe119	5.03	21.63	37.74	1.81	1.66	33.10	0.05	0.03	101.05
G1 c7 Line 002	18MPe119	5.05	21.70	37.58	1.78	1.70	33.12	0.04	0.04	101.01
G1 c7 Line 003	18MPe119	4.96	21.71	37.74	1.74	1.79	33.06	0.02	0.01	101.02
G1 c7 Line 004	18MPe119	4.90	21.64	37.56	1.82	1.81	33.01	0.04	0.01	100.79
G1 c7 Line 005	18MPe119	7.49	6.27	42.13	0.14	0.38	23.14	0.03	17.76	97.35
G1 c7 Line 006	18MPe119	4.75	21.55	37.64	1.81	2.10	32.81	0.01	0.03	100.70
G1 c7 Line 007	18MPe119	4.52	21.55	37.59	2.17	2.27	32.78	0.02	0.03	100.93
G1 c7 Line 008	18MPe119	4.46	21.61	37.64	2.07	2.41	32.90	0.00	0.07	101.16
G1 c7 Line 009	18MPe119	4.19	21.37	37.55	1.91	2.84	32.92	0.02	0.00	100.80
G1 c7 Line 010	18MPe119	3.93	21.61	37.39	2.00	3.35	32.81	0.01	0.05	101.15
G1 c7 Line 011	18MPe119	3.60	21.48	37.29	2.03	4.19	32.69	0.03	0.01	101.33
G1 c7 Line 012	18MPe119	2.93	21.43	37.15	1.98	5.48	32.21	0.01	0.01	101.20
G1 c13 Line 001	18MPe119	1.13	25.79	31.11	0.08	18.89	19.88	0.00	0.07	96.96
G1 c13 Line 002	18MPe119	1.01	22.77	34.07	0.08	20.27	20.73	0.00	0.13	99.06
G1 c13 Line 003	18MPe119	0.81	20.92	35.97	0.12	21.55	21.08	0.01	0.08	100.54
G1 c13 Line 004	18MPe119	0.79	20.81	36.05	0.08	21.49	21.23	0.03	0.11	100.60
G1 c13 Line 005	18MPe119	0.56	20.74	35.88	0.08	22.10	20.84	0.00	0.10	100.30
G1 c13 Line 006	18MPe119	0.32	20.66	35.52	0.08	23.95	19.91	0.00	0.13	100.56

G1 c13 Line 007	18MPe119	0.32	20.66	35.68	0.09	24.30	19.54	0.05	0.10	100.74
G1 c13 Line 008	18MPe119	0.22	20.72	35.43	0.09	24.73	19.28	0.00	0.10	100.58
G1 c13 Line 009	18MPe119	0.26	20.75	35.62	0.07	24.49	19.19	0.01	0.13	100.53
G1 c13 Line 010	18MPe119	0.56	20.70	35.51	0.08	22.67	20.72	0.00	0.10	100.33
G1 c13 Line 011	18MPe119	0.93	20.67	35.77	0.10	21.79	20.72	0.00	0.12	100.09
G1 c13 Line 012	18MPe119	1.00	20.64	36.19	0.07	22.20	20.26	0.00	0.06	100.42
G1 d6 Line 001	17Mi604	2.87	21.52	37.14	3.09	7.75	28.60	0.03	0.00	101.00
G1 d6 Line 002	17Mi604	3.11	21.33	37.23	3.10	7.57	28.22	0.03	0.00	100.59
G1 d6 Line 003	17Mi604	3.15	21.48	37.39	3.15	7.59	28.03	0.02	0.02	100.83
G1 d6 Line 004	17Mi604	3.18	21.53	37.28	3.38	7.61	28.05	0.03	0.01	101.07
G1 d6 Line 005	17Mi604	3.17	21.55	37.53	3.64	7.31	27.86	0.04	0.01	101.11
G1 d6 Line 006	17Mi604	3.11	21.31	37.58	3.79	7.50	27.14	0.05	0.00	100.48
G1 d6 Line 007	17Mi604	3.06	21.36	37.20	3.87	7.50	27.84	0.04	0.00	100.87
G1 d6 Line 008	17Mi604	3.11	21.37	37.36	3.67	7.44	27.58	0.02	0.02	100.57
G1 d6 Line 009	17Mi604	3.12	21.37	37.36	3.48	7.40	27.91	0.04	0.00	100.68
G1 d6 Line 010	17Mi604	3.17	21.40	37.07	3.38	7.49	28.21	0.03	0.02	100.77
G1 d6 Line 011	17Mi604	3.17	21.40	37.30	3.16	7.57	28.15	0.04	0.01	100.80
G1 d6 Line 012	17Mi604	3.08	21.19	36.91	2.95	7.73	28.42	0.03	0.00	100.32
G1 d11 Line 001	17Mi604	3.31	21.51	37.07	1.80	6.90	30.19	0.00	0.01	100.79
G1 d11 Line 002	17Mi604	3.32	21.41	37.21	1.79	6.81	30.32	0.02	0.00	100.88
G1 d11 Line 003	17Mi604	0.00	0.06	100.83	0.02	0.12	0.79	0.00	0.01	101.83
G1 d11 Line 004	17Mi604	3.38	21.10	38.26	1.74	6.60	30.13	0.01	0.00	101.22
G1 d11 Line 005	17Mi604	3.39	21.48	37.33	1.76	6.86	30.22	0.03	0.03	101.10
G1 d11 Line 006	17Mi604	3.41	21.59	37.29	1.70	6.65	30.08	0.02	0.01	100.75
G1 d11 Line 007	17Mi604	3.27	21.46	37.14	1.71	6.92	29.61	0.00	0.00	100.11
G1 d11 Line 008	17Mi604	3.05	21.66	37.40	1.69	7.28	30.28	0.03	0.02	101.40
G1 d11 Line 009	17Mi604	3.19	21.47	37.47	1.73	7.06	30.06	0.00	0.00	100.98
G1 d11 Line 010	17Mi604	3.27	21.55	37.46	1.76	6.81	30.11	0.00	0.00	100.96
G1 d11 Line 011	17Mi604	3.22	21.58	37.40	1.69	6.97	30.47	0.00	0.02	101.36
G1 d11 Line 012	17Mi604	3.23	22.03	37.96	1.55	6.94	30.66	0.01	0.00	102.38

G1 d30 Line 001	17Mi604	1.93	21.41	36.87	1.59	9.88	29.14	0.03	0.01	100.87
G1 d30 Line 002	17Mi604	1.95	21.56	36.96	1.63	10.46	29.06	0.03	0.03	101.68
G1 d30 Line 003	17Mi604	1.93	21.31	36.94	1.65	10.52	28.91	0.02	0.01	101.30
G1 d30 Line 004	17Mi604	1.87	21.17	36.93	1.70	10.65	28.74	0.01	0.04	101.10
G1 d30 Line 005	17Mi604	1.93	21.52	37.04	1.75	10.68	28.53	0.01	0.04	101.50
G1 d30 Line 006	17Mi604	1.86	21.60	36.81	1.73	10.69	28.55	0.01	0.09	101.34
G1 d30 Line 007	17Mi604	1.91	21.32	36.89	1.69	10.81	28.76	0.00	0.05	101.43
G1 d30 Line 008	17Mi604	1.88	21.52	37.05	1.64	10.75	28.44	0.03	0.05	101.35
G1 d30 Line 009	17Mi604	1.86	21.30	36.87	1.64	10.82	28.36	0.00	0.05	100.90
G1 d30 Line 010	17Mi604	1.96	21.48	37.03	1.59	10.65	28.71	0.00	0.01	101.43
G1 d30 Line 011	17Mi604	1.89	21.30	36.98	1.61	10.48	28.94	0.01	0.00	101.22
G1 d30 Line 012	17Mi604	1.88	21.35	37.04	1.71	10.13	29.42	0.00	0.02	101.55
G1 d40 Line 001	17Mi604	3.37	21.43	37.31	1.50	9.76	27.94	0.05	0.02	101.37
G1 d40 Line 002	17Mi604	3.47	21.61	37.29	1.48	9.53	28.07	0.03	0.00	101.48
G1 d40 Line 003	17Mi604	3.47	21.56	37.23	1.57	9.55	27.94	0.04	0.00	101.36
G1 d40 Line 004	17Mi604	3.58	21.47	37.12	1.55	9.33	28.08	0.05	0.01	101.20
G1 d40 Line 005	17Mi604	3.44	21.64	37.30	1.66	9.42	27.77	0.05	0.02	101.29
G1 d40 Line 006	17Mi604	3.54	21.54	37.19	1.53	9.43	28.20	0.04	0.03	101.50
G1 d40 Line 007	17Mi604	3.49	21.55	37.42	1.59	9.30	27.94	0.01	0.01	101.31
G1 d40 Line 008	17Mi604	3.51	21.46	37.44	1.64	9.15	28.15	0.04	0.00	101.39
G1 d40 Line 009	17Mi604	3.59	21.43	37.43	1.51	9.22	28.09	0.02	0.00	101.29
G1 d40 Line 010	17Mi604	3.55	21.55	37.47	1.49	9.51	28.25	0.03	0.00	101.85
G1 d40 Line 011	17Mi604	3.33	21.67	37.31	1.54	9.76	27.69	0.07	0.00	101.38
G1 d40 Line 012	17Mi604	3.06	21.54	37.35	1.65	10.61	27.34	0.03	0.02	101.60
G1 d50 Line 001	17Mi604	2.92	21.39	37.07	1.57	8.11	29.93	0.02	0.00	101.01
G1 d50 Line 002	17Mi604	3.00	21.61	37.09	1.55	7.99	29.78	0.00	0.05	101.07
G1 d50 Line 003	17Mi604	3.08	21.42	37.16	1.55	8.38	29.52	0.02	0.00	101.13
G1 d50 Line 004	17Mi604	3.11	21.34	37.29	1.60	8.19	29.56	0.01	0.01	101.11
G1 d50 Line 005	17Mi604	3.15	21.57	37.15	1.61	8.19	29.78	0.01	0.00	101.46
G1 d50 Line 006	17Mi604	3.13	21.34	37.10	1.56	8.16	29.68	0.01	0.01	100.99

G1 d50 Line 007	17Mi604	3.09	21.50	37.05	1.62	8.00	29.83	0.02	0.02	101.12
G1 d50 Line 008	17Mi604	3.08	21.43	37.08	1.53	8.29	29.82	0.00	0.00	101.23
G1 d50 Line 009	17Mi604	3.06	21.63	37.07	1.54	8.18	29.55	0.04	0.02	101.08
G1 d50 Line 010	17Mi604	3.02	21.47	37.18	1.63	8.19	29.97	0.03	0.01	101.50
G1 d50 Line 011	17Mi604	3.06	21.39	37.17	1.58	8.05	29.89	0.01	0.03	101.17
G1 d50 Line 012	17Mi604	2.85	21.31	37.14	1.53	8.16	29.79	0.02	0.02	100.82

8.1.3 Appendix E: Results of Ar-Ar dating of amphiboles and mica

Sample: 18MPe250
Project: Alaska
Owner: Bahlburg

Exp-Nr: 8827
Material: 1.00 mg Bt

Irradiation: FGA023P4H7 (End date: 2016-05-19 12:33:00)
Measurement: 2016-08-17 16:58:24
Device: CO2-Laser
Air: 298.6
J-Value: 0.0043380 f-value: 0.998981
J-Value Error: 0.0000110 f-value Error: 0.000177
Reference Standard(s):

Interfering isotope production ratios:
ca3637 = 0.000227 +/- 0.000002
ca3937 = 0.000602 +/- 0.000006
k3839 = 0.01211 +/- 0.00061
k4039 = 0.00183 +/- 0.00009

Decay constants:
lambda40 = 5.5492e-010 +/- 9.3000e-013 1/a
lambda39 = 0.002577 +/- 0.000026 1/a
lambda37 = 7.2438 +/- 0.0214 1/a

ALF ARGONLAB FREIBERG

Fit model: automatic **All errors are 1s!**

Nr.	Step	39Ar(K) (V)	39Ar(K) (%)	39Ar (10e-14 mol)	40Ar* (V)	36Ar_atm (V)	40Ar* (%)	40Ar/36Ar	37Ar/36Ar	37Ar/39Ar	K/Ca	K/Ca Error	40Ar*/39Ar(K)	40Ar*/39Ar(K) Error	Age (Ma)	Age Error(Ma)
1	13.2%	0.7486	100.0	25.24	1.713	0.0193	22.9	387.5	0.17	0.004	19.507	0.349	2.29	0.03	**17.80**	**0.21**

J - value = #BEZUG!
J-error [%] = #BEZUG!

Age spectra data

Nr.	39Ar%	Age (Ma)	Age_err (Ma)
1	100.0	17.80	0.21

Isochron Data

39/36	err	40/36	err
38.867	0.135	387.52	1.34

Inverse Isochron Data

39/40	err	36/40	err
0.000000	0.000010	0.003384	0.000010
0.100298	0.000050	0.002581	0.000009

Blank intercepts:

exp.#	Step	36Ar (V)	±σ36 (V)	37Ar (V)	±σ37 (V)	38Ar (V)	±σ38 (V)	39Ar (V)	±σ39 (V)	40Ar (V)	±σ40 (V)
8824	0.0%	-0.00464	0.00004	-0.00223	0.00004	-0.00247	0.00004	0.02645	0.00003	-0.00455	0.00014

Blank corrected intensity intercepts:

Nr.	Step	36Ar (V)	±σ36 (V)	37Ar (V)	±σ37 (V)	38Ar (V)	±σ38 (V)	39Ar (V)	±σ39 (V)	40Ar (V)	±σ40 (V)
1	13.2%	0.01919	0.00006	0.00332	0.00006	0.01247	0.00006	0.74738	0.00031	7.46519	0.00159

Sample: 18EPe939
Project: Alaska
Owner: Bahlburg

Exp-Nr: 8832
Material: 1.00 mg Bt

Irradiation: FGA023P4H18 (End date: 2016-05-19 12:33:00)
Measurement: 2016-08-17 21:15:45
Device: CO2-Laser
Air: 298.6
J-Value: 0.0043380 f-value: 0.998977
J-Value Erro 0.0000110 f-value Error: 0.000181
Reference Standard(s):

Interfering isotope production ratios:
ca3637 = 0.000227 +/- 0.000002
ca3937 = 0.000602 +/- 0.000006
k3839 = 0.01211 +/- 0.00061
k4039 = 0.00183 +/- 0.00009

Decay constants:
lambda40 = 5.5492e-010 +/- 9.3000e-013 1/a
lambda39 = 0.002577 +/- 0.000026 1/a
lambda37 = 7.2438 +/- 0.0214 1/a

Fit model: automatic All errors are 1s!

Nr.	Step	39Ar(K) (V)	39Ar(K) (%)	39Ar (10e-14 mol)	40Ar* (V)	36Ar_atm (V)	40Ar* (%)	40Ar/36Ar	37Ar/36Ar	37Ar/39Ar	K/Ca	K/Ca Error	40Ar*/39Ar(K)	40Ar*/39Ar(K) Error	Age (Ma)	Age Error(Ma)
1	13.8%	0.0307	100.0	1.04	0.174	0.0003	66.1	880.1	0.29	0.003	30.779	29.609	5.68	0.69	43.8	5.3

J - value = #BEZUG!
J-error [%] = #BEZUG!

Age spectra data

Nr.	39Ar%	Age (Ma)	Age_err (Ma)
1	100.0	43.85	5.28

Isochron Data

39/36	err	40/36	err
102.510	24.305	880.63	208.81

Inverse Isochron Data

39/40	err	36/40	err
0.116405	0.000552	0.001136	0.000269
0.000000	0.000010	0.003384	0.000010

Blank intercepts:

exp.#	Step	36Ar (V)	±σ36 (V)	37Ar (V)	±σ37 (V)	38Ar (V)	±σ38 (V)	39Ar (V)	±σ39 (V)	40Ar (V)	±σ40 (V)
8830	0.0%	-0.00467	0.00005	-0.00226	0.00007	-0.00255	0.00004	0.02647	0.00006	-0.00433	0.00014

Blank corrected intensity intercepts:

Nr.	Step	36Ar (V)	±σ36 (V)	37Ar (V)	±σ37 (V)	38Ar (V)	±σ38 (V)	39Ar (V)	±σ39 (V)	40Ar (V)	±σ40 (V)
1	13.8%	0.00030	0.00007	0.00009	0.00008	0.00061	0.00006	0.03066	0.00009	0.26387	0.00095

Sample: 18MPe37

Project: Alaska
Owner: Bahlburg

Exp-Nr: 8835
Material: 1.00 mg Hbl

Irradiation: FGA023P4H1 (End date: 2016-05-19 12:33:00)
Measurement 2016-08-18 13:30:01
Device: CO2-Laser
Air: 298.6
J-Value: 0.0043380 f-value: 0.998958
J-Value Erro 0.0000110 f-value Error: 0.000200
Reference Standard(s):

Interfering isotope production ratios:

ca3637 = 0.000227 +/- 0.000002
ca3937 = 0.000602 +/- 0.000006
k3839 = 0.01211 +/- 0.00061
k4039 = 0.00183 +/- 0.00009

Decay constants:

lambda40 = 5.5492e-010 +/- 9.3000e-013 1/a
lambda39 = 0.002577 +/- 0.000026 1/a
lambda37 = 7.2438 +/- 0.0214 1/a

Fit model: automatic **All errors are 1s!**

Nr.	Step	39Ar(K) (V)	39Ar(K) (%)	39Ar (10e-14 mol)	40Ar* (V)	36Ar_atm (V)	40Ar* (%)	40Ar/36Ar	37Ar/36Ar	37Ar/39Ar	K/Ca	K/Ca Error	40Ar*/39Ar(K)	40Ar*/39Ar(K) Error	Age (Ma)	Age Error(Ma)
1	14.1%	0.0043	5.6	0.15	0.040	0.0003	29.0	360.0	103.73	8.979	0.009	0.000	9.33	7.47	*71.48*	*56.09*
2	14.2%	0.0017	2.2	0.06	-0.005	0.0001	-34.9	173.1	157.95	6.820	0.012	0.001	-2.67	12.61	*-20.99*	*99.76*
3	14.3%	0.0048	6.1	0.16	0.019	0.0002	23.4	327.5	115.36	5.804	0.014	0.000	3.93	3.96	*30.47*	*30.47*
4	14.4%	0.0047	6.1	0.16	0.001	0.0001	4.8	192.9	278.27	7.871	0.011	0.000	0.27	4.10	*2.10*	*31.99*
5	14.5%	0.0046	5.9	0.15	0.057	0.0002	47.4	511.0	71.84	3.662	0.023	0.000	12.50	4.44	*95.14*	*32.90*
6	14.6%	0.0577	74.1	1.95	0.275	0.0002	83.5	1532.9	112.22	0.417	0.205	0.001	4.76	0.34	36.8	2.6

J - value = #BEZUG!
J-error [%] = #BEZUG!

Age spectra data

Nr.	39Ar%	Age (Ma)	Age_err (Ma)
1	5.6	71.48	56.09
2	2.2	-20.99	99.76
3	6.1	30.47	30.47
4	6.1	2.10	31.99
5	5.9	95.14	32.90
6	74.1	36.82	2.59

Isochron Data

39/36	err	40/36	err
13.054	4.277	420.36	137.05
28.917	35.332	221.40	270.54
23.162	7.123	389.65	119.74
55.865	42.750	313.61	240.33
21.508	6.869	567.39	181.03
318.804	114.958	1815.63	654.72

Inverse Isochron Data

39/40	err	36/40	err
0.000000	0.000010	0.003384	0.000010
0.031054	0.001037	0.002379	0.000776
0.130612	0.009315	0.004517	0.005519
0.059442	0.001154	0.002566	0.000789
0.178131	0.008366	0.003189	0.002444
0.037907	0.000657	0.001762	0.000562
0.175588	0.000608	0.000551	0.000199

Blank intercepts:

exp.#	Step	36Ar (V)	±σ36 (V)	37Ar (V)	±σ37 (V)	38Ar (V)	±σ38 (V)	39Ar (V)	±σ39 (V)	40Ar (V)	±σ40 (V)
8833	0.0%	-0.00462	0.00005	-0.00227	0.00005	-0.00251	0.00004	0.02646	0.00005	-0.00431	0.00016

Blank corrected intensity intercepts:

Nr.	Step	36Ar (V)	±σ36 (V)	37Ar (V)	±σ37 (V)	38Ar (V)	±σ38 (V)	39Ar (V)	±σ39 (V)	40Ar (V)	±σ40 (V)
1	14.1%	0.00039	0.00011	0.04005	0.00012	0.00023	0.00009	0.00447	0.00014	0.13944	0.00091
2	14.2%	0.00008	0.00007	0.01192	0.00008	0.00007	0.00006	0.00175	0.00008	0.01310	0.00068
3	14.3%	0.00024	0.00006	0.02827	0.00007	0.00017	0.00006	0.00488	0.00008	0.08050	0.00083
4	14.4%	0.00014	0.00006	0.03819	0.00008	0.00018	0.00006	0.00486	0.00008	0.02656	0.00117
5	14.5%	0.00024	0.00007	0.01695	0.00007	0.00018	0.00006	0.00464	0.00007	0.12097	0.00091
6	14.6%	0.00021	0.00007	0.02400	0.00007	0.00097	0.00006	0.05772	0.00009	0.32887	0.00102

Sample: 18EPe941
Project: Alaska
Owner: Bahlburg

Exp-Nr: 8839
Material: 1.00 mg Hbl

Irradiation: FGA023P4H49 (End date: 2016-05-19 12:33:00)
Measurement: 2016-08-18 21:17:56
Device: CO2-Laser
Air: 298,6
J-Value: 0.0043380 f-value: 0.998950
J-Value Erro 0.0000110 f-value Error: 0.000210
Reference Standard(s):

Interfering isotope production ratios:
ca3637 = 0.000227 +/- 0.000002
ca3937 = 0.000602 +/- 0.000006
k3839 = 0.01211 +/- 0.00061
k4039 = 0.00183 +/- 0.00009

Decay constants:
lambda40 = 5.5492e-010 +/- 9.3000e-013 1/a
lambda39 = 0.002577 +/- 0.000026 1/a
lambda37 = 7.2438 +/- 0.0214 1/a

Fit model: automatic **All errors are 1s!**

Nr.	Step	39Ar(K) (V)	39Ar(K) (%)	39Ar (10e-14 mol)	40Ar* (V)	36Ar_atm (V)	40Ar* (%)	40Ar/36Ar	37Ar/36Ar	37Ar/39Ar	K/Ca	K/Ca Error	40Ar*/39Ar(K)	40Ar*/39Ar(K) Error	Age (Ma)	Age Error(Ma)
1	15.1%	0.0079	48.5	0.27	0.152	0.0002	74.0	839.6	193.55	5.843	0.014	0.000	19.16	2.79	**143.9**	**20.2**
2	15.2%	0.0084	51.5	0.28	0.149	0.0001	80.4	1128.8	184.55	3.557	0.024	0.000	17.70	2.41	**133.3**	**17.5**

J - value = #BEZUG!
J-error [%] = #BEZUG!

Age spectra data

Nr.	39Ar%	Age (Ma)	Age_err (Ma)
1	48.5	143.91	20.16
2	51.5	133.34	17.51

Isochron Data

39/36	err	40/36	err
44.432	18.322	1150.08	474.10
69.033	38.101	1520.72	839.34

Inverse Isochron Data

39/40	err	36/40	err
0.000000	0.000010	0.003384	0.000010
0.038634	0.000639	0.000870	0.000358
0.045395	0.000768	0.000658	0.000363

Blank intercepts:

exp.#	Step	36Ar (V)	$\pm\sigma_{36}$ (V)	37Ar (V)	$\pm\sigma_{37}$ (V)	38Ar (V)	$\pm\sigma_{38}$ (V)	39Ar (V)	$\pm\sigma_{39}$ (V)	40Ar (V)	$\pm\sigma_{40}$ (V)
8838	0.0%	-0.00459	0.00005	-0.00216	0.00006	-0.00247	0.00006	0.02658	0.00006	-0.00371	0.00024

Blank corrected intensity intercepts:

Nr.	Step	36Ar (V)	$\pm\sigma_{36}$ (V)	37Ar (V)	$\pm\sigma_{37}$ (V)	38Ar (V)	$\pm\sigma_{38}$ (V)	39Ar (V)	$\pm\sigma_{39}$ (V)	40Ar (V)	$\pm\sigma_{40}$ (V)
1	15.1%	0.00024	0.00007	0.04710	0.00010	0.00092	0.00008	0.00808	0.00011	0.20493	0.00189
2	15.2%	0.00016	0.00007	0.03019	0.00009	0.00090	0.00007	0.00851	0.00010	0.18523	0.00222

Sample: 17Pe87
Project: Alaska
Owner: Bahlburg

Exp-Nr: 8841
Material: 1.00 mg Hbl

Irradiation: FGA023P4H51 (End date: 2016-05-19 12:33:00)
Measurement: 2016-08-18 22:40:46
Device: CO2-Laser
Air: 298.6
J-Value: 0.0043380 f-value: 0.998948
J-Value Erro 0.0000110 f-value Error: 0.000211
Reference Standard(s):

Interfering isotope production ratios:
ca3637 = 0.000227 +/- 0.000002
ca3937 = 0.000602 +/- 0.000006
k3839 = 0.01211 +/- 0.00061
k4039 = 0.00183 +/- 0.00009

Decay constants:
lambda40 = 5.5492e-010 +/- 9.3000e-013 1/a
lambda39 = 0.002577 +/- 0.000026 1/a
lambda37 = 7.2438 +/- 0.0214 1/a

Fit model: automatic **All errors are 1s!**

Nr.	Step	39Ar(K) (V)	39Ar(K) (%)	39Ar (10e-14 mol)	40Ar* (V)	36Ar_atm (V)	40Ar* (%)	40Ar/36Ar	37Ar/36Ar	37Ar/39Ar	K/Ca	K/Ca Error	40Ar*/39Ar(K)	40Ar*/39Ar(K) Error	Age (Ma)	Age Error(Ma)
1	15.4%	0.0101	100.0	0.34	0.196	0.0003	72.2	941.3	88.80	2.524	0.033	0.000	19.50	2.47	**146.3**	**17.8**

J - value = #BEZUG!
J-error [%] = #BEZUG!

Age spectra data

Nr.	39Ar%	Age (Ma)	Age_err (Ma)
1	100.0	146.32	17.83

Isochron Data

39/36	err	40/36	err
39.859	13.090	1075.80	353.19

Inverse Isochron Data

39/40	err	36/40	err
0.000000	0.000010	0.003384	0.000010
0.037050	0.000443	0.000930	0.000305

Blank intercepts:

exp.#	Step	36Ar (V)	±σ36 (V)	37Ar (V)	±σ37 (V)	38Ar (V)	±σ38 (V)	39Ar (V)	±σ39 (V)	40Ar (V)	±σ40 (V)
8838	0.0%	-0.00459	0.00005	-0.00216	0.00006	-0.00247	0.00006	0.02658	0.00006	-0.00371	0.00024

Blank corrected intensity intercepts:

Nr.	Step	36Ar (V)	±σ36 (V)	37Ar (V)	±σ37 (V)	38Ar (V)	±σ38 (V)	39Ar (V)	±σ39 (V)	40Ar (V)	±σ40 (V)
1	15.4%	0.00029	0.00008	0.02554	0.00011	0.00210	0.00008	0.01014	0.00010	0.27164	0.00162

Sample: 18MPe37
Project: Alaska
Owner: Bahlburg

Exp-Nr: 8844
Material: 1.00 mg Bt

Irradiation: FGA023P4H57 (End date: 2016-05-19 12:33:00)
Measurement 2016-08-19 00:47:35
Device: CO2-Laser
Air: 298.6
J-Value: 0.0043380 f-value: 0.998946
J-Value Erro 0.0000110 f-value Error: 0.000214
Reference Standard(s):

Interfering isotope production ratios:
ca3637 = 0.000227 +/- 0.000002
ca3937 = 0.000602 +/- 0.000006
k3839 = 0.01211 +/- 0.00061
k4039 = 0.00183 +/- 0.00009

Decay constants:
lambda40 = 5.5492e-010 +/- 9.3000e-013 1/a
lambda39 = 0.002577 +/- 0.000026 1/a
lambda37 = 7.2438 +/- 0.0214 1/a

Fit model: automatic **All errors are 1s!**

Nr.	Step	39Ar(K) (V)	39Ar(K) (%)	39Ar (10e-14 mol)	40Ar* (V)	36Ar_atm (V)	40Ar* (%)	40Ar/36Ar	37Ar/36Ar	37Ar/39Ar	K/Ca	K/Ca Error	40Ar*/39Ar(K)	40Ar*/39Ar(K) Error	Age (Ma)	Age Error(Ma)
1	15.8%	0.0212	100.0	0.71	0.150	0.0001	78.4	1386.1	0.00	0.000	Inf	Inf	7.07	1.31	**54.46**	**9.91**

J - value = #BEZUG!
J-error [%] = #BEZUG!

Age spectra data

Nr.	39Ar%	Age (Ma)	Age_err (Ma)
1	100.0	54.46	9.91

Isochron Data

39/36	err	40/36	err
153.796	103.420	1386.38	932.25

Inverse Isochron Data

39/40	err	36/40	err
0.000000	0.000010	0.003384	0.000010
0.110934	0.000547	0.000721	0.000485

Blank intercepts:

exp.#	Step	36Ar (V)	±σ36 (V)	37Ar (V)	±σ37 (V)	38Ar (V)	±σ38 (V)	39Ar (V)	±σ39 (V)	40Ar (V)	±σ40 (V)
8838	0.0%	-0.00459	0.00005	-0.00216	0.00006	-0.00247	0.00006	0.02658	0.00006	-0.00371	0.00024

Blank corrected intensity intercepts:

Nr.	Step	36Ar (V)	±σ36 (V)	37Ar (V)	±σ37 (V)	38Ar (V)	±σ38 (V)	39Ar (V)	±σ39 (V)	40Ar (V)	±σ40 (V)
1	15.8%	0.00014	0.00009	0.00000	0.00010	0.00029	0.00009	0.02115	0.00009	0.19101	0.00040

Single grain furnace step heating experiment of a large hornblende mineral (7.3 mg)

Sample: **18MPe37**
Project: Alaska
Owner: Bahlburg

Exp-Nr: **8809**
Material: 7.26 mg Hbl

Irradiation: FGA023P8H2 (End date: 2016-05-19 12:33:00)
Measurement 2016-08-11 14:22:04
Device: HTC
Air: 298.6 +/- 0.3
J-Value: **0.0043785** f-value: 0.999067
J-Value Erro 0.0000091 f-value Error: 0.000171
Reference Standard: DRF1 - 25.682 +/- 0.030 Ma
Total gas age: 48.76 Ma

Interfering isotope production ratios:
ca3637 = 0.000227 +/- 0.000002
ca3937 = 0.000602 +/- 0.000006
k3839 = 0.01211 +/- 0.00061
k4039 = 0.00183 +/- 0.00009

Decay constants:
lambda40 = 5.5492e-010 +/- 9.3000e-013 1/a
lambda39 = 0.002577 +/- 0.000026 1/a
lambda37 = 7.2438 +/- 0.0214 1/a

Fit model: automatic **All errors are 1s!**

Nr.	Step	39Ar(K) (V)	39Ar(K) (%)	39Ar (10e-14 mol)	40Ar* (V)	36Ar_atm (V)	40Ar* (%)	40Ar/36Ar	37Ar/36Ar	37Ar/39Ar	K/Ca	K/Ca Error	40Ar*/39Ar(K)	40Ar*/39Ar(K) Error	Age (Ma)	Age Error(Ma)
1	661°C	0.0016	0.5	0.05	0.040	0.0056	2.3	305.6	0.38	1.329	0.073	0.003	24.89	9.12	186.39	64.92
2	839°C	0.0127	4.2	0.43	0.079	0.0011	19.9	369.5	7.67	0.643	0.152	0.002	6.19	1.28	48.22	9.84
3	954°C	0.0702	23.5	2.37	0.399	0.0011	55.1	613.3	64.77	1.088	0.090	0.000	5.69	0.24	44.36	1.82
4	999°C	0.0471	15.8	1.59	0.274	0.0003	77.4	868.2	285.01	2.449	0.040	0.000	5.81	0.32	45.31	2.48
5	1032°C	0.0279	9.3	0.94	0.167	0.0001	84.7	1167.8	334.76	2.006	0.049	0.000	5.96	0.59	46.45	4.55
6	1109°C	0.0925	30.9	3.12	0.612	0.0003	87.2	1096.2	439.60	3.014	0.032	0.000	6.61	0.15	51.44	1.18
7	1147°C	0.0086	2.9	0.29	0.049	0.0001	65.0	634.3	213.50	2.939	0.033	0.000	5.73	1.55	44.64	11.91
8	1228°C	0.0384	12.8	1.30	0.255	0.0007	56.1	549.6	159.37	3.395	0.029	0.000	6.64	0.41	51.62	3.18

J - value = #BEZUG!
J-error [%] = #BEZUG!

Age spectra data

Nr.	39Ar%	Age (Ma)	Age_err (Ma)
1	0.5	186.39	64.92
2	**4.2**	**48.22**	**9.84**
3	**23.5**	**44.36**	**1.82**
4	**15.8**	**45.31**	**2.48**
5	**9.3**	**46.45**	**4.55**
6	**30.9**	**51.44**	**1.18**
7	**2.9**	**44.64**	**11.91**
8	**12.8**	**51.62**	**3.18**

Isochron Data

Nr.	39/36	err	40/36	err
1	0.287	0.010	305.73	2.65
2	12.013	0.621	373.00	19.20
3	64.402	3.272	665.15	33.79
4	176.019	33.328	1322.12	250.33
5	278.251	153.446	1957.85	1079.68
6	307.709	48.379	2333.45	366.87
7	96.976	48.706	854.11	428.95
8	57.505	4.581	680.23	54.17

Inverse Isochron Data

Nr.	39/40	err	36/40	err
	0.000000	0.000010	0.003384	0.000010
1	0.000937	0.000030	0.003271	0.000028
2	0.032206	0.000155	0.002681	0.000138
3	0.096823	0.000125	0.001503	0.000076
4	0.133134	0.000211	0.000756	0.000143
5	0.142121	0.000380	0.000511	0.000282
6	0.131869	0.000125	0.000429	0.000067
7	0.113540	0.000749	0.001171	0.000588
8	0.084537	0.000165	0.001470	0.000117

Blank intercepts:

exp.#	Step	36Ar (V)	±σ36 (V)	37Ar (V)	±σ37 (V)	38Ar (V)	±σ38 (V)	39Ar (V)	±σ39 (V)	40Ar (V)	±σ40 (V)
8808	(1280°C)	-0.00458	0.00004	-0.00223	0.00005	-0.00250	0.00004	0.02638	0.00005	-0.00003	0.00014
8807	(1010°C)	-0.00465	0.00005	-0.00225	0.00005	-0.00252	0.00005	0.02643	0.00005	-0.00311	0.00014
8806	(721°C)	-0.00466	0.00004	-0.00226	0.00004	-0.00253	0.00004	0.02639	0.00005	-0.00368	0.00015

Blank corrected intensity intercepts:

Nr.	Step	36Ar (V)	±σ36 (V)	37Ar (V)	±σ37 (V)	38Ar (V)	±σ38 (V)	39Ar (V)	±σ39 (V)	40Ar (V)	±σ40 (V)
1	661°C	0.00556	0.00005	0.00213	0.00006	0.00136	0.00005	0.00160	0.00005	1.70470	0.00030
2	839°C	0.00106	0.00005	0.00814	0.00007	0.00053	0.00006	0.01268	0.00006	0.39365	0.00017
3	954°C	0.00118	0.00006	0.07635	0.00009	0.00116	0.00005	0.07032	0.00009	0.72494	0.00019
4	999°C	0.00041	0.00005	0.11588	0.00009	0.00065	0.00004	0.04741	0.00007	0.35396	0.00015
5	1032°C	0.00017	0.00006	0.05621	0.00008	0.00054	0.00005	0.02808	0.00007	0.19664	0.00017
6	1109°C	0.00064	0.00005	0.28059	0.00012	0.00370	0.00005	0.09326	0.00008	0.70163	0.00021
7	1147°C	0.00012	0.00004	0.02540	0.00007	0.00024	0.00005	0.00866	0.00005	0.07567	0.00018
8	1228°C	0.00082	0.00005	0.13142	0.00009	0.00118	0.00005	0.03878	0.00007	0.45450	0.00017

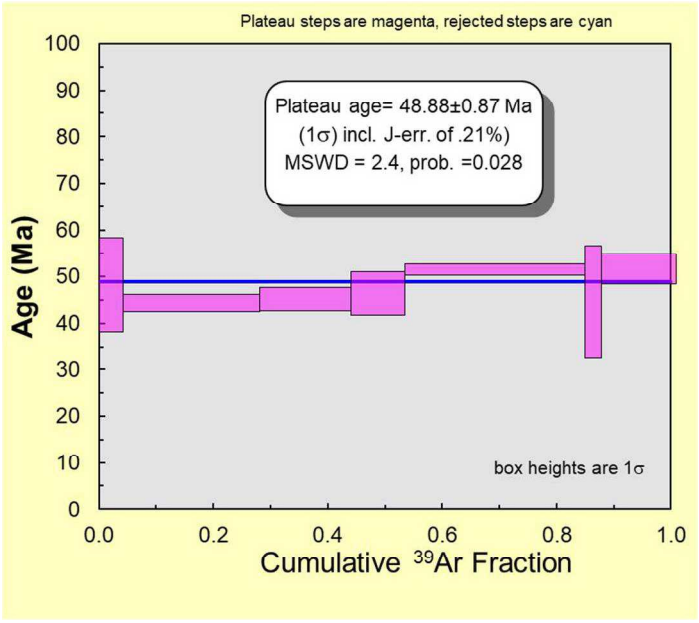
Plateau steps are magenta, rejected steps are cyan
Plateau age= 48.88±0.87 Ma
(1σ) incl. J-err. of .21%)
MSWD = 2.4, prob. =0.028
box heights are 1σ
Age (Ma)
Cumulative 39Ar Fraction

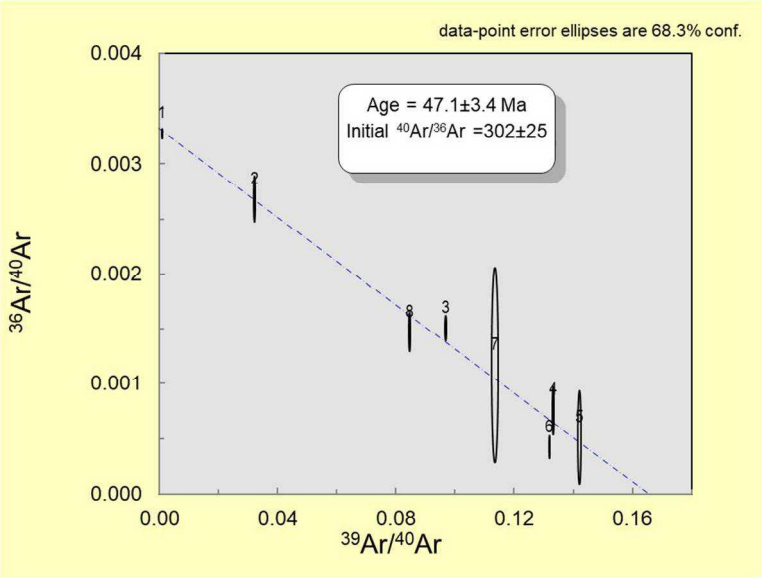
data-point error ellipses are 68.3% conf.
Age = 47.1±3.4 Ma
Initial 40Ar/36Ar =302±25
36Ar/40Ar
39Ar/40Ar

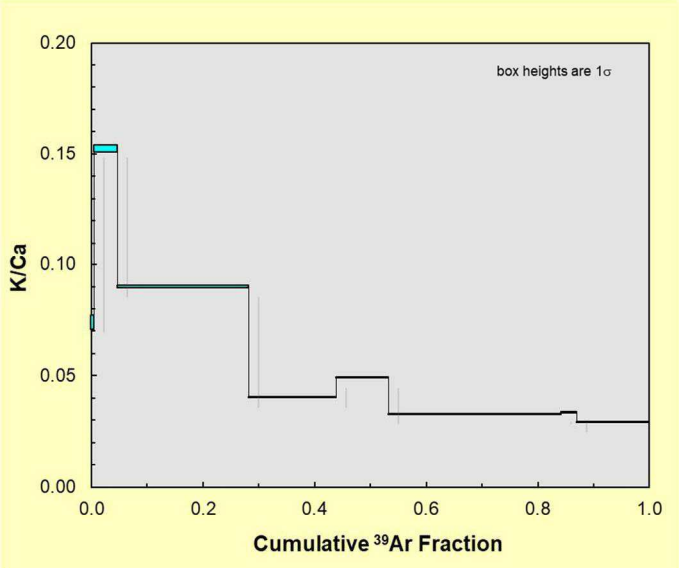
box heights are 1σ
K/Ca
Cumulative 39Ar Fraction

8.1.4 Appendix F: Details on amphibole and garnet as provenance indicators

8.1.4.1 Amphibole as provenance indicator

Amphiboles have complex geochemical and physical properties and are common in many igneous and metamorphic rocks (Leake, 1978; Mange and Maurer, 1992; Leake et al., 2004). Their geochemistry depends on source rock geochemistry and P-T conditions, allowing analysis of their major element geochemistry to reveal information on the genetic type of the source rock (Mange and Morton, 2007; Andò et al., 2014).

We classify the amphiboles according to the rules of the IMA 2004 (International Mineralogical Association) (Leake et al., 2004) to evaluate changes in the compositional spectra with depositional age. For information on metamorphic grade, we plot the SiO_2 vs. TiO_2 content and Al^{IV} vs. Al^{VI} values of amphiboles. The Ti content is considered to depend more on temperature than on pressure (Leake, 1965). TiO_2 values of up to 1.5 wt% are typical for amphibolite facies conditions while higher TiO_2 contents are more typical for granulite conditions or igneous source rocks (Andò et al., 2014). Continuous spectra of increasing Ti with reduction of Si are typical for rising metamorphic grade of the source rock, as Ti is replacing Si with higher metamorphic grade (Fleet and Bernett, 1978; Andò et al., 2014). Metamorphic amphiboles have higher Al^{VI} values than igneous ones, very likely caused by different pressure conditions during crystallization but also depending on magma composition (Leake, 1965; Fleet and Bernett, 1978). $Al^{IV}/Al^{VI} = 2$ is considered to be the boundary between low pressure metamorphic amphiboles (>2) and high pressure amphiboles (<2) (representing ca. 5 kbar; Leake, 1965; Fleet and Bernett, 1978). In igneous calciferous amphiboles, Al^{IV} increases with rising crystallization temperature and $Al^{IV}/Al^{VI} \geq 3.3$ is considered the limiting value for unaltered igneous amphibole (Fleet and Bernett, 1978). Testing of this approach by Li et al. (2015) showed that most igneous grains (gabbro, (grano)diorite, syenite, granite) as well as greenschist facies metamorphic grains have Al^{IV}/Al^{VI} values ≥ 3.3 while garnets from gneiss and amphibolites show values between 1.0 and 3.3.

8.1.4.2 Garnet as provenance indicator

Garnet comprises many different compositional types and is a relatively stable heavy mineral (Morton, 1984). Its mineral structure incorporates a large variety of major elements making it suitable for geochemical analysis using electron microprobe (Mange and Morton, 2007). Garnet composition depends on bulk geochemistry and P-T conditions of the source rocks (Mange and Morton, 2007). Natural garnets are solid solutions of different endmembers. Almandine ($Fe_3Al_2Si_3O_{12}$), pyrope ($Mg_3Al_2Si_3O_{12}$), spessartine ($Mn_3Al_2Si_3O_{12}$), grossular ($Ca_3Al_2Si_3O_{12}$), andradite ($Ca_3(Fe,Ti)_2Si_3O_{12}$) and uvarovite ($Ca_3Cr_2Si_3O_{12}$) are the most common ones (Krippner et al., 2014). The complex controls on garnet geochemistry and overlapping of compositional groups make garnet discrimination imperfect (Tolosana-Delgado et al., in press). Different bi- and triangular plots are used in the literature to identify the genetic type of source rocks based on garnet geochemistry (Wright, 1938; Teraoka et al., 1997, 1998; Mange and Morton, 2007; Aubrecht et al., 2009). Krippner et al. (2014) reviewed and tested those diagrams, concluding that the strict boundaries separating fields for certain source rocks are overstating their discriminatory power as many compositional fields overlap, with success rates of correct and unambiguous classification being low for many lithologies. The discrimination of amphibolite facies metasediments, which is a prominent lithology in the source area of the Surveyor fan sediments, is difficult in all these diagrams. To overcome these problems, a multivariate discrimination scheme for garnets has been developed (Tolosana-Delgado et al., in press). It provides probabilities for the affiliation of a garnet to one of five main source rock types (eclogite-, amphibolite- and granulite- facies metamorphic rocks, ultramafic and igneous rocks). The scheme has been tested to confidently differentiate igneous and metamorphic garnets (correct classification >90%). This is important for the discrimination of source areas of Surveyor fan sediments as wide parts of the terrestrial catchment consist of amphibolite facies metamorphic rocks and igneous intrusions.

The scheme requires setting prior probabilities that reflect a subjective likelihood for a garnet to belong to each group, without considering the composition of the garnet itself.

Choosing these values needs knowledge of the abundance of the different rock types in the source area and respective garnet fertilities (Tolosana-Delgado et al., in press). At the southern Alaska continental margin, the exposition of different rock types might have changed over time due to erosion and the low grade or non-metamorphic sediments on the Yakutat terrane might provide material from a wide variety of source rocks with respective abundances. Therefore we use the predefined prior "global" (Tolosana-Delgado et al., in press) that reflects the average abundances of garnet bearing rocks and their garnet fertilities in the average crust. We tested the settings with literature data on amphibolite facies metamorphic rocks from the source area of this study. 80 % were assigned to amphibolite facies rocks using the discrimination scheme with the prior global while 20 % were assigned to have ultramafic source rocks. Therefore, we keep in mind that grains assigned to be ultramafic might have an amphibolite facies source. Only a small amount of greenschist facies metamorphic garnets has been incorporated in the setup of the multivariate discrimination scheme. These grains have been included with the amphibolite facies garnets (Tolosana-Delgado et al., in press). Therefore, the discrimination scheme does not distinguish between amphibolite and greenschist facies garnets. Input from greenschist facies sources might therefore be wrongly assigned to have an amphibolite source.

To display the diversity of the garnet compositions and changes therein, we use the triangular diagram of Mange and Morton (2007) that has almandine + spessartine, grossular, and pyrope as apices, which are the most abundant garnet endmembers in our samples (fig. 3A). The discrimination fields are not intended to be diagnostic for certain garnet bearing rock types but evaluation of natural garnet populations indicates the respective genetic types (Mange and Morton, 2007) and application of this diagram to a large data set has shown the main orientation of discrimination fields to agree with natural garnet data (Tolosana-Delgado et al., in press). Strong overlap in the lower left part (i.e., Fe and/or Mn rich) of group Ci of three facies groups occur in relevant proportions and igneous rocks as well as amphibolite facies metasedimentary rocks might plot in the same field (Bi-type garnets; Krippner et al., 2014) and could therefore be misinterpreted. We keep the discrimination fields but to avoid misleading indications for provenance we refer to the garnets in the different fields as "x-type" garnet where x is the fieldname in the triangular diagram.

8.1.4.3 References

Aubrecht, R., Méres, Š., Sýkora, M., Mikuš, T., 2009. Provenance of the detrital garnets and spinels from the Albian sediments of the Czorsztyn Unit (Pieniny Klippen Belt, Western Carpathians, Slovakia). Geol. Carpa. 60, 463-483.

Andò, S., Morton, A., Garzanti, E., 2014. Metamorphic grade of source rocks revealed by chemical fingerprints of detrital amphibole and garnet. In: Scott, R.A.; Smyth, H.R., Morton, A.C., Richardson, N., (Eds.), Sediment Provenance Studies in Hydrocarbon Exploration and Production. Geological Society, London, Special Publications 386, 351-371.

Fleet, M.E., Barnett, R.L., 1978. Al^{IV}/Al^{VI} partitioning in calciferous amphiboles from the Frood mine Sudbury, Ontario. Can. Min. 16, 527-532.

Krippner, A., Meinhold, G., Morton, A.C., von Eynatten, H., 2014. Evaluation of garnet discrimination diagrams using geochemical data of garnets derived from various host rocks. Sed. Geol. 306, 36-52.

Leake, B.E., 1965. The relationship between composition of calciferous amphibole and grade of metamorphism. In: Pitcher, W.S., Flinn, G.W. (Eds.), Controls of Metamorphism. Oliver and Boyd, Edinburgh, pp. 299-318.

Leake, B.E., 1978. Nomenclature of Amphiboles. Am. Min. 63, 1023-1052.

Leake, B.E., Woolley, A.R., Birch, W.D., Burke, E.A., Ferraris, G., Grice, J.D., Hawthorne, F.C., Kisch, H.J., Krivovichev, V.G., Schumacher, J.C., Stephenson, N.C.N., Whitaker, E.J.W., 2004. Nomenclature of amphiboles: Additions and revisions to the International Mineralogical Association's amphibole nomenclature. Mineral. Mag. 68, 209- 2015.

Li, G., Yan, W., Zhong, L., Xia, Z., Wang, S., 2015. Provenance of heavy mineral deposits on the northwestern shelf of the South China Sea, evidence from single-mineral chemistry. Mar. Geol. 363, 112-124.
Mange, M.A., Maurer, H.F.W., 1992. Heavy Minerals in Colour. Chapman & Hall, London, 147 p.
Mange, M.A., Morton, A.C., 2007. Chapter 13, Geochemistry of Heavy Minerals. In: Mange, M.A., Wright, D.K. (Eds.), Heavy Minerals in use Developments in Sedimentology. Elsevier, Amsterdam, pp. 345-391.
Morton, A.C., 1984. Stability of Detrital Heavy Minerals in Tertiary Sandstones from the North Sea Basin. Clay Min. 19, 287-308.
Teraoka, Y., Suzuki, M., Hayashi, T., Kawakami, K., 1997. Detrital garnets from Paleozoic and Mesozoic sandstones in the Onogawa area, East Kyushu, Southwest Japan. Bulletin of the Faculty of School Education, Hiroshima University, Part II 19, 87–101 (in Japanese with English abstract).
Teraoka, Y., Suzuki, M., Kawakami, K., 1998. Provenance of Cretaceous and Paleogene sediments in the Median Zone of Southwest Japan. Bulletin of the Geological Society of Japan 49, 395–411 (in Japanese with English abstract).
Tolosana-Delgado, R., Eynatten, H., Krippner, A. Meinhold, G., in press. A multivariate discrimination scheme of detrital garnet chemistry for use in sedimentary provenance analysis. Sed. Geol., in press, doi.org/10.1016/j.sedgeo.2017.11.003.
Wright, W., 1938. The composition and occurrence of garnets. Am. Min. 23, 436-499.

8.4 Appendix for Huber et al., 2018; The Journal of Geology

8.4.1 Appendix A: Details of U-Pb dating, (U-Th)/He dating, REE and Hf-isotope measurements

8.4.1.1 U-Pb dating

For U-Pb isotopic analyses, calibration was done using the GJ1 zircon reference material (Jackson et al., 2004). Precision and accuracy were monitored by analyzing the 91500 reference zircon (Wiedenbeck et al., 1995) over the course of this study. An in-house Excel-spreadsheet (Kooijman et al., 2012), with common Pb correction based on the Pb evolution model of Stacey and Kramers (1975) was used for data reduction. For grains younger 1000 Ma we report $^{206}Pb/^{238}U$ ages, for grains older 1000 Ma we report $^{207}Pb/^{206}Pb$ ages. We excluded all grains >1000Ma that are more than 10 % discordant. The degree of concordance is defined as the ratio of the ($^{206}Pb/^{238}U$) and the ($^{207}Pb/^{206}Pb$) ages. Most of the younger zircons are of Cretaceous or even younger age, for these grains essentially only the $^{206}Pb/^{238}U$ ages can be used and a test for concordance is not possible. Some ages had to be rejected because of very high common Pb that could not be corrected properly. For details of instrument settings see Tab.A1.

Tab. A1: LA-ICP-MS metadata following the guideline of (Horstwood et al., 2016).

Laboratory and Sample Preparation	
Laboratory name	Institut für Mineralogie Westfälische Wilhelms-Universität Münster
Sample type/mineral	Detrital/Metamorphic/Magmatic Zircons
Sample preparation	Conventional mineral separation/1 inch mount 0.25µm final polish
Imaging	CL, 10kV, 20 mm WD
Laser Ablation System	
Make, Model, Type	Photon Machines, Analyte G2, Excimer Laser
Ablation cell	HelEx 2-volume cell
Laser wavelength	193 nm
Pulse width	4 ns
Fluence	3-4 J/cm2
Repetition rate	10 Hz
Ablation duration	37 s
Ablation pit depth/ ablation rate	~0.1µm/pulse equals 37 µm pit depth measured using SEM
Spot diameter	25/35 µm
Sampling mode/ pattern	static
Carrier gas	He in the cell, Ar sampling and cooling gas
Cell carrier gas flow	0.8 l min -1 for MFC1, 0.5 l min -1 for MFC2
ICP-MS Instrument	
Make, Model, Type	ThermoFisher Element 2 Single Collector ICP-MS
Sample introduction	Ablation aerosol
RF power	1250 W
Sample and cooling gas flow	1 l min -1/ 16 l min-1
Detection system	SEM
Masses measured	202, 204, 206, 207, 238
Settling time	1 ms/amu
Sample time	40 ms (202, 204, 207) 10 ms (206), 4 ms (238)

Sweep time	160 ms (202, 204, 207) 40 ms (206), 10 ms (238)
Integration time	0.56 s
Number of runs	91
Background time	12 s
Ablation time	37 s
Sensitivity as useful yield	~0.3% U
SEM Deatime	25 ns
Data Processing	
Gas blank	12 s on-peak zero substracted
Calibration strategy	GJ1 as primary reference material, 91500 to precision and accuracy
Reference material information	91500 (Wiedenbeck et al., 1995) GJ1 (Jackson et al., 2004), in-house ID-TIMS (unpubl.)
Data processing	in-house Excel spreadsheet (Kooijman et al., 2012)
Mass fractionation and mass bias	external calibration, least-squares linear regression to t_0
Common Pb correction	applied if estimated common 206Pb to the total measured 206Pb exceeds 1 % and thus approaches the analytical uncertainty of the Pb-isotope ratio measurement
Uncertainty level and error propagation	Ages are quoted at 2s absolute and relative (%), quadratic addition of the precision of individual analysis and external reproducibility obtained from the reference zircon during analytical session
Quality control	n= 71 analyses of 91500 reference zircon 0.17889 (± 2.9 %, 2σ) for $^{206}Pb/^{23}8U$, 1.857 (± 4 %, 2σ) for 207Pb/235U 0.0753 (± 2.6 %, 2σ) for 207Pb/206Pb

8.4.1.2 Hf isotope analysis

Hf-isotopy was measured using a Thermo-Finnigan NEPTUNE multi collector ICP-MS at Goethe University Frankfurt (GUF) coupled to a RESOlution S-155 (Resonetics) 193 nm ArF excimer laser (CompexPro 102, Coherent) following the method described by Gerdes and Zeh (2006, 2009) and Zeh and Gerdes (2012). Spots of 40 µm in diameter were drilled with a repetition rate of 5.5 Hz and an energy density of 6 J/cm^2 during 50s of data acquisition. Laser spots were set directly 'on top' of the U–Pb spots, or immediately beside but within the same zone as determined by CL. For calculation of $\varepsilon(Hf)_t$ values the decay constant of 1.867 × 10–11 (average of Scherer et al., 2001; Söderlund et al., 2004) and the values for the chondritic uniform reservoir (CHUR, $^{176}Lu/^{177}Hf$ =0.0336, $^{176}Hf/^{177}Hf$ = 0.282785; (Bouvier et al., 2008; Söderlund et al., 2004) were used. A two stage depleted mantle Hf model age (TDM, in Ga) was calculated from the initial$^{176}Hf/^{177}$ Hf of each zircon at the time of crystallization by using$^{176}Hf/^{177}Hf$ = 0.28325 and$^{176}Lu/^{177}Hf$ = 0.0384 for the bulk earth (Bouvier et al., 2008) and $^{176}Lu/^{177}Hf$ = 0.0113 for the average crust.

All data were adjusted relative to the JMC475 of $^{176}Hf/^{177}Hf$ ratio = 0.282160 and quoted uncertainties are quadratic additions of the within run precision of each analysis and the reproducibility of the JMC475 (2SD = 0.0028%, n = 8). Accuracy and daily reproducibility of the method was verified by repeated analyses of reference zircon GJ-1 and Temora, which yielded a $^{176}Hf/^{177}Hf$ of 0.282009 ±0.000021 (2 SD, n=30) and 0.282670 ±0.000025 (n=23), respectively. This is in perfect agreement the LA-MC-ICPMS long-term average of GJ-1

(0.282010 ±0.000025; n > 800) and Temora (0.282483 ±0.000023, n > 250) reference zircon at GUF.

8.4.1.3 REE analysis

REE analyses were performed on the same machine used for U-Pb dating. For quantification, internal standard concentrations of Si were determined previously by electron microprobe. The NIST 612 reference material was used as the external standard. The Glitter software (version 4.4.4; Griffin et al., 2008) was used to calculate the concentrations of the measured elements. For monitoring of accuracy, the 91500 reference zircon (Wiedenbeck et al., 1995) and BIR-1G reference glass were measured along with the unknowns.

8.4.1.4 (U-Th)/He dating

The crystals were inspected for inclusions under 250x magnification and cross-polarized light. Only inclusion- and fissure-free, intact, mostly euhedral grains that exceeded 70 µm in width were selected. The shape parameters were determined and archived by multiple digital microphotographs; besides the total length and width the proportion of the length of the prismatic and pyramidal zones was also considered.

The crystals were wrapped in platinum capsules of ca. 1x1 mm size. The Pt capsules were heated in the full-metal extraction line by an infra-red laser for 2 minutes in high vacuum. The extracted gas was purified using a SAES Ti-Zr getter kept at 450 °C. The chemically inert noble gases and a minor amount of other rest gases were then expanded into a Hiden triple-filter quadrupol mass spectrometer equipped with a positive ion counting detector. Beyond the detection of helium the partial pressures of some rest gases were continuously monitored (H_2, CH_4, H_2O, N_2, Ar and CO_2). He blanks were estimated using the same procedure on empty Pt tubes (max. 0.0003 and 0.0008 ncc 4He; cold and hot blanks, respectively). Crystals were checked for degassing of He by sequential reheating and He measurement. The He signal was processed and evaluated by the factory-made software of the mass spectrometer (MASsoft, HIDEN). During standard and sample measurements 240 readings of the mass spectrometer were recorded.

Following degassing, samples were retrieved from the gas extraction line, spiked with calibrated ^{230}Th and ^{233}U solutions. The zircon crystals were dissolved in pressurized teflon bombs using a mixture of double distilled 48% HF and 65% HNO_3. Each sample batch was prepared with a series of procedural blanks and spiked normals to check the purity and calibration of the reagents and spikes. Spiked solutions were analyzed by a Perkin Elmer Elan DRC II or by a Thermo iCAP Q ICP-MS assembled with an APEX micro-flow nebulizer. Procedural U and Th blanks by this method are usually very stable in a measurement session and below 1.5 pg. Sm, Pt and Zr were determined by external calibration. The oxide formation rate and the PtAr - U interference was always monitored, but the effects of these isobaric argides were negligible relatively to the signal of actinides.

The ejection correction factors (Ft) were determined for the single crystals by a modified algorithm of Farley et al., (1996) using an in-house spread sheet. Note that alternative methods result in different Ft values. The (U-Th-Sm)/He ages were calculated by the Taylor Expansion Method (after Des Patterson). The Sm content was also considered for age calculation. The uncertainty of single-crystal ages contain the estimated error of Ft.

8.4.1.5 References cited

Bouvier, A., Vervoort, J.D., Patchett, P.J., 2008. The Lu–Hf and Sm–Nd isotopic composition of CHUR: Constraints from unequilibrated chondrites and implications for the bulk composition of terrestrial planets. Earth Planet. Sci. Lett. 27, 48–57.

Farley, K.A., Wolf, R.A., Silver, L.T. 1996. The effects of long alpha-stopping distance on (U-Th)/He ages. Geochim. Cosmochim. Acta, 60, 4223-4229.

Gerdes, A., Zeh, A., 2006. Combined U–Pb and Hf isotope LA-(MC-)ICP-MS analyses of detrital zircons: Comparison with SHRIMP and new constraints for the provenance and age of an Armorican metasediment in Central Germany. Earth Planet. Sci. Lett. 249, 47–61.

Gerdes, A., Zeh, A., 2009. Zircon formation versus zircon alteration — New insights from combined U–Pb and Lu–Hf in-situ LA-ICP-MS analyses, and consequences for the interpretation of Archean zircon from the Central Zone of the Limpopo Belt. Chemical Geology, 261, 230-243.

Griffin, W.L., Powell, W.J., Pearson, N.J., O' Reilly, S.Y. 2008. GLITTER: Data reduction software for laser ablation ICP-MS. In: Sylvester, P. (Ed.). Mineralogical society of Canada Short Course Series, Vancouver, British Columbia, p. 204–207.

Horstwood, M.S.A., Košler, J., Gehrels, G., Jackson, S.E., McLean, N.M., Paton, C., Pearson, N.J., Sircombe, K., Sylvester, P., Vermeesch, P., Bowring, J.F., and Condon, D.J., Schoene, B., 2016. Community-Derived Standards for LA-ICP-MS U-(Th-)Pb Geochronology - Uncertainty Propagation, Age Interpretation and Data Reporting. Geostand. Geoanal. Res. 40, 311–332.

Jackson, S.E.; Pearson, N.J.; Griffin, W.L.; and Belousova, E.A. 2004. The application of laser ablation-inductively coupled plasmamass

spectrometry to in situ U-Pb zircon geochronology. Chem. Geol. 211, 47–69.

Kooijman, E., Berndt, J., Metzger, K., 2012. U-Pb dating of zircon by laser ablation ICP-MS: Recent improvements and new insights. Eur. J. Mineral. 24, 5–21.

Scherer, E., Munker, C., and Mezger, K. 2001. Calibration of the lutetium-hafnium clock. Science (N.Y.) 293, 683–687.

Söderlund, U., Patchett, P., Vervoort, J.D., Isachsen, C.E., 2004. The 176Lu decay constant determined by Lu–Hf and U–Pb isotope systematics of Precambrian mafic intrusions. Earth Planet. Sc. Lett. 219, 311–324.

Stacey, J.S., Kramers, J.D., 1975. Approximation of terrestrial lead isotope evolution by a two-stage model. Earth Planet. Sc. Lett. 26, 207–221.

Wiedenbeck, M., Allé, P., Corfu, F., Griffin, W.L., Meier, M., Oberli, F., Quadt, A.V., Roddikk, J.C., and Spiegel, W., 1995. Three natural zircon standards for u-Th-Pb, Lu-Hf, Trace Elementand REE analyses. Geostand. Geoanal. Res. 19, 1–23.

Zeh, A., Gerdes, A., 2012. U–Pb and Hf isotope record of detrital zircons from gold-bearing sediments of the Pietersburg Greenstone Belt (South Africa)—Is there a common provenance with the Witwatersrand Basin? Precambr. Res. 204–205, 46-56.

8.4.2 Appendix B: U-Pb data

Appendix B: U-Pb ages from site U1417 and U1418

Analysis	Ratios							Ages (Ma)									
	$^{206}Pb/^{238}U$	±2σ	$^{207}Pb/^{235}U$	±2σ	$^{207}Pb/^{206}Pb$	±2σ	rho:	$^{206}Pb/^{238}U$	±2σ	±2σ%	$^{207}Pb/^{235}U$	±2σ	±2σ%	$^{207}Pb/^{206}Pb$	±2σ	±2σ%	Concor-dance %
								18MPI3									
Z1c10c	0.3008	0.0047	4.39	0.11	0.1059	0.002	0.63	1695	23	1.4	1711	20	1.2	1730	35	2	0.98
z1c11r	0.01261	0.00085	0.104	0.016	0.0596	0.0085	0.43	80.8	5.4	6.7	100	15	15	588	314	53	-
Z1c12c	0.01093	0.00032	0.0816	0.0057	0.0542	0.0034	0.42	70	2.1	3	79.7	5.4	6.8	379	143	38	-
z1c12r	0.01027	0.00036	0.0721	0.0036	0.0509	0.0018	0.7	65.9	2.3	3.5	70.7	3.4	4.9	236	83	35	-
Z1c13c	0.02398	0.00053	0.185	0.015	0.056	0.0042	0.28	152.8	3.3	2.2	173	12	7.2	454	168	37	-
z1c13r	0.02385	0.00092	0.181	0.01	0.055	0.0022	0.69	151.9	5.8	3.8	168.7	8.6	5.1	411	90	22	-
z1c15r	0.00811	0.00033	0.0586	0.0039	0.0524	0.0027	0.62	52	2.1	4.1	57.8	3.7	6.5	303	119	39	-
z1c16c	0.01713	0.00067	0.1194	0.0084	0.0505	0.003	0.55	109.5	4.2	3.9	114.5	7.7	6.7	220	137	62	-
Z1c17c	0.01222	0.0003	0.0806	0.0048	0.0478	0.0026	0.42	78.3	1.9	2.5	78.7	4.5	5.7	92	107	117	-
z1c17r	0.0117	0.00065	0.0797	0.0074	0.0494	0.0037	0.6	75	4.1	5.5	77.8	6.9	8.9	167	166	99	-
z1c18r	0.00848	0.00031	0.0556	0.0027	0.0475	0.0015	0.76	54.4	2	3.6	54.9	2.6	4.7	76	74	97	-
Z1c19c	0.00942	0.00023	0.059	0.0043	0.0454	0.0031	0.35	60.4	1.5	2.5	58.2	4.1	7	-	63	-	-
z1c19r	0.00953	0.00062	0.068	0.011	0.0515	0.0076	0.41	61.2	4	6.5	67	10	15.6	264	285	108	-
Z1c1c	0.0186	0.001	0.131	0.01	0.0509	0.0029	0.69	118.8	6.3	5.3	124.7	9.2	7.3	238	131	55	-
Z1c1c	0.0183	0.0012	0.126	0.012	0.0498	0.0034	0.68	117.2	7.3	6.2	120	10	8.7	184	158	86	-
z1c1r	0.0195	0.0011	0.145	0.012	0.0542	0.0031	0.7	124.2	6.9	5.5	138	10	7.5	379	129	34	-
Z1c20c	0.00801	0.00024	0.0548	0.004	0.0496	0.0033	0.42	51.4	1.6	3	54.2	3.8	7	178	153	86	-
z1c20r	0.00742	0.00033	0.0495	0.0027	0.0484	0.0016	0.81	47.7	2.1	4.4	49.1	2.6	5.4	117	77	65	-
z1c21c	0.01578	0.00089	0.105	0.038	0.048	0.017	0.16	101	5.7	5.6	101	35	34.6	102	392	386	-
z1c24r	0.01177	0.00054	0.079	0.012	0.0488	0.0072	0.3	75.5	3.4	4.5	77	11	14.9	136	225	165	-
Z1c25c	0.01232	0.00028	0.0868	0.0061	0.0511	0.0034	0.33	78.9	1.8	2.3	84.5	5.7	6.8	245	154	63	-
z1c25r	0.293	0.013	4.23	0.21	0.1047	0.002	0.92	1655	66	4	1679	40	2.4	1710	35	2	0.97
Z1c26c	0.3093	0.0044	4.66	0.1	0.1093	0.0019	0.63	1737	22	1.2	1760	19	1.1	1788	32	2	0.97
z1c26r	0.01217	0.00052	0.0838	0.0041	0.0499	0.0012	0.87	78	3.3	4.3	81.7	3.9	4.7	191	56	29	-
z1c27c	0.01426	0.00073	0.0949	0.0066	0.0483	0.0023	0.74	91.3	4.7	5.1	92.1	6.1	6.7	113	110	98	-
z1c28r	0.01407	0.00071	0.0985	0.007	0.0508	0.0026	0.71	90.1	4.5	5	95.3	6.5	6.8	230	117	51	-
z1c2c	0.00841	0.00039	0.0553	0.0084	0.0477	0.0069	0.3	54	2.5	4.6	54.7	8	14.7	84	197	236	-
Z1c2r	0.00862	0.00041	0.0578	0.004	0.0487	0.0024	0.69	55.3	2.6	4.8	57.1	3.9	6.8	131	118	90	-
Z1c3c	0.0268	0.0013	0.18	0.01	0.0488	0.0013	0.88	170.3	8.4	4.9	168.3	8.9	5.3	140	65	46	-
z1c3c	0.0254	0.0016	0.213	0.024	0.0608	0.0058	0.55	162	10	6.2	196	20	10.4	631	207	33	-
Z1c4c	0.0077	0.00037	0.0516	0.0034	0.0487	0.0022	0.73	49.4	2.3	4.7	51.1	3.3	6.4	133	106	80	-
z1c4r	0.00809	0.00021	0.0551	0.0027	0.0494	0.002	0.55	52	1.4	2.6	54.5	2.6	4.7	166	95	57	-
z1c5c	0.0705	0.004	0.6	1.9	0.066	0.19	0.02	439	24	5.5	503.8	-	-	809	1616	200	-

Z1c6r	0.01983	0.00094	0.1332	0.0088	0.0487	0.0022	0.72	126.6	5.9	4.7	126.9	7.9	6.2	134	107	80	-
z1c6c	0.01935	0.00048	0.1374	0.0057	0.0515	0.0017	0.6	123.5	3	2.5	130.7	5.1	3.9	263	76	29	-
Z1c7r	0.0276	0.0013	0.194	0.01	0.051	0.0013	0.89	175.4	8.2	4.7	180.1	8.8	4.9	242	57	23	-
z1cc	0.02867	0.00068	0.2018	0.0066	0.051	0.0012	0.72	182.2	4.3	2.3	186.7	5.6	3	243	52	21	-
z1c8c	0.0112	0.0028	0.37	0.88	0.238	0.56	0.1	72	18	24.8	319	774	242.9	3108	2463	79	-
Z1c9r	0.01539	0.00089	0.1086	0.0096	0.0512	0.0034	0.65	98.4	5.7	5.8	104.7	8.8	8.4	249	155	62	-
z1c9c	0.01598	0.00081	0.118	0.01	0.0536	0.0039	0.57	102.2	5.1	5	113.3	9.5	8.4	353	166	47	-
z1d10c	0.01322	0.00093	0.0985	0.0075	0.054	0.0016	0.92	84.6	5.9	7	95.3	7	7.3	372	67	18	-
z1d11c	0.0022	0.00023	0.0165	0.002	0.0542	0.0033	0.86	14.2	1.5	10.3	16.6	2	11.9	379	139	37	-
Z1d12r	0.01375	0.00055	0.0903	0.0063	0.0477	0.0027	0.58	88	3.5	4	87.8	5.8	6.6	83	106	128	-
z1d12c	0.01417	0.00095	0.0916	0.0064	0.04689	0.00098	0.95	90.7	6	6.6	89	6	6.7	44	46	106	-
z1d13	0.00917	0.00035	0.0627	0.0033	0.0496	0.0018	0.71	58.8	2.2	3.8	61.8	3.2	5.1	178	87	49	-
z1d15	0.0106	0.00041	0.076	0.0043	0.052	0.0021	0.68	67.9	2.6	3.8	74.4	4	5.4	286	94	33	-
z1d16	0.00969	0.00044	0.0515	0.0083	0.0385	0.006	0.28	62.2	2.8	4.5	51	8	15.7		0	-	-
Z1d17c	0.000381	7.8E-05	0.0025	0.0016	0.047	0.029	0.31	2.5	0.5	20.5	2.5	1.6	65.2	52	550	1062	-
z1d17	0.000395	0.00007	0.0044	0.0013	0.081	0.019	0.61	2.5	0.5	17.8	4.5	1.3	29	1221	465	38	-
z1d18	0.0264	0.0012	0.21	0.019	0.0576	0.0045	0.5	167.8	7.5	4.5	193	16	8.2	516	172	33	-
Z1d19c	0.02592	0.00098	0.18	0.016	0.0504	0.0041	0.42	165	6.1	3.7	168	14	8.2	214	187	87	-
z1d19	0.0529	0.0019	0.404	0.019	0.0555	0.0018	0.74	332	11	3.4	345	14	4	431	72	17	-
Z1d1c	0.02199	0.00078	0.1478	0.0071	0.0487	0.0016	0.74	140.2	4.9	3.5	139.9	6.3	4.5	135	76	56	-
z1d1	0.02258	0.00063	0.1472	0.006	0.0473	0.0014	0.69	144	4	2.8	139.4	5.3	3.8	62	66	106	-
Z1d21c	0.01302	0.00044	0.087	0.0038	0.0484	0.0014	0.76	83.4	2.8	3.3	84.7	3.6	4.2	120	68	57	-
z1d21	0.01319	0.00088	0.09	0.019	0.0496	0.0099	0.32	84.5	5.6	6.6	88	18	20.2	179	294	165	-
z1d23	0.02126	0.00082	0.1506	0.0079	0.0514	0.0018	0.74	135.6	5.2	3.8	142.5	7	4.9	258	81	32	-
z1d24	0.00942	0.00031	0.0614	0.0034	0.0473	0.0021	0.59	60.5	2	3.3	60.5	3.3	5.4	62	83	134	-
z1d25	0.0112	0.00041	0.0734	0.0043	0.0476	0.0022	0.62	71.8	2.6	3.6	72	4.1	5.7	78	92	118	-
z1d26	0.01315	0.00045	0.0908	0.0049	0.0501	0.002	0.64	84.2	2.9	3.4	88.2	4.5	5.1	198	95	48	-
Z1d27c	0.01259	0.00064	0.082	0.0056	0.0472	0.0022	0.74	80.7	4.1	5.1	80	5.3	6.6	62	84	136	-
z1d27	0.01294	0.00041	0.0889	0.004	0.0498	0.0016	0.7	82.9	2.6	3.2	86.5	3.7	4.3	187	75	40	-
Z1d28c	0.00812	0.00043	0.0535	0.0043	0.0478	0.0028	0.67	52.1	2.8	5.3	52.9	4.1	7.8	87	112	128	-
z1d28	0.0079	0.00025	0.0529	0.0022	0.0485	0.0013	0.75	50.7	1.6	3.1	52.3	2.1	4.1	125	65	52	-
Z1d29c	0.01178	0.00063	0.0776	0.0054	0.0478	0.0022	0.76	75.5	4	5.3	75.9	5.1	6.8	90	97	109	-
z1d29	0.01171	0.00041	0.0792	0.0048	0.0491	0.0024	0.58	75.1	2.6	3.5	77.4	4.5	5.8	151	116	77	-
z1d2	0.0142	0.00035	0.1007	0.0044	0.0514	0.0018	0.56	90.9	2.2	2.4	97.5	4	4.1	261	82	32	-
Z1d30c	0.0205	0.0011	0.1409	0.0098	0.0499	0.0021	0.8	130.6	7.2	5.5	133.9	8.7	6.5	192	97	50	-
z1d30	0.01996	0.00067	0.1493	0.0079	0.0542	0.0022	0.63	127.4	4.2	3.3	141.3	7	5	381	93	24	-
z1d31	0.012	0.00038	0.0812	0.0034	0.049	0.0014	0.75	76.9	2.4	3.2	79.2	3.2	4.1	150	65	44	-
Z1d32c	0.01903	0.00098	0.134	0.01	0.0511	0.0028	0.69	121.5	6.2	5.1	127.7	9	7	245	125	51	-
z1d32	0.01922	0.00067	0.1284	0.0062	0.0485	0.0016	0.72	122.7	4.2	3.5	122.6	5.6	4.6	121	80	66	-
z1d33	0.00897	0.00034	0.0644	0.0039	0.052	0.0025	0.62	57.6	2.1	3.7	63.3	3.7	5.9	287	108	38	-
z1d34	0.01013	0.00036	0.0695	0.0051	0.0497	0.0032	0.49	65	2.3	3.5	68.2	4.8	7.1	183	149	82	-

Z1d35c	0.0364	0.0022	0.282	0.023	0.0562	0.0032	0.72	230	14	5.9	252	19	7.4	461	128	28	-
z1d35	0.01155	0.00029	0.083	0.0048	0.0522	0.0027	0.43	74	1.8	2.5	81	4.5	5.6	292	120	41	-
Z1d36c	0.0122	0.00078	0.08	0.012	0.0475	0.0062	0.44	78.2	5	6.4	78	11	14	75	179	240	-
z1d36	0.01188	0.0003	0.0814	0.0031	0.0497	0.0014	0.67	76.2	1.9	2.5	79.5	2.9	3.6	180	65	36	-
z1d37	0.01433	0.00038	0.1057	0.0067	0.0535	0.0031	0.42	91.7	2.4	2.6	102	6.1	6	350	130	37	-
z1d38	0.01147	0.00027	0.0758	0.0026	0.0479	0.0012	0.68	73.5	1.7	2.3	74.2	2.4	3.3	95	59	62	-
z1d39	0.01154	0.00046	0.0796	0.0066	0.0501	0.0036	0.49	73.9	2.9	4	77.8	6.2	7.9	198	168	85	-
z1d3	0.00982	0.00028	0.0646	0.0025	0.0477	0.0013	0.72	63	1.8	2.8	63.6	2.4	3.8	86	64	75	-
z1d40	0.01139	0.00036	0.0753	0.0031	0.048	0.0012	0.78	73	2.3	3.2	73.8	2.9	3.9	97	60	62	-
z1d41	0.01383	0.00035	0.092	0.0034	0.0483	0.0013	0.7	88.5	2.3	2.5	89.4	3.1	3.5	112	62	55	-
z1d4	0.01006	0.00077	0.0657	0.0062	0.0474	0.0025	0.82	64.5	4.9	7.7	64.6	5.9	9.1	69	96	139	-
z1d44	0.00883	0.00042	0.0605	0.0046	0.0497	0.003	0.62	56.7	2.7	4.7	59.6	4.4	7.4	180	139	77	-
z1d45	0.01191	0.00042	0.0823	0.0035	0.0501	0.0012	0.84	76.3	2.7	3.5	80.3	3.3	4.1	200	54	27	-
Z1d45c	0.015	0.00076	0.0994	0.0059	0.0481	0.0015	0.86	95.9	4.8	5.1	96.2	5.5	5.7	102	72	71	-
Z1d46c	0.0106	0.00057	0.0775	0.0062	0.053	0.0031	0.67	68	3.6	5.3	75.8	5.8	7.7	328	135	41	-
z1d46	0.00884	0.00033	0.0601	0.0038	0.0493	0.0025	0.6	56.7	2.1	3.8	59.3	3.6	6.1	164	117	71	-
z1d47	0.0054	0.0013	0.094	0.078	0.126	0.099	0.3	35	8.7	24.7	92	73	79.3	2041	1510	74	-
Z1d48c	0.01537	0.0005	0.111	0.0092	0.0524	0.004	0.39	98.3	3.2	3.2	106.9	8.4	7.9	302	175	58	-
z1d48	0.01517	0.00057	0.12	0.019	0.0573	0.0088	0.23	97	3.6	3.7	115	17	15	502	345	69	-
z1d49	0.00836	0.00033	0.0584	0.0043	0.0507	0.0032	0.53	53.7	2.1	3.9	57.6	4.1	7.2	225	146	65	-
z1d51	0.00836	0.00035	0.074	0.004	0.0642	0.0023	0.76	53.7	2.2	4.1	72.5	3.8	5.3	749	75	10	-
z1d50	0.00789	0.00029	0.0523	0.0034	0.0481	0.0025	0.57	50.6	1.9	3.7	51.8	3.3	6.3	105	113	107	-
z1d52	0.0085	0.0003	0.0582	0.0028	0.0496	0.0017	0.72	54.6	1.9	3.5	57.4	2.7	4.7	177	79	45	-
z1d53	0.0089	0.00034	0.0597	0.0028	0.0487	0.0014	0.8	57.1	2.1	3.8	58.9	2.7	4.6	132	67	51	-
z1d54	0.028	0.0011	0.2022	0.0099	0.0524	0.0016	0.79	177.8	6.8	3.8	187	8.4	4.5	304	68	22	-
z1d55	0.00772	0.00032	0.0555	0.0032	0.0521	0.0022	0.7	49.6	2	4.1	54.8	3.1	5.7	290	95	33	-
Z1d56c	0.2819	0.0052	3.948	0.088	0.1016	0.0012	0.84	1601	26	1.6	1624	18	1.1	1653	22	1	0.97
z1d6	0.0257	0.0017	0.186	0.014	0.0524	0.0018	0.88	164	11	6.5	173	12	6.8	303	79	26	-
z1d60	0.00806	0.00019	0.0533	0.0019	0.0479	0.0012	0.68	51.8	1.2	2.4	52.7	1.8	3.4	95	61	64	-
z1d7	0.0103	0.00071	0.0791	0.007	0.0557	0.0031	0.78	66	4.5	6.9	77.3	6.6	8.6	441	125	28	-
Z1d7c	0.00949	0.00039	0.0597	0.0064	0.0457	0.0045	0.38	60.9	2.5	4.1	58.9	6.2	10.5	-	102	-	-
z1d8	0.00723	0.00051	0.0536	0.0047	0.0537	0.0028	0.8	46.5	3.3	7.1	53	4.6	8.6	358	119	33	-
Z1d8r	0.00788	0.00033	0.011	0.0051	0.0101	0.0047	0.09	50.6	2.1	4.2	11.1	5.1	46	-	0	-	-
Z1d9c	0.01175	0.00045	0.0852	0.0063	0.0526	0.0033	0.52	75.3	2.9	3.8	83	5.9	7.1	312	144	46	-
z1d9r	0.01067	0.0007	0.0733	0.006	0.0498	0.0024	0.81	68.4	4.5	6.6	71.8	5.6	7.8	188	111	59	-
Z1e12c	0.01661	0.00065	0.113	0.011	0.0492	0.0045	0.4	106.2	4.1	3.9	108	10	9.4	156	177	114	-
z1e2r	0.01609	0.00039	0.1066	0.0045	0.0481	0.0016	0.57	102.9	2.4	2.4	102.9	4.1	4	103	81	79	-
Z1e3c	0.01348	0.00063	0.142	0.016	0.0766	0.0078	0.41	86.3	4	4.6	135	14	10.5	1110	205	18	-
z1e3r	0.01306	0.00032	0.0893	0.0035	0.0496	0.0016	0.61	83.7	2	2.4	86.9	3.3	3.8	176	74	42	-
Z1e5c	0.01073	0.00093	0.082	0.015	0.0553	0.0092	0.46	68.8	5.9	8.6	80	14	18	424	376	89	-
Z1e6c	0.01112	0.00032	0.0707	0.004	0.0461	0.0022	0.51	71.3	2	2.9	69.3	3.8	5.4	2	57	2435	-

z1e6r	0.0115	0.00035	0.08	0.0052	0.0505	0.0029	0.47	73.7	2.2	3	78.2	4.9	6.2	218	132	61	-
z1e7r	0.00806	0.00019	0.0502	0.0016	0.04517	0.00092	0.76	51.7	1.2	2.4	49.7	1.5	3.1	-	1.1	-	-
z1e8c	0.00816	0.00021	0.0494	0.0017	0.04388	0.00098	0.75	52.4	1.3	2.6	49	1.6	3.3	-	0	-	-
z1e9r	0.01093	0.0003	0.0709	0.003	0.047	0.0016	0.63	70.1	1.9	2.7	69.6	2.9	4.1	51	64	125	-
z1e10r	0.01124	0.00029	0.0698	0.0024	0.045	0.001	0.75	72	1.9	2.6	68.5	2.3	3.4	-	0.78	-	-
Z2d10c	0.02045	0.00063	0.1009	0.0049	0.0358	0.0013	0.63	130.5	4	3	97.6	4.5	4.6	-	0	-	-
z2d10r	0.01933	0.00078	0.1364	0.0083	0.0512	0.0023	0.66	123.4	5	4	129.8	7.4	5.7	249	105	42	-
z2d11c	0.0105	0.00039	0.0733	0.0035	0.0506	0.0015	0.79	67.4	2.5	3.7	71.9	3.3	4.6	224	68	30	-
Z2d11r	0.00977	0.00041	0.0668	0.0054	0.0496	0.0035	0.51	62.7	2.6	4.1	65.7	5.2	7.9	175	163	93	-
Z2d12c	0.044	0.0013	0.317	0.013	0.0524	0.0014	0.75	277.3	8.1	2.9	279.9	9.8	3.5	302	60	20	-
z2d12r	0.0433	0.0015	0.314	0.013	0.0525	0.0012	0.84	273.3	9.4	3.4	277	10	3.6	308	51	16	-
Z2d13c	0.0256	0.0012	0.493	0.064	0.139	0.017	0.36	163.2	7.4	4.6	407	43	10.6	2220	210	9	-
z2d13r	0.0266	0.0014	0.182	0.055	0.05	0.015	0.18	169.5	8.9	5.3	170	47	27.6	176	374	213	-
Z2d14c	0.01596	0.00057	0.0988	0.0067	0.0449	0.0026	0.53	102.1	3.6	3.5	95.7	6.2	6.4	-	37	-	-
z2d14r	0.01669	0.00062	0.1127	0.0052	0.049	0.0013	0.81	106.7	3.9	3.7	108.4	4.7	4.4	146	64	44	-
Z2d15c	0.01088	0.0005	0.0715	0.0058	0.0477	0.0031	0.57	69.7	3.2	4.6	70.1	5.5	7.8	83	116	141	-
z2d15r	0.01137	0.00042	0.0756	0.0035	0.0482	0.0013	0.81	72.9	2.7	3.7	74	3.3	4.4	110	64	58	-
Z2d16c	0.01318	0.00041	0.0867	0.004	0.0477	0.0016	0.68	84.4	2.6	3.1	84.4	3.7	4.4	85	81	95	-
z2d16r	0.01235	0.00044	0.0837	0.0038	0.0492	0.0013	0.79	79.1	2.8	3.5	81.7	3.5	4.3	157	64	41	-
Z2d17c	0.00825	0.00032	0.0553	0.0064	0.0486	0.0053	0.34	52.9	2.1	3.9	54.6	6.2	11.3	128	184	143	-
z2d17r	0.00807	0.00033	0.0569	0.0033	0.0512	0.0021	0.71	51.8	2.1	4.1	56.2	3.1	5.6	249	93	37	-
Z2d19c	0.01356	0.00051	0.0899	0.0083	0.0481	0.0041	0.41	86.8	3.2	3.7	87.5	7.7	8.8	105	146	140	-
Z2d19r	0.01373	0.00043	0.0907	0.0042	0.0479	0.0016	0.69	87.9	2.8	3.1	88.1	3.9	4.4	94	79	84	-
Z2d21c	0.02845	0.00082	0.24	0.014	0.0612	0.0032	0.49	180.8	5.2	2.9	218	12	5.4	645	112	17	-
Z2d22c	0.01099	0.00039	0.082	0.0054	0.0541	0.003	0.54	70.4	2.5	3.5	80	5	6.3	377	124	33	-
Z2d22r	0.01068	0.00038	0.0746	0.0041	0.0507	0.0022	0.63	68.5	2.4	3.5	73.1	3.9	5.4	228	99	44	-
Z2d23c	0.01203	0.00056	0.087	0.016	0.0525	0.0096	0.25	77.1	3.5	4.6	85	15	18	305	337	110	-
Z2d23r	0.0091	0.00029	0.0606	0.0031	0.0483	0.002	0.61	58.4	1.8	3.1	59.8	3	5	114	96	84	-
z2d1r	0.00892	0.0003	0.0695	0.0042	0.0565	0.0029	0.55	57.2	1.9	3.3	68.2	4	5.8	473	112	24	-
Z2d1c	0.00828	0.00042	0.0444	0.0071	0.0389	0.0059	0.31	53.2	2.7	5	44.1	6.9	15.7	-	0	-	-
z2d2r	0.01161	0.0003	0.0895	0.0043	0.0559	0.0023	0.53	74.4	1.9	2.6	87	4.1	4.7	449	92	20	-
Z2d2c	0.01123	0.00042	0.0751	0.0044	0.0485	0.0022	0.63	72	2.7	3.7	73.5	4.2	5.7	122	108	88	-
z2d3r	0.00867	0.00022	0.0643	0.0031	0.0538	0.0022	0.52	55.6	1.4	2.5	63.3	3	4.7	364	94	26	-
Z2d3c	0.00899	0.00039	0.0639	0.0053	0.0515	0.0037	0.52	57.7	2.5	4.4	62.8	5.1	8.1	264	164	62	-
Z2d4c	0.0277	0.0011	0.1964	0.0098	0.0513	0.0016	0.78	176.4	6.7	3.8	182.1	8.3	4.6	256	73	28	-
z2d4r	0.00903	0.00029	0.0605	0.0025	0.0486	0.0013	0.78	57.9	1.8	3.2	59.6	2.4	4	127	61	48	-
Z2d5c	0.00821	0.00045	0.0541	0.0054	0.0478	0.0039	0.56	52.7	2.9	5.5	53.5	5.2	9.7	90	137	152	-
z2d5r	0.01777	0.00037	0.147	0.01	0.0602	0.004	0.3	113.5	2.3	2.1	139.6	9.1	6.5	610	145	24	-
z2d6r	0.03273	0.00083	0.224	0.014	0.0497	0.0029	0.4	207.6	5.2	2.5	206	12	5.8	182	136	75	-
z2d7c	0.03326	0.00082	0.2362	0.0093	0.0515	0.0016	0.62	210.9	5.1	2.4	215.3	7.6	3.5	263	71	27	-
z2d8c	0.2128	0.0063	2.56	0.11	0.0873	0.0026	0.7	1244	34	2.7	1290	31	2.4	1367	58	4	0.91

Z2d8r	0.0089	0.00038	0.0588	0.0032	0.048	0.0016	0.78	57.1	2.4	4.2	58.1	3.1	5.3	98	81	83	-
Z2d9c	0.0253	0.001	0.184	0.012	0.0527	0.0027	0.61	161.2	6.3	3.9	171	10	6	315	117	37	-
z2d9r	0.0255	0.0011	0.24	0.024	0.0683	0.0061	0.45	162.3	7.2	4.4	219	20	9	878	186	21	-
Z3cm1c	0.014	0.0004	0.0916	0.0031	0.04745	0.00085	0.85	89.6	2.5	2.8	89	2.9	3.2	72	43	59	-
Z3m1r	0.01419	0.0006	0.0942	0.0045	0.0481	0.001	0.9	90.9	3.8	4.2	91.4	4.1	4.5	105	49	47	-
Z3m2r	0.01409	0.00056	0.0971	0.0067	0.05	0.0028	0.58	90.2	3.6	4	94.1	6.2	6.5	195	130	67	-
Z3m2c	0.01442	0.00047	0.1004	0.0055	0.0505	0.0022	0.6	92.3	3	3.2	97.1	5	5.2	217	102	47	-
Z3m3c	0.01439	0.00045	0.0945	0.0046	0.0476	0.0018	0.63	92.1	2.8	3.1	91.7	4.3	4.7	80	84	105	-
Z3m4c	0.01014	0.00032	0.0653	0.0036	0.0467	0.0022	0.56	65.1	2	3.1	64.2	3.5	5.4	34	70	209	-
Z3m4r	0.00829	0.00035	0.0527	0.0029	0.0461	0.0016	0.76	53.2	2.2	4.2	52.2	2.8	5.4	5	44	890	-
Z3m5r	0.00831	0.00049	0.0514	0.0053	0.0449	0.0038	0.57	53.3	3.1	5.8	50.9	5.1	10.1	-	66	-	-
Z3m5c	0.00854	0.00026	0.0582	0.0029	0.0495	0.0019	0.62	54.8	1.7	3	57.5	2.7	4.8	170	90	53	-
Z3m6r	0.008	0.00047	0.052	0.0054	0.0471	0.004	0.57	51.4	3	5.9	51.4	5.2	10.1	55	124	224	-
Z3m6r	0.00779	0.00036	0.0512	0.0047	0.0476	0.0038	0.49	50	2.3	4.5	50.7	4.6	9	81	131	161	-
Z3m7r	0.01021	0.00039	0.0696	0.0038	0.0494	0.002	0.69	65.5	2.5	3.8	68.3	3.6	5.3	169	93	55	-
Z3m7c	0.00955	0.00029	0.0617	0.0023	0.04684	0.00098	0.82	61.3	1.9	3	60.8	2.2	3.6	41	45	110	-
Z3m8c	0.01104	0.00036	0.0791	0.0054	0.0519	0.0031	0.48	70.8	2.3	3.3	77.3	5.1	6.6	282	137	49	-
Z3m8r	0.01082	0.00051	0.0787	0.0059	0.0528	0.0031	0.63	69.4	3.2	4.7	76.9	5.6	7.2	318	133	42	-
Z3m9r	0.275	0.011	3.81	0.18	0.1005	0.0024	0.86	1566	56	3.6	1595	38	2.4	1633	44	2.7	0.96
Z3m9c	0.2862	0.0079	3.95	0.13	0.1	0.0017	0.85	1622	40	2.5	1623	26	1.6	1625	32	2	1
Z3m10r	0.0122	0.00049	0.0876	0.0053	0.052	0.0023	0.67	78.2	3.1	4	85.2	4.9	5.8	287	102	36	-
Z3m10c	0.01241	0.00048	0.0819	0.0043	0.0479	0.0017	0.74	79.5	3.1	3.9	79.9	4.1	5.1	92	84	91	-
Z3m11c	0.01218	0.0007	0.0801	0.0053	0.0477	0.0016	0.86	78	4.4	5.7	78.3	5	6.4	87	79	91	-
Z3m11c	0.01145	0.00068	0.0753	0.0054	0.0477	0.002	0.82	73.4	4.3	5.9	73.7	5.1	7	84	89	107	-
Z3m12r	0.01097	0.00048	0.0719	0.0038	0.0475	0.0013	0.84	70.4	3.1	4.4	70.5	3.6	5.1	76	67	88	-
Z3m12c	0.01079	0.00053	0.0718	0.0054	0.0483	0.0028	0.65	69.2	3.4	4.9	70.4	5.2	7.3	112	121	108	-
								18MPI2									
z1c1r	0.0195	0.0011	0.145	0.012	0.0542	0.0031	0.7	124.2	6.9	5.5	138	10	7.5	379	129	34	-
Z1c1c	0.01805	0.00091	0.062	0.014	0.0249	0.0054	0.22	115.3	5.7	5	61	13	21.7		0	-	-
Z1c10c	0.3008	0.0047	4.39	0.11	0.1059	0.002	0.63	1695	23	1.4	1711	20	1.2	1730	35	2	0.98
Z1c12c	0.01093	0.00032	0.0816	0.0057	0.0542	0.0034	0.42	70	2.1	3	79.7	5.4	6.8	379	143	38	-
z1c12r	0.01027	0.00036	0.0721	0.0036	0.0509	0.0018	0.7	65.9	2.3	3.5	70.7	3.4	4.9	236	83	35	-
Z1c13c	0.02131	0.0007	0.131	0.013	0.0446	0.0041	0.34	135.9	4.4	3.2	125	11	9.1	-	67	-	-
z1c18r	0.00848	0.00031	0.0556	0.0027	0.0475	0.0015	0.76	54.4	2	3.6	54.9	2.6	4.7	76	74	97	-
z1c15r	0.00811	0.00033	0.0586	0.0039	0.0524	0.0027	0.62	52	2.1	4.1	57.8	3.7	6.5	303	119	39	-
z1c16c	0.01713	0.00067	0.1194	0.0084	0.0505	0.003	0.55	109.5	4.2	3.9	114.5	7.7	6.7	220	137	62	-
z1c17r	0.0117	0.00065	0.0797	0.0074	0.0494	0.0037	0.6	75	4.1	5.5	77.8	6.9	8.9	167	166	99	-
Z1c17c	0.01222	0.0003	0.0806	0.0048	0.0478	0.0026	0.42	78.3	1.9	2.5	78.7	4.5	5.7	92	107	117	-
z1c18r	0.00848	0.00031	0.0556	0.0027	0.0475	0.0015	0.76	54.4	2	3.6	54.9	2.6	4.7	76	74	97	-
Z1c18c	0.0084	0.00028	0.0195	0.0089	0.0169	0.0077	0.07	53.9	1.8	3.4	19.6	8.9	45.3	-	0	-	-
z1c19r	0.00953	0.00062	0.068	0.011	0.0515	0.0076	0.41	61.2	4	6.5	67	10	15.6	264	285	108	-

Z1c19c	0.00942	0.00023	0.059	0.0043	0.0454	0.0031	0.35	60.4	1.5	2.5	58.2	4.1	7	-	63	-	-
z1c2c	0.00841	0.00039	0.0553	0.0084	0.0477	0.0069	0.3	54	2.5	4.6	54.7	8	14.7	84	197	236	-
Z1c2r	0.00862	0.00041	0.0578	0.004	0.0487	0.0024	0.69	55.3	2.6	4.8	57.1	3.9	6.8	131	118	90	-
z1c20r	0.00742	0.00033	0.0495	0.0027	0.0484	0.0016	0.81	47.7	2.1	4.4	49.1	2.6	5.4	117	77	65	-
Z1c20c	0.00801	0.00024	0.0548	0.004	0.0496	0.0033	0.42	51.4	1.6	3	54.2	3.8	7	178	153	86	-
z1c21	0.01578	0.00089	0.105	0.038	0.048	0.017	0.16	101	5.7	5.6	101	35	34.6	102	392	386	-
z1c24r	0.01177	0.00054	0.079	0.012	0.0488	0.0072	0.3	75.5	3.4	4.5	77	11	14.9	136	225	165	-
z1c3r	0.0242	0.0016	0.199	0.022	0.0599	0.0051	0.61	154	10	6.5	185	18	9.9	599	186	31	-
Z1c3c	0.0268	0.0013	0.18	0.01	0.0488	0.0013	0.88	170.3	8.4	4.9	168.3	8.9	5.3	140	65	46	-
z1c4r	0.00781	0.00024	0.0547	0.0026	0.0508	0.0019	0.63	50.2	1.5	3	54.1	2.5	4.7	231	86	37	-
Z1c4c	0.0077	0.00037	0.0516	0.0034	0.0487	0.0022	0.73	49.4	2.3	4.7	51.1	3.3	6.4	133	106	80	-
z1c6r	0.01935	0.00048	0.1374	0.0057	0.0515	0.0017	0.6	123.5	3	2.5	130.7	5.1	3.9	263	76	29	-
Z1c6c	0.01983	0.00094	0.1332	0.0088	0.0487	0.0022	0.72	126.6	5.9	4.7	126.9	7.9	6.2	134	107	80	-
z1c7r	0.02578	0.0007	0.1783	0.0067	0.0501	0.0013	0.72	164.1	4.4	2.7	166.6	5.8	3.5	202	61	30	-
Z1c7c	0.0255	0.0012	0.1775	0.009	0.0506	0.0012	0.89	162.1	7.2	4.5	165.9	7.8	4.7	221	54	24	-
Z1c9c	0.01318	0.00068	0.0871	0.0068	0.0479	0.0028	0.66	84.4	4.3	5.1	84.8	6.4	7.5	95	115	120	-
z1c9r	0.0139	0.00063	0.1024	0.0089	0.0535	0.0039	0.52	89	4	4.5	99	8.2	8.3	348	167	48	-
Z4a10r	0.01203	0.00036	0.0792	0.0042	0.0478	0.0021	0.57	77.1	2.3	3	77.4	3.9	5.1	89	94	106	-
Z4a11c	0.01551	0.00041	0.1027	0.0037	0.048	0.0012	0.72	99.2	2.6	2.6	99.3	3.4	3.5	102	60	59	-
Z4a11r	0.015	0.00041	0.0973	0.0042	0.047	0.0015	0.64	96	2.6	2.7	94.3	3.9	4.1	52	64	124	-
Z4a1c	0.02849	0.00078	0.1973	0.007	0.0502	0.0012	0.76	181.1	4.9	2.7	182.8	6	3.3	205	54	26	-
Z4a1r	0.02855	0.00061	0.2015	0.0088	0.0512	0.002	0.49	181.4	3.8	2.1	186.4	7.5	4	250	88	35	-
Z4a2r	0.00987	0.00028	0.0681	0.0033	0.05	0.002	0.59	63.3	1.8	2.8	66.9	3.1	4.7	197	91	46	-
Z4a4c	0.00937	0.00034	0.0616	0.0045	0.0477	0.003	0.5	60.1	2.2	3.6	60.7	4.3	7.1	84	113	136	-
Z4a5c	0.00831	0.00027	0.0545	0.003	0.0476	0.0021	0.59	53.3	1.7	3.2	53.9	2.9	5.4	78	90	115	-
Z4a6c	0.01123	0.0003	0.0748	0.0036	0.0483	0.0019	0.56	72	1.9	2.7	73.2	3.4	4.7	114	95	83	-
Z4a6r	0.01123	0.00029	0.0759	0.0028	0.049	0.0013	0.71	72	1.9	2.6	74.3	2.6	3.6	150	61	41	-
Z4a7c	0.0083	0.0003	0.0589	0.0046	0.0515	0.0035	0.46	53.3	1.9	3.6	58.1	4.4	7.5	262	158	60	-
Z4a7r	0.00885	0.00024	0.0748	0.0051	0.0613	0.0038	0.4	56.8	1.5	2.7	73.2	4.8	6.5	649	134	21	-
Z4a8c	0.0414	0.0013	0.311	0.012	0.0544	0.0012	0.82	261.3	8	3.1	274.6	9.2	3.3	390	49	13	-
Z4a9c	0.02223	0.00072	0.15	0.0083	0.0489	0.0022	0.59	141.7	4.6	3.2	141.9	7.3	5.2	144	105	73	-
Z4a3c	0.00909	0.00055	0.043	0.012	0.0343	0.0096	0.21	58.3	3.5	6	43	12	28	-	0	-	-
Z3c10c	0.01431	0.00056	0.0979	0.0053	0.0497	0.0018	0.73	91.6	3.6	3.9	94.9	4.9	5.1	179	85	48	-
Z3c10r	0.01466	0.00071	0.0981	0.0053	0.0485	0.0012	0.89	93.8	4.5	4.8	95	4.9	5.2	126	57	45	-
Z3c11r	0.01453	0.00099	0.094	0.013	0.0467	0.0055	0.5	93	6.3	6.8	91	12	13.1	34	148	433	-
Z3c12c	0.01094	0.00044	0.0817	0.0058	0.0542	0.0031	0.57	70.2	2.8	4	79.8	5.4	6.8	378	131	35	-
Z3c12r	0.00838	0.00042	0.0596	0.0054	0.0516	0.0039	0.55	53.8	2.7	5	58.8	5.2	8.8	269	175	65	-
Z3c13c	0.007	0.00031	0.0463	0.0029	0.048	0.0021	0.71	45	2	4.5	46	2.8	6.2	99	100	102	-
Z3c13r	0.00754	0.00048	0.0496	0.0065	0.0477	0.0055	0.48	48.4	3	6.3	49.2	6.3	12.8	86	169	197	-
Z3c14c	0.00864	0.00041	0.0586	0.0053	0.0491	0.0038	0.51	55.5	2.6	4.7	57.8	5.1	8.9	155	164	106	-

Z3c14r	0.00828	0.00039	0.058	0.0049	0.0508	0.0035	0.56	53.2	2.5	4.7	57.3	4.7	8.2	233	161	69	-
Z3c15r	0.00764	0.00047	0.0228	0.0051	0.0216	0.0046	0.28	49.1	3	6.1	22.9	5	21.9	-	0	-	-
Z3c15c	0.01538	0.00065	0.103	0.012	0.0486	0.005	0.38	98.4	4.1	4.2	100	11	10.7	128	178	139	-
Z3c16c	0.01275	0.00055	0.0858	0.0042	0.0488	0.0011	0.88	81.7	3.5	4.3	83.6	3.9	4.7	139	55	39	-
Z3c16r	0.0091	0.0004	0.0606	0.0038	0.0483	0.0021	0.7	58.4	2.5	4.3	59.8	3.6	6	116	104	90	-
Z3c17c	0.00721	0.00032	0.0525	0.0034	0.0528	0.0024	0.69	46.3	2	4.4	52	3.2	6.2	321	105	33	-
Z3c18c	0.01476	0.00057	0.0966	0.0047	0.0475	0.0014	0.79	94.4	3.6	3.8	93.6	4.4	4.7	73	71	98	-
Z3c18r	0.01438	0.00061	0.101	0.0062	0.0509	0.0023	0.69	92	3.9	4.2	97.7	5.7	5.9	238	102	43	-
Z3c19c	0.0243	0.0016	0.183	0.029	0.0546	0.0079	0.41	154.7	9.9	6.4	171	25	14.6	396	330	83	-
Z3c19r	0.0238	0.0012	0.17	0.014	0.0519	0.0033	0.63	151.8	7.7	5.1	160	12	7.6	280	145	52	-
Z3c1c	0.0218	0.0011	0.1545	0.0095	0.0513	0.0019	0.8	139.3	6.8	4.9	145.9	8.4	5.7	255	85	33	-
Z3c1r	0.0218	0.001	0.158	0.01	0.0527	0.0024	0.72	139	6.4	4.6	149.3	9	6	316	102	32	-
Z3c2c	0.0119	0.00045	0.0844	0.005	0.0514	0.0023	0.64	76.3	2.9	3.8	82.3	4.7	5.7	261	105	40	-
Z3c2r	0.01176	0.0008	0.0741	0.0087	0.0457	0.0043	0.58	75.4	5.1	6.8	72.6	8.2	11.3	-	98	-	-
Z3c20c	0.01569	0.00063	0.0715	0.0057	0.0331	0.0023	0.5	100.4	4	4	70.2	5.4	7.8	-	0	-	-
Z3c20r	0.01548	0.00065	0.1063	0.0063	0.0498	0.0021	0.71	99	4.1	4.1	102.5	5.8	5.6	185	97	52	-
Z3c21c	0.00875	0.00039	0.0582	0.0032	0.0482	0.0016	0.81	56.2	2.5	4.4	57.5	3.1	5.4	111	77	69	-
Z3c21r	0.01351	0.00065	0.0911	0.0053	0.0489	0.0016	0.83	86.5	4.1	4.7	88.5	4.9	5.5	142	77	54	-
Z3c22c	0.00935	0.0005	0.0582	0.0054	0.0451	0.0034	0.58	60	3.2	5.3	57.4	5.2	9	-	63	-	-
Z3c22r	0.00961	0.00054	0.0645	0.0059	0.0487	0.0035	0.61	61.7	3.5	5.6	63.5	5.7	8.9	132	147	111	-
Z3c23c	0.0306	0.0013	0.222	0.011	0.0526	0.0016	0.82	194.3	8.1	4.2	203.4	9.5	4.7	310	67	22	-
Z3c23r	0.00863	0.00036	0.0585	0.0029	0.0492	0.0013	0.85	55.4	2.3	4.1	57.7	2.7	4.7	155	61	39	-
Z3c25c	0.01455	0.0006	0.0963	0.0049	0.048	0.0015	0.8	93.1	3.8	4.1	93.4	4.6	4.9	99	73	73	-
Z3c25r	0.01643	0.0007	0.107	0.0071	0.0473	0.0024	0.64	105	4.4	4.2	103.2	6.5	6.3	62	90	144	-
Z3c26c	0.0086	0.00036	0.0576	0.0035	0.0485	0.0021	0.71	55.2	2.3	4.2	56.8	3.3	5.8	126	100	80	-
Z3c26r	0.00856	0.00042	0.0587	0.0043	0.0498	0.0027	0.66	55	2.7	4.8	58	4.1	7.1	184	128	69	-
Z3c27c	0.054	0.0022	0.397	0.019	0.0534	0.0013	0.85	339	13	4	340	14	4.1	345	56	16	-
Z3c28c	0.0234	0.001	0.1586	0.0093	0.0491	0.0019	0.74	149.2	6.4	4.3	149.5	8.2	5.5	154	92	60	-
Z3c29c	0.0054	0.00026	0.0361	0.0033	0.0485	0.0038	0.52	34.7	1.6	4.7	36	3.3	9	124	150	121	-
Z3c30c	0.01001	0.00031	0.0666	0.0029	0.0483	0.0015	0.71	64.2	2	3.1	65.5	2.8	4.2	113	73	65	-
Z3c30r	0.00957	0.00044	0.0679	0.0042	0.0514	0.0022	0.74	61.4	2.8	4.6	66.7	4	6	261	96	37	-
Z3c31c	0.01352	0.00043	0.0923	0.0041	0.0495	0.0015	0.73	86.6	2.8	3.2	89.6	3.8	4.2	171	71	41	-
Z3c32c	0.00856	0.00035	0.0576	0.0054	0.0488	0.0041	0.44	54.9	2.2	4.1	56.9	5.2	9.1	140	163	117	-
Z3c32r	0.00909	0.0005	0.0655	0.0061	0.0523	0.0039	0.59	58.3	3.2	5.5	64.4	5.8	9	298	172	58	-
Z3c34c	0.0116	0.00039	0.0876	0.0049	0.0548	0.0025	0.59	74.3	2.5	3.3	85.3	4.6	5.4	404	101	25	-
Z3c35c	0.015	0.00053	0.1045	0.0071	0.0505	0.003	0.52	95.9	3.4	3.5	100.9	6.6	6.5	220	136	62	-
Z3c36c	0.0136	0.00045	0.0893	0.0049	0.0476	0.0021	0.61	87.1	2.9	3.3	86.9	4.5	5.2	81	91	111	-
Z3c36r	0.01302	0.00062	0.0848	0.005	0.0472	0.0016	0.81	83.4	4	4.7	82.6	4.7	5.6	60	69	116	-
Z3c37c	0.01611	0.00052	0.1079	0.0041	0.04856	0.00097	0.85	103	3.3	3.2	104	3.8	3.6	127	47	37	-
Z3c37r	0.01708	0.00076	0.113	0.0059	0.048	0.0013	0.85	109.2	4.8	4.4	108.7	5.4	5	99	64	65	-
Z3c38c	0.0087	0.00046	0.0786	0.0076	0.0655	0.0053	0.55	55.9	2.9	5.3	76.8	7.1	9.3	790	170	22	-

Z3c39r	0.0243	0.0013	0.126	0.016	0.0376	0.0043	0.44	154.8	8.5	5.5	120	14	12	-	0	-	-
Z3c3c	0.0135	0.00065	0.0836	0.0056	0.0449	0.0021	0.72	86.4	4.2	4.8	81.5	5.2	6.4	-	24	-	-
Z3c3r	0.01369	0.00051	0.0922	0.0038	0.04881	0.00094	0.89	87.7	3.2	3.7	89.5	3.6	4	139	45	33	-
Z3c3r	0.0123	0.00053	0.0845	0.0042	0.0499	0.0012	0.88	78.8	3.4	4.3	82.4	3.9	4.7	189	55	29	-
Z3c40c	0.016	0.00048	0.102	0.0099	0.0462	0.0043	0.31	102.3	3.1	3	98.7	9.1	9.3	11	110	1027	-
Z3c40r	0.01566	0.00072	0.1029	0.0061	0.0477	0.0018	0.77	100.2	4.5	4.5	99.4	5.6	5.7	82	85	104	-
Z3c41c	0.01551	0.00049	0.1092	0.0051	0.051	0.0018	0.67	99.2	3.1	3.1	105.2	4.7	4.5	242	81	33	-
Z3c42c	0.00713	0.0005	0.0606	0.0096	0.0616	0.0088	0.44	45.8	3.2	6.9	59.7	9.2	15.4	662	309	47	-
Z3c42r	0.00934	0.00051	0.061	0.011	0.0475	0.0083	0.3	59.9	3.2	5.4	60	11	17.8	73	222	303	-
Z3c43c	0.02133	0.00077	0.1452	0.0084	0.0494	0.0022	0.62	136	4.8	3.6	137.7	7.4	5.4	166	106	64	-
Z3c45c	0.01762	0.00081	0.1311	0.0073	0.054	0.0017	0.82	112.6	5.1	4.5	125.1	6.6	5.3	369	73	20	-
Z3c45r	0.0013	0.0076	0.009	0.053	0.0508	0.0028	1	9	49	570.7	9	53	569	232	128	55	-
Z3c46c	0.0302	0.001	0.214	0.011	0.0515	0.002	0.67	191.6	6.5	3.4	197.3	9.3	4.7	265	88	33	-
Z3c47c	0.01464	0.00048	0.0968	0.004	0.048	0.0012	0.79	93.7	3	3.2	93.8	3.7	3.9	98	60	61	-
Z3c4c	0.0131	0.0005	0.0879	0.0039	0.0487	0.0011	0.86	83.9	3.2	3.8	85.5	3.6	4.2	131	53	40	-
Z3c4r	0.01285	0.00058	0.0845	0.005	0.0477	0.0018	0.77	82.3	3.7	4.5	82.4	4.7	5.7	83	85	102	-
Z3c5c	0.01359	0.00074	0.0889	0.0068	0.0474	0.0025	0.71	87	4.7	5.4	86.4	6.3	7.3	70	96	138	-
Z3c5r	0.0136	0.0019	0.087	0.014	0.0464	0.0039	0.85	87	12	13.6	85	13	15.5	20	105	536	-
Z3c6c	0.00672	0.00035	0.0582	0.0049	0.0628	0.0042	0.61	43.1	2.2	5.2	57.4	4.7	8.2	703	144	20	-
Z3c6r	0.00697	0.00038	0.0551	0.0047	0.0574	0.0037	0.65	44.7	2.5	5.5	54.5	4.5	8.3	507	143	28	-
Z3c7c	0.0091	0.00035	0.0614	0.0031	0.0489	0.0016	0.77	58.4	2.2	3.9	60.5	3	4.9	143	76	53	-
Z3c7r	0.0094	0.00045	0.0678	0.0041	0.0523	0.0019	0.79	60.3	2.9	4.7	66.6	3.9	5.8	299	84	28	-
Z3c8r	0.00777	0.00037	0.0617	0.0051	0.0576	0.0038	0.58	49.9	2.4	4.7	60.7	4.8	8	513	147	29	-
Z3c9c	0.02462	0.00096	0.1736	0.0092	0.0511	0.0018	0.73	156.8	6	3.8	162.5	8	4.9	247	83	34	-
Z3c9r	0.026	0.0012	0.184	0.015	0.0515	0.0035	0.57	165.2	7.8	4.7	172	13	7.7	265	158	59	-
Z3c44r	0.00826	0.00029	0.0584	0.0033	0.0512	0.0023	0.62	53	1.9	3.5	57.6	3.2	5.5	251	103	41	-
Z3c44c	0.00865	0.0004	0.0612	0.0035	0.0513	0.0018	0.79	55.5	2.5	4.6	60.3	3.4	5.6	254	81	32	-
								18MPI1									
Z3e1c	0.01664	0.00062	0.1105	0.0078	0.0482	0.0029	0.52	106.4	3.9	3.7	106.4	7.2	6.7	108	122	113	-
Z3e10c	0.00699	0.00041	0.0463	0.007	0.0481	0.0067	0.39	44.9	2.6	5.8	46	6.8	14.8	105	202	194	-
Z3e10r	0.00945	0.00062	0.06	0.02	0.046	0.015	0.19	60.7	3.9	6.5	59	20	33	7	329	4872	-
Z3e11c	0.01798	0.00035	0.132	0.011	0.0532	0.0044	0.23	114.9	2.2	1.9	126	10	8.1	337	190	56	-
Z3e11r	0.01842	0.00096	0.139	0.014	0.0548	0.0048	0.51	117.7	6.1	5.2	132	13	9.5	403	195	48	-
Z3e12c	0.00886	0.0004	0.0577	0.0076	0.0472	0.0058	0.34	56.9	2.5	4.4	57	7.3	12.7	62	166	269	-
Z3e13c	0.01087	0.00052	0.0711	0.0059	0.0474	0.0032	0.57	69.7	3.3	4.8	69.7	5.6	8.1	71	113	160	-
Z3e13r	0.01079	0.00023	0.0737	0.0032	0.0496	0.0019	0.5	69.2	1.5	2.2	72.2	3	4.2	174	88	50	-
Z3e14r	0.00843	0.0003	0.0552	0.0034	0.0475	0.0024	0.59	54.1	1.9	3.6	54.5	3.2	6	72	93	129	-
Z3e14r	0.01256	0.00056	0.08	0.012	0.0463	0.0069	0.29	80.5	3.6	4.5	78	12	14.9	12	168	1370	-
Z3e15c	0.01035	0.00022	0.0718	0.0039	0.0503	0.0025	0.39	66.4	1.4	2.1	70.4	3.7	5.3	209	116	56	-
Z3e15r	0.0105	0.00019	0.0689	0.0024	0.0476	0.0014	0.51	67.3	1.2	1.8	67.7	2.3	3.4	79	72	91	-
Z3e16c	0.00997	0.00029	0.0654	0.005	0.0476	0.0034	0.38	64	1.8	2.9	64.4	4.8	7.4	79	120	152	-

Z3e17c	0.00909	0.00038	0.0637	0.0087	0.0508	0.0066	0.31	58.3	2.4	4.2	62.7	8.3	13.3	233	254	109	-
Z3e18c	0.01591	0.00036	0.1048	0.0037	0.0478	0.0013	0.64	101.8	2.3	2.3	101.2	3.4	3.4	87	65	75	-
Z3e18r	0.01503	0.00064	0.1002	0.0057	0.0484	0.0018	0.75	96.2	4.1	4.2	97	5.3	5.4	117	89	77	-
Z3e19c	0.02679	0.0005	0.1808	0.0043	0.04896	0.00075	0.77	170.4	3.1	1.8	168.8	3.7	2.2	146	36	24	-
Z3e19r	0.0268	0.0015	0.185	0.011	0.05002	0.00089	0.95	170.6	9.6	5.6	172.3	9.4	5.5	196	41	21	-
Z3e20c	0.01104	0.00022	0.082	0.011	0.0539	0.0068	0.16	70.8	1.4	2	80.1	9.9	12.3	367	289	79	-
Z3e20r	0.01035	0.00059	0.0776	0.0066	0.0544	0.0034	0.68	66.4	3.8	5.7	75.9	6.2	8.2	386	140	36	-
Z3e21c	0.01121	0.00028	0.0761	0.0033	0.0493	0.0018	0.58	71.8	1.8	2.5	74.5	3.1	4.2	160	84	52	-
Z3e21r	0.00844	0.00051	0.0569	0.0043	0.0489	0.0023	0.79	54.2	3.2	6	56.1	4.2	7.4	141	111	78	-
Z3e22c	0.01516	0.00084	0.0997	0.0066	0.0477	0.0017	0.84	97	5.3	5.5	96.5	6.1	6.3	84	84	99	-
Z3e22r	0.01428	0.0003	0.0975	0.0052	0.0495	0.0024	0.39	91.4	1.9	2.1	94.4	4.8	5.1	171	115	67	-
Z3e23c	0.00767	0.00021	0.0486	0.0024	0.0459	0.0019	0.56	49.3	1.3	2.7	48.2	2.3	4.8	-	44	-	-
Z3e25c	0.02943	0.00091	0.2131	0.0089	0.0525	0.0015	0.74	187	5.7	3.1	196.1	7.4	3.8	308	63	21	-
Z3e26c	0.01356	0.00034	0.0915	0.0045	0.049	0.0021	0.51	86.8	2.2	2.5	88.9	4.2	4.7	146	99	68	-
Z3e26r	0.01418	0.0008	0.0957	0.0081	0.049	0.003	0.67	90.7	5.1	5.6	92.8	7.5	8	146	143	98	-
Z3e27c	0.02536	0.00084	0.1731	0.009	0.0495	0.002	0.64	161.5	5.3	3.3	162.1	7.8	4.8	172	93	54	-
Z3e28c	0.00992	0.00059	0.0696	0.0058	0.0509	0.0029	0.72	63.6	3.8	5.9	68.3	5.5	8	236	134	57	-
Z3e28r	0.0118	0.0003	0.0803	0.0043	0.0493	0.0023	0.48	75.6	1.9	2.6	78.4	4	5.1	164	109	66	-
Z3e29r	0.00969	0.00028	0.0671	0.0049	0.0502	0.0033	0.4	62.1	1.8	2.9	65.9	4.6	7	205	155	75	-
Z3e2c	0.01523	0.00058	0.0971	0.0063	0.0463	0.0024	0.58	97.4	3.7	3.8	94.1	5.8	6.2	11	67	589	-
Z3e2r	0.0144	0.00041	0.0992	0.0054	0.05	0.0023	0.52	92.1	2.6	2.9	96.1	5	5.2	195	109	56	-
Z3e30c	0.02724	0.00095	0.17	0.012	0.0453	0.0028	0.5	173.2	5.9	3.4	159	10	6.5	-	50	-	-
Z3e30r	0.0295	0.0017	0.189	0.017	0.0464	0.0032	0.65	187	11	5.8	176	14	8.2	19	87	463	-
Z3e31c	0.01421	0.00051	0.0961	0.007	0.0491	0.0031	0.5	91	3.3	3.6	93.2	6.5	6.9	150	146	97	-
Z3e31r	0.01556	0.00089	0.1038	0.0068	0.0484	0.0015	0.87	99.5	5.6	5.7	100.3	6.2	6.2	118	76	64	-
Z3e32c	0.02443	0.0006	0.1661	0.0053	0.0493	0.001	0.77	155.6	3.8	2.4	156	4.6	3	163	48	30	-
Z3e32r	0.0262	0.0014	0.181	0.012	0.0501	0.0019	0.81	166.4	8.8	5.3	169	10	6.1	200	90	45	-
Z3e33r	0.017	0.0011	0.117	0.019	0.0502	0.0076	0.38	108.5	6.7	6.2	113	17	15.5	203	261	128	-
Z3e33c	0.01545	0.00058	0.1018	0.0074	0.0478	0.003	0.51	98.8	3.7	3.7	98.4	6.8	6.9	89	115	129	-
Z3e34c	0.01077	0.00028	0.0728	0.0067	0.049	0.0043	0.28	69.1	1.8	2.6	71.4	6.3	8.8	149	171	115	-
Z3e34r	0.01133	0.00065	0.079	0.012	0.0506	0.0071	0.38	72.6	4.1	5.7	77	11	14.6	222	259	117	-
Z3e35c	0.00957	0.00052	0.0571	0.0073	0.0433	0.005	0.42	61.4	3.3	5.4	56.4	7	12.4	-	56	-	-
Z3e35r	0.01013	0.00051	0.0681	0.0038	0.0488	0.0011	0.92	65	3.3	5	66.9	3.6	5.4	137	52	38	-
Z3e36c	0.01462	0.00042	0.0995	0.0066	0.0493	0.0029	0.44	93.6	2.7	2.9	96.3	6.1	6.3	164	140	85	-
Z3e36r	0.01581	0.00082	0.1097	0.009	0.0503	0.0032	0.63	101.1	5.2	5.1	105.7	8.3	7.8	211	150	71	-
Z3e37c	0.01031	0.00031	0.0676	0.0031	0.0475	0.0016	0.67	66.1	2	3	66.4	2.9	4.4	77	78	101	-
Z3e37r	0.0096	0.0005	0.0652	0.0047	0.0493	0.0025	0.72	61.6	3.2	5.2	64.1	4.5	7	160	117	73	-
38r	0.00857	0.00029	0.0568	0.004	0.0481	0.003	0.48	55	1.8	3.3	56.1	3.8	6.8	104	122	117	-
Z3e38c	0.00827	0.00054	0.0551	0.0051	0.0483	0.0032	0.7	53.1	3.4	6.5	54.4	4.9	9.1	115	132	115	-
Z3e39c	0.01539	0.0005	0.1036	0.0073	0.0488	0.0031	0.46	98.4	3.2	3.2	100.1	6.7	6.7	140	140	100	-
Z3e39r	0.01426	0.00077	0.0862	0.0074	0.0438	0.0029	0.63	91.3	4.9	5.3	83.9	6.9	8.2	-	18	-	-

Z3e3c	0.01245	0.00044	0.081	0.0036	0.0472	0.0012	0.8	79.7	2.8	3.5	79.1	3.4	4.3	60	61	102	-
Z3e3r	0.01202	0.00034	0.0873	0.0061	0.0526	0.0034	0.4	77	2.2	2.8	84.9	5.7	6.8	314	147	47	-
Z3e40c	0.01286	0.00054	0.0825	0.0054	0.0465	0.0024	0.63	82.4	3.4	4.1	80.5	5.1	6.4	24	71	301	-
Z3e41c	0.02452	0.00065	0.1754	0.0084	0.0519	0.0021	0.55	156.2	4.1	2.6	164.1	7.3	4.4	280	92	33	-
Z3e41r	0.0249	0.0013	0.174	0.013	0.0506	0.0027	0.7	158.4	8.1	5.1	163	11	6.9	225	125	55	-
Z4e43c	0.0365	0.00083	0.27	0.024	0.0537	0.0047	0.25	231.1	5.2	2.2	243	19	8	359	197	55	-
Z3e43r	0.01114	0.00041	0.0715	0.005	0.0466	0.0027	0.53	71.4	2.6	3.7	70.2	4.7	6.7	27	81	298	-
Z4e42r	0.2352	0.0059	2.845	0.083	0.0877	0.0013	0.86	1361	31	2.3	1367	22	1.6	1377	29	2.1	0.99
Z3e42r	0.225	0.011	2.65	0.13	0.0853	0.0015	0.94	1309	56	4.3	1314	37	2.9	1321	34	2.6	0.99
Z3e44c	0.01465	0.00052	0.0953	0.0061	0.0471	0.0025	0.56	93.8	3.3	3.5	92.4	5.6	6.1	57	89	157	-
Z4e44r	0.01207	0.00033	0.0793	0.0044	0.0477	0.0023	0.49	77.4	2.1	2.7	77.5	4.1	5.3	83	96	116	-
Z3e45c	0.03385	0.0009	0.237	0.012	0.0507	0.0021	0.54	214.6	5.6	2.6	215.7	9.6	4.4	228	96	42	-
Z4e46c	0.01572	0.00042	0.1049	0.0045	0.0484	0.0016	0.62	100.5	2.6	2.6	101.3	4.1	4.1	119	79	67	-
Z3e46r	0.01677	0.0007	0.1186	0.0075	0.0513	0.0024	0.66	107.2	4.4	4.1	113.8	6.8	6	254	109	43	-
Z4e47c	0.01089	0.00031	0.0749	0.0039	0.0499	0.0021	0.56	69.8	2	2.9	73.3	3.6	5	188	100	53	-
Z4e48c	0.00881	0.00083	0.1	0.021	0.082	0.015	0.45	56.5	5.3	9.4	97	19	19.8	1254	368	29	-
Z4e49c	0.0679	0.0025	0.522	0.024	0.0557	0.0015	0.8	424	15	3.6	426	16	3.7	441	61	14	0.96
Z3e49r	0.01072	0.00085	0.07	0.015	0.0476	0.0092	0.38	68.7	5.4	7.9	69	14	20.2	80	242	305	-
Z3e4c	0.01328	0.00049	0.091	0.014	0.0499	0.0073	0.24	85	3.1	3.6	89	13	14.4	192	250	130	-
Z3e4r	0.01301	0.00033	0.087	0.0061	0.0485	0.0032	0.35	83.3	2.1	2.5	84.7	5.7	6.8	124	136	110	-
Z4e50	0.0296	0.00087	0.213	0.015	0.0521	0.0035	0.41	188	5.5	2.9	196	13	6.6	290	152	53	-
Z4e51r	0.01039	0.00043	0.0705	0.0054	0.0492	0.0032	0.53	66.6	2.7	4.1	69.2	5.2	7.4	159	152	96	-
Z3e51c	0.00958	0.00047	0.0633	0.0074	0.0479	0.0051	0.42	61.5	3	4.9	62.3	7.1	11.4	96	166	173	-
Z4e52r	0.01584	0.00048	0.105	0.0075	0.0481	0.0031	0.43	101.3	3.1	3	101.4	6.9	6.8	102	124	121	-
Z3e52c	0.01098	0.00057	0.069	0.0073	0.0456	0.0042	0.49	70.4	3.6	5.2	67.8	7	10.3	-	93	-	-
Z4e53r	0.01249	0.00041	0.0827	0.0046	0.048	0.0022	0.59	80	2.6	3.3	80.6	4.4	5.4	99	101	103	-
Z4e54r	0.0081	0.00029	0.0541	0.0039	0.0484	0.003	0.5	52	1.9	3.6	53.5	3.8	7.1	119	130	109	-
Z3e54c	0.00792	0.0003	0.054	0.0033	0.0495	0.0023	0.63	50.8	1.9	3.8	53.4	3.2	5.9	171	111	65	-
Z4e55r	0.01061	0.0003	0.0689	0.0063	0.0471	0.0041	0.3	68.1	1.9	2.8	67.6	6	8.9	52	125	239	-
Z3e55c	0.01103	0.00069	0.0724	0.0078	0.0476	0.0042	0.58	70.7	4.4	6.2	71	7.4	10.4	81	139	171	-
Z3e56c	0.00882	0.00029	0.0578	0.005	0.0475	0.0038	0.37	56.6	1.8	3.2	57	4.8	8.5	75	128	172	-
Z3e56r	0.00887	0.00037	0.058	0.0049	0.0475	0.0035	0.5	56.9	2.4	4.1	57.3	4.7	8.2	73	119	163	-
Z3e57c	0.0112	0.00028	0.0735	0.0072	0.0476	0.0045	0.26	71.8	1.8	2.5	72	6.8	9.5	80	145	182	-
Z3e57r	0.01121	0.00065	0.088	0.012	0.057	0.0067	0.44	71.8	4.1	5.8	86	11	12.6	492	263	54	-
Z3e58r	0.01229	0.00022	0.0821	0.0029	0.0484	0.0015	0.51	78.8	1.4	1.8	80.1	2.7	3.4	121	72	59	-
Z3e59c	0.01393	0.00046	0.0953	0.0048	0.0496	0.0019	0.66	89.2	2.9	3.3	92.4	4.5	4.8	176	89	50	-
Z3e59r	0.01417	0.00028	0.0957	0.0038	0.049	0.0017	0.51	90.7	1.8	2	92.8	3.5	3.8	147	80	54	-
Z3e5r	0.0325	0.0012	0.2289	0.0096	0.051	0.0011	0.85	206.5	7.2	3.5	209.3	7.9	3.8	241	51	21	-
Z3e6r	0.0357	0.001	0.255	0.013	0.0518	0.0023	0.56	226.2	6.5	2.9	231	11	4.7	275	100	36	-
Z3e6c	0.0368	0.0011	0.25	0.013	0.0492	0.0021	0.57	233.2	6.8	2.9	226	11	4.7	157	101	64	-
Z3e60c	0.2402	0.0075	3.06	0.14	0.0924	0.0031	0.68	1388	39	2.8	1423	35	2.5	1475	64	4.4	0.94

Z3e60r	0.254	0.0038	2.995	0.063	0.0855	0.0012	0.73	1459	20	1.4	1406	16	1.1	1328	28	2.1	1.1
Z3e61c	0.01065	0.00041	0.0691	0.0058	0.0471	0.0035	0.45	68.3	2.6	3.8	67.9	5.5	8.1	52	111	213	-
Z3e61r	0.01128	0.00023	0.0741	0.0033	0.0477	0.0019	0.46	72.3	1.5	2	72.6	3.1	4.3	82	87	106	-
Z3e62c	0.01609	0.0006	0.1117	0.0095	0.0503	0.0038	0.44	102.9	3.8	3.7	107.5	8.7	8	210	177	84	-
Z3e62r	0.01567	0.00025	0.1039	0.0035	0.0481	0.0014	0.47	100.2	1.6	1.6	100.4	3.2	3.2	105	70	67	-
Z3e63c	0.00889	0.00038	0.0628	0.0055	0.0513	0.0039	0.49	57	2.4	4.3	61.9	5.2	8.5	253	176	69	-
Z3e63r	0.01069	0.00026	0.0732	0.0053	0.0497	0.0034	0.34	68.6	1.7	2.4	71.8	5	7	180	159	88	-
Z3e64c	0.02534	0.00044	0.173	0.0054	0.0495	0.0013	0.56	161.3	2.8	1.7	162	4.7	2.9	172	61	35	-
Z3e65r	0.01353	0.00028	0.0923	0.0045	0.0495	0.0022	0.42	86.6	1.8	2.1	89.6	4.2	4.7	170	104	61	-
Z3e65c	0.01346	0.00048	0.0866	0.0062	0.0466	0.0029	0.5	86.2	3.1	3.6	84.3	5.8	6.8	31	86	277	-
Z3e66c	0.00955	0.00024	0.0618	0.0028	0.047	0.0018	0.54	61.3	1.5	2.5	60.9	2.7	4.4	47	68	145	-
Z3e66c	0.01009	0.00036	0.0664	0.0038	0.0477	0.0022	0.61	64.7	2.3	3.5	65.3	3.7	5.6	85	95	112	-
Z3e67c	0.01473	0.00024	0.098	0.0037	0.0482	0.0016	0.44	94.3	1.5	1.6	94.9	3.4	3.6	112	80	71	-
Z3e67c	0.0146	0.0004	0.1018	0.0046	0.0506	0.0018	0.61	93.4	2.6	2.7	98.4	4.2	4.3	221	82	37	-
Z3e6r	0.0357	0.001	0.255	0.013	0.0518	0.0023	0.56	226.2	6.5	2.9	231	11	4.7	275	100	36	-
Z3e7c	0.00891	0.00034	0.0588	0.005	0.0478	0.0036	0.45	57.2	2.2	3.8	58	4.8	8.2	91	131	144	-
Z3e7r	0.00804	0.00056	0.0543	0.0088	0.049	0.0071	0.43	51.6	3.6	7	53.7	8.4	15.7	148	229	154	-
Z3e8c	0.0397	0.0012	0.276	0.012	0.0503	0.0016	0.68	251.1	7.3	2.9	247.3	9.6	3.9	211	75	36	-
Z3e8r	0.0413	0.0017	0.299	0.021	0.0525	0.0029	0.61	261	11	4.1	265	16	6	306	125	41	-
Z3e9c	0.01	0.00018	0.0651	0.0024	0.0472	0.0015	0.48	64.1	1.1	1.7	64	2.3	3.6	62	69	111	-
Z3e9r	0.01022	0.00043	0.0804	0.0089	0.057	0.0059	0.38	65.6	2.7	4.2	78.5	8.4	10.7	492	228	46	-
Z4b10c	0.01223	0.00022	0.0783	0.0036	0.0464	0.002	0.4	78.3	1.4	1.8	76.5	3.4	4.4	20	59	297	-
Z4b10r	0.00948	0.00035	0.0647	0.0045	0.0495	0.0029	0.54	60.8	2.3	3.7	63.7	4.3	6.7	173	136	79	-
Z4b11c	0.0095	0.00069	0.066	0.01	0.0502	0.0068	0.48	60.9	4.4	7.3	64.6	9.6	14.9	202	245	121	-
Z4b13c	0.01023	0.00039	0.061	0.011	0.043	0.0073	0.22	65.6	2.5	3.8	60	10	17	-	104	-	-
Z4b13r	0.00971	0.00028	0.0446	0.0037	0.0333	0.0026	0.36	62.3	1.8	2.9	44.3	3.6	8	-	0	-	-
Z4b14c	0.01255	0.00056	0.0912	0.0062	0.0527	0.0028	0.65	80.4	3.5	4.4	88.6	5.8	6.6	316	119	38	-
Z4b14r	0.01758	0.0004	0.1177	0.0081	0.0486	0.0031	0.33	112.4	2.6	2.3	113	7.4	6.5	126	136	108	-
Z4b15r	0.01347	0.00029	0.0893	0.0037	0.0481	0.0017	0.53	86.2	1.9	2.2	86.8	3.4	3.9	103	83	81	-
Z4b15c	0.01358	0.00048	0.0972	0.0075	0.0519	0.0035	0.46	86.9	3.1	3.5	94.1	6.9	7.3	281	156	56	-
Z4b16r	0.02423	0.00063	0.1685	0.0078	0.0504	0.0019	0.56	154.4	4	2.6	158.1	6.8	4.3	215	89	41	-
Z4b16c	0.02555	0.00066	0.1741	0.0085	0.0494	0.0021	0.53	162.6	4.1	2.5	162.9	7.4	4.5	167	97	58	-
Z4b17c	0.01176	0.00051	0.0757	0.0089	0.0467	0.0051	0.37	75.4	3.2	4.3	74.1	8.4	11.3	33	138	414	-
Z4b17r	0.01103	0.00043	0.0721	0.0057	0.0474	0.0033	0.49	70.7	2.7	3.9	70.7	5.4	7.6	72	114	158	-
Z4b18c	0.01974	0.00047	0.135	0.0065	0.0496	0.0021	0.5	126	3	2.4	128.6	5.8	4.5	177	97	55	-
Z4b18r	0.01889	0.0006	0.1302	0.0068	0.05	0.0021	0.61	120.6	3.8	3.2	124.3	6.1	4.9	195	96	49	-
Z4b19c	0.011	0.00052	0.0848	0.0064	0.0559	0.0033	0.62	70.5	3.3	4.7	82.6	6	7.3	449	133	30	-
Z4b19r	0.00892	0.00031	0.0627	0.005	0.051	0.0036	0.44	57.2	2	3.4	61.8	4.8	7.7	243	165	68	-
Z4b1c	0.01957	0.00066	0.1386	0.008	0.0514	0.0024	0.58	124.9	4.2	3.3	131.8	7.1	5.4	258	107	42	-
Z4b1r	0.01999	0.00053	0.1487	0.0089	0.054	0.0029	0.45	127.6	3.4	2.6	140.8	7.8	5.6	370	120	32	-
Z4b20c	0.00782	0.0002	0.0564	0.0028	0.0523	0.0022	0.53	50.2	1.3	2.6	55.7	2.7	4.8	300	95	32	-

Z4b20r	0.00764	0.00026	0.0547	0.0041	0.052	0.0034	0.46	49.1	1.7	3.4	54.1	3.9	7.2	284	151	53	-
Z4b21c	0.0086	0.0002	0.0569	0.002	0.048	0.0013	0.64	55.2	1.3	2.3	56.2	1.9	3.4	98	64	66	-
Z4b21r	0.00854	0.00022	0.0561	0.0029	0.0476	0.0022	0.49	54.8	1.4	2.6	55.4	2.8	5.1	82	93	114	-
Z4b22	0.00752	0.00017	0.0476	0.0024	0.0459	0.0021	0.46	48.3	1.1	2.3	47.2	2.3	4.9	-	48	-	-
Z4b22c	0.00771	0.00021	0.0503	0.0019	0.0473	0.0013	0.71	49.5	1.3	2.7	49.8	1.9	3.7	65	64	98	-
Z4b23c	0.01109	0.0005	0.0763	0.007	0.0499	0.004	0.5	71.1	3.2	4.5	74.7	6.6	8.8	190	183	96	-
Z4b23r	0.01097	0.00033	0.0699	0.0043	0.0462	0.0025	0.48	70.3	2.1	3	68.6	4.1	6	9	67	776	-
Z4b24c	0.01798	0.00057	0.136	0.011	0.0547	0.0041	0.39	114.9	3.6	3.1	129.1	9.8	7.6	399	167	42	-
Z4b24r	0.01795	0.00043	0.1206	0.0062	0.0487	0.0022	0.46	114.7	2.7	2.4	115.6	5.6	4.9	135	108	80	-
Z4b25r	0.01113	0.00056	0.0729	0.0081	0.0475	0.0047	0.46	71.4	3.6	5	71.4	7.7	10.7	73	146	200	-
Z4b26c	0.00943	0.00035	0.064	0.0032	0.0492	0.0016	0.76	60.5	2.3	3.7	63	3	4.8	159	75	47	-
Z4b26r	0.00799	0.00023	0.0532	0.0026	0.0483	0.002	0.58	51.3	1.5	2.9	52.6	2.6	4.9	114	96	84	-
Z4b27c	0.01359	0.00076	0.099	0.018	0.053	0.0091	0.31	87	4.9	5.6	96	17	17.2	329	339	103	-
Z4b27r	0.01385	0.0005	0.0932	0.0047	0.0488	0.0017	0.72	88.7	3.2	3.6	90.5	4.3	4.8	139	82	59	-
Z4b28c	0.01262	0.00038	0.0916	0.0054	0.0527	0.0027	0.51	80.8	2.4	3	89	5	5.7	315	116	37	-
Z4b28r	0.01296	0.00056	0.0706	0.008	0.0395	0.0041	0.38	83	3.6	4.3	69.3	7.5	10.9	-	0	-	-
Z4b29c	0.0087	0.00039	0.0582	0.004	0.0485	0.0025	0.66	55.9	2.5	4.5	57.5	3.8	6.7	124	121	97	-
Z4b29r	0.00863	0.0002	0.0565	0.0019	0.0475	0.0011	0.69	55.4	1.3	2.3	55.8	1.8	3.3	74	57	77	-
Z4b2c	0.02864	0.00052	0.2025	0.0088	0.0513	0.002	0.42	182	3.2	1.8	187.2	7.4	4	254	91	36	-
Z4b2r	0.02822	0.00087	0.1962	0.0089	0.0504	0.0017	0.68	179.4	5.5	3	181.9	7.6	4.2	215	78	36	-
Z4b30	0.1316	0.0051	1.226	0.093	0.0676	0.0044	0.51	797	29	3.6	813	42	5.2	856	136	16	0.93
Z4b30r	0.01248	0.00032	0.0829	0.0032	0.0482	0.0014	0.67	80	2	2.6	80.9	3	3.7	108	67	62	-
Z4b31c	0.01417	0.00053	0.0934	0.0047	0.0478	0.0016	0.74	90.7	3.4	3.7	90.7	4.4	4.9	91	81	90	-
Z4b31r	0.01456	0.00075	0.09	0.013	0.0447	0.0059	0.36	93.2	4.7	5.1	87	12	13.5	-	111	-	-
Z4b32r	0.00502	0.00028	0.0448	0.0085	0.065	0.012	0.29	32.3	1.8	5.6	44.5	8.3	18.6	762	391	51	-
Z4b32d	0.0054	0.00051	0.0208	0.0084	0.028	0.011	0.23	34.7	3.2	9.3	20.9	8.4	39.9	-	0	-	-
Z4b3c	0.0077	0.0003	0.0504	0.0027	0.0475	0.0018	0.71	49.4	1.9	3.8	49.9	2.6	5.2	75	81	108	-
Z4b3r	0.00733	0.00022	0.048	0.0042	0.0475	0.0039	0.34	47.1	1.4	3	47.6	4.1	8.6	77	131	171	-
Z4b4c	0.01243	0.00052	0.0864	0.0063	0.0504	0.003	0.58	79.7	3.3	4.2	84.1	5.9	7	213	138	65	-
Z4b4r	0.01254	0.00023	0.0822	0.0029	0.0476	0.0014	0.53	80.3	1.5	1.8	80.2	2.7	3.3	78	70	89	-
Z4b5c	0.0513	0.0014	0.374	0.015	0.0529	0.0015	0.71	322.6	8.8	2.7	323	11	3.4	325	62	19	-
Z4b6r	0.00536	0.00024	0.0324	0.0034	0.0438	0.0041	0.44	34.5	1.6	4.5	32.4	3.3	10.2	-	46	-	-
Z4b7r	0.02088	0.00072	0.1402	0.0098	0.0487	0.003	0.49	133.2	4.5	3.4	133.2	8.7	6.6	134	136	101	-
Z4b8c	0.01798	0.00034	0.1255	0.0048	0.0506	0.0017	0.5	114.9	2.2	1.9	120	4.4	3.6	223	78	35	-
Z4b8r	0.01757	0.00051	0.134	0.01	0.0553	0.0038	0.38	112.3	3.2	2.9	127.7	9	7.1	425	156	37	-
Z4b9c	0.01089	0.00026	0.0729	0.0029	0.0485	0.0016	0.59	69.8	1.7	2.4	71.4	2.8	3.9	125	77	61	-
Z4b9r	0.00815	0.00027	0.054	0.0028	0.048	0.002	0.63	52.3	1.7	3.3	53.4	2.7	5.1	101	97	96	-
Z4d1r	0.0131	0.00055	0.0835	0.0048	0.0463	0.0018	0.73	83.9	3.5	4.2	81.5	4.5	5.5	11	51	467	-
Z4d10r	0.00771	0.00034	0.066	0.0073	0.0621	0.0063	0.4	49.5	2.2	4.4	64.9	6.9	10.7	679	218	32	-
Z4d10c	0.00798	0.00018	0.0531	0.0033	0.0483	0.0028	0.37	51.2	1.2	2.3	52.6	3.2	6.1	113	122	108	-
Z4d11c	0.01087	0.00028	0.0723	0.0035	0.0482	0.002	0.53	69.7	1.8	2.5	70.8	3.3	4.7	110	97	88	-

Z4d11r	0.01051	0.00027	0.0726	0.0028	0.0501	0.0014	0.67	67.4	1.7	2.6	71.1	2.7	3.7	198	67	34	-
Z4d12c	0.00885	0.00022	0.0603	0.0042	0.0494	0.0032	0.36	56.8	1.4	2.5	59.5	4	6.7	169	152	90	-
Z4d12r	0.00879	0.00032	0.0582	0.006	0.0481	0.0047	0.35	56.4	2.1	3.6	57.5	5.8	10.1	103	159	154	-
Z4d13c	0.00987	0.0004	0.0675	0.0079	0.0496	0.0054	0.35	63.3	2.6	4	66.3	7.5	11.3	174	205	118	-
Z4d13r	0.00813	0.00038	0.0583	0.0053	0.052	0.0041	0.51	52.2	2.4	4.6	57.6	5.1	8.8	286	179	63	-
Z4d14r	0.00813	0.00018	0.0523	0.0026	0.0467	0.0021	0.44	52.2	1.1	2.2	51.8	2.5	4.8	34	68	203	-
Z4d14r	0.00787	0.00036	0.0608	0.0042	0.0561	0.0029	0.66	50.5	2.3	4.5	60	4	6.7	455	115	25	-
Z4d15r	0.01579	0.0003	0.1121	0.0061	0.0515	0.0026	0.35	101	1.9	1.9	107.9	5.6	5.2	263	117	44	-
Z4d15r	0.01258	0.00055	0.0837	0.0061	0.0483	0.0028	0.61	80.6	3.5	4.4	81.6	5.7	6.9	112	121	108	-
Z4d16c	0.00783	0.00033	0.0526	0.0029	0.0488	0.0018	0.76	50.3	2.1	4.2	52.1	2.8	5.4	138	85	62	-
Z4d16r	0.00823	0.00012	0.054	0.0019	0.0476	0.0016	0.4	52.8	0.8	1.4	53.4	1.9	3.5	80	78	97	-
Z4d19c	0.01034	0.00034	0.0695	0.0033	0.0488	0.0017	0.68	66.3	2.1	3.2	68.2	3.1	4.6	137	82	60	-
Z4d19r	0.00825	0.00041	0.0628	0.0047	0.0552	0.0031	0.66	53	2.6	5	61.8	4.5	7.3	420	126	30	-
Z4d20r	0.00913	0.00027	0.0602	0.0052	0.0478	0.0039	0.34	58.6	1.7	3	59.3	5	8.4	89	136	153	-
Z4d21r	0.01223	0.00089	0.0411	0.0095	0.0244	0.0054	0.32	78.4	5.7	7.3	40.9	9.3	22.7	-	0	-	-
Z4d21c	0.013	0.00045	0.0884	0.0071	0.0493	0.0035	0.43	83.2	2.9	3.4	86	6.6	7.7	163	161	99	-
Z4d23c	0.00991	0.00028	0.0661	0.0034	0.0484	0.0021	0.54	63.6	1.8	2.8	65	3.3	5	117	103	88	-
Z4d24r	0.0271	0.0012	0.198	0.014	0.0531	0.003	0.63	172.4	7.8	4.5	184	12	6.6	331	127	38	-
Z4d25c	0.01313	0.00034	0.092	0.0072	0.0508	0.0037	0.33	84.1	2.2	2.6	89.3	6.7	7.5	231	171	74	-
Z4d25r	0.01288	0.00053	0.0876	0.0054	0.0493	0.0022	0.67	82.5	3.4	4.1	85.3	5	5.9	163	107	65	-
Z4d26c	0.01097	0.00055	0.0705	0.0062	0.0466	0.0034	0.57	70.3	3.5	5	69.1	5.9	8.5	27	96	352	-
Z4d26r	0.01142	0.00031	0.0751	0.0043	0.0477	0.0024	0.48	73.2	2	2.7	73.5	4	5.5	83	99	119	-
Z4d27r	0.01078	0.00054	0.0745	0.0053	0.0501	0.0025	0.7	69.1	3.4	4.9	73	5	6.8	200	118	59	-
Z4d28c	0.02713	0.00077	0.183	0.011	0.049	0.0025	0.49	172.6	4.8	2.8	170.8	9.1	5.3	146	118	81	-
Z4d29r	0.02595	0.00049	0.1791	0.0055	0.0501	0.0012	0.61	165.1	3.1	1.9	167.3	4.8	2.8	198	57	29	-
Z4d2c	0.01873	0.00047	0.131	0.011	0.0506	0.004	0.3	119.6	2.9	2.5	124.8	9.6	7.7	225	181	81	-
Z4d2r	0.01151	0.00037	0.0753	0.004	0.0474	0.002	0.6	73.8	2.3	3.2	73.7	3.8	5.1	71	84	119	-
Z4d3r	0.0081	0.00034	0.0551	0.0035	0.0493	0.0024	0.66	52	2.2	4.2	54.4	3.4	6.2	164	112	68	-
Z4d3c	0.00787	0.00027	0.0525	0.0029	0.0484	0.0021	0.63	50.5	1.8	3.5	52	2.8	5.4	119	101	85	-
Z4d4c	0.00861	0.00029	0.0574	0.004	0.0484	0.003	0.48	55.3	1.8	3.3	56.7	3.9	6.8	117	128	109	-
Z4d4r	0.00812	0.0004	0.105	0.012	0.094	0.01	0.42	52.1	2.5	4.9	102	11	11.1	1510	202	13	-
Z4d5c	0.01225	0.00043	0.0832	0.0037	0.0493	0.0014	0.78	78.5	2.7	3.5	81.2	3.5	4.3	162	66	41	-
Z4d6c	0.00912	0.00034	0.0622	0.0046	0.0495	0.0031	0.51	58.5	2.2	3.7	61.3	4.4	7.1	171	148	86	-
Z4d6r	0.00859	0.00028	0.064	0.0047	0.054	0.0035	0.44	55.1	1.8	3.2	62.9	4.5	7.1	372	148	40	-
Z4d7c	0.01145	0.00054	0.009	0.013	0.006	0.0084	0.03	73.4	3.5	4.7	10	13	139.5	-	0	-	-
Z4d7r	0.01235	0.00055	0.089	0.012	0.0522	0.0066	0.34	79.1	3.5	4.5	86	11	12.8	295	280	95	-
Z4d8c	0.01141	0.00064	0.082	0.011	0.0523	0.0062	0.43	73.1	4.1	5.6	80	10	12.7	299	274	92	-
Z4d8r	0.00627	0.00039	0.0418	0.007	0.0484	0.0076	0.37	40.3	2.5	6.1	41.6	6.9	16.5	117	225	192	-
Z4d9c	0.029	0.0011	0.2	0.01	0.0501	0.0017	0.76	184.2	7.2	3.9	185.3	8.9	4.8	201	80	40	-
Z4d9r	0.02834	0.0003	0.1936	0.0037	0.04954	0.0008	0.56	180.1	1.9	1.1	179.7	3.2	1.8	174	37	22	-
Z4e10	0.02661	0.00063	0.2023	0.0098	0.0551	0.0023	0.49	169.3	4	2.3	187.1	8.3	4.4	418	95	23	-

Z4e12c	0.00803	0.00026	0.0534	0.0031	0.0482	0.0024	0.56	51.5	1.7	3.3	52.8	3	5.7	110	111	100	-
Z4e12r	0.00732	0.00041	0.0498	0.0047	0.0494	0.0037	0.6	47	2.6	5.6	49.4	4.6	9.2	167	167	100	-
Z4e14c	0.0263	0.00062	0.1753	0.007	0.0483	0.0016	0.59	167.4	3.9	2.3	164	6.1	3.7	116	77	66	-
Z4e14r	0.0246	0.00132	0.173	0.015	0.0508	0.0033	0.64	156.9	8.3	5.3	162	13	7.8	231	150	65	-
Z4e16c	0.0109	0.00035	0.0841	0.0053	0.056	0.003	0.51	69.9	2.2	3.2	82	5	6	451	120	27	-
Z4e16r	0.0112	0.00056	0.08	0.0063	0.0518	0.0032	0.63	71.8	3.6	5	78.1	5.9	7.6	275	141	51	-
Z4e17c	0.01051	0.00019	0.0777	0.0041	0.0536	0.0027	0.33	67.4	1.2	1.8	75.9	3.9	5.1	354	114	32	-
Z4e18c	0.00762	0.00027	0.0518	0.0048	0.0493	0.0042	0.38	48.9	1.7	3.5	51.3	4.6	9	164	176	107	-
Z4e18r	0.00861	0.00015	0.0587	0.0023	0.0494	0.0018	0.43	55.3	1	1.7	57.9	2.3	3.9	169	84	50	-
Z4e19c	0.00851	0.00016	0.057	0.0026	0.0486	0.002	0.41	54.6	1	1.8	56.3	2.5	4.4	128	97	76	-
Z4e19r	0.00846	0.00027	0.0586	0.0042	0.0503	0.0032	0.44	54.3	1.7	3.1	57.8	4	7	208	150	72	-
Z4e1r	0.00878	0.00019	0.0596	0.0029	0.0493	0.0021	0.45	56.4	1.2	2.2	58.8	2.8	4.7	160	102	64	-
Z4e20c	0.00781	0.00016	0.0508	0.0019	0.0472	0.0015	0.56	50.2	1	2.1	50.3	1.8	3.6	58	65	112	-
Z4e20r	0.00774	0.0002	0.0444	0.0029	0.0416	0.0025	0.39	49.7	1.3	2.5	44.2	2.8	6.4	-	0	-	-
Z4e21c	0.01344	0.00034	0.0898	0.0052	0.0484	0.0025	0.43	86.1	2.2	2.5	87.3	4.9	5.6	121	120	99	-
Z4e22	0.00576	0.00018	0.0375	0.0031	0.0473	0.0036	0.38	37	1.2	3.2	37.4	3.1	8.2	62	118	189	-
Z4e2c	0.00837	0.00041	0.055	0.0034	0.0477	0.0018	0.8	53.7	2.6	4.8	54.4	3.2	5.9	84	85	100	-
Z4e2r	0.00824	0.00024	0.0536	0.0035	0.0472	0.0028	0.45	52.9	1.6	2.9	53.1	3.4	6.4	61	98	161	-
Z4e3c	0.00697	0.00018	0.005	0.0057	0.0052	0.006	0.02	44.8	1.2	2.6	5	5.8	115.8	-	0	-	-
Z4e3r	0.0071	0.00022	0.0456	0.0042	0.0466	0.004	0.34	45.6	1.4	3.1	45.3	4.1	9	28	112	400	-
Z4e4c	0.01193	0.00037	0.08	0.0072	0.0487	0.0041	0.35	76.4	2.4	3.1	78.2	6.8	8.6	132	159	121	-
Z4e4r	0.01221	0.00043	0.0893	0.0079	0.0531	0.0043	0.4	78.2	2.8	3.5	86.9	7.4	8.5	332	185	56	-
Z4e5c	0.02228	0.0004	0.151	0.0049	0.0492	0.0013	0.55	142	2.5	1.8	142.8	4.3	3	156	64	41	-
Z4e5r	0.02303	0.00044	0.1598	0.0063	0.0503	0.0018	0.48	146.8	2.7	1.9	150.5	5.6	3.7	209	81	39	-
Z4e6c	0.00912	0.00018	0.0603	0.0027	0.0479	0.0019	0.45	58.5	1.2	2	59.4	2.6	4.3	95	93	98	-
Z4e6r	0.00883	0.00054	0.082	0.014	0.067	0.011	0.35	56.7	3.5	6.1	80	14	16.9	853	348	41	-
Z4e7r	0.00807	0.00015	0.055	0.0022	0.0494	0.0017	0.46	51.8	1	1.8	54.3	2.1	3.9	166	83	50	-
Z4e8r	0.0116	0.00057	0.0588	0.0062	0.0368	0.0034	0.47	74.4	3.7	4.9	58	6	10.3	-	0	-	-
Z4e8c	0.01241	0.00022	0.0816	0.0024	0.0477	0.0011	0.61	79.5	1.4	1.8	79.6	2.2	2.8	83	55	66	-
Z4e9c	0.01279	0.00064	0.089	0.0059	0.0505	0.0022	0.75	81.9	4.1	5	86.6	5.5	6.4	217	102	47	-
Z4e9r	0.01364	0.0003	0.0894	0.0035	0.0475	0.0015	0.55	87.3	1.9	2.2	86.9	3.3	3.8	75	76	100	-
								18EPI									
Z3f1c	0.008	0.00021	0.0529	0.0026	0.0479	0.002	0.53	51.4	1.3	2.6	52.3	2.5	4.7	97	96	99	-
Z3f1r	0.00782	0.00023	0.0501	0.0023	0.0465	0.0016	0.65	50.2	1.5	3	49.7	2.2	4.5	23	52	224	-
Z3f10c	0.00838	0.00017	0.0564	0.0025	0.0489	0.0019	0.47	53.8	1.1	2.1	55.7	2.4	4.3	141	93	66	-
Z3f10r	0.00866	0.00022	0.0589	0.0039	0.0493	0.003	0.4	55.6	1.4	2.6	58.1	3.7	6.4	164	141	86	-
Z3f11c	0.01089	0.00016	0.0732	0.0033	0.0488	0.0021	0.33	69.8	1	1.5	71.8	3.1	4.3	136	99	73	-
Z3f11r	0.00741	0.00029	0.046	0.0046	0.045	0.0042	0.39	47.6	1.8	3.9	45.7	4.5	9.8	-	79	-	-
Z3f12c	0.01553	0.00021	0.1035	0.0032	0.0484	0.0014	0.43	99.3	1.3	1.3	100	3	3	117	67	57	-
Z3f12r	0.00839	0.00028	0.0589	0.0069	0.0509	0.0057	0.28	53.8	1.8	3.3	58.1	6.6	11.4	236	239	101	-
Z3f13c	0.01468	0.00021	0.0999	0.0043	0.0493	0.002	0.34	94	1.4	1.4	96.6	3.9	4.1	164	94	58	-

Z3f13r	0.01427	0.00032	0.0987	0.0053	0.0501	0.0024	0.42	91.4	2.1	2.2	95.5	4.9	5.1	201	113	56	-
Z3f15r	0.00772	0.00027	0.0473	0.0031	0.0444	0.0025	0.53	49.6	1.7	3.5	46.9	3	6.4	-	22	-	-
Z3f15r	0.00789	0.00026	0.0515	0.0024	0.0473	0.0016	0.68	50.7	1.6	3.2	50.9	2.4	4.6	64	73	113	-
Z3f16c	0.00938	0.00017	0.0704	0.0029	0.0545	0.002	0.44	60.2	1.1	1.8	69.1	2.7	4	391	83	21	-
Z3f16r	0.00796	0.00033	0.0506	0.0036	0.0461	0.0027	0.58	51.1	2.1	4.1	50.2	3.5	6.9	5	69	1360	-
Z3f17c	0.00972	0.00021	0.0633	0.0029	0.0473	0.0019	0.48	62.3	1.3	2.2	62.4	2.7	4.4	64	78	122	-
Z3f17r	0.00878	0.00029	0.0586	0.0044	0.0484	0.0033	0.44	56.3	1.9	3.3	57.9	4.2	7.3	121	136	113	-
Z3f18r	0.01534	0.0003	0.0746	0.0044	0.0352	0.002	0.33	98.2	1.9	1.9	73	4.1	5.7	-	0	-	-
Z3f18r	0.01551	0.00039	0.1035	0.0048	0.0484	0.0019	0.54	99.2	2.5	2.5	100	4.4	4.4	118	92	79	-
Z4319r	0.02312	0.00033	0.157	0.0045	0.0493	0.0012	0.5	147.3	2.1	1.4	148.1	3.9	2.6	160	58	36	-
Z3f19c	0.02242	0.00056	0.1552	0.0092	0.0502	0.0027	0.42	142.9	3.5	2.5	146.5	8.1	5.5	205	126	61	-
Z3f20r	0.01002	0.00035	0.0192	0.0023	0.0139	0.0016	0.3	64.2	2.2	3.5	19.3	2.2	11.6	-	0	-	-
Z3f20c	0.01042	0.00026	0.0673	0.0078	0.0469	0.0053	0.22	66.8	1.7	2.5	66.2	7.4	11.2	42	146	349	-
Z3f21r	0.01432	0.00065	0.035	0.016	0.0176	0.0078	0.1	91.7	4.1	4.5	35	15	43.9	-	0	-	-
Z3f21c	0.01504	0.00068	0.09	0.014	0.0435	0.0063	0.3	96.2	4.3	4.5	88	13	14.6	-	93	-	-
Z3f22c	0.0419	0.0012	0.33	0.033	0.0572	0.0055	0.29	264.4	7.6	2.9	290	25	8.8	500	214	43	-
Z3f23c	0.00969	0.00029	0.0564	0.0047	0.0423	0.0033	0.36	62.2	1.8	3	55.8	4.5	8.1	-	0	-	-
Z3f23r	0.00748	0.00023	0.0545	0.0036	0.0529	0.0031	0.47	48	1.5	3.1	53.9	3.5	6.5	323	133	41	-
Z3f24c	0.0091	0.00036	0.0664	0.0059	0.0529	0.0042	0.45	58.4	2.3	4	65.3	5.6	8.5	327	179	55	-
Z3f25c	0.00985	0.00036	0.0714	0.0052	0.0526	0.0033	0.5	63.2	2.3	3.6	70	5	7.1	311	145	47	-
Z3f26c	0.01547	0.00053	0.1129	0.0077	0.0529	0.0031	0.51	99	3.4	3.4	108.6	7	6.4	325	133	41	-
Z3f2r	0.00758	0.00019	0.0487	0.0058	0.0466	0.0054	0.21	48.7	1.2	2.5	48.3	5.6	11.6	30	143	478	-
Z3f3r	0.00837	0.0002	0.0609	0.0042	0.0528	0.0034	0.35	53.7	1.3	2.4	60.1	4	6.7	320	147	46	-
Z3f3r	0.00851	0.0002	0.0558	0.0029	0.0476	0.0022	0.47	54.6	1.3	2.4	55.2	2.8	5	78	91	117	-
Z3f3r	0.00851	0.0002	0.0558	0.0029	0.0476	0.0022	0.47	54.6	1.3	2.4	55.2	2.8	5	78	91	117	-
Z3f4c	0.00792	0.00018	0.056	0.0026	0.0513	0.0021	0.49	50.9	1.2	2.3	55.4	2.5	4.5	255	93	36	-
Z3f4r	0.008	0.00027	0.0523	0.0035	0.0474	0.0028	0.51	51.4	1.8	3.4	51.8	3.4	6.6	71	102	144	-
Z3f5c	0.01206	0.00029	0.0782	0.0065	0.0471	0.0037	0.29	77.3	1.9	2.4	76.5	6.1	8	52	115	221	-
Z3f5r	0.00879	0.00032	0.0566	0.0036	0.0467	0.0024	0.58	56.4	2.1	3.6	55.9	3.4	6.1	35	77	219	-
Z3f6c	0.00869	0.00012	0.0595	0.0021	0.0497	0.0016	0.4	55.7	0.8	1.4	58.7	2	3.4	179	76	42	-
Z3f6r	0.00834	0.00037	0.0128	0.0025	0.0111	0.0021	0.23	53.5	2.3	4.4	12.9	2.5	19.2	-	0	-	-
Z3f7c	0.00751	0.00027	0.0513	0.0057	0.0495	0.0052	0.32	48.2	1.7	3.6	50.8	5.5	10.9	172	201	117	-
Z3f7r	0.00741	0.00028	0.0491	0.0039	0.048	0.0033	0.48	47.6	1.8	3.8	48.7	3.7	7.7	101	128	127	-
Z3f8c	0.01227	0.00036	0.0801	0.0046	0.0474	0.0023	0.52	78.6	2.3	2.9	78.2	4.3	5.5	67	90	134	-
Z3f8r	0.01146	0.00055	0.092	0.013	0.0579	0.0076	0.34	73.4	3.5	4.8	89	12	13.4	528	291	55	-
Z3f9r	0.02447	0.00072	0.043	0.015	0.0128	0.0045	0.08	155.8	4.5	2.9	43	15	34.5	-	0	-	-
Z3f9c	0.02478	0.00067	0.168	0.011	0.0493	0.003	0.41	157.8	4.2	2.7	158	9.6	6.1	160	141	88	-
Z4319r	0.02312	0.00033	0.157	0.0045	0.0493	0.0012	0.5	147.3	2.1	1.4	148.1	3.9	2.6	160	58	36	-
Z4327r	0.01711	0.00035	0.1142	0.0051	0.0484	0.0019	0.46	109.3	2.2	2	109.8	4.6	4.2	120	93	78	-
Z4f1c	0.00714	0.00022	0.0484	0.0029	0.0492	0.0025	0.52	45.9	1.4	3.1	48	2.8	5.8	157	118	75	-
Z4f1r	0.00802	0.00015	0.0531	0.0025	0.0481	0.0021	0.4	51.5	1	1.9	52.6	2.4	4.6	103	101	99	-

Z4f2c	0.0257	0.00059	0.1752	0.0064	0.0494	0.0014	0.63	163.6	3.7	2.3	163.9	5.5	3.4	169	66	39	-
Z4f2r	0.02408	0.00071	0.162	0.012	0.0487	0.0035	0.38	153.4	4.5	2.9	152	11	7.2	134	147	109	-
Z4f3r	0.00928	0.00017	0.0636	0.0024	0.0497	0.0016	0.5	59.6	1.1	1.9	62.6	2.3	3.6	181	75	41	-
Z4f4r	0.00695	0.0003	0.0461	0.0042	0.0481	0.0038	0.47	44.6	1.9	4.2	45.7	4	8.8	104	141	135	-
Z4f4c	0.01448	0.00039	0.101	0.024	0.051	0.012	0.12	92.7	2.5	2.7	98	22	22.3	222	342	154	-
Z4f5c	0.00867	0.00022	0.0563	0.0021	0.0471	0.0013	0.67	55.6	1.4	2.5	55.6	2	3.6	55	60	109	-
Z4f5r	0.00787	0.00016	0.051	0.003	0.047	0.0026	0.35	50.5	1	2	50.5	2.9	5.7	50	88	174	-
								17PI									
Z2a2c	0.01002	0.00039	0.0657	0.0059	0.0476	0.0039	0.43	64.2	2.5	3.9	64.6	5.6	8.7	78	130	167	-
Z2a3c	0.01113	0.0004	0.0753	0.0044	0.049	0.0023	0.62	71.4	2.6	3.6	73.7	4.1	5.6	150	108	72	-
Z2a4c	0.0086	0.00032	0.059	0.0037	0.0497	0.0026	0.59	55.2	2.1	3.7	58.2	3.6	6.2	182	120	66	-
Z2a1c	0.00879	0.00044	0.002	0.011	0.0017	0.0092	0.01	56.4	2.8	5	2	11	542.4	-	0	-	-
Z3a1r	0.00672	0.00085	0.89	0.24	0.96	0.23	0.46	43.1	5.4	12.5	646	131	20.3	5181	349	7	-
Z3a2c	0.01179	0.00034	0.0837	0.0066	0.0515	0.0038	0.37	75.5	2.2	2.9	81.6	6.1	7.5	264	168	64	-
Z3a2r	0.01201	0.00054	0.075	0.014	0.0454	0.0082	0.24	77	3.4	4.5	74	13	18	-	177	-	-
Z3a4c	0.038	0.0011	0.269	0.018	0.0513	0.0031	0.44	240.6	7	2.9	242	15	6	256	140	55	-
Z3a4r	0.0378	0.0012	0.261	0.016	0.05	0.0026	0.52	239.1	7.3	3.1	235	13	5.4	196	121	61	-
Z3a5r	0.00911	0.00034	0.0735	0.006	0.0586	0.0043	0.45	58.4	2.2	3.7	72	5.7	7.9	551	160	29	-
Z3a5c	0.00972	0.00044	0.0656	0.0044	0.049	0.0024	0.68	62.4	2.8	4.5	64.5	4.2	6.5	146	114	78	-
Z3a6	0.01073	0.00051	0.0708	0.008	0.0479	0.0049	0.41	68.8	3.2	4.7	69.5	7.6	11	93	161	172	-
Z3a7c	0.01034	0.00022	0.0677	0.0036	0.0475	0.0023	0.41	66.3	1.4	2.2	66.5	3.4	5.1	74	93	125	-
Z3a7r	0.00885	0.00023	0.0631	0.0028	0.0517	0.0019	0.59	56.8	1.5	2.6	62.1	2.7	4.4	271	84	31	-
Z3a9r	0.01488	0.00057	0.036	0.042	0.017	0.02	0.03	95.2	3.6	3.8	35	41	116.2	-	0	-	-
Z3a9c	0.01589	0.00061	0.101	0.012	0.0461	0.0053	0.32	101.6	3.9	3.8	98	11	11.5	3	129	4276	-
Z3a8r	0.028	0.00087	0.192	0.013	0.0497	0.003	0.46	178	5.5	3.1	178	11	6.2	183	141	77	-
Z3a8c	0.02739	0.0007	0.188	0.01	0.0499	0.0023	0.48	174.2	4.4	2.5	175.3	8.6	4.9	191	109	57	-
Z3a11r	0.00447	0.00032	0.0509	0.0071	0.083	0.01	0.5	28.8	2	7	50.4	6.9	13.7	1258	239	19	-
Z3a11	0.00455	0.00017	0.0317	0.0053	0.0505	0.0083	0.22	29.3	1.1	3.7	31.7	5.2	16.5	217	279	129	-
Z3a10r	0.0114	0.0004	0.073	0.027	0.047	0.017	0.09	73.1	2.5	3.5	72	25	35.4	27	363	1347	-
Z3a10c	0.01089	0.00024	0.0745	0.0038	0.0496	0.0023	0.43	69.8	1.5	2.2	73	3.6	4.9	178	107	60	-
Z3a12r	0.0213	0.0011	0.143	0.021	0.0486	0.0068	0.34	135.8	6.9	5.1	135	19	14	128	215	168	-
Z3a12	0.02192	0.00044	0.1526	0.0068	0.0505	0.002	0.45	139.8	2.8	2	144.2	6	4.1	218	92	42	-
Z3a13r	0.0274	0.0011	0.189	0.011	0.0502	0.0021	0.67	173.9	6.6	3.8	176	9.3	5.3	203	98	48	-
Z3a13c	0.02759	0.00058	0.1825	0.007	0.048	0.0015	0.55	175.4	3.7	2.1	170.2	6	3.5	98	75	77	-
Z3a14r	0.018	0.0014	0.169	0.019	0.0683	0.0056	0.7	114.7	9	7.9	159	17	10.5	877	169	19	-
Z3i1	0.0434	0.0012	0.333	0.016	0.0556	0.0022	0.58	273.8	7.5	2.7	292	12	4.2	437	88	20	-
Z3i1c	0.04381	0.00094	0.319	0.013	0.0529	0.0018	0.53	276.4	5.8	2.1	281	10	3.5	323	79	24	-
Z3i2c	0.01336	0.0003	0.0863	0.0031	0.0468	0.0013	0.62	85.6	1.9	2.2	84.1	2.9	3.4	42	53	128	-
Z3i2r	0.0236	0.0011	0.175	0.021	0.0539	0.0061	0.38	150.2	6.8	4.5	164	18	11.2	369	255	69	-
								17Pi									
z1f2r	0.00921	0.0002	0.0666	0.0035	0.0525	0.0025	0.41	59.1	1.3	2.1	65.5	3.3	5	306	108	35	-

z1f2c	0.00975	0.00031	0.0653	0.0029	0.0486	0.0016	0.7	62.5	2	3.1	64.3	2.8	4.4	129	76	59	-
z1f5r	0.00887	0.00014	0.0606	0.0021	0.0495	0.0015	0.45	56.9	0.9	1.5	59.7	2	3.3	173	71	41	-
Z1f5c	0.0125	0.00042	0.17	0.013	0.0986	0.0067	0.44	80.1	2.7	3.4	159	11	7	1598	128	8	-
Z1f6c	0.00552	0.00054	0.006	0.015	0.007	0.02	0.04	35.5	3.5	9.8	6	15	264.2	-	0	-	-
z1f6r	0.0058	0.00018	0.0432	0.0034	0.054	0.0039	0.4	37.3	1.2	3.1	42.9	3.3	7.6	371	161	43	-
z1f7r	0.03794	0.0009	0.268	0.014	0.0513	0.0025	0.44	240	5.6	2.3	241	12	4.8	252	112	44	-
z1f8r	0.01013	0.00027	0.0672	0.0042	0.0481	0.0027	0.42	65	1.7	2.7	66	4	6.1	104	117	112	-
z1f9r	0.02613	0.00062	0.1944	0.0077	0.0539	0.0017	0.6	166.3	3.9	2.3	180.4	6.6	3.6	369	72	19	-
z1f10r	0.00868	0.00029	0.0573	0.0034	0.0479	0.0024	0.56	55.7	1.8	3.3	56.6	3.3	5.8	94	103	110	-
z2b1r	0.01753	0.00089	0.121	0.0071	0.05	0.0014	0.87	112.1	5.6	5	116	6.4	5.5	197	67	34	-
z2b2r	0.00876	0.00043	0.0585	0.0033	0.0485	0.0014	0.86	56.2	2.7	4.9	57.8	3.2	5.5	122	68	56	-
Z2b2c	0.00871	0.00028	0.0585	0.0027	0.0487	0.0016	0.7	55.9	1.8	3.2	57.7	2.6	4.5	136	78	57	-
Z2b3c	0.00908	0.00031	0.0629	0.0033	0.0503	0.002	0.65	58.2	2	3.4	62	3.1	5.1	208	92	44	-
z2b3r	0.00942	0.00048	0.0677	0.0043	0.0521	0.002	0.8	60.5	3.1	5.1	66.5	4.1	6.1	289	86	30	-
Z2b4c	0.00531	0.00016	0.033	0.0037	0.0452	0.0048	0.27	34.1	1	3	33	3.6	11	-	98	-	-
z2b4r	0.00522	0.00026	0.0365	0.0022	0.0508	0.0018	0.82	33.6	1.7	4.9	36.4	2.2	6	230	81	35	-
Z2b6c	0.01626	0.00054	0.1166	0.0056	0.052	0.0018	0.69	104	3.4	3.3	112	5.1	4.6	285	81	28	-
z2b6r	0.01672	0.00088	0.1102	0.0069	0.0478	0.0016	0.85	106.9	5.6	5.2	106.2	6.3	5.9	90	78	87	-
z2b7r	0.00809	0.00043	0.0553	0.0036	0.0495	0.0019	0.81	51.9	2.8	5.4	54.6	3.5	6.4	174	90	52	-
z2b8r	0.01957	0.00094	0.1342	0.0073	0.0498	0.0012	0.89	124.9	6	4.8	127.9	6.5	5.1	184	57	31	-
z2b9	0.0083	0.00041	0.0581	0.0032	0.0508	0.0013	0.89	53.3	2.6	4.9	57.4	3.1	5.4	231	58	25	-
z2b10	0.01059	0.00059	0.108	0.01	0.074	0.0058	0.58	67.9	3.8	5.6	104.2	9.6	9.2	1043	159	15	-
z2b11	0.0332	0.0034	1.9	0.4	0.415	0.077	0.48	210	21	10	1079	142	13.2	3963	283	7	-
Z3b1r	0.03069	0.00039	0.2127	0.0055	0.0502	0.0011	0.49	194.9	2.4	1.2	195.8	4.6	2.4	207	53	26	-
Z3b1c	0.0293	0.0012	0.205	0.01	0.0508	0.0013	0.84	186.2	7.7	4.1	189.6	8.6	4.5	233	61	26	-
Z3b2r	0.00898	0.0005	0.0637	0.0087	0.0515	0.0064	0.41	57.6	3.2	5.5	62.7	8.3	13.3	263	264	100	-
Z3b2c	0.0085	0.00025	0.0549	0.0037	0.0468	0.0029	0.43	54.6	1.6	2.9	54.3	3.6	6.6	40	90	224	-
Z3b3r	0.0298	0.0013	0.211	0.014	0.0514	0.0026	0.65	189.1	7.8	4.2	194	12	5.9	258	115	44	-
Z3b3c	0.02985	0.00052	0.2057	0.0085	0.05	0.0019	0.42	189.6	3.2	1.7	190	7.1	3.8	195	87	45	-
Z3b4c	0.01138	0.00018	0.0747	0.0025	0.0477	0.0014	0.48	72.9	1.1	1.6	73.2	2.3	3.2	82	69	83	-
Z3b5c	0.00728	0.00013	0.0475	0.0021	0.0473	0.0019	0.4	46.7	0.8	1.8	47.1	2.1	4.4	67	81	121	-
Z3b5r	0.00723	0.00072	0.05	0.011	0.05	0.01	0.43	46.5	4.6	9.9	49	11	22.2	184	301	164	-
Z3b6c	0.01085	0.00041	0.0711	0.0053	0.0475	0.0031	0.5	69.6	2.6	3.8	69.7	5	7.2	76	111	147	-
Z3b6r	0.00888	0.00034	0.0583	0.005	0.0476	0.0037	0.44	57	2.2	3.8	57.6	4.8	8.4	81	128	157	-
Z3b7r	0.00808	0.00037	0.0525	0.0034	0.0471	0.0021	0.71	51.9	2.4	4.6	52	3.3	6.3	56	81	143	-
Z3b7c	0.00825	0.00021	0.0506	0.0033	0.0445	0.0027	0.38	53	1.3	2.5	50.2	3.2	6.4	-	29	-	-
Z3b8r	0.00718	0.00035	0.0462	0.0044	0.0467	0.0038	0.52	46.1	2.3	4.9	45.9	4.2	9.2	32	107	333	-
Z3b8c	0.00656	0.00045	0.0422	0.0067	0.0467	0.0066	0.43	42.1	2.9	6.8	42	6.5	15.4	35	172	489	-
Z3b8r	0.00812	0.00037	0.0472	0.0034	0.0422	0.0024	0.62	52.1	2.4	4.5	46.8	3.3	7.1	-	0	-	-
Z3b9r	0.00786	0.00031	0.0542	0.0036	0.0501	0.0027	0.6	50.5	2	3.9	53.6	3.5	6.4	198	124	62	-
Z3b9c	0.00808	0.00022	0.0539	0.0032	0.0484	0.0026	0.46	51.9	1.4	2.7	53.3	3.1	5.8	117	119	102	-

Z3b10c	0.02462	0.00064	0.174	0.012	0.0514	0.0032	0.38	156.8	4	2.6	163	10	6.2	257	144	56	-
Z3b11c	0.01643	0.00024	0.1109	0.0028	0.049	0.001	0.58	105.1	1.5	1.4	106.8	2.5	2.4	146	48	33	-
Z3b11r	0.01352	0.00051	0.09	0.0059	0.0483	0.0026	0.57	86.5	3.2	3.7	87.5	5.5	6.3	113	118	104	-
Z3b12c	0.01154	0.0005	0.0739	0.0078	0.0465	0.0045	0.41	74	3.2	4.3	72.4	7.4	10.2	21	119	558	-
Z3b13c	0.00925	0.00014	0.0637	0.0052	0.0499	0.004	0.18	59.3	0.9	1.5	62.7	5	8	193	185	96	-
Z3b13r	0.00891	0.00045	0.0658	0.0077	0.0536	0.0057	0.43	57.2	2.9	5.1	64.8	7.4	11.4	353	241	68	-
Z3b14c	0.00806	0.00019	0.0461	0.0026	0.0414	0.0022	0.41	51.8	1.2	2.3	45.7	2.5	5.6	-	0	-	-
Z3b14r	0.00798	0.00039	0.0574	0.0056	0.0522	0.0045	0.49	51.2	2.5	4.9	56.7	5.4	9.6	293	196	67	-
Z3b15c	0.05128	0.00096	0.376	0.01	0.0531	0.001	0.7	322.4	5.9	1.8	323.7	7.4	2.3	334	44	13	-
Z3b15r	0.0533	0.002	0.399	0.019	0.0543	0.0015	0.79	335	12	3.6	341	13	3.9	385	64	17	-
Z3b16r	0.01915	0.00071	0.1368	0.0074	0.0518	0.0021	0.68	122.3	4.5	3.6	130.2	6.6	5.1	278	91	33	-
Z3b16c	0.01951	0.00042	0.1412	0.0084	0.0525	0.0029	0.36	124.6	2.6	2.1	134.1	7.4	5.5	307	126	41	-
Z3b17c	0.00881	0.0002	0.0599	0.0023	0.0493	0.0015	0.6	56.5	1.3	2.3	59.1	2.2	3.7	164	71	43	-
Z3b17r	0.00838	0.00034	0.0546	0.0039	0.0472	0.0028	0.57	53.8	2.2	4	54	3.7	6.9	61	97	159	-
Z3b18r	0.03064	0.00071	0.2237	0.0098	0.053	0.002	0.53	194.5	4.4	2.3	205	8.1	3.9	327	84	26	-
Z3b19r	0.00741	0.00038	0.0527	0.0046	0.0515	0.0036	0.59	47.6	2.4	5.1	52.1	4.4	8.5	265	162	61	-
Z3b19	0.00749	0.00027	0.0505	0.0047	0.049	0.0042	0.39	48.1	1.7	3.6	50.1	4.5	9.1	146	168	115	-
Z3b20r	0.2323	0.0087	2.78	0.12	0.0869	0.0018	0.87	1346	46	3.4	1351	32	2.4	1359	40	3	0.99
Z3b20c	0.2369	0.0048	2.858	0.066	0.08748	0.00098	0.87	1371	25	1.8	1371	17	1.3	1371	22	1.6	1
Z3b21c	0.01107	0.00041	0.0796	0.006	0.0522	0.0034	0.49	70.9	2.6	3.7	77.8	5.6	7.2	293	149	51	-
Z3b21r	0.01058	0.00026	0.0727	0.0033	0.0499	0.0019	0.54	67.8	1.7	2.5	71.3	3.2	4.4	189	90	48	-
Z3b22c	0.00913	0.00026	0.0599	0.0037	0.0476	0.0026	0.46	58.6	1.7	2.8	59.1	3.6	6	79	103	129	-
Z3b23r	0.00903	0.00044	0.061	0.011	0.0489	0.0089	0.26	58	2.8	4.8	60	11	18.3	145	262	181	-
Z3b23c	0.02671	0.00064	0.192	0.01	0.0523	0.0025	0.45	169.9	4	2.4	178.7	8.7	4.9	297	109	37	-
Z3b24c	0.01395	0.0003	0.0932	0.0042	0.0485	0.0019	0.48	89.3	1.9	2.1	90.5	3.9	4.3	121	94	77	-
Z3b24r	0.01388	0.00044	0.0939	0.0064	0.049	0.0029	0.47	88.9	2.8	3.2	91.1	5.9	6.5	150	141	94	-
Z3b25r	0.0063	0.00037	0.025	0.012	0.029	0.014	0.12	40.5	2.3	5.8	25	12	49.2	-	0	-	-
Z3b26c	0.00837	0.00021	0.0565	0.0024	0.049	0.0016	0.61	53.7	1.4	2.5	55.8	2.3	4.1	146	78	53	-
Z3b26r	0.00778	0.00033	0.0517	0.0031	0.0481	0.0021	0.7	50	2.1	4.2	51.1	3	5.9	107	102	96	-
Z3b27c	0.0095	0.00019	0.0623	0.0037	0.0476	0.0027	0.34	60.9	1.2	2	61.4	3.6	5.8	77	103	133	-
Z3b28r	0.00651	0.0002	0.0428	0.0026	0.0477	0.0024	0.52	41.8	1.3	3.1	42.5	2.5	5.9	84	101	120	-
Z3b29r	0.0204	0.00058	0.148	0.014	0.0526	0.0048	0.3	130.2	3.7	2.8	140	12	8.9	311	208	67	-
Z3b29c	0.0207	0.00078	0.1439	0.0079	0.0504	0.002	0.69	132.1	4.9	3.7	136.5	7	5.2	214	93	43	-
Z3b30r	0.00811	0.00025	0.031	0.0031	0.0277	0.0026	0.31	52.1	1.6	3.1	31	3	9.7	-	0	-	-
Z3b30c	0.00832	0.00019	0.0559	0.0026	0.0487	0.002	0.49	53.4	1.2	2.3	55.3	2.5	4.6	136	96	71	-
Z3b31r	0.00819	0.00025	0.0555	0.0027	0.0492	0.0018	0.64	52.6	1.6	3.1	54.9	2.6	4.7	157	87	56	-
Z3b31c	0.00834	0.0002	0.0551	0.0021	0.0479	0.0015	0.62	53.6	1.3	2.4	54.5	2.1	3.8	95	72	76	-
Z3b32r	0.01415	0.00039	0.0972	0.0038	0.0498	0.0014	0.71	90.6	2.5	2.8	94.2	3.5	3.7	186	63	34	-
Z3b32c	0.01442	0.00034	0.0973	0.0033	0.049	0.0012	0.7	92.3	2.2	2.4	94.3	3.1	3.2	146	57	39	-
Z3b33r	0.00882	0.00037	0.0574	0.0049	0.0472	0.0035	0.49	56.6	2.4	4.2	56.7	4.7	8.3	59	113	193	-
Z3b33c	0.01062	0.0003	0.0736	0.0051	0.0503	0.0032	0.41	68.1	1.9	2.8	72.1	4.8	6.7	207	147	71	-

Z3b34c	0.01147	0.0003	0.0749	0.0026	0.0473	0.0011	0.75	73.5	1.9	2.6	73.3	2.4	3.3	66	53	81	-
Z3b34r	0.01101	0.00033	0.0756	0.0034	0.0498	0.0017	0.67	70.6	2.1	3	74	3.2	4.4	188	79	42	-
Z3b35r	0.0289	0.0014	0.193	0.017	0.0484	0.0037	0.52	183.7	8.6	4.7	179	15	8.3	117	145	124	-
Z3b35c	0.02682	0.00095	0.185	0.017	0.05	0.0041	0.4	170.6	6	3.5	172	14	8.2	196	188	96	-
Z3b36c	0.00893	0.00031	0.0558	0.0039	0.0453	0.0027	0.51	57.3	2	3.5	55.1	3.7	6.7	-	50	-	-
Z3b36r	0.00923	0.00023	0.0613	0.0035	0.0481	0.0025	0.43	59.3	1.5	2.5	60.4	3.3	5.5	106	111	105	-
Z3b37c	0.00841	0.00022	0.0568	0.0022	0.049	0.0014	0.68	54	1.4	2.6	56.1	2.1	3.8	147	66	45	-
Z3b38r	0.01531	0.00037	0.1059	0.0046	0.0502	0.0018	0.55	98	2.3	2.4	102.2	4.2	4.1	202	84	42	-
Z3b38c	0.01452	0.00047	0.0962	0.0038	0.0481	0.0011	0.82	92.9	3	3.2	93.2	3.5	3.7	102	53	52	-
Z3b39c	0.00964	0.0005	0.0631	0.0045	0.0474	0.0023	0.73	61.9	3.2	5.2	62.1	4.3	6.9	71	91	129	-
Z3b40r	0.00875	0.00029	0.059	0.0025	0.0489	0.0014	0.77	56.2	1.8	3.3	58.2	2.4	4.2	143	65	46	-
Z3b41c	0.01223	0.00042	0.0832	0.0044	0.0493	0.002	0.64	78.4	2.7	3.4	81.1	4.2	5.1	164	96	58	-
Z3b41r	0.01309	0.00045	0.007	0.0066	0.0039	0.0036	0.04	83.8	2.9	3.4	7.1	6.6	93.3	-	0	-	-
Z3b42c	0.00881	0.00028	0.0579	0.0029	0.0477	0.0018	0.63	56.6	1.8	3.1	57.2	2.7	4.8	84	86	103	-
Z3b42r	0.0087	0.00028	0.0566	0.0033	0.0472	0.0023	0.55	55.9	1.8	3.2	55.9	3.1	5.6	59	85	145	-
Z3b43r	0.01184	0.00034	0.0771	0.0037	0.0472	0.0018	0.6	75.9	2.2	2.8	75.4	3.5	4.6	61	75	123	-
Z3b43c	0.01241	0.00038	0.0836	0.0041	0.0488	0.0019	0.62	79.5	2.4	3	81.5	3.9	4.8	139	92	66	-
Z3b44c	0.02362	0.00082	0.167	0.011	0.0514	0.0029	0.53	150.5	5.2	3.4	157.1	9.5	6.1	258	128	50	-
Z3b44r	0.023	0.0014	0.169	0.014	0.0533	0.0033	0.7	146.4	8.7	5.9	158	13	7.9	342	139	41	-
Z3b45c	0.01969	0.00062	0.1382	0.0077	0.0509	0.0024	0.56	125.7	3.9	3.1	131.5	6.9	5.3	238	107	45	-
Z3b45r	0.02015	0.00052	0.1507	0.0075	0.0542	0.0023	0.52	128.6	3.3	2.6	142.5	6.6	4.6	381	96	25	-
Z3b46r	0.01126	0.00046	0.0797	0.0081	0.0513	0.0047	0.41	72.2	3	4.1	77.8	7.6	9.7	255	213	84	-
Z3b46c	0.01172	0.0002	0.0768	0.0041	0.0475	0.0024	0.32	75.1	1.3	1.7	75.1	3.9	5.2	76	96	126	-
Z3b47r	0.02679	0.00096	0.19	0.013	0.0514	0.003	0.52	170.4	6	3.5	177	11	6.3	259	135	52	-
Z3b47c	0.02782	0.00071	0.187	0.011	0.0487	0.0027	0.42	176.9	4.4	2.5	174.1	9.6	5.5	136	129	95	-
Z3b48r	0.01447	0.00032	0.0957	0.004	0.048	0.0017	0.53	92.6	2	2.2	92.8	3.7	4	98	84	86	-
Z3b48c	0.01453	0.00025	0.099	0.0043	0.0494	0.002	0.4	93	1.6	1.7	95.8	4	4.1	166	93	56	-
Z3b49c	0.0093	0.00014	0.0644	0.0024	0.0502	0.0017	0.42	59.7	0.9	1.5	63.3	2.3	3.6	204	78	38	-
Z3b50r	0.02425	0.00076	0.177	0.013	0.053	0.0034	0.43	154.4	4.8	3.1	166	11	6.6	330	148	45	-
Z3b50c	0.0232	0.0004	0.157	0.0076	0.0491	0.0022	0.35	147.9	2.5	1.7	148	6.7	4.5	151	106	70	-
Z3b51c	0.00791	0.00013	0.057	0.0042	0.0523	0.0038	0.22	50.8	0.8	1.6	56.3	4	7.2	297	165	55	-
Z3b51r	0.00768	0.00038	0.0505	0.0045	0.0477	0.0035	0.55	49.3	2.4	4.9	50	4.3	8.7	85	126	149	-
Z3b52r	0.00674	0.00024	0.0449	0.007	0.0483	0.0073	0.23	43.3	1.6	3.6	44.6	6.8	15.2	113	218	193	-
Z3b52c	0.00671	0.00021	0.0437	0.0022	0.0472	0.0018	0.63	43.1	1.4	3.1	43.4	2.1	4.9	60	75	125	-
Z3b53c	0.01116	0.00018	0.0721	0.0038	0.0469	0.0024	0.31	71.5	1.2	1.6	70.7	3.6	5.1	43	80	185	-
Z3b53r	0.01168	0.00034	0.067	0.0055	0.0416	0.0032	0.35	74.9	2.2	2.9	65.8	5.2	8	-	0	-	-
Z3b54c	0.01097	0.00016	0.0719	0.0027	0.0476	0.0017	0.39	70.3	1	1.4	70.5	2.6	3.6	77	79	102	-
Z3b54r	0.01099	0.00036	0.0754	0.0038	0.0498	0.0019	0.66	70.5	2.3	3.3	73.8	3.6	4.8	184	88	48	-
Z3b55r	0.01462	0.00049	0.0965	0.0064	0.0479	0.0027	0.51	93.5	3.1	3.3	93.6	5.9	6.3	94	112	119	-
Z3b55c	0.01408	0.00025	0.0929	0.0039	0.0479	0.0018	0.42	90.1	1.6	1.7	90.2	3.6	4	93	90	96	-
Z3b56r	0.01713	0.00023	0.1174	0.0041	0.0497	0.0016	0.38	109.5	1.5	1.3	112.7	3.7	3.3	182	75	41	-

Z3b57r	0.01858	0.00046	0.1235	0.0048	0.0482	0.0015	0.63	118.7	2.9	2.4	118.2	4.3	3.7	109	71	65	-
Z3b57c	0.01882	0.00033	0.1293	0.0042	0.0498	0.0014	0.54	120.2	2.1	1.8	123.5	3.8	3.1	186	64	34	-
Z3b58r	0.01202	0.00053	0.093	0.013	0.0558	0.0076	0.31	77	3.4	4.4	90	12	13.7	446	307	69	-
Z3b58c	0.01208	0.00038	0.0994	0.0079	0.0597	0.0043	0.4	77.4	2.4	3.2	96.3	7.3	7.6	592	158	27	-
Z3b59r	0.03088	0.00092	0.242	0.016	0.0569	0.0034	0.45	196	5.8	2.9	220	13	6	489	132	27	-
Z3b59c	0.03258	0.00095	0.228	0.02	0.0507	0.0042	0.33	206.7	5.9	2.9	208	16	7.9	228	190	84	-
Z3b60c	0.01232	0.0002	0.085	0.003	0.0501	0.0015	0.46	78.9	1.3	1.6	82.9	2.8	3.3	198	72	36	-
Z3b60r	0.01248	0.0003	0.0811	0.0033	0.0471	0.0016	0.58	80	1.9	2.4	79.2	3.1	3.9	56	67	120	-
Z3b61c	0.00949	0.00018	0.0618	0.0022	0.0472	0.0014	0.55	60.9	1.2	1.9	60.9	2.1	3.4	62	65	106	-
Z3b61r	0.00966	0.00017	0.0637	0.0033	0.0478	0.0023	0.35	62	1.1	1.8	62.7	3.2	5	89	100	113	-
Z3b62r	0.00842	0.0003	0.0409	0.0045	0.0352	0.0036	0.33	54.1	1.9	3.6	40.7	4.4	10.7	-	0	-	-
Z3b62c	0.00868	0.0003	0.0564	0.0067	0.0472	0.0054	0.29	55.7	1.9	3.4	55.7	6.5	11.6	58	155	266	-
Z3b63r	0.01198	0.00033	0.0787	0.0041	0.0476	0.0021	0.52	76.8	2.1	2.7	76.9	3.9	5	81	91	113	-
Z3b63c	0.01191	0.00013	0.0781	0.002	0.0476	0.0011	0.43	76.3	0.8	1.1	76.4	1.9	2.4	79	54	68	-
Z3b64r	0.00824	0.00025	0.0507	0.0042	0.0447	0.0034	0.37	52.9	1.6	3	50.3	4	8	-	51	-	-
Z3b64c	0.00827	0.00023	0.0551	0.0028	0.0483	0.0021	0.53	53.1	1.4	2.7	54.5	2.7	5	116	104	90	-
Z3b56c	0.00746	0.00013	0.0505	0.003	0.0491	0.0027	0.3	47.9	0.9	1.8	50	2.9	5.7	153	131	86	-
Z3b65r	0.00793	0.00019	0.0536	0.0031	0.049	0.0026	0.42	50.9	1.2	2.4	53	3	5.7	148	124	84	-
Z3b66r	0.03741	0.0008	0.263	0.013	0.0509	0.0022	0.44	236.7	5	2.1	237	10	4.3	237	101	42	-
Z3b66c	0.0363	0.0013	0.252	0.02	0.0504	0.0037	0.44	229.8	8	3.5	228	17	7.2	213	169	79	-
Z3b67r	0.02346	0.00064	0.1647	0.0084	0.0509	0.0022	0.53	149.5	4	2.7	154.8	7.3	4.7	237	100	42	-
Z3b67c	0.02297	0.00064	0.1623	0.0083	0.0512	0.0022	0.54	146.4	4	2.7	152.7	7.2	4.7	252	98	39	-
Z3b68c	0.01365	0.00037	0.1011	0.0063	0.0537	0.003	0.43	87.4	2.3	2.7	97.8	5.8	6	359	127	36	-
Z3b68r	0.01397	0.00039	0.0951	0.006	0.0494	0.0028	0.45	89.4	2.5	2.8	92.2	5.5	6	166	131	79	-
Z3b69r	0.00852	0.00029	0.0601	0.0042	0.0512	0.0031	0.49	54.7	1.9	3.4	59.3	4	6.8	249	140	56	-
Z3b69c	0.00867	0.00014	0.0572	0.0023	0.0478	0.0018	0.4	55.7	0.9	1.6	56.5	2.2	4	90	88	98	-
Z3b70c	0.02871	0.00043	0.1993	0.0082	0.0503	0.0019	0.37	182.5	2.7	1.5	184.5	6.9	3.7	211	88	42	-
Z3b70r	0.02782	0.00087	0.202	0.016	0.0525	0.0038	0.39	176.9	5.5	3.1	186	14	7.3	309	167	54	-
Z3b71c	0.0087	0.00014	0.0579	0.0044	0.0482	0.0036	0.21	55.9	0.9	1.6	57.1	4.3	7.5	110	139	127	-
Z3b71r	0.00917	0.00032	0.0631	0.0042	0.0499	0.0029	0.52	58.8	2.1	3.5	62.1	4.1	6.5	191	134	70	-
Z3b72c	0.01044	0.00015	0.0689	0.0023	0.0479	0.0014	0.44	66.9	1	1.5	67.7	2.2	3.2	94	70	75	-
Z3b73c	0.01232	0.00024	0.0952	0.0099	0.0561	0.0057	0.19	78.9	1.5	1.9	92.3	9.1	9.9	455	227	50	-
Z3b73r	0.01283	0.00056	0.1034	0.0078	0.0584	0.0036	0.58	82.2	3.6	4.4	99.9	7.2	7.2	545	134	25	-
Z3b74r	0.0564	0.0016	0.428	0.018	0.055	0.0017	0.67	353.8	9.6	2.7	361	13	3.5	411	70	17	-
Z3b74	0.05667	0.00095	0.436	0.016	0.0558	0.0018	0.46	355.3	5.8	1.6	367	11	3.1	445	73	16	-
Z3b75c	0.01105	0.00032	0.0788	0.0057	0.0517	0.0034	0.4	70.9	2	2.9	77	5.4	7	272	153	56	-
Z3b75r	0.01036	0.00073	0.08	0.011	0.0559	0.007	0.49	66.4	4.7	7	78	11	13.8	449	280	62	-
Z3b76r	0.00911	0.00029	0.066	0.0044	0.0525	0.0031	0.48	58.4	1.8	3.1	64.9	4.2	6.4	309	133	43	-
Z3b77c	0.01134	0.00021	0.0756	0.0028	0.0484	0.0016	0.49	72.7	1.3	1.8	74	2.7	3.6	118	77	65	-
Z3b77r	0.01137	0.00041	0.0753	0.0049	0.048	0.0026	0.55	72.9	2.6	3.6	73.7	4.6	6.3	101	112	111	-
Z3b78r	0.00846	0.00025	0.0577	0.0032	0.0495	0.0023	0.53	54.3	1.6	2.9	57	3.1	5.4	172	111	64	-

Z3b78c	0.01037	0.00034	0.0787	0.0041	0.0551	0.0023	0.62	66.5	2.1	3.2	77	3.9	5	415	92	22	-
Z3b79c	0.00893	0.00021	0.0487	0.0031	0.0395	0.0023	0.38	57.3	1.4	2.4	48.3	3	6.2		0	-	-
Z3b79r	0.00849	0.00041	0.0557	0.0047	0.0476	0.0033	0.57	54.5	2.6	4.8	55	4.5	8.3	78	118	152	-
Z3b81c	0.02219	0.0004	0.1561	0.0063	0.051	0.0018	0.45	141.5	2.5	1.8	147.3	5.5	3.8	242	83	34	-
Z3b81r	0.0229	0.00133	0.156	0.015	0.0494	0.0038	0.6	146	8.4	5.7	147	13	9	165	169	102	-
Z3b82c	0.01236	0.00018	0.0818	0.0033	0.048	0.0018	0.36	79.2	1.2	1.5	79.9	3.1	3.9	100	90	90	-
Z3b83r	0.00876	0.00047	0.0627	0.0088	0.0519	0.0067	0.39	56.2	3	5.4	61.8	8.4	13.6	282	277	98	-
Z3b83c	0.00871	0.00017	0.0628	0.0034	0.0523	0.0027	0.35	55.9	1.1	1.9	61.9	3.3	5.3	299	117	39	-
Z3b84c	0.01526	0.00023	0.1059	0.0042	0.0503	0.0018	0.39	97.6	1.5	1.5	102.2	3.8	3.7	210	84	40	-
Z3b84r	0.01497	0.00067	0.106	0.0058	0.0514	0.0016	0.82	95.8	4.3	4.5	102.3	5.3	5.2	257	71	28	-
Z3b85c	0.0188	0.00034	0.1392	0.0085	0.0537	0.0031	0.3	120.1	2.2	1.8	132.4	7.6	5.7	359	132	37	-
Z3b86c	0.00857	0.00022	0.0563	0.004	0.0476	0.0032	0.37	55	1.4	2.6	55.6	3.8	6.9	81	115	143	-
Z3b86r	0.00797	0.00048	0.0549	0.0061	0.05	0.0046	0.55	51.2	3.1	6	54.3	5.8	10.7	194	198	102	-
Z3b87r	0.00867	0.00039	0.0573	0.0038	0.048	0.0023	0.69	55.6	2.5	4.5	56.6	3.6	6.4	99	103	105	-
Z3b87c	0.00822	0.00014	0.0536	0.0017	0.0473	0.0012	0.53	52.8	0.9	1.6	53	1.6	3	63	62	99	-
Z3b88c	0.0083	0.0002	0.0528	0.0039	0.0461	0.0032	0.33	53.3	1.3	2.4	52.2	3.7	7.1	5	82	1542	-
Z3b89r	0.01165	0.00063	0.0848	0.0094	0.0528	0.0051	0.49	74.7	4	5.4	82.6	8.8	10.6	319	220	69	-
Z3b89c	0.01081	0.00043	0.0695	0.0045	0.0466	0.0023	0.62	69.3	2.8	4	68.2	4.2	6.2	31	74	238	-
Z3b90c	0.01123	0.00025	0.0775	0.0041	0.0501	0.0024	0.42	72	1.6	2.2	75.8	3.9	5.1	199	112	56	-
Z3b90r	0.01187	0.00054	0.0746	0.0079	0.0455	0.0043	0.43	76.1	3.4	4.5	73	7.5	10.2		95	-	-
Z3b91c	0.0649	0.0015	0.492	0.017	0.055	0.0014	0.69	405.2	9.3	2.3	406	12	2.8	411	56	14	-
Z3b91r	0.0646	0.0029	0.503	0.027	0.0564	0.0017	0.83	404	17	4.3	414	18	4.4	470	67	14	-
Z3b92c	0.01431	0.00047	0.0583	0.0057	0.0296	0.0027	0.34	91.6	3	3.3	57.6	5.5	9.6		0	-	-
Z3b92r	0.01368	0.00081	0.1	0.013	0.0532	0.0062	0.45	87.6	5.2	5.9	97	12	12.5	337	268	79	-
Z3b93r	0.0086	0.00042	0.0534	0.0047	0.045	0.0033	0.56	55.2	2.7	4.9	52.8	4.5	8.5		57	-	-
Z3b93c	0.00879	0.00019	0.0577	0.003	0.0476	0.0022	0.42	56.4	1.2	2.2	57	2.9	5	81	94	117	-
Z3b94c	0.00376	0.00036	0.0317	0.004	0.0611	0.005	0.76	24.2	2.3	9.6	31.7	4	12.5	644	178	28	-
Z3b95c	0.02169	0.00049	0.1499	0.0067	0.0501	0.0019	0.5	138.3	3.1	2.2	141.9	5.9	4.2	201	90	45	-
Z3b95r	0.02	0.0012	0.144	0.014	0.0523	0.0042	0.59	127.8	7.5	5.8	137	13	9.4	297	185	62	-
Z3b96r	0.01537	0.00086	0.107	0.018	0.0507	0.0078	0.34	98.3	5.4	5.5	104	16	15.6	228	275	121	-
Z3b96c	0.01484	0.00032	0.1009	0.0046	0.0493	0.002	0.47	95	2	2.1	97.6	4.2	4.3	163	93	57	-
Z3b97c	0.01146	0.00021	0.0784	0.0027	0.0496	0.0015	0.52	73.4	1.3	1.8	76.7	2.6	3.3	179	69	39	-
Z3b97r	0.01076	0.00055	0.0729	0.0052	0.0491	0.0025	0.72	69	3.5	5.1	71.5	4.9	6.9	155	117	76	-
Z3b98c	0.01009	0.00017	0.0694	0.0022	0.0498	0.0014	0.51	64.7	1.1	1.7	68.1	2.1	3.1	188	65	34	-
Z3b98r	0.00982	0.00042	0.0659	0.0034	0.0487	0.0014	0.82	63	2.7	4.2	64.8	3.2	5	134	70	52	-
Z3b99c	0.0118	0.00035	0.085	0.012	0.0522	0.0073	0.2	75.6	2.2	2.9	83	11	13.7	294	293	100	-
Z3b99r	0.01175	0.00066	0.077	0.0095	0.0476	0.0052	0.45	75.3	4.2	5.5	75.4	8.9	11.8	78	160	206	-
Z3b100c	0.00863	0.00031	0.0569	0.004	0.0478	0.0029	0.52	55.4	2	3.6	56.2	3.8	6.8	91	113	125	-
Z3b100r	0.00846	0.00034	0.0539	0.0039	0.0463	0.0028	0.55	54.3	2.1	4	53.3	3.7	7	11	75	667	-
								17Mi2									
z1a1r	0.00951	0.00026	0.0646	0.0037	0.0493	0.0025	0.48	61	1.7	2.7	63.6	3.5	5.5	162	117	72	-

Z1a1c	0.00891	0.00039	0.0682	0.0058	0.0555	0.0041	0.52	57.2	2.5	4.4	67	5.5	8.3	433	163	38	-
z1a2r	0.0476	0.0011	0.369	0.016	0.0562	0.0021	0.52	299.7	6.5	2.2	319	12	3.7	459	82	18	-
Z1a2c	0.0506	0.0025	0.375	0.029	0.0538	0.0033	0.63	318	15	4.8	323	22	6.7	362	137	38	-
z1a3r	0.01021	0.00024	0.0676	0.0035	0.048	0.0022	0.46	65.5	1.5	2.4	66.4	3.3	5	100	102	102	-
z1a4-3c	0.00999	0.00031	0.0654	0.0034	0.0474	0.002	0.6	64.1	2	3.1	64.3	3.3	5.1	72	84	117	-
z1a5r	0.01018	0.00019	0.0671	0.003	0.0478	0.0019	0.42	65.3	1.2	1.9	65.9	2.8	4.3	90	91	101	-
z1a5c	0.00984	0.00022	0.0654	0.0032	0.0482	0.0021	0.45	63.1	1.4	2.2	64.3	3.1	4.8	110	105	95	-
z1a7c	0.01245	0.00031	0.0986	0.0043	0.0574	0.002	0.57	79.7	2	2.5	95.4	4	4.2	508	78	15	-
z1a8r	0.00766	0.0002	0.0523	0.0023	0.0495	0.0018	0.59	49.2	1.3	2.6	51.8	2.2	4.3	174	83	48	-
z1a8c	0.008	0.00017	0.0519	0.0032	0.0471	0.0027	0.34	51.4	1.1	2.1	51.4	3.1	6	53	92	174	-
z1a10r	0.00864	0.00021	0.0581	0.0035	0.0488	0.0027	0.41	55.4	1.4	2.4	57.4	3.4	5.9	139	130	93	-
Z1a10c	0.0084	0.00031	0.0537	0.0029	0.0464	0.0018	0.68	53.9	2	3.7	53.1	2.8	5.3	18	55	311	-
z1a11r	0.00801	0.00031	0.0552	0.0046	0.0499	0.0037	0.46	51.4	2	3.8	54.5	4.4	8.1	192	173	90	-
z1a12r	0.01224	0.00024	0.0865	0.0033	0.0513	0.0017	0.52	78.4	1.6	2	84.2	3.1	3.7	252	76	30	-
z1a13c	0.01236	0.00027	0.0816	0.0033	0.0479	0.0016	0.55	79.2	1.7	2.2	79.6	3.1	3.9	93	79	85	-
z1a17r	0.00977	0.00018	0.0655	0.0029	0.0486	0.002	0.41	62.7	1.1	1.8	64.4	2.8	4.3	130	96	74	-
z1a18c	0.00982	0.00027	0.0647	0.004	0.0478	0.0027	0.43	63	1.7	2.7	63.7	3.9	6.1	89	109	122	-
z1a19r	0.00996	0.00025	0.0648	0.0045	0.0472	0.0031	0.37	63.9	1.6	2.5	63.8	4.3	6.7	59	103	175	-
z1a20r	0.00849	0.0002	0.0561	0.0029	0.048	0.0022	0.45	54.5	1.3	2.3	55.5	2.8	5.1	97	102	105	-
z1a21c	0.00799	0.00033	0.0572	0.0041	0.0519	0.003	0.58	51.3	2.1	4.1	56.4	3.9	6.9	282	133	47	-
z1a22r	0.0089	0.00014	0.0577	0.0019	0.047	0.0014	0.48	57.1	0.9	1.6	57	1.9	3.3	52	60	117	-
z1a23r	0.00904	0.00031	0.0704	0.0047	0.0566	0.0033	0.52	58	2	3.5	69.1	4.5	6.5	474	128	27	-
z1a23c	0.0117	0.00036	0.0766	0.0062	0.0475	0.0035	0.38	75	2.3	3	75	5.8	7.7	75	122	161	-
z1a25r	0.00846	0.00032	0.0541	0.0033	0.0464	0.0022	0.61	54.3	2	3.7	53.5	3.2	6	20	66	327	-
z1a25c	0.01131	0.00024	0.0747	0.0034	0.0479	0.002	0.46	72.5	1.5	2.1	73.2	3.3	4.4	96	95	99	-
z1a27r	0.01105	0.00019	0.0775	0.0033	0.0508	0.002	0.39	70.9	1.2	1.7	75.7	3.2	4.2	233	92	39	-
z1a27c	0.0072	0.00029	0.0491	0.0034	0.0494	0.0028	0.58	46.2	1.9	4	48.6	3.3	6.8	169	133	79	-
z1a29r	0.01165	0.00038	0.076	0.041	0.047	0.025	0.06	74.7	2.4	3.2	74	39	51.9	64	503	786	-
z1a29c	0.00678	0.00022	0.0461	0.0031	0.0494	0.0029	0.47	43.5	1.4	3.2	45.8	3	6.6	167	139	83	-
z1a31r	0.00805	0.00017	0.0619	0.0034	0.0558	0.0028	0.38	51.7	1.1	2.1	61	3.2	5.3	444	113	25	-
z1a31c	0.0075	0.00038	0.0486	0.0033	0.047	0.0022	0.74	48.2	2.4	5.1	48.2	3.2	6.7	51	79	154	-
z1a33r	0.00787	0.00019	0.0543	0.0029	0.05	0.0024	0.46	50.5	1.2	2.4	53.7	2.8	5.2	197	111	56	-
z1a33c	0.00771	0.00014	0.0527	0.0022	0.0496	0.0019	0.44	49.5	0.9	1.8	52.2	2.1	4.1	178	88	49	-
Z1a35c	0.00721	0.00042	0.0004	0.0054	0.0004	0.0055	0	46.3	2.7	5.7	0.4	5.5	1316.1	-	0	-	-
z1a35r	0.00677	0.00019	0.0436	0.002	0.0466	0.0018	0.59	43.5	1.2	2.8	43.3	2	4.6	31	60	191	-
z1a36r	0.00857	0.0002	0.0615	0.0036	0.052	0.0028	0.39	55	1.3	2.3	60.6	3.5	5.7	286	125	44	-
Z1a36c	0.00883	0.00027	0.0614	0.0059	0.0505	0.0046	0.32	56.6	1.7	3	60.5	5.6	9.3	217	207	96	-
z1a37r	0.00984	0.00021	0.0711	0.0034	0.0524	0.0022	0.46	63.1	1.4	2.2	69.7	3.2	4.6	304	97	32	-
z1a37c	0.00974	0.00039	0.0653	0.0052	0.0486	0.0033	0.51	62.5	2.5	4	64.2	4.9	7.7	129	141	109	-
z1a39r	0.00839	0.00023	0.0546	0.0045	0.0472	0.0037	0.33	53.8	1.5	2.7	54	4.3	8	61	118	194	-
z1a39c	0.01183	0.00047	0.0774	0.0045	0.0474	0.002	0.68	75.8	3	4	75.7	4.3	5.6	71	85	119	-

z1a41	0.01166	0.00024	0.08	0.0029	0.0498	0.0015	0.57	74.7	1.5	2.1	78.2	2.8	3.5	186	70	38	-
z1a42r	0.01142	0.00029	0.0773	0.0039	0.0491	0.0021	0.5	73.2	1.8	2.5	75.6	3.7	4.8	153	102	67	-
z1a42c	0.01126	0.00026	0.0823	0.005	0.0531	0.003	0.38	72.1	1.7	2.3	80.3	4.7	5.9	332	129	39	-
z1a44r	0.00874	0.0006	0.0619	0.0074	0.0514	0.005	0.58	56.1	3.8	6.8	61	7	11.5	260	224	86	-
z1a44c	0.01098	0.00033	0.0719	0.0047	0.0475	0.0028	0.46	70.4	2.1	3	70.5	4.5	6.3	73	103	141	-
z1a46r	0.00799	0.00032	0.0514	0.0044	0.0466	0.0035	0.47	51.3	2	4	50.9	4.2	8.3	31	101	328	-
Z1a46c	0.00767	0.00017	0.05	0.0021	0.0473	0.0017	0.54	49.2	1.1	2.3	49.5	2	4.1	64	73	114	-
z1a47r	0.00952	0.00018	0.065	0.0024	0.0495	0.0015	0.53	61.1	1.2	1.9	64	2.3	3.5	172	73	42	-
z1a47c	0.00736	0.00027	0.051	0.011	0.051	0.011	0.17	47.3	1.7	3.7	51	11	21.2	224	328	146	-
z1a51r	0.01061	0.00035	0.071	0.0034	0.0485	0.0016	0.7	68.1	2.3	3.3	69.7	3.2	4.6	126	80	64	-
Z1a51c	0.02576	0.00061	0.1819	0.0073	0.0512	0.0017	0.59	164	3.8	2.3	169.7	6.3	3.7	250	75	30	-
z1a53r	0.01777	0.00052	0.1194	0.0045	0.0487	0.0012	0.78	113.5	3.3	2.9	114.5	4.1	3.6	135	56	42	-
z1a53c	0.00826	0.00029	0.0451	0.0092	0.0396	0.008	0.17	53	1.8	3.5	44.8	9	20	-	39	-	-
z1a55r	0.00883	0.00053	0.0603	0.0046	0.0495	0.0024	0.77	56.7	3.4	5.9	59.4	4.5	7.5	173	114	66	-
z1a55c	0.00943	0.00029	0.0629	0.0026	0.0484	0.0014	0.73	60.5	1.8	3	61.9	2.5	4.1	117	68	58	-
z1a57r	0.00753	0.00052	0.0516	0.006	0.0497	0.0047	0.6	48.4	3.3	6.9	51.1	5.8	11.4	181	193	107	-
z1a58r	0.0162	0.00036	0.107	0.005	0.0479	0.002	0.48	103.6	2.3	2.2	103.2	4.6	4.4	95	95	99	-
z1a59r	0.01112	0.00017	0.0728	0.0022	0.0475	0.0013	0.49	71.3	1.1	1.5	71.3	2.1	3	73	63	87	-
z1a59c	0.01081	0.00021	0.0706	0.0026	0.0474	0.0015	0.53	69.3	1.3	1.9	69.3	2.5	3.6	69	71	103	-
z1a61r	0.01236	0.00023	0.0829	0.0034	0.0487	0.0018	0.45	79.2	1.4	1.8	80.9	3.2	3.9	132	86	66	-
Z1a61c	0.01186	0.00031	0.081	0.0046	0.0495	0.0025	0.46	76	2	2.6	79.1	4.3	5.5	173	119	68	-
z1a62r	0.01252	0.00031	0.085	0.0036	0.0492	0.0017	0.58	80.2	1.9	2.4	82.8	3.4	4.1	158	81	51	-
Z1a62c	0.01305	0.00035	0.0866	0.0041	0.0481	0.0019	0.57	83.6	2.2	2.7	84.3	3.8	4.5	106	91	86	-
z1a63r	0.02089	0.00051	0.156	0.01	0.0543	0.0033	0.38	133.3	3.2	2.4	147.6	9	6.1	385	137	35	-
Z1a63c	0.02093	0.00052	0.1426	0.0073	0.0494	0.0022	0.48	133.5	3.3	2.4	135.4	6.5	4.8	167	104	62	-
z1a64r	0.00931	0.0003	0.063	0.0036	0.0491	0.0023	0.57	59.7	1.9	3.2	62	3.5	5.6	152	111	73	-
Z1a64c	0.00886	0.00024	0.0638	0.003	0.0522	0.002	0.57	56.8	1.5	2.7	62.8	2.9	4.6	295	88	30	-
z1a66r	0.01048	0.0003	0.0679	0.0033	0.047	0.0018	0.59	67.2	1.9	2.9	66.7	3.1	4.7	49	70	143	-
Z1a66c	0.01009	0.0002	0.0717	0.0027	0.0515	0.0017	0.51	64.7	1.3	1.9	70.3	2.6	3.7	264	76	29	-
z1a67r	0.01217	0.00031	0.0816	0.0034	0.0486	0.0016	0.61	78	2	2.5	79.6	3.2	4	129	78	61	-
Z1a67c	0.01176	0.0003	0.0807	0.0044	0.0498	0.0024	0.46	75.4	1.9	2.5	78.8	4.2	5.3	184	114	62	-
z1a68r	0.00803	0.00011	0.0525	0.0048	0.0474	0.0043	0.15	51.6	0.7	1.4	51.9	4.6	8.9	69	136	197	-
Z1a68c	0.00764	0.00029	0.0004	0.0041	0.0004	0.0038	0	49.1	1.9	3.8	0.4	4.1	938.6	-	0	-	-
Z1a69c	0.01146	0.00041	0.0793	0.0044	0.0502	0.0021	0.65	73.5	2.6	3.6	77.5	4.1	5.4	204	98	48	-
Z1a69r	0.01185	0.00045	0.0752	0.0069	0.046	0.0038	0.41	75.9	2.9	3.8	73.6	6.5	8.8	-	94	-	-
z1a70r	0.00861	0.0002	0.0588	0.0039	0.0495	0.003	0.36	55.3	1.3	2.4	58	3.7	6.4	172	143	83	-
Z1a70c	0.00867	0.00023	0.063	0.0051	0.0527	0.0041	0.33	55.7	1.5	2.7	62	4.9	7.9	314	176	56	-
Z1a71r	0.0079	0.00018	0.0514	0.0029	0.0472	0.0024	0.39	50.7	1.1	2.2	50.9	2.8	5.5	61	90	148	-
Z1a71c	0.00756	0.0002	0.0502	0.0028	0.0481	0.0023	0.48	48.6	1.3	2.7	49.7	2.7	5.4	105	108	103	-
z1a73r	0.01194	0.00062	0.0928	0.0077	0.0564	0.0036	0.63	76.5	4	5.2	90.2	7.1	7.9	467	142	30	-
Z1a73c	0.013	0.00074	0.0897	0.0099	0.0501	0.0047	0.52	83.2	4.7	5.6	87.3	9.2	10.5	198	202	102	-

z1a74r	0.03217	0.00059	0.288	0.018	0.065	0.0038	0.3	204.1	3.7	1.8	257	14	5.5	774	125	16	-
Z1a74c	0.03278	0.00089	0.238	0.024	0.0526	0.0052	0.26	207.9	5.5	2.7	217	20	9.3	313	227	73	-
Z1a75c	0.00926	0.00036	0.003	0.012	0.0024	0.0093	0.01	59.4	2.3	3.9	3	12	385.5	-	0	-	-
z1a75r	0.00931	0.00027	0.0637	0.0048	0.0496	0.0034	0.39	59.7	1.7	2.9	62.7	4.5	7.2	177	161	91	-
z1a76c	0.00908	0.00032	0.0603	0.0043	0.0482	0.0029	0.5	58.2	2.1	3.6	59.4	4.1	6.9	108	123	114	-
Z1a76r	0.00874	0.00028	0.0576	0.004	0.0478	0.0029	0.47	56.1	1.8	3.2	56.9	3.8	6.7	90	114	127	-
z1a77r	0.00846	0.00024	0.0567	0.0023	0.0487	0.0015	0.67	54.3	1.5	2.8	56	2.3	4	132	72	55	-
Z1a77c	0.00838	0.00026	0.0588	0.0031	0.0509	0.0022	0.6	53.8	1.7	3.1	58	3	5.1	237	98	41	-
z1a78c	0.00875	0.00015	0.0599	0.0031	0.0497	0.0024	0.34	56.1	1	1.7	59.1	2.9	5	180	113	63	-
Z1a78c	0.00849	0.00041	0.0556	0.0074	0.0475	0.0059	0.36	54.5	2.6	4.8	54.9	7.1	13	73	172	236	-
z1a79r	0.0162	0.00039	0.1109	0.0047	0.0497	0.0017	0.57	103.6	2.5	2.4	106.8	4.3	4	180	80	45	-
Z1a79c	0.01573	0.0005	0.1044	0.0057	0.0481	0.0022	0.58	100.6	3.2	3.1	100.8	5.3	5.2	106	104	99	-
z1a81c	0.00909	0.00017	0.0616	0.0026	0.0491	0.0018	0.46	58.3	1.1	1.9	60.7	2.5	4.1	154	88	57	-
z1a81c	0.00929	0.00044	0.0661	0.0063	0.0516	0.0042	0.5	59.6	2.8	4.7	65	6	9.2	266	190	71	-
z1a82r	0.02003	0.00037	0.1252	0.0073	0.0453	0.0025	0.32	127.8	2.4	1.8	119.8	6.6	5.5	-	46	-	-
Z1a82c	0.02087	0.00067	0.1403	0.0064	0.0488	0.0016	0.7	133.2	4.2	3.2	133.3	5.7	4.3	136	76	56	-
z1a84r	0.00803	0.0003	0.0535	0.0033	0.0483	0.0024	0.6	51.5	1.9	3.7	52.9	3.2	6	115	113	99	-
z1a85r	0.01003	0.00025	0.0656	0.003	0.0475	0.0019	0.54	64.3	1.6	2.5	64.5	2.9	4.5	72	81	113	-
Z1a85c	0.01	0.00035	0.0718	0.0042	0.0521	0.0025	0.59	64.1	2.2	3.4	70.4	4	5.7	291	109	38	-
z1a86c	0.00822	0.00017	0.0553	0.0027	0.0488	0.0021	0.43	52.8	1.1	2.1	54.7	2.6	4.7	139	103	74	-
Z1a86c	0.00783	0.00031	0.0039	0.0061	0.0036	0.0057	0.02	50.3	2	3.9	3.9	6.2	158.5	-	0	-	-
z1a87r	0.01435	0.00024	0.1062	0.0047	0.0537	0.0022	0.37	91.8	1.5	1.6	102.5	4.3	4.2	358	92	26	-
Z1a87c	0.01467	0.00041	0.1014	0.0092	0.0501	0.0043	0.31	93.9	2.6	2.7	98.1	8.5	8.6	200	194	97	-
z1a88r	0.01381	0.00025	0.091	0.0027	0.0478	0.0011	0.6	88.4	1.6	1.8	88.4	2.5	2.8	89	56	63	-
z189r	0.01347	0.00029	0.0924	0.003	0.0498	0.0013	0.64	86.3	1.8	2.1	89.8	2.8	3.2	184	59	32	-
z189c	0.01396	0.00029	0.0949	0.004	0.0493	0.0018	0.49	89.4	1.8	2	92.1	3.7	4.1	162	87	53	-
z1a93c	0.00728	0.00027	0.0515	0.0034	0.0513	0.0029	0.55	46.8	1.7	3.6	51	3.3	6.5	255	129	51	-
z1a95c	0.00864	0.00016	0.0588	0.0028	0.0494	0.0022	0.38	55.4	1	1.8	58	2.7	4.7	165	104	63	-
z1a96r	0.00849	0.00032	0.059	0.0031	0.0504	0.0018	0.72	54.5	2	3.7	58.2	3	5.1	212	85	40	-
z1a97c	0.00804	0.00015	0.0528	0.0018	0.0476	0.0014	0.53	51.6	0.9	1.8	52.2	1.8	3.4	80	71	88	-
z1a98c	0.00824	0.00018	0.0587	0.0021	0.0517	0.0014	0.64	52.9	1.2	2.2	57.9	2	3.4	271	62	23	-
z1b2c	0.0273	0.0011	0.1858	0.0088	0.0494	0.0013	0.84	173.7	6.8	3.9	173	7.6	4.4	165	61	37	-
Z1b2r	0.00831	0.00029	0.0543	0.0032	0.0474	0.0023	0.58	53.4	1.8	3.4	53.7	3.1	5.8	68	90	131	-
z1b3c	0.00725	0.00027	0.0467	0.002	0.04672	0.00094	0.88	46.5	1.7	3.7	46.3	1.9	4.1	35	41	117	-
Z1b3r	0.00699	0.00032	0.0462	0.003	0.0479	0.0022	0.71	44.9	2	4.5	45.8	2.9	6.3	96	100	105	-
z1b5r	0.02461	0.00094	0.1629	0.007	0.04801	0.00093	0.89	156.7	5.9	3.8	153.3	6.1	4	100	46	46	-
Z1b5c	0.0248	0.0011	0.17	0.01	0.0498	0.0019	0.78	157.7	7.2	4.6	159.7	8.8	5.5	188	87	46	-
z1b6r	0.509	0.019	12.74	0.52	0.1814	0.0029	0.92	2654	81	3.1	2661	38	1.4	2666	26	1	1
z1b7r	0.00639	0.00028	0.0456	0.0028	0.0518	0.0023	0.71	41	1.8	4.4	45.3	2.8	6.1	277	101	36	-
z1b9c	0.00619	0.00025	0.0423	0.0024	0.0496	0.002	0.7	39.8	1.6	4	42.1	2.4	5.6	178	94	53	-
z1b10c	0.01136	0.00034	0.0776	0.0061	0.0495	0.0036	0.39	72.8	2.2	3	75.8	5.7	7.5	172	166	96	-

z1b11r	0.01347	0.00041	0.0941	0.0041	0.0507	0.0015	0.71	86.3	2.6	3	91.4	3.8	4.1	227	70	31	-
Z1b11c	0.01306	0.00059	0.0873	0.0046	0.0485	0.0013	0.87	83.6	3.8	4.5	85	4.3	5	123	61	49	-
z1b12r	0.00973	0.00031	0.0704	0.003	0.0524	0.0015	0.75	62.4	2	3.1	69	2.8	4.1	305	64	21	-
Z1b12c	0.01034	0.00053	0.0685	0.0044	0.048	0.0019	0.8	66.3	3.4	5.1	67.3	4.2	6.2	101	92	91	-
z1b13r	0.00829	0.00026	0.0558	0.0029	0.0488	0.002	0.61	53.2	1.7	3.2	55.1	2.8	5.1	138	97	70	-
z1b13c	0.00794	0.00025	0.0531	0.002	0.0485	0.00096	0.84	51	1.6	3.1	52.5	1.9	3.6	124	47	38	-
z1b15r	0.03309	0.00098	0.2357	0.0086	0.0517	0.0011	0.8	209.8	6.1	2.9	214.9	7.1	3.3	271	50	18	-
Z1b15c	0.033	0.0017	0.166	0.016	0.0365	0.0029	0.53	209	10	5	156	14	8.8	-	0	-	-
z1b16r	0.01809	0.00059	0.1238	0.0061	0.0496	0.0019	0.65	115.6	3.7	3.2	118.5	5.5	4.7	178	87	49	-
Z1b16c	0.01837	0.0009	0.1291	0.0075	0.051	0.0016	0.84	117.3	5.7	4.9	123.3	6.8	5.5	239	73	31	-
z1b18r	0.00427	0.00024	0.0349	0.0028	0.0593	0.0033	0.71	27.5	1.5	5.6	34.9	2.7	7.8	579	123	21	-
z1b19c	0.00911	0.00036	0.0601	0.0027	0.04785	0.00098	0.88	58.4	2.3	3.9	59.2	2.5	4.3	92	49	53	-
z1b20r	0.00958	0.0004	0.0655	0.0033	0.0496	0.0014	0.83	61.5	2.6	4.2	64.5	3.2	4.9	178	66	37	-
z1b21r	0.00788	0.00033	0.0607	0.0031	0.0558	0.0016	0.82	50.6	2.1	4.2	59.8	3	5	446	65	15	-
Z1b21c	0.00793	0.00037	0.0573	0.0038	0.0524	0.0024	0.71	50.9	2.4	4.7	56.6	3.6	6.4	302	107	35	-
z1b22r	0.0079	0.00032	0.0529	0.0028	0.0485	0.0016	0.77	50.8	2	4	52.3	2.7	5.1	124	79	64	-
Z1b22c	0.00795	0.00035	0.0563	0.003	0.0514	0.0015	0.84	51	2.3	4.4	55.6	2.9	5.1	258	66	25	-
z1b23r	0.00828	0.00033	0.0555	0.003	0.0486	0.0019	0.72	53.1	2.1	3.9	54.8	2.9	5.3	130	90	69	-
Z1b23c	0.00872	0.00041	0.0567	0.0043	0.0472	0.0028	0.62	56	2.7	4.7	56	4.2	7.5	58	98	169	-
z1b24r	0.0108	0.00045	0.0708	0.0057	0.0476	0.0033	0.51	69.2	2.8	4.1	69.5	5.4	7.8	78	117	150	-
Z1b24c	0.01028	0.00049	0.024	0.0032	0.0169	0.0021	0.35	65.9	3.1	4.7	24.1	3.2	13.3	-	0	-	-
z1b25r	0.01573	0.00062	0.1064	0.005	0.049	0.0013	0.83	100.6	3.9	3.9	102.7	4.6	4.5	150	61	41	-
z1b25c	0.01567	0.00066	0.1078	0.0061	0.0499	0.0019	0.75	100.2	4.2	4.2	103.9	5.6	5.4	190	87	46	-
z1b27r	0.00822	0.00036	0.0568	0.0049	0.0501	0.0037	0.5	52.8	2.3	4.3	56.1	4.7	8.4	198	174	88	-
Z1b27c	0.0076	0.00037	0.0496	0.0035	0.0473	0.0025	0.69	48.8	2.4	4.9	49.1	3.4	7	65	92	142	-
z1b28	0.00779	0.0003	0.0583	0.0034	0.0543	0.0024	0.65	50	1.9	3.8	57.5	3.3	5.7	383	100	26	-
z1b30r	0.0162	0.00062	0.1187	0.0072	0.0531	0.0025	0.64	103.6	3.9	3.8	113.9	6.5	5.7	334	105	32	-
Z1b30c	0.01608	0.00093	0.13	0.025	0.059	0.011	0.3	102.8	5.9	5.7	124	23	18.4	551	416	75	-
								17Mi1									
Z3j1c	0.01097	0.00019	0.073	0.0022	0.0482	0.0012	0.59	70.4	1.2	1.8	71.5	2.1	2.9	110	57	52	-
Z3j1r	0.00737	0.0002	0.0473	0.0035	0.0466	0.0032	0.37	47.3	1.3	2.7	47	3.4	7.1	29	92	318	-
Z3j2c	0.00853	0.00016	0.0572	0.0027	0.0487	0.0021	0.4	54.8	1	1.8	56.5	2.6	4.5	131	101	77	-
Z3j2r	0.00879	0.00016	0.0572	0.0024	0.0472	0.0018	0.43	56.4	1	1.8	56.5	2.3	4.1	59	74	125	-
Z3j3c	0.00823	0.00019	0.0532	0.0031	0.0469	0.0025	0.41	52.8	1.2	2.3	52.6	2.9	5.6	44	82	189	-
Z3j4r	0.01358	0.00024	0.0932	0.0037	0.0498	0.0018	0.44	87	1.5	1.7	90.5	3.4	3.8	184	83	45	-
Z3j4c	0.01403	0.00022	0.0938	0.0032	0.0485	0.0015	0.46	89.8	1.4	1.6	91	3	3.3	123	72	58	-
Z3j5c	0.01127	0.00015	0.0757	0.0021	0.0487	0.0012	0.49	72.3	1	1.4	74.1	2	2.7	134	57	43	-
Z3j5r	0.0072	0.00016	0.0466	0.0021	0.047	0.0018	0.5	46.2	1	2.2	46.3	2	4.4	50	70	142	-
Z3j6c	0.01001	0.00032	0.062	0.0072	0.0449	0.005	0.28	64.2	2.1	3.2	61.1	6.8	11.2	-	96	-	-
Z3j6r	0.00963	0.00015	0.0657	0.0029	0.0495	0.002	0.36	61.8	1	1.6	64.6	2.7	4.2	171	95	56	-
Z3j7c	0.00827	0.00021	0.0297	0.0059	0.026	0.0051	0.13	53.1	1.3	2.5	29.7	5.8	19.6	-	0	-	-

Z3j7r	0.00798	0.00014	0.0531	0.0018	0.0482	0.0014	0.5	51.2	0.9	1.7	52.5	1.8	3.4	110	70	64	-
Z3j8c	0.0103	0.00067	0.0695	0.005	0.0489	0.0015	0.91	66.1	4.3	6.5	68.2	4.7	6.9	145	70	48	-
Z3j8r	0.01072	0.00016	0.0725	0.0021	0.0491	0.0012	0.53	68.7	1	1.5	71.1	2	2.8	152	57	38	-
Z3j9c	0.00785	0.00016	0.056	0.0034	0.0517	0.0029	0.34	50.4	1	2	55.3	3.3	5.9	273	131	48	-
Z3j9r	0.00785	0.00012	0.0551	0.0018	0.0509	0.0014	0.47	50.4	0.8	1.5	54.5	1.7	3.1	237	65	27	-
Z3j10c	0.01531	0.00038	0.1108	0.0035	0.0525	0.001	0.79	97.9	2.4	2.5	106.7	3.2	3	308	44	14	-
Z3j10r	0.01486	0.00037	0.1019	0.0048	0.0498	0.002	0.53	95.1	2.4	2.5	98.6	4.4	4.5	184	94	51	-
Z3j11c	0.01207	0.00024	0.0831	0.006	0.0499	0.0035	0.27	77.4	1.5	1.9	81	5.6	6.9	191	162	85	-
Z3j11r	0.01043	0.00016	0.0695	0.0017	0.04833	0.00091	0.63	66.9	1	1.5	68.2	1.6	2.4	115	44	39	-
Z3j12r	0.00784	0.00022	0.0522	0.0032	0.0483	0.0026	0.46	50.3	1.4	2.8	51.6	3	5.9	112	117	104	-
Z3j12c	0.00788	0.00026	0.0524	0.0031	0.0482	0.0024	0.55	50.6	1.6	3.2	51.8	3	5.8	110	111	101	-
Z3j13c	0.01062	0.00025	0.0696	0.004	0.0476	0.0025	0.41	68.1	1.6	2.4	68.3	3.8	5.6	77	99	128	-
Z3j14r	0.0079	0.00025	0.0539	0.0028	0.0495	0.002	0.61	50.7	1.6	3.1	53.3	2.7	5	170	96	56	-
Z3j14c	0.00778	0.00022	0.0526	0.0031	0.049	0.0026	0.47	49.9	1.4	2.8	52	3	5.8	148	123	83	-
Z3j15c	0.00834	0.0002	0.0541	0.0032	0.0471	0.0025	0.42	53.5	1.3	2.4	53.5	3	5.7	54	88	162	-
Z3j15r	0.00799	0.00031	0.0543	0.0031	0.0492	0.0021	0.68	51.3	2	3.9	53.7	3	5.6	159	98	62	-
Z3j16c	0.3068	0.0035	4.94	0.13	0.1167	0.0028	0.43	1725	17	1	1809	23	1.2	1907	43	2.3	0.9
Z3j16r	0.312	0.011	4.72	0.27	0.1096	0.0052	0.58	1751	52	3	1770	49	2.8	1792	86	4.8	0.98
Z3j17c	0.0423	0.0013	0.704	0.03	0.1207	0.0037	0.69	267.2	7.8	2.9	541	18	3.3	1967	55	2.8	-
Z3j17r	0.00658	0.00028	0.0422	0.005	0.0465	0.0051	0.36	42.3	1.8	4.3	41.9	4.8	11.5	22	133	593	-
Z3j18c	0.0399	0.0014	0.3	0.013	0.0546	0.0015	0.79	252.2	8.7	3.4	267	10	3.9	395	61	15	-
Z3j18r	0.00715	0.00026	0.0542	0.0024	0.055	0.0014	0.83	45.9	1.7	3.7	53.6	2.3	4.3	414	55	13	-
Z3j19c	0.01089	0.00014	0.0742	0.0035	0.0494	0.0022	0.27	69.8	0.9	1.3	72.7	3.3	4.5	168	105	63	-
Z3j19r	0.01065	0.0004	0.0698	0.0045	0.0476	0.0025	0.58	68.3	2.5	3.7	68.5	4.3	6.2	78	99	127	-
Z3j20c	0.00845	0.00029	0.0559	0.0051	0.048	0.004	0.38	54.2	1.9	3.5	55.3	4.9	8.8	101	144	142	-
Z3j20r	0.01108	0.00041	0.0782	0.0055	0.0512	0.0031	0.53	71	2.6	3.7	76.4	5.2	6.8	248	139	56	-
Z3j21c	0.00836	0.00035	0.0531	0.0034	0.0461	0.0022	0.65	53.6	2.2	4.2	52.5	3.3	6.3	1	57	3961	-
Z3j21r	0.00822	0.00021	0.0553	0.0032	0.0488	0.0026	0.43	52.8	1.3	2.5	54.6	3.1	5.7	137	125	91	-
Z3j22c	0.00807	0.00033	0.0575	0.0066	0.0517	0.0055	0.36	51.8	2.1	4.1	56.8	6.3	11.2	272	247	91	-
Z3j22r	0.00809	0.00024	0.0557	0.0045	0.05	0.0037	0.37	51.9	1.5	2.9	55	4.3	7.8	193	174	90	-
Z3j23c	0.03056	0.00085	0.225	0.019	0.0534	0.0042	0.33	194	5.3	2.7	206	16	7.5	345	179	52	-
Z3j23r	0.0326	0.0015	0.225	0.016	0.05	0.0027	0.65	207	9.2	4.5	206	13	6.3	194	125	64	-
Z3j24c	0.00976	0.00019	0.0678	0.0024	0.0504	0.0015	0.55	62.6	1.2	1.9	66.6	2.3	3.4	212	69	33	-
Z3j24r	0.00973	0.00044	0.0641	0.0049	0.0478	0.003	0.59	62.4	2.8	4.5	63.1	4.7	7.4	90	115	128	-
Z3j25c	0.0079	0.00016	0.0536	0.0026	0.0492	0.0022	0.41	50.7	1	2	53.1	2.5	4.7	159	103	65	-
Z3j26c	0.01283	0.00016	0.0859	0.0029	0.0486	0.0015	0.37	82.2	1	1.3	83.7	2.7	3.3	127	75	59	-
Z3j27c	0.0126	0.00035	0.0872	0.0052	0.0502	0.0026	0.47	80.7	2.2	2.8	84.9	4.8	5.7	204	122	60	-
Z3j28r	0.00897	0.00022	0.0614	0.005	0.0496	0.0038	0.3	57.6	1.4	2.4	60.5	4.8	7.9	177	174	98	-
Z3j28c	0.0252	0.0012	0.177	0.011	0.051	0.0023	0.71	160.7	7.3	4.5	165.9	9.9	6	240	105	44	-
Z3j29r	0.00796	0.00013	0.0523	0.0018	0.0476	0.0014	0.49	51.1	0.9	1.7	51.7	1.7	3.3	81	71	87	-
Z3j29c	0.00814	0.00014	0.053	0.0018	0.0472	0.0014	0.51	52.3	0.9	1.7	52.5	1.7	3.3	61	64	105	-

Z3j30c	0.02092	0.00029	0.1412	0.0032	0.04895	0.00088	0.61	133.5	1.8	1.4	134.1	2.9	2.1	146	42	29	-
Z3j30r	0.01979	0.00084	0.1347	0.0074	0.0494	0.0017	0.78	126.3	5.3	4.2	128.3	6.6	5.1	165	80	48	-
Z3j31c	0.01887	0.00047	0.1326	0.0093	0.051	0.0033	0.36	120.5	3	2.5	126.4	8.3	6.6	239	151	63	-
Z3j32c	0.01218	0.00031	0.08	0.0043	0.0476	0.0022	0.47	78	2	2.5	78.2	4	5.1	82	95	116	-
Z3j32r	0.01184	0.00066	0.0789	0.0069	0.0483	0.0033	0.64	75.9	4.2	5.6	77.1	6.5	8.4	115	133	116	-
Z3j33c	0.01101	0.00021	0.0706	0.0027	0.0465	0.0015	0.51	70.6	1.4	1.9	69.3	2.6	3.7	25	51	205	-
Z3j33r	0.00994	0.00045	0.0636	0.0042	0.0464	0.0022	0.69	63.8	2.9	4.5	62.6	4	6.4	19	65	350	-
Z3j34c	0.00934	0.00027	0.0652	0.0038	0.0506	0.0026	0.5	59.9	1.7	2.9	64.1	3.6	5.7	222	117	53	-
Z3j34r	0.00904	0.0004	0.0616	0.0045	0.0495	0.0028	0.61	58	2.6	4.5	60.7	4.3	7.1	170	134	79	-
Z3j35c	0.01314	0.00027	0.0865	0.0031	0.0478	0.0014	0.58	84.1	1.7	2	84.3	2.9	3.4	88	69	78	-
Z3j35r	0.01291	0.00056	0.0863	0.0056	0.0485	0.0023	0.67	82.7	3.5	4.3	84	5.2	6.2	123	114	93	-
Z3j36c	0.01208	0.0005	0.0804	0.0051	0.0483	0.0023	0.66	77.4	3.2	4.2	78.5	4.7	6	113	110	98	-
Z3j36r	0.01197	0.00021	0.0791	0.0028	0.0479	0.0015	0.51	76.7	1.4	1.8	77.3	2.6	3.4	94	72	76	-
Z3j37c	0.00804	0.0002	0.0522	0.0037	0.0471	0.0031	0.36	51.6	1.3	2.5	51.7	3.6	6.9	56	103	184	-
Z3j37r	0.00833	0.00038	0.0563	0.0038	0.049	0.0024	0.68	53.5	2.4	4.6	55.6	3.6	6.6	147	116	79	-
Z3j38r	0.02767	0.00036	0.1952	0.0051	0.0512	0.0012	0.49	176	2.2	1.3	181	4.3	2.4	248	53	21	-
Z3j38c	0.0272	0.00114	0.189	0.011	0.0505	0.0021	0.7	172.8	7.2	4.1	175.8	9.6	5.5	217	99	45	-
Z3j39c	0.00893	0.00016	0.0617	0.008	0.0501	0.0065	0.14	57.3	1	1.8	60.8	7.7	12.7	200	238	119	-
Z3j39r	0.00898	0.00021	0.0584	0.0038	0.0471	0.0028	0.37	57.6	1.4	2.4	57.6	3.6	6.3	56	97	172	-
Z3j40c	0.00891	0.00042	0.0591	0.0042	0.0481	0.0026	0.66	57.2	2.7	4.7	58.4	4	6.9	106	114	108	-
Z3j40r	0.00836	0.00032	0.0561	0.0039	0.0487	0.0028	0.56	53.7	2.1	3.9	55.4	3.7	6.7	133	131	99	-
Z3j41c	0.00921	0.00016	0.0614	0.0025	0.0484	0.0018	0.42	59.1	1	1.7	60.5	2.4	4	117	89	76	-
Z3j41r	0.00928	0.00033	0.0214	0.0043	0.0168	0.0033	0.18	59.6	2.1	3.5	21.5	4.3	19.7	-	0	-	-
Z3j43c	0.01917	0.00054	0.1274	0.0086	0.0482	0.0029	0.42	122.4	3.4	2.8	121.8	7.7	6.3	110	124	113	-
Z3j44c	0.00836	0.00031	0.0557	0.0062	0.0483	0.005	0.33	53.7	2	3.7	55	5.9	10.8	114	172	150	-
Z3j44r	0.00775	0.00014	0.0516	0.002	0.0484	0.0016	0.47	49.7	0.9	1.8	51.1	1.9	3.7	117	80	68	-
Z3j45c	0.00846	0.00019	0.0582	0.0043	0.0499	0.0035	0.3	54.3	1.2	2.2	57.5	4.1	7.1	192	163	85	-
Z3j45r	0.00836	0.00027	0.0548	0.0042	0.0475	0.0033	0.42	53.7	1.8	3.3	54.2	4.1	7.5	75	117	156	-
Z3j46c	0.02927	0.0009	0.21	0.023	0.0521	0.0056	0.28	186	5.7	3	194	20	10.1	292	246	84	-
Z3j46r	0.0286	0.0013	0.188	0.035	0.0478	0.0087	0.24	181.6	8.1	4.4	175	30	17.2	88	235	269	-
Z3j47c	0.02212	0.00051	0.1517	0.0075	0.0498	0.0022	0.47	141	3.2	2.3	143.4	6.6	4.6	184	102	56	-
Z3j47r	0.00801	0.00018	0.0526	0.0039	0.0476	0.0033	0.31	51.4	1.2	2.3	52	3.7	7.2	80	119	149	-
Z3j48c	0.00857	0.00025	0.0626	0.0046	0.053	0.0036	0.4	55	1.6	2.9	61.6	4.4	7.2	327	155	47	-
Z3j48r	0.00827	0.00014	0.0554	0.0018	0.0486	0.0013	0.53	53.1	0.9	1.7	54.8	1.7	3.2	129	65	50	-
Z3j49c	0.01067	0.00029	0.0714	0.0029	0.0486	0.0014	0.68	68.4	1.9	2.7	70.1	2.7	3.9	127	70	55	-
Z3j49r	0.01353	0.00041	0.0901	0.0051	0.0483	0.0023	0.53	86.6	2.6	3	87.6	4.7	5.4	115	112	97	-
Z3j50c	0.00858	0.00013	0.0585	0.002	0.0495	0.0015	0.44	55.1	0.8	1.5	57.8	1.9	3.3	172	72	42	-
Z3j51c	0.022	0.00032	0.1504	0.0039	0.0496	0.001	0.57	140.3	2	1.4	142.2	3.4	2.4	175	49	28	-
Z3j52c	0.00867	0.00017	0.0564	0.0034	0.0472	0.0027	0.33	55.7	1.1	2	55.8	3.3	5.9	59	95	160	-
Z3j52r	0.00842	0.00029	0.0565	0.0045	0.0487	0.0035	0.43	54	1.9	3.5	55.8	4.3	7.8	134	147	110	-
Z3j53c	0.01377	0.00029	0.0917	0.0058	0.0483	0.0029	0.33	88.1	1.8	2.1	89.1	5.4	6	114	124	109	-

Z3j53r	0.01334	0.00043	0.0934	0.0059	0.0507	0.0028	0.5	85.4	2.7	3.2	90.6	5.5	6.1	229	128	56	-
Z3j55c	0.00673	0.00027	0.045	0.0043	0.0486	0.0042	0.42	43.2	1.7	4	44.7	4.1	9.3	127	159	125	-
Z3j55c	0.00729	0.00028	0.0489	0.0045	0.0486	0.0041	0.41	46.8	1.8	3.8	48.4	4.4	9.1	130	159	122	-
Z3j56c	0.00976	0.0003	0.0668	0.0036	0.0496	0.0022	0.56	62.6	1.9	3	65.7	3.4	5.2	178	104	59	-
Z3j56r	0.01003	0.00027	0.0669	0.0035	0.0484	0.0022	0.52	64.3	1.8	2.7	65.8	3.3	5.1	119	105	89	-
z1h1	0.00606	0.0003	0.0375	0.0024	0.0448	0.0019	0.77	39	1.9	5	37.4	2.4	6.4	-	17	-	-
z1h2r	0.00846	0.00018	0.0539	0.0022	0.0463	0.0017	0.51	54.3	1.1	2.1	53.3	2.2	4	11	47	435	-
z1h2c	0.00859	0.00027	0.0546	0.0025	0.0461	0.0016	0.67	55.2	1.7	3.1	54	2.4	4.5	2	41	2263	-
Z15hr	0.01096	0.00023	0.0734	0.0027	0.0486	0.0015	0.56	70.2	1.4	2.1	71.9	2.5	3.5	128	71	56	-
z1h5c	0.00911	0.00027	0.0608	0.0033	0.0484	0.0022	0.55	58.4	1.7	3	60	3.1	5.2	121	106	88	-
z1h9	0.00772	0.00015	0.0485	0.0015	0.0456	0.0011	0.63	49.5	1	2	48.1	1.5	3.1	-	18	-	-
z1h10r	0.00849	0.00016	0.0544	0.0015	0.04649	0.00092	0.69	54.5	1	1.9	53.8	1.4	2.7	23	35	152	-
Z1h10c	0.01093	0.00024	0.0708	0.0027	0.047	0.0015	0.58	70.1	1.5	2.2	69.5	2.6	3.7	47	60	127	-
Z1h11c	0.00877	0.00019	0.0603	0.0018	0.0498	0.001	0.74	56.3	1.2	2.2	59.4	1.7	2.9	187	47	25	-
z2h1r	0.00791	0.0002	0.0524	0.002	0.048	0.0014	0.65	50.8	1.3	2.5	51.8	1.9	3.7	99	68	69	-
z2h2r	0.01092	0.00037	0.0707	0.0047	0.047	0.0027	0.5	70	2.3	3.3	69.4	4.5	6.4	50	91	183	-
z2h3r	0.00882	0.00022	0.0593	0.0021	0.0487	0.0012	0.7	56.6	1.4	2.5	58.5	2	3.5	134	60	45	-
z2h4r	0.00861	0.00022	0.056	0.0026	0.0472	0.0018	0.56	55.2	1.4	2.5	55.3	2.5	4.5	59	74	125	-
Z4g1c	0.00974	0.0003	0.0641	0.003	0.0477	0.0017	0.67	62.5	1.9	3.1	63.1	2.8	4.5	87	82	94	-
Z4g1r	0.00826	0.00029	0.0581	0.0038	0.051	0.0028	0.54	53	1.9	3.5	57.3	3.6	6.3	241	125	52	-

8.4.3 Appendix C: Hf-isotopic data

LA-MC-ICPMS Lu-Hf isotope data of zircon from IODP 341 sites U1417 and U1418.

sample	$^{176}Yb/^{177}Hf$ [a]	±2s	$^{176}Lu/^{177}Hf$ [a]	±2s	$^{178}Hf/^{177}Hf$	$^{180}Hf/^{177}Hf$	Sig_{Hf} [b]	$^{176}Hf/^{177}Hf$	±2s [c]	$^{176}Hf/^{177}Hf_{(t)}$ [d]	$eHf_{(t)}$ [d]	±2s [c]	T_{NC} [e]	age [f]	±2s
							(V)						(Ga)	(Ma)	
18MPI3															
z2d23	0.0242	23	0.00073	5	1.46712	1.88652	10	0.282756	24	0.282754	0.6	0.8	0.92	77	4
z21	0.0433	37	0.00132	9	1.46723	1.88700	16	0.283016	35	0.283011	12.0	1.2	0.38	181	5
19	0.0319	26	0.00101	6	1.46711	1.88675	11	0.282817	20	0.282816	3.0	0.7	0.80	87	3
17	0.0398	32	0.00108	7	1.46711	1.88652	10	0.282762	21	0.282761	0.3	0.7	0.92	53	2
15	0.0264	26	0.00080	7	1.46709	1.88655	11	0.282886	23	0.282885	5.1	0.8	0.67	70	3
14	0.0492	41	0.00154	10	1.46715	1.88671	10	0.282823	25	0.282820	3.5	0.9	0.78	102	4
12	0.0689	75	0.00187	17	1.46714	1.88673	11	0.282789	25	0.282780	6.0	0.9	0.79	277	8
11	0.0266	23	0.00083	6	1.46711	1.88676	10	0.282890	19	0.282889	5.1	0.7	0.66	63	3
8	0.0489	45	0.00135	10	1.46725	1.88657	5	0.282940	38	0.282908	32.4	1.4	0.10	1244	34
9	0.0423	35	0.00120	7	1.46707	1.88656	9	0.282984	23	0.282981	10.5	0.8	0.44	161	6
7	0.0335	28	0.00111	7	1.46711	1.88661	10	0.283006	26	0.283001	12.3	0.9	0.38	211	5
5	0.0490	41	0.00125	8	1.46711	1.88695	9	0.282808	22	0.282806	1.9	0.8	0.83	53	3
4	0.0568	48	0.00162	11	1.46711	1.88664	12	0.282910	20	0.282905	8.2	0.7	0.59	176	7
2	0.0290	24	0.00084	5	1.46715	1.88677	10	0.282580	21	0.282578	-5.7	0.8	1.26	72	3
1	0.0271	22	0.00080	5	1.46713	1.88651	8	0.282762	23	0.282761	0.3	0.8	0.92	53	3
z2c1	0.0926	81	0.00262	18	1.46705	1.88667	9	0.282870	35	0.282869	3.6	1.2	0.72	27	1
3	0.0613	50	0.00170	10	1.46702	1.88694	11	0.282786	33	0.282782	3.2	1.2	0.84	150	4
z3e1	0.0220	24	0.00068	6	1.46712	1.88660	13	0.282999	15	0.282998	9.9	0.5	0.43	106	4
2	0.0278	23	0.00080	5	1.46730	1.88659	8	0.282917	24	0.282916	6.8	0.9	0.60	97	4
3	0.0312	34	0.00100	8	1.46728	1.88667	8	0.282745	24	0.282743	0.3	0.8	0.94	80	3
4	0.0341	28	0.00097	6	1.46717	1.88659	10	0.282797	24	0.282796	2.3	0.8	0.84	85	3
5	0.0965	86	0.00274	19	1.46715	1.88655	9	0.282937	24	0.282926	9.6	0.9	0.53	206	7
6	0.0372	42	0.00112	10	1.46725	1.88664	10	0.282974	26	0.282970	11.7	0.9	0.44	233	7

7	0.0330	27	0.00091	5	1.46729	1.88663	9	0.282750	28	0.282749	0.0	1.0	0.94	57	2
8	0.0815	79	0.00228	18	1.46711	1.88664	10	0.283056	25	0.283045	14.8	0.9	0.28	251	7
9	0.0291	25	0.00090	6	1.46713	1.88679	10	0.282825	18	0.282824	2.8	0.6	0.79	64	1
10	0.0299	24	0.00087	5	1.46718	1.88671	9	0.282880	22	0.282879	4.7	0.8	0.69	61	4
11	0.0206	17	0.00061	4	1.46716	1.88677	8	0.282897	26	0.282896	6.5	0.9	0.63	115	2
12	0.0204	16	0.00059	4	1.46714	1.88673	9	0.282839	26	0.282839	3.2	0.9	0.76	57	3
13	0.0517	50	0.00140	11	1.46714	1.88677	10	0.283009	20	0.283008	9.4	0.7	0.43	70	3
14cdf	0.0194	18	0.00062	5	1.46727	1.88669	11	0.282722	22	0.282721	-0.5	0.8	0.98	80	4
14r	0.0190	16	0.00059	4	1.46710	1.88676	10	0.282759	23	0.282758	0.3	0.8	0.92	54	2
15	0.0218	22	0.00061	5	1.46719	1.88656	9	0.282783	29	0.282782	1.4	1.0	0.87	66	1
16	0.0240	20	0.00076	5	1.46712	1.88676	11	0.282717	22	0.282717	-1.0	0.8	1.00	64	2
17	0.0369	32	0.00101	7	1.46720	1.88673	8	0.282757	25	0.282756	0.3	0.9	0.93	58	2
18	0.0354	35	0.00108	9	1.46715	1.88673	10	0.283014	27	0.283012	10.3	1.0	0.41	102	2
19	0.0485	53	0.00152	13	1.46715	1.88677	11	0.282864	25	0.282859	6.4	0.9	0.68	170	3
20	0.0219	18	0.00067	4	1.46715	1.88670	9	0.282716	24	0.282715	-0.9	0.9	1.00	71	1
21c	0.0112	19	0.00030	5	1.46716	1.88679	11	0.282734	19	0.282733	-0.2	0.7	0.96	72	2
22	0.0270	23	0.00083	6	1.46715	1.88669	8	0.282927	29	0.282925	7.1	1.0	0.58	97	5
23	0.0354	30	0.00096	6	1.46719	1.88670	12	0.282768	16	0.282767	0.4	0.6	0.91	49	1
26	0.0170	15	0.00050	3	1.46720	1.88675	11	0.282960	20	0.282959	8.1	0.7	0.52	87	2
27	0.0373	30	0.00097	6	1.46711	1.88671	10	0.282842	22	0.282839	5.5	0.8	0.72	161	5
28	0.0189	17	0.00055	4	1.46730	1.88666	8	0.282679	39	0.282678	-2.4	1.4	1.07	64	4
28r	0.0103	10	0.00034	2	1.46712	1.88668	9	0.282699	35	0.282698	-1.4	1.2	1.03	76	2
29	0.0207	19	0.00056	4	1.46714	1.88678	9	0.282895	22	0.282895	5.3	0.8	0.65	62	2
30	0.0132	11	0.00039	2	1.46711	1.88671	11	0.282865	24	0.282863	6.6	0.8	0.67	173	6
31	0.0381	32	0.00113	7	1.46712	1.88678	9	0.282662	27	0.282661	-2.4	0.9	1.10	91	3
32	0.0250	20	0.00078	5	1.46712	1.88672	10	0.282964	22	0.282962	9.7	0.8	0.48	156	4
33	0.0211	17	0.00065	4	1.46714	1.88679	9	0.282816	27	0.282815	3.2	1.0	0.79	99	4
34	0.0304	26	0.00093	6	1.46718	1.88670	10	0.282696	23	0.282695	-1.7	0.8	1.04	69	2
36	0.0253	21	0.00079	5	1.46716	1.88650	11	0.282885	24	0.282883	5.6	0.9	0.66	94	3
37	0.0206	27	0.00068	8	1.46711	1.88668	9	0.282718	28	0.282717	-0.9	1.0	1.00	66	3
38	0.0194	22	0.00059	5	1.46714	1.88652	9	0.282692	26	0.282691	-2.1	0.9	1.05	53	2
39	0.0309	31	0.00090	7	1.46717	1.88674	11	0.282979	21	0.282977	9.0	0.7	0.48	98	3

40	0.0321	27	0.00103	7	1.46712	1.88657	11	0.282974	22	0.282973	8.5	0.8	0.49	82	3
41	0.0239	26	0.00077	7	1.46711	1.88653	7	0.282848	24	0.282845	5.6	0.8	0.71	156	4
42	0.0630	52	0.00166	10	1.46711	1.88671	13	0.281942	20	0.281900	-0.4	0.7	2.05	1377	29
43c	0.0283	24	0.00083	5	1.46712	1.88671	10	0.282676	24	0.282672	1.1	0.9	1.02	231	5
43r	0.0130	10	0.00043	3	1.46714	1.88668	11	0.282673	24	0.282672	-2.4	0.9	1.08	71	3
44	0.0361	30	0.00098	6	1.46716	1.88662	12	0.282775	23	0.282774	1.7	0.8	0.88	94	3
46	0.0392	36	0.00119	8	1.46714	1.88671	9	0.282899	28	0.282897	6.2	1.0	0.63	101	3
49c	0.0254	31	0.00086	8	1.46727	1.88679	7	0.282729	33	0.282722	7.2	1.2	0.84	424	15
49r	0.0218	18	0.00070	4	1.46723	1.88663	11	0.282720	24	0.282719	-0.8	0.8	0.99	69	5
50	0.0351	29	0.00102	6	1.46725	1.88669	7	0.282866	21	0.282862	6.9	0.7	0.67	188	5
51	0.0192	16	0.00068	4	1.46711	1.88653	7	0.282965	36	0.282964	7.8	1.3	0.52	67	3
52c	0.0265	21	0.00070	4	1.46717	1.88674	11	0.283083	18	0.283081	12.7	0.6	0.27	101	3
52r	0.0228	19	0.00062	4	1.46713	1.88670	11	0.283079	19	0.283078	11.9	0.7	0.29	70	4
54	0.0585	67	0.00155	15	1.46713	1.88663	11	0.282807	22	0.282805	1.8	0.8	0.83	51	2
55	0.0166	15	0.00054	4	1.46711	1.88659	10	0.283018	24	0.283017	9.8	0.8	0.41	71	4
56	0.0283	23	0.00075	5	1.46718	1.88679	10	0.282712	23	0.282712	-1.3	0.8	1.01	57	2
57	0.0194	16	0.00063	4	1.46714	1.88679	8	0.283053	21	0.283052	11.0	0.7	0.34	72	2
59	0.0382	39	0.00123	11	1.46713	1.88650	10	0.282892	20	0.282890	5.7	0.7	0.65	89	3
61	0.0271	22	0.00085	5	1.46717	1.88662	12	0.283083	21	0.283082	12.0	0.7	0.28	68	3
62	0.0267	28	0.00079	7	1.46710	1.88660	8	0.282847	24	0.282846	4.4	0.8	0.73	103	4
63	0.0150	13	0.00048	3	1.46722	1.88679	11	0.283039	19	0.283039	10.2	0.7	0.37	57	2
65	0.0213	18	0.00065	4	1.46712	1.88672	10	0.283071	23	0.283070	12.0	0.8	0.30	86	3
66	0.0281	25	0.00097	7	1.46720	1.88663	5	0.282981	33	0.282980	8.3	1.2	0.49	61	2
67	0.0285	25	0.00092	6	1.46718	1.88671	10	0.282897	19	0.282896	6.0	0.7	0.64	94	2
18MPI2															
z1d3	0.0439	39	0.00130	9	1.46716	1.88657	8	0.282854	25	0.282852	3.8	0.9	0.74	65	5
6	0.0258	23	0.00080	6	1.46714	1.88670	10	0.282402	23	0.282400	-10.0	0.8	1.57	164	11
7	0.0296	34	0.00084	8	1.46716	1.88670	9	0.282777	22	0.282776	1.0	0.8	0.89	61	3
8	0.0236	24	0.00080	7	1.46713	1.88667	7	0.282678	23	0.282677	-2.8	0.8	1.08	46	3
9	0.0517	42	0.00153	9	1.46717	1.88671	11	0.282587	23	0.282585	-5.6	0.8	1.25	68	4
10	0.0504	46	0.00137	10	1.46718	1.88680	8	0.282864	25	0.282861	4.6	0.9	0.71	85	6
12	0.0530	44	0.00183	12	1.46719	1.88656	9	0.283048	26	0.283045	11.2	0.9	0.35	88	4

17	0.0721	73	0.00200	16	1.46716	1.88666	10	0.283075	26	0.283075	10.3	0.9	0.32	2	1
16	0.0454	37	0.00137	9	1.46718	1.88672	10	0.282724	25	0.282723	-0.8	0.9	0.99	62	3
27	0.0293	24	0.00089	6	1.46712	1.88679	11	0.282948	20	0.282947	7.5	0.7	0.54	81	4
28	0.0334	27	0.00101	6	1.46711	1.88679	11	0.282795	25	0.282794	1.5	0.9	0.85	52	3
33	0.0419	34	0.00119	7	1.46715	1.88675	11	0.282843	25	0.282840	4.9	0.9	0.73	131	7
36	0.0254	26	0.00081	7	1.46717	1.88671	7	0.282078	27	0.282077	-23.3	1.0	2.22	78	5
42	0.1324	185	0.00436	55	1.46720	1.88662	5	0.282967	36	0.282967	6.4	1.3	0.54	0	0
53	0.0306	25	0.00095	6	1.46719	1.88671	10	0.282900	19	0.282899	5.3	0.7	0.65	57	2
z4a1	0.0301	24	0.00097	6	1.46711	1.88672	11	0.282610	24	0.282606	-2.3	0.8	1.17	181	5
2	0.0446	39	0.00118	8	1.46716	1.88672	9	0.282764	24	0.282763	0.6	0.8	0.91	63	2
3	0.0158	13	0.00057	4	1.46711	1.88651	7	0.283068	34	0.283067	11.3	1.2	0.32	58	4
4	0.0283	25	0.00077	5	1.46718	1.88671	9	0.282796	19	0.282795	1.7	0.7	0.85	60	2
5	0.0335	32	0.00092	7	1.46712	1.88676	12	0.282814	22	0.282813	2.2	0.8	0.82	53	2
6	0.0310	26	0.00098	6	1.46720	1.88671	9	0.282680	24	0.282679	-2.2	0.8	1.07	72	2
7	0.0165	16	0.00051	4	1.46716	1.88671	10	0.282979	21	0.282979	8.0	0.7	0.49	53	2
8	0.0292	26	0.00081	6	1.46714	1.88660	8	0.282770	24	0.282766	5.2	0.8	0.82	261	8
9	0.0324	30	0.00086	6	1.46729	1.88668	9	0.282863	38	0.282863	2.7	1.3	0.74	0	0
10	0.0235	19	0.00073	5	1.46717	1.88679	10	0.283014	25	0.283013	9.8	0.9	0.42	77	2
11	0.0296	24	0.00096	6	1.46713	1.88676	11	0.282879	22	0.282877	5.5	0.8	0.67	99	3
z3c1	0.0445	38	0.00150	11	1.46730	1.88678	7	0.282741	30	0.282737	1.4	1.1	0.93	139	7
z3c2	0.0480	39	0.00142	9	1.46718	1.88657	7	0.282578	27	0.282576	-5.7	1.0	1.27	76	3
3	0.0201	17	0.00063	4	1.46722	1.88668	11	0.282857	20	0.282856	4.4	0.7	0.72	86	4
6	0.0372	32	0.00111	7	1.46718	1.88676	10	0.282700	23	0.282699	-2.1	0.8	1.04	43	2
7	0.0178	16	0.00058	4	1.46711	1.88665	9	0.282685	23	0.282684	-2.3	0.8	1.06	58	2
9	0.0532	43	0.00176	11	1.46712	1.88674	9	0.283039	27	0.283034	12.3	0.9	0.34	157	6
12	0.0373	43	0.00119	12	1.46717	1.88670	10	0.282820	23	0.282818	2.7	0.8	0.80	70	3
13	0.0296	27	0.00088	6	1.46711	1.88671	9	0.282715	24	0.282715	-1.5	0.8	1.01	45	2
14	0.0455	40	0.00130	8	1.46714	1.88660	11	0.282821	30	0.282819	2.4	1.1	0.80	55	3
15	0.0141	13	0.00048	4	1.46717	1.88655	8	0.282875	25	0.282874	5.3	0.9	0.68	98	4
16c	0.0242	21	0.00076	5	1.46719	1.88671	9	0.282870	22	0.282869	4.8	0.8	0.70	82	3
16r	0.0062	5	0.00024	2	1.46714	1.88671	10	0.282854	24	0.282853	3.7	0.9	0.74	58	3
18	0.0354	29	0.00122	8	1.46713	1.88679	8	0.282911	22	0.282909	6.5	0.8	0.61	94	4

19	0.0208	17	0.00063	4	1.46718	1.88667	11	0.283014	24	0.283012	11.5	0.9	0.38	155	10
20	0.0344	30	0.00102	8	1.46719	1.88656	10	0.282920	26	0.282918	6.9	0.9	0.59	100	4
22	0.0422	35	0.00128	8	1.46711	1.88679	7	0.283060	28	0.283059	11.0	1.0	0.33	60	3
23	0.0256	23	0.00072	6	1.46713	1.88679	8	0.282684	22	0.282682	0.7	0.8	1.02	194	8
25	0.0221	18	0.00082	5	1.46713	1.88660	9	0.282885	20	0.282883	5.5	0.7	0.66	93	4
26	0.0349	29	0.00113	7	1.46712	1.88665	7	0.282754	33	0.282753	0.1	1.2	0.93	55	2
29	0.1147	140	0.00325	30	1.46717	1.88660	7	0.282914	57	0.282912	5.3	2.0	0.63	35	2
30	0.0245	20	0.00075	5	1.46713	1.88674	9	0.282795	23	0.282794	1.8	0.8	0.85	64	2
31	0.0223	19	0.00083	5	1.46714	1.88655	10	0.282936	22	0.282935	7.2	0.8	0.56	87	3
32	0.0245	28	0.00068	6	1.46725	1.88667	8	0.282994	28	0.282994	8.6	1.0	0.46	55	2
36	0.0509	50	0.00174	13	1.46712	1.88657	7	0.282865	33	0.282862	4.6	1.2	0.71	87	3
37	0.0239	20	0.00080	5	1.46713	1.88675	11	0.282331	24	0.282329	-13.8	0.9	1.73	103	3
40	0.0421	37	0.00152	11	1.46715	1.88670	9	0.282882	25	0.282879	5.6	0.9	0.67	102	3
42	0.0162	15	0.00056	5	1.46711	1.88670	9	0.283060	27	0.283059	11.0	1.0	0.33	60	3
44	0.0198	18	0.00072	6	1.46715	1.88672	10	0.282887	32	0.282886	4.8	1.1	0.67	56	3
45	0.0198	90	0.00042	14	1.46717	1.88665	7	0.282583	31	0.282582	-4.7	1.1	1.24	113	5
46	0.0447	46	0.00141	12	1.46711	1.88670	8	0.282974	24	0.282969	10.8	0.9	0.46	192	7
18MPI1															
z3cm1	0.0421	41	0.00123	9	1.46717	1.88656	9	0.282496	24	0.282494	-8.3	0.8	1.42	90	3
2	0.0332	29	0.00092	6	1.46711	1.88671	9	0.283007	26	0.283006	9.8	0.9	0.42	90	4
5	0.0364	31	0.00108	7	1.46712	1.88669	10	0.282721	22	0.282719	-1.1	0.8	1.00	55	2
6	0.0419	56	0.00112	13	1.46722	1.88660	9	0.282740	29	0.282739	-0.5	1.0	0.96	51	3
10	0.0330	28	0.00097	6	1.46711	1.88654	9	0.282818	26	0.282816	2.9	0.9	0.80	80	3
11	0.0474	93	0.00141	24	1.46717	1.88671	8	0.282939	26	0.282937	7.1	0.9	0.56	78	4
z4b1	0.0509	49	0.00155	14	1.46711	1.88661	8	0.283008	23	0.283005	10.5	0.8	0.41	125	4
2	0.0288	28	0.00094	8	1.46720	1.88664	11	0.282333	20	0.282330	-12.1	0.7	1.70	182	3
4	0.0385	32	0.00107	7	1.46714	1.88674	8	0.282960	26	0.282958	7.9	0.9	0.52	80	3
5	0.0444	73	0.00120	19	1.46712	1.88664	10	0.282653	26	0.282646	2.3	0.9	1.03	323	9
6	0.0289	29	0.00092	8	1.46714	1.88650	8	0.282980	25	0.282979	7.6	0.9	0.50	34	2
7	0.0328	28	0.00103	7	1.46710	1.88670	9	0.282849	20	0.282846	5.1	0.7	0.72	133	5
8	0.0192	16	0.00061	4	1.46713	1.88672	11	0.282961	21	0.282960	8.7	0.8	0.50	115	2
9	0.0259	23	0.00088	6	1.46728	1.88670	9	0.282883	25	0.282882	5.0	0.9	0.68	70	2

10	0.0297	25	0.00094	6	1.46718	1.88676	9	0.283049	25	0.283047	11.0	0.9	0.35	78	1
13	0.0195	16	0.00066	5	1.46717	1.88670	7	0.282768	26	0.282768	0.8	0.9	0.90	66	2
14	0.0290	25	0.00083	5	1.46717	1.88667	8	0.282968	26	0.282967	8.2	0.9	0.50	80	4
15	0.0139	11	0.00042	3	1.46719	1.88678	11	0.282911	23	0.282910	6.4	0.8	0.61	87	3
16	0.0220	19	0.00069	5	1.46719	1.88672	9	0.282770	21	0.282768	3.0	0.7	0.86	163	4
17	0.0257	28	0.00079	7	1.46720	1.88670	8	0.282980	27	0.282979	8.5	1.0	0.48	75	3
18	0.0238	20	0.00080	6	1.46712	1.88670	9	0.282867	21	0.282865	5.6	0.7	0.69	126	3
19	0.0138	13	0.00044	3	1.46718	1.88670	9	0.283076	24	0.283076	11.8	0.9	0.29	71	3
20	0.0383	34	0.00107	7	1.46712	1.88677	9	0.282766	24	0.282765	0.4	0.9	0.91	50	1
22	0.0404	39	0.00113	9	1.46717	1.88674	9	0.282782	26	0.282781	0.9	0.9	0.88	50	1
23	0.0190	20	0.00063	6	1.46719	1.88673	9	0.283006	23	0.283005	9.3	0.8	0.43	71	3
24	0.0193	15	0.00058	3	1.46710	1.88656	9	0.282979	21	0.282978	9.4	0.7	0.47	115	4
25	0.0190	22	0.00056	5	1.46711	1.88663	9	0.283053	24	0.283053	11.1	0.8	0.34	71	4
26	0.0609	50	0.00171	11	1.46719	1.88670	7	0.282713	27	0.282711	-1.3	1.0	1.01	61	2
27	0.0189	17	0.00052	4	1.46710	1.88675	10	0.282993	20	0.282992	9.3	0.7	0.45	87	5
28	0.0292	24	0.00083	5	1.46716	1.88654	9	0.282913	24	0.282912	6.3	0.9	0.61	81	2
29	0.0298	25	0.00089	6	1.46718	1.88670	10	0.282704	24	0.282703	-1.7	0.8	1.03	56	3
30	0.0330	27	0.00096	6	1.46717	1.88664	11	0.282172	23	0.282157	-4.4	0.8	1.79	797	29
31	0.0297	24	0.00084	5	1.46710	1.88662	10	0.282911	22	0.282910	6.4	0.8	0.61	91	3
32	0.0051	6	0.00016	2	1.46716	1.88671	10	0.282719	21	0.282719	-1.6	0.8	1.01	32	2
z4d1	0.0395	33	0.00128	8	1.46715	1.88680	8	0.282863	25	0.282861	4.5	0.9	0.71	84	3
3	0.0409	39	0.00135	11	1.46720	1.88671	9	0.282865	28	0.282864	3.9	1.0	0.72	51	2
4	0.0283	39	0.00084	10	1.46717	1.88664	10	0.282857	23	0.282856	3.7	0.8	0.73	55	2
5	0.0260	25	0.00083	7	1.46717	1.88659	10	0.282848	20	0.282847	3.9	0.7	0.74	78	3
6	0.0182	18	0.00059	5	1.46713	1.88671	10	0.283021	23	0.283020	9.6	0.8	0.41	59	2
7	0.0183	15	0.00058	4	1.46715	1.88679	9	0.283059	25	0.283058	11.3	0.9	0.33	73	3
8	0.0191	16	0.00052	3	1.46720	1.88674	9	0.283028	27	0.283027	10.2	0.9	0.39	73	4
9	0.0373	31	0.00139	9	1.46710	1.88674	9	0.282848	26	0.282843	6.2	0.9	0.70	184	7
10	0.0241	22	0.00077	6	1.46717	1.88675	9	0.282845	21	0.282844	3.2	0.8	0.76	51	1
11	0.0195	17	0.00065	4	1.46717	1.88676	10	0.282995	20	0.282995	9.0	0.7	0.45	70	2
12	0.0379	35	0.00106	8	1.46714	1.88671	8	0.282837	22	0.282836	3.1	0.8	0.77	57	1
13	0.0154	14	0.00046	3	1.46713	1.88670	10	0.282824	20	0.282823	2.8	0.7	0.79	63	3

14	0.0222	19	0.00072	5	1.46713	1.88679	10	0.282857	25	0.282856	3.7	0.9	0.73	52	1
15	0.0204	18	0.00062	4	1.46717	1.88675	10	0.282946	25	0.282945	7.9	0.9	0.54	101	2
16	0.0259	21	0.00084	5	1.46718	1.88665	9	0.282968	29	0.282967	7.6	1.0	0.52	50	2
19	0.0212	17	0.00064	4	1.46720	1.88670	10	0.282988	21	0.282987	8.6	0.7	0.47	66	2
20	0.0166	14	0.00052	3	1.46711	1.88671	9	0.282687	25	0.282686	-2.2	0.9	1.06	59	2
21c	0.0184	15	0.00052	3	1.46713	1.88674	11	0.283040	21	0.283039	10.8	0.7	0.36	83	3
22	0.0212	18	0.00060	4	1.46712	1.88653	8	0.282843	24	0.282843	2.1	0.9	0.78	0	0
23	0.0329	32	0.00090	7	1.46712	1.88676	9	0.283056	24	0.283055	11.0	0.8	0.34	64	2
24	0.0475	42	0.00141	10	1.46711	1.88673	11	0.282932	22	0.282927	8.9	0.8	0.54	172	8
25	0.0236	19	0.00068	4	1.46713	1.88671	10	0.282935	21	0.282934	7.1	0.8	0.57	84	2
26	0.0131	12	0.00044	3	1.46716	1.88652	10	0.282948	25	0.282948	7.3	0.9	0.55	70	4
27	0.0127	11	0.00040	2	1.46710	1.88673	10	0.282949	19	0.282948	7.3	0.7	0.55	69	3
28	0.0289	23	0.00091	6	1.46714	1.88670	9	0.282419	24	0.282416	-9.2	0.8	1.54	173	5
z4e1	0.0156	13	0.00048	3	1.46712	1.88680	10	0.282748	23	0.282747	-0.1	0.8	0.94	56	1
3	0.0401	37	0.00126	9	1.46713	1.88668	9	0.283074	22	0.283073	11.2	0.8	0.31	45	1
4	0.0281	23	0.00083	5	1.46711	1.88679	10	0.283052	20	0.283051	11.1	0.7	0.34	76	2
5	0.0293	24	0.00093	6	1.46716	1.88673	10	0.282953	18	0.282951	9.0	0.6	0.51	142	3
6	0.0087	8	0.00029	2	1.46720	1.88678	10	0.282734	18	0.282734	-0.5	0.6	0.97	59	1
7	0.0431	36	0.00124	8	1.46711	1.88668	9	0.282765	29	0.282764	0.4	1.0	0.91	52	1
8	0.0236	20	0.00076	5	1.46717	1.88675	11	0.282997	22	0.282996	9.2	0.8	0.45	80	1
10	0.0558	70	0.00166	18	1.46710	1.88678	8	0.282955	30	0.282950	9.6	1.1	0.50	169	4
12	0.0605	57	0.00160	13	1.46714	1.88670	11	0.282889	32	0.282887	4.8	1.1	0.67	52	2
14	0.0289	30	0.00099	8	1.46714	1.88672	9	0.283022	17	0.283019	12.0	0.6	0.37	167	4
16	0.0263	23	0.00085	6	1.46715	1.88671	9	0.282911	23	0.282910	6.0	0.8	0.62	70	2
17	0.0220	18	0.00070	5	1.46717	1.88661	10	0.282783	26	0.282782	1.4	0.9	0.87	67	1
18	0.0523	46	0.00150	10	1.46728	1.88664	8	0.282794	27	0.282793	1.4	1.0	0.86	49	2
19	0.0355	29	0.00111	7	1.46715	1.88671	8	0.282895	26	0.282893	5.0	0.9	0.66	55	1
20	0.0416	34	0.00114	7	1.46713	1.88676	10	0.282781	26	0.282780	0.9	0.9	0.88	50	1
22	0.0565	47	0.00163	10	1.46710	1.88675	10	0.283009	25	0.283007	8.7	0.9	0.44	37	1
12	0.0294	26	0.00096	7	1.46712	1.88670	10	0.283034	20	0.283033	10.3	0.7	0.38	69	3
18EPI															
z3f1	0.0154	15	0.00044	3	1.46720	1.88676	10	0.282814	24	0.282814	2.2	0.8	0.82	51	1

2	0.0477	42	0.00136	10	1.46718	1.88662	8	0.282760	27	0.282758	0.1	0.9	0.92	49	1
3	0.0507	41	0.00133	8	1.46714	1.88680	11	0.282779	20	0.282777	0.9	0.7	0.89	54	1
4	0.0635	52	0.00172	11	1.46710	1.88667	7	0.282754	29	0.282753	0.0	1.0	0.93	51	1
5c	0.0256	26	0.00070	6	1.46718	1.88668	11	0.282699	39	0.282698	-1.3	1.4	1.03	77	2
5r	0.0213	24	0.00066	7	1.46716	1.88671	10	0.282831	26	0.282831	2.9	0.9	0.78	56	2
6	0.0450	38	0.00118	8	1.46715	1.88672	11	0.282796	24	0.282795	1.6	0.9	0.85	56	1
7	0.0307	25	0.00075	5	1.46718	1.88659	9	0.282870	23	0.282869	4.1	0.8	0.71	48	2
8	0.0248	23	0.00075	6	1.46718	1.88671	10	0.283002	26	0.283001	9.4	0.9	0.44	79	2
9	0.0155	14	0.00045	3	1.46715	1.88677	10	0.282861	20	0.282859	6.1	0.7	0.68	156	5
10	0.0458	53	0.00132	12	1.46720	1.88676	10	0.282668	21	0.282667	-3.0	0.7	1.10	54	1
11	0.0228	19	0.00071	5	1.46711	1.88668	7	0.282745	22	0.282744	0.1	0.8	0.94	70	1
12	0.0453	37	0.00130	8	1.46711	1.88662	9	0.282863	27	0.282860	4.9	1.0	0.71	99	1
12r	0.0392	32	0.00118	7	1.46711	1.88667	8	0.282872	31	0.282871	4.2	1.1	0.70	54	2
13	0.0280	25	0.00088	6	1.46715	1.88670	10	0.282932	24	0.282931	7.2	0.8	0.57	94	1
16	0.0342	31	0.00095	7	1.46718	1.88653	11	0.283060	22	0.283059	11.0	0.8	0.33	60	1
17	0.0218	18	0.00066	4	1.46713	1.88672	12	0.282828	20	0.282827	2.9	0.7	0.78	62	1
18	0.0296	25	0.00093	6	1.46718	1.88673	9	0.282940	22	0.282938	7.6	0.8	0.55	98	2
19	0.0290	24	0.00093	6	1.46714	1.88671	9	0.282847	24	0.282845	5.3	0.8	0.72	143	4
20	0.0260	26	0.00079	6	1.46714	1.88679	9	0.282115	29	0.282114	-22.3	1.0	2.16	67	2
21c	0.0300	27	0.00092	6	1.46714	1.88678	8	0.282980	25	0.282979	9.0	0.9	0.48	96	4
23	0.0516	42	0.00142	9	1.46714	1.88673	9	0.282776	23	0.282773	1.7	0.8	0.88	96	15
27	0.0342	29	0.00101	7	1.46713	1.88671	7	0.283088	32	0.283086	13.1	1.1	0.26	109	2
17PI															
z3a1	0.0747	61	0.00194	12	1.46711	1.88670	9	0.283170	21	0.283169	14.5	0.7	0.12	43	5
2	0.0262	23	0.00074	5	1.46717	1.88680	9	0.283040	21	0.283039	10.7	0.7	0.36	76	2
4	0.0619	50	0.00195	12	1.46725	1.88669	6	0.282938	34	0.282929	10.4	1.2	0.51	239	7
6	0.0217	19	0.00072	5	1.46712	1.88671	9	0.283008	20	0.283007	9.4	0.7	0.43	69	3
7c	0.0419	35	0.00112	7	1.46718	1.88670	10	0.282790	27	0.282789	1.6	1.0	0.86	66	1
7r	0.0507	41	0.00143	9	1.46717	1.88669	8	0.282781	27	0.282780	1.1	0.9	0.88	57	1
8	0.0320	26	0.00088	5	1.46711	1.88671	11	0.283034	24	0.283031	12.6	0.9	0.34	174	4
9	0.0196	16	0.00058	4	1.46719	1.88675	11	0.283022	23	0.283021	10.6	0.8	0.39	102	4
10	0.0484	44	0.00141	11	1.46716	1.88665	13	0.283018	21	0.283016	9.8	0.8	0.41	73	3

11	0.0268	22	0.00078	5	1.46717	1.88663	9	0.282810	34	0.282810	1.5	1.2	0.83	29	1
12	0.0554	54	0.00155	12	1.46720	1.88679	12	0.282992	22	0.282988	10.3	0.8	0.44	140	3
13	0.0408	33	0.00116	7	1.46710	1.88669	11	0.283028	18	0.283024	12.3	0.6	0.35	175	4
14	0.0268	26	0.00086	7	1.46716	1.88651	9	0.282992	22	0.282990	9.8	0.8	0.44	115	9
17Pi															
z3b1	0.0337	28	0.00098	6	1.46711	1.88680	9	0.282648	23	0.282645	-0.8	0.8	1.09	186	8
2	0.0508	72	0.00150	18	1.46716	1.88674	9	0.282733	24	0.282731	-0.7	0.8	0.97	55	2
3	0.0241	20	0.00079	5	1.46716	1.88665	9	0.282422	26	0.282419	-8.7	0.9	1.53	190	3
5	0.0217	18	0.00065	4	1.46714	1.88675	10	0.282796	17	0.282795	1.4	0.6	0.85	47	1
6	0.0286	23	0.00083	5	1.46713	1.88675	12	0.283008	22	0.283007	9.4	0.8	0.43	70	3
6r	0.0516	45	0.00138	9	1.46711	1.88679	13	0.282837	20	0.282835	3.0	0.7	0.77	57	2
7	0.0431	70	0.00120	17	1.46711	1.88670	10	0.282833	23	0.282831	2.8	0.8	0.78	53	1
8	0.0381	32	0.00097	6	1.46719	1.88673	10	0.282933	25	0.282932	6.1	0.9	0.59	42	3
9	0.0613	49	0.00161	10	1.46711	1.88671	11	0.282855	22	0.282854	3.6	0.8	0.74	52	1
12	0.0269	22	0.00081	5	1.46713	1.88677	9	0.282670	24	0.282669	-2.5	0.8	1.09	74	3
13	0.0385	33	0.00105	7	1.46720	1.88650	11	0.282942	25	0.282941	6.8	0.9	0.56	59	1
14	0.0306	28	0.00085	6	1.46717	1.88671	10	0.282807	23	0.282807	1.9	0.8	0.83	52	1
15	0.0509	42	0.00158	10	1.46714	1.88671	10	0.282953	24	0.282944	12.8	0.9	0.45	322	6
17	0.0236	22	0.00073	6	1.46712	1.88679	8	0.282732	23	0.282731	-0.6	0.8	0.97	57	1
19	0.0482	40	0.00134	9	1.46720	1.88669	9	0.282817	26	0.282816	2.2	0.9	0.81	48	2
20	0.0720	64	0.00186	13	1.46712	1.88674	12	0.281956	22	0.281908	-0.2	0.8	2.03	1371	22
21c	0.0394	38	0.00121	10	1.46719	1.88672	9	0.283028	25	0.283026	10.1	0.9	0.39	71	3
22	0.0588	58	0.00165	13	1.46716	1.88671	9	0.282768	27	0.282767	0.6	1.0	0.90	59	2
23	0.0357	30	0.00109	7	1.46712	1.88673	9	0.282647	26	0.282644	-1.2	0.9	1.10	170	4
24	0.0320	28	0.00104	7	1.46716	1.88664	9	0.283007	21	0.283005	9.8	0.8	0.43	89	2
26	0.0407	35	0.00109	7	1.46718	1.88670	10	0.282774	26	0.282772	0.7	0.9	0.90	54	1
27	0.0366	36	0.00107	9	1.46720	1.88665	10	0.282745	26	0.282744	-0.1	0.9	0.95	61	1
29	0.0395	35	0.00107	7	1.46713	1.88659	9	0.282862	27	0.282860	5.6	1.0	0.69	132	5
30	0.0389	33	0.00105	7	1.46710	1.88673	10	0.282858	26	0.282857	3.7	0.9	0.73	53	1
31	0.0697	71	0.00187	15	1.46720	1.88658	10	0.282810	26	0.282808	2.0	0.9	0.83	54	1
32	0.0393	36	0.00149	11	1.46710	1.88671	9	0.282949	23	0.282946	7.7	0.8	0.54	92	2
34	0.0261	21	0.00075	4	1.46719	1.88671	11	0.282894	21	0.282893	5.5	0.7	0.65	74	2

35	0.0312	32	0.00102	9	1.46718	1.88672	9	0.282990	20	0.282987	10.9	0.7	0.43	171	6
36	0.0697	56	0.00187	11	1.46715	1.88670	11	0.282815	21	0.282813	2.3	0.7	0.81	57	2
38	0.0532	49	0.00169	12	1.46716	1.88676	7	0.282998	25	0.282996	9.5	0.9	0.44	93	3
41	0.0188	15	0.00054	3	1.46719	1.88653	10	0.282954	22	0.282953	7.7	0.8	0.53	78	3
42	0.0359	32	0.00097	7	1.46710	1.88680	12	0.282774	20	0.282773	0.8	0.7	0.89	57	2
43c	0.0249	20	0.00076	5	1.46717	1.88673	11	0.282675	23	0.282673	-2.2	0.8	1.08	80	2
44	0.0158	13	0.00052	3	1.46719	1.88671	9	0.282842	26	0.282841	5.3	0.9	0.72	150	5
45	0.0389	36	0.00128	9	1.46713	1.88671	10	0.283029	24	0.283026	11.3	0.8	0.37	126	4
46	0.0221	18	0.00064	4	1.46718	1.88675	9	0.282932	23	0.282931	6.8	0.8	0.58	75	1
47c	0.0259	21	0.00071	4	1.46713	1.88679	10	0.282840	17	0.282838	5.8	0.6	0.72	177	4
48	0.0216	20	0.00071	6	1.46713	1.88658	9	0.282871	26	0.282869	5.0	0.9	0.69	93	2
50	0.0201	19	0.00067	5	1.46716	1.88673	9	0.282934	20	0.282932	8.5	0.7	0.54	148	3
51	0.0586	48	0.00158	10	1.46713	1.88670	11	0.282826	23	0.282825	2.5	0.8	0.79	51	1
52c	0.0599	48	0.00159	10	1.46713	1.88655	7	0.282849	27	0.282847	3.2	1.0	0.75	43	1
53	0.0100	8	0.00032	2	1.46720	1.88680	10	0.282620	21	0.282620	-4.2	0.8	1.18	75	2
54	0.0229	19	0.00062	4	1.46715	1.88672	10	0.282850	20	0.282849	3.8	0.7	0.74	70	1
55	0.0293	24	0.00115	7	1.46714	1.88660	8	0.282617	30	0.282615	-4.0	1.0	1.19	90	2
57	0.0231	19	0.00071	4	1.46719	1.88670	8	0.282677	22	0.282676	-1.2	0.8	1.06	120	2
58	0.0202	17	0.00058	4	1.46717	1.88662	10	0.283010	21	0.283009	9.6	0.7	0.42	77	2
59	0.0425	46	0.00131	12	1.46713	1.88677	9	0.283015	24	0.283010	12.5	0.9	0.37	207	6
61	0.0189	16	0.00057	4	1.46716	1.88673	11	0.282855	22	0.282854	3.8	0.8	0.73	61	1
62	0.0215	18	0.00067	4	1.46719	1.88680	9	0.282693	22	0.282692	-2.0	0.8	1.05	56	2
63	0.0064	5	0.00015	1	1.46718	1.88679	11	0.282902	19	0.282902	5.8	0.7	0.63	76	1
64	0.0255	22	0.00079	5	1.46715	1.88678	11	0.282712	19	0.282711	-1.4	0.7	1.01	53	1
66	0.0325	27	0.00102	7	1.46718	1.88679	9	0.282951	24	0.282947	10.8	0.9	0.48	230	8
67	0.0546	52	0.00167	12	1.46721	1.88671	8	0.282619	28	0.282615	-2.8	1.0	1.16	146	4
68	0.0172	14	0.00051	3	1.46716	1.88670	10	0.282989	18	0.282988	9.1	0.6	0.46	87	2
69	0.0466	40	0.00125	8	1.46714	1.88674	10	0.282796	23	0.282795	1.6	0.8	0.85	56	1
70	0.0217	18	0.00057	3	1.46711	1.88677	9	0.282804	22	0.282803	4.7	0.8	0.78	182	3
71	0.0323	28	0.00104	7	1.46716	1.88674	10	0.282782	20	0.282781	1.2	0.7	0.88	59	2
73	0.0238	20	0.00082	5	1.46717	1.88677	8	0.283029	34	0.283028	10.3	1.2	0.39	79	2
74	0.0266	22	0.00071	4	1.46712	1.88671	10	0.281970	25	0.281965	-21.1	0.9	2.33	355	6

75	0.0399	40	0.00106	9	1.46717	1.88673	9	0.282884	23	0.282882	5.0	0.8	0.67	71	2
76	0.0520	52	0.00159	13	1.46719	1.88674	10	0.282892	22	0.282890	5.0	0.8	0.66	58	2
77	0.0305	26	0.00088	6	1.46719	1.88669	10	0.282888	26	0.282887	5.2	0.9	0.66	73	1
78	0.0584	50	0.00164	11	1.46720	1.88667	11	0.282775	25	0.282773	1.0	0.9	0.89	66	2
79	0.0261	21	0.00072	4	1.46710	1.88679	10	0.282831	16	0.282830	2.9	0.6	0.78	57	1
80	0.0372	39	0.00105	9	1.46714	1.88660	7	0.282886	26	0.282886	3.6	0.9	0.69	0	0
81	0.0101	10	0.00035	3	1.46716	1.88664	10	0.282848	21	0.282847	5.3	0.7	0.71	141	3
83	0.0210	17	0.00066	4	1.46715	1.88671	9	0.282768	22	0.282768	0.6	0.8	0.90	56	1
84	0.0511	43	0.00159	10	1.46710	1.88671	9	0.282656	23	0.282654	-2.5	0.8	1.11	98	1
87	0.0640	52	0.00181	11	1.46719	1.88670	9	0.282826	23	0.282824	2.6	0.8	0.79	53	1
86	0.0229	19	0.00072	5	1.46716	1.88653	10	0.282691	20	0.282690	-2.1	0.7	1.05	55	1
88	0.0219	18	0.00061	4	1.46713	1.88670	10	0.282798	23	0.282797	1.6	0.8	0.85	53	1
89	0.0172	14	0.00056	3	1.46711	1.88657	11	0.283035	22	0.283034	10.4	0.8	0.38	69	3
90	0.0339	28	0.00093	6	1.46717	1.88664	9	0.282971	22	0.282969	8.1	0.8	0.50	72	2
91	0.0168	14	0.00051	3	1.46718	1.88656	11	0.282840	25	0.282836	10.8	0.9	0.63	405	9
92	0.0307	25	0.00096	6	1.46710	1.88660	8	0.283022	24	0.283020	10.3	0.9	0.40	92	3
95	0.0206	17	0.00067	4	1.46716	1.88674	9	0.282821	25	0.282819	4.3	0.9	0.77	138	3
97	0.0354	30	0.00106	7	1.46712	1.88675	9	0.282801	24	0.282800	2.1	0.9	0.83	73	1
98	0.0304	25	0.00096	6	1.46717	1.88679	10	0.282784	22	0.282783	1.4	0.8	0.87	65	1
z1f6	0.0449	38	0.00120	8	1.46717	1.88659	11	0.283027	22	0.283026	9.4	0.8	0.41	37	1
7	0.0284	31	0.00083	7	1.46708	1.88663	7	0.282722	30	0.282718	3.0	1.1	0.93	240	6
8	0.0227	19	0.00066	4	1.46707	1.88655	9	0.282806	19	0.282805	2.2	0.7	0.83	65	2
9	0.0294	24	0.00094	6	1.46713	1.88666	10	0.282585	25	0.282583	-3.5	0.9	1.22	166	4
10	0.0328	51	0.00098	14	1.46715	1.88666	10	0.282817	24	0.282816	2.3	0.9	0.81	56	2
z2b7	0.0301	29	0.00102	7	1.46711	1.88673	8	0.282829	33	0.282828	2.7	1.2	0.79	52	3
6	0.0460	37	0.00146	9	1.46704	1.88658	10	0.283000	22	0.282997	9.8	0.8	0.44	104	3
4	0.0454	38	0.00116	7	1.46707	1.88653	12	0.282946	24	0.282945	6.4	0.8	0.57	34	1
3	0.0289	24	0.00088	6	1.46725	1.88670	8	0.282689	35	0.282688	-2.1	1.2	1.06	58	2
2	0.0290	27	0.00088	6	1.46727	1.88675	9	0.282765	35	0.282765	0.5	1.3	0.91	56	2
17Mi2															
z1a	0.0326	28	0.00086	6	1.46715	1.88663	8	0.282833	26	0.282832	2.9	0.9	0.78	57	3
2	0.0741	84	0.00204	20	1.46712	1.88678	10	0.282913	24	0.282910	5.9	0.9	0.62	64	2

3	0.0245	23	0.00072	5	1.46711	1.88672	7	0.282826	26	0.282825	2.8	0.9	0.79	63	1
5	0.0386	40	0.00117	10	1.46718	1.88655	9	0.282701	28	0.282700	-1.6	1.0	1.03	63	1
7	0.0224	21	0.00066	5	1.46713	1.88674	8	0.282883	25	0.282882	5.2	0.9	0.67	80	2
8	0.0346	29	0.00100	6	1.46718	1.88674	7	0.282900	28	0.282899	5.2	1.0	0.65	51	1
10	0.0540	50	0.00143	11	1.46719	1.88677	10	0.282802	22	0.282800	1.7	0.8	0.84	54	2
12	0.0431	35	0.00128	8	1.46717	1.88660	10	0.282858	24	0.282856	4.3	0.8	0.72	79	2
17	0.0328	27	0.00106	7	1.46719	1.88670	7	0.282726	28	0.282725	-0.7	1.0	0.98	63	1
19	0.0248	26	0.00086	7	1.46716	1.88652	7	0.282767	30	0.282766	0.8	1.0	0.90	64	2
20	0.0516	42	0.00162	10	1.46714	1.88675	9	0.282649	26	0.282647	-3.7	0.9	1.14	51	2
22	0.0464	38	0.00123	7	1.46719	1.88677	12	0.282827	19	0.282825	2.7	0.7	0.79	57	1
23	0.0379	33	0.00112	8	1.46713	1.88667	7	0.282790	29	0.282788	1.8	1.0	0.86	75	2
25	0.0259	22	0.00079	5	1.46716	1.88671	10	0.282735	24	0.282734	-0.2	0.8	0.96	72	2
27	0.0513	49	0.00139	11	1.46711	1.88677	9	0.282738	25	0.282737	-0.7	0.9	0.97	46	2
29c	0.0444	45	0.00122	10	1.46717	1.88656	8	0.282804	26	0.282803	2.3	0.9	0.83	75	2
29r	0.0216	26	0.00061	6	1.46711	1.88676	9	0.282782	26	0.282781	0.8	0.9	0.88	44	1
31	0.0832	96	0.00232	22	1.46719	1.88665	9	0.282808	40	0.282806	1.8	1.4	0.83	48	2
34	0.0540	45	0.00153	10	1.46711	1.88671	9	0.282833	29	0.282831	2.7	1.0	0.78	49	1
35	0.0245	20	0.00071	4	1.46716	1.88668	10	0.282698	24	0.282698	-2.1	0.8	1.04	46	3
36	0.0192	17	0.00055	4	1.46710	1.88680	10	0.282757	23	0.282756	0.2	0.8	0.93	57	2
37	0.0698	59	0.00187	12	1.46712	1.88654	11	0.282795	24	0.282793	1.7	0.8	0.85	62	3
39	0.0110	14	0.00036	4	1.46718	1.88660	8	0.282836	33	0.282836	3.0	1.2	0.77	54	1
41	0.0380	41	0.00111	10	1.46716	1.88680	12	0.282960	20	0.282958	7.8	0.7	0.52	75	2
42	0.0375	39	0.00112	10	1.46716	1.88658	10	0.282954	28	0.282952	7.5	1.0	0.54	72	2
44	0.0170	14	0.00056	4	1.46712	1.88679	10	0.282999	26	0.282998	9.1	0.9	0.45	70	2
46	0.0219	19	0.00070	5	1.46712	1.88662	11	0.282811	24	0.282811	2.0	0.8	0.82	49	1
47c	0.0593	48	0.00154	9	1.46715	1.88671	12	0.282986	25	0.282984	8.1	0.9	0.48	47	2
51	0.0303	24	0.00098	6	1.46715	1.88678	10	0.282926	16	0.282923	8.5	0.6	0.56	164	4
53	0.0464	38	0.00124	8	1.46711	1.88663	7	0.282752	24	0.282751	0.0	0.8	0.94	53	2
55	0.0388	40	0.00116	10	1.46715	1.88653	8	0.282859	30	0.282857	3.9	1.1	0.73	60	2
57	0.0566	67	0.00171	18	1.46717	1.88662	4	0.282658	38	0.282656	-3.5	1.3	1.12	48	3
59	0.0197	19	0.00057	4	1.46719	1.88651	8	0.282830	26	0.282829	3.1	0.9	0.78	69	1
61	0.0248	20	0.00070	4	1.46713	1.88678	9	0.282904	20	0.282903	5.8	0.7	0.63	76	2

62	0.0279	26	0.00099	8	1.46712	1.88670	11	0.282893	22	0.282891	5.6	0.8	0.65	84	2
63	0.0181	16	0.00056	4	1.46710	1.88679	9	0.282778	23	0.282777	2.7	0.8	0.85	134	3
64	0.0311	29	0.00095	7	1.46711	1.88671	10	0.282876	21	0.282875	4.4	0.7	0.69	57	2
66	0.0473	44	0.00149	11	1.46715	1.88656	7	0.282842	26	0.282840	3.4	0.9	0.76	65	1
68	0.0918	86	0.00267	20	1.46717	1.88677	9	0.282950	26	0.282947	6.8	0.9	0.56	49	2
69	0.0545	75	0.00150	18	1.46719	1.88671	10	0.283053	23	0.283051	11.0	0.8	0.34	73	3
70	0.0315	28	0.00099	7	1.46712	1.88679	10	0.282802	31	0.282801	1.8	1.1	0.84	56	1
73	0.0258	24	0.00077	5	1.46714	1.88678	10	0.283025	20	0.283024	10.3	0.7	0.39	83	5
74	0.0238	24	0.00076	6	1.46716	1.88667	9	0.282847	24	0.282844	6.7	0.9	0.69	208	6
76	0.0240	20	0.00082	5	1.46711	1.88679	9	0.282883	22	0.282882	4.7	0.8	0.68	58	2
77	0.0354	29	0.00099	6	1.46712	1.88672	10	0.282763	21	0.282762	0.4	0.7	0.92	54	2
78	0.0278	22	0.00077	5	1.46721	1.88663	10	0.282774	21	0.282774	0.8	0.7	0.89	55	3
79	0.0337	29	0.00120	8	1.46716	1.88664	8	0.282922	26	0.282920	7.0	0.9	0.59	101	3
80	0.0365	32	0.00118	8	1.46718	1.88671	9	0.282587	23	0.282585	-5.7	0.8	1.26	60	3
82	0.0247	22	0.00078	5	1.46719	1.88661	10	0.282869	23	0.282867	5.8	0.8	0.68	133	4
84	0.0446	36	0.00120	7	1.46715	1.88672	10	0.282880	24	0.282879	4.5	0.8	0.69	52	2
86	0.0355	29	0.00100	6	1.46711	1.88679	10	0.282767	21	0.282766	0.4	0.8	0.91	50	2
87	0.0326	28	0.00097	7	1.46715	1.88662	12	0.283042	23	0.283040	11.1	0.8	0.36	94	3
89	0.0236	20	0.00076	5	1.46719	1.88670	8	0.282982	23	0.282981	8.9	0.8	0.47	89	2
z1b2	0.0216	18	0.00066	4	1.46716	1.88671	10	0.282796	21	0.282793	4.2	0.7	0.81	174	7
6	0.0262	22	0.00071	5	1.46710	1.88660	8	0.281174	25	0.281138	2.4	0.9	2.95	2666	26
7	0.0493	63	0.00133	15	1.46718	1.88673	10	0.282753	22	0.282752	-0.3	0.8	0.94	41	2
9	0.0233	19	0.00074	5	1.46715	1.88680	12	0.282753	22	0.282753	-0.3	0.8	0.94	40	2
10	0.0416	34	0.00121	7	1.46713	1.88664	10	0.282946	24	0.282945	7.3	0.8	0.55	73	2
12	0.0461	58	0.00129	14	1.46715	1.88675	8	0.282755	26	0.282753	0.3	0.9	0.93	66	3
16	0.0418	34	0.00137	8	1.46712	1.88651	9	0.282888	26	0.282885	6.2	0.9	0.65	117	6
18	0.0628	51	0.00178	11	1.46718	1.88668	9	0.282843	27	0.282842	2.6	1.0	0.77	27	2
19	0.0431	36	0.00129	8	1.46711	1.88678	9	0.282849	21	0.282848	3.5	0.7	0.75	58	2
21c	0.0288	23	0.00093	6	1.46720	1.88664	11	0.282752	21	0.282751	-0.1	0.7	0.94	51	2
22	0.0405	33	0.00115	8	1.46712	1.88652	9	0.282780	23	0.282779	0.9	0.8	0.88	51	2
28	0.0247	20	0.00074	5	1.46728	1.88669	10	0.282606	24	0.282606	-5.2	0.9	1.22	50	2
17Mi1															

z3j1	0.0506	41	0.00152	9	1.46710	1.88671	8	0.282975	27	0.282973	8.2	0.9	0.50	70	1
2	0.0142	11	0.00048	3	1.46716	1.88653	10	0.282716	23	0.282716	-1.2	0.8	1.00	55	1
3	0.0318	26	0.00094	6	1.46724	1.88662	9	0.282790	24	0.282789	1.3	0.8	0.86	53	1
4	0.0212	18	0.00062	4	1.46719	1.88671	9	0.282461	23	0.282460	-9.5	0.8	1.49	90	1
5c	0.0135	13	0.00039	3	1.46713	1.88677	10	0.282671	22	0.282671	-2.4	0.8	1.09	72	1
5r	0.0157	13	0.00047	3	1.46711	1.88671	11	0.282676	23	0.282675	-2.9	0.8	1.09	46	1
6	0.0344	28	0.00098	6	1.46719	1.88666	8	0.282782	28	0.282780	1.3	1.0	0.88	64	2
7	0.0398	34	0.00108	7	1.46713	1.88671	10	0.282939	24	0.282938	6.6	0.8	0.57	53	1
8	0.0317	26	0.00085	5	1.46715	1.88679	10	0.282768	26	0.282767	0.8	0.9	0.90	66	4
9	0.0618	51	0.00168	11	1.46710	1.88678	11	0.282903	24	0.282902	5.3	0.9	0.64	50	1
10	0.0385	34	0.00120	8	1.46711	1.88668	8	0.282308	31	0.282306	-14.8	1.1	1.78	98	2
11	0.0250	26	0.00072	6	1.46715	1.88670	9	0.282886	20	0.282885	5.3	0.7	0.67	77	2
12	0.0315	26	0.00087	6	1.46713	1.88680	11	0.282815	22	0.282814	2.1	0.8	0.82	51	2
13	0.0309	27	0.00085	6	1.46729	1.88665	7	0.282911	25	0.282910	5.9	0.9	0.62	68	2
14	0.0660	54	0.00176	11	1.46718	1.88674	11	0.282660	29	0.282659	-3.4	1.0	1.12	50	1
15	0.0870	79	0.00238	19	1.46730	1.88663	9	0.282831	34	0.282828	2.7	1.2	0.79	54	1
16	0.0155	13	0.00042	3	1.46721	1.88675	8	0.281709	26	0.281695	4.5	0.9	2.21	1907	43
17	0.0374	32	0.00111	7	1.46718	1.88660	10	0.282720	23	0.282715	3.5	0.8	0.92	267	8
17r	0.0274	22	0.00076	5	1.46716	1.88671	11	0.282710	25	0.282710	-1.7	0.9	1.02	42	2
18	0.0224	18	0.00064	4	1.46713	1.88661	9	0.282822	24	0.282819	6.8	0.9	0.72	252	9
19	0.0232	20	0.00073	5	1.46717	1.88678	10	0.282626	18	0.282625	-4.1	0.6	1.18	70	1
20	0.0244	20	0.00072	5	1.46719	1.88670	10	0.282903	25	0.282903	5.4	0.9	0.64	54	2
21c	0.0260	21	0.00081	5	1.46718	1.88675	9	0.282720	22	0.282719	-1.1	0.8	1.00	54	2
22	0.0563	54	0.00147	12	1.46711	1.88676	10	0.282844	26	0.282842	3.2	0.9	0.76	52	2
23	0.0211	18	0.00073	5	1.46727	1.88671	8	0.282951	24	0.282948	10.1	0.9	0.49	194	5
24	0.0469	38	0.00134	8	1.46714	1.88655	11	0.282649	21	0.282647	-3.5	0.7	1.13	63	1
28	0.0506	44	0.00136	10	1.46718	1.88676	10	0.282751	32	0.282749	0.0	1.1	0.94	58	1
28r	0.0373	41	0.00101	10	1.46711	1.88680	11	0.282760	21	0.282757	2.6	0.7	0.88	161	7
29	0.0349	28	0.00094	6	1.46719	1.88673	12	0.282767	18	0.282766	0.5	0.6	0.91	52	1
30	0.0784	78	0.00223	21	1.46728	1.88671	9	0.282813	34	0.282807	3.8	1.2	0.80	133	2
31	0.0309	25	0.00094	6	1.46716	1.88663	8	0.282912	28	0.282910	7.1	1.0	0.60	121	3
32	0.0160	13	0.00051	3	1.46719	1.88679	10	0.282955	25	0.282954	7.7	0.9	0.53	78	2

33	0.0170	15	0.00050	3	1.46711	1.88664	9	0.282855	29	0.282854	4.0	1.0	0.73	71	1
34	0.0578	49	0.00167	11	1.46710	1.88670	8	0.282986	26	0.282984	8.4	0.9	0.48	60	2
35	0.0318	30	0.00114	9	1.46726	1.88669	4	0.282918	41	0.282917	6.5	1.4	0.60	84	2
36	0.0303	24	0.00084	5	1.46720	1.88678	10	0.282859	24	0.282857	4.3	0.8	0.72	77	3
37	0.0186	16	0.00061	4	1.46730	1.88667	8	0.282965	19	0.282965	7.5	0.7	0.52	52	1
38	0.0299	25	0.00095	6	1.46720	1.88659	8	0.282687	27	0.282684	0.3	0.9	1.02	173	7
39	0.0877	80	0.00243	18	1.46727	1.88667	7	0.282834	27	0.282832	2.9	1.0	0.78	57	1
41r	0.0204	18	0.00067	5	1.46712	1.88679	10	0.282810	23	0.282809	2.2	0.8	0.82	60	2
53	0.0323	27	0.00108	7	1.46713	1.88668	6	0.282767	32	0.282765	1.3	1.1	0.90	88	2
43c	0.0184	16	0.00062	4	1.46717	1.88671	9	0.282866	25	0.282864	5.5	0.9	0.69	122	3
44	0.0412	33	0.00116	7	1.46714	1.88671	11	0.282877	24	0.282876	4.4	0.8	0.69	54	2
45	0.0328	27	0.00090	6	1.46719	1.88679	14	0.282844	17	0.282843	3.3	0.6	0.76	54	1
46	0.0242	20	0.00071	4	1.46713	1.88671	9	0.283006	23	0.283003	11.9	0.8	0.39	186	6
47c	0.0355	33	0.00102	7	1.46713	1.88678	10	0.282820	18	0.282817	4.3	0.7	0.77	141	3
47r	0.0292	24	0.00090	6	1.46719	1.88674	8	0.282838	23	0.282837	3.0	0.8	0.77	51	1
48	0.0286	23	0.00075	5	1.46720	1.88670	11	0.282869	22	0.282868	4.2	0.8	0.71	55	2
56	0.0132	11	0.00041	3	1.46712	1.88673	13	0.282861	18	0.282860	4.1	0.6	0.72	63	2
49c	0.0423	41	0.00126	10	1.46710	1.88670	9	0.282993	21	0.282992	8.8	0.7	0.46	68	2
49r	0.0935	83	0.00254	18	1.46717	1.88671	10	0.283042	22	0.283038	10.9	0.8	0.36	87	3
52c	0.0440	62	0.00114	14	1.46722	1.88664	11	0.282736	19	0.282735	-0.5	0.7	0.97	56	1
z4f1	0.0372	30	0.00102	6	1.46719	1.88672	11	0.282756	20	0.282755	0.0	0.7	0.93	46	1
2	0.0243	27	0.00070	6	1.46714	1.88672	9	0.282751	25	0.282749	2.4	0.9	0.90	164	4
3	0.0276	22	0.00090	5	1.46718	1.88651	10	0.282727	26	0.282726	-0.8	0.9	0.98	60	1
4	0.0202	18	0.00055	4	1.46714	1.88670	9	0.282742	24	0.282741	0.5	0.9	0.94	93	3
5	0.0271	26	0.00090	8	1.46710	1.88671	10	0.282764	27	0.282763	0.4	1.0	0.91	56	1
z2h3	0.0209	17	0.00066	4	1.46718	1.88676	10	0.282646	21	0.282645	-3.7	0.7	1.14	57	1
4	0.0300	24	0.00079	5	1.46711	1.88668	11	0.282914	20	0.282913	5.7	0.7	0.62	55	1
z4g1	0.0447	38	0.00122	8	1.46710	1.88671	12	0.282826	21	0.282825	2.8	0.7	0.79	62	2
z1c1	0.0266	26	0.00097	8	1.46715	1.88671	8	0.283032	24	0.283029	11.4	0.9	0.36	124	7
6	0.0255	20	0.00099	6	1.46719	1.88666	9	0.282996	23	0.282994	10.2	0.8	0.43	127	6
7	0.0277	28	0.00097	8	1.46715	1.88670	11	0.282725	23	0.282722	1.8	0.8	0.94	182	4
12	0.0204	18	0.00068	5	1.46712	1.88661	9	0.282787	25	0.282787	1.6	0.9	0.86	70	2

17	0.0210	20	0.00070	5	1.46712	1.88660	9	0.282972	23	0.282971	8.3	0.8	0.50	78	2
18	0.0369	37	0.00115	9	1.46724	1.88662	7	0.282567	35	0.282566	-6.6	1.2	1.30	54	2
25	0.0262	23	0.00079	6	1.46713	1.88676	8	0.281846	35	0.281845	-31.5	1.3	2.66	79	2
Temora (n=23)	0.0450	354	0.00119	91	1.46713	1.88661	23	0.282680	25	0.282670	5.2	0.8	0.95	417	3
GJ-1 (n=30)	0.0090	3	0.00025	0	1.46714	1.88664	9	0.282012	21	0.282009	-14.0	0.7	2.15	606	6
JMC 475 (n=6)					1.46718	1.88669	11	0.282145	8						

Quoted uncertainties (absolute) relate to the last quoted figure. The effect of the inter-element fractionation on the Lu/Hf was estimated to be about 6 % or less based on analyses of the GJ-1 zircon. Accuracy and reproducibility was checked by repeated analyses (n = 30 and 23, respectively) of reference zircon GJ-1 and Temora (data given as mean with 2 standard deviation uncertainties)

(a) 176Yb/177Hf = (176Yb/173Yb)true x (173Yb/177Hf)meas x (M173(Yb)/M177(Hf))b(Hf), b(Hf) = ln(179Hf/177Hf true / 179Hf/177Hfmeasured)/ ln (M179(Hf)/M177(Hf)), M=mass of respective isotope. The 176Lu/177Hf were calculated in a similar way by using the 175Lu/177Hf and b(Hf).

(b) Mean Hf signal in volt.

(c) Uncertainties are quadratic additions of the within-run precision and the daily reproducibility of the 40ppb-JMC475 solution. Uncertainties for the JMC475 quoted at 2SD (2 standard deviation).

(d) Initial 176Hf/177Hf and eHf calculated using the apparent Pb-Pb age determined by LA-ICP-MS dating (see column f), and the CHUR parameters:

176Lu/177Hf = 0.0336, and 176Hf/177Hf = 0.282785 (Bouvier et al., 2008).

(e) two stage model age in billion years using the measured 176Lu/177Lu of each spot (first stage = age of zircon), a value of 0.0113 for the average continental crust (second stage), and a juvenile crust (NC) 176Lu/177Lu and 176Hf/177Hf of 0.0384 and 0.28314, respectively.

(f) apparentU-Pb age determined by LA-ICP-MS

seq1

GJ1-001	0.0090	7	0.00025	2	1.46716	1.88651	10	0.282007	21	0.282004	-14.2	0.8	2.16	604	5	105
GJ1-002	0.0090	7	0.00025	2	1.46711	1.88667	10	0.282001	21	0.281998	-14.4	0.8	2.17	604	5	105
GJ1-030	0.0091	7	0.00026	2	1.46719	1.88657	10	0.282021	22	0.282018	-13.7	0.8	2.14	604	5	105
GJ1-031	0.0090	7	0.00026	2	1.46718	1.88667	10	0.282015	23	0.282012	-13.9	0.8	2.15	604	5	105
GJ1-060	0.0091	7	0.00025	2	1.46713	1.88651	9	0.281997	26	0.281994	-14.5	0.9	2.18	604	5	105
GJ1-061	0.0090	7	0.00026	2	1.46713	1.88676	9	0.282009	22	0.282006	-14.1	0.8	2.16	604	5	105
GJ1-092	0.0091	7	0.00025	2	1.46705	1.88656	9	0.282007	23	0.282004	-14.1	0.8	2.16	604	5	105
GJ1-093	0.0090	7	0.00025	2	1.46715	1.88658	9	0.282003	21	0.282000	-14.3	0.8	2.17	604	5	105

GJ1-124	0.0090	7	0.00025	2	1.46712	1.88662	8	0.282022	22	0.282020	-13.6	0.8	2.13	604	5	105
GJ1-125	0.0088	7	0.00025	2	1.46711	1.88659	9	0.282006	19	0.282003	-14.2	0.7	2.16	604	5	105
GJ1-498	0.0086	7	0.00025	2	1.46716	1.88662	9	0.282003	25	0.282000	-14.3	0.9	2.17	604	5	105
GJ1-449	0.0088	7	0.00025	2	1.46713	1.88677	9	0.281997	23	0.281994	-14.5	0.8	2.18	604	5	0
GJ1-497	0.0087	7	0.00025	2	1.46719	1.88662	10	0.282004	21	0.282001	-14.3	0.7	2.17	604	5	0
GJ1-396	0.0088	7	0.00025	2	1.46712	1.88666	9	0.282005	25	0.282002	-14.2	0.9	2.17	604	5	0
GJ1-347	0.0088	7	0.00025	2	1.46711	1.88672	9	0.282023	23	0.282020	-13.6	0.8	2.13	604	5	0
GJ1-346	0.0089	7	0.00025	2	1.46714	1.88663	9	0.282013	18	0.282010	-14.0	0.6	2.15	604	5	0
GJ1-295	0.0088	7	0.00025	2	1.46713	1.88671	9	0.282001	21	0.281998	-14.4	0.7	2.17	604	5	0
GJ1-294	0.0090	7	0.00025	2	1.46713	1.88661	9	0.282030	20	0.282028	-13.3	0.7	2.12	604	5	0
GJ1-245	0.0089	7	0.00025	2	1.46713	1.88667	9	0.282013	24	0.282010	-13.9	0.9	2.15	604	5	0
GJ1-244	0.0089	7	0.00025	2	1.46715	1.88670	9	0.282031	21	0.282028	-13.3	0.7	2.12	604	5	0
GJ1-185	0.0089	7	0.00025	2	1.46714	1.88671	10	0.282015	20	0.282012	-13.9	0.7	2.15	604	5	0
GJ1-184	0.0089	7	0.00025	2	1.46713	1.88670	9	0.281999	24	0.281996	-14.4	0.9	2.18	604	5	0
GJ1-124	0.0090	7	0.00026	2	1.46711	1.88668	10	0.282034	18	0.282031	-13.2	0.6	2.11	604	5	0
GJ1-123	0.0090	7	0.00026	2	1.46715	1.88664	9	0.282008	27	0.282005	-14.1	1.0	2.16	604	5	0
GJ1-093	0.0091	7	0.00026	2	1.46718	1.88661	10	0.282014	21	0.282011	-13.9	0.7	2.15	604	5	0
GJ1-092	0.0091	7	0.00026	2	1.46716	1.88664	9	0.282016	21	0.282013	-13.9	0.7	2.15	604	5	0
GJ1-031	0.0091	7	0.00026	2	1.46713	1.88671	10	0.282012	18	0.282009	-14.0	0.6	2.15	604	5	0
GJ1-030	0.0090	7	0.00026	2	1.46711	1.88662	10	0.282033	21	0.282030	-13.2	0.7	2.11	604	5	0
GJ1-002	0.0090	7	0.00026	2	1.46711	1.88664	11	0.282008	24	0.282005	-14.1	0.8	2.16	604	5	0
GJ1-001	0.0092	7	0.00026	2	1.46715	1.88662	11	0.282010	21	0.282007	-14.1	0.7	2.16	604	5	0
30	0.0090	3	0.00025	0	1.46714	1.88664	9.4	0.282012	21	0.282009	-14.0	0.7	2.15			
TM-003	0.0428	34	0.00111	7	1.46715	1.88670	25	0.282707	13	0.282699	6.2	0.5	0.89	417	5	100
TM-004	0.0343	29	0.00094	6	1.46717	1.88654	25	0.282676	14	0.282668	5.2	0.5	0.95	417	5	100
TM-032	0.0832	84	0.00218	17	1.46712	1.88654	21	0.282706	20	0.282689	5.9	0.7	0.91	417	5	100
TM-033	0.0396	32	0.00100	6	1.46716	1.88650	24	0.282675	16	0.282667	5.1	0.6	0.95	417	5	100
TM-062	0.0858	82	0.00224	17	1.46716	1.88656	21	0.282683	17	0.282665	5.1	0.6	0.96	417	5	100

TM-063	0.0343	29	0.00085	6	1.46706	1.88662	21	0.282675	16	0.282668	5.2	0.6	0.95	417	5	100
TM-094	0.0877	88	0.00229	19	1.46709	1.88663	20	0.282677	18	0.282659	4.8	0.6	0.97	417	5	100
TM-095	0.0499	40	0.00134	8	1.46714	1.88652	25	0.282690	15	0.282679	5.5	0.5	0.93	417	5	100
TM-122	0.0290	29	0.00074	6	1.46712	1.88662	20	0.282679	15	0.282673	5.3	0.5	0.94	417	5	100
TM-123	0.0392	40	0.00098	8	1.46714	1.88662	19	0.282666	18	0.282659	4.8	0.6	0.97	417	5	100
TM-495	0.0378	30	0.00099	6	1.46712	1.88664	24	0.282671	13	0.282663	5.0	0.5	0.96	417	5	100
TM-496	0.0440	36	0.00117	7	1.46710	1.88679	22	0.282674	17	0.282665	5.0	0.6	0.96	417	5	100
TM-398	0.0347	28	0.00094	6	1.46717	1.88655	26	0.282679	15	0.282672	5.3	0.5	0.94	417	5	100
TM-399	0.0324	26	0.00091	6	1.46715	1.88653	26	0.282664	14	0.282657	4.8	0.5	0.97	417	5	100
TM-296	0.0413	38	0.00111	8	1.46706	1.88658	22	0.282673	16	0.282664	5.0	0.6	0.96	417	5	100
TM-297	0.0302	24	0.00083	5	1.46718	1.88655	25	0.282665	16	0.282658	4.8	0.6	0.97	417	5	100
TM-246	0.0502	43	0.00133	9	1.46712	1.88667	22	0.282677	14	0.282666	5.1	0.5	0.95	417	5	100
TM-247	0.0422	35	0.00111	7	1.46722	1.88664	22	0.282704	15	0.282696	6.1	0.5	0.90	417	5	100
TM-126	0.0412	35	0.00108	7	1.46708	1.88651	21	0.282667	16	0.282659	4.8	0.6	0.97	417	5	100
TM-095	0.0460	37	0.00131	8	1.46714	1.88680	25	0.282685	16	0.282675	5.4	0.6	0.94	417	5	100
TM-094	0.0238	19	0.00070	4	1.46713	1.88664	24	0.282680	15	0.282675	5.4	0.5	0.94	417	5	100
TM-004	0.0414	33	0.00106	6	1.46715	1.88676	24	0.282678	14	0.282669	5.2	0.5	0.95	417	5	100

8.4.4 Appendix D: REE data

Sample	identifier	La	Ce	Pr	Nd	Sm	Eu	Gd	Tb	Dy	Ho	Er	Tm	Yb	U/Pb age (Ma)	type
18MPl2	z1cr4	0.035	2.05	0.262	1.08	10.28	0.4	50.3	98.68	198.22	356.72	597.36	897.13	1250.73	51.97	unknown
	z1cr2	30.26	64.18	27	26.13	28.48	14.62	68.47	121.4	230.4	401.87	664.8	1044.57	1490.35	54.01	unknown
	z1dr50	15.61	20.12	9.04	7.19	9.01	5.46	28.04	52.9	111.18	207.55	361.75	629.61	968.79	53.65	unknown
	z1dr38	50.24	69.77	59.49	44.19	43.42	8.27	75.96	116.45	207.78	374.73	635.79	1021.27	1457.53	73.52	unknown
	z1dr29	0.203	16.78	0.44	1.09	5.83	2.83	19.02	45.3	96.44	168.5	308.99	566.28	899.83	75.06	unknown
	z2cr3	0.092	45.89	0.8	1.97	18.86	19.13	70.48	132.66	233.36	413.78	694.63	1147.56	1741.57	80.09	unknown
	z1dr30	0.102	17.28	0.75	1.1	11.1	4.1	35.29	67.1	147.29	272.04	491.12	809.56	1272.33	127.42	unknown
	z1cr7	0.058	9.12	0.154	0.399	2.57	4.95	14.5	24.77	63.71	123.56	250.11	470.61	788.13	175.42	unknown
	z1dr56	0.0179	16.39	0.93	3.62	28.91	18.58	139.58	269.49	563.85	983.89	1586.1	2424.92	3310.76	1628.92	unknown
17Pi	z2br4	0.476	3.94	1.57	3.05	15.92	10.16	92.79	168.27	356.69	656.74	1092.35	1579.72	1970.43	33.56	magmatic
	z1fr6	22.93	34.8	21.24	22.93	30.5	7.33	70.06	132.65	253.76	449.09	737.75	1132.96	1575.14	37.27	magmatic
	z2br2	0.818	21.7	3.08	6.49	51.73	26.11	159.29	275.23	447.39	693.97	925.33	1423.35	1960.98	56.22	magmatic
	z2br6	0.094	25.64	0.177	0.93	5.74	8.63	30.36	61.63	136.34	275.98	549.58	1010.38	1632.28	51.94	unknown
	z2br8	127.97	126.35	78.12	62.54	47.54	49.87	84.59	131.05	227.6	393.71	659.8	1092.53	1582.03	53.30	unknown
	z2br3	97.86	97	66.75	56.33	38.96	12.47	59.83	87.24	169.25	298.53	515.53	844.34	1263.05	60.46	magmatic
	z1fr3	15.6	35.61	14.08	14.05	20.38	6.56	60.08	119.11	229.61	418.08	695.76	1180.31	1748.96	62.54	magmatic
	z2br9	0.686	49.41	1.9	4.57	28.57	31.08	107.02	170.99	281.9	434.68	647.22	981.75	1338.49	106.91	magmatic
17Mi2	z1ar32	0.061	2.62	2.59	6.93	56.44	0.61	222.77	455.61	919.76	1586.29	2559.55	3845.8	5219.14	48.15	magmatic
	z1ar33	0.175	1.65	0.33	1.15	7.68	0.79	35.95	73.04	139.99	263.35	432.24	662.03	916.26	50.55	magmatic
	z1ar71	6.89	8.7	7.53	8.93	18.99	1.02	57.74	100.4	187.96	329.76	548.76	812.94	1083.65	50.72	magmatic
	z1ar9	0.041	1.569	0.74	2.99	22.75	4.97	100.59	183.98	327.39	553.88	853.27	1245.77	1724.91	51.36	magmatic
	z1a68	5.17	32.78	4.62	5.58	15.12	5.33	68.81	134.85	300.05	630.18	1142.04	1849.47	2725.14	51.58	magmatic
	z1br23	0.524	9.53	0.77	2.29	12	7.98	40.68	77.67	132.71	234.67	387.51	654.67	1015.41	53.13	magmatic
	z1ar77	0.399	1.709	0.78	1.87	15.86	1.46	82.36	157.28	312.38	554.96	902.33	1368.73	1841.36	54.29	magmatic
	z1ar21	0.525	18.71	0.97	1.41	7.47	9.34	47.55	83.59	171.47	318.68	560.53	908.2	1451.8	54.49	magmatic
	z1ar36	0.039	3.34	0	1.17	13.51	2.47	54	106.44	167.5	257	347.58	476.23	678.51	56.64	magmatic
	z1ar55	2.15	23.84	1.86	3.03	16.82	8.31	78.85	171.58	351.88	625.04	1055.1	1680.3	2380.79	56.66	magmatic
	z1br20	0.066	12.54	0.79	1.77	11.7	9.3	54.22	107.27	202.98	370.62	647.37	1064.43	1603.13	58.45	magmatic
	z1ar38	0	0.626	0.74	2.82	29.39	1.29	145.63	278.1	537.69	914.94	1379.53	1991.15	2585.36	62.48	magmatic
	z1ar17	0.087	4.04	0.6	1.15	6.2	2.16	37.04	83.2	174.03	322.22	575.66	1004.56	1614.37	62.67	magmatic
	z1ar19	0	9.65	0.63	2.46	12.82	12.18	39.37	62.4	119.05	200.35	336	576.95	891.79	63.02	magmatic
	z1ar25	7.34	34.1	5.81	6.54	21.16	18.43	70.03	113.76	197.57	326.51	529.58	837.46	1254.1	54.29	metamorphic
	z1ar30	0.074	2.96	2.01	6.19	38.1	4.71	153.81	290.27	560.87	955.33	1500.14	2183.73	2878.41	43.53	metamorphic
	z1ar28	0.183	1.51	0.75	2.44	12.39	0.79	71.66	141.62	281.91	469.12	761.95	1131.68	1570.59	46.23	metamorphic
	z1ar6	126.37	110.58	90.56	75.63	46.75	15.76	60.8	83.24	138.55	238.99	405.51	655.98	964.45	63.09	magmatic

z1br6	0.105	15	1.34	4.11	17.13	16.83	64.41	99.21	166.12	254.51	378.92	550.26	740.91	63.09	magmatic
z1ar4	2.07	6.67	2.27	2.76	9.97	3.85	31.15	55.64	99.52	174.91	287.83	481.9	713.94	64.10	magmatic
z1ar5	4.09	12.94	3.44	3.9	10.86	7.5	45.57	84.31	160.49	293.18	501.87	785.86	1125.5	65.29	magmatic
z1ar66	0.236	10.31	0.57	1.66	11.02	5.6	47.82	90.57	174.65	306.46	540.84	845.67	1310	67.23	magmatic
z1ar60	7.36	16.73	8.89	10.96	28.75	10.99	131.85	238.57	411	656.19	987.2	1389.7	1810.06	69.30	magmatic
z1ar59	0.373	4.79	0.52	1.29	9.88	7.35	50.74	92.1	150.42	257.94	413.19	634.1	953.52	71.31	magmatic
z1ar43	14.16	19.68	10.46	8.88	10.16	5.06	32.27	59.17	115.57	210.58	376.47	643.69	990.84	72.15	magmatic
z1ar61	0.182	2.06	0.289	1.01	8.89	1.92	39.19	75.76	146.73	253.18	445.28	729.18	1058.15	75.97	magmatic
z1a67	0	12.21	0.289	0.95	5.64	7.12	26.05	55.5	111.51	211.05	398.29	695.25	1101.08	78.00	magmatic
z1ar13	23.87	38.21	14.9	12.6	24.12	9.01	76.86	135.86	272.86	496.76	866.75	1445.49	2186.45	79.16	magmatic
z1br13	0	0.389	0.148	1.2	12.44	0.42	83.45	210.46	492.05	936.7	1674.83	2805.04	3981.73	79.16	magmatic
z1ar89	0	10.17	0.103	0.76	4.11	7.92	24.43	46.75	90.44	166.05	294.54	504.18	798.61	89.37	magmatic
z1ar87	5.23	16.91	5.55	6.44	12.54	3.65	42.74	81.07	163.63	307.62	539.24	897.9	1342.79	91.84	magmatic
z1br26	18.55	24.75	6.58	5.57	4.68	5.68	18.1	35.67	70.61	140.26	261.65	480.35	771	100.22	magmatic
z1br15	0	4.92	0.119	0.349	1.71	4.38	12.96	22.17	50.66	98.76	215.43	419.1	815.65	209.82	magmatic
z1ar2	0.86	5.52	1.52	2.85	17.05	8.09	87.23	161.33	313.98	580.49	959.73	1428.52	2023.82	299.75	magmatic
z1ar58	0.034	22.98	0.63	1.66	10.88	8.79	56.63	106.53	202.74	383.25	673.27	1144.48	1790.17	103.56	unkown
z1ar45	0.058	11.62	0.81	2.04	14.42	13.38	45.35	78.7	137.39	226.94	394.48	644.19	1006.41	70.37	metamorphic
z1ar24	0	14.85	1.08	4.26	22.21	15.66	86.98	152.21	279.23	477.15	767.97	1150.89	1568.59	74.95	metamorphic
z1ar40	0.048	2.55	0.132	0.45	4.9	3.19	33.37	73.63	108.78	154	227.36	349.04	504.67	75.83	metamorphic

8.4.5 Appendix E: (U-Th)/He data

		He		U238			Th232				Sm			Ejection	*Uncorr.*	Ft-Corr.	
Sample	aliq.	vol. [ncc]	1σ [%]	mass [ng]	1σ [%]	conc. [ppm]	mass [ng]	1σ [%]	conc. [ppm]	Th/U ratio	mass [ng]	1σ [%]	conc. [ppm]	correct. (Ft)	*He-age [Ma]*	He-age [Ma]	2σ [Ma]
U1417-Pliocene																	
	z1	**15.43**	1.3	**2.95**	1.8	569	**0.66**	2.4	128	0.22	**0.003**	2.4	1	**0.796**	*41.1*	**51.6**	3.8
	z2	**12.09**	1.3	**1.65**	1.8	385	**0.43**	2.4	101	0.26	**0.023**	2.4	5	**0.773**	*56.8*	**73.5**	5.9
	z3	**3.67**	1.3	**2.57**	1.8	369	**0.47**	2.4	67	0.18	**0.004**	2.4	1	**0.806**	*11.3*	**14.1**	1.0
	z4	**3.23**	1.4	**2.45**	1.8	234	**0.38**	2.4	37	0.16	**0.006**	2.4	1	**0.850**	*10.5*	**12.4**	0.8
	z5	**9.29**	1.3	**2.48**	1.8	1429	**0.53**	2.4	306	0.21	**0.016**	2.4	9	**0.695**	*29.4*	**42.4**	4.3
	z6	**1.72**	1.4	**0.22**	2.1	122	**0.07**	2.5	39	0.32	**0.001**	2.4	1	**0.699**	*58.6*	**83.9**	8.5
	z7	**16.14**	1.3	**3.83**	1.8	1732	**0.52**	2.4	234	0.13	**0.005**	2.4	2	**0.717**	*33.8*	**47.1**	4.5
	z8	**1.88**	1.4	**1.44**	1.8	525	**0.26**	2.4	95	0.18	**0.003**	2.4	1	**0.737**	*10.4*	**14.1**	1.3
	z9	**7.27**	1.3	**1.92**	1.8	598	**0.52**	2.4	162	0.27	**0.005**	2.4	2	**0.734**	*29.4*	**40.1**	3.6
	z10	**4.28**	1.3	**0.88**	1.8	147	**0.42**	2.4	70	0.47	**0.002**	2.4	0	**0.789**	*36.3*	**45.9**	3.5
	z11	**5.85**	0.9	**0.78**	1.8	537	**0.21**	2.4	144	0.27	**0.025**	14.0	17	**0.732**	*58.0*	**79.3**	7.0
	z12	**0.90**	1.1	**0.34**	1.9	154	**0.16**	2.4	70	0.46	**0.004**	14.0	2	**0.711**	*19.7*	**27.7**	2.6
	z13	**5.20**	0.9	**0.56**	1.8	257	**0.26**	2.4	119	0.46	**0.006**	14.0	3	**0.693**	*68.6*	**98.9**	9.8
	z14	**12.56**	0.9	**1.91**	1.8	644	**0.49**	2.4	166	0.26	**0.019**	14.0	6	**0.730**	*51.1*	**70.0**	6.2
	z15	**13.40**	0.8	**3.40**	1.8	1297	**0.83**	2.4	318	0.25	**0.019**	14.0	7	**0.726**	*30.8*	**42.4**	3.8
	z16	**19.07**	0.9	**5.02**	1.8	1439	**0.57**	2.4	162	0.11	**0.013**	14.0	4	**0.742**	*30.6*	**41.2**	3.6
	z17	**0.81**	1.1	**0.19**	2.0	100	**0.12**	2.4	64	0.64	**0.004**	14.0	2	**0.707**	*30.2*	**42.7**	4.1
	z18	**3.67**	0.9	**0.74**	1.8	245	**0.29**	2.4	95	0.39	**0.009**	14.0	3	**0.752**	*37.5*	**49.9**	4.2
	z19	**7.48**	0.8	**1.76**	1.8	885	**0.40**	2.4	200	0.23	**0.015**	14.0	8	**0.681**	*33.3*	**48.9**	5.0
	z20	**5.51**	0.9	**1.53**	1.8	562	**0.57**	2.4	210	0.37	**0.018**	14.0	7	**0.700**	*27.4*	**39.2**	3.8
	z21	**1.95**	0.9	**0.59**	1.8	305	**0.24**	2.4	124	0.41	**0.010**	14.0	5	**0.699**	*25.1*	**35.8**	3.5
	z22	**1.40**	1.0	**0.30**	1.9	214	**0.16**	2.4	111	0.52	**0.007**	14.0	5	**0.677**	*34.0*	**50.2**	5.2
	z23	**5.03**	0.9	**2.92**	1.8	650	**0.65**	2.4	143	0.22	**0.029**	14.0	7	**0.775**	*13.6*	**17.5**	1.3
	z24	**22.21**	0.9	**1.67**	1.8	444	**0.75**	2.4	199	0.45	**0.030**	14.0	8	**0.727**	*99.1*	**136.3**	12.2

	z25	**12.86**	0.8	**3.55**	1.8	847	**1.02**	2.4	242	0.29	**0.022**	14.0	5	**0.770**	*28.0*	**36.4**	2.8
	z26	**6.38**	0.9	**0.49**	1.8	154	**0.17**	2.4	53	0.34	**0.006**	14.0	2	**0.745**	*98.4*	**132.1**	11.2
	z27	**19.67**	0.8	**7.55**	1.8	740	**1.30**	2.4	128	0.17	**0.011**	14.0	1	**0.798**	*20.7*	**26.0**	1.8
	z28	**6.41**	0.9	**1.33**	1.8	456	**0.54**	2.4	186	0.41	**0.043**	14.0	15	**0.741**	*36.4*	**49.1**	4.2
	z29	**11.80**	0.9	**1.98**	1.8	751	**0.88**	2.4	336	0.45	**0.041**	14.0	16	**0.729**	*44.6*	**61.2**	5.5
	z30	**2.10**	0.9	**0.76**	1.8	248	**0.21**	2.4	70	0.28	**0.016**	14.0	5	**0.722**	*21.5*	**29.7**	2.7
	z31	**1.26**	1.0	**0.32**	1.9	126	**0.08**	2.4	32	0.26	**0.004**	14.0	2	**0.724**	*30.4*	**42.0**	3.9
	z32	**1.61**	0.9	**0.77**	1.8	307	**0.21**	2.4	86	0.28	**0.018**	14.0	7	**0.724**	*16.2*	**22.3**	2.0
	z33	**2.28**	0.9	**1.04**	1.8	405	**0.18**	2.4	70	0.17	**0.005**	14.0	2	**0.712**	*17.4*	**24.5**	2.3
U1417-Miocene1,2																	
	z1	**8.69**	1.3	**3.94**	1.8	631	**0.60**	2.4	95	0.15	**0.309**	15.7	49	**0.788**	*17.6*	**22.4**	1.7
	z2	**2.09**	1.3	**1.31**	1.8	424	**0.26**	2.4	85	0.20	**0.004**	2.4	1	**0.732**	*12.6*	**17.2**	1.6
	z3	**14.23**	1.3	**5.92**	1.8	812	**0.67**	2.4	92	0.11	**0.005**	2.4	1	**0.801**	*19.4*	**24.2**	1.8
	z4	**7.18**	1.3	**3.10**	1.8	654	**0.31**	2.4	65	0.10	**0.008**	2.4	2	**0.751**	*18.7*	**24.9**	2.1
	z5	**23.05**	1.3	**2.21**	1.8	1197	**0.24**	2.4	131	0.11	**0.004**	2.4	2	**0.731**	*83.6*	**114.4**	10.5
	z6	**2.26**	1.3	**0.93**	1.8	458	**0.25**	2.4	122	0.27	**0.004**	2.4	2	**0.680**	*18.9*	**27.9**	2.9
	z7	**7.03**	1.3	**3.53**	1.8	661	**0.56**	2.4	104	0.16	**0.007**	2.4	1	**0.782**	*15.9*	**20.3**	1.6
	z8	**4.63**	1.3	**3.04**	1.8	1028	**0.35**	2.4	117	0.11	**0.120**	15.7	41	**0.724**	*12.3*	**17.0**	1.6
	z9	**1.25**	1.4	**0.71**	1.8	266	**0.20**	2.4	73	0.27	**0.005**	2.4	2	**0.731**	*13.7*	**18.7**	1.7
	z10	**16.80**	1.3	**4.04**	1.8	661	**0.33**	2.4	54	0.08	**0.004**	2.4	1	**0.789**	*33.7*	**42.7**	3.3
	z11	**10.29**	0.8	**3.30**	1.8	628	**0.94**	2.4	179	0.28	**0.010**	14.0	2	**0.783**	*24.1*	**30.8**	2.3
	z12	**2.90**	0.9	**1.61**	1.8	570	**0.46**	2.4	163	0.29	**0.007**	14.0	3	**0.716**	*14.0*	**19.5**	1.8
	z13	**6.47**	0.8	**4.84**	1.8	1381	**0.36**	2.4	102	0.07	**0.008**	14.0	2	**0.728**	*10.9*	**14.9**	1.3
	z14	**7.84**	0.9	**2.84**	1.8	576	**0.48**	2.4	98	0.17	**0.009**	14.0	2	**0.797**	*22.0*	**27.6**	2.0
	z15	**6.18**	0.9	**1.63**	1.8	685	**0.28**	2.4	117	0.17	**0.008**	14.0	3	**0.670**	*30.2*	**45.1**	4.8
	z16	**12.49**	0.9	**1.38**	1.8	307	**0.57**	2.4	126	0.41	**0.020**	14.0	4	**0.724**	*68.1*	**94.0**	8.5
	z17	**3.20**	0.9	**1.40**	1.8	414	**0.34**	2.4	101	0.24	**0.018**	14.0	5	**0.735**	*17.9*	**24.4**	2.1
	z18	**0.33**	1.3	**0.50**	1.8	261	**0.32**	2.4	165	0.63	**0.012**	14.0	6	**0.696**	*4.8*	**6.9**	0.7
	z19	**19.24**	0.9	**3.89**	1.8	502	**1.01**	2.4	131	0.26	**0.033**	14.0	4	**0.786**	*38.5*	**49.0**	3.6
	z20	**5.22**	0.9	**1.19**	1.8	447	**0.41**	2.4	152	0.34	**0.012**	14.0	5	**0.693**	*33.4*	**48.2**	4.8
	z21	**3.21**	0.9	**1.04**	1.8	416	**0.45**	2.4	180	0.43	**0.023**	14.0	9	**0.695**	*23.1*	**33.2**	3.3

z22	**7.18**	1.1	**2.39**	1.8	779	**0.13**	2.4	44	0.06	**0.006**	14.0	2	**0.706**	*24.5*	**34.7**	3.4
z23	**11.99**	0.8	**1.31**	1.8	242	**0.73**	2.4	134	0.56	**0.053**	14.0	10	**0.819**	*66.5*	**81.1**	5.3
z24	**2.28**	0.9	**0.77**	1.8	134	**0.41**	2.4	71	0.53	**0.033**	14.0	6	**0.734**	*21.8*	**29.6**	2.6
z25	**27.18**	0.8	**6.23**	1.8	1934	**1.45**	2.4	449	0.23	**0.030**	14.0	9	**0.748**	*34.1*	**45.7**	3.8
z26	**1.88**	1.0	**1.62**	1.8	351	**0.39**	2.4	84	0.24	**0.015**	14.0	3	**0.753**	*9.1*	**12.1**	1.0
z27	**6.50**	0.8	**2.47**	1.8	701	**0.49**	2.4	141	0.20	**0.020**	14.0	6	**0.709**	*20.8*	**29.4**	2.8
z28	**4.19**	0.9	**0.92**	1.8	385	**0.31**	2.4	129	0.33	**0.004**	14.0	2	**0.691**	*34.7*	**50.2**	5.0
z29	**5.45**	0.9	**1.22**	1.8	527	**0.46**	2.4	198	0.38	**0.015**	14.0	6	**0.716**	*34.0*	**47.5**	4.4
z30	**12.43**	0.9	**6.51**	1.8	2376	**0.13**	2.4	48	0.02	**0.012**	14.0	4	**0.721**	*15.7*	**21.8**	2.0
z31	**5.91**	0.8	**3.39**	1.8	1439	**0.21**	2.4	91	0.06	**0.009**	14.0	4	**0.668**	*14.2*	**21.3**	2.3
z32	**6.12**	0.9	**2.06**	1.8	443	**0.86**	2.4	185	0.42	**0.027**	14.0	6	**0.760**	*22.4*	**29.5**	2.4
z33	**5.77**	0.8	**1.61**	1.8	520	**0.33**	2.4	106	0.20	**0.022**	14.0	7	**0.710**	*28.3*	**39.9**	3.8
z34	**21.20**	0.9	**2.86**	1.8	646	**0.59**	2.4	133	0.21	**0.015**	14.0	3	**0.799**	*58.2*	**72.8**	5.2
z35	**14.30**	0.8	**5.74**	1.8	3446	**2.65**	2.4	1589	0.46	**0.023**	14.0	14	**0.666**	*18.6*	**27.9**	3.0
z36	**8.71**	0.9	**1.77**	1.8	418	**0.86**	2.4	204	0.49	**0.024**	14.0	6	**0.799**	*36.4*	**45.6**	3.2
z37	**0.45**	1.2	**0.37**	1.9	200	**0.06**	2.5	32	0.16	**0.006**	14.0	3	**0.646**	*9.8*	**15.2**	1.7

Note. Amount of helium is given in nano-cubic-cm in standard temperature and pressure.

Amount of radioactive elements are given in nanograms.

Ejection correct. (Ft): correction factor for alpha-ejection (according to Farley et al., 1996 and Hourigan et al., 2005).

Uncertainties of helium and the radioactive element contents are given as 1 sigma, in relative error %.

Uncertaintiy of the single grain age is given as 2 sigma in Ma and it includs both the analytical uncertainty and the estimated uncertainty of the Ft.

References: Farley, K.A.; Wolf, R.A. and Silver, L.T. 1996. The effects of long alpha-stopping distances on (U-Th)/He ages. Geochimica et Cosmochimica Acta, 60, 4223–4229, 1996. doi:10.1016/S0016-7037(96)00193-7.

Hourigan, J. K.; P. W. Reiners; and M. T. Brandon 2005. U-Th zonation-dependent alpha-ejection in (U-Th)/He chronometry, Geochim. Cosmochim. Acta, 69(13), 3349–3365. doi:10.1016/j.gca.2005.01.024.

8.4.6 Appendix F: ε(Hf) values calculated from ε(Nd) values from literature

$\varepsilon(Hf)_t$ values calculated from ε(Nd) values from literature for different plutons of the Sanak-Baranof Plutonic belt

εNd(T)	εHf(calc.)	T (Ma)	Name	type	source
-2.6	-0.664	50	Rude River Pluton	granodiorite	Baker et al. (1992)
-3.3	-1.602	50	Rude River Pluton	granodiorite	Baker et al. (1992)
2.02	5.5268	50	McKinley peak Pluton	granodiorite	Baker et al. (1992)
1.11	4.3074	50	McKinley peak Pluton	granodiorite	Baker et al. (1992)
1.22	4.4548	50	McKinley peak Pluton	granodiorite	Baker et al. (1992)
2.07	5.5938	50	McKinley peak Pluton	granodiorite	Baker et al. (1992)
-2.4	-0.396	50	Sheep Bay Pluton	granodiorite	Baker et al. (1992)
-0.8	1.748	50	Sheep Bay Pluton	granodiorite	Baker et al. (1992)
-1.2	1.212	50	Sheep Bay Pluton	granodiorite	Baker et al. (1992)
10.3	16.622	50	Basalts/Basaltic Tuff		Baker et al. (1992)
11	17.56	50	Basalts/Basaltic Tuff		Baker et al. (1992)
7.94	13.4596	50	Tonalite/Dacite		Baker et al. (1992)
7.1	12.334	50	Nunatak Fjord	diorite	Sisson et al. (2003)
3.5	7.51	50	Mount Draper	tonalite	Sisson et al. (2003)
2.1	5.634	50	Nunatak Fjord	gabbro	Sisson et al. (2003)
2.1	5.634	50	Nunatak Fjord	gabbro	Sisson et al. (2003)
9.6	15.684	50	Nunatak Fjord	amphibolite	Sisson et al. (2003)
-1	1.48	50	Van Cleve Glacier	tonalite	Sisson et al. (2003)
-0.6	2.016	50	Van Cleve Glacier	tonalite	Sisson et al. (2003)
-2.3	-0.262	50	Novatak Glacier	tonalite	Sisson et al. (2003)
3.1	6.974	50	Mount Draper	granite	Sisson et al. (2003)
8.3	13.942	50	Nunatak Fjord	felsic dike	Sisson et al. (2003)
5.3	9.922	50	Nunatak Fjord	amphiblite	Sisson et al. (2003)
8.6	14.344	50	Nunatak Fjord	gabbro	Sisson et al. (2003)
1.3	4.562	50	Mount Stamy	leucosome	Sisson et al. (2003)
7.6	13.004	50	Nunatak Fjord	amphibolite	Sisson et al. (2003)

Note. ε(Hf) values were calculated from ε(Nd) values from Baker et al. (1992); Sissson et al. (2003) using the equation for the crustal array from Vervoort et al. (1999).

Sources: Barker, F.; Farmer, G.L.; Ayuso, R.A.; Plafker, G.; and Lull, J.S. 1992. The 50 Ma granodiorite of the eastern Gulf of Alaska: Melting in an accretionary prism in the forearc. J. Geophys. Res. 97 (B5), 6757-6778.

Vervoort, J.D., Patchett, P., Blichert-Toft, J., Albarède, F. 1999. Relationships between Lu–Hf andSm–Nd isotopic systems in the global sedimentary system. Earth Planet. Sci. Lett. 168 (1-2),79–99. 10.1016/S0012-821X(99)00047-3.

Sisson, V.B.; Poole, A.R.; Harris, N.R.; Burner, H.C.; Pavlis, T.L.; Copeland, P.; Donelick, R.A.; and McLelland, W.C. 2003. Geochemical and geochronologic constraints for genesis of a tonalitetrondjemite suite and associated mafic intrusive rocks in the eastern Chugach Mountains, Alaska: A record of ridge-transform subduction. In Sisson, V. B.; Roeske, S. M.; and Pavlis, T. L. eds., Geology of a transpressional orogen developed during ridge-trench interaction along the North Pacific margin. Geol. S. Am. S. 371, 293–326.

8.5 Appendix for Huber and Bahlburg, 2018; to be submitted

8.5.1 Appendix A: IODP codes of the samples

sample name	IODP identifier
17Pe87	341-U1417C-11H-2-W 70/72-BAHL
17Pe93	341-U1417C-11H-6-W 66/68-BAHL
17Pe146	341-U1417D-17H-6-W 28/29-BAHL
17Pe181	341-U1417D-25H-1-W 148/150-BAHL
17Pe243	341-U1417D-40X-1-W 52/54-BAHL
17Pi400	341-U1417E-7R-2-W 15/24-BAHL
17Mi438	341-U1417E-11R-1-W 22/66-BAHL
17Mi602	341-U1417E-28R-2-W 0/13-BAHL
17Mi642	341-U1417E-32R-1-W 113/120-BAHL
17Mi704	341-U1417E-39R-4-W 144/149-BAHL
18MPe4	341-U1418A-1H-4-W 17/25-BAHL
18MPe96	341-U1418A-11H-5-W 86/89-BAHL
18MPe106	341-U1418D-12H-CC-W 6/8-BAHL
18MPe158	341-U1418E-11H-3-W 81/83-BAHL
18MPe171	341-U1418A-25H-1-W 87/91-BAHL
18MPe280	341-U1418D-35X-3-W 53/58-BAHL
18EPe900	341-U1418F-68R-1-W 27/33-BAHL
18EPe939	341-U1418F-72R-1-W 1/19-BAHL

8.5.2 Appendix B: Geochemical data of pyroxene in wt% from sites U1417 and U1418

sample name	Na_2O	MgO	SiO_2	Al_2O_3	K_2O	CaO	FeO	TiO_2	Cr_2O_3	MnO	Total
17Pe87	0.17	3.53	49.40	3.18	0.00	19.08	12.95	1.89	0.01	0.36	99.86
17Pe87	0.94	10.63	52.30	19.21	0.03	17.15	4.97	0.03	0.03	0.21	93.96
17Pe87	0.33	16.92	51.14	3.57	0.05	12.57	16.78	0.84	0.03	0.19	98.72
17Pe87	0.09	2.61	52.66	2.12	0.09	12.05	16.41	0.22	0.04	0.30	97.23
17Pe87	0.93	16.04	53.62	1.51	0.05	12.14	15.80	0.08	0.02	0.27	97.51
17Pe87	0.21	16.57	47.32	11.36	0.11	11.63	9.77	0.44	0.20	0.17	97.17
17Pe87	2.20	9.01	31.58	11.83	0.01	13.99	15.15	13.01	0.01	0.23	91.80
17Pe87	0.42	16.61	41.32	5.35	0.27	19.41	5.39	22.40	0.02	0.07	96.37
17Pe243	1.84	10.38	51.17	2.76	0.12	11.18	19.13	0.25	0.04	0.54	96.01
17Pe243	1.44	9.61	52.88	3.61	0.01	12.17	13.62	0.10	0.01	0.29	97.56
17Pe243	0.32	10.28	51.00	5.48	0.04	11.89	14.14	0.28	0.00	0.32	97.14
17Pe243	0.18	15.47	48.48	5.36	0.01	17.43	12.38	1.09	0.00	0.29	98.88
17Pe243	0.66	18.63	49.70	4.80	0.13	11.66	17.16	1.81	0.00	0.26	95.87
17Pe243	0.77	18.58	38.25	9.52	0.22	13.39	14.56	13.97	0.10	0.22	96.62
17Pe243	0.21	16.63	45.22	11.95	0.11	11.54	12.57	0.43	0.02	0.21	95.84
17Pe243	1.08	15.62	37.04	7.15	0.12	21.37	2.18	27.27	0.06	0.01	98.72
17Pe243	0.20	15.01	48.73	7.17	0.26	11.67	15.66	0.31	0.12	0.25	96.37
17Pe243	0.69	14.54	45.15	12.31	0.25	11.61	15.19	0.33	0.07	0.23	96.74
17Pe243	0.31	17.41	45.81	11.32	0.21	11.23	13.52	0.25	0.07	0.25	96.03
17Pe243	0.57	6.18	44.71	9.07	0.22	10.74	19.76	0.30	0.03	0.27	95.53
17Pe243	0.47	16.96	39.03	8.92	0.17	10.59	16.58	17.77	0.01	0.86	100.30
17Pe243	0.16	5.90	50.14	5.10	0.09	11.50	15.53	0.22	0.01	0.30	96.26

17Pe243	1.68	6.74	46.61	7.15	0.33	11.90	20.74	1.07	0.00	0.28	97.07
17Pe243	1.09	13.45	48.29	7.87	0.07	13.51	17.39	0.10	0.00	0.23	96.90
17Pe243	0.09	16.39	35.21	2.18	0.02	23.58	4.33	29.30	0.02	0.11	97.14
17Pe243	0.39	13.76	46.83	8.48	0.29	11.44	17.90	0.39	0.02	0.32	96.35
17Pe243	0.02	0.10	52.00	4.06	0.14	12.01	14.17	0.21	0.03	0.25	96.60
17Pe243	0.59	11.63	50.38	4.56	0.28	12.20	18.30	0.40	0.02	0.33	97.24
17Pe243	0.48	12.86	44.36	5.57	0.20	13.34	17.88	3.97	0.04	0.30	95.59
17Pe243	0.40	13.61	46.24	9.43	0.29	11.52	14.76	0.36	0.04	0.52	96.46
17Pe243	1.78	14.39	51.45	4.20	0.10	13.22	15.20	0.09	0.00	0.33	97.60
17Pe243	0.03	5.96	46.85	7.27	0.14	9.78	18.24	0.12	0.02	0.35	94.29
17Pe243	0.10	2.05	24.49	2.18	0.00	21.04	12.29	39.43	0.02	0.98	100.53
17Pe243	0.41	12.58	55.28	2.39	0.12	11.62	16.31	0.12	0.00	0.35	98.02
17Pe243	0.02	0.01	52.83	2.19	0.08	12.56	15.47	0.93	0.00	0.35	97.24
17Pe243	0.80	11.44	53.11	4.06	0.04	11.93	11.93	0.16	0.03	0.25	97.19
17Pe243	1.51	12.46	53.80	2.37	0.02	12.32	11.07	0.54	0.00	0.23	96.06
17Pe243	1.21	8.46	48.92	8.47	0.06	11.65	14.73	0.23	0.08	0.26	97.65
17Pe243	1.21	10.55	49.36	7.13	0.10	11.62	13.56	0.29	0.03	0.29	95.89
17Pi400	1.59	11.56	52.81	7.26	0.13	11.18	16.74	0.20	0.03	0.23	100.79
17Pi400	1.00	11.93	32.29	14.00	0.02	9.44	15.53	11.22	0.05	0.23	93.83
17Pi400	5.25	0.53	46.97	6.06	0.16	9.27	21.09	0.12	0.00	0.54	94.82
17Pi400	1.32	12.53	55.84	1.29	0.01	12.50	10.88	0.00	0.05	0.31	97.71
17Pi400	0.20	13.24	51.20	5.95	0.15	11.48	10.36	0.13	1.27	0.21	97.45
17Pi400	1.26	11.43	54.41	1.64	0.05	12.20	13.39	0.27	0.03	0.36	97.56
17Pi400	0.16	16.09	53.09	3.39	0.11	12.56	10.69	1.91	0.11	0.22	97.30
17Pi400	0.11	12.05	55.59	1.69	0.08	12.24	10.21	0.02	0.04	0.20	97.78
17Pi400	0.29	10.29	54.91	1.67	0.08	12.50	13.06	0.09	0.01	0.14	98.11
17Pi400	0.40	15.51	54.55	2.62	0.13	12.27	7.90	0.16	0.05	0.28	97.24
17Pi400	0.18	13.94	53.02	4.49	0.06	12.80	7.00	0.31	0.12	0.15	97.30
17Pi400	0.25	12.97	43.56	13.03	0.45	11.37	17.22	0.44	0.00	0.23	96.16
17Pi400	1.55	10.98	40.38	15.73	0.32	13.97	16.32	1.78	0.08	0.27	95.60
17Pi400	0.01	0.03	54.40	2.55	0.09	12.14	10.40	0.07	0.02	0.33	97.42
17Pi400	0.01	2.12	33.59	3.36	0.82	13.59	10.93	16.66	0.06	0.10	85.17
17Pi400	0.19	12.47	43.94	10.35	1.28	11.64	17.94	1.19	0.00	0.54	97.13
17Pi400	0.46	12.91	42.11	12.16	0.68	11.30	22.23	0.03	0.00	0.25	97.18
17Pi400	0.17	16.90	46.79	8.30	0.42	11.53	13.43	1.20	0.02	0.40	96.62
17Pi400	0.92	10.38	55.24	1.47	0.04	12.41	11.40	0.14	0.02	0.18	97.39
17Pi400	0.53	12.73	52.76	2.45	0.01	11.39	15.01	0.43	0.02	0.34	96.56
17Pi400	0.54	11.84	30.61	0.65	0.01	27.15	0.64	40.79	0.02	0.01	100.01
17Pi400	1.64	10.89	49.80	5.87	0.18	12.02	15.50	0.39	0.04	0.12	96.14
17Pi400	0.03	17.27	44.05	10.85	1.09	12.14	13.42	0.81	0.04	0.23	96.90
17Pi400	1.78	11.65	47.20	1.76	0.00	21.83	10.31	7.73	0.00	0.39	99.18
17Pi400	0.22	15.07	55.69	1.21	0.05	12.77	11.20	0.02	0.04	0.21	98.05
17Mi642	0.66	13.50	54.60	0.94	0.01	12.46	13.74	0.04	0.00	0.26	97.01
17Mi642	0.44	15.66	47.33	10.38	0.03	10.51	13.97	0.52	0.03	0.34	96.90
17Mi642	0.29	16.60	49.55	5.04	0.06	10.93	19.49	0.10	0.01	0.36	96.88
17Mi642	0.51	9.42	43.37	15.90	0.08	14.77	6.23	0.13	0.00	0.14	82.64
17Mi642	0.34	13.03	45.06	11.16	0.14	11.64	15.10	0.44	0.02	0.25	96.18
17Mi642	0.50	14.38	55.45	1.78	0.00	12.48	8.03	0.00	0.08	0.21	97.98
17Mi642	3.35	1.22	52.42	2.09	0.13	11.85	18.32	0.12	0.02	0.34	97.09
17Mi642	1.07	15.16	45.17	13.42	0.05	17.54	14.17	0.15	0.03	0.28	97.98

17Mi642	1.47	12.32	48.69	5.94	0.48	10.86	16.86	0.79	0.03	0.80	96.69
17Mi642	0.01	17.72	43.51	2.15	0.09	18.53	8.34	16.64	0.03	0.19	98.35
17Mi642	1.11	14.72	46.60	9.23	0.37	11.29	15.43	1.10	0.03	0.59	96.73
17Mi642	0.32	17.60	55.68	0.74	0.05	12.04	12.61	0.00	0.00	0.27	97.47
17Mi642	1.08	11.35	54.45	1.05	0.07	12.47	14.34	0.03	0.00	0.29	97.43
17Mi642	0.38	13.04	46.68	9.72	0.21	11.75	14.07	0.34	0.07	0.23	97.04
17Mi642	0.96	11.29	47.67	5.03	0.53	11.50	21.63	0.37	0.00	0.37	96.76
17Mi642	0.98	9.02	44.76	10.53	0.24	11.68	15.96	0.45	0.01	0.29	95.68
17Mi642	0.80	16.41	44.24	11.30	0.23	11.77	16.35	0.88	0.01	0.26	96.84
17Mi642	0.51	15.80	46.94	11.15	0.31	14.22	16.30	0.49	0.05	0.29	97.41
17Mi642	0.34	14.75	52.05	2.58	0.22	11.78	17.15	0.58	0.01	0.43	97.63
17Pi400	0.30	14.49	50.53	4.69	0.00	18.43	8.26	1.34	0.19	0.22	99.37
18MPe171	1.62	10.18	53.84	1.12	0.04	12.03	16.49	0.14	0.00	0.30	97.18
18MPe171	0.33	7.34	46.07	10.93	0.19	11.24	14.51	0.50	0.05	0.26	96.28
18MPe171	0.69	12.15	28.70	0.58	0.00	26.21	0.62	42.46	0.08	0.06	98.75
18MPe171	0.16	14.80	42.42	16.94	0.05	15.22	13.56	0.05	0.00	0.08	90.46
18MPe171	0.97	12.82	53.99	0.81	0.02	12.11	17.20	0.13	0.01	0.38	97.31
18MPe171	0.99	10.35	53.10	1.19	0.10	11.74	17.63	0.05	0.04	0.31	97.53
18MPe171	0.17	1.85	52.83	1.62	0.00	17.88	9.61	0.83	0.06	0.27	100.17
18MPe171	1.12	11.25	43.55	5.67	0.12	17.28	13.10	1.90	0.02	0.28	93.22
18MPe171	0.11	19.84	51.37	3.32	0.19	11.76	14.84	0.07	0.00	0.36	95.17
18MPe171	0.38	11.42	49.77	5.59	0.51	10.86	16.80	0.24	0.02	0.43	96.59
18MPe171	0.28	6.89	54.23	6.09	0.14	9.99	12.93	0.11	0.02	0.29	96.33
18MPe171	0.43	8.45	55.28	1.29	0.04	12.64	10.38	0.01	0.11	0.29	97.34
18MPe171	1.09	11.00	43.33	11.44	0.23	10.39	15.62	0.28	0.04	0.25	95.02
18MPe171	0.36	15.72	52.08	3.25	0.17	11.05	17.25	0.07	0.01	0.40	97.21
18MPe171	0.24	14.50	48.39	10.29	0.02	12.57	2.76	19.18	0.00	0.45	99.45
18MPe171	0.49	12.87	51.44	2.53	0.00	20.31	8.65	0.57	0.30	0.24	99.32
18MPe171	0.36	13.37	56.04	2.69	0.09	11.43	15.32	0.02	0.02	0.38	99.84
18MPe171	0.42	10.35	53.59	1.22	0.04	12.34	16.16	0.00	0.02	0.43	97.25
18MPe171	0.28	9.64	47.32	9.48	0.09	11.63	14.98	0.34	0.08	0.29	96.90
18MPe171	1.26	12.04	54.09	1.94	0.04	13.06	10.79	0.34	0.43	0.19	97.12
18MPe171	0.43	12.58	50.60	2.79	0.02	10.93	18.44	0.08	0.30	0.21	95.53
18MPe171	0.47	11.05	48.53	2.32	0.09	14.41	15.82	2.90	0.01	0.31	94.96
18MPe171	0.00	0.09	59.57	1.32	0.05	11.31	8.50	0.10	0.00	0.45	97.20
18MPe171	0.18	11.66	51.52	1.00	0.02	14.05	13.90	0.32	0.00	0.49	95.42
18MPe280	5.77	0.02	50.91	3.38	0.25	12.18	18.16	0.07	0.02	0.30	97.11
18MPe280	5.31	8.24	50.78	6.15	0.05	12.10	9.78	0.05	0.01	0.23	97.02
18MPe280	5.46	0.21	36.48	9.66	0.05	29.27	0.49	0.06	0.02	0.03	81.85
18MPe280	0.34	14.80	34.24	8.94	0.00	19.64	5.27	21.22	0.00	0.09	94.01
18MPe280	0.26	11.94	51.50	1.83	0.00	18.16	10.80	0.66	0.09	0.34	99.08
18MPe280	0.35	14.31	30.49	8.77	0.00	16.70	7.02	21.42	0.06	0.09	92.38
18MPe280	0.56	11.28	53.17	3.06	0.10	12.38	12.91	0.13	0.04	0.30	97.27
18MPe280	1.18	16.70	39.90	4.58	0.03	21.83	2.43	26.28	0.05	0.07	99.54
18MPe280	0.73	3.87	54.48	1.97	0.03	11.53	16.11	0.00	0.00	0.35	98.07
18MPe280	0.30	15.40	33.64	4.77	0.02	22.14	3.80	29.28	0.03	0.10	95.92
18MPe280	0.03	7.79	51.36	5.06	0.18	12.36	14.20	0.19	0.06	0.51	97.25
18MPe280	0.34	14.84	49.34	6.67	0.25	13.12	14.36	1.78	0.04	0.62	97.92
18MPe280	2.11	2.27	49.76	7.67	0.22	12.08	13.95	0.22	0.07	0.33	97.33
18MPe280	0.79	12.82	36.45	3.21	0.09	23.03	6.45	24.64	0.01	0.11	97.69

18MPe280	0.86	1.27	47.37	7.60	0.38	12.11	17.19	0.07	0.06	0.19	96.54
18MPe280	0.49	12.84	53.73	2.30	0.38	11.68	12.80	0.53	0.01	0.27	96.85
18MPe280	0.81	10.93	53.23	1.49	0.05	12.33	17.77	0.10	0.03	0.37	97.57
18MPe280	0.59	12.44	54.02	2.49	0.05	12.55	13.70	0.10	0.05	0.28	97.89
18EPe900	0.30	13.27	54.71	2.50	0.08	12.59	10.37	0.10	0.06	0.25	97.74
18EPe900	0.26	16.82	34.21	2.25	0.03	24.15	2.59	29.92	0.07	0.05	95.87
18EPe900	0.10	2.50	44.19	12.83	0.28	11.51	16.14	0.45	0.06	0.29	96.83
18EPe900	1.20	9.88	47.73	7.67	0.17	13.07	13.06	2.68	0.01	0.26	97.07
18EPe900	0.68	11.73	48.36	13.07	0.24	11.64	12.09	0.43	0.19	0.22	100.65
18EPe900	2.20	12.20	46.77	11.80	0.13	8.02	13.85	0.18	0.00	0.21	96.96
18EPe900	1.40	14.60	50.33	8.10	0.16	11.70	9.96	0.26	0.17	0.22	98.03
18EPe900	1.83	15.31	49.86	7.48	0.09	12.09	9.78	0.31	0.20	0.19	97.00
18EPe900	1.24	15.76	52.80	2.33	0.08	12.46	15.77	0.03	0.00	0.26	97.19
18EPe900	0.16	13.30	49.28	6.92	0.04	11.86	15.62	0.09	0.26	0.30	97.35
18EPe900	0.91	12.06	48.65	7.26	0.33	10.41	14.54	1.10	0.05	0.34	96.59
18EPe900	0.82	13.09	32.23	5.47	0.03	19.56	6.22	23.48	0.00	0.10	93.27
18EPe900	0.37	10.73	49.57	4.03	0.13	12.62	16.66	2.32	0.03	0.24	96.70
18EPe900	0.42	14.57	53.12	2.97	0.08	12.05	13.50	0.03	0.04	0.32	97.10
18EPe900	0.45	10.91	50.64	4.48	0.22	12.31	18.10	0.22	0.04	0.34	97.71
18EPe900	0.02	6.16	53.88	3.50	0.08	12.46	9.68	0.11	0.05	0.22	97.23
18EPe900	0.26	15.44	33.79	1.57	0.00	25.18	1.45	32.61	0.02	0.05	97.38
18EPe900	1.26	8.60	55.39	1.03	0.04	10.29	12.29	0.00	0.02	0.37	96.40
18EPe900	1.20	9.04	53.49	2.09	0.02	11.60	11.84	0.02	0.10	0.27	96.21
18EPe900	1.47	12.80	49.04	12.35	0.25	10.53	13.84	0.29	0.03	0.17	97.71
18EPe900	0.19	9.76	54.59	2.75	0.05	12.62	10.22	0.03	0.00	0.28	97.57
18EPe900	0.14	16.71	49.13	2.18	0.03	16.10	8.44	7.87	0.04	0.19	97.54
18EPe939	0.20	12.64	50.66	4.86	0.07	12.16	10.61	0.57	0.34	0.23	96.71
18EPe939	0.48	15.19	53.39	3.77	0.05	12.09	11.04	0.06	0.03	0.25	97.00
18EPe939	0.21	15.50	52.76	3.54	0.09	12.19	12.55	0.14	0.52	0.21	97.09
18EPe939	1.00	12.24	52.87	3.17	0.05	12.41	12.50	0.33	0.40	0.23	96.74
18EPe939	0.82	12.69	45.73	12.66	0.10	11.56	13.21	0.40	0.03	0.28	97.11
18EPe939	0.36	10.46	50.16	6.71	0.15	12.16	11.08	0.11	0.10	0.26	96.96
18EPe939	0.54	14.33	46.08	8.79	0.26	13.42	11.59	2.85	0.04	0.26	97.08
18EPe939	0.81	13.18	56.32	0.47	0.01	13.22	9.88	0.00	0.05	0.11	97.80
18EPe939	0.27	13.57	49.02	8.52	0.21	12.38	10.91	0.25	0.16	0.22	97.50
18EPe939	0.59	9.76	54.40	2.85	0.00	12.80	7.88	0.45	0.18	0.18	96.66
18EPe939	1.35	5.05	51.71	5.91	0.20	11.85	15.82	0.26	0.07	0.26	98.51
18EPe939	1.76	12.03	51.89	3.92	0.24	12.13	15.11	0.27	0.03	0.25	97.25
18EPe939	1.78	1.75	47.37	9.92	0.20	11.66	14.85	0.33	0.12	0.25	96.96
18EPe939	0.72	11.47	37.17	9.03	0.19	9.03	18.80	11.08	0.07	0.93	96.29
18EPe939	1.17	10.44	47.62	9.70	0.24	11.57	13.87	0.33	0.08	0.24	96.89
18EPe939	1.55	11.81	53.65	1.80	0.10	12.11	14.23	0.19	0.03	0.35	97.21
18EPe939	0.75	9.68	53.67	1.66	0.06	12.53	13.49	0.09	0.02	0.31	96.78
18EPe939	3.17	3.21	51.51	5.10	0.01	11.38	15.53	0.15	0.04	0.32	97.64
18EPe939	0.89	8.09	53.74	3.04	0.07	12.20	15.27	2.43	0.00	0.33	99.10
18EPe939	0.46	8.98	54.02	1.37	0.02	12.40	13.66	0.10	0.02	0.30	96.76
18EPe939	0.15	2.25	53.10	2.64	0.01	12.07	13.45	0.41	0.01	0.29	96.76
18EPe939	0.96	9.73	53.29	3.10	0.06	11.95	13.36	0.03	0.00	0.24	97.21
18EPe939	0.77	16.89	53.32	3.09	0.08	12.08	12.70	0.11	0.07	0.30	97.14
18EPe939	1.24	13.19	54.02	2.71	0.06	12.42	11.73	0.02	0.04	0.28	97.16

18EPe939	1.41	11.94	55.02	4.70	0.17	10.11	13.16	0.59	0.01	0.21	96.68
18EPe939	1.00	12.24	54.04	2.80	0.10	11.80	13.94	0.02	0.01	0.34	97.21
18EPe939	0.37	14.38	53.11	3.16	0.10	12.38	10.63	0.35	0.13	0.20	96.16
18EPe939	0.24	14.70	51.24	4.12	0.01	11.34	11.32	0.07	0.07	0.24	95.29
18EPe939	0.93	12.67	41.09	5.38	0.07	17.50	9.01	14.56	0.06	0.19	97.80
18EPe939	0.72	11.29	52.10	3.41	0.07	12.15	15.53	0.12	0.00	0.31	97.05
18EPe939	0.20	14.67	52.55	3.51	0.12	12.37	13.69	0.01	0.00	0.29	97.43
18EPe939	0.51	14.27	45.09	8.67	0.02	17.20	1.48	22.72	0.00	0.05	99.80
18EPe939	0.49	14.68	52.43	4.91	0.05	12.39	8.96	0.18	0.10	0.17	96.84
18EPe939	0.41	14.99	47.73	10.36	0.09	11.66	11.96	0.41	0.07	0.28	96.99
18EPe939	0.31	15.56	45.54	12.35	0.08	11.58	12.83	0.37	0.10	0.27	96.47
18EPe939	1.43	11.28	24.22	7.45	0.02	37.79	0.56	0.02	0.00	0.01	75.74